EUROPEAN COMMISSION

Radiation Protection 140

Cosmic Radiation Exposure of Aircraft Crew

Compilation of Measured and Calculated Data

Final Report of
EURADOS WG 5

to

the Group of Experts established under
Article 31 of the Euratom treaty

Directorate-General for Energy and Transport
Directorate H — Nuclear Energy
Unit H.4 — Radiation Protection

2004

This report was produced by the European Radiation Dosimetry Group (EURADOS) for the European Commission and represents that organisation's views on the subject matter. These views have not been adopted or in any way approved by the Commission and should not be relied upon as a statement of the Commission's views.

The European Commission does not guarantee the accuracy of the data included in this report, nor does it accept responsibility for any use made thereof.

Luxembourg: Office for Official Publications of the European Communities, 2004

ISBN 92-894-8448-9

Printed in Belgium

PRINTED ON WHITE CHLORINE-FREE BLEACHED PAPER

Text completed on 20 May 2004

FOREWORD

Already in 1913, the Nobel Prize winner Victor F. Hess discovered and described the ionising radiation of cosmic origin. The technical developments of civil aviation, supersonic flights and space travel, together with more accurate knowledge about cosmic radiation, motivated in 1966 the International Commission on Radiological Protection, ICRP, to consider the biological effects of the varying solar radiation and the relatively constant galactic radiation, and to recommend for aircrew preventive measures in specific cases. The 1990 ICRP Recommendations stated that exposures to cosmic radiation during flight in jet aircraft should be included as part of occupational exposure of aircrew.

With the protection of aircrew, a new occupational radiation protection area was opened with many unknown parameters. Therefore, in 1991, the Radiation Protection Unit jointly with scientific experts in this field, the aviation companies, regulatory bodies and the social partners developed a work programme aimed at laying down appropriate European radiation protection legislation and to ensure its uniform conversion into practical radiation protection measures. From the beginning of this work programme, the association of institutes in the European Dosimetry Group, EURADOS, provided considerable expertise and co-ordinated important research projects.

The 1996 European Council Directive on the protection of the workers and the general public against the dangers arising from ionising radiation allows for the 1990 ICRP recommendations. Specific requirements are incorporated into this European radiation protection legislation aimed at establishing a radiological protection system for aircrew.

This report, prepared by a specific EURADOS Working Group delivers the successful conclusion of the above mentioned work programme.

The European Commission thanks EURADOS for the intensive support and in particular the scientists and experts for their personal efforts. Their strong commitment was essential for the success of the entire work programme.

Indispensable for achieving the envisaged objectives was also the constructive dialogue between the group of experts established pursuant to Article 31 of the Euratom Treaty and EURADOS. As a result of this fruitful co-operation, the now presented publication provides guidelines, recommendations and practical solutions for applying radiological protection measures for air crew exposed to cosmic radiation, based on the most recent scientific knowledge.

Augustin JANSSENS
Head of Unit

Cosmic Radiation Exposure of Aircraft Crew

Compilation of Measured and Calculated Data

A Report of EURADOS WG 5

to

Group of Experts established under

Article 31 of the EURATOM Treaty

Edited by

L. Lindborg, D. T. Bartlett, P. Beck, I. R. McAulay, K. Schnuer,
H. Schraube and F. Spurný

European Radiation Dosimetry Group

EURADOS Working Group 5 on Aircraft Crew Exposure

D.T. Bartlett[1], P. Beck[2], P. Bilski[3], J.-F. Bottollier-Depois[4], L. Lindborg[5] (Chairman from 2003), H. Schraube[6], F. Spurný[7] and F. Wissmann[8], E. Felsberger[9] (resigned in 2002), W. Heinrich[10], B. Lewis[11], D. O´Sullivan[12], G. Reitz[13], U. Schrewe[14] (Chairman 2000 to 2002), and L. Tommasino[15], G. Dietze[8] for Article 31, I. McAulay[16] for Article 31, J. Siedenburg[17] (2004) and A. Ruge (2000 –2003) for JAA, K. Schnuer[18] for EC and K. Ulbak[19] for Article 31.

Contributions were also received from:
J.C. Saez-Vergara[(20)], H. Roos[(21)], G.A. Taylor[(22)], R. Grillmaier[(23)], W. Friedberg[(24)], K. O'Brien[(25)], M. Pelliccioni[(26)], B. Wiegel[(8)] and their colleagues.

(1) National Radiological Protection Board (NRPB), Chilton Didcot, UK
(2) ARC Seibersdorf Research (ARCS), Seibersdorf, Austria
(3) Institute of Nuclear Physics, Krakow, Poland
(4) Institute for Radiation Protection and Nuclear Safety (IRSN) , Paris, France
(5) Swedish Radiation Protection Authority (SSI), Stockholm, Sweden
(6) Forschungszentrum für Umwelt und Gesundheit (GSF), Institut für Strahlenschutz, Neuherberg, Germany
(7) Nuclear Physics Institute, Academy of Sciences of Czech Republic, Prague
(8) Physikalisch-Technische Bundesanstalt (PTB), Braunschweig, Germany
(9) IASON Labormedizin GesmbH. & Co KG, Austria
(10) Universität, Siegen, Germany
(11) Royal Military College of Canada (RMC), Kingston, Ontario, Canada
(12) Dublin Institute for Advanced Studies (DIAS), Dublin, Ireland
(13) Deutsches Zentrum für Luft und Raumfahrt (DLR), Institut für Luft- und Raumfahrtmedizin, Köln, Germany
(14) Fachhochschule, Hannover, Germany
(15) National Agency for Environmental Protection and Technical Services (APAT), Rome, Italy
(16) Trinity College, Dublin, Ireland
(17) Central Joint Aviation Authority (JAA), Hoofdorp, The Netherlands
(18) European Commission, DG TREN H4, Luxembourg
(19) Statens Institut for Straalehygiejne (SIS), Knapholm, Denmark
(20) CIEMAT, Dosimetría de Radiaciones, Madrid, Spain
(21) Radiobiologisches Institut, Ludwig-Maximilians-Universität München, Germany
(22) National Physical Laboratory, Teddington, U.K.
(23) Fachrichtung Biophysik, Universität des Saarlandes, Homburg/Saar, Germany
(24) Civil Aerospace Medical Institute, Federal Aviation Administration, Oklahoma City, USA
(25) Northern Arizona University, Flagstaff, Arizona, USA
(26) INFN, Laboratori Nazionali di Frascati, Frascati, Italy

Cosmic Radiation Exposure of Aircraft Crew:

Compilation of Measured and Calculated Data

Contents

Preface

The knowledge of cosmic radiation dosimetry onboard aircraft has increased dramatically during the last ten years and new results are continuously being reported. To guide authorities as well as companies concerned with exposure to cosmic radiation, the Article 31 group of experts[1], proposed in February 2000 to the Directorate DG XI Environment. "*that a EURADOS working group is installed with the aim to validate the existing dose rate data in flight altitudes and to evaluate a data set which might become the basis for a recommendation of the Article 31 experts group*".

In 2002, taking into account the experience acquired by the members and first analysis of data, the following objective was agreed:

" The objective of the working group is to bring together all recent, available, preferably published, experimental data and results of calculations, with detailed descriptions of methods of measurement and calculation, in particular from European research groups.

The purpose is to provide a data set for all Member States for the assessment of individual doses and/or to assess the validity of different approaches, and to provide an input to technical recommendations by the Article 31 group of experts and the EC.

The quantity of interest is effective dose, E(ISO), but the comparison of measurement results obtained by different methods or groups, and comparison of measurement results and the results of calculations will be done in terms of the operational quantity ambient dose equivalent, H(10).*

The report giving the results of the investigations is to be published by the EC DG ENV."

In May 2000 the chairman of EURADOS invited a number of experts with experiences of cosmic ray dosimetry to form a working group (WG 5) on Aircrew Dosimetry. Three observers from the Article 31 Group of Experts as well as one observer from the Joint Aviation Authorities (JAA) were also appointed. The European Commission funded the meetings. Full meetings were organised in January 2001 and in November 2001. An editorial group started late in 2002 to finalise a draft report, which was submitted to the Group of Experts under Article 31 in June 2003.

The European Radiation Dosimetry Group (EURADOS) is an international society, which has the objectives to advance the scientific understanding of the dosimetry of ionising radiation and to ensure compatibility of the dosimetric procedures used within the EU. EURADOS in co-operation with the Directorates General XI and XII [2] published a report in 1996 titled "Exposure of air crew to cosmic radiation" (European Commission, DG Environment, Nuclear Safety and Civil Protection Radiation Protection 85;ECSC-EC-EAEC, Brussels, Luxembourg, 1996 (ISBN 92-827-7994-7) EURADOS report 1996-01.

The methods and results now reported have been obtained through the work of a number of scientists within EU, USA and Canada. Some of the work has been supported by Contracts with the European Commission, Directorate General XII, Science, Research and Development, Radiation Protection Research Action such as Contracts F13P-CT92-0026, F14P-CT950011a and FIGM-CT2000-00068. EURADOS is currently partly supported under Contract no FIR1-CT-2000-20104.

Ian McAulay
Chairman of the Article 31 Group of Experts

Pascal Pihet
Chairman of Eurados

[1] The Group of Experts is established under Article 31 of the Euratom Treaty
[2] Currently DG TREN and DG RTD respectively

I Introduction

I.1 General introduction

The exposure of aircraft crew to cosmic radiation has received a great deal of attention during the last decade. The recommendation by the International Commission on Radiological Protection (ICRP) in 1990, that exposure to cosmic radiation in the operation of jet aircraft should be recognised as occupational exposure, initiated a number of new dose measurements onboard aircraft. Computer programs suitable for predicting route doses were further developed and new ones were designed. (For reviews see the proceedings of the workshops in Luxembourg, 1991 [WRE93] and in Dublin, 1998 [WRE99]). A large fraction of the available dose measurements results published during the last ten years is compiled in this report and descriptions of the instruments and techniques used are also included. The measured results are compared with results calculated for the same routes using different computer programs designed for this purpose. One aim of this report has been to investigate whether estimates of route dose agree within the uncertainties accepted for work in radiation protection generally.

The report is written at the request of the radiation protection expert group established under Article 31 of the Euratom treaty. It does not deal in detail with the quantities used in radiation protection or with background information on radiation protection principles. Basic reports dealing with those matters are from the ICRP [ICRP91] and the ICRU [ICRU1993], [ICRU98], and also others [BAR99]. Some information on the radiation fields at cruising altitudes as well as the influence of solar activity on the dose rate is included. More detailed information can be found in the literature, for instance [EUR96] or [HEI99].

Although the report is written for radiation protection experts, the intention has been to make the content understandable for a broader audience of interested persons such as those working in the aviation industry or as members of aircraft crew.

I.2 Working Group 5 progress

The working group members (WG) were recruited from groups which had been engaged in this dosimetry field during the period to 2000. Other groups became interested in participating, and a few additional members joined the WG in late 2000 and early 2001. Groups identified after this time were invited to report their values together with information on the flight routes to the WG. From late 2002, it was not possible to accept data from new groups for practical reasons.

Four subgroups were set up in 2001 (the name of the coordinator of each group is underlined):
Codes and Measurement Methods for Air Crew Dose Assessments,
D. Bartlett, W. Heinrich, D. O'Sullivan and Ulrich Schrewe
Route Dose Tabulation,
P. Bilski and L. Tommasino
Comparison of Dose Rates at Different Flight Altitudes and at Different Geomagnetic Latitudes,
P. Beck, L. Lindborg, Fr. Spurny, W. Reitz and Fr. Wissman
A Comparison of Route Doses calculated with Different Computer Codes,
J.-F. Bottollier, E. Felsberger, B. Lewis and H. Schraube

In 2002, the work had proceeded to the stage that an editorial group was suggested with the coordinators as members. All coordinators with the exception of P. Bilski were able to accept. Additional members of the editorial group were F. Spurný and L. Lindborg. E. Felsberger resigned as member of the working group in 2002. A draft version was presented to the Article 31 group of experts and this was accepted in late October 2003. A final draft was presented to the EURADOS General Assembly in March 2004.

I.3 Legal considerations

Cosmic radiation has been known for almost a century and for many years airlines cruising at very high altitudes have had their aircraft equipped with instruments to detect possible sudden increases in the dose rate due to solar activities [BAG99]. The annual average dose to aircraft crew may become similar to or even larger than that of other occupationally exposed groups [BAR99], [SPU02], [JWD03]. In Publication 60, the ICRP suggested the inclusion of exposure to elevated levels of natural radiation as occupational exposure.

The legal consequences of the ICRP recommendation were considered by the European Council in its Basic Safety Standards (Directive 96/29/Euratom) [BSS96]. The protection of air crew (Article 42) is therein formulated as

"*Each Member State shall make arrangements for undertakings operating aircraft to take account of exposure to cosmic radiation of air crew who are liable to be subject to exposure to more than 1 mSv per year. The undertakings shall take appropriate measures, in particular:*

to assess the exposure of the crew concerned,
to take into account the assessed exposure when organizing working schedules with a view to reducing the doses of highly exposed aircrew,
to inform the workers concerned of the health risks their work involves,
to apply Article 10 to female air crew."

Article 10 deals with special protection during pregnancy and breastfeeding. Its first paragraph reads:

"*As soon as a pregnant woman informs the undertaking, in accordance with national legislation and/or national practice, of her condition, the protection of the child to be born shall be comparable with that provided for members of the public. The conditions for the pregnant women in the context of her employment shall therefore be such that the equivalent dose to the child to be born will be as low as reasonably achievable and that it will be unlikely that this dose will exceed 1 mSv during at least the remainder of the pregnancy*."

Technical guidance on ways to include in regulations "a significant increase in exposure due to natural radiation sources" was issued by the Commission in 1997 [EUR97]. A special section is concerned with the protection of air crew. Three paragraphs are cited from that document. Part of paragraph 66 reads:

"*For air crew whose annual dose falls in the range 1-6 mSv there should be individual estimates of the dose. These estimates of dose should be made available to the individual concerned. For flights below 15 km these may be carried out using an appropriate computer program and internationally agreed information."*

Paragraph 67 deals with situations when a larger dose may occur and reads:

"It will normally be possible to adjust rostering so that no individual exceeds 6 mSv per year. However, for air crew whose dose is likely to exceed 6 mSv, record keeping in the sense of the Directive is recommended with appropriate medical surveillance."

Paragraph 68 finally concludes:

"It would be unnecessary and unhelpful to declare supervised or controlled areas in aircraft"

Civil aviation is an international business and it is essential that it be regulated in a similar way in different countries. The civil aviation authorities co-operate through an organisation called the Joint

Aviation Authorities (JAA)[1]. It is an associated body of the European Civil Aviation Conference (ECAC) representing the civil aviation regulatory authorities of a number of European States, which have agreed to co-operate in developing and implementing common safety regulatory standards and procedures. It issues Joint Aviation Requirements (JARs), which usually are implemented as national regulations. The European radiation protection Basic Safety Standards Directive [BSS96] is considered in JAR-OPS 1.390 [JAR01].

I.4 Quantities

There are two quantities used in this report. One is the protection quantity effective dose (E), which is most often used in regulations. This quantity is related, through probability coefficients, to the stochastic health effects in humans that ionising radiation might cause. E may be used to quantify the degree of protection a regulatory body considers reasonable. E is, however, not a measurable quantity. Therefore, for measurements a quantity called ambient dose equivalent, $H^*(10)$, is defined. The two quantities can be related to each other. However, while $H^*(10)$ is independent of the irradiation geometry, E is not. . To be able to convert a value of $H^*(10)$ into a value of E, and in some instances to be able to correctly interpret the indication of an instrument, the direction distribution of the radiation field has to be known. In this report, as a simplifying assumption, the radiation field onboard aircraft is taken to be isotropic. The movement of crew may tend to make the field approximately isotropic and the high energies of some radiation components will result in the radiation field geometry being a less important parameter. However, the possible error introduced needs to be quantified. Both E and $H^*(10)$ have the same unit, sievert (Sv). Sometimes, when it is less important, or when it is obvious which quantity is meant, the general word dose is used instead of the precise names. The cosmic radiation exposure of the body is essentially uniform and the maternal abdomen provides no effective shielding to the foetus. As a result, the magnitude of equivalent dose to the foetus can be put equal to that of the effective dose received by the mother.

Doses on board aircraft are generally predictable, and unforeseen exposures such as may occur in other radiological workplaces cannot occur (with the rare exceptions of the extremely intense and high energy solar particle events) [ICRP97].

Calculations can be made directly of effective dose per unit time as a function of geographic location, altitude and solar cycle phase, for the assumed field geometry (taken as isotropic). When folded with flight and staff roster information, estimates of effective dose for individuals are obtained. The role of calculations in this procedure is unusual in routine radiation protection. Because effective dose is not directly measurable, in order to validate assessed values of effective dose based on calculations, calculations are also made of ambient dose equivalent rate or ambient dose equivalent and these compared with values determined by measurements traceable to national standards. The validation of calculations of ambient dose equivalent calculations for a particular calculation method or program can be taken as a validation of the calculation of effective dose by the same computer code. This step in the process may need to be confirmed

The alternative is to establish, *a priori*, that the operational quantity ambient dose equivalent is a good estimator of effective dose and equivalent dose to the foetus for the radiation fields being considered, in the same way that the use of the operational quantity personal dose equivalent is justified for the estimation of effective dose for radiation workers. For most workplace fields, $H^*(10)$ overestimates E, but for exposure of cosmic radiation the reverse is the case. This is principally a result of the radiation weighting factor of 5 for protons. Changes of the values of radiation weighting factors are under discussion. If a proton weighting factor of 2 is adopted as proposed [ICRP 03], $H^*(10)$ would be an acceptable estimate for E for air crew exposure. However, a change to the weighting factor for neutrons is also proposed: the effect of this proposed change needs to be evaluated (see, for example, FER04). Ambient dose equivalent rate as a function of geographic location, altitude and solar cycle

[1] For further information see www.jaa.nl

phase is then calculated and folded with flight and staff roster information. The calculations of ambient dose equivalent rate or route doses have to be validated by measurements traceable to national standards.

I.5 The collection of material for the report

Groups engaged in dosimetry onboard aircraft, with preferably published results, were invited to report their values together with information on the flight routes. They were also asked to describe their instruments and measurement procedures. Most groups submitted the requested information, and their measurement procedures supplied are presented in Appendix A. For practical reason a deadline for inclusion of groups had to be determined as late in 2002. Results from the groups cover the period from 1993 to 2003.

All computer programs, which were known to the WG for calculation of effective dose and/or ambient dose equivalent on board aircraft, were identified. Descriptions of the programs were requested, and these are presented in Appendix B as supplied by the originator of the program. Those programs were then used to calculate the dose for the flights for which measurement results had been reported. It was, however, not practical to use this procedure for all flights. Originally it was hoped to have all programs available in such a way that an independent check could have been made. However, this did not prove possible.

I.6 Content of the report

Chapter II contains an introduction to the cosmic radiation fields and to cosmic radiation dosimetry. The influence of solar activity on the dose rate is also considered.

In Chapter III experimental and calculated dose rate values are compared and presented in a few different ways to demonstrate the dependence on flight altitude, geomagnetic co-ordinates and solar potential.

Chapter IV presents a comparison of measured and calculated route dose values. The agreement between calculations and experiments as well as between different codes is discussed.

Chapter V summarises the uncertainties in dose measurements, which are accepted by the radiation protection community. The methods and procedures used to obtain the experimental results in Chapter III and IV are summarised and the experimental uncertainties as well as those connected with calculations are also reviewed. The interpretation of the results in Chapter III and IV depend of course on them.

Chapter VI gives a summary, recommendations and requirements for future work.

The two Appendices describe the measurement methods (Appendix A) and the codes used for calculation of route dose or route dose rate values (Appendix B). The descriptions should be relevant for the time period when the results were reported to the working group. It is realised that during the period improvements have been made in the methods and those have sometimes been added in the appendices.

I.6 References

[BAG99] Bagshaw, M. *Cosmic Radiation – An Aircraft Manufacturer's View*. Radiat. Prot. Dosim. **86** 335-336 (1999).

[BAR99] Bartlett, D.T. *Radiation Protection Concepts and Quantities for the Occupational Exposure to Cosmic radiation.* Radiat. Prot. Dosim. **86** 263-268 (1999).

[BSS96] EURATOM. *Council Directive 96/29/EURATOM of 13 May 1996 Laying Down the Basic Safety Standards for Protection of the Health of Workers and the General Public Against the Dangers Arising from Ionising Radiation.*. Official J. European Communities 39, L159.

[EUR96] European Commission Radiation Protection 85. *Exposure of Air crew to Cosmic Radiation. A report of EURADOS working group 11* EURADOS Report 1996-01. Editors: I.R. McAulay, D.T. Bartlett, G. Dietze, H.G. Menzel, K. Schnuer and U.J. Schrewe. ISBN 92-827-7994-7.

[EUR97] European Commission Radiation Protection 88. *Recommendations for the implementation of Title VII of the European Basic Safety Standards Directive (BSS) concerning significant increase in exposure due to natural radiation sources.* (1996) ISBN 92-827-5336-0.

[FER04] Ferrari, A, Pelliccioni, M. and Villari, R. Evaluation of the Influence of Aircraft Shielding on the Aircrew Exposure through an Aircraft Mathematical Model, Radiat. Prot. Dosim. 108 91-108 (2004).

[HEI99] Heinrich, W., Roesler, S. and Schraube, H. *Physics of Cosmic Radiation Fields*. Radiat. Prot. Dosim. **86** 253-258 (1999).

[ICRP91] International Commission on Radiological Protection. *Publication 60 Recommendations of the International Commission on Radiological Protection.* (Oxford:Pergamon Press) (1991).

[ICRP03] International Commission on Radiological Protection *Publication 92 Relative Biological Effectiveness* (*RBE*), *Quality Factor* (*Q*), *and Radiation Weighting Factor* (W_R). (Oxford:Pergamon Press) (2003).

[ICRP97] International Commission on Radiological Protection. *Publication 75 General Principles for the Radiation Protection of Workers*. (Oxford:Pergamon Press) (1997).

[ICRU93] International Commission on Radiation Units and Measurements. *Report 51 "Quantities and Units in Radiation Protection Dosimetry*. (Bethesda:ICRU) (1998).

[ICRU98] International Commission on Radiation Units and Measurements. *Report 57 Conversion Coefficients for use into Radiological Protection Against External Radiation*. (Bethesda:ICRU) (1998).

[JAR01] Joint Aviation Authorities. *Joint Aviation Requirements JAR-OPS 1 Commercial Air Transportation (Aeroplanes) Subpart D – Operational Procedures JAR-OPS-1.390 Cosmic radiation,* (2001).

[JWD03] van Dijk, J. W. E. *Dose assessment of Aircraft Crew in the Netherlands*, Radiat. Prot. Dosim. **106** 25-32 (2003).

[SPU02] Spurný, F., Malušek, A., and Kovář I. *Individual dosimetry of Czech company aircrew 1998-2000",* Inter.Conf. on Occupational Radiation Protection: Protecting of Workers against Exposure to Ionising Radiation, IAEA, Geneva, August 26-30, . 397-400.

[WRE93] Proceedings of a Workshop on *Radiation Exposure of Civil Aircrew*, Luxembourg, June 25-27, 1991, Radiat. Prot. Dosim. **48** (1993).

[WRE99] Proceedings of an International Conference on Cosmic Radiation and Aircrew Exposure, Dublin, July 1-3, 1998, Radiat. Prot. Dosim. **86** (1999).

II Cosmic radiation environment at aircraft altitudes and dosimetry

II.1 Cosmic radiation

The earth is continuously bombarded with high-energy ionising radiation from outer space. The intensity of the cosmic radiation is partly decreased by the magnetic field associated with the Sun's solar wind and by the Earth's magnetic field. Many important data on the cosmic radiation in general and near the Earth's surface were presented in a previous EURADOS Report on the topic [EUR96]. Some basic characteristics are repeated here and some further information is added on the influence of solar particle events and magnetic disturbances.

The cosmic radiation field (in the Earth´s atmosphere), to which aircraft crew members are exposed, has two different origins: energetic particles from the universe in general (usually referred to as galactic cosmic radiation) and from the Sun.

Galactic energetic charged particles (galactic cosmic radiation (GCR)) are mostly protons (~85 %) and helium ions (~12 %), the rest includes nuclei of all known elements and some electrons. Their energy extends up to about 10^{20} eV. The GCR interacts with the atmosphere producing secondary radiation, which together with the primary incident particles give rise to radiation exposure throughout the atmosphere decreasing in intensity with depth from the altitude of supersonic aircraft down to sea level.

The dose from GCR varies not only with altitude but also with the geomagnetic coordinates (longitude and latitude) being larger towards the poles and smaller near the equator. It also depends on the solar activity, which varies according to a cycle about 11 years long. The GCR contribution to the aircraft crew exposure is about 95 %. GCR exposure is fairly stable and predictable.

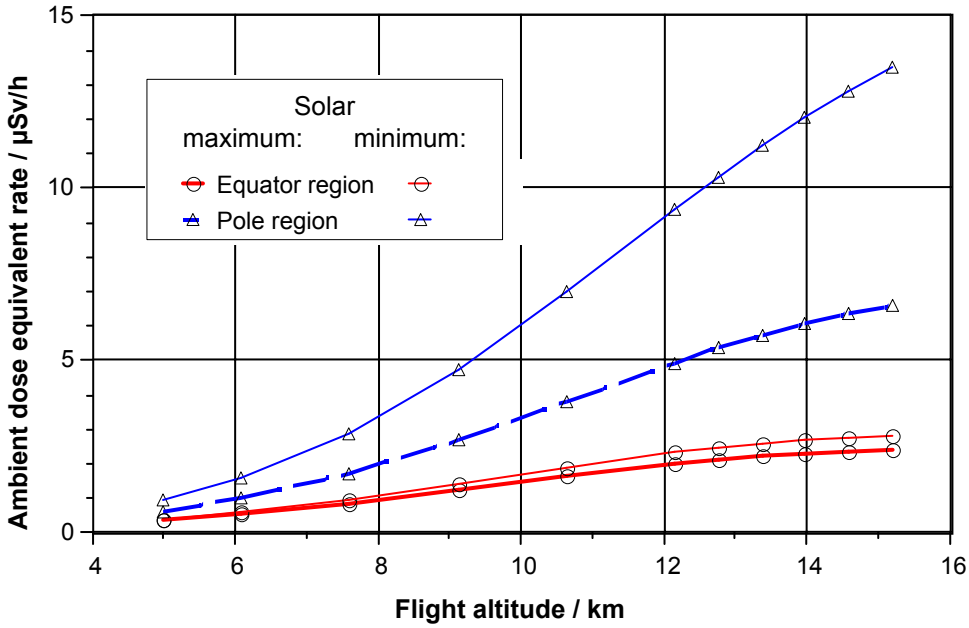

Figure II.1 Calculated ambient dose equivalent rate, dH*(10)/dt, for conditions close to solar maximum activity (Jan.1990) and close to solar minimum (Jan. 1998), both at zero-meridian (λ=0°) and geographic latitude ϕ of 0° (red lines) resp. 90°(blue lines).(For uncertainties in calculated values see CH.IV.6 and Ch.V.5)

Figure II.1 shows the variation of the ambient dose equivalent rate as a function of flight altitude. The calculations were made for conditions close to solar maximum activity in January 1990 and close to the solar minimum activity in January 1998. The calculations were made with EPCARD and show results for both the equatorial and polar regions.

Solar energetic charged particles can contribute to the aircraft crew exposure through occasional so-called solar particle events (SPE's). These are produced by sudden, sporadic releases of energy in the solar atmosphere (solar flares), and by coronal mass ejections (CMEs). During such events a large number of mainly high-energy protons is produced and an increased fluence of particles at aviation altitudes may be observed. Only a small fraction of the SPEs, on average one per year, causes an increased dose rate at aviation altitudes. Those events can be observed with neutron monitors at ground level: ground level events (GLEs). The largest events often take place on either side of the period of maximum solar activity as measured by sunspot number. Any rise in dose rate associated with an event is quite rapid, usually taking place in minutes. The duration may be hours to several days. The prediction of which events will give rise to significant increases in dose rate at aircraft altitudes is not currently possible. Estimation of the doses to aircraft crew in the event of a GLE must be made retrospectively. Principally it is possible due to the existence of a number of geomagnetically dispersed, ground level neutron monitors, and because the observed neutron fluence at ground level is primarily caused by the cosmic radiation.

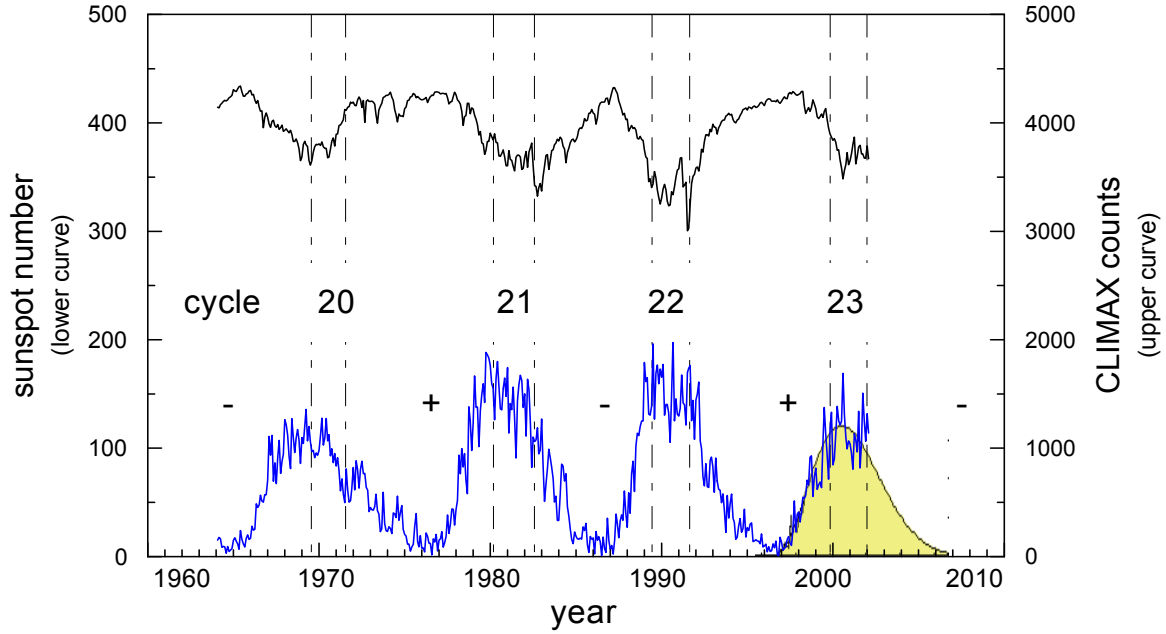

Figure II.2 Sunspot number (lower curve) and monthly averaged Climax neutron monitor count rate per hour (divided by 100) for solar cycles 20 through 23 (from 1964 to begin of 2002). Solar cycle 23 is expected to last until approximately the year 2008. The vertical dashed lines indicate the periods (around 2 years each) of solar reversal; +/- specifies the respective polarity of the field model of NASA Johnson Space Center (Badhwar, 1997). The shaded area is the solar activity predicted by the NASA Marshall Space Flight Center.

Figure II.2 shows how the neutron monitor count rate has varied with the number of sunspot during the time period from1960 to the present. The sunspot number reflects the actitiy of the sun and a smoothed curve is used to identify the maxima and minima of the sun activitity. The neutron fluence sometimes also decreases as an effect of increased solar wind and the increases in associated magnetic field. Those effects decrease the intensity of the GCR at the top of the atmosphere. Such events are called "Forbush decreases", they may occur a handful of times each year [FOR37], [CRR96] and [CAN00]. They may last for several days.

While the GLEs may increase the dose to aircraft crew, the dose is diminished during Forbush decreases. Reductions of more than 20 % of the normal dose rate have been reported.

The effect of Forbush decreases on route doses can be calculated as they happen by FREE, which can also be used to calculate retrospectively the effect on route doses of a solar particle event, Appendix B 5. Contributions to route doses from GLE´s are regularly estimated by Lantos and co-workers [LAF03] and their results made available to users of SIEVERT and EPCARD, within an inter-institutional cooperation. The validation of these procedures is not within the scope of this report.

The short term of increase of the dose rate due to solar particle events can be quite substantial. The uncertainties related to them, when assessed by calculation, were recently reviewed by Lantos and Fuller [LAN03]. They use in their analysis a semi-empirical model mostly based on Concorde measurements, particularly those obtained during GLE 42 (29/09/89) and GLE 59 (14/07/00). They state, as some other authors have previously, that the estimation of the increased dose rate due to a SPE for a given flight, in absence of experimentally measured data, is affected by a large relative uncertainty of at least several tens of percents. The large uncertainties mostly result from the anisotropy and localised nature of the events and the variability of the energy spectra of the protons. The more important a solar flare is, the higher is the uncertainty in the estimate of the increased dose rate. It should, however, also be mentioned that the estimation of the increased dose during GLE 60 agrees well with the estimation deduced from on-board measured data (Chapter V).

When all 64 GLE's observed since 1942 are considered, Lantos and Fuller conclude that only 18 have presented a likelihood of an increase in the effective dose of more than 30 μSv and only 4 by more than 1 mSv. The importance of the contribution of SPEs to the total exposure of air crew to cosmic radiation is, according to these authors, therefore rather limited.

Long-term monitoring onboard a Czech Airlines aircraft permitted the registration during 2001 several Forbush decreases and one solar flare – GLE 60. The extent of their influence is shown in Table 1 [SPD01], [SPD03] and [SPU04], where the ratios of the experimental values divided by values calculated with the EPCARD code are shown, EPCARD does not include effects of SPEs for these extreme situations. The measurements were made by means of a Si-spectrometer MDU (see Annex I – A.4).

Table II.1 Influence of SPE and Forbush decreases on the dose measured onboard aircraft during 2001 and 2003.

Flight route			Ratio MDU/EPCARD, H*(10)		
			"low LET"	"high LET"	Total
PRG-JFK	01 04 14	no extreme	1.00	0.96	0.98
JFK-PRG	01 04 16	no extreme	1.01	1.01	1.01
PRG-JFK	01 04 15	GLE 60	1.24	1.68	1.44
PRG-JFK	01 04 12	Forbush	0.92	0.78	0.84
PRG-JFK	01 11 06	Forbush	0.89	0.85	0.87
PRG-SOF	03 10 25	no extreme	0.95	1.00	0.98
SOF-PRG	03 10 29	Forbush	0.88	0.62	0.74

The ratio is larger than one in the case of the solar flare, and lower than one during the Forbush decreases. Measurements during Forbush decreases have also been reported by Kyllönen et al. [KYL01], Figure II.3. They report reductions of the dose equivalent rate with up to 20% similar to the results in the table.

The typical total effective dose for a trans-Atlantic flight is about 50 μSv. The additional dose during GLE 60 corresponds therefore to about 20 μSv, which is small as compared to the typical annual effective dose of aircraft crew (~2 mSv). The maximum estimated value of the dose equivalent rate during a GLE of several mSv per hour occurred in February 1956 [ARM69] at a subsonic flight

altitude, i.e. 10^3 times higher than during GLE 60 [SPD01]. The extra dose at aircraft altitudes for a flight during this event might have been a significant fraction of the annual dose limit for occupational workers. However, for the largest event, which has occurred since 1956, GLE 42 on 29th of September 1989, the estimated additional dose equivalent for a flight was a few hundred μSv [OBR96, LAN03]. It must always be noted that solar particle events can produce markedly anisotropic particle fluence rates, and therefore large local differences in the dose rate.

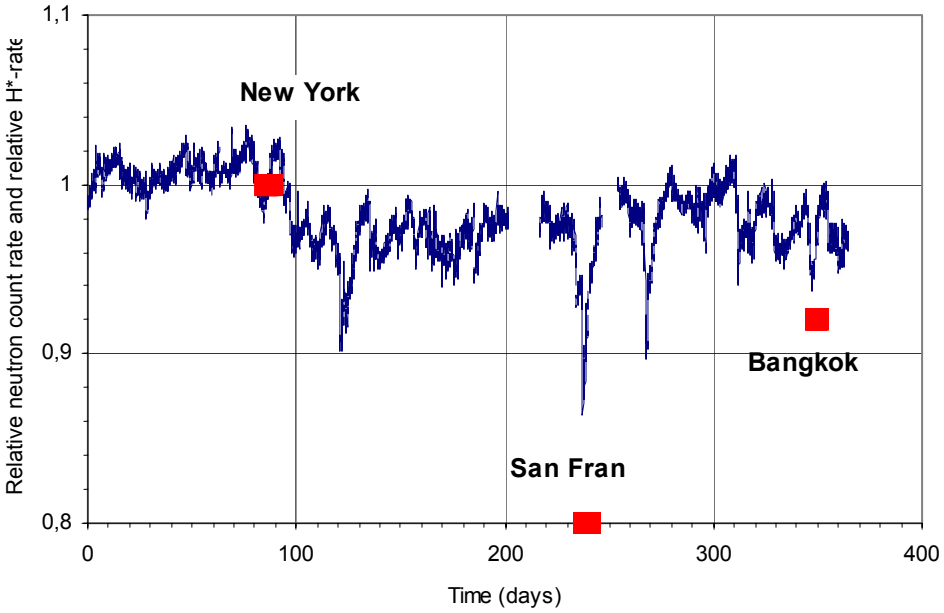

Figure II.3 The influence of Forbush decreases on the ambient dose equivalent rate. The curve shows the relative count rate as measured by the Climax neutron monitor on ground. The red squares show the observed ambient dose equivalent rate for comparable geomagnetic positions normalised to the same flight level. The measurements were made in 1998. When the fluence reduces the dose rate also reduces.

II.2 Radiation dose components at aviation altitudes

The relative contributions to H^* and E due to the different particle types are depicted in figures II.4, II.5, II.6 and II.7. The calculations were made for civil flight routes at approximately solar maximum and minimum conditions [SHL02]. The data of ambient dose equivalent and effective dose are given for a number of destinations from Munich and Frankfurt.

For both quantities, the hadron (neutrons and protons) component contributes more than fifty percent to the total dose. Due to the radiation-weighting factor of 5 for protons (ICRP60, Council directive 96/29/EURATOM and European Member State national regulations), the proton contribution to the effective dose is the next most important after the neutrons, and the total hadron component may be up to 80% of the total effective dose. When considering ambient dose equivalent, neutrons are the major contributor followed by electrons.

The change from solar maximum to solar minimum condition does not change the relative dose contributions greatly. The dose fractions are also relatively constant for different flight levels and a particular location [SHL00] at normal flight altitudes. The contribution to the two quantities from energetic primary heavy charged particles (HZE) or fragments is not significant [DOS99].

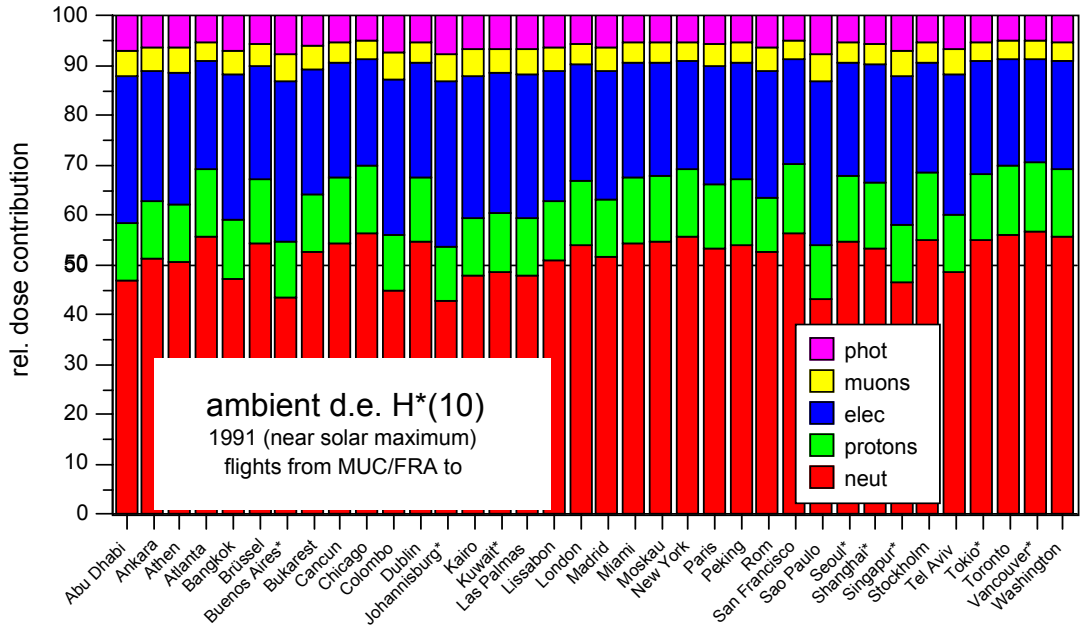

Figure II.4 Relative contribution to ambient dose equivalent, $H^*(10)$, for various destinations near solar maximum condition (1991) for 37000 ft flight altitude, as calculated with EPCARDv3.2. Data are shown in alphabetic order.

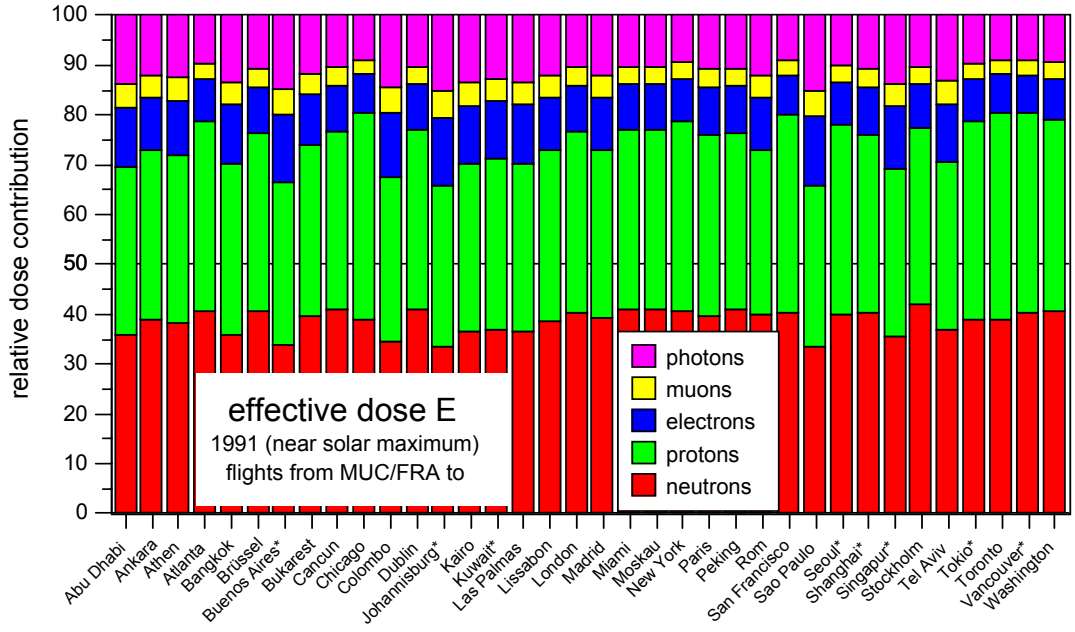

Figure II.5 Relative contribution to effective dose, E, for various destinations near solar maximum condition (1991) for 37000 ft flight altitude as calculated with EPCARDv.3.2.

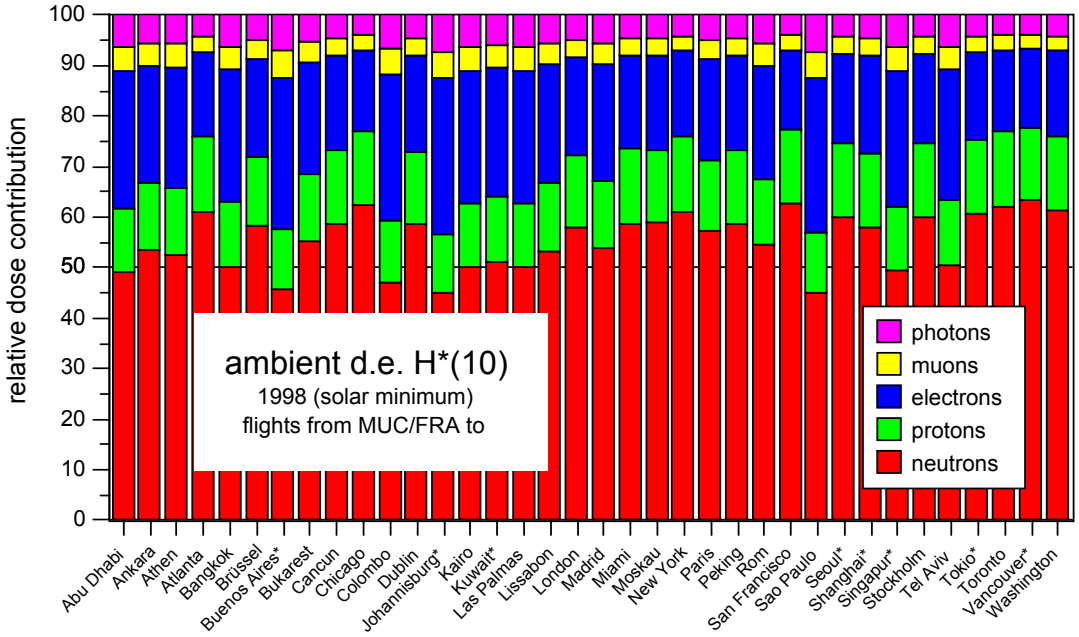

Figure II.6 Relative contribution to ambient dose equivalent for various destinations near solar minimum condition (1998) for 37000 ft flight altitude.

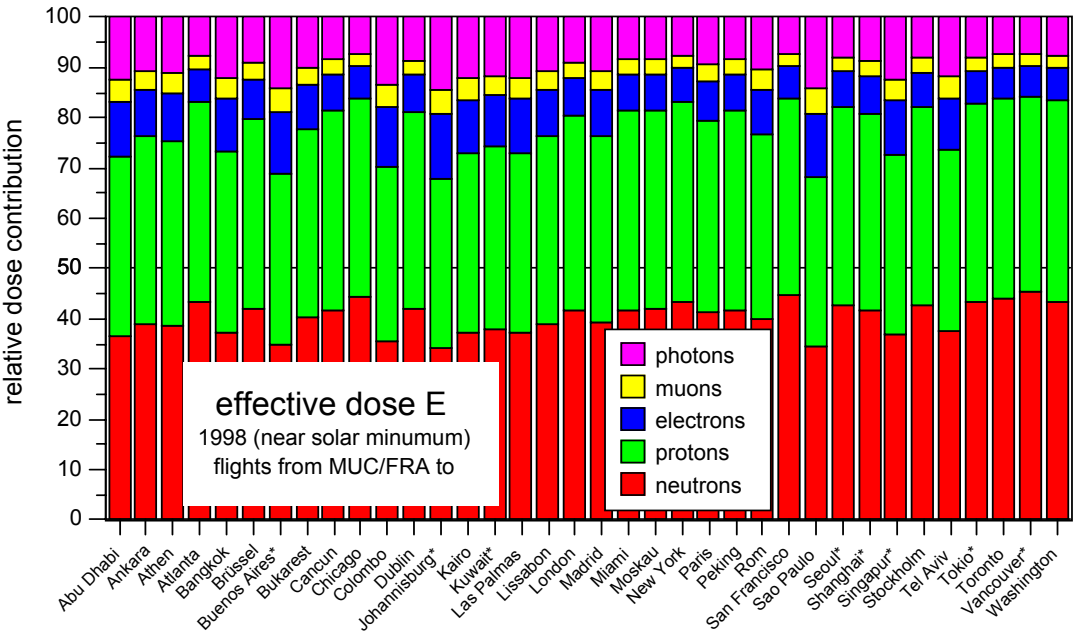

Figure II.7 Relative contribution to effective dose for various destinations near solar minimum condition (1998) for 37000 ft flight altitude.

II.3 Measurement requirements

It is recommended that instruments for dose measurements on board aircraft determine the operational quantity, ambient dose equivalent, $H^*(10)$. Instruments sensitive to neutrons as well as to low-LET radiations are required. Some instruments, such as tissue equivalent proportional counters (TEPC), silicon semiconductor LET spectrometers and recombination ionization chambers [ZIE96] [GOL99], are capable of measuring both high and low-LET dose components, as well as the approximate LET distribution or mean LET, and therefore dose equivalent using the quality factor, $Q(L)$, [ICRU93]. For

this reason such instruments, in particular the TEPC, have been suggested as reference instruments for cosmic radiation measurements [LKB99].

Alternatively, for dosimetric purposes the field can be divided into low ($\leq$ 5 keV μm^{-1}) and high (> 5-10 keV μm^{-1}) LET particle components, or into two slightly different components, the non-neutron component and the neutron component, which includes the dose equivalent contribution by high-energy protons. The deposition by low-LET particles can be determined using ionization chambers, scintillation counters, silicon-based detectors, or passive luminescence detectors (OSL, RPL and TL) or ion storage device. The high-LET component can be measured using special neutron survey meters (with an extended energy range response), passive etched track detectors, bubble detectors (superheated drop detectors) or fission foils with damage track detectors.

It is essential for the measurement of complex radiation fields that the instruments used are fully characterized for measurements of $H^*(10)$. Ideally, an isotropic instrument response and little energy dependence of response for the different particle types to be measured are required. For instruments not responding to all radiation components, the influence on the signal from other radiations should be understood. Response characterization is usually made at national standards laboratories. For some particles, such as protons, high-energy neutrons and high-energy electrons those laboratories have limited possibilities to offer services, and calculations may be used as an alternative, or in conjunction with measurements. Traceability to international standards is achieved through measurements at national dosimetry standards laboratories.

At present little information is published concerning instrument responses to electrons and protons mainly as a lack of suitable high-energy radiation fields. For neutrons, characterization may be carried out for neutron energies up to 19 MeV in ISO reference fields, supplemented at higher energies in the quasi- monoenergetic high-energy neutron fields at iThemba LABS, Capetown, The Svedberg Laboratory, Uppsala, and Université Catholique, Louvain-la-Neuve. The CERN/European Union high-energy Reference Field (CERF) facility offers a neutron radiation field similar to the neutron component in aircraft [SAA99]. It has allowed comparisons of response characteristics of different instruments, dosemeters and spectrometers as well as comparisons of measured and predicted responses. The distribution of the cosmic radiation in energy covers a very wide energy range. The distributions apparently do not change very much with geographic position and flight level [GCW03], [SHL00] and this is probably one reason why so many different types of instruments can be used, if they are correctly calibrated.

II.4 Dose calculations

There are a number of radiation transport codes used to calculate the radiation field at aircraft altitudes and at sea level produced by galactic cosmic radiation, for example LUIN, FLUKA, GEANT, LAHET, MCNPX and MARS. There are similar number of methods in current use, which are based on the results of such calculations to compute dose to aircraft crew, for example CARI (using LUIN), EPCARD (using FLUKA), FREE (using PLOTINUS related to LUIN), PC-AIRE (using experimental measurements with fitting), SIEVERT (using the data from CARI, and since January 2004 from EPCARD), and the algorithm of Pelliccioni (using FLUKA). At present, none of these consider the influence of the aircraft on the particle fluence. (But see FER04)

The radiation transport codes take as input the cosmic radiation field at the top of the atmosphere and solve, either analytically or by Monte Carlo simulation, the radiation transport equations which describe the interactions of each particle with the constituents of the atmosphere, in order to calculate the field at a given aircraft altitude and geographic location. The effect on particle trajectories of the Earth's magnetic field is included in approximations using tables of rigidity cut-offs. The CARI and FREE program takes account of the variation in the Sun's magnetic field on the intensity of the cosmic radiation at the top of the atmosphere by applying an equivalent heliocentric electrostatic field- the heliocentric potential, the magnitude of which is related to the instantaneous

value of the count rate of ground level neutron monitors. In EPCARD the solar cycle modulation is taken into account by deriving a solar deceleration potential based on ground level neutron monitor count rates averaged over 28 days. This is then used to modify the intensity and energy distribution of cosmic radiation at a distance from the Sun of 60 to 100 AU (an AU, astronomical unit, is the average Sun to Earth separation) with a time-lag of 95 days which is approximately the travel time for this distance for the lower energy component of the galactic cosmic radiation, which is most affected. The programs, which calculate dose rates and route doses, use the results of the transport calculations together with details of an aircraft's flight path. The route doses can be used for the dose assessment for a crew member.

II.5 References

[ARM69] Armstrong, T.W., Alsmiller, R.G. and Barish, J. *Calculation of the Radiation Hazard at Supersonic Aircraft Altitudes Produced by an Energetic Solar Flare*, Nucl. Sci. Eng. **37** 337-342 (1969)

[CAN00] Cane, H.V. *Coronal Mass Ejections and Forbush Decreases*, Space Science Reviews **93** 53-77 (2000).

[DOS99] O´Sullivan, D. *Study of Radiation Fields and Dosimetry at Aviation Altitudes.* Final Report, January 1996 – June 1999. Contract Number: F14P-CT950011 DIAS Report 99-9-1 (1999).

[EUR96] EURADOS Report 1996-01. *Exposure of Air Crew to Cosmic Radiation*. Eds.: I.R. McAulay, D.T. Bartlett, G. Dietze, A. Menzel, K. Schnuer, and U.J. Schrewe, IBSN 92-827-7994-7, Luxembourg 1996.

[CRR96] Cane, H.V., Richardsson, J. G. and Rosenvinge, T.T. *Cosmic Ray Decreases 1964 – 1994.* Journal of Geophysical Research, **101** A10 21561–21572 (1996).

[FER04] Ferrari, A, Pelliccioni, M. and Villari, R. *Evaluation of the Influence of Aircraft Shielding on the Aircrew Exposure through an Aircraft Mathematical Model,* Radiat. Prot. Dosim. **108** 91-108 (2004).

[FOR37] Forbush, S.E. *On the Effects in Cosmic Ray Intensity Observed During the Recent Magnetic Storms.* Phys. Rev. **50** 1108 –1109 (1937).

[GCW03] Goldhagen, P., Clem, M. and Wilson, J.W. *New results from Measurements of the Energy Spectrum of Cosmic-Ray Induced Neutrons aboard an ER-2 Airplane and on the Ground*. 34th COSPAR Scientific Assembly, Houston, October 2002, Adv. Space Research **32** (2003).

[GOL 99] Golnik, N., Silari, M. and Otto, T. *On the Use of a Recombination Chamber for Radiation Measurements in CERN-EU High-Energy Reference Radiation Fields*, Radiat. Prot. Dosim. **86** 173-179 (1999).

[ICRU93] ICRU. Report 51. *Quantities and Units in Radiation Protection Dosimetry*. Bethesda, 1993.

[KYL01] Kyllönen, J.-E., Lindborg, L. and Samuelsson, G. *Cosmic Radiation Measurements On-board Aircraft with the Variance Method*. Radiat. Prot. Dosim. **93** 197-205 (2001).

[LAN03] Lantos, P. and Fuller, N. *History of the Solar Flare Radiation Doses on-board Aircraft using a Semi-empirical Model and Concorde Measurements.* Radiat. Prot. Dosim. **104** 199-210 (2003).

[LKB99] Lindborg, L., Kyllönen, J. E., Beck, P., Bottolier, J.F. and Gerdung, S. *The use of TEPC for Reference Dosimetry*. Radiat. Prot. Dosim. **86** 285-288 (1999).

[OBR96] O'Brien, K., Friedberg, W., Sauer, H.H. and Smart, D.F. *Atmospheric Cosmic Rays and Solar Energetic Particles at Aircraft Altitudes*, Environ. Int. **22** Suppl. 1 S9-S44 (1996).

[SAA99] Schrewe, U.J., Alberts, W.G., Alevra, A.V., Ferrari, A. Otto, T. and Silari, M. *Calibration Problems , Calibration Procedures and Reference fields for Dosimetry at Flight Altitudes*. Radiat. Prot. Dosim. **86** 289-295 (1999).

[SHL00] Schraube, H., Heinrich,W., Leuthold, G., Mares, V. and Roesler, S. *Aviation Route Dose Calculation and its Numerical Basis.* Tenth International Congress of the International Radiation Protection Association (IRPA-10), Hiroshima, Japan, T-4-4 2000. http://www.irpa.net/irpa10/cdrom/01230.pdf

[SHL02] Schraube, H., Heinrich, W., Leuthold, G., Roesler, S., and Schraube, G. *Collating of data for the determination of the exposure of aviation personnel due to cosmic radiation, concluded by 21 Dec 2000, and Calculation of radiation fields at air craft flight altitude during the period of solar maximum activity by 15 Nov 2000.* Joint Report to The Council of the Dublin Institute for Advanced Studies (DIAS) 2002.

[SPD01] Spurný F., and Datchev Ts. *Measurements in an Aircraft during an Intense Solar Flare*, GLE 60, on the 15th April 2001. Radiat. Prot. Dosim. **95** 2873-275 (2001).

[SPU04] Spurný F., Kudela, K. and Dacev, C. *Airplane Radiation Dose Decrease during a Strong Forbush Decrease* Submitted to Radiat Prot. Dosim. 2004.

[SPD03] Spurný, F. and Datchev, Ts. *Long-term Monitoring of Onboard Aircraft Exposure Level with Si-diode based Spectrometer.* Solicited speech, 34th COSPAR Scientific Assembly, Houston, Advances Space Research **32** 53-58 (2003).

[ZIE 96] Zielczyński, M., Golnik, N. and Shvidkij, S V. *Recombination Chamber and a Measuring System with Sensitivity Sufficient for In-Flight and Low-Level Dosimetr*, Nukleonika **41** 127-132 (1996).

III Measured and calculated ambient dose equivalent rate data at aircraft altitudes

III.1 In-flight measurements

The in-flight radiation exposure depends on the latitude, longitude and altitude. This dependence is caused by the influence of the Earth's geomagnetic field on cosmic rays and their subsequent transport through the atmosphere. The additional influence of the Sun's varying activity during the eleven-year solar cycle also affects the radiation exposure. The parameters used describing these effects are the heliocentric potential (HCP), and the solar deceleration potential (SDP), both in units of megavolts (MV). The differences between the two approaches are described in Ch IV.5. The comparison of time differential in-flight data has ideally to be done exactly at the same flight position (altitude, longitude and latitude) and under the same solar condition (HCP or SDP). Usually the UTC time combines the link from all in-flight measurement data. Because of insufficient experimental data, the influence of solar events - which can lead to higher radiation exposure at flight altitudes - is not analysed.

Time differential results from measurements on board aircraft as reported for thirteen active and one passive radiation protection instruments, and for the computer code EPCARDv3.2, are given in this section. EPCARDv3.2 calculations are based on cosmic ray Monte Carlo Simulations by FLUKA [SRA02]. The in-flight measurements were made between May 1992 and April 2003 and are summarized in Table III.1. Table III.2 shows a list of instruments used, with their abbreviations and the measurement integration time. For the ionization chambers and neutron monitors, an integration time of 5 to 10 minutes was agreed. For TEPC instruments the measurement time chosen was from 25 minutes up to 60 minutes to get adequate accuracy [see Chapter V]. For passive dosemeters integration time of 32 hours over 16 flights was used [BAR02], [BAR04]. Detailed description of the instruments, measurement method and the calibration procedures are given in Annex A. Table III.3 shows an overview of the in-flight investigations.

Table III.1: List of analysed in-flight investigations

Institute	Primary investigator	Dose assessment method	Number of data[1]	Time Period
APAT	Tommasino	TEPC (tissue equivalent proportional counter) and other active instruments	55	1997
ARCS	Beck	TEPC and other active instruments	1767	1997 – 2003
CIEMAT	Saez-Vergara	TEPC and other active instruments	5680	2001 – 2002
GSF	Schraube, Regulla	active instruments	308	1992 – 1993
IRSN	Bottollier	TEPC	49	2002
NPI	Spurny	Si-spectra dosemeter (MDU-Liulin)	811	2001
NPL	Taylor	TEPC	146	2000-2003
NRPB	Bartlett	track detectors and TLDs	19	1997 – 2003
PTB	Schrewe	active instruments	1240	1997 – 1999
PTB	Wiegel	Bonner Spheres, Ionization Chamber	43	1998
RMC	Lewis	TEPC	342	1999
SSI	Lindborg	TEPC	66	1998 – 2003

[1] EURADOS Aircrew In-Flight Data Base.

Table III.2: List of dose assessment methods during in-flight investigations

Abbreviation	Dose assessment method measurement / calculation	Measurement intervals
NM+IC (ARCS)	Combined neutron monitor (NM) LB6411 and ionization chamber (IC) RSS [BEC99a], [BEC99b]	5 min
NMX+IC (PTB)	Combined neutron monitor NE-NM2 with lead converter (NMX) and ionization chamber [SRE99a], [SRE99b]	5 - 20 min
ACREM (ARCS)	Combined GM detector and transport code calculations [BEC99a], [BEC99b]	5 min
NMX+Halle(GSF)	Combined neutron monitor NE-NM2 with lead converter (NMX) and low level scintillation detector DLM7908 [REG93], [REG96]	6 min
TEPC-log (ARCS)	TEPC detector, 12 cm sphere, logarithmic amplifier [BEC99a], [BEC99b], [BEC04]	30 – 60 min
TEPC (ARCS)	TEPC (HAWK) [BEC03], [BEC04]	30 - 60 min
TEPC (RMC)	TEPC (FAR WEST detector) [GRE00] [LEW01]	25 min
TEPC (SSI)	TEPC instruments based on the variance method [KYL01]	30 - 60 min
TEPC (CIEMAT)	TEPC (HAWK) [SAE02] [ROM04] [SAE04a] [SAE04b]	25 min
NMX+IC (CIEMAT)	Combined neutron monitor with tungsten converter (NMX) SWENDI-2 and ionization chamber (IC) RSS [SAE02] [ROM04] [SAE04a] [SAE04b]	5 min
LIULIN (NPI)	Si-Spectra-dosemeter developed originally for space (MDU-Liulin) [SPU03]	30 min
Track Detector (NRPB)	Box with 36 PADC and 30 TL dosemeters [BAR00], [BAR01], [BAR03]	16 × 120 min
TEPC (NPL-PPARC)	TEPC (HAWK) [TAY02]	30 min
EPCARDv3.2	European Program Package for the Calculation of Aviation Route Doses [SRA02]	single point calculation
TEPC (IRSN)	TEPC (HAWK) [BOT04]	30 min
TEPC (APAT)	TEPC (HANDI) [TOM99], [CUR01a], [CUR01b]	60 min
NMX+IC (APAT)	Combined neutron monitor LINUS with tungsten converter (NMX) and ionization chamber RSS (IC) [TOM99]	5 min
BSS+IC (PTB)	Bonner Spheres (BSS) and ionization chamber (IC) [WIE02], [BEC99a].	30 - 60 min

Table III.3: Summary of overall data of all in-flight investigations

Description	Data
Number of analysed flights	368
Time period	May 1992 – April 2003
Range of sunspot numbers	5 – 170
Range of heliocentric potential	474 MV – 1 187 MV
Range of solar deceleration potential	472 MV – 1 322 MV
Range of geographical longitude	180° West to 180° East
Range of geographical latitude	87° North to 62° South
Range of vertical cut off rigidity	0 – 17.4 GV
Range of barometric altitude	Up to 16 500 m
Measured mean ambient dose equivalent rate	3.8 ± 0.8 µSv h^{-1} [(a)]
Most frequent measured ambient dose equivalent rate	2.5 ± 0.5 µSv h^{-1} [(a)]
Maximum measured ambient dose equivalent rate	19.2 ± 12.4 µSvh^{-1}[(a)]
Number of analysed data sets	10 526

[(a)] … confidence level of the uncertainty is 2s.

III.2 Comparison of time differential data

To evaluate the time differential data, measurements and calculations have to be analysed for the same, or similar, flight location (latitude, longitude, altitude) and the same, or similar, solar activity (HCP or DSP). The parameter used for the flight altitude is the standard barometric altitude (SBA), which is the altitude determined by a barometric altimeter by reference to a pressure level and calculated according to the standard atmosphere definition. The SI unit used is metre. In aviation the parameter flight level (FL) is also used, which is one hundredth of the standard barometric altitude expressed in feet. Figure III.1 shows three dimensional world maps of the effective dose rate distributions for two different flight altitudes 10 058 m (FL 330) and 11 887 m (FL 390), calculated with the cosmic ray transport code LUIN [OBR71]. The heliocentric potential (HCP) used for these calculations was 500 MV. The Sun's activity has ranged during the last 50 years from about HCP = 250 MV to about 1 600 MV. The influence of the Earth's magnetic field results in more shielding against cosmic rays near the equator than at the poles, which leads to lower radiation exposure in the equatorial region than the polar Regions. Additionally it can be concluded that at higher altitudes the increase of the radiation exposure at the poles is much larger than at lower altitudes.

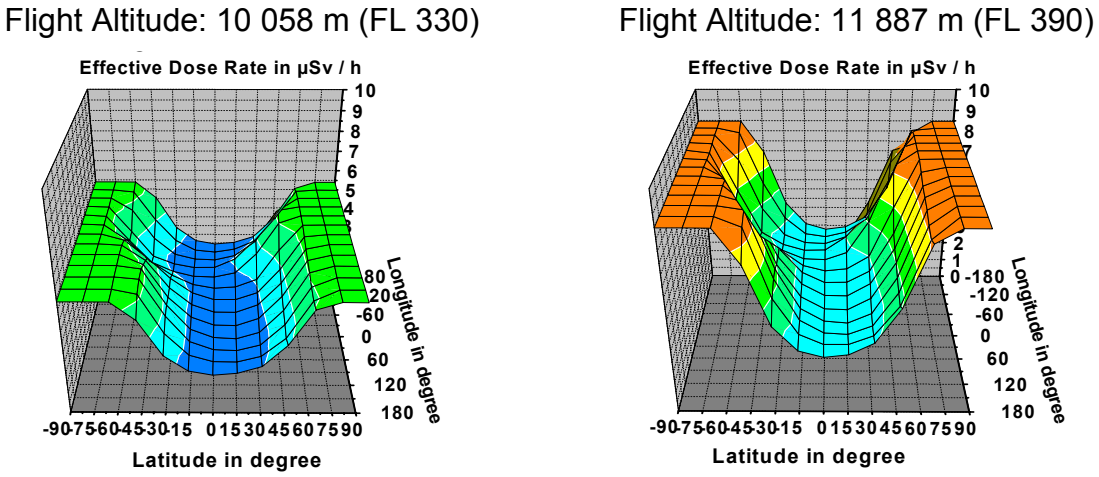

Figure III. 1: Calculation of a 3D-World-Dose-Map for the effective dose rate distribution at standard barometric altitude of 10 058 m (FL 330) and 11 887 m (FL 390) for a heliocentric potential of 500 MV.

For an appropriate two dimensional comparison of the in-flight measurements and the calculation, for all geographical co-ordinates, geomagnetic latitudes have been calculated using a simplified dipole model for the Earth magnetic field [STR97]:

$$B_{\mathrm{m}} = \arcsin\left[\sin\left(B_{\mathrm{p}}\right)\cdot\sin\left(B_{\mathrm{g}}\right)+\cos\left(B_{\mathrm{p}}\right)\cdot\cos\left(B_{\mathrm{g}}\right)\cdot\cos\left(L_{\mathrm{g}}-L_{\mathrm{p}}\right)\right]$$

B_{m} ... geomagnetic latitude in degrees.
B_p, L_{p} … latitude and longitude of the magnetic north pole (1990: 79.13°N, 288.88°E) in degrees.
B_{g}, L_{g} ... geographical latitude and longitude in degrees.

Another approach is to compare the data under the same condition of the magnetic vertical cut-off rigidity r_{c}. A charged cosmic ray particle has to pass the Earth's magnetic field. Depending on the strength of the magnetic field, a particle with a certain momentum is able to pass or not. Obviously at the poles, the strength of the magnetic field is lower compared to the equator region (see Figure III.1). Cut off rigidity is a measure of the penetration of a cosmic ray particle through the Earth's magnetic field. Rigidity is defined as:

$$r = p/Q$$

p … momentum of the particle
Q … charge of the particle

The unit of rigidity is $\mathrm{kg\cdot m\cdot s^{-2}\cdot A^{-1}}$ or T·m. A frequently used unit is V (or GV) in a system of units where momentum is given in $\mathrm{eV\cdot c^{-1}}$(or $\mathrm{GeV\cdot c^{-1}}$) and where rigidity is c times momentum per unit charge, p·c / Q, or where c is put equal to unity.

Figure III.2 shows the distribution of the vertical cut-off rigidity r_{c} in GV for 20 km SBA based on the Earth's magnetic conditions in 1990 [SHE68], [SHE01]. A lower r_{c} shows a lower magnetic shielding, and higher values show a higher shielding. For all further data comparisons these parameter values have been used.

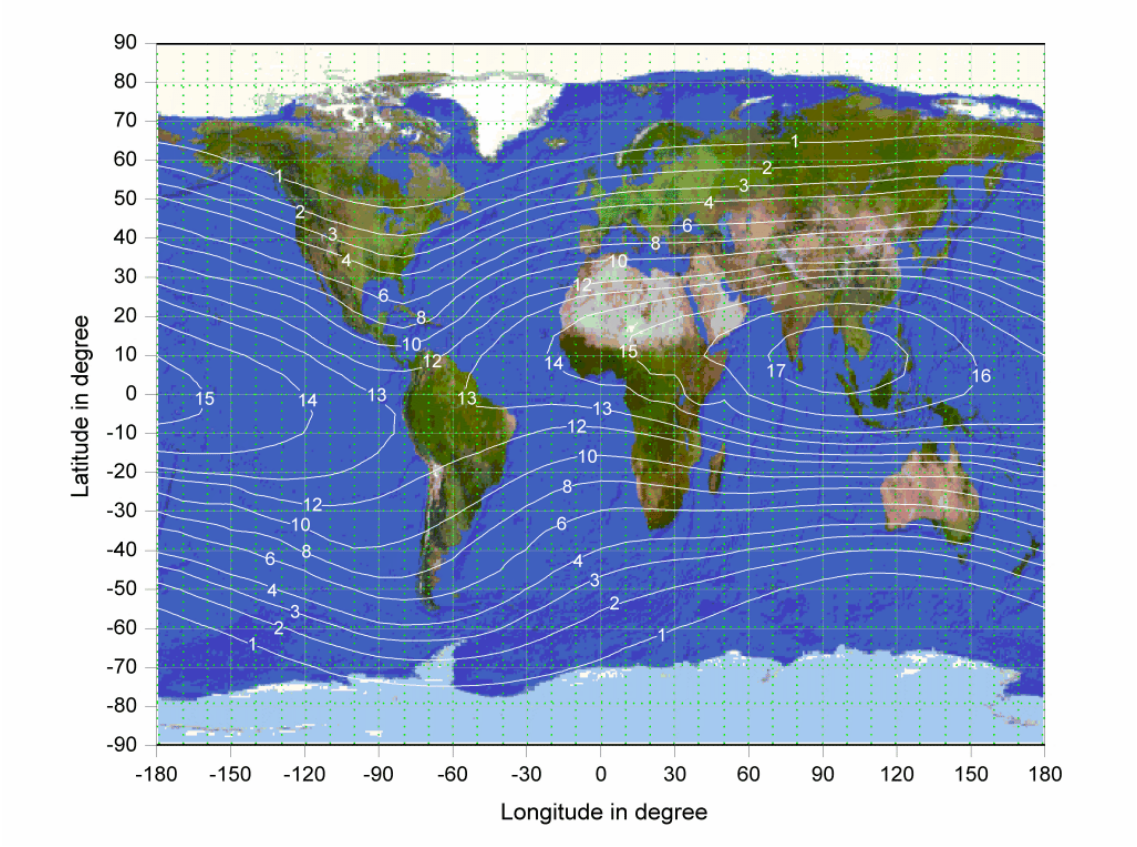

Figure III.2: Vertical Cosmic Ray Cut-off Rigidity in GV based on data in 1990 at 20km altitude.

III.3 Results

For comparison of the measurement results with calculated results, three different kinds of diagrams have been used:

1. Dependence of the ambient dose equivalent rate, $\dot{H}^*(10)$, on the geomagnetic latitude, at the same standard barometric altitude (SBA). SBA from 9 448 m (FL 310) up to 16 459 m (FL 540) have been analysed in steps of 305 m (FL 10) in a range of ±152.5 m (±FL 5). Values of the solar deceleration potentials have been selected from 470 MV to 610 MV, 611MV to 750 MV, 950 MV to 1140 MV, 1 141 MV to 1 330 MV.
2. Dependence of the ambient dose equivalent rate, $\dot{H}^*(10)$, on the vertical cut off rigidity r_c in GV, at the same standard barometric altitude. SBA from 9 448 m (FL 310) up to 16 459 m (FL 540) have been analysed in steps of 305 m (FL 10) in a range of ±152.5 m (±FL 5). Values of the solar deceleration potentials have been selected from 470 MV to 610 MV, 611MV to 750 MV, 950 MV to 1140 MV, 1 141 MV to 1 330 MV.
3. Dependence of the ambient dose equivalent rate, $\dot{H}^*(10)$, on the standard barometric altitude for two different vertical cut off rigidities: $r_c \leq 2$ GV, $r_c \geq 12$ GV. Values of the solar deceleration potentials have been selected from 470 MV to 610 MV, 611MV to 750 MV, 950 MV to 1140 MV, 1 141 MV to 1 330 MV.

Figure III.3 shows all routes of in-flight measurements between May 1992 and February 2003, on a map of the cut off rigidity r_c. Figures III.4 to III.71 show the results for ambient dose equivalent rate versus geomagnetic latitude and cut off rigidity for different flight levels and different solar activity. The mean value of the ambient dose equivalent rate for all experimental data within an r_c interval of

± 0.5 GV (indicated with "Avg.exp") were determined together with its standard deviation, *s*. Each mean value shows thus the mean ambient dose equivalent rate, for at least three measured data, for the following parameter ranges: r_c: ±0.5GV, SBA: ±152.5 m (FL±5), SDP: ±70MV (470MV - 750 MV) and SDP: ±95MV (950 MV- 1 330 MV). The vertical uncertainty bars in the diagrams show ±2*s*. The mean relative uncertainty (2*s*) for all r_c intervals for the experimental results is 20%. In the way the average value is calculated all experimental values are given the same weight. Thus if one specific instrument has delivered many results in a specific interval it will affect the average value significantly.

Figures III.72 to III.79 show ambient dose equivalent rate versus standard barometric altitude (different flight levels) for ranges of vertical cut off rigidity of $r_c \leq 2$ GV and $r_c \geq 12$ GV. The region of $r_c \leq 2$GV characterise the polar regions, $r_c \geq 12$ GV the equatorial region. The mean ambient dose eauivalent rate ("Avg. exp.") is here the mean of all results below 2 GV or above 12 GV and for SBA: ±152.5 m (FL±5) and SDP: ±70MV (470MV - 750 MV) and SDP: ±95MV (950 MV- 1 330 MV). The vertical uncertainty bars shown are ±2*s*. The mean relative uncertainty (2*s*) for all r_c intervals and the experimental values becomes here 25%.

The EURADOS Air Crew In-Flight Database does not contain experimental data for every possible in-flight condition and solar activity. For conditions where measurement results are not available, there is no figure given.

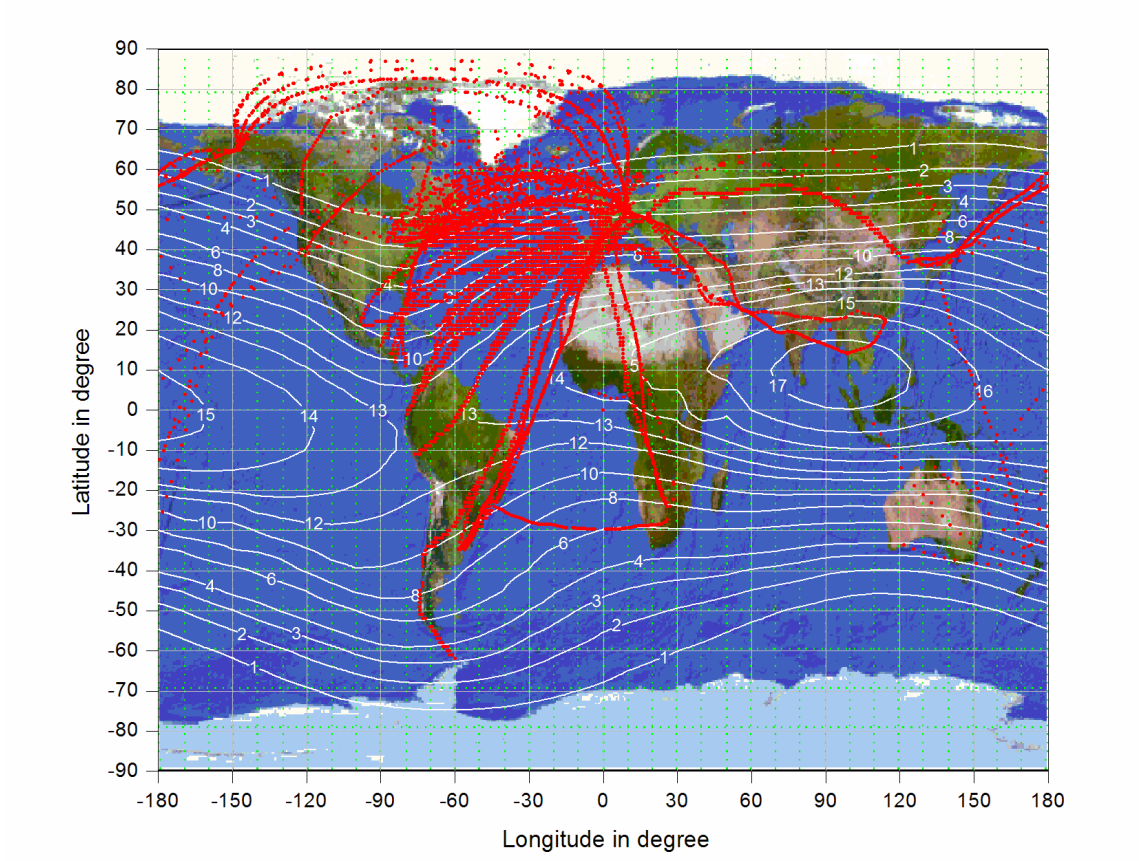

Figure III.3: Investigated flight routes between May 1992 and April 2003.

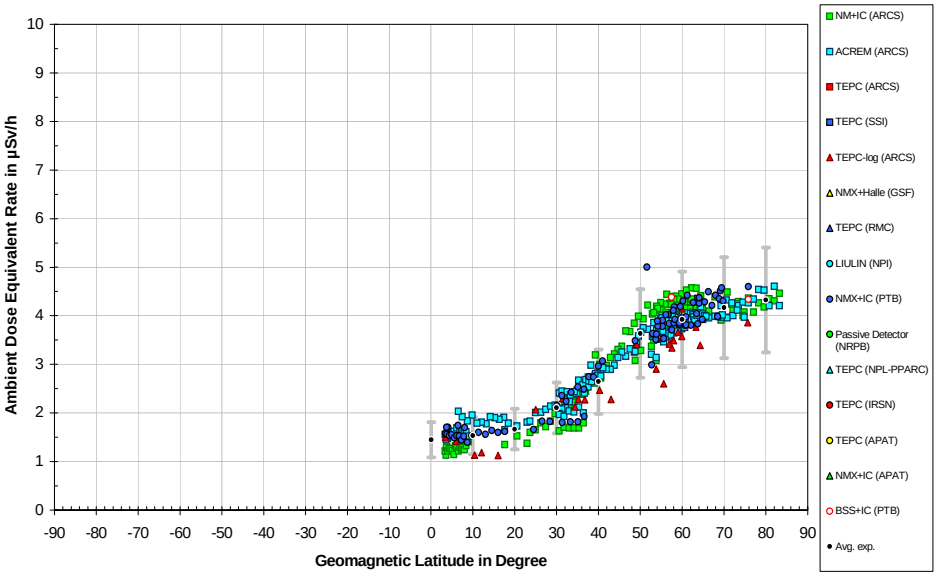

Figure III. 4 Ambient dose equivalent rate dH*(10)/dt vs. geomagnetic latitude between May 1992 and May 2003 for standard barometric altitude 9448 m (FL 310) and for solar deceleration potential in the range of 470 MV - 610 MV.

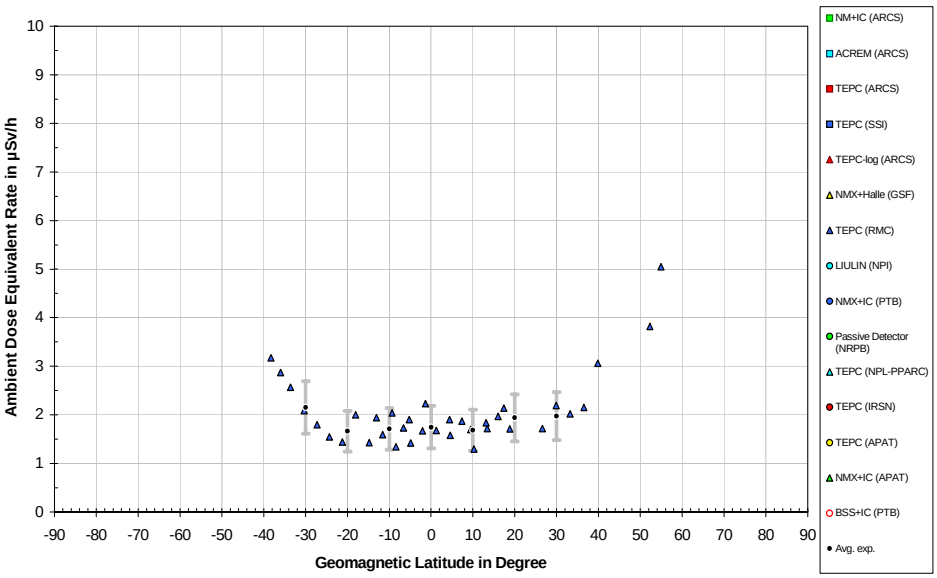

Figure III. 5 Ambient dose equivalent rate dH*(10)/dt vs. geomagnetic latitude between May 1992 and May 2003 for standard barometric altitude 9448 m (FL 310) and for solar deceleration potential in the range of 610 MV - 750 MV.

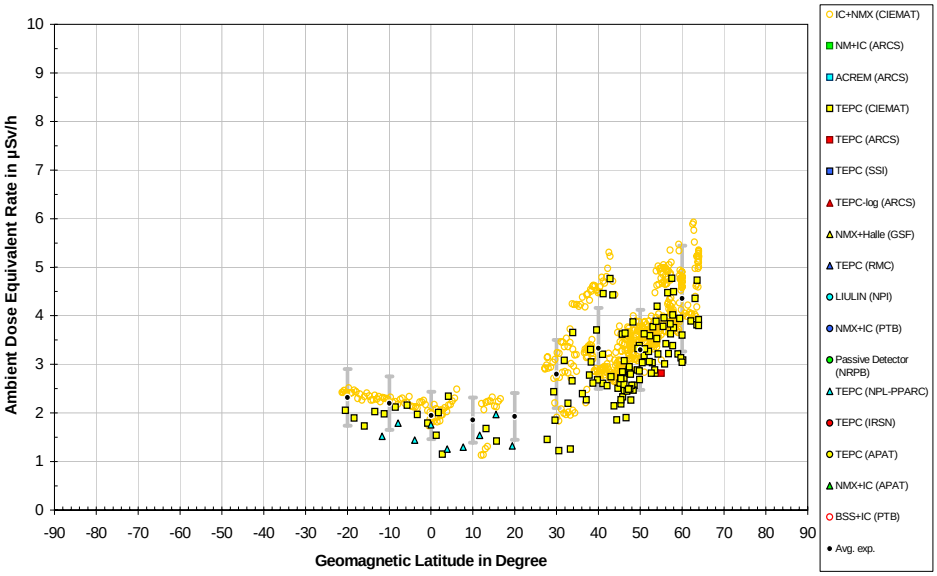

Figure III. 6 Ambient dose equivalent rate dH*(10)/dt vs. geomagnetic latitude between May 1992 and May 2003 for standard barometric altitude 9448 m (FL 310) and for solar deceleration potential in the range of 950 MV - 1140 MV.

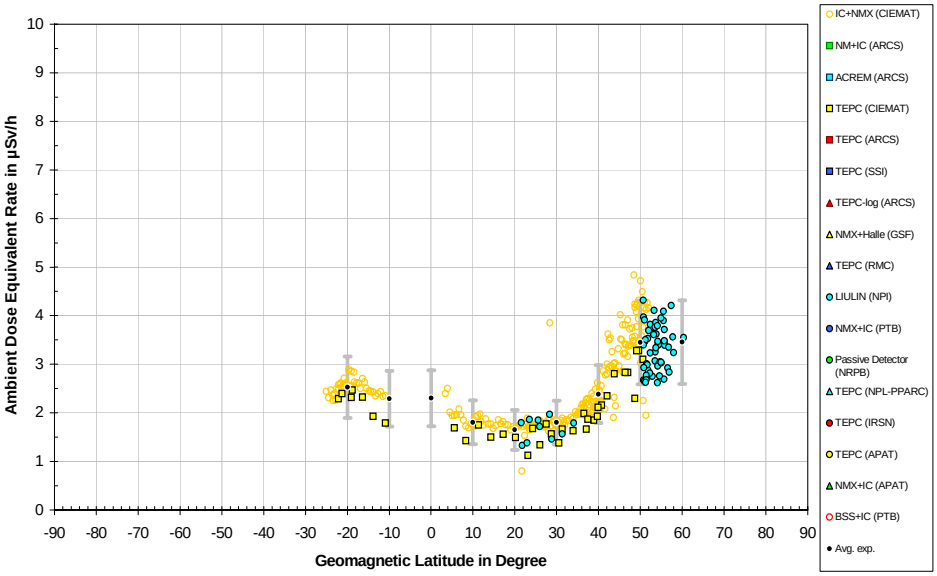

Figure III. 7 Ambient dose equivalent rate dH*(10)/dt vs. geomagnetic latitude between May 1992 and May 2003 for standard barometric altitude 9448 m (FL 310) and for solar deceleration potential in the range of 1140 MV - 1330 MV.

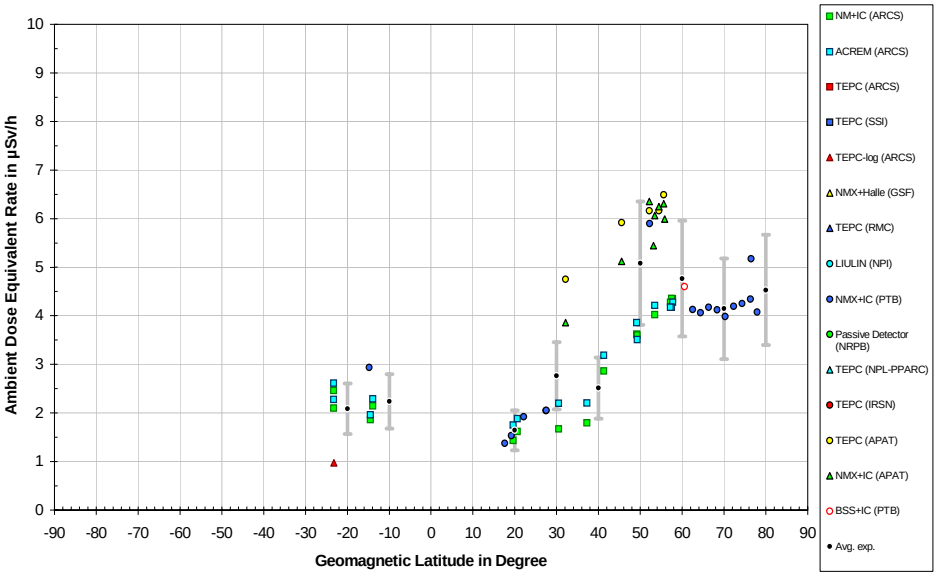

Figure III. 8 Ambient dose equivalent rate dH*(10)/dt vs. geomagnetic latitude between May 1992 and May 2003 for standard barometric altitude 9753 m (FL 320) and for solar deceleration potential in the range of 470 MV - 610 MV.

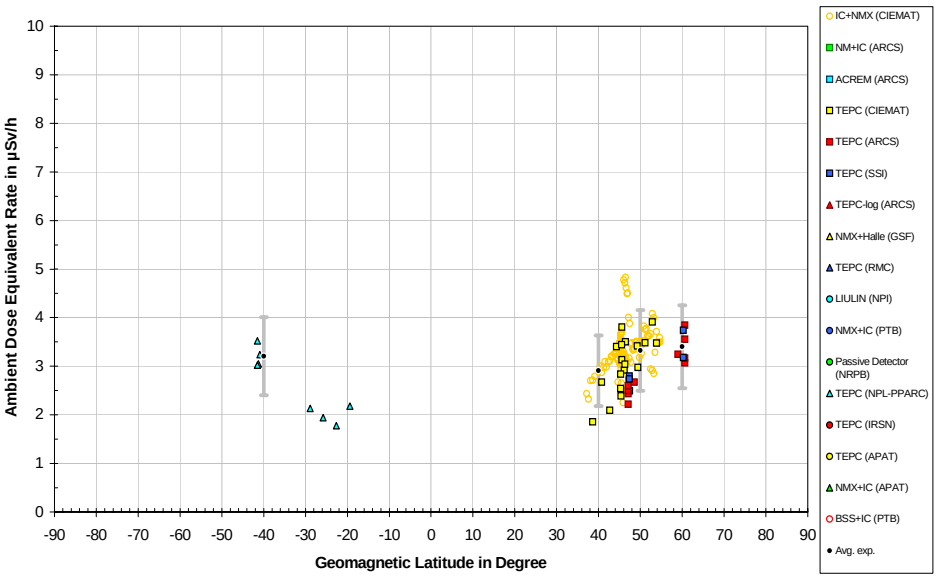

Figure III. 9 Ambient dose equivalent rate dH*(10)/dt vs. geomagnetic latitude between May 1992 and May 2003 for standard barometric altitude 9753 m (FL 320) and for solar deceleration potential in the range of 950 MV - 1140 MV.

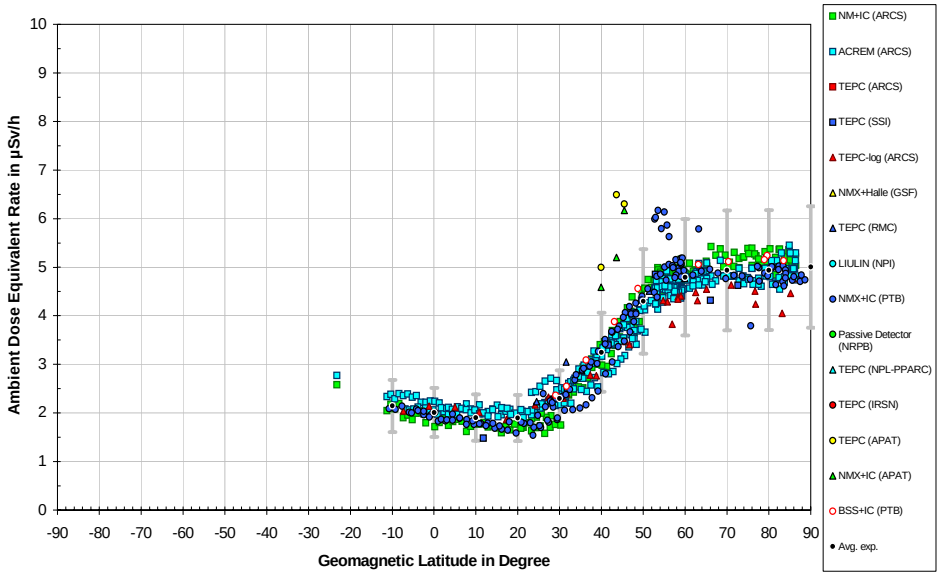

Figure III. 10 Ambient dose equivalent rate dH*(10)/dt vs. geomagnetic latitude between May 1992 and May 2003 for standard barometric altitude 10058 m (FL 330) and for solar deceleration potential in the range of 470 MV - 610 MV.

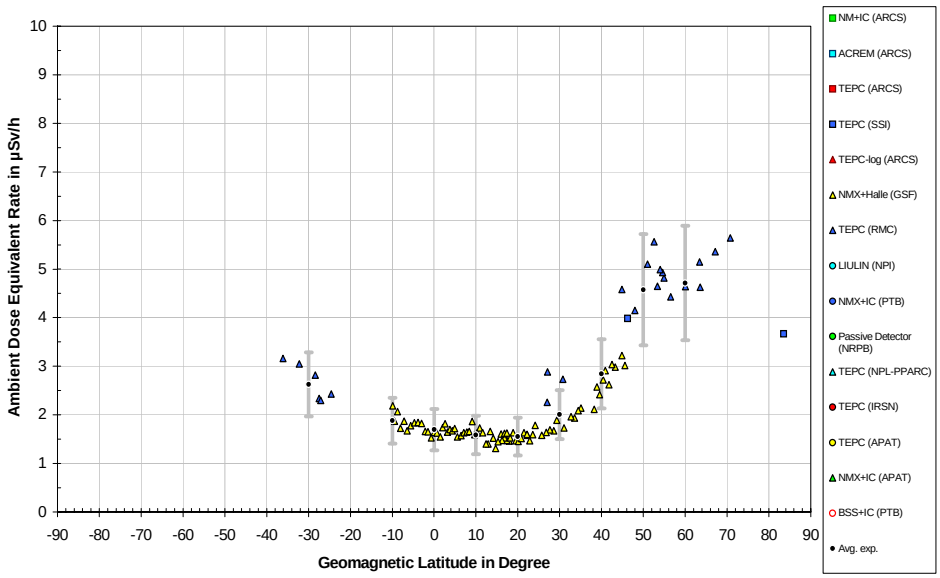

Figure III. 11 Ambient dose equivalent rate dH*(10)/dt vs. geomagnetic latitude between May 1992 and May 2003 for standard barometric altitude 10058 m (FL 330) and for solar deceleration potential in the range of 610 MV - 750 MV.

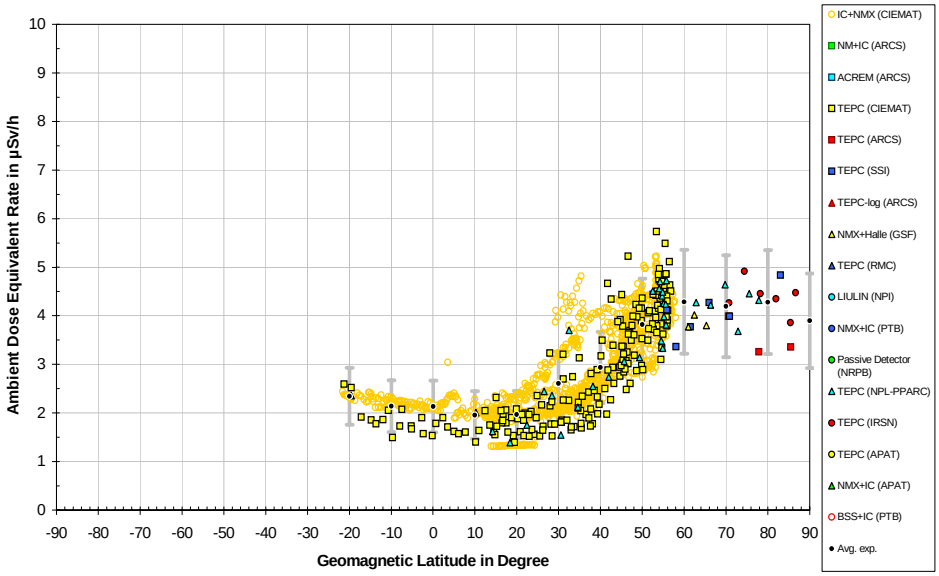

Figure III. 12 Ambient dose equivalent rate dH*(10)/dt vs. geomagnetic latitude between May 1992 and May 2003 for standard barometric altitude 10058 m (FL 330) and for solar deceleration potential in the range of 950 MV - 1140 MV.

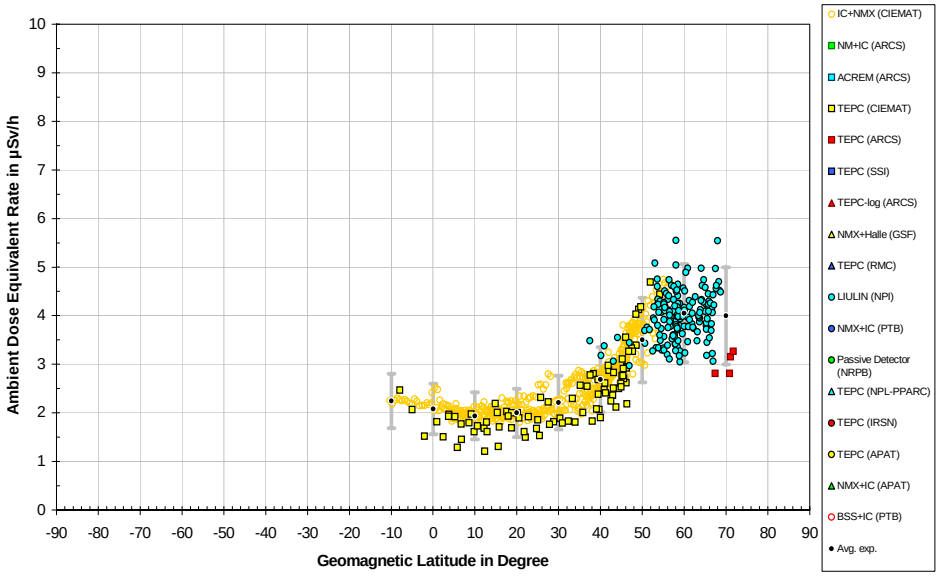

Figure III. 13 Ambient dose equivalent rate dH*(10)/dt vs. geomagnetic latitude between May 1992 and May 2003 for standard barometric altitude 10058 m (FL 330) and for solar deceleration potential in the range of 1140 MV - 1330 MV.

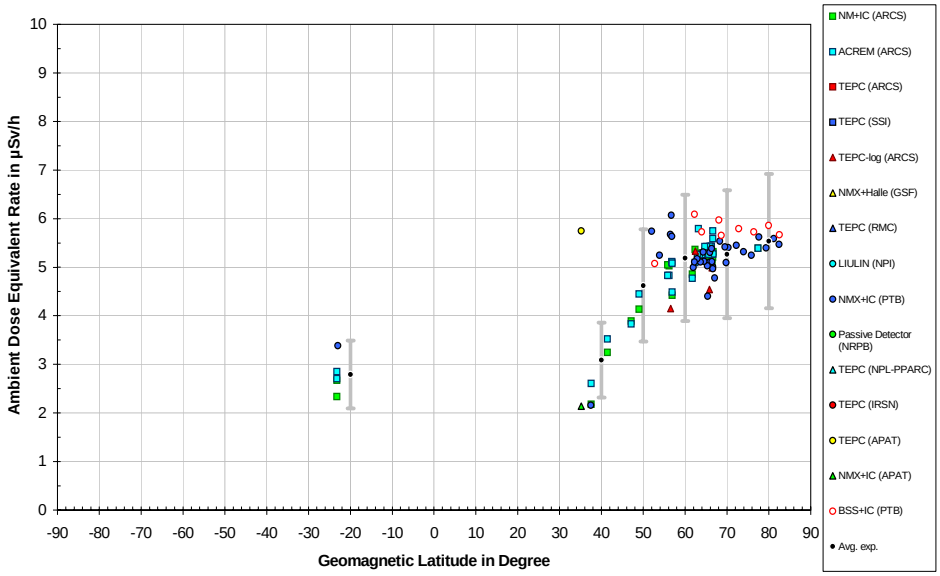

Figure III. 14 Ambient dose equivalent rate dH*(10)/dt vs. geomagnetic latitude between May 1992 and May 2003 for standard barometric altitude 10363 m (FL 340) and for solar deceleration potential in the range of 470 MV - 610 MV.

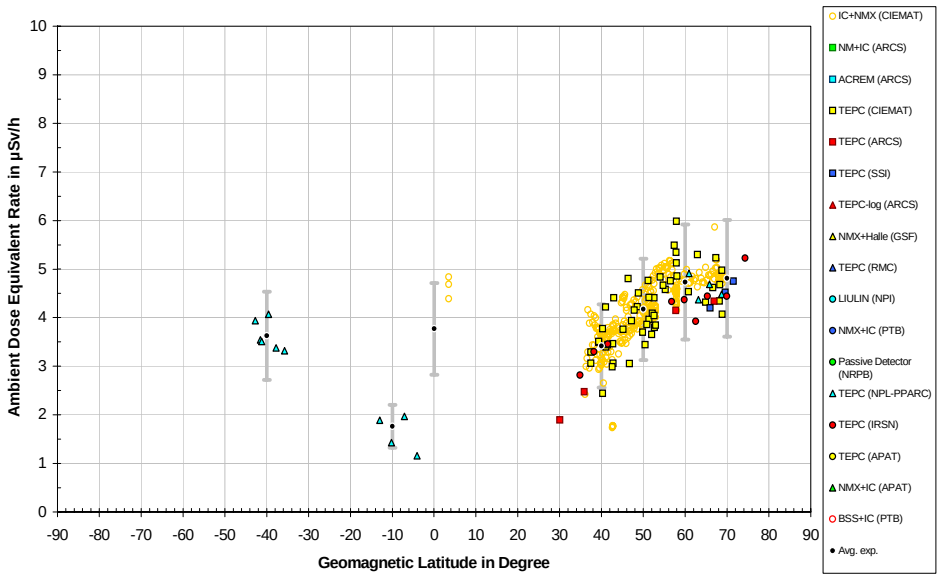

Figure III. 15 Ambient dose equivalent rate dH*(10)/dt vs. geomagnetic latitude between May 1992 and May 2003 for standard barometric altitude 10363 m (FL 340) and for solar deceleration potential in the range of 950 MV - 1140 MV.

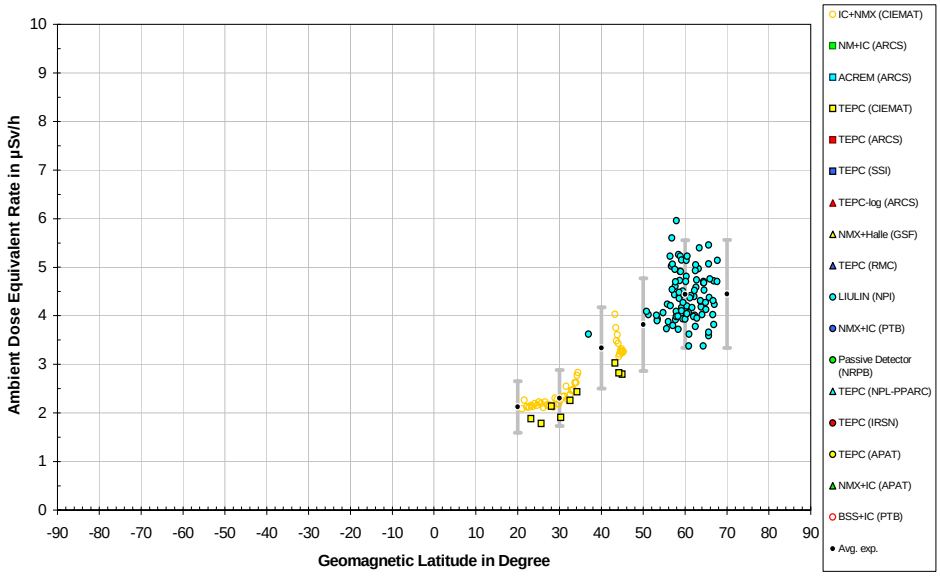

Figure III. 16 Ambient dose equivalent rate dH*(10)/dt vs. geomagnetic latitude between May 1992 and May 2003 for standard barometric altitude 10363 m (FL 340) and for solar deceleration potential in the range of 1140 MV - 1330 MV.

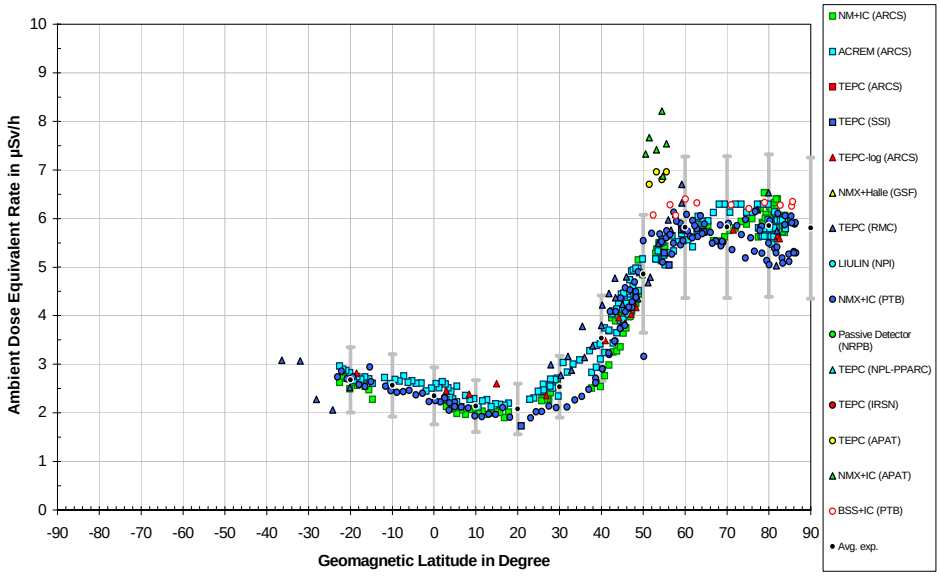

Figure III. 17 Ambient dose equivalent rate dH*(10)/dt vs. geomagnetic latitude between May 1992 and May 2003 for standard barometric altitude 10668 m (FL 350) and for solar deceleration potential in the range of 470 MV - 610 MV.

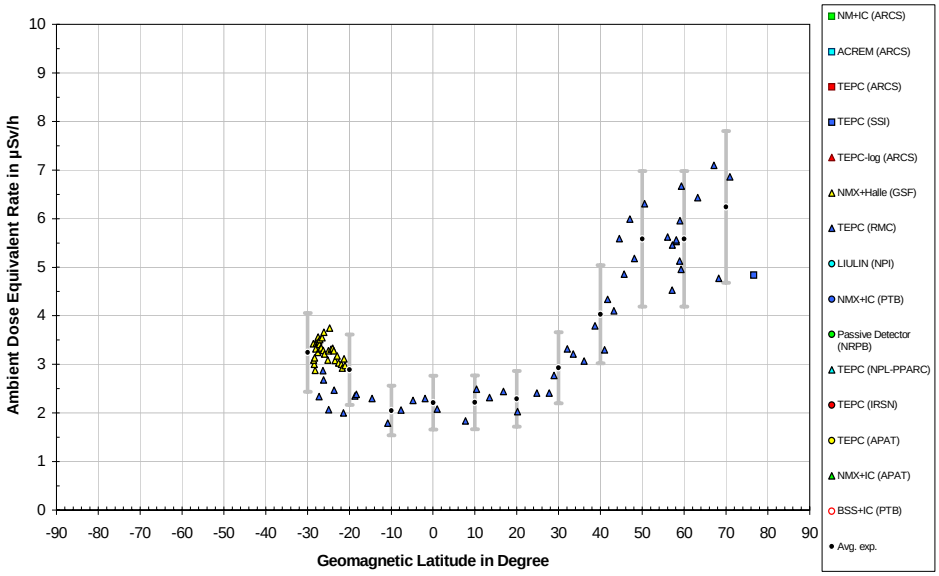

Figure III. 18 Ambient dose equivalent rate dH*(10)/dt vs. geomagnetic latitude between May 1992 and May 2003 for standard barometric altitude 10668 m (FL 350) and for solar deceleration potential in the range of 610 MV - 750 MV.

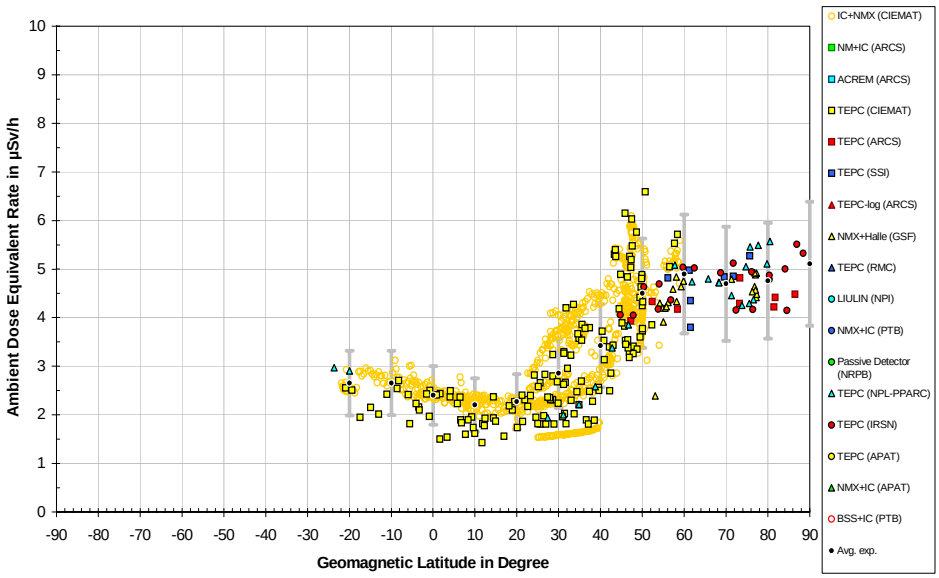

Figure III. 19 Ambient dose equivalent rate dH*(10)/dt vs. geomagnetic latitude between May 1992 and May 2003 for standard barometric altitude 10668 m (FL 350) and for solar deceleration potential in the range of 950 MV - 1140 MV.

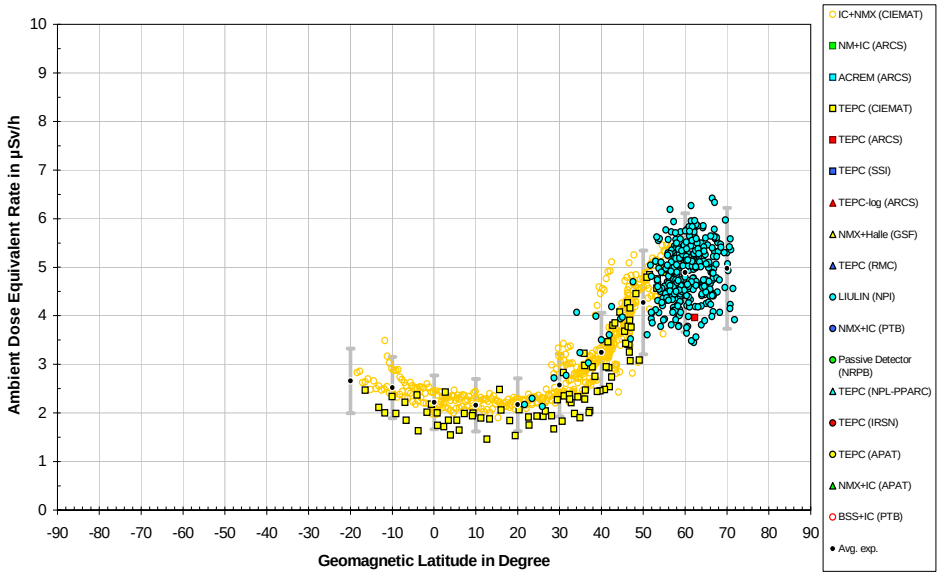

Figure III. 20 Ambient dose equivalent rate dH*(10)/dt vs. geomagnetic latitude between May 1992 and May 2003 for standard barometric altitude 10668 m (FL 350) and for solar deceleration potential in the range of 1140 MV - 1330 MV.

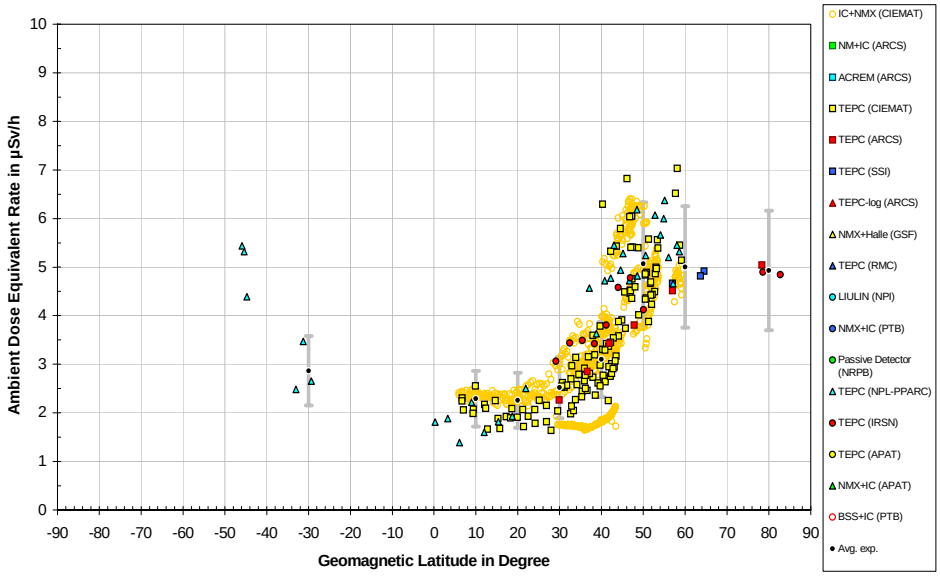

Figure III. 21 Ambient dose equivalent rate dH*(10)/dt vs. geomagnetic latitude between May 1992 and May 2003 for standard barometric altitude 10972 m (FL 360) and for solar deceleration potential in the range of 950 MV - 1140 MV.

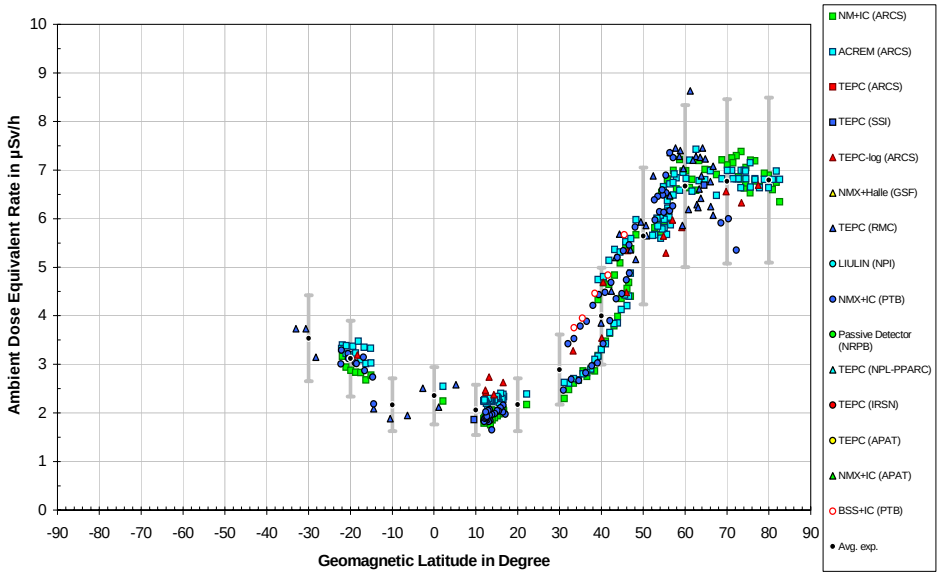

Figure III. 22 Ambient dose equivalent rate dH*(10)/dt vs. geomagnetic latitude between May 1992 and May 2003 for standard barometric altitude 11277 m (FL 370) and for solar deceleration potential in the range of 470 MV - 610 MV.

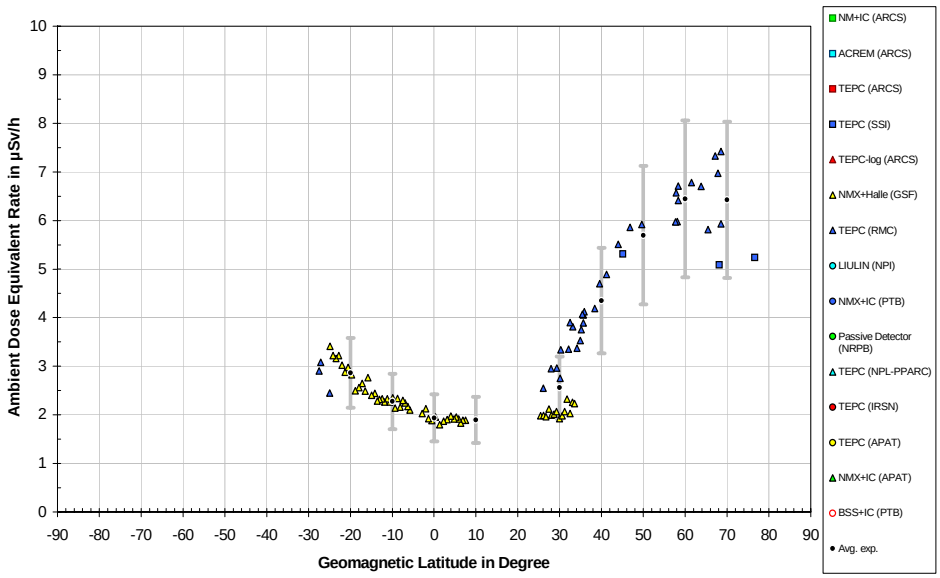

Figure III. 23 Ambient dose equivalent rate dH*(10)/dt vs. geomagnetic latitude between May 1992 and May 2003 for standard barometric altitude 11277 m (FL 370) and for solar deceleration potential in the range of 610 MV - 750 MV.

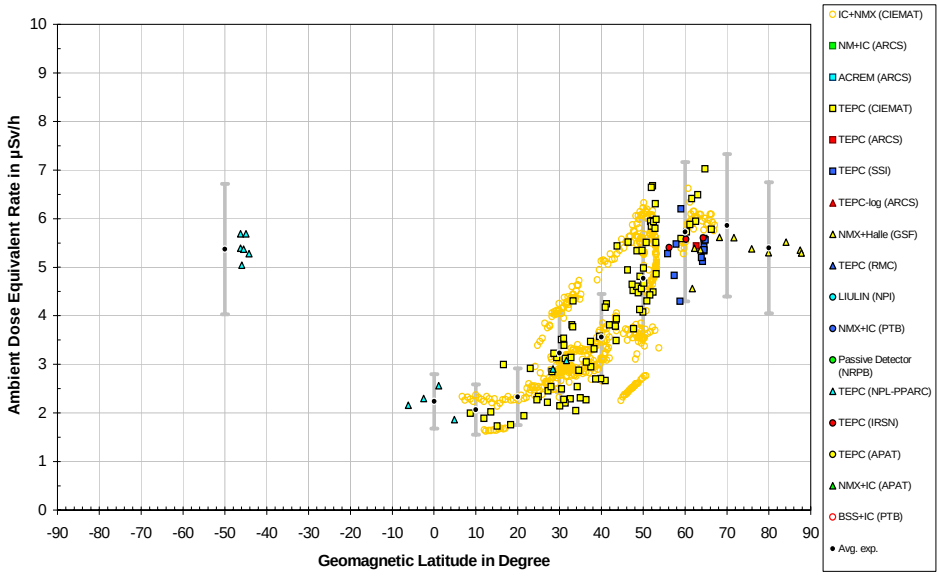

Figure III. 24 Ambient dose equivalent rate dH*(10)/dt vs. geomagnetic latitude between May 1992 and May 2003 for standard barometric altitude 11277 m (FL 370) and for solar deceleration potential in the range of 950 MV - 1140 MV.

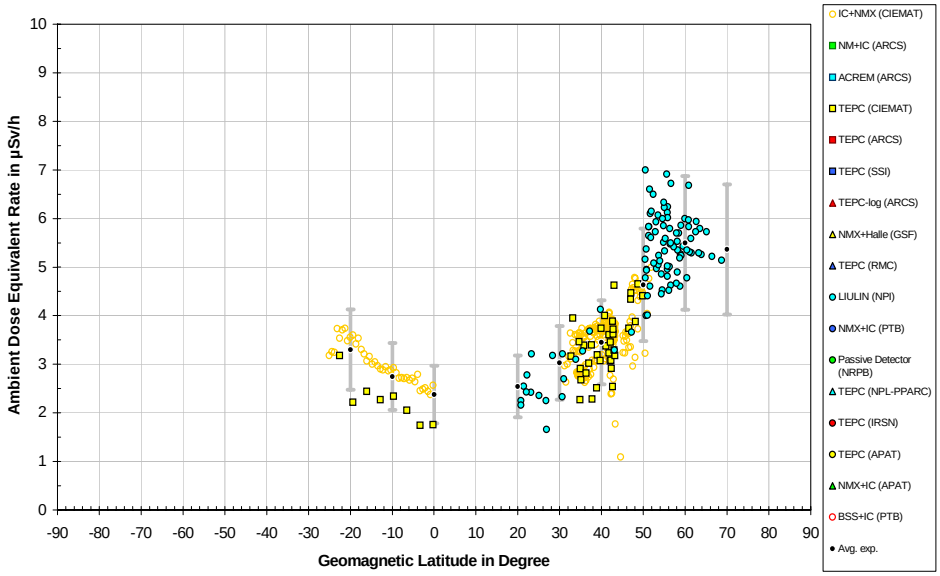

Figure III. 25 Ambient dose equivalent rate dH*(10)/dt vs. geomagnetic latitude between May 1992 and May 2003 for standard barometric altitude 11277 m (FL 370) and for solar deceleration potential in the range of 1140 MV - 1330 MV.

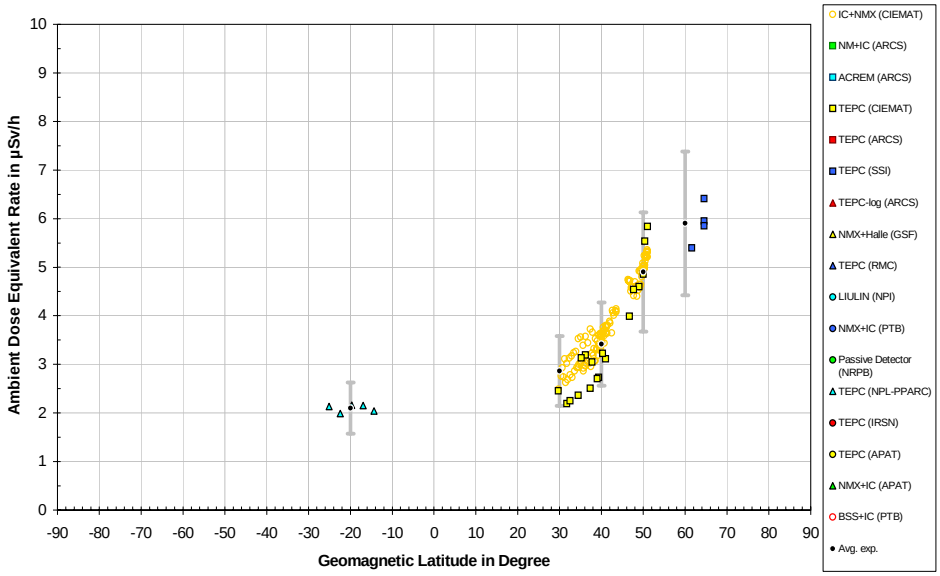

Figure III. 26 Ambient dose equivalent rate dH*(10)/dt vs. geomagnetic latitude between May 1992 and May 2003 for standard barometric altitude 11582 m (FL 380) and for solar deceleration potential in the range of 950 MV - 1140 MV.

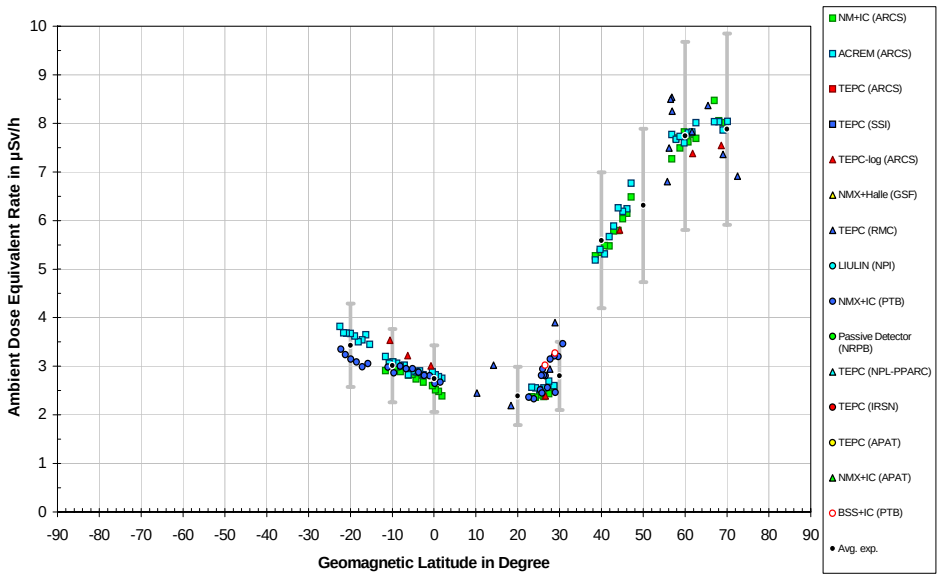

Figure III. 27 Ambient dose equivalent rate dH*(10)/dt vs. geomagnetic latitude between May 1992 and May 2003 for standard barometric altitude 11887 m (FL 390) and for solar deceleration potential in the range of 470 MV - 610 MV.

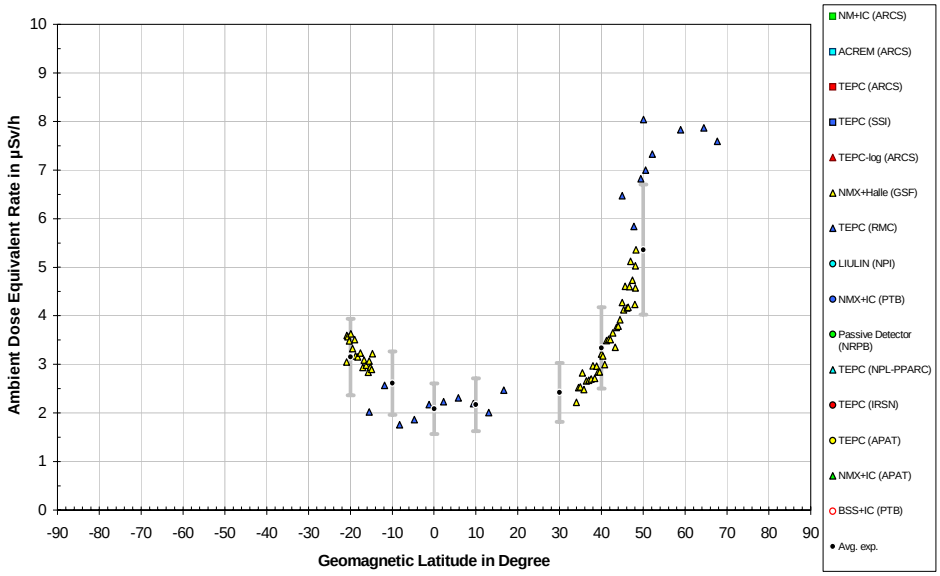

Figure III. 28 Ambient dose equivalent rate dH*(10)/dt vs. geomagnetic latitude between May 1992 and May 2003 for standard barometric altitude 11887 m (FL 390) and for solar deceleration potential in the range of 610 MV - 750 MV.

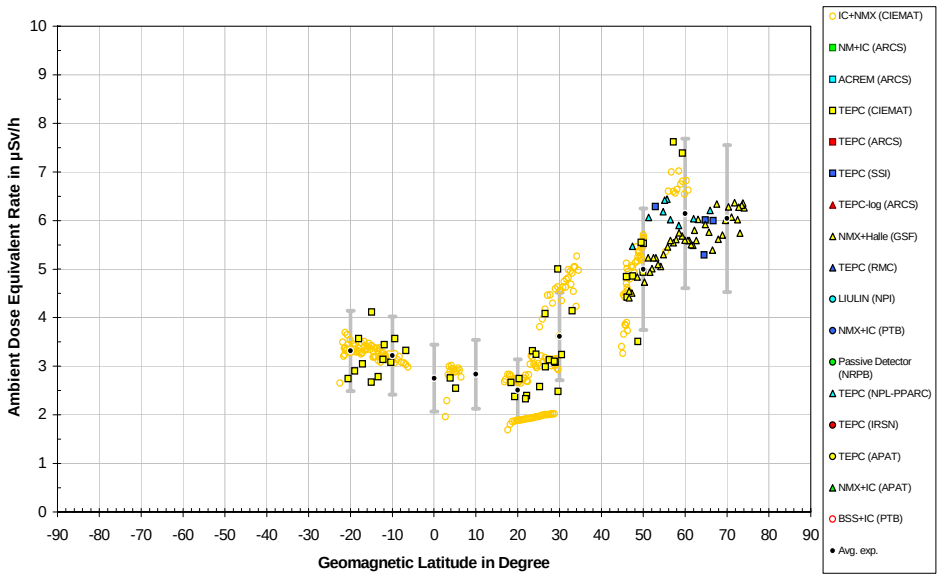

Figure III. 29 Ambient dose equivalent rate dH*(10)/dt vs. geomagnetic latitude between May 1992 and May 2003 for standard barometric altitude 11887 m (FL 390) and for solar deceleration potential in the range of 950 MV - 1140 MV.

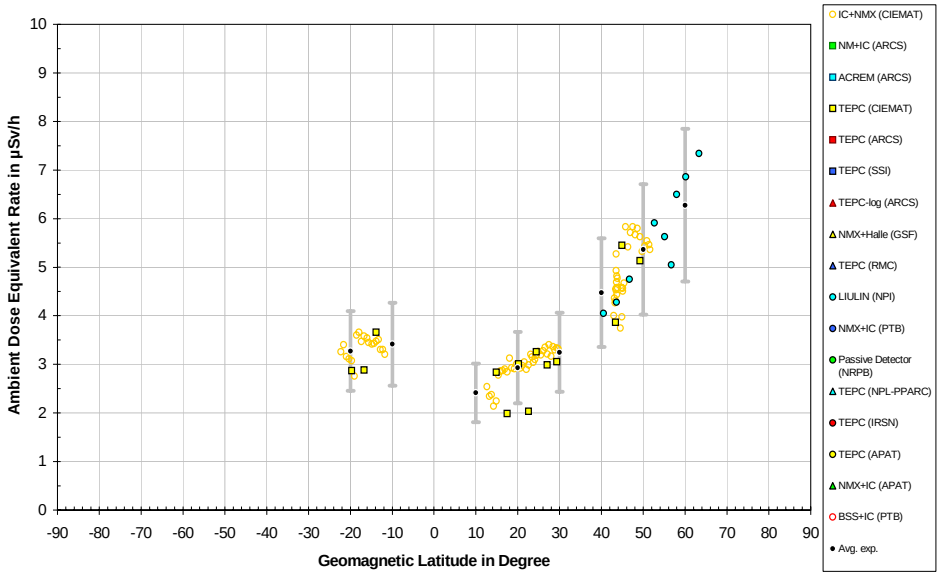

Figure III. 30 Ambient dose equivalent rate dH*(10)/dt vs. geomagnetic latitude between May 1992 and May 2003 for standard barometric altitude 11887 m (FL 390) and for solar deceleration potential in the range of 1140 MV - 1330 MV.

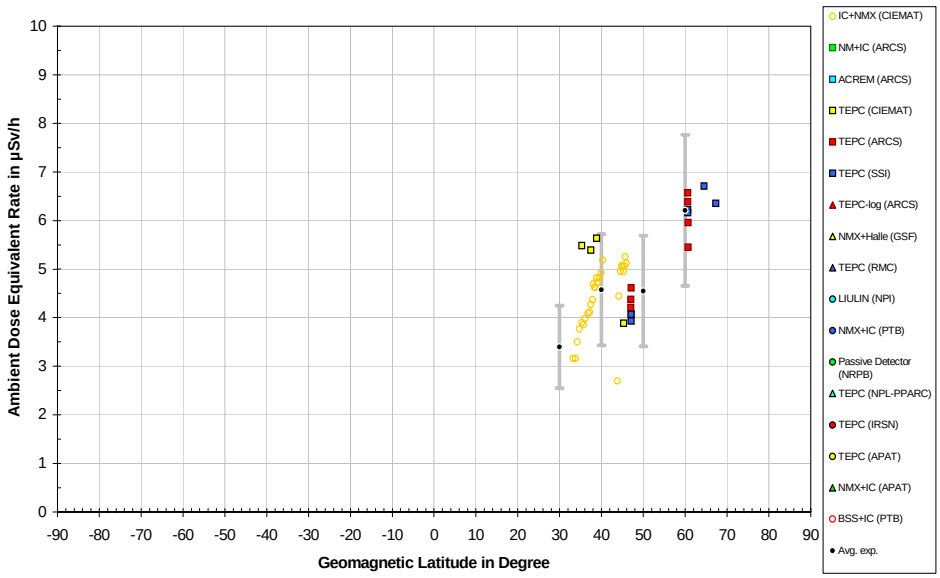

Figure III. 31 Ambient dose equivalent rate dH*(10)/dt vs. geomagnetic latitude between May 1992 and May 2003 for standard barometric altitude 12192 m (FL 400) and for solar deceleration potential in the range of 950 MV - 1140 MV.

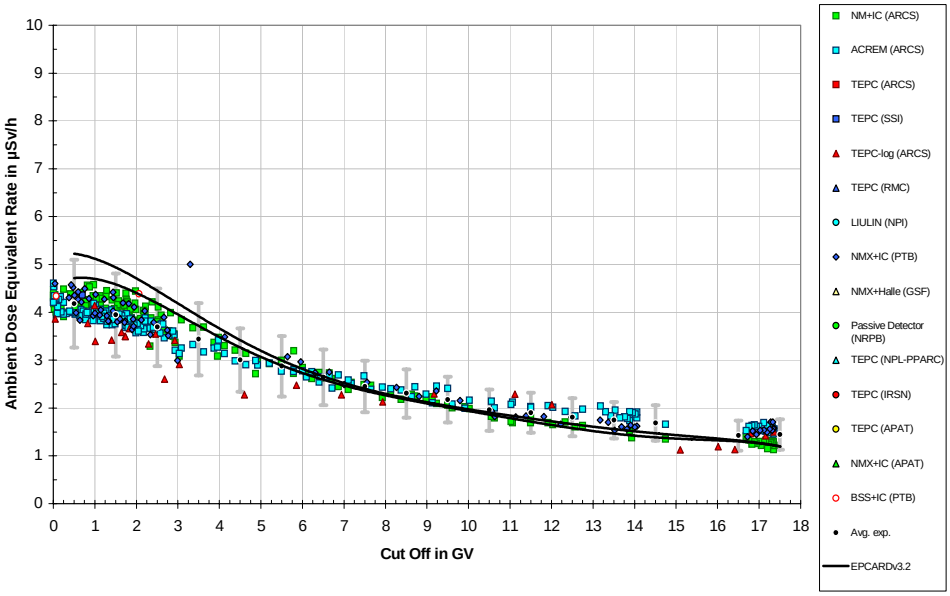

Figure III. 32 Ambient dose equivalent rate dH*(10)/dt vs. vertical cut off rigidity rc between May 1992 and May 2003 for standard barometric altitude 9448 m (FL 310) and for solar deceleration potential in the range of 470 MV - 610 MV.

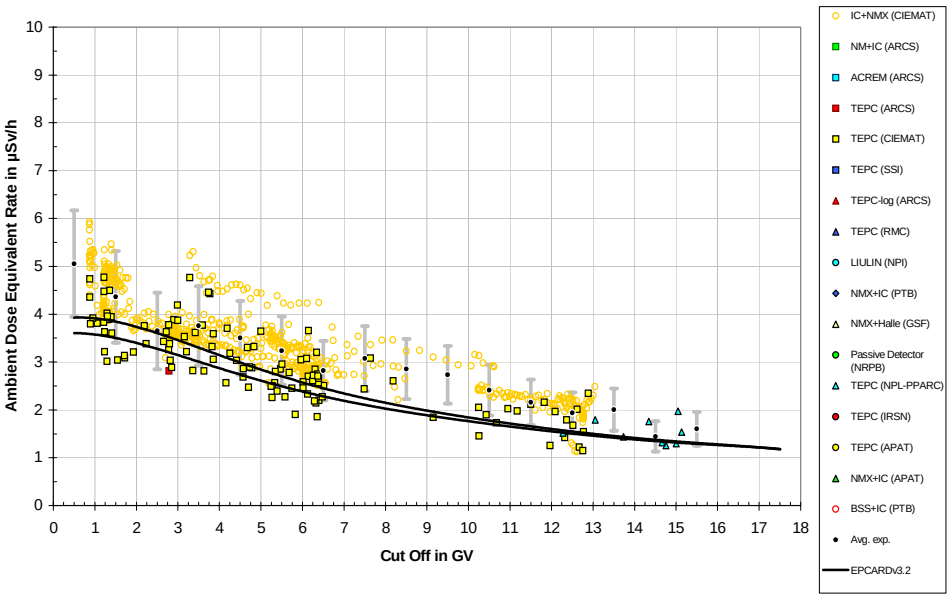

Figure III. 33 Ambient dose equivalent rate dH*(10)/dt vs. vertical cut off rigidity rc between May 1992 and May 2003 for standard barometric altitude 9448 m (FL 310) and for solar deceleration potential in the range of 950 MV - 1140 MV.

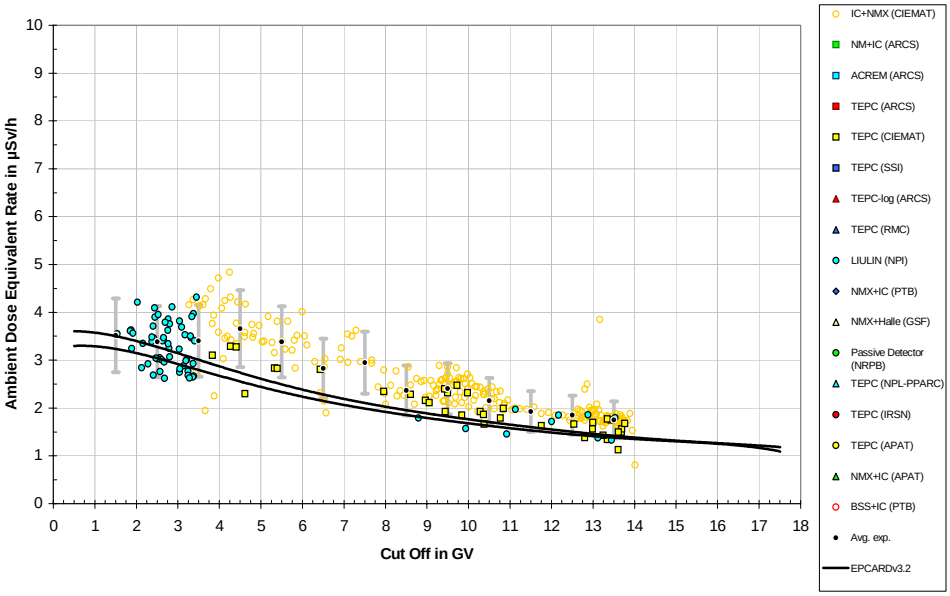

Figure III. 34 Ambient dose equivalent rate dH*(10)/dt vs. vertical cut off rigidity rc between May 1992 and May 2003 for standard barometric altitude 9448 m (FL 310) and for solar deceleration potential in the range of 1140 MV - 1330 MV.

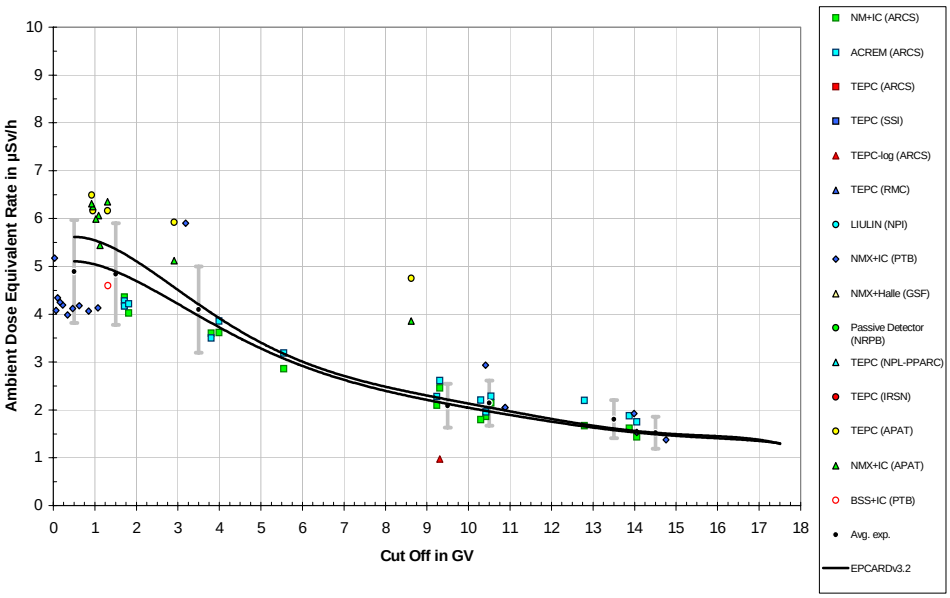

Figure III. 35 Ambient dose equivalent rate dH*(10)/dt vs. vertical cut off rigidity rc between May 1992 and May 2003 for standard barometric altitude 9753 m (FL 320) and for solar deceleration potential in the range of 470 MV - 610 MV.

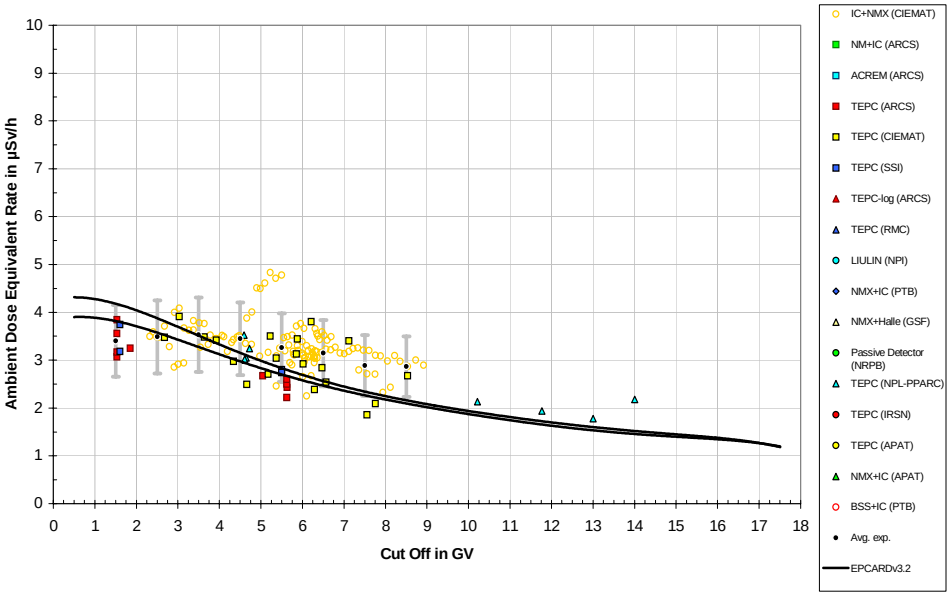

Figure III. 36 Ambient dose equivalent rate dH*(10)/dt vs. vertical cut off rigidity rc between May 1992 and May 2003 for standard barometric altitude 9753 m (FL 320) and for solar deceleration potential in the range of 950 MV - 1140 MV.

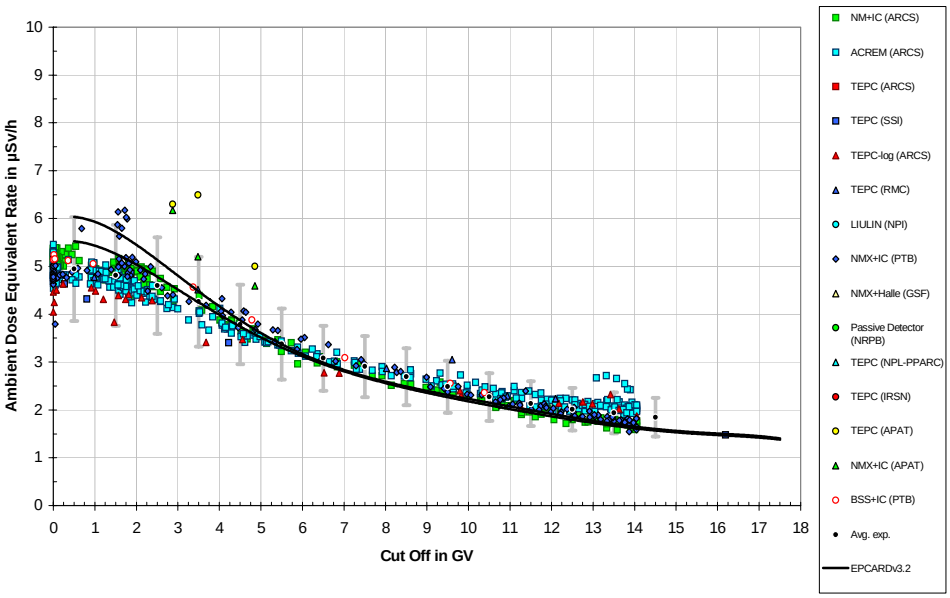

Figure III. 37 Ambient dose equivalent rate dH*(10)/dt vs. vertical cut off rigidity rc between May 1992 and May 2003 for standard barometric altitude 10058 m (FL 330) and for solar deceleration potential in the range of 470 MV - 610 MV.

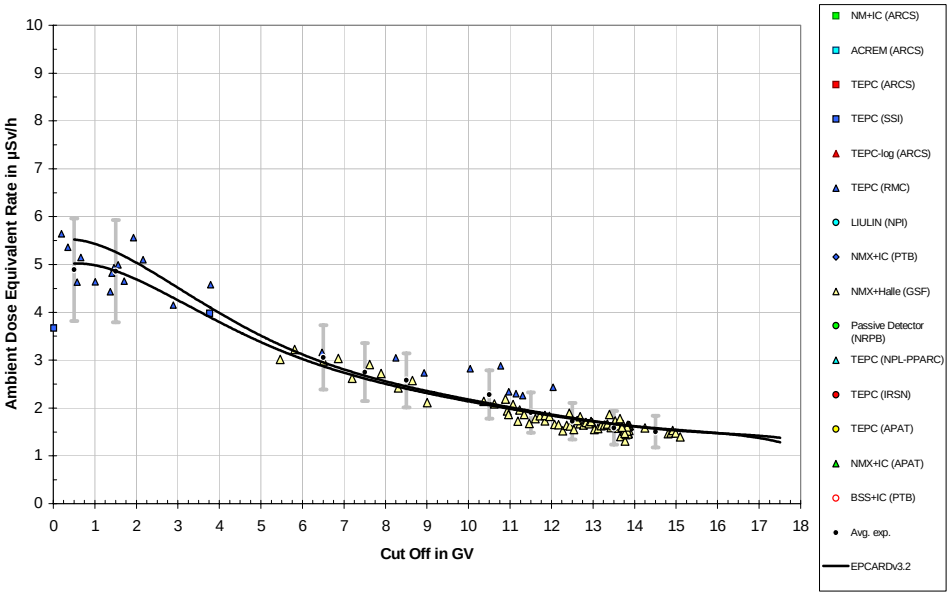

Figure III. 38 Ambient dose equivalent rate dH*(10)/dt vs. vertical cut off rigidity rc between May 1992 and May 2003 for standard barometric altitude 10058 m (FL 330) and for solar deceleration potential in the range of 610 MV - 750 MV.

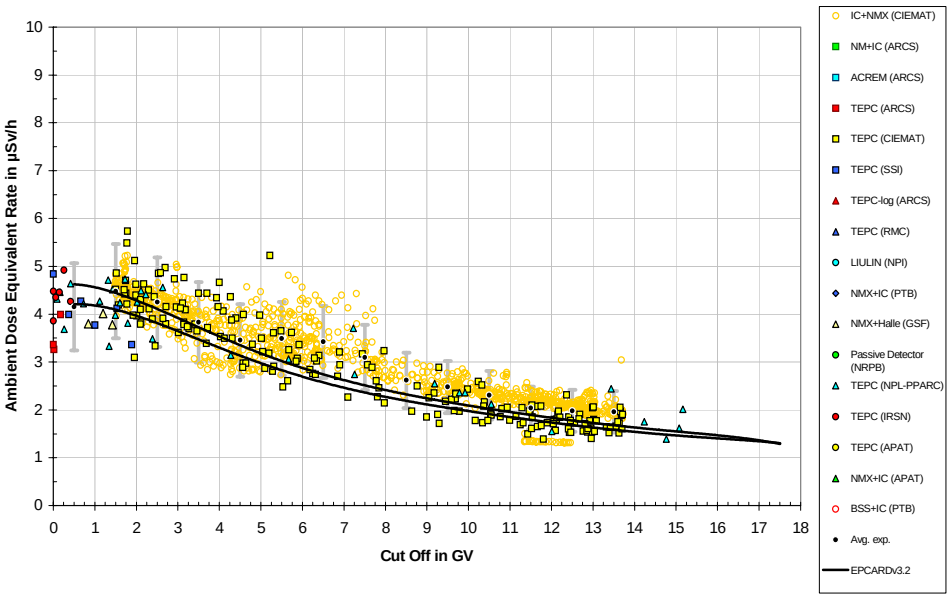

Figure III. 39 Ambient dose equivalent rate dH*(10)/dt vs. vertical cut off rigidity rc between May 1992 and May 2003 for standard barometric altitude 10058 m (FL 330) and for solar deceleration potential in the range of 950 MV - 1140 MV.

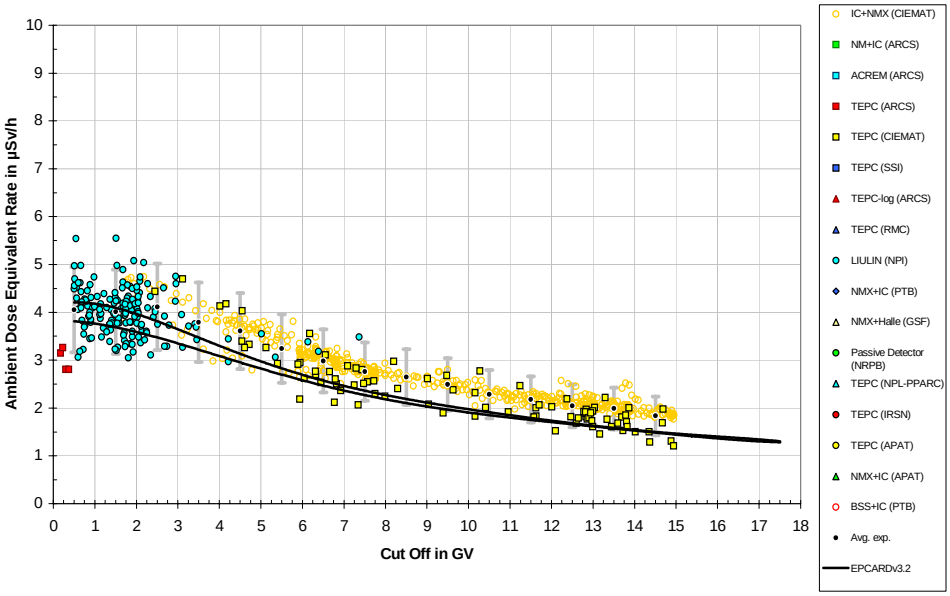

Figure III. 40 Ambient dose equivalent rate dH*(10)/dt vs. vertical cut off rigidity rc between May 1992 and May 2003 for standard barometric altitude 10058 m (FL 330) and for solar deceleration potential in the range of 1140 MV - 1330 MV.

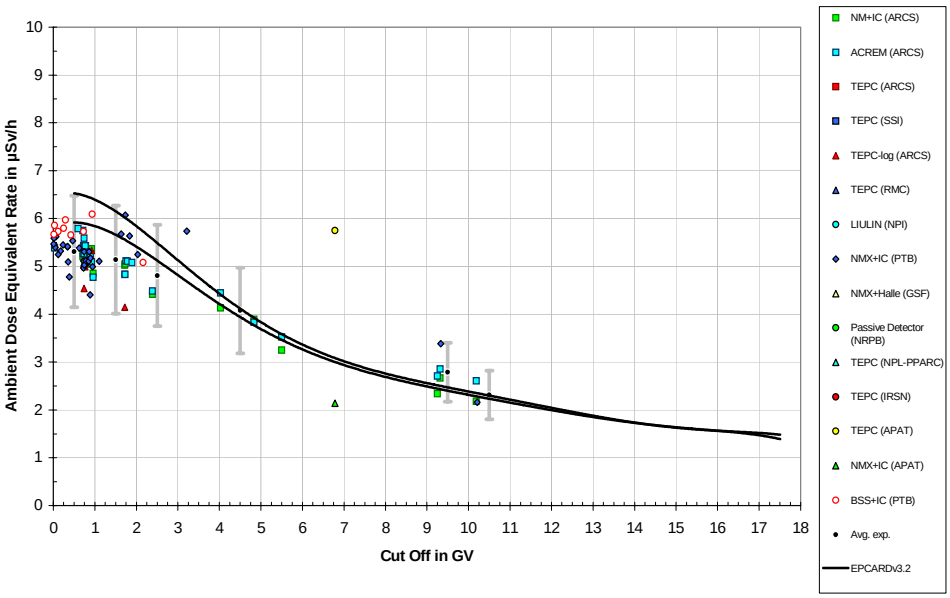

Figure III. 41 Ambient dose equivalent rate dH*(10)/dt vs. vertical cut off rigidity rc between May 1992 and May 2003 for standard barometric altitude 10363 m (FL 340) and for solar deceleration potential in the range of 470 MV - 610 MV.

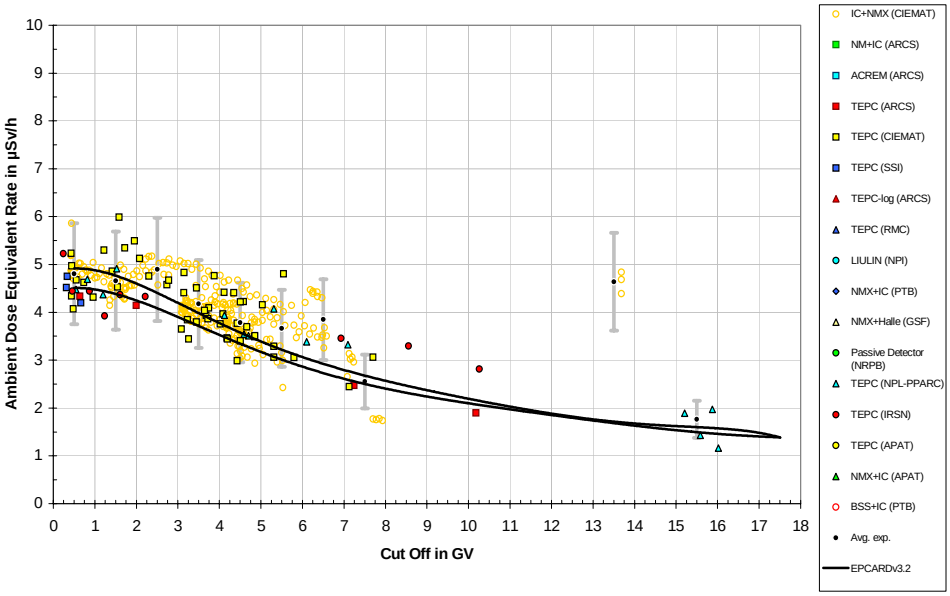

Figure III. 42 Ambient dose equivalent rate dH*(10)/dt vs. vertical cut off rigidity rc between May 1992 and May 2003 for standard barometric altitude 10363 m (FL 340) and for solar deceleration potential in the range of 950 MV - 1140 MV.

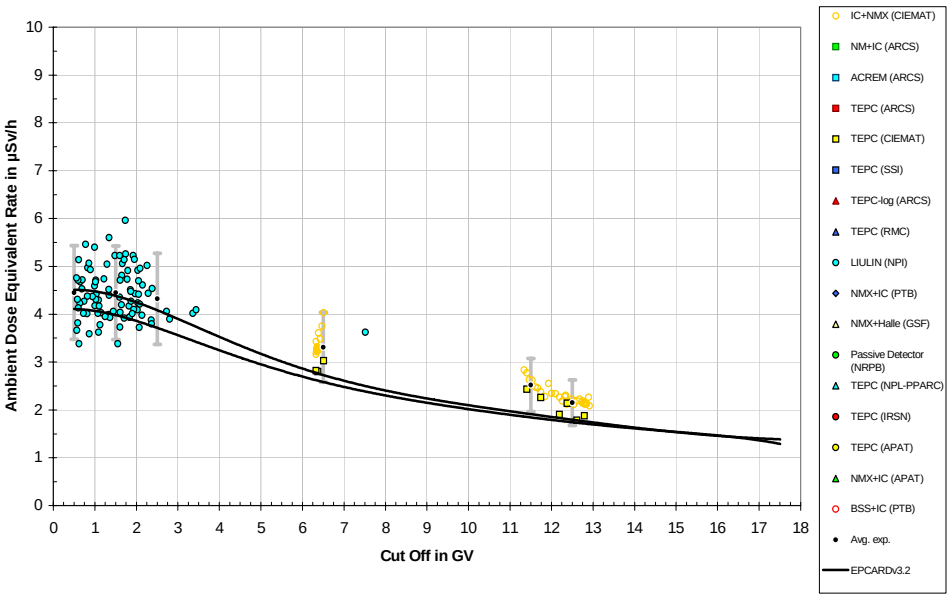

Figure III. 43 Ambient dose equivalent rate dH*(10)/dt vs. vertical cut off rigidity rc between May 1992 and May 2003 for standard barometric altitude 10363 m (FL 340) and for solar deceleration potential in the range of 1140 MV - 1330 MV.

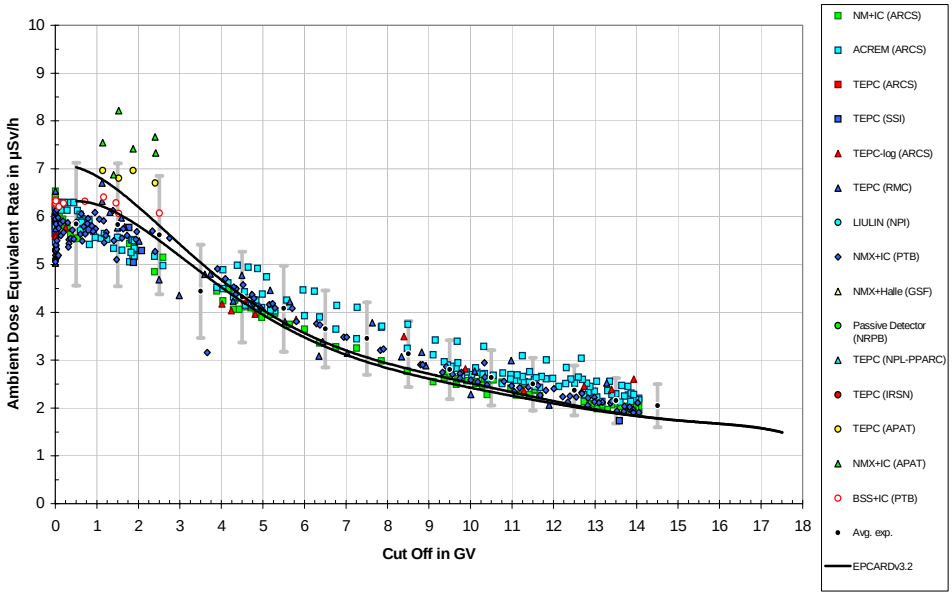

Figure III. 44 Ambient dose equivalent rate dH*(10)/dt vs. vertical cut off rigidity rc between May 1992 and May 2003 for standard barometric altitude 10668 m (FL 350) and for solar deceleration potential in the range of 470 MV - 610 MV.

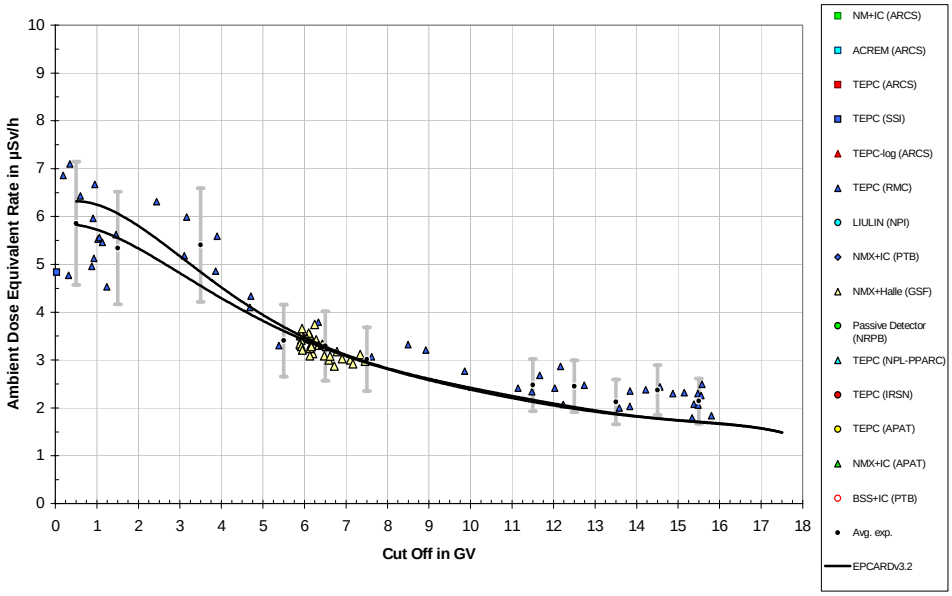

Figure III. 45 Ambient dose equivalent rate dH*(10)/dt vs. vertical cut off rigidity rc between May 1992 and May 2003 for standard barometric altitude 10668 m (FL 350) and for solar deceleration potential in the range of 610 MV - 750 MV.

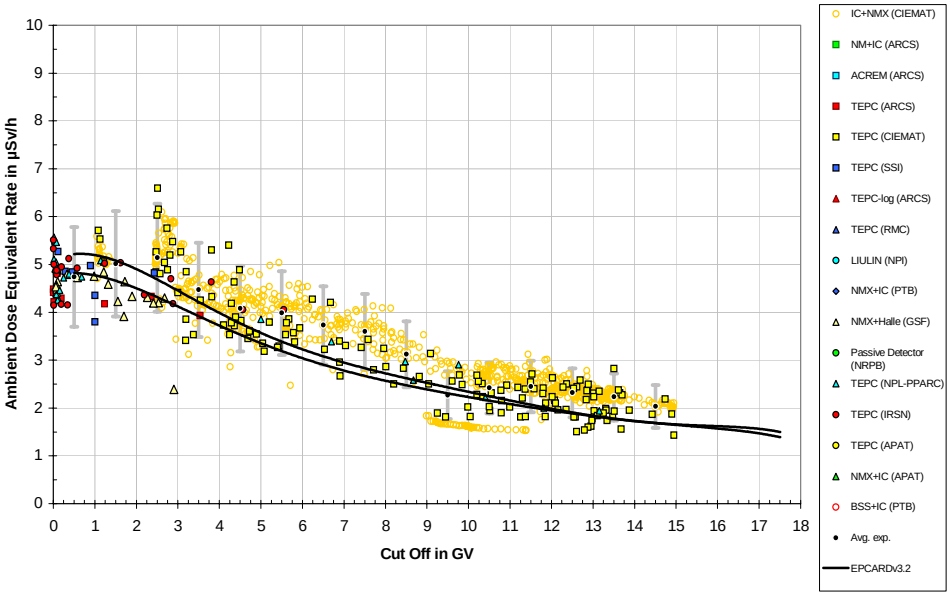

Figure III. 46 Ambient dose equivalent rate dH*(10)/dt vs. vertical cut off rigidity rc between May 1992 and May 2003 for standard barometric altitude 10668 m (FL 350) and for solar deceleration potential in the range of 950 MV - 1140 MV.

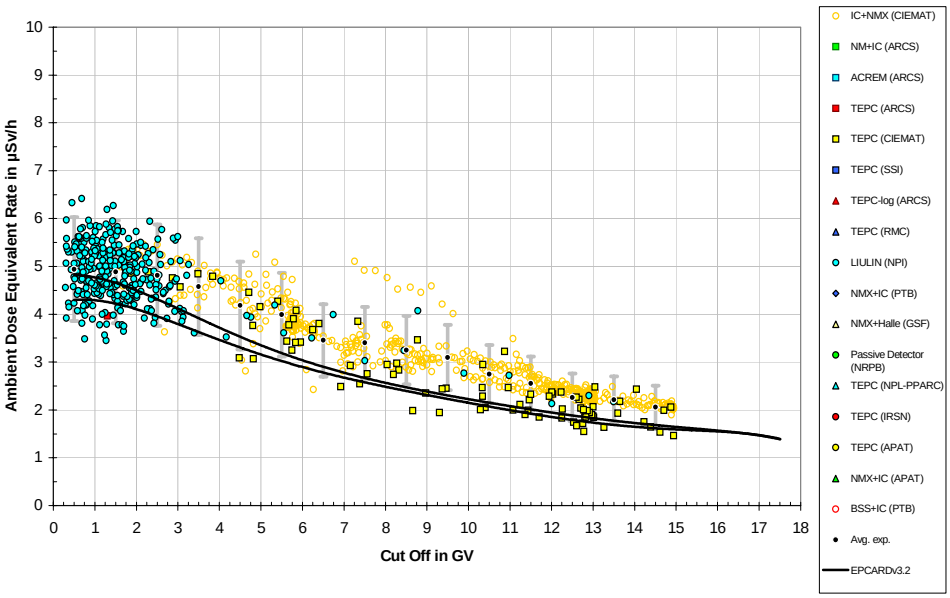

Figure III. 47 Ambient dose equivalent rate dH*(10)/dt vs. vertical cut off rigidity rc between May 1992 and May 2003 for standard barometric altitude 10668 m (FL 350) and for solar deceleration potential in the range of 1140 MV - 1330 MV.

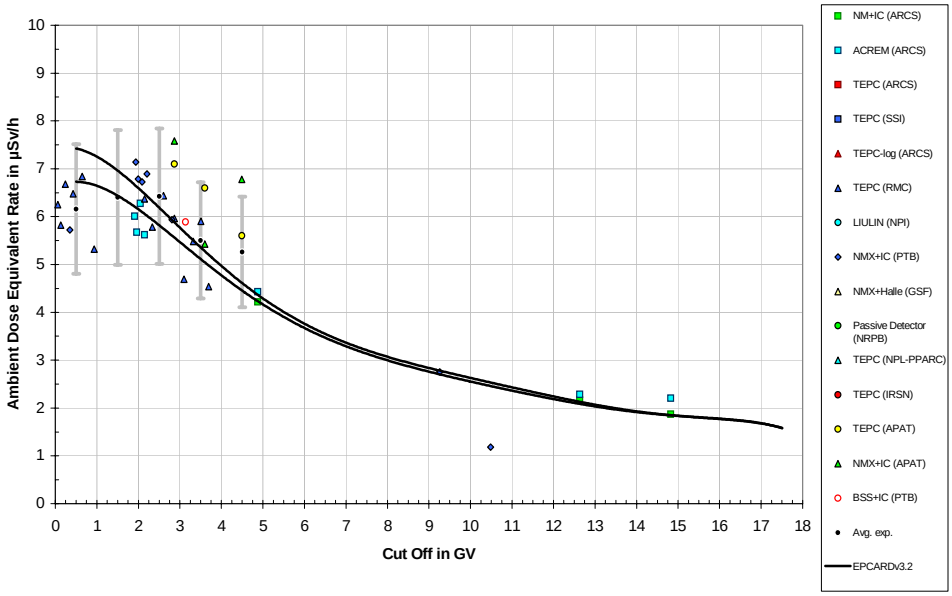

Figure III. 48 Ambient dose equivalent rate dH*(10)/dt vs. vertical cut off rigidity rc between May 1992 and May 2003 for standard barometric altitude 10972 m (FL 360) and for solar deceleration potential in the range of 470 MV - 610 MV.

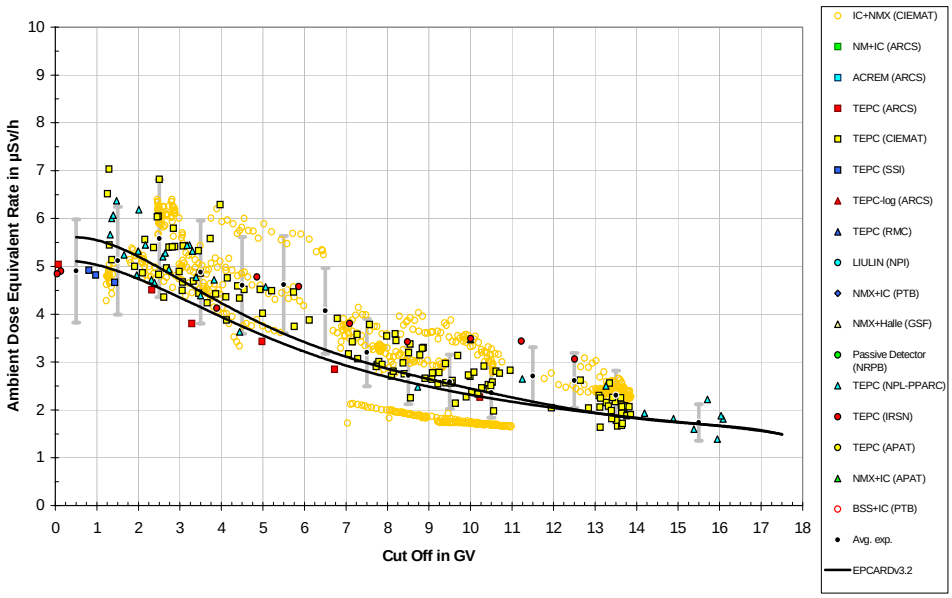

Figure III. 49 Ambient dose equivalent rate dH*(10)/dt vs. vertical cut off rigidity rc between May 1992 and May 2003 for standard barometric altitude 10972 m (FL 360) and for solar deceleration potential in the range of 950 MV - 1140 MV.

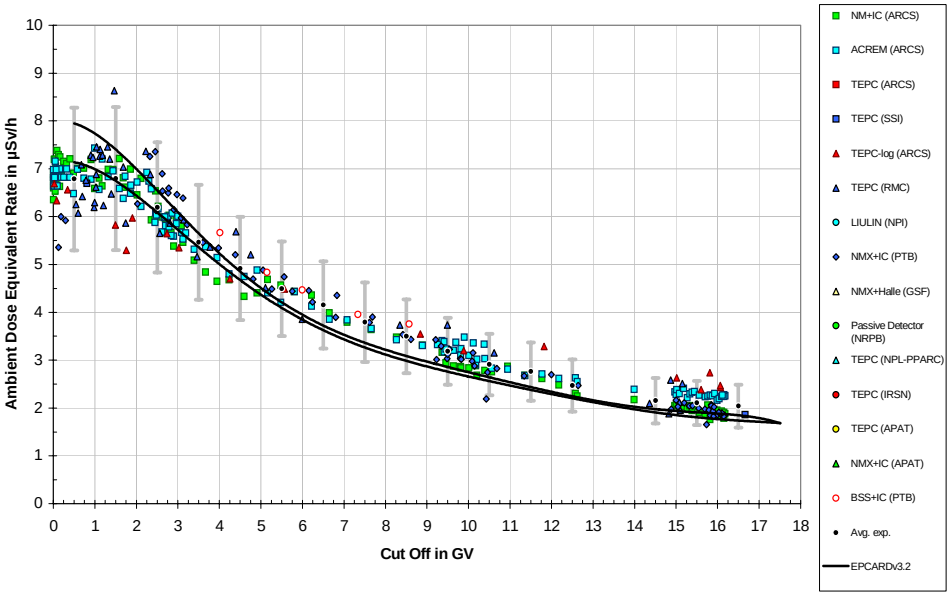

Figure III. 50 Ambient dose equivalent rate dH*(10)/dt vs. vertical cut off rigidity rc between May 1992 and May 2003 for standard barometric altitude 11277 m (FL 370) and for solar deceleration potential in the range of 470 MV - 610 MV.

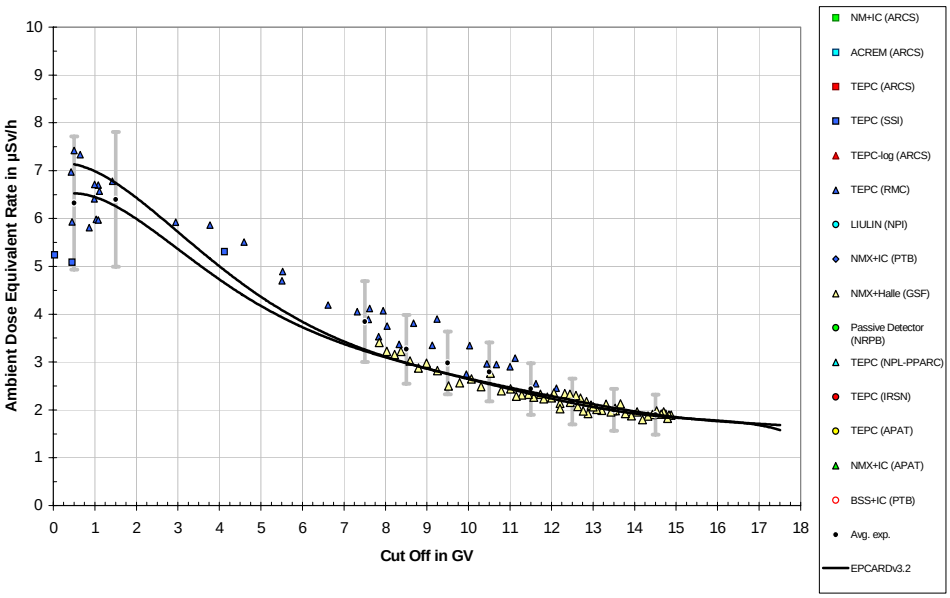

Figure III. 51 Ambient dose equivalent rate dH*(10)/dt vs. vertical cut off rigidity rc between May 1992 and May 2003 for standard barometric altitude 11277 m (FL 370) and for solar deceleration potential in the range of 610 MV - 750 MV.

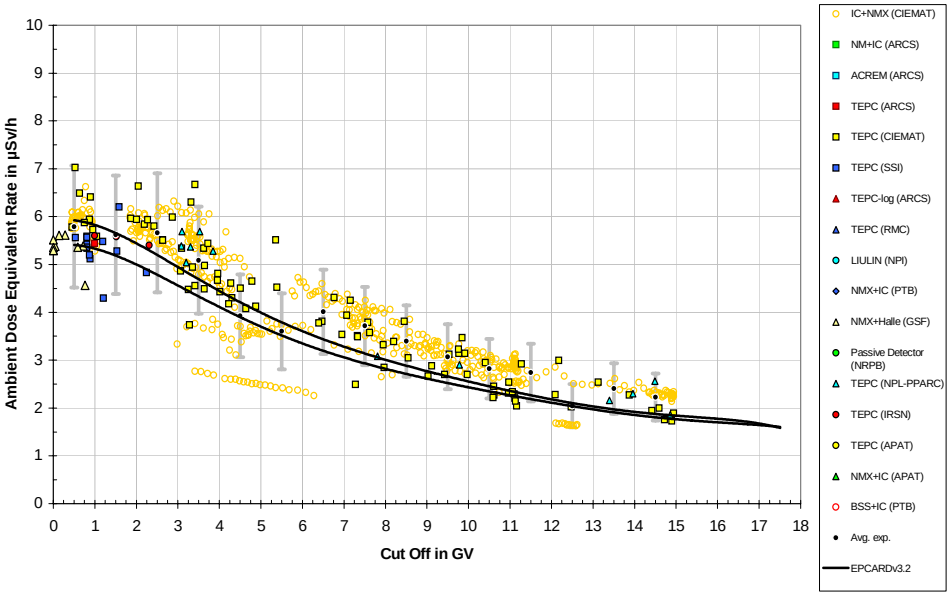

Figure III. 52 Ambient dose equivalent rate dH*(10)/dt vs. vertical cut off rigidity rc between May 1992 and May 2003 for standard barometric altitude 11277 m (FL 370) and for solar deceleration potential in the range of 950 MV - 1140 MV.

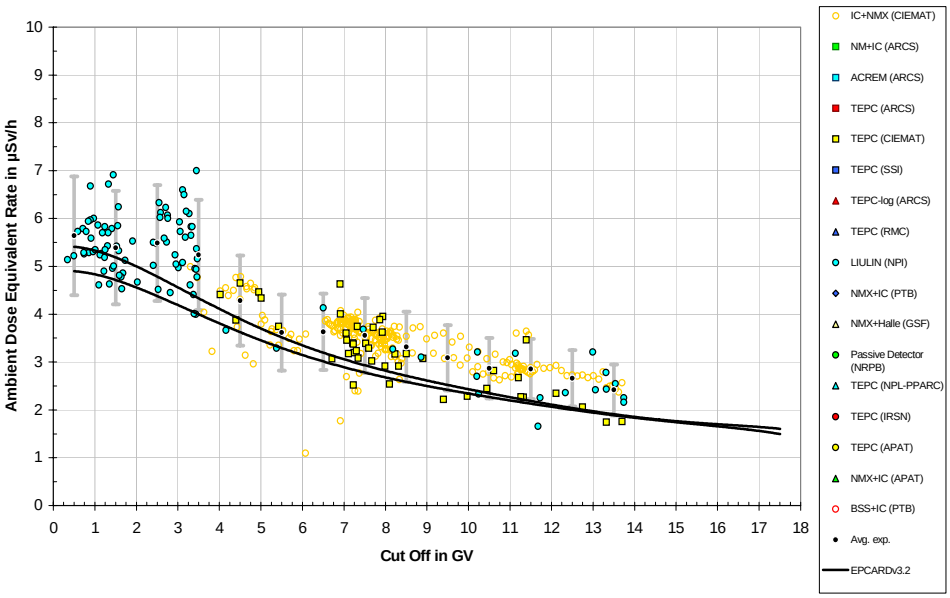

Figure III. 53 Ambient dose equivalent rate dH*(10)/dt vs. vertical cut off rigidity rc between May 1992 and May 2003 for standard barometric altitude 11277 m (FL 370) and for solar deceleration potential in the range of 1140 MV - 1330 MV.

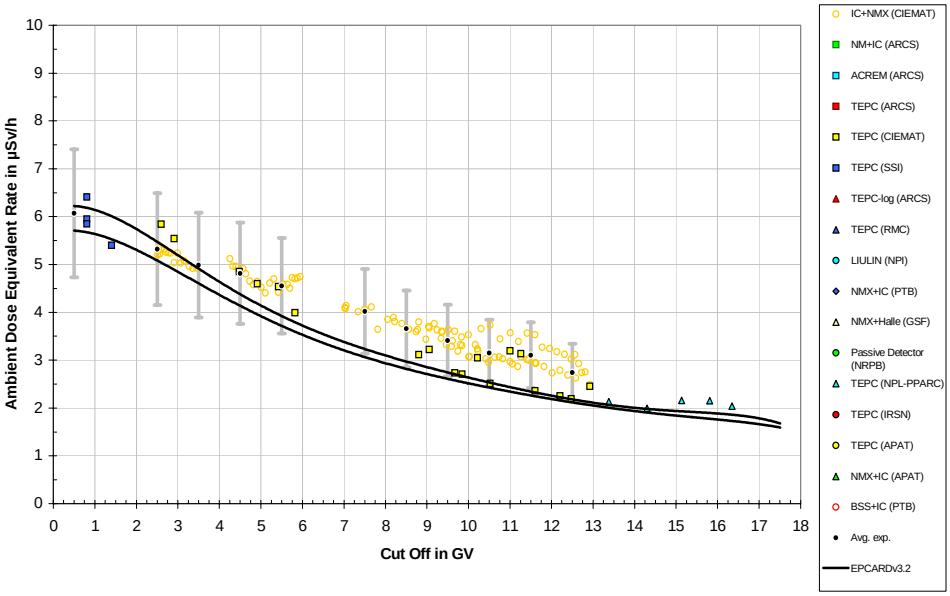

Figure III. 54 Ambient dose equivalent rate dH*(10)/dt vs. vertical cut off rigidity rc between May 1992 and May 2003 for standard barometric altitude 11582 m (FL 380) and for solar deceleration potential in the range of 950 MV - 1140 MV.

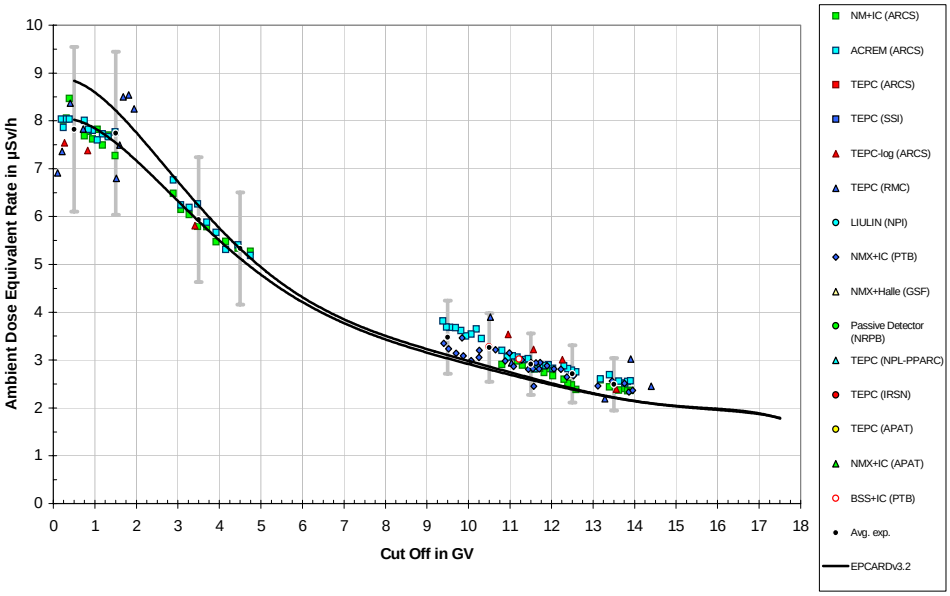

Figure III. 55 Ambient dose equivalent rate dH*(10)/dt vs. vertical cut off rigidity rc between May 1992 and May 2003 for standard barometric altitude 11887 m (FL 390) and for solar deceleration potential in the range of 470 MV - 610 MV.

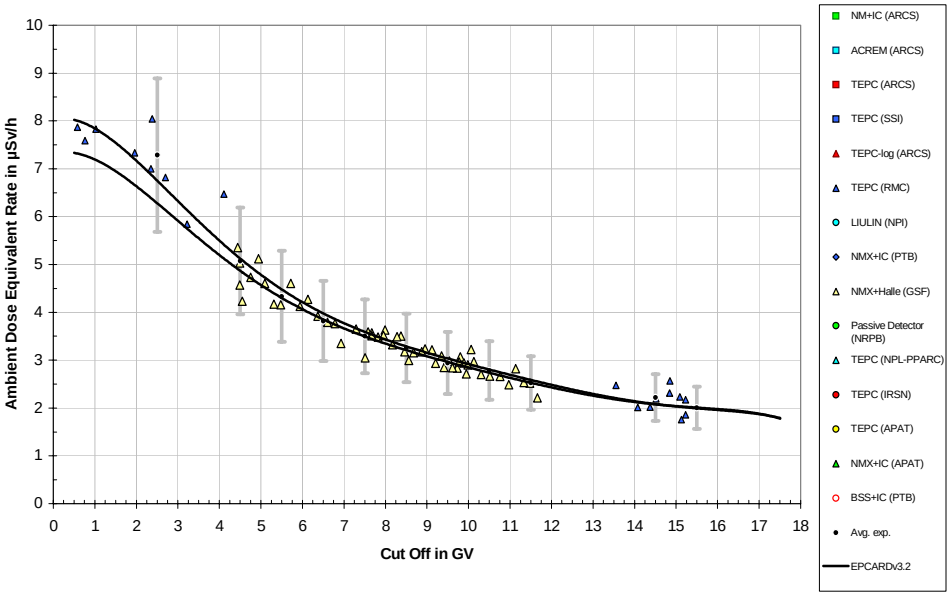

Figure III. 56 Ambient dose equivalent rate dH*(10)/dt vs. vertical cut off rigidity rc between May 1992 and May 2003 for standard barometric altitude 11887 m (FL 390) and for solar deceleration potential in the range of 610 MV - 750 MV.

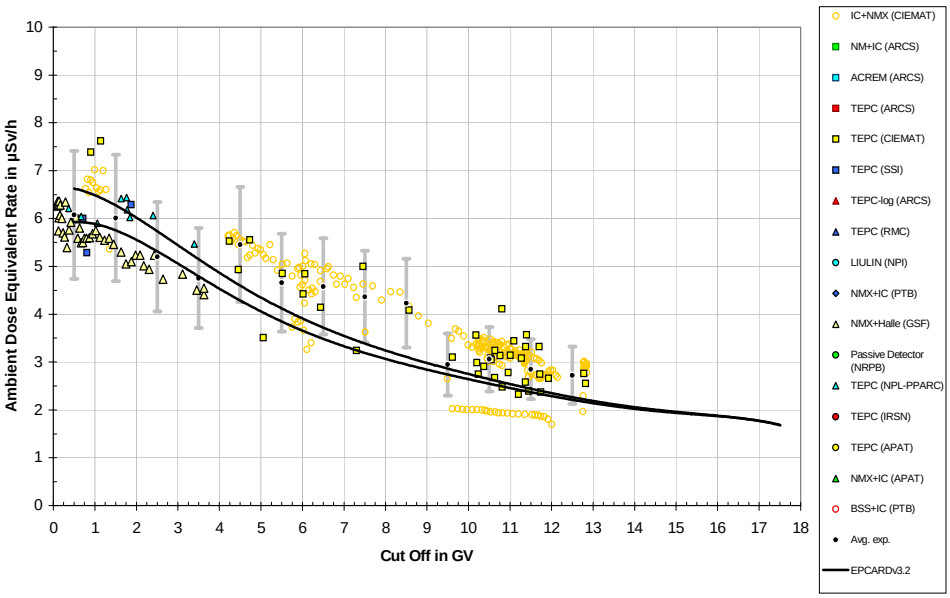

Figure III. 57 Ambient dose equivalent rate dH*(10)/dt vs. vertical cut off rigidity rc between May 1992 and May 2003 for standard barometric altitude 11887 m (FL 390) and for solar deceleration potential in the range of 950 MV - 1140 MV.

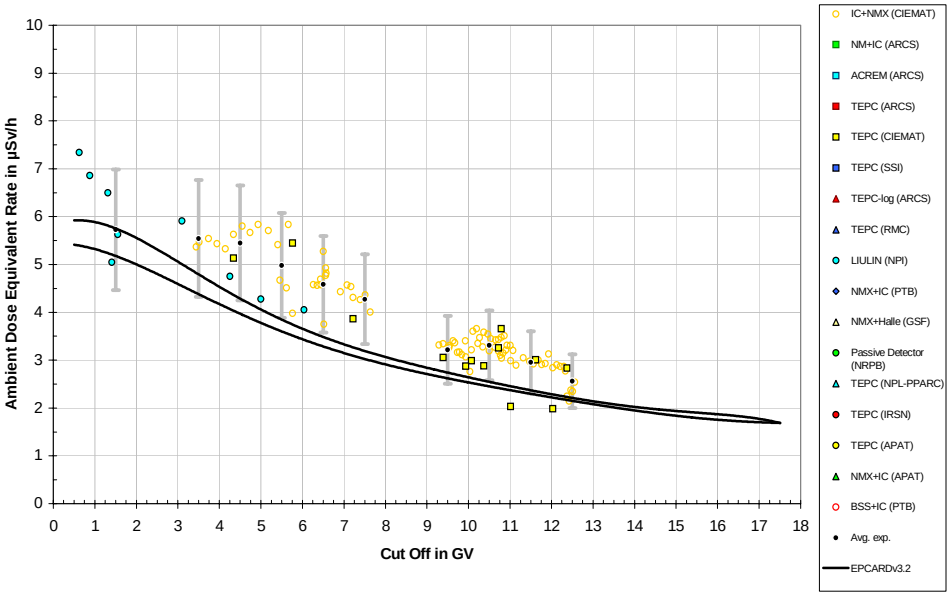

Figure III. 58 Ambient dose equivalent rate dH*(10)/dt vs. vertical cut off rigidity rc between May 1992 and May 2003 for standard barometric altitude 11887 m (FL 390) and for solar deceleration potential in the range of 1140 MV - 1330 MV.

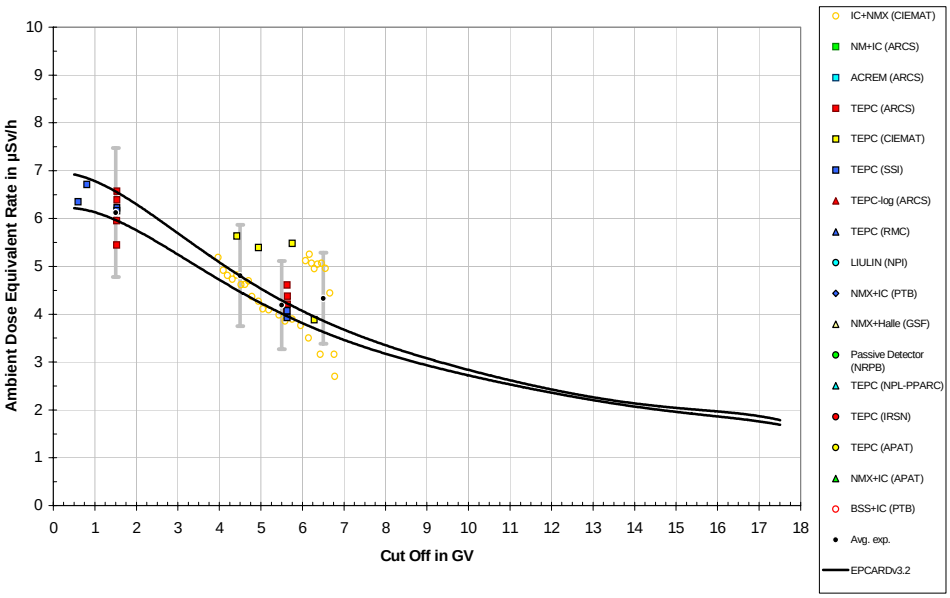

Figure III. 59 Ambient dose equivalent rate dH*(10)/dt vs. vertical cut off rigidity rc between May 1992 and May 2003 for standard barometric altitude 12192 m (FL 400) and for solar deceleration potential in the range of 950 MV - 1140 MV.

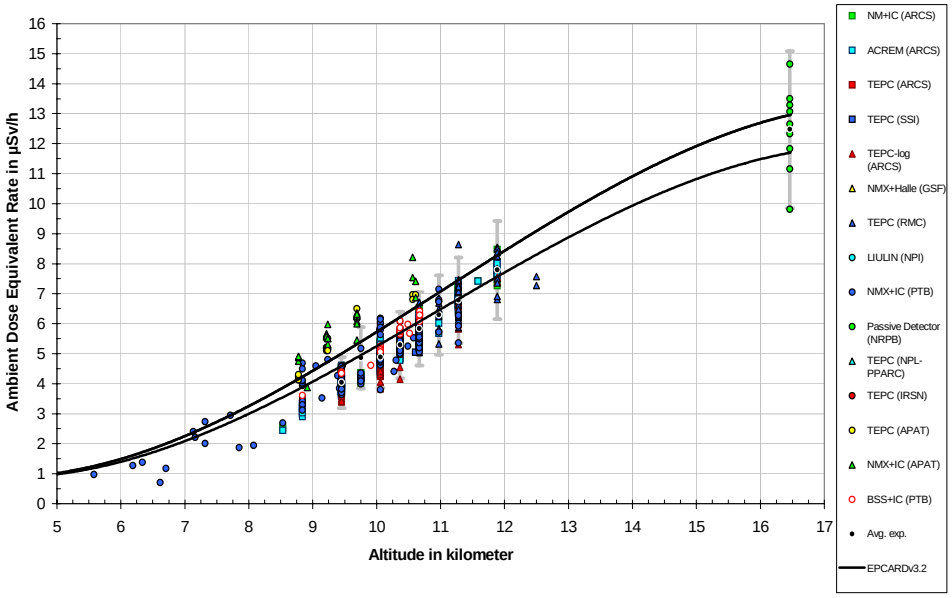

Figure III. 60 Ambient dose equivalent rate dH*(10)/dt vs. standard barometric altitude between May 1992 and May 2003 for vertical cut off rigidity rc ≤2 GV and solar deceleration potential in the range of 470 MV - 610 MV.

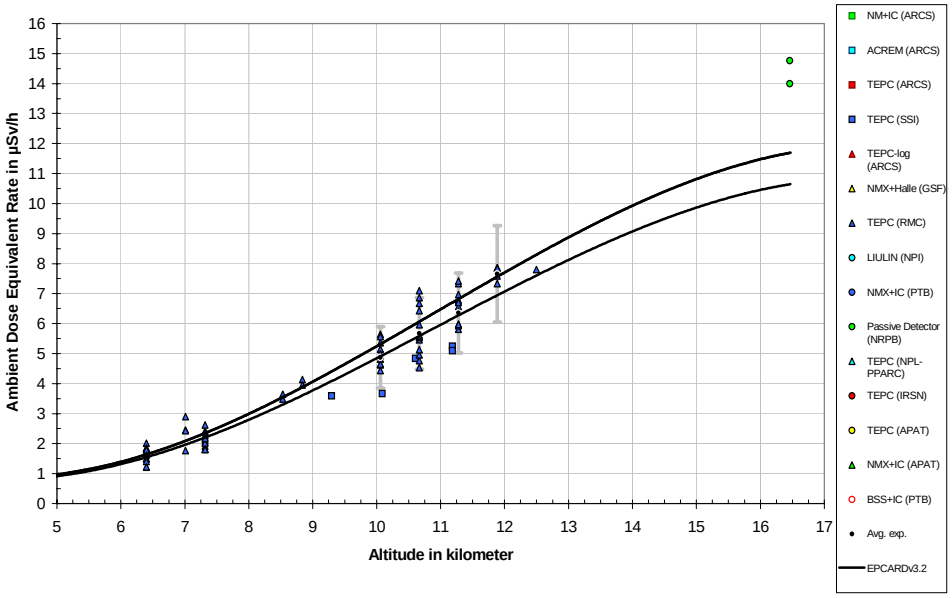

Figure III. 61 Ambient dose equivalent rate dH*(10)/dt vs. standard barometric altitude between May 1992 and May 2003 for vertical cut off rigidity rc ≤2 GV and solar deceleration potential in the range of 610 MV - 750 MV.

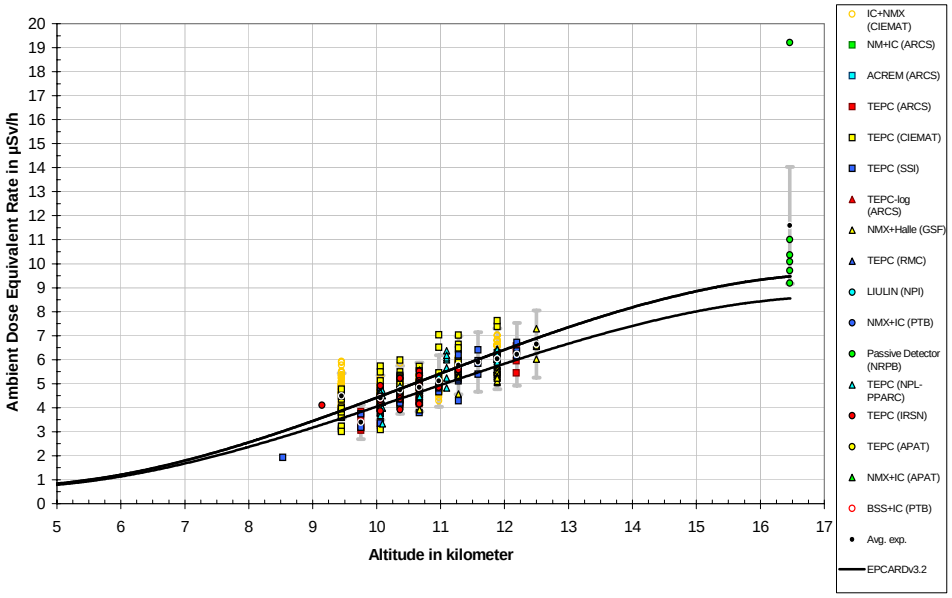

Figure III. 62 Ambient dose equivalent rate dH*(10)/dt vs. standard barometric altitude between May 1992 and May 2003 for vertical cut off rigidity rc ≤2 GV and solar deceleration potential in the range of 950 MV - 1140 MV.

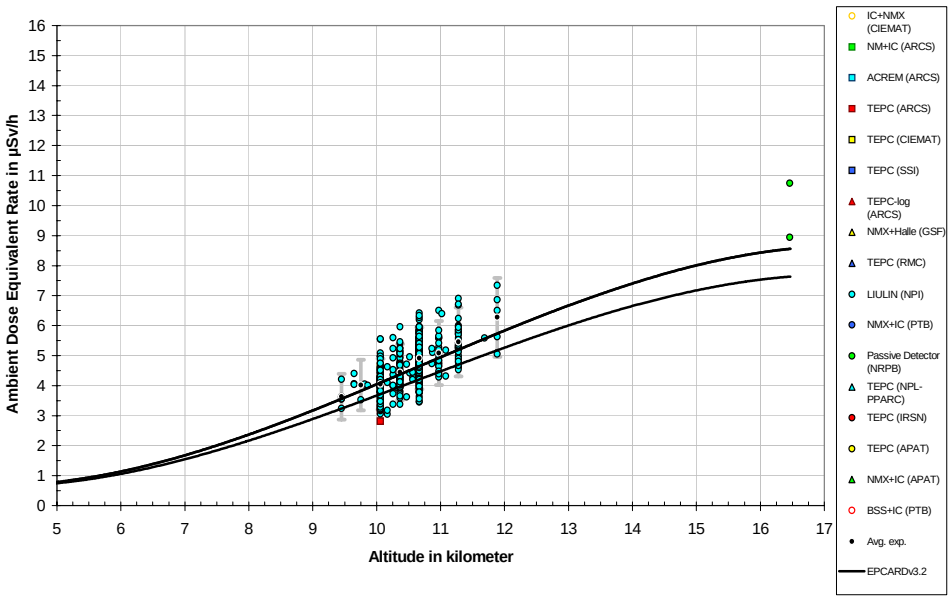

Figure III. 63 Ambient dose equivalent rate dH*(10)/dt vs. standard barometric altitude between May 1992 and May 2003 for vertical cut off rigidity rc ≤2 GV and solar deceleration potential in the range of 1140 MV - 1330 MV.

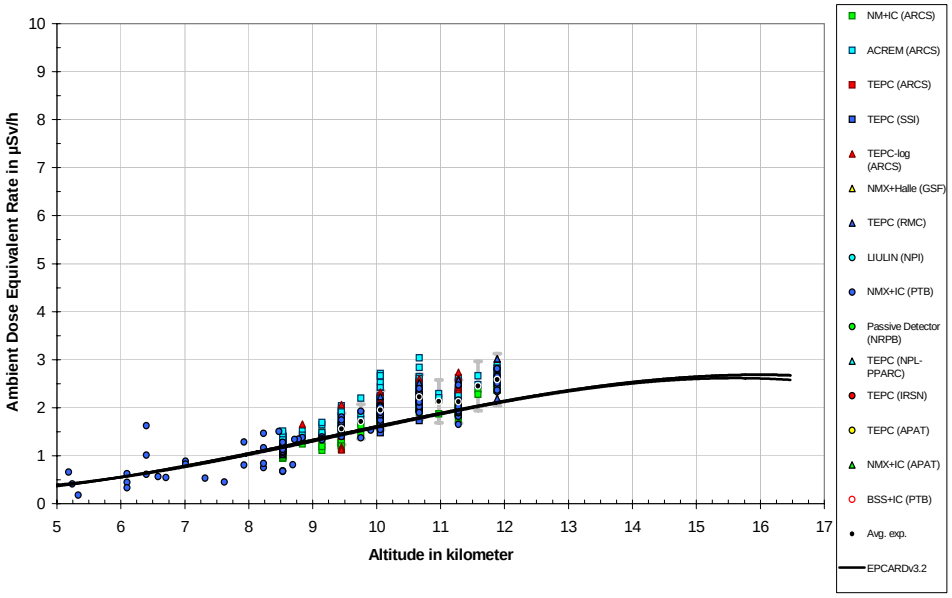

Figure III. 64 Ambient dose equivalent rate dH*(10)/dt vs. standard barometric altitude between May 1992 and May 2003 for vertical cut off rigidity rc ≥12 GV and solar deceleration potential in the range of 470 MV - 610 MV.

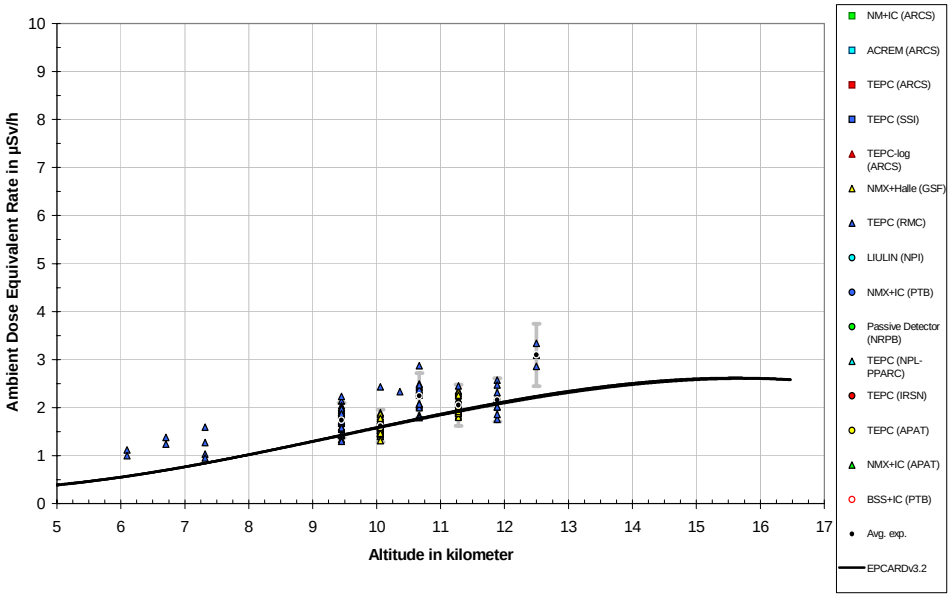

Figure III. 65 Ambient dose equivalent rate dH*(10)/dt vs. standard barometric altitude between May 1992 and May 2003 for vertical cut off rigidity rc ≥12 GV and solar deceleration potential in the range of 610 MV - 750 MV.

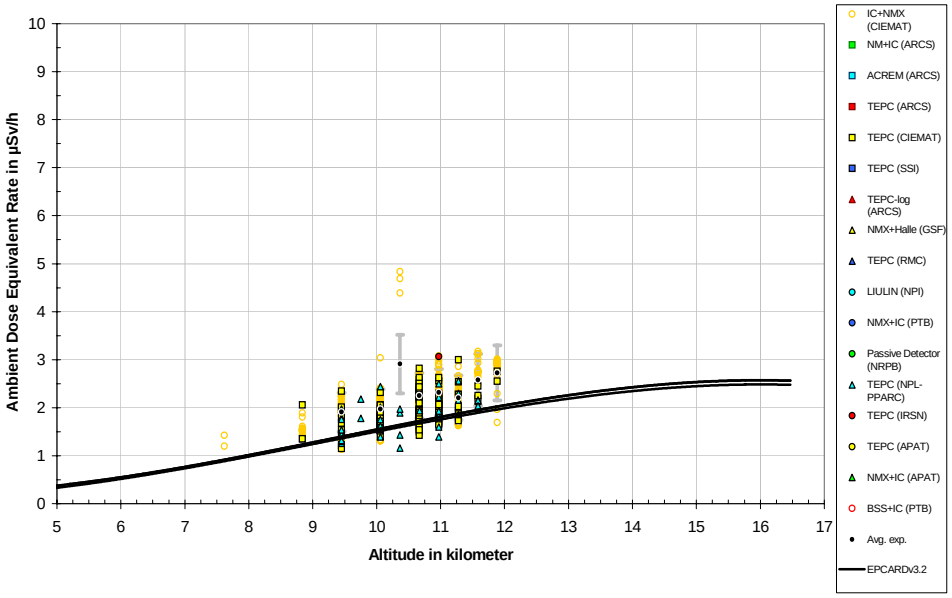

Figure III. 66 Ambient dose equivalent rate dH*(10)/dt vs. standard barometric altitude between May 1992 and May 2003 for vertical cut off rigidity rc ≥12 GV and solar deceleration potential in the range of 950 MV - 1140 MV.

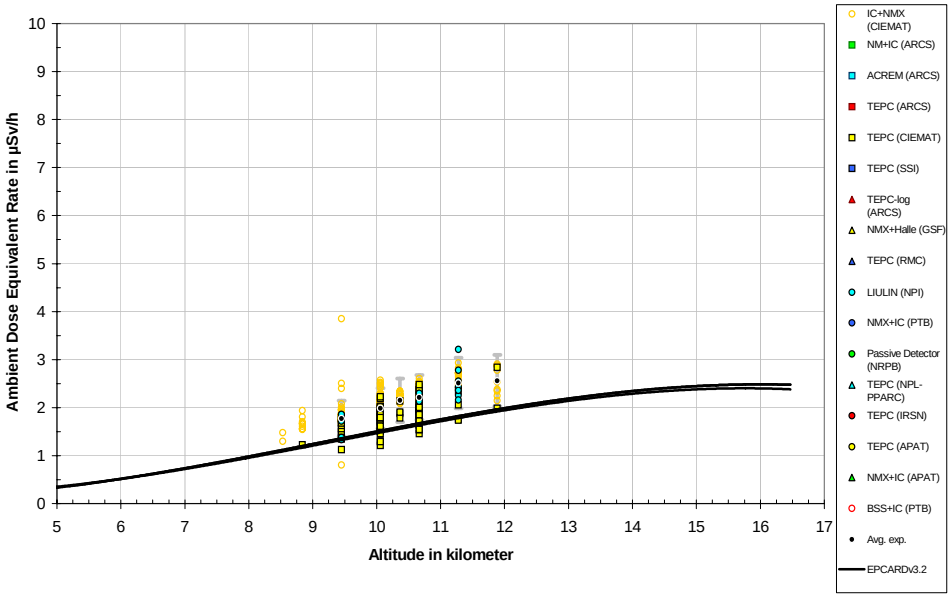

Figure III. 67 Ambient dose equivalent rate dH*(10)/dt vs. standard barometric altitude between May 1992 and May 2003 for vertical cut off rigidity rc ≥12 GV and solar deceleration potential in the range of 1140 MV - 1330 MV.

III.4 Conclusion

The current database includes some 10 500 ambient dose equivalent rate values determined by different active and passive, neutron and non-neutron radiation monitors, and several TEPC instruments. Results of the computer code EPCARDv3.2 were calculated for comparable situations. For each type of instrument, the dose rate was averaged over a time period such that the statistical uncertainty was low enough to allow analysis. This averaging was made before the data were put into the data base by the experimenter. The data cover a wide range of geographic longitudes (180° west to 180° east), latitudes (87° north to 62° south), standard barometric altitudes up to 16 459 m (FL 540) and almost one solar cycle (474 MV ≤ HCP < 1 187 MV, 472 MV ≤ SDP < 1 322 MV). The results present a good overview of the northern hemisphere. Some geographical locations and solar conditions were not covered by the current data. This should be taken into account for future investigations. Mean values of measurement results (Avg.exp) have been calculated for certain values of the parameters (r_c, SBA, SDP) and for defined ranges. The overall measured mean ambient dose equivalent rate was 3.8 $\mu Sv \cdot h^{-1}$; the most frequent measured ambient dose equivalent rate was 2.5 $\mu Sv \cdot h^{-1}$.

Typically a mean uncertainty in the grouped measured results of about 20% (2s) is observed for a specified interval of parameter values, but larger uncertainties of up to 70% (2*s*) are observed. In general a systematic dependency of the uncertainty of the ambient dose equivalent rate is noticed: lower ambient dose equivalent rate measurements show a higher standard deviation. Finally, when comparing the measured values with calculated values (EPCARDv3.2) for similar conditions, two relative standard deviations become 25% (2*s*).

There were insufficient relevant experimental results to be able to determine the influence of solar particle events. It is strongly recommended that solar events are considered in future studies.

III.5 References

[BAR00] Bartlett, D.T., Hager, L.G., Irvine, D. and Bagshaw, M. *Measurements on Concorde of the Cosmic Radiation Field at Aviation Altitudes*. Radiat. Prot. Dosim. **91** 365-376 (2000).

[BAR01] Bartlett, D T, Hager, L G, Tanner, R J, and Steele, J.D. *Measurements of the High Energy Neutron Component of Cosmic Radiation Fields in Aircraft Using Etched Track Dosemeters* Radiat. Meas. **33** (3) 243-253 (2001).

[BAR02] Bartlett, D.T., Tanner, R.J. and Hager, L.G *The High Energy Neutron Response Characteristics of a Passive Survey Instrument for the Determination of Cosmic Radiation Fields in Aircraft*. Radiat Prot. Dosim. **100** 519-524 (2002).

[BAR03] Bartlett, D T, Hager, L G, and Tanner, R J. *The Determination Using Passive Dosemeters for Aircraft Crew Dose: Results for 1997 ER-2 Flights*. IN Atmospheric Ionizing Radiation (AIR): Analysis, Results and Lessons Learned from the June 1997 ER-2 Campaign, Eds. Wilson, J.W., Jones, I.W., Maiden, D L. and Goldhagen, P. 321-332, (NASA: Langley, VA, USA) (February 2003).

[BAR04] See Bartlett, D.T., Hager, L.G and Tanner, R.J., this report Appendix.

[BEC99a] Beck, P., Ambrosi, P., Schrewe, U., O'Brien, K., *ACREM, Aircrew Radiation Exposure Monitoring*, OEFZS Report OEFZS-G-0008, November (1999)

[BEC99b] Beck, P., Bartlett D., O'Brien, K., Schrewe U.J., *In-Flight investigation and Routine Measurements*, Radiat. Prot. Dosim. **86** 303-308 (1999).

[BEC03] Beck, P., *DOSMAX, Dosimetry of Aircrew Exposure to Radiation During Solar Maximum*: Annex 2 of the Annual Progress Report, European Commission Contract No: FIGM-CT2000-00068, 2003.

[BEC04] See Beck, P., Rollet S., Stehno G., this report Appendix A 10.

[BOT04] Bottollier-Depois J.F., Trompier, F., Clairand, I., Spurny, F., Bartlett, D., Beck, P., Lewis, B. Lindborg, L., O'Sullivan, D., Roos, H., and Tommasino, L., *Exposure of Aircraft to Cosmic Radiation: On-board Intercomparison of Various Detectors*, Rad. Prot. Dos., 2004 (in press).

[CUR01a] Curzio, W.G., Grillmaier E., O'Sullivan D., Pelliccioni M., Piermattei S. and Tommasino L. *The Italian National Survey of Aircrew Exposure: I Characterization of Advanced Instrumentation*. Radiation Protection Dosimetry, **93** 115-123 (2001),

[CUR01b] Curzio G., Grillmaier E., O'Sullivan D., Pelliccioni M., Piermattei S., and Tommasino L. *The Italian National Survey of Aircrew Exposure: II On-board Measurements and Results.Radiation Protection and Dosimetry*. **93** 125-133 (2001).

[GRE00] Green, A.R., McCall, M.J., Lewis, B.J. and Bennett, L.G.I. *Cosmic Radiation Exposure of Aircrew* Transport Canada Report RMC-CCE-NSE-00-02, **1 - 2**, March 2000**.**

[KYL01] Kyllönen, J.-E., Lindborg, L., and Samuelsson, G. *Cosmic Radiation Measurements On-board Aircraft with the Variance Method*. Radiat. Prot. Dosim. **93** 197-205 (2001).

[LEW01] Lewis, B.J., McCall, M.J. Green, A.R., Bennett, L.G.I., Pierre, M., Schrewe, U.J., O'Brien, K. and Felsberger, E. *Aircrew Exposure from Cosmic Radiation on Commercial Airline Routes* Radiat. Prot. Dosim. **93** 293-314 (2001).

[OBR71] O'Brien, K., *Cosmic-ray propagation in the atmosphere*, Nuovo Cimento **A 3**, 52-78, (1971).

[OSU99] O'Sullivan, D, Tommasino, L., Schraube, H., Grillmaier, R., Bartlett, D.T., Lindborg, L., Heinrich, W and Silari, M. *Investigations of Radiation Fields at Aircraft Altitudes*, Final Report of European Commission contract no. F14P-CT950011 (Dublin Institute for Advanced Studies: Dublin) (1999).

[OSU99a] O'Sullivan, D., Zhou, D., Heinrich, W., Roesler, S., Donnelly, J., Flood, E. and Tommasino, L. *Cosmic Rays and Dosimetry at Aviation Altitudes*, Radiat. Meas. **31** 579-584. (1999).

[REG93] Regulla, D. and David, J., *Measurements of cosmic radiation on board Lufthansa aircraft on the major intercontinental flight routes*. Radiat. Prot. Dosim. **48**(1) 65-72 (1993).

[REG96] Regulla, D. and Schraube, H., *Radiation exposure of aircrews in civil aviation*. In: Strahlenbiologie und Strahlenschutz. 28.Jahrestagung des Fachverbands für Strahlenschutz e.V., Hannover, 23.-25.10.1996 (Hrsg.: G. Heinemann, H. Pfob). Köln: Verlag TÜV Rheinland, .375-380 (1996).

[ROM04] Romero, A.M., Saez-Vergara, J.C., Rodriguez, R. and Domínguez-Mompell, R. *Study of the Ratio of Ionising to Neutron Dose Components of Cosmic Radiation at Typical Commercial Flight Altitudes* Accepted for publication in Radiat.Prot.Dosim. (2004).

[SAE02] Saez Vergara, J.C., Romero, A.M., Rodriguez, R., Muñiz J.L., Dominguez-Mompell, R. Merelo, F., Ortiz, P., Ruano. J. *Monitoring of the Cosmic Radiation at IBERIA Commercial Flights: One Year Experience of In-flight Measurements.* Proceedings of the Radiation Protection and Shielding Division Topical Meeting, Santa Fe, 2002. ISBN: 0-89448-667-5, CD ROM (2002).

[SAE04a] See Saez Vergara J.C., Dominguez-Mompell Román R., this report Appendix A 7.

[SAE04b] Saez Vergara, J.C., Romero, A.M., Rodriguez, R. and Dominguez-Mompell,R. *In-flight Measured and Predicted Ambient Dose Equivalent and Latitude Differences on Effective Dose Estimates***.** Accepted for publication in Radiat.Prot.Dosim. (2004).

[SAE02b] Saez Vargara, J.C, Romero, A.M., Rodrigues, R., Muniz, J.L., Domingues-Mompell, Merelo, R.F., Ortiz, P., *Medida de la radiacion cosmica en los vuelos de IBERIA L.A.E (I): Instrumentacion, Metodologia y Calibracion. (II): Analisis de los resultaados obtenidos en las medidas experimentales en vuelo. (III): Estimacion inicial de la dosisefectiva anual recibida por las tripulaciones*. Radioproteccion. Numero

Extraordinario IX Congreso Nacional de la Sociedad Esponla de Proteccion radiologia (2002).

[SHE01] Shea M.A., Smart D.F, *Vertical Cutoff Rigidities for Cosmic Ray Stations Since 1955*, 27th International Cosmic Ray Conference, Contributed Papers, 10, 4063-4066, (2001).

[SHE68] Shea M.A., Smart D.F, McCall, J.R., *A Five Degree by Fifteen Degree World Grid of Trajectory-Determined Vertical Cutoff Rigidities*, Can.J.Phys., **46** S1098-S1101, (1968).

[SPU03] Spurný, F. and Datchev, Ts. *Long-term Monitoring of Onboard Aircraft Exposure with Si-diode based Spectrometer*. 34th COSPAR Scientific Assembly, Houston, October 10-19, 2002, Adv. Space Research **32** N01, 53-58, (2003).

[SRA02] Schraube, H., Leuthold, G., Heinrich, W., Roesler, S., Mares, V. and Schraube, G., *EPCARD - European Program Package for the calculation of aviation route doses - User's Manual*. GSF - National Research Center on Environment and Health, GSF-Bericht 08/02 ISSN 0721 - 1694 (2002).

[SRE99a] Schrewe, U.J., *ACREM Air Crew Radiation Exposure Monitoring Results from the in-flight measurement program of the PTB: Summary of the Radiation Monitoring Data*. PTB Laboratorbericht PTB-6.31-99-1, Braunschweig, (1999).

[SRE99b] Schrewe, U. J., *Global Measurements of the Radiation Exposure of Civil Air Crew from 1997 to 1999.* Rad. Prot. Dosim. **91** 347-364 (2000)

[STR97] Strahlenschutzkommission: *Die Ermittlung der durch kosmische Strahlung verursachten Strahlenbelastung des fliegenden Personals*. Report. Stellungnahme der Deutschen Strahlenschutzkommission (1997).

[TAY02] Taylor, G.C., Bentley, R.D., Conroy, T.J., Hunter, R., Jones, J.B.L., Pond, A. and Thomas, D.J., *The Evaluation and Use of a Portable TEPC System for Measuring In-Flight Exposure to Cosmic Radiation*, Rad. Prot. Dosim. **99**(1-4) 435-438 (2002).

[TOM96] Tommasino L., Caggiati F., Cavaioli M., Notaro M., Teodori R., and Zhou D., *Passive Multidetector Stack for the Assessment of Aircrew Exposure*. Environment International **22** S: 115-119 (1996)

[TOM99] Tommasino, L., *In-flight measurements of radiation fields and doses*. Radiat. Prot. Dosim., **86** 297-301 (1999).

[WIE02] Wiegel B., Alevra A.V., Matzke M., Schrewe U.J. and Wittstock J., *Spectrometry with the PTB Neutron Multisphere Spectrometer (NEMUS) at Flight Altitudes and at Ground Level*, Nucl. Instrum. Meth. A476, 52-57 (2002).

IV Comparison of calculated and measured route doses and selected dose rate data for scheduled flights

IV.1 Introduction

This chapter is devoted to a phenomenological, comparative study of calculated radiation doses obtained along civil flight routes. Furthermore, a comparison with experimental data is included for a number of flights, for which data are available either from integrating (passive or active) devices or dose rate measuring instruments after integration over the time differential data (see Chapter III).

Four computer codes were used in this study: CARI, EPCARD, FREE and PCAIRE. The most recent version CARI-6 (July 2001) [CJG04] (see Appendix B.4) is employed and the respective actual data for the heliocentric potential provided by CAMI [CJG04]. The version EPCARDv3.2 [SLH02] (see Annex B.2) is employed, whose data set will be valid for the rest of solar cycle 23 until solar minimum conditions (approximately 2007) and further until the next solar reversal (approximately 2009). Actual data of the Climax monitor are used by the program to derive the solar deceleration potential. Both programs have been available to the scientific public, and hence any interested scientist may reproduce the results. For the two other computer codes, PCAIREv6.5 (see Appendix B.3) and FREEv1.0 (see Apendix B.5), data were provided by the authors of the codes. None of the computer codes takes account of an influence from the aircraft itself on the air crew dose.

As described in Appendix B.4, the code CARI takes data of the LUIN-code that is based on a general analytical solution of the transport equation of the cosmic radiation field. The code EPCARD is based on FLUKA MC-calculations of the radiation field under all solar and geomagnetic conditions. The code FREEv1.0 was originally based on data of the transport code LUIN, and the calculations within this chapter were conducted herewith. In meantime, an improved code, PLOTINUS (see Appendix B.5), became available as data base of FREE, which takes into account short-term variations of the solar modulation, too. PCAIRE uses a hybrid method with analytical fits to $H^*(10)$ experimental data and uses a scaling ratio to convert to effective dose results based on LUIN and on FLUKA calculations.

The data presented comprise dose values in terms both of effective dose and ambient dose equivalent, and the contributions of the various cosmic ray components calculated with EPCARD. From CARI the results of effective dose are reported. The results of PCAIRE and FREE were reported in terms of ambient dose equivalent. Flight schemes were taken for flights conducted by members of the EURADOS working group WG5 on “Air crew dosimetry”, by a Spanish co-operative group (J.C.Vergara et al., CIEMAT/IBERIA), by the U.K. National Physical Laboratory (NPL), and for a selection of worldwide public destinations in order to receive a fairly systematic survey.

The aim of this chapter was initially to show a phenomenological picture of the dose results from the various calculation approaches obtained for an appropriate selection of flight routes. Experimental data were then added. It should be emphasised that not all experimental data were well suited for this purpose. A number of flights was dedicated to measure time differential dose rates (see Chapter III) rather than to determine integrated doses. For these flights, part of the experiments only started when stable flight conditions were reached, or, in some case, the measurements were interrupted due to operational necessities.

Additionally, a selection of experimental data is used for comparison with and verification of calculated dose rates.

IV.2 Basic conditions

Two data sets were employed to study the behaviour of the codes under different flight conditions:

1. a number of flights conducted by the various laboratories for experimental studies and
2. an arbitrary number of flights obtained from official flight schedules between two airports and worldwide destinations.

Both data sets cover a half period (i.e. 11 years) of solar modulation (solar cycle no. 22 to no. 23) including two maxima and a minimum of solar activity. As the solar maximum, occurring during the end of 1989 and begin of 1990, was the most intensive one since the 1956, it is assumed that the data set includes the extreme values of solar modulation, at least for the time being.

The comparison of calculated data extend in first instance to the "total effective dose, E", obtained by the codes as a measure for radiation risk and as required by the European Directive. Furthermore, the operational quantity, $H^*(10)$, will be reported and the contributions of the various particles to both quantities.

IV.3 In-flight measurement results and comparison with calculations

The experimental data have partly been published elsewhere, partly they are intentionally published the first time in this report for the purpose of broaden the experimental basis of the study. The respective method of experimental techniques is described in Appendix A, the methods of calculating cosmic radiation fields and route doses described in Appendix B.

In the figures IV.2 through IV.15, the dose data are presented for each flight on the basis of the specific flight data reported. The dose data comprise effective dose, E, calculated with CARI and EPCARD, and ambient dose equivalent, $H^*(10)$, both experimentally determined, and calculated with EPCARD, FREE and PCAIRE, as far as available. Each figure consists of at least two parts: i) effective dose and ambient dose equivalent calculated by the respective program, the experimental findings, and the ratio of effective dose values obtained from EPCARD and CARI; ii) the ratio of calculated to experimental ambient dose eqivalent values.

General observations. Although the figures should be self-explanatory, a few general observations may be stated:

- When comparing the two codes, CARI and EPCARD, which delivered explicitely values for the quantity effective dose, it is seen that the results of EPCARD are up to 30% higher than those of CARI for northern routes, for very high flight levels (Concorde-flights) even up to 50% (see also clause IV.5 and 6). For southern routes the ratios invert, and the EPCARD results may be lower by up to around 20%.
- The calculations of EPCARD indicate that the effective dose, E, is generally higher than the ambient dose equivalent, $H^*(10)$, by up to approximately 30%. This is essentially due to the weighting factor 5 for protons, used for calculating the effective dose, as required by the Council Directive 96/29/EURATOM.
- The data of total ambient dose equivalent, $H^*(10)$, as obtained by the three codes EPCARD, FREE and PCAIRE, generally, with a few exceptions, do not deviate by more than 20% from each other.
- While presenting the experimental data, it is assumed that the experimental devices employed, indicate the operational quantity, $H^*(10)$. This may be have been achieved by calibration of the respective device under laboratory standard conditions. Subsequent application of correction factors may allow for deviations from the standard condition, e.g. due to different particle energy

spectra, or particle contributions not present in the calibration situation. Alternatively, estimated deviations may be taken into account, when the overall uncertainty is considered (see Chapter V and Annex A). No further corrections were applied in the present analysis.

- The agreement between the reported experimental data, H^*_{exp}, of the total route doses and doses $H^*(10)$ obtained with EPCARD, FREE and PCAIRE, was generally within ±30%, for both active and passive devices.

Table IV.1 List of data sets available for the calculation of integral aviation doses during experimental flights

Institution	Author(s) or primary investigator	Number of measure-ments	Period of time	Measured integral data (method)	For details see figure
IRSN	Bottollier	8	1996-1998	TEPC	IV.2
SSI	Kyllönen/Lindborg	20	1998-2003	TEPC	IV.3, 4
NRPB	Bartlett/Hager	18	1997-2002	Track detectors and TLDs	IV.5
DIAS	O'Sullivan/Zhou	18	1993-2002	Track detectors	IV.6
ANPA	Tommasino	24	1997-2002	LINUS, IC, TEPC, ANPA-stack	IV.7
GSF	Schraube/Regulla	21	1990-1993	NM, NMX, Sci, IC	IV.8
Uni Kiel	Reitz/Beaujean	27	1996-2003	DOSTEL	IV.9
CAS	Spurny	86	1991-1999	TEPC+multidetector	IV.10.a, b
PTB (ACREM)	Schrewe	39	1997-1999	NM, NMX, Sci, IC	IV.11.a, b
ARCS (ACREM)	Beck	39	1997-1999	TEPC, IC, NM, GM	IV.12.a, b
RMC	Lewis	65	1999	TEPC	IV.13.a, b, c
IBERIA	Saez-Vergara	69	2001	TEPC, SWENDI, IC, etc.	IV.14.a, b
NPL	Taylor	46	2000	TEPC	IV.15.a, b

LINUS, NM, NMX, SWENDI = neutron moderator detectors
TEPC = tissue equivalent proportional counters
IC = high pressure ionisation chambers
Sci = Scintillation dose rate meter

Specific observations. The tissue equivalent proportional counter (TEPC) was the experimental device favoured by eight groups (see Table IV.1), who employed it either as the only instrumentation or in combination with other devices. One of the problems is its relatively low sensitivity, which results in higher statistical uncertainties than observed with other devices. Furthermore, events from low-LET particles are much more frequent than high LET-particles, but contribute less to the total dose equivalent. Thus, the uncertainty analysis is more complicated.

In order to find some information on the total statistical weight of the data, the following evaluation was done: The data of RMC obtained with TEPC were used, as the experimental data were reported for both short and long haul flights in a range of dose equivalent between 1 and 60 μSv. (It should be recalled that the daily natural radiation background is around 2 μSv at ground level).

Figure IV.13c. depicts that the scatter of the ratio of calculated data to the experimental ones decreases with increasing dose. This is true for all calculated data. It suggests that a minimum of 20 μSv is required to keep the uncertainties well below ±30%. The uncertainties are due to the stochastic nature of the measurements and due to the fact that for short distance flights the uncertainties in defining the

flight profile may increase.

In Figure IV.1 the same data are plotted versus $H^*(10)$: The data calculated with EPCARD, FREE and PCAIRE are again normalised to the experimental findings. It should be emphasised that the PCAIRE results are not independent from the RMC measurements, as the experimental data are part of PCAIRE. Nevertheless, they are well suited to demonstrate the importance of the statistical uncertainties at low integral doses. This figure may give some indication for requirements of experimental verification of calculated dose data. However, the determination of the "true" value remains an important problem. The shape of the data in Figure IV.1 exhibits some similarities with the trumpet curve for defining acceptance limits for the test of individual dosemeters in accordance ISO standard 14146 [ISO00].

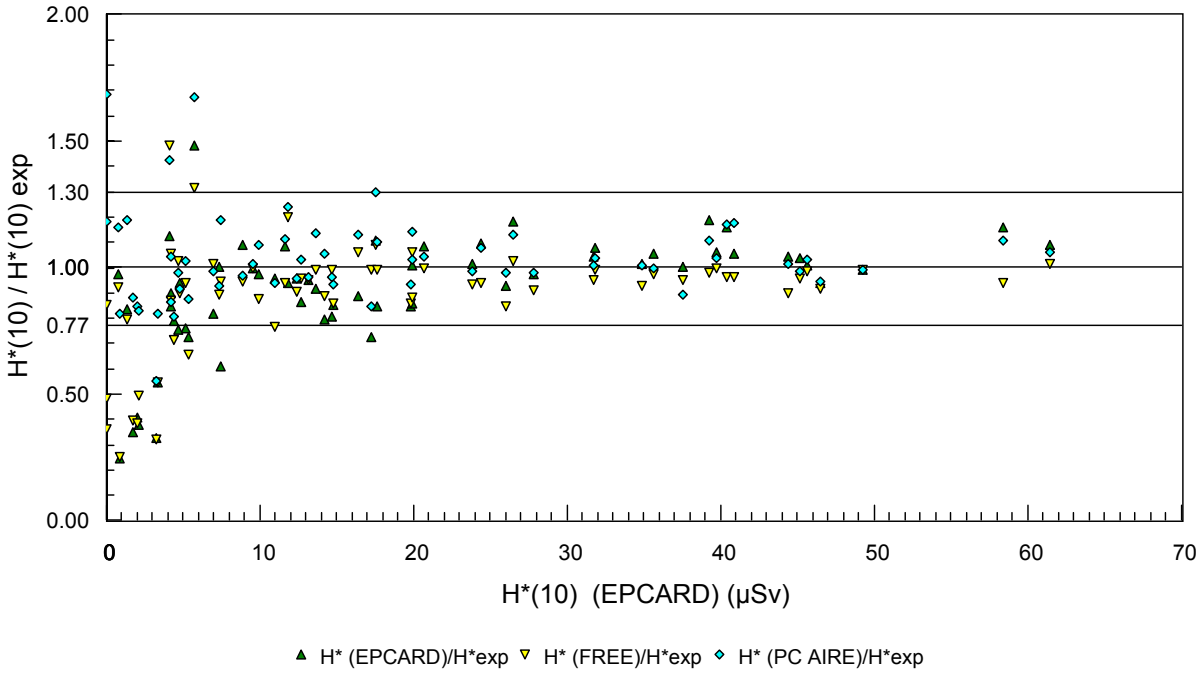

Figure IV.1 Ratio of calculated route doses to experimental data of RMC, when using EPCARD, FREE and PCAIRE.

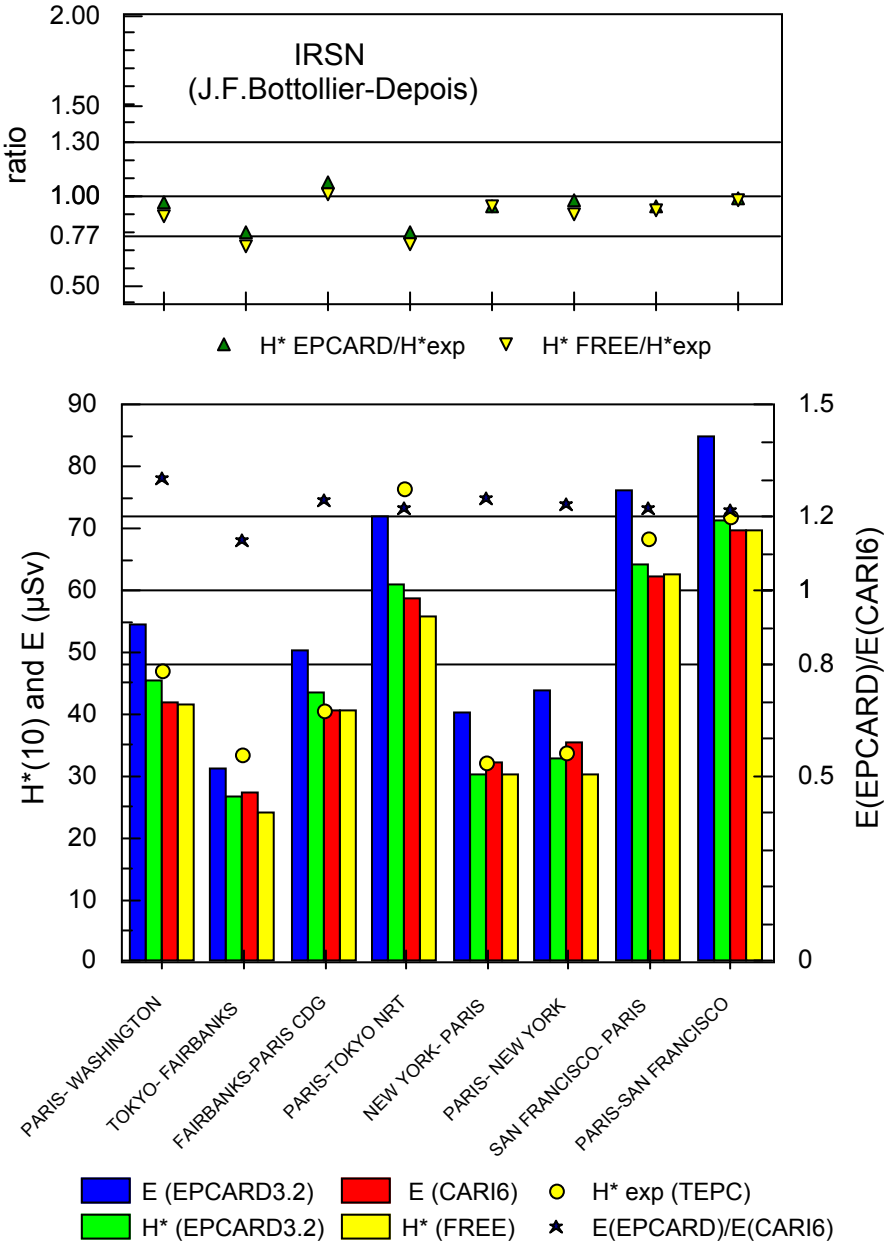

Figure IV.2 Calculated doses for flights of IRSN (1996-1998), and experimental data obtained with TEPC. The ratio of effective doses obtained with EPCARD and CARI6, respectively, is depicted together with a ± 20% band (right scale). Top of figure: Ratio of calculated operational quantity, H*(10), and experimental data. An uncertainty band of ±30% (i.e. factor 1.3) is included.

NOTE: If the figures are printed in b/w, it should be noted that the legends to the data presented are to be read column by column.

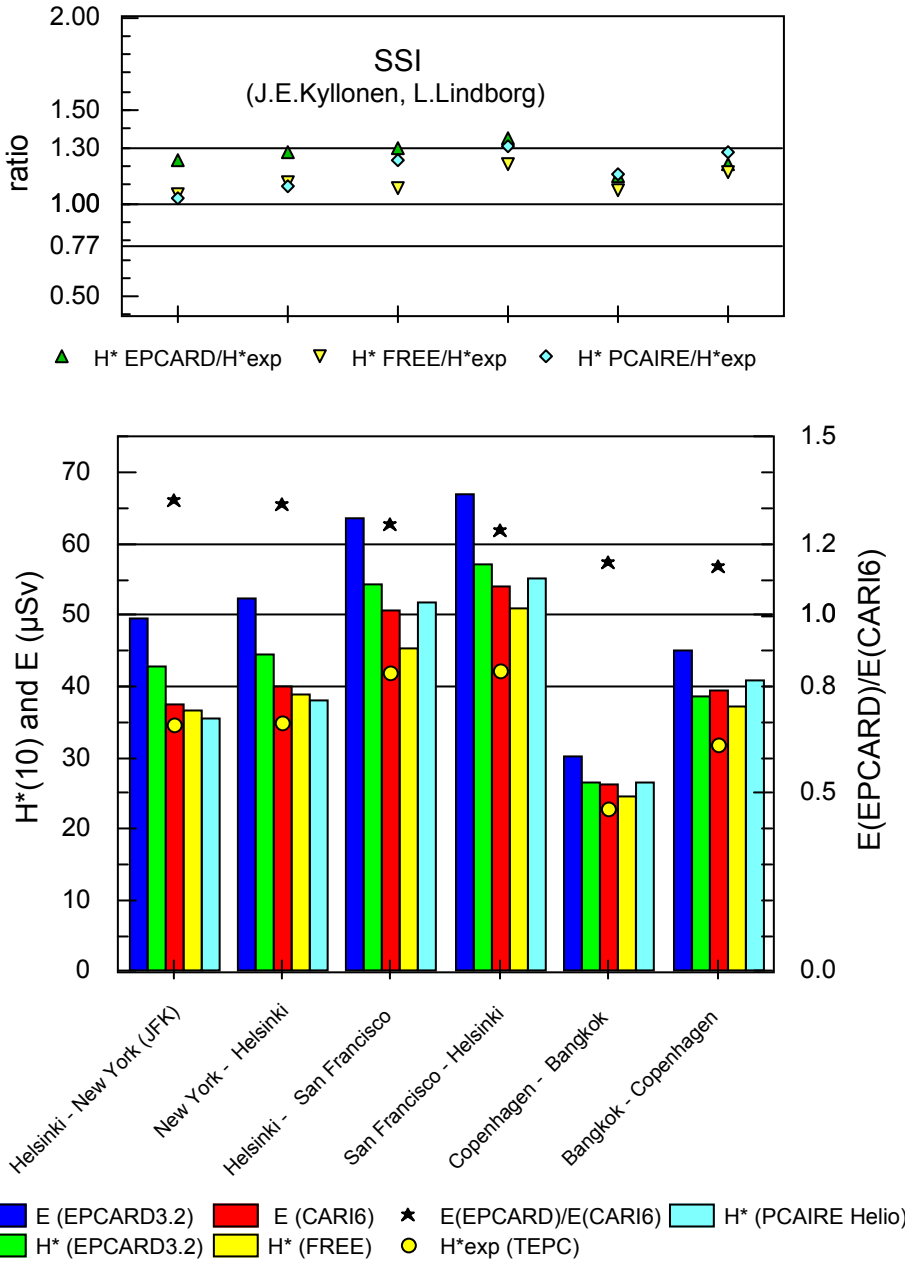

Figure IV.3 Calculated doses for flights of SSI (1998), and experimental data obtained with TEPC. The calculations were conducted with CARI, EPCARD, FREE and PCAIRE. "PCAIRE Helio" indicates the use of the heliocentric potential during calculation. The ratio of effective doses obtained with EPCARD and CARI6, respectively, is depicted together with a ± 20% band (right scale). Top of figure: Ratio of calculated operational quantity, H*(10), and experimental data. An uncertainty band of ±30% (i.e. factor 1.3) is included. The flights to and from San Francisco were performed during Forbush decreases. Also the Bangkok flights were made during a period of reduced neutron fluence (see Figure II.3).

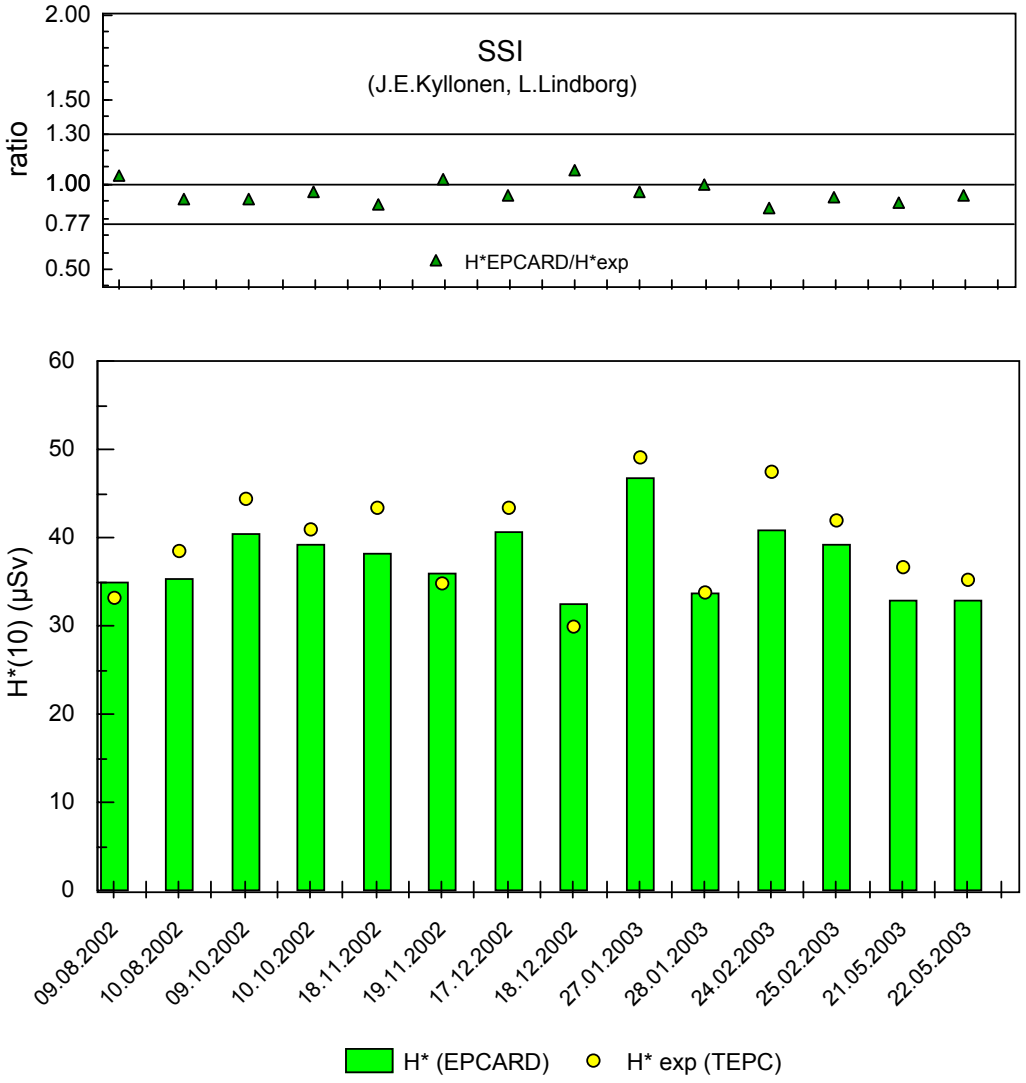

Figure IV.4 Calculated doses for a specific flight mission conducted by SSI (2002-2003) from Stockholm via Iceland to USA, and experimental data obtained with TEPC.
Two bars depict one return route starting from Stockholm, respectively. The calculations were conducted with EPCARD, only. Top of figure: Ratio of calculated operational quantity, *H**(10), and the experimental data.

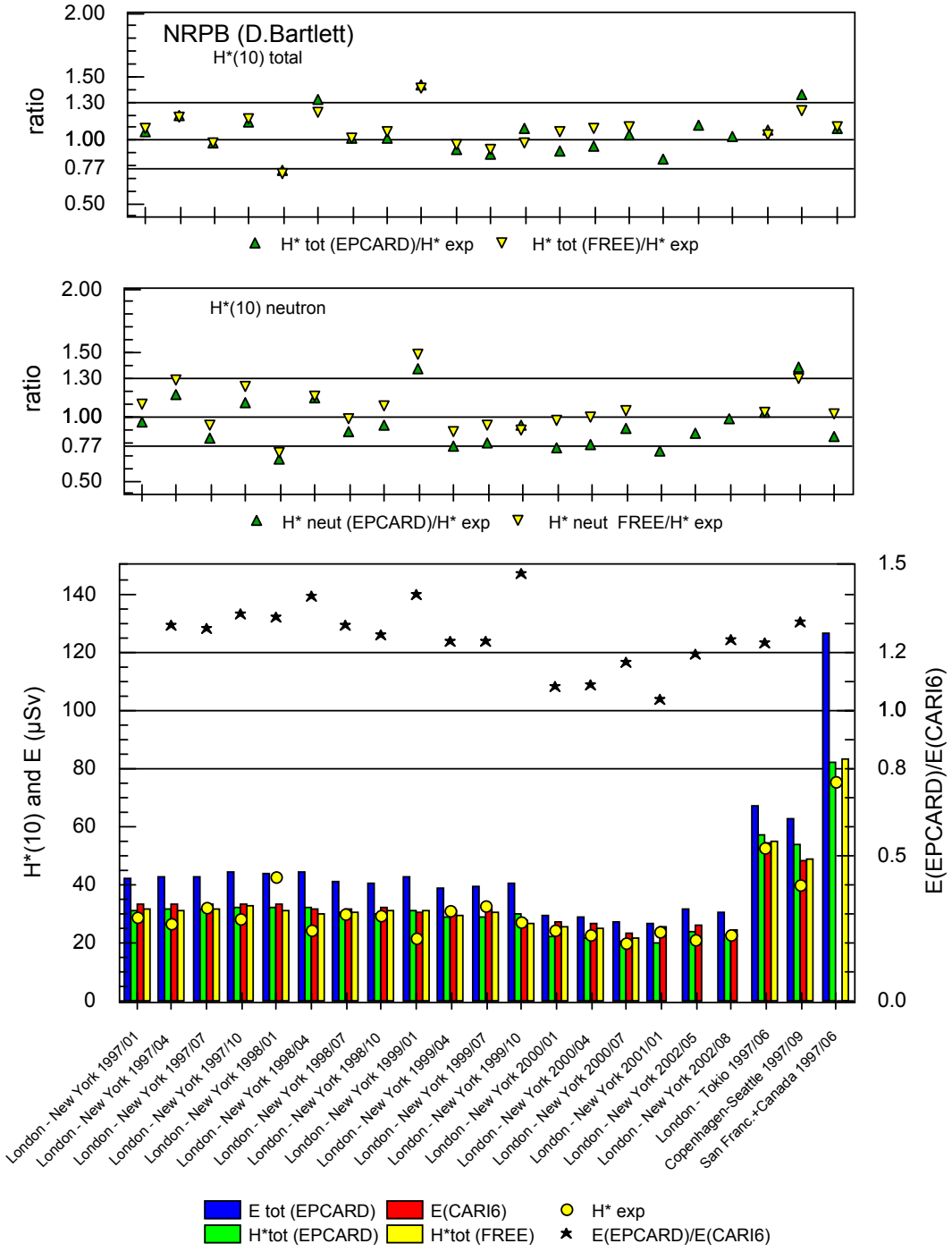

Figure IV.5 Calculated doses for flights of NRPB (1997-2002), and experimental data obtained with integrating passive devices.
Lower part of figure: The calculations were conducted with CARI, EPCARD and FREE. The ratio of effective doses obtained with EPCARD and CARI, respectively, is depicted together with a ± 20% band (right scale). Top of figure: Ratio of calculated operational quantity, H*(10), and experimental data, for total dose and neutron dose equivalent, respectively. The experimental data H*(10) for neutrons include neutron like reactions of protons. An uncertainty band of ±30% (i.e. factor 1.3) is included.

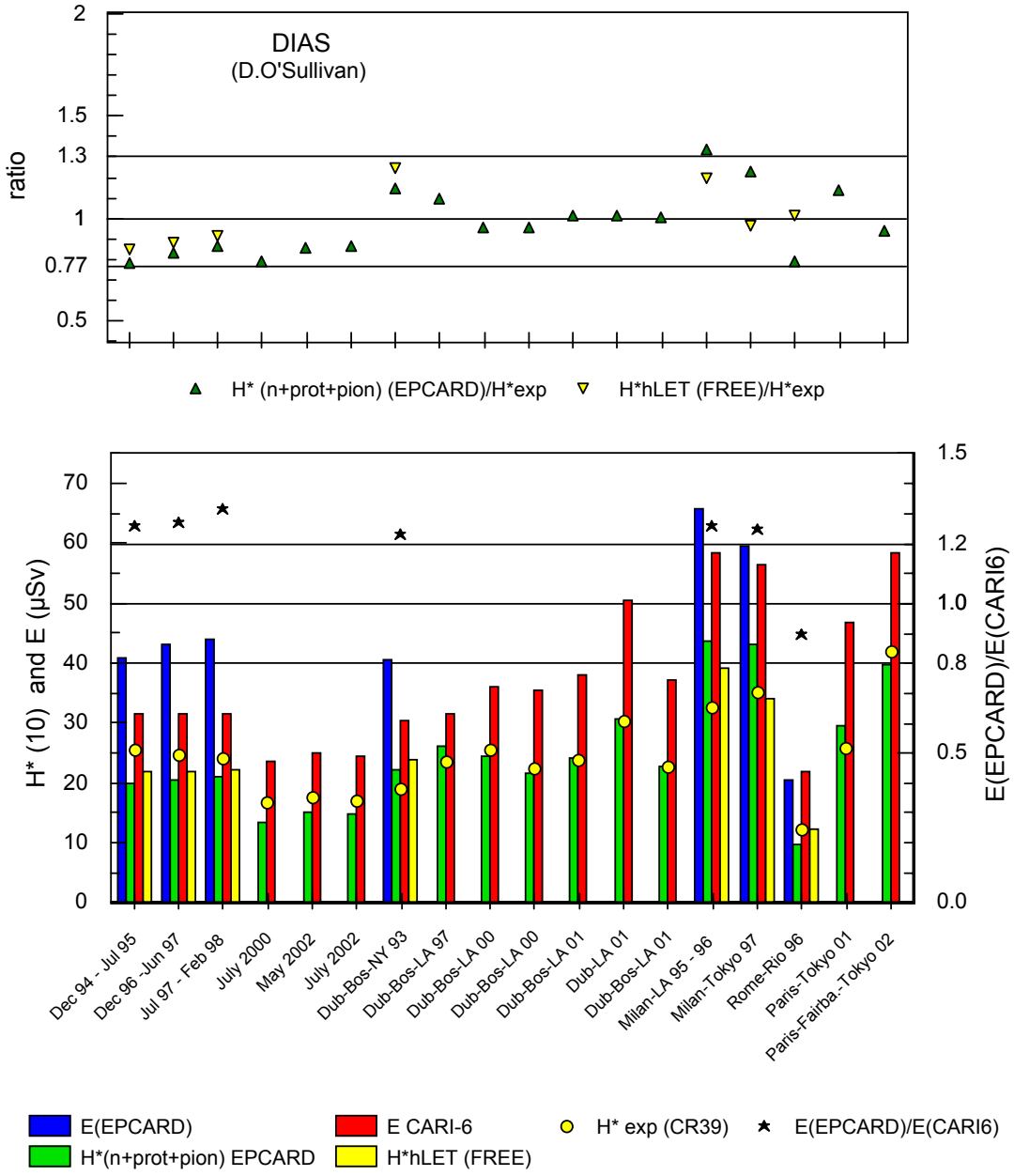

Figure IV.6 Calculated and experimental mean dose rates for flights of DIAS (1993-2002). Experimental data are obtained with PADC detectors (CR-39) and determined for stopping power of >5 keV/µm, i.e. particle energies of < 10MeV in the case of protons; H*(10) is for the same conditions. E_{CARI6} and E_{EPCARD} depict the total effective dose determined with CARI-6 and EPCARD, respectively. Flight groups from left to right were with: British Airways - Concorde (6 missions), Aer Lingus (7), Alitalia (3), and Air France (2).

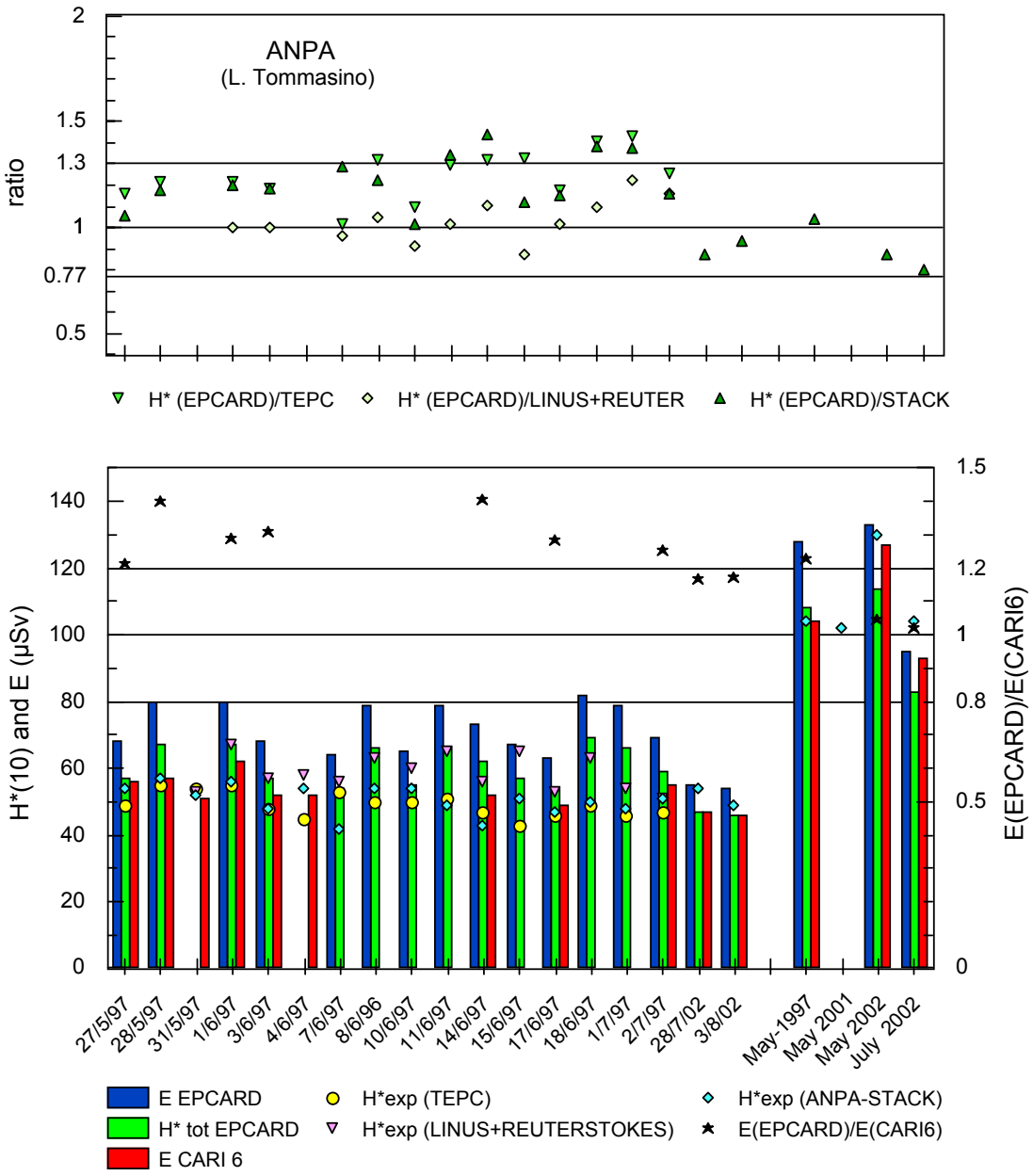

Figure IV.7 Calculated and experimental mean doses for flights of ANPA (1997-2002). Experimental data are obtained with TEPC, the LINUS/ReuterStokes-combination and the ANPA-stack. The data displayed for the year 1997 were obtained on the route Milan - Tokyo - Milan, for the years 2001 and 2002 on the routes Paris - Tokyo and Rome - Tokyo, respectively.

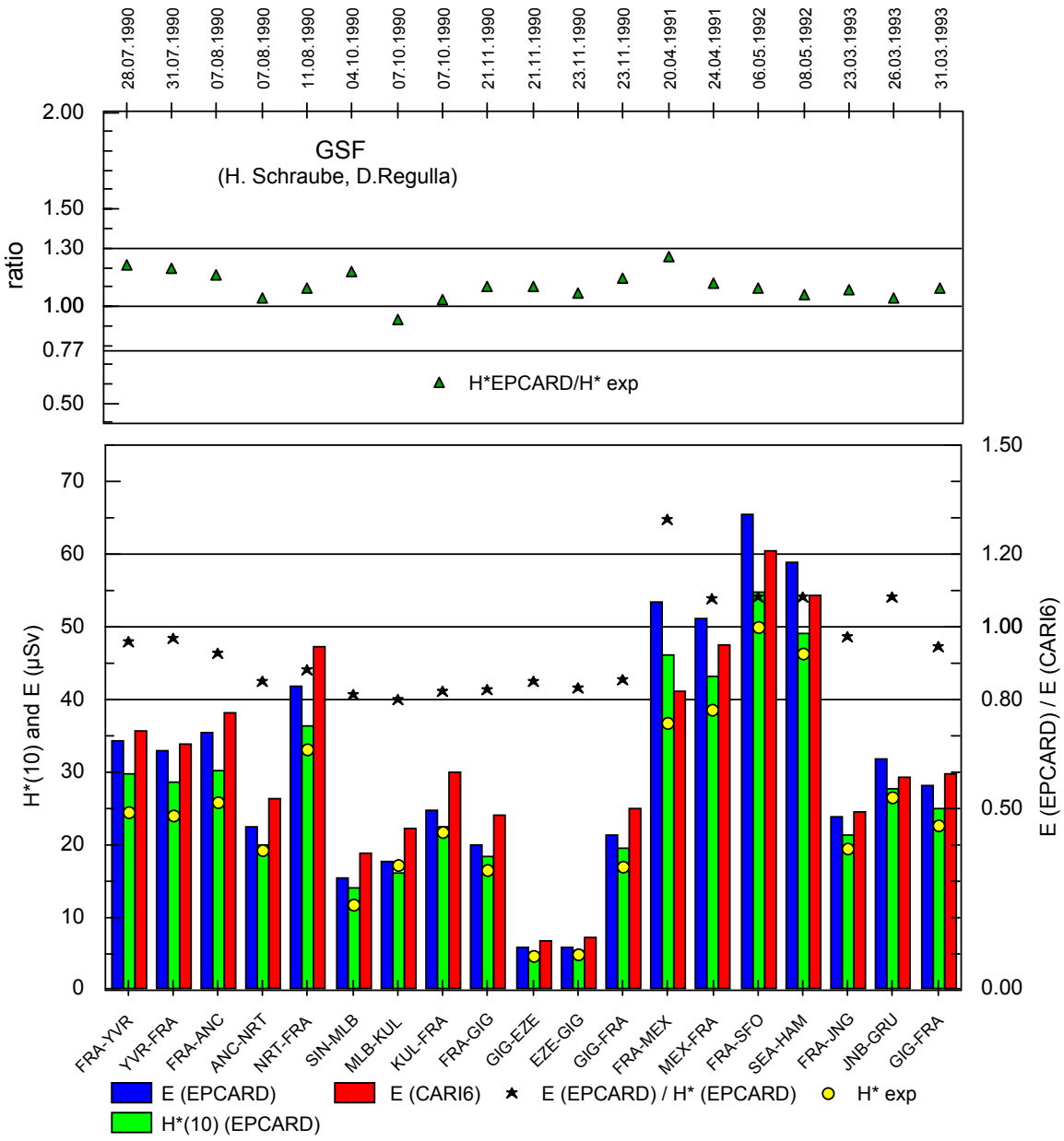

Figure IV.8 Calculated doses for flights of GSF (1990-1993) and experimental data obtained with NM, NMX and scintillation counter. Lower part of figure: The ratio of effective doses obtained with EPCARD and CARI6, respectively, is depicted together with a ± 20% band (right scale). Top of figure: Ratio of calculated operational quantity, H*(10), and experimental data. An uncertainty band of ±30% (i.e. factor 1.3) is included.

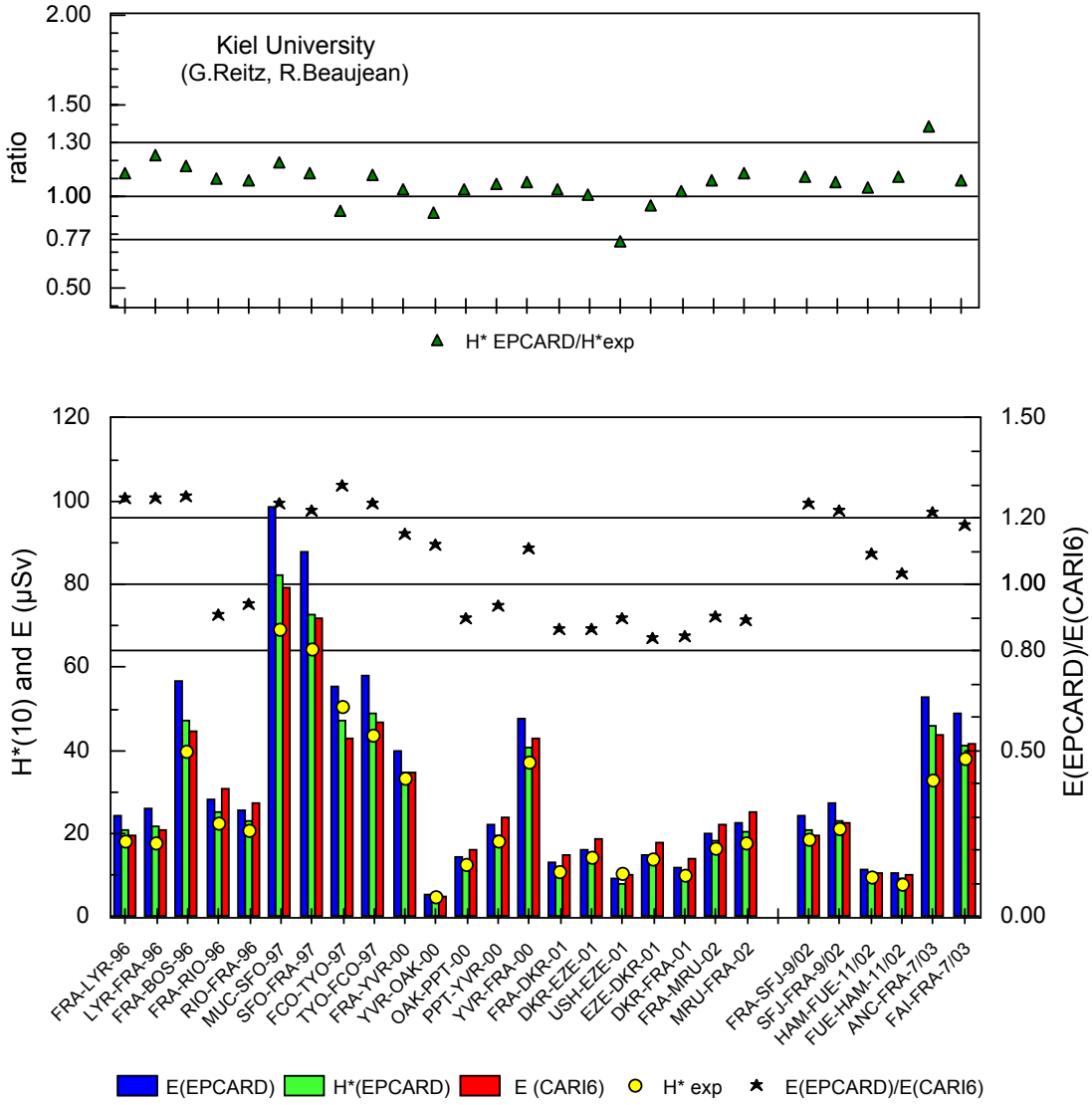

Figure IV.9 Calculated doses for flights of Uni Kiel (1996-2003), and experimental data obtained with DOSTEL. The ratio of effective doses obtained with EPCARD and CARI6, respectively, is depicted together with a ± 20% band (right scale). Top of figure: Ratio of calculated operational quantity, H*(10), and experimental data. An uncertainty band of ±30% (i.e. factor 1.3) is included.

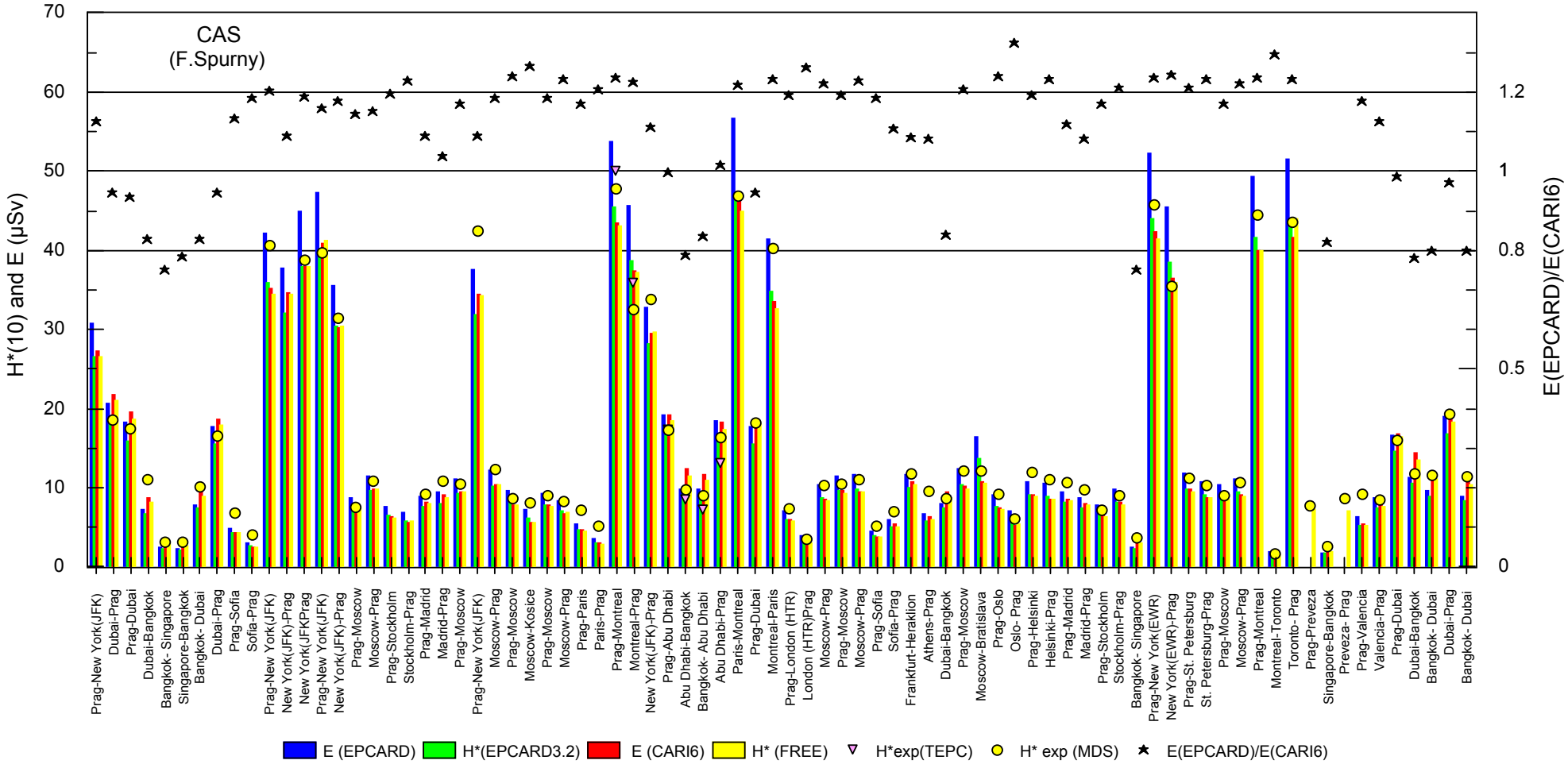

Figure IV.10a Calculated doses for flights of CAS (1991-1999) and experimental findings with TEPC and a multidetector system (MDS). The calculations were conducted with CARI, EPCARD, FREE and PCAIRE. The ratio of effective doses obtained with EPCARD and CARI, respectively, is depicted together with a ± 20% band (right scale).

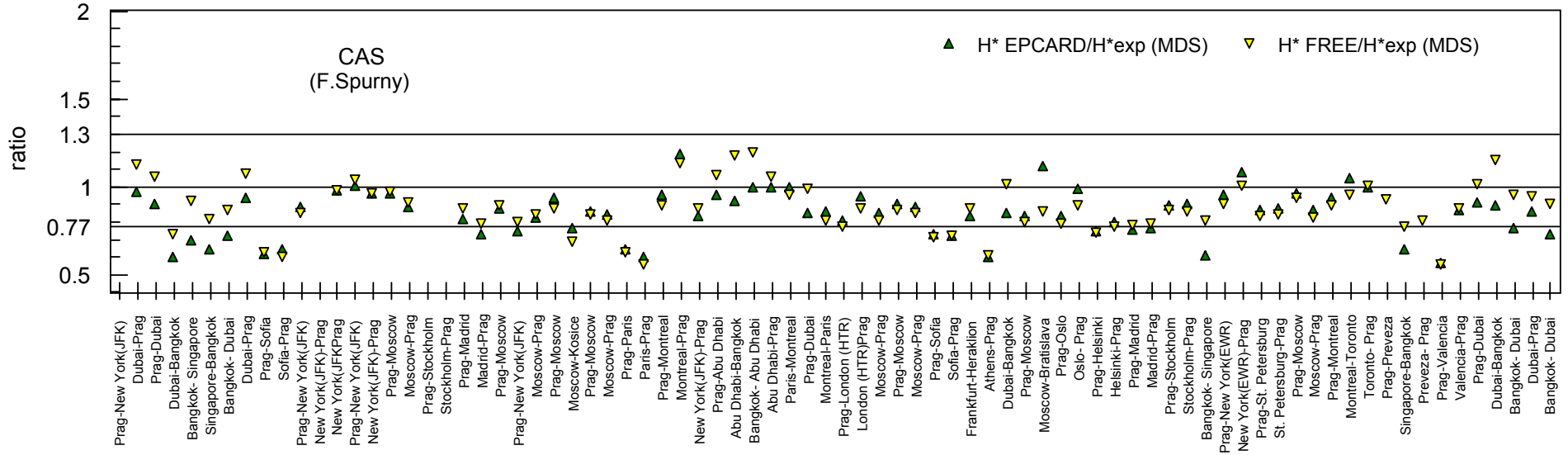

Figure IV.10b Ratio of calculated doses, H*(10), to the experimental findings with a multidetector system (MDS) for flights of CAS (1991-1999). An uncertainty band of ±30% (i.e. factor 1.3) is indicated.

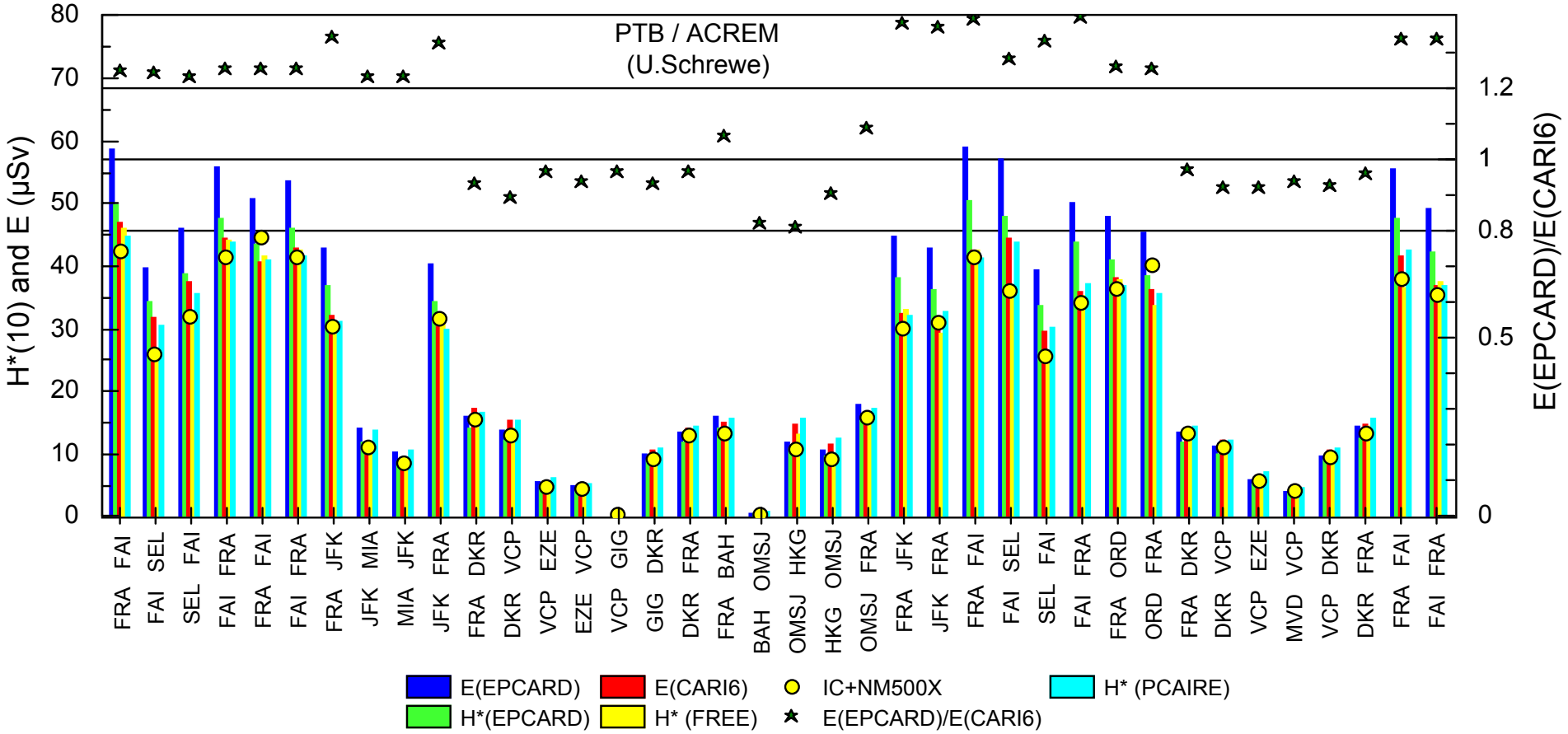

Figure IV.11a Calculated doses for flights of PTB/ACREM (1997-1999), and experimental data obtained from the evaluated results of ACREM. The calculations were conducted with CARI, EPCARD, FREE and PCAIRE. The ratio of effective doses obtained with EPCARD and CARI, respectively, is depicted together with a ± 20% band (right scale).

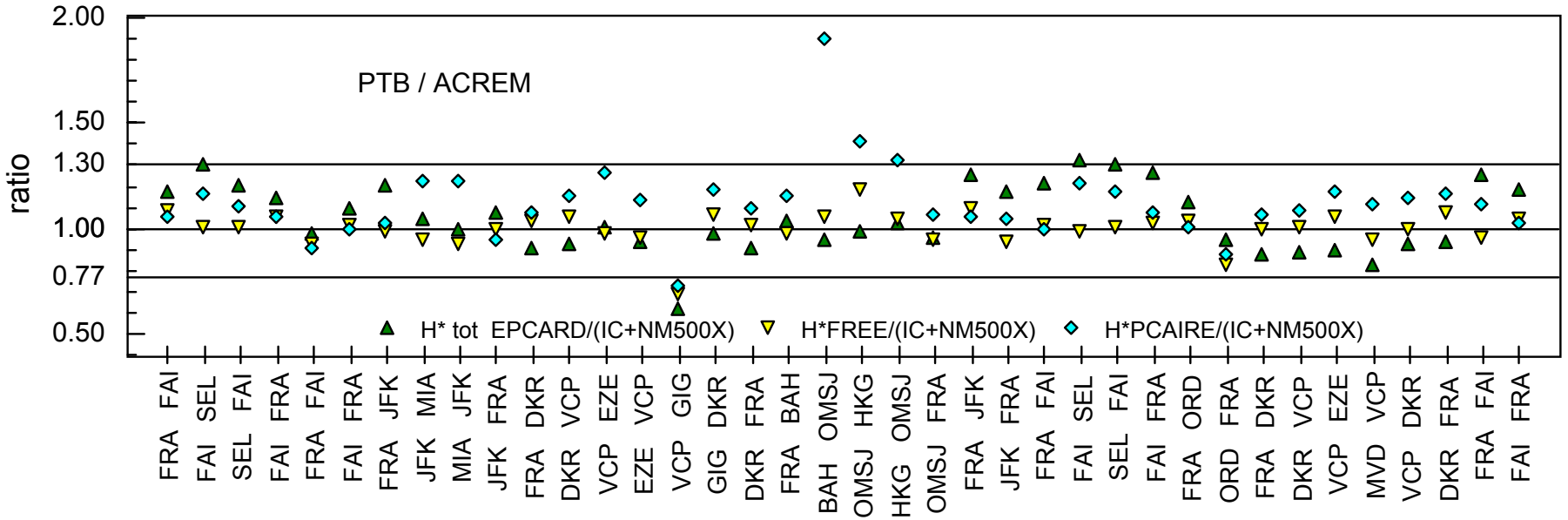

Figure IV.11b Ratio of calculated operational quantity, $H^*(10)$, and experimental data for PTB/ACREM flights. An uncertainty band of ±30% (i.e. factor 1.3) is indicated.

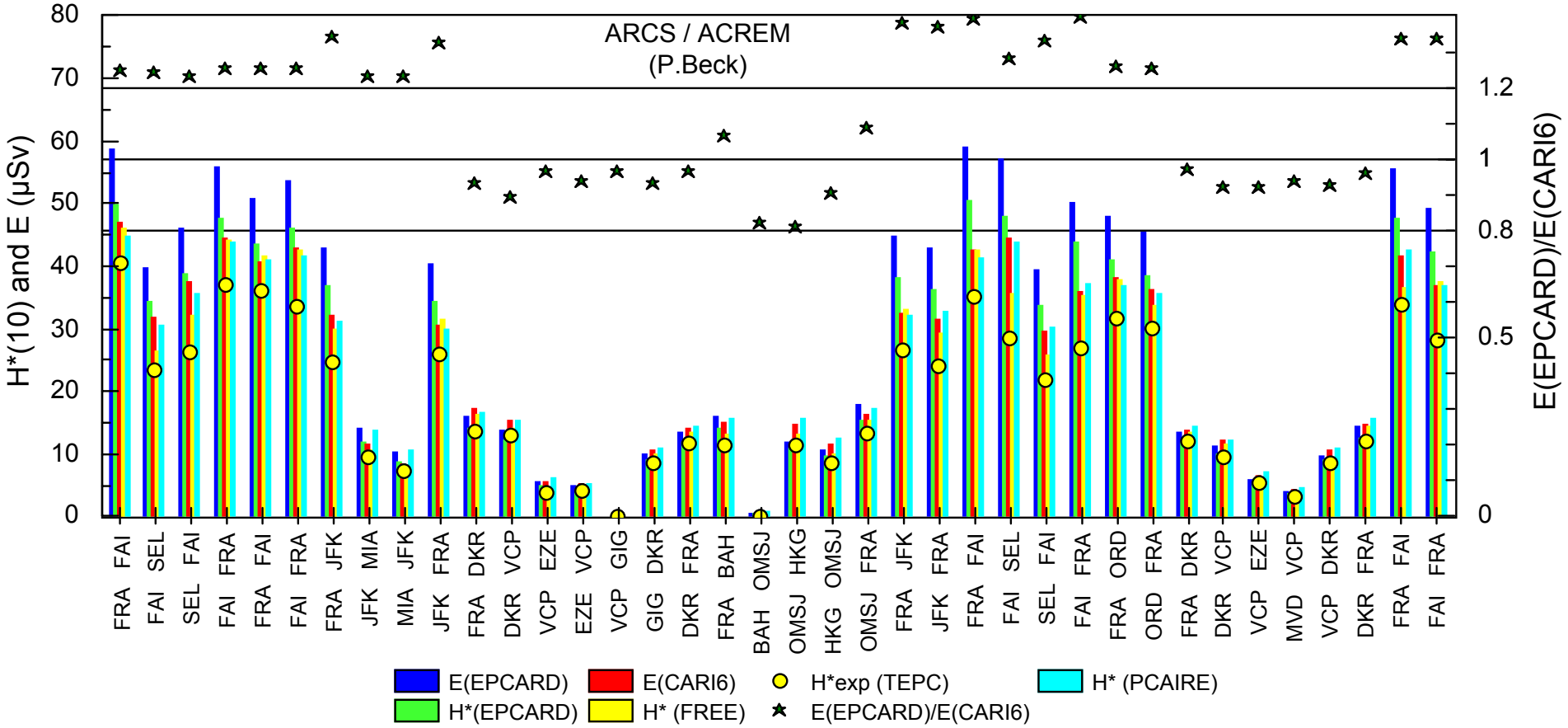

Figure IV.12a Calculated doses for flights of ARCS/ACREM (1997-1999), and experimental data obtained from TEPC measurements.

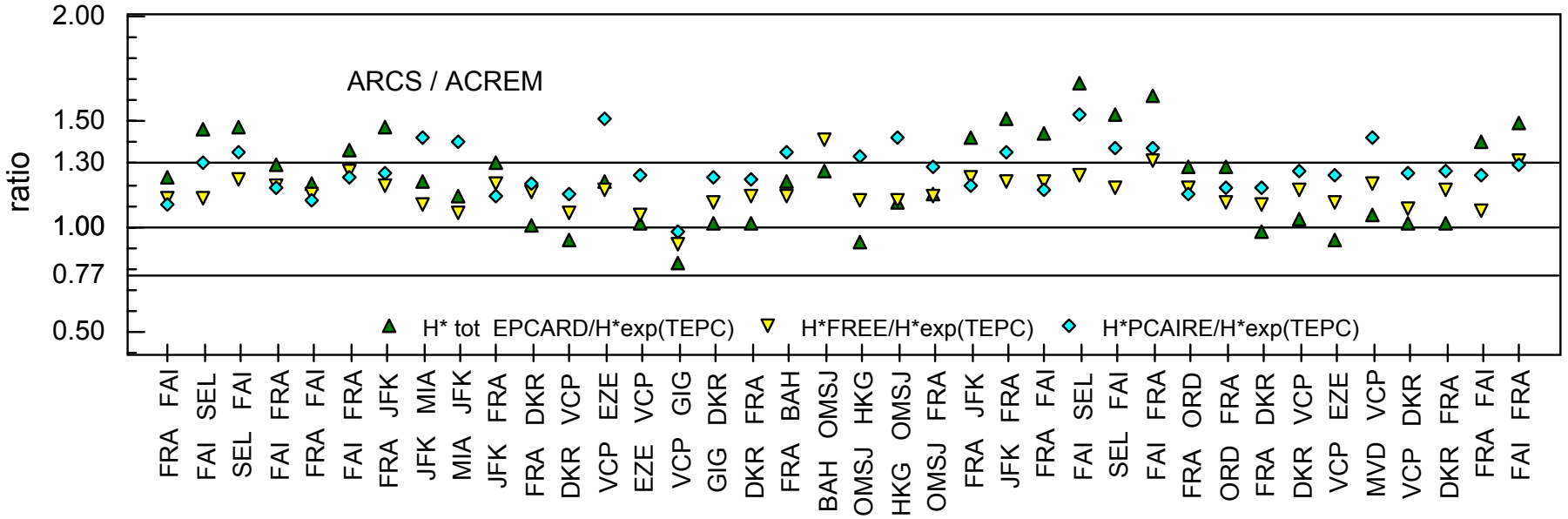

Figure IV.12b Ratio of calculated operational quantity, *H**(10), and experimental data for ARCS/ACREM flights. An uncertainty band of ±30% (i.e. factor 1.3) is indicated.

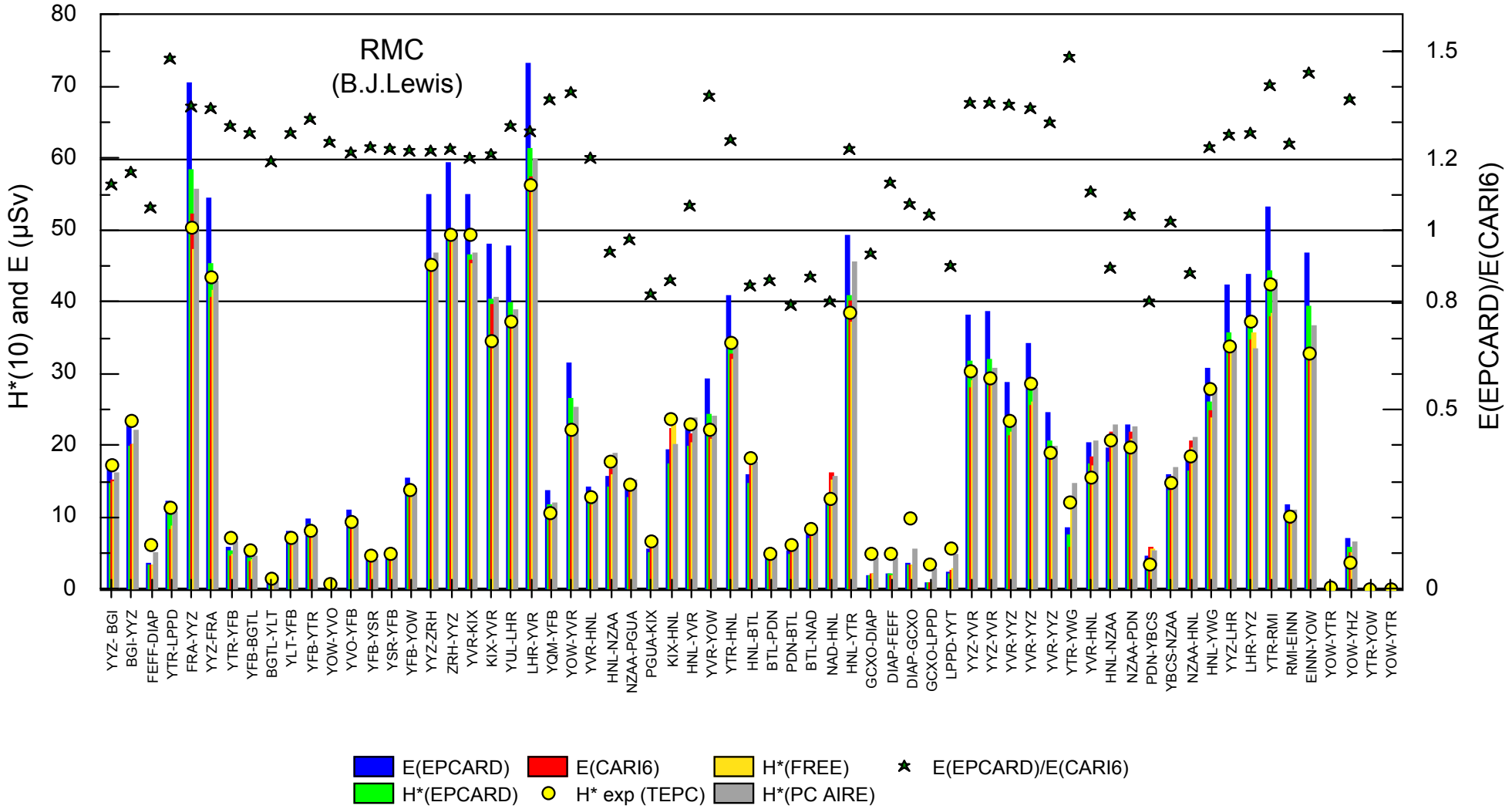

Figure IV.13a Calculated doses and experimental findings for flights of RMC (1999).

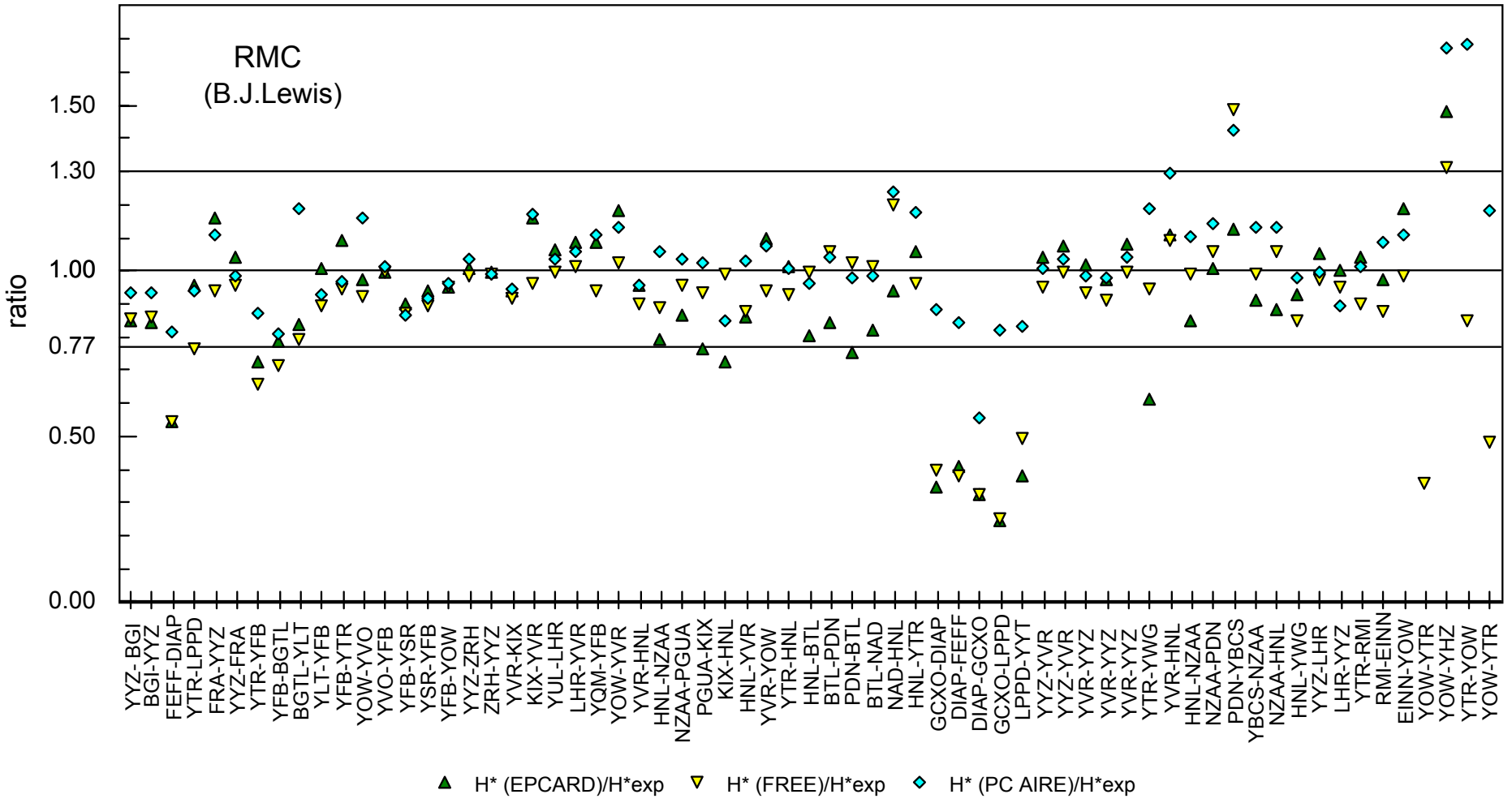

Figure IV.13b Ratio of calculated operational quantity, *H**(10), and experimental data for flights of RMC (1999). PCAIRE calculation done employing the solar deceleration potential.

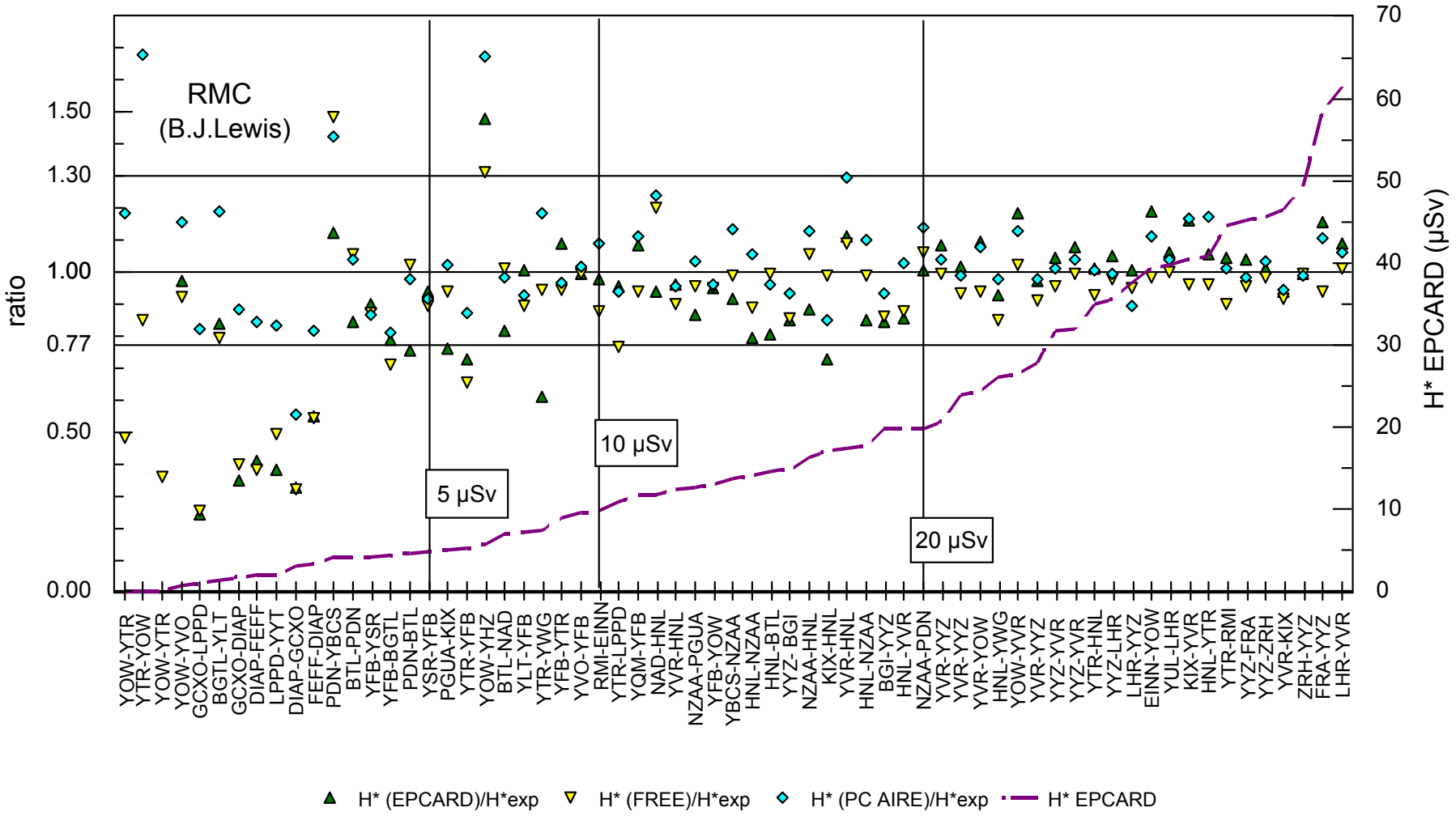

Figure IV.13c Same presentation as in figure IV.13.b, sorted with increasing total calculated ambient dose equivalent $H^*(10)$ (right scale).

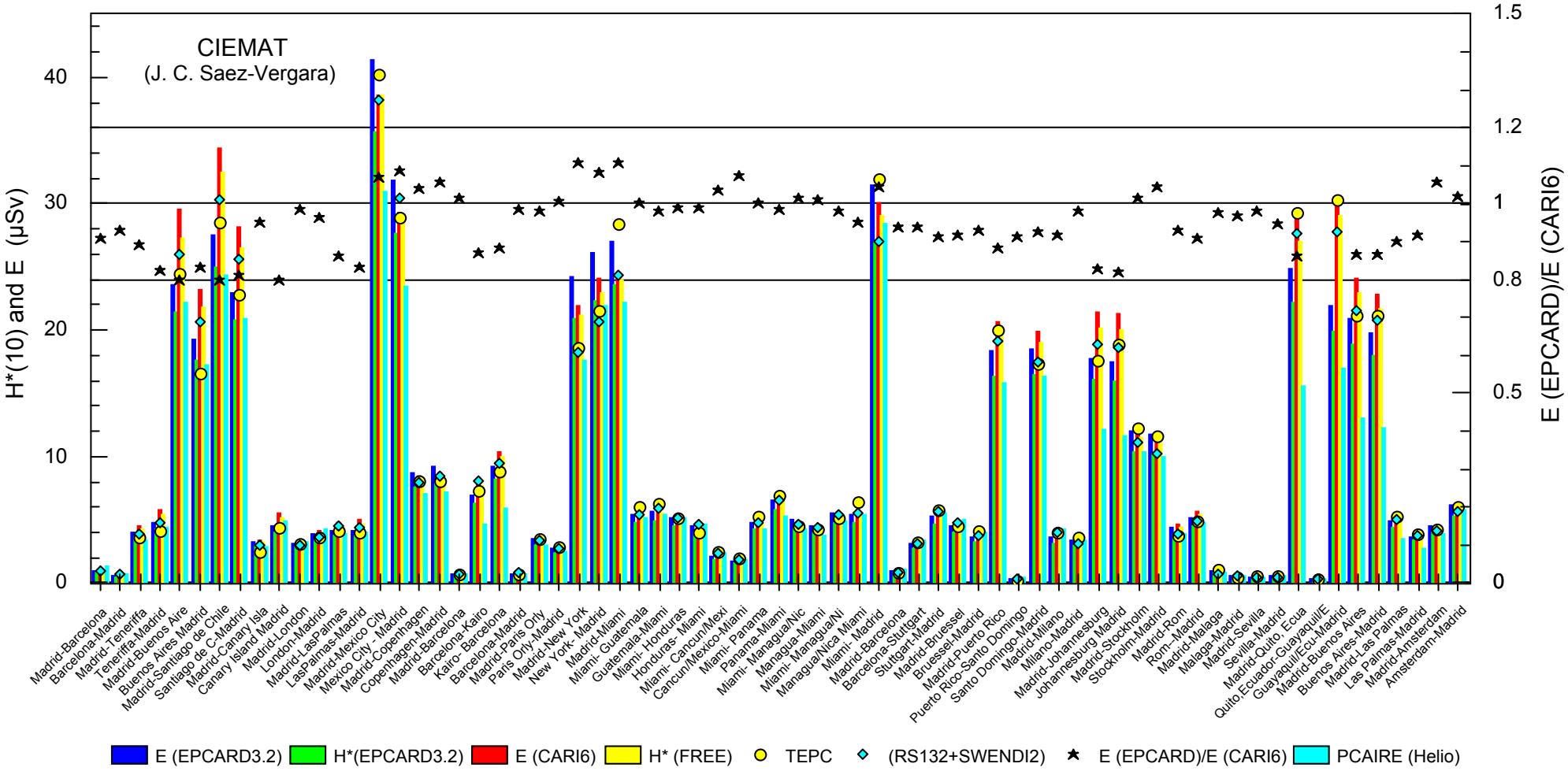

Figure IV.14a Calculated doses and experimental findings of flights of CIEMAT/IBERIA. Experimental data obtained with TEPC and with RS132/SWENDI-combination. The ratio of effective doses obtained with EPCARD and CARI6 is depicted together with a ± 20% band (right scale).

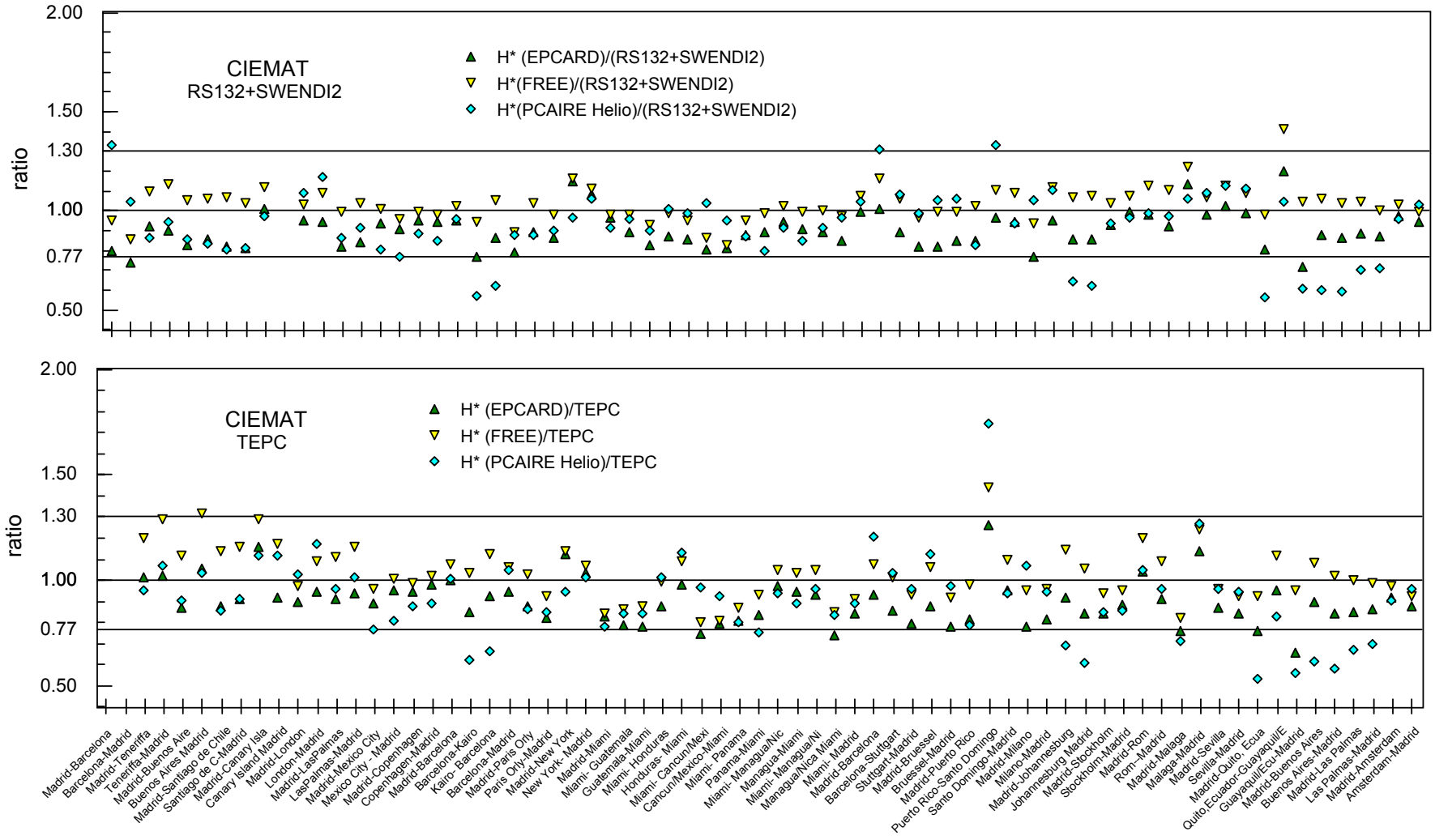

Figure IV.14b Ratios of calculated and experimental data for flights of CIEMAT. An uncertainty band of ±30% (i.e. factor 1.3) is included

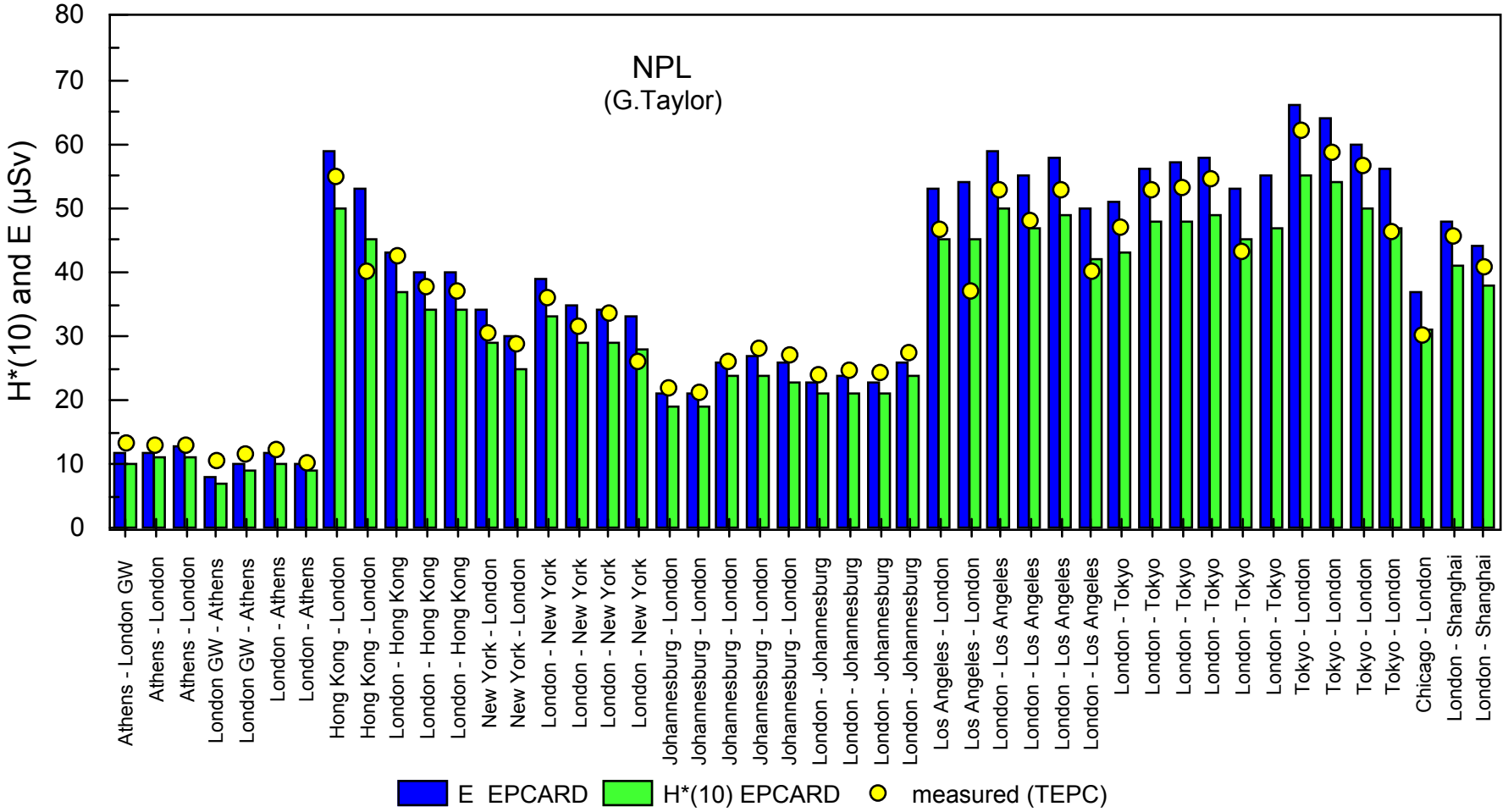

Figure IV.15a Calculated doses for flights of NPL and experimental findings with TEPC. The calculations of effective dose and ambient dose equivalent were conducted with EPCARD only.

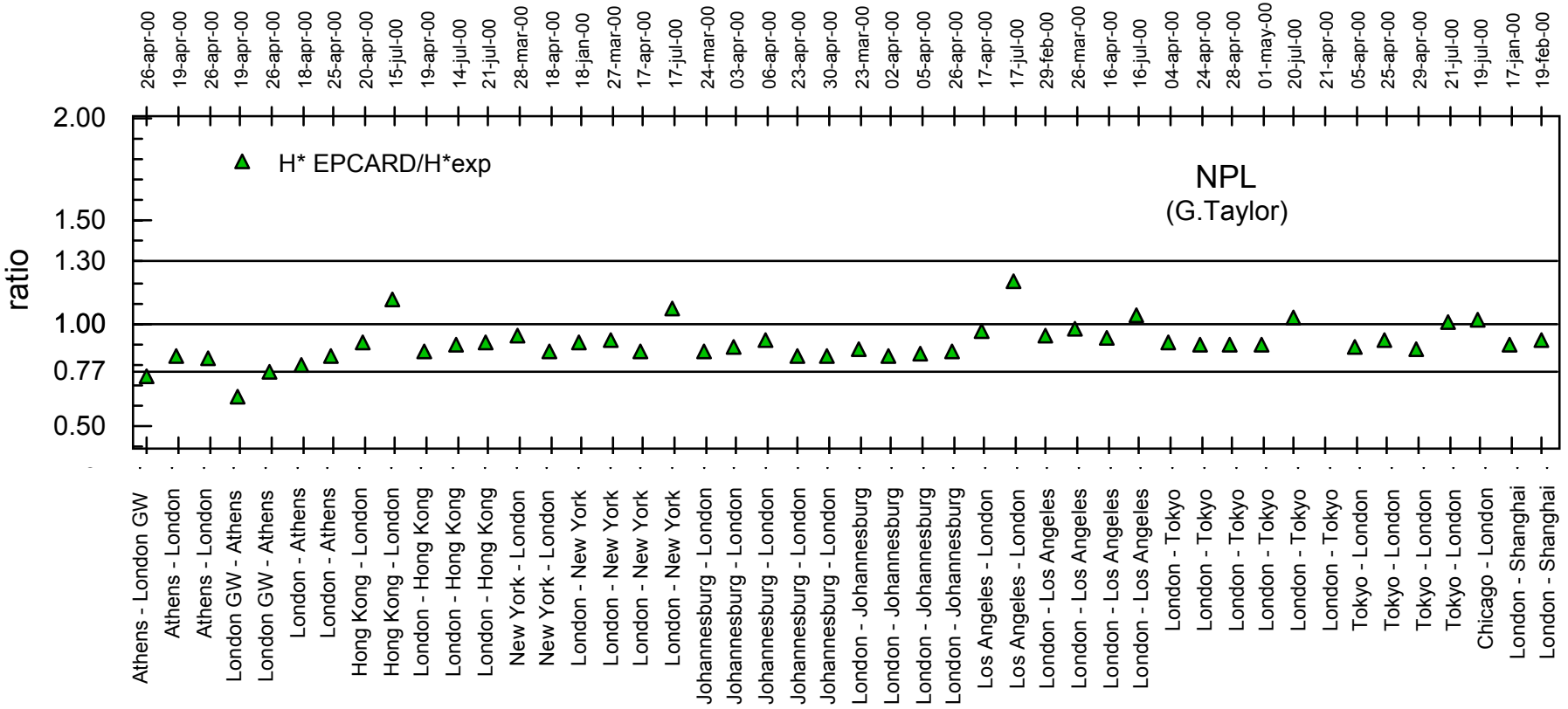

Figure IV.15b Ratios of calculated and experimental data for flights of NPL. An uncertainty band of ±30% (i.e. factor 1.3) is indicateded..

IV.4 Calculated doses of scheduled flights

These flights are arbitrarily chosen from the regular flight schedule from Munich and Frankfurt (Germany) to worldwide destinations (this data set may be extended to further connections between any other airport pairs required). The flight conditions were simplified in such, that the full "elapsed" time from the official schedule was used as total flight time, and an ascent to the flight level and descent to the destination airport was taken as 30 min, respectively. Only one flight level is used for each destination and the shortest distance (i.e. great circle navigation) is assumed between top of climb and top of descent or, in this case, the two cities.

The Figure IV.16 shows the results for $H^*(10)$ and E obtained with EPCARD for January 2002 sorted by increasing flight time. Figure IV.17 depicts the results of effective dose obtained by CARI and EPCARD, respectively, and the ratio of both results. The data are sorted by increasing effective dose obtained from EPCARD. A flight altitude of 37000 ft is assumed. It is observed that all ratios are well between 0.8 and 1.1, i.e. within ±15%.

The presentation in Figure IV.17 may give some impression on the importance of the differences observed: While for the northern (long distance) routes with the highest dose values, EPCARD delivers around 5% higher effective doses than CARI6, the southern routes are estimated by up to 20% lower by EPCARD. For the short-range destinations in Europe, both programs deliver approximately the same data.

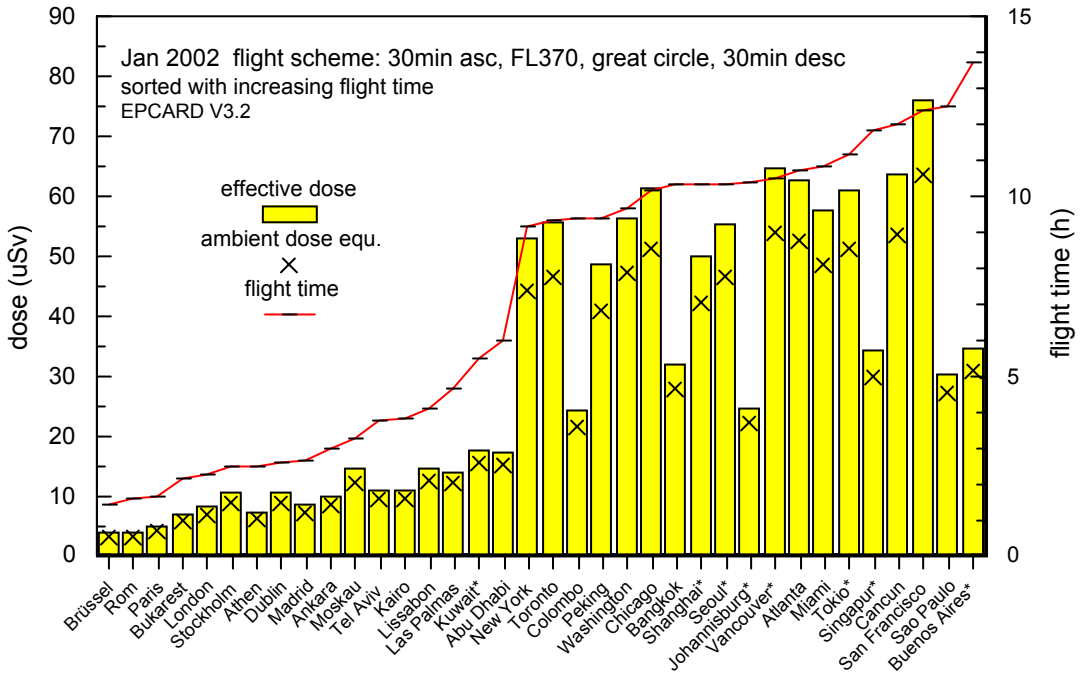

Figure IV.16 Effective dose, ambient dose equivalent (left scale) and total flight time (right scale) for selected scheduled flights for January 2002. The flights are from Munich and Frankfurt (*) assuming a simplified flight profile with ascent and descent of 30min, respectively, and a constant flight level of 37000ft.

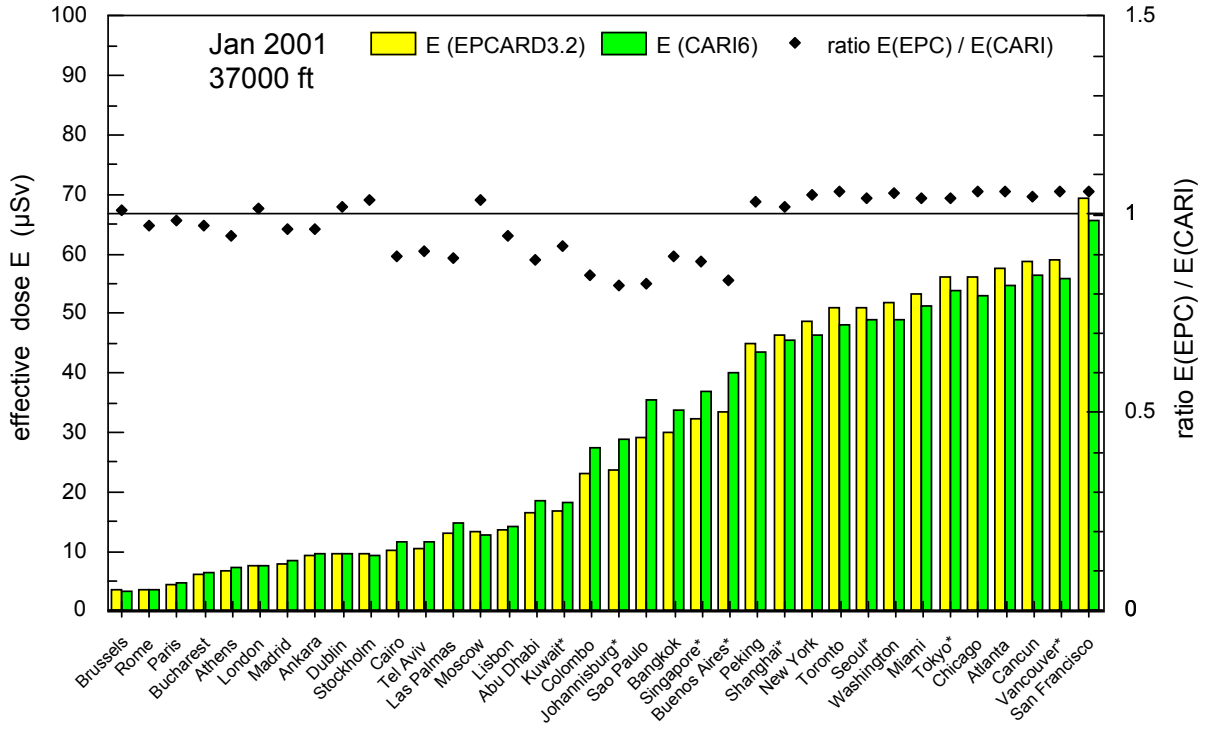

Figure IV.17 Effective dose, *E*, for the scheduled flights of figure IV.16, but for January 2001, calculated with EPCARDv3.2 and CARI6, in the order of increasing effective dose.

IV.5 Solar modulation effects

In order to study the dependence of the calculated doses from the solar modulation, it had been proposed to refer to the same solar potential, and to vary it in both the codes. However, CARI and EPCARD use different models to describe the solar modulation: CARI employs the heliocentric potential [OFD92] and EPCARD the solar deceleration potential [BAD97], both describing the time variable shielding effect of the sun's magnetic field against the galactic cosmic rays. The deceleration potential relates to the IGY neutron monitor at Climax (39.37 N, 253.82 E, cutoff 2.97 GV, altitude 3400 m). The heliocentric potential is currently based on neutron counts from the Apatity NM64-monitor (67.57°N, 33.40°E, cutoff ca. 0.5 GV, elevation 181 m). Both monitors are sensitive to energetic cosmic rays.

Figure IV.18 depicts the count rate of the Climax monitor within the time period from 1957 until middle of 2001, together with the ratios of the two solar potentials: the decelaration potential is calculated from the relations given by Badhwar [BAD97] using the Climax data, the heliocentric potential was obtained from the Civil Aerospace Medical Institute [CJG04]. The ratio is close to one only over some short periods of time, while during other time periods a factor between 0.8 and 1.6 is observed.

The reason for these differences in the potential is of fundamental importance. To model doses at aviation altitudes, the energy spectra of cosmic ray particles entering the atmosphere are needed as input data. For the LUIN code these spectra are referred to as the boundary condition.

For the calculations, which support the fundamental data used in EPCARD a standard primary cosmic ray particle model developed by NASA for radiation protection purposes in space was used. It starts with an energy spectrum without any effects of solar modulation. This spectrum is generally called the local interstellar spectrum (LIS). It represents the particle fluxes close to our solar system but without any effects caused by the sun. The solar shielding effect against primary cosmic rays, i.e. the effect that cosmic ray particles moving towards the sun are slowed down and deflected by the solar

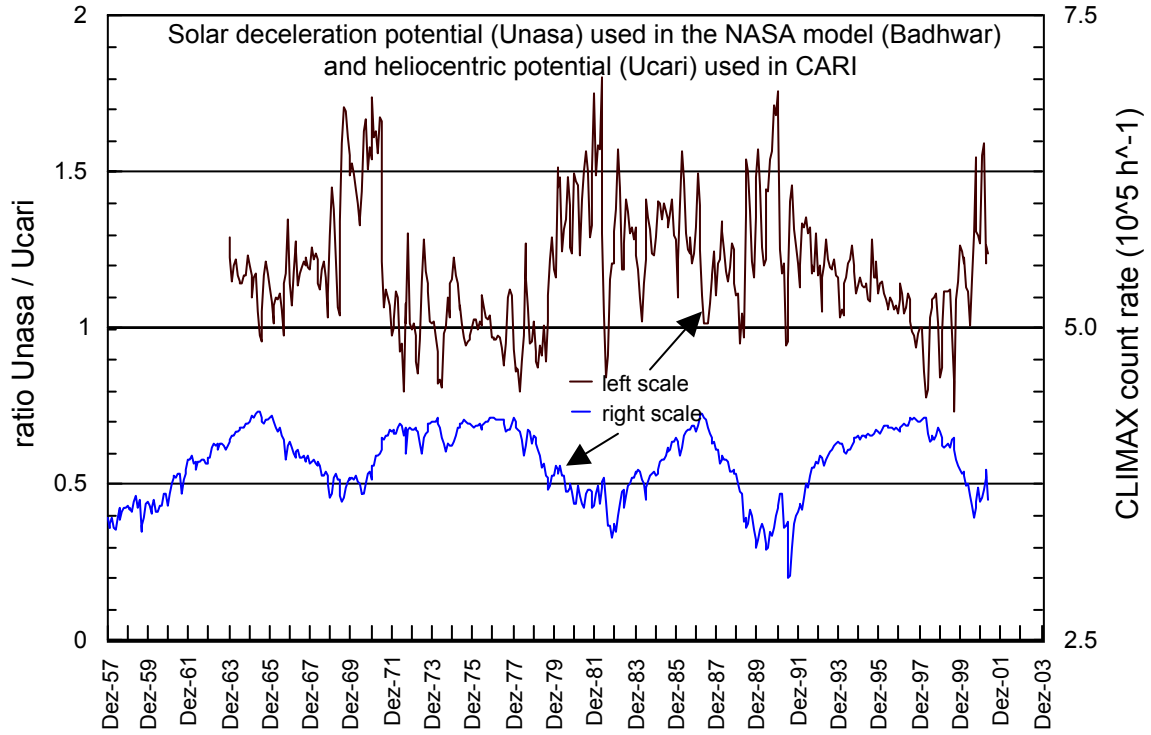

Figure IV.18 Monthly averaged count rate of the Climax monitor depicted in the lower curve (right scale) for the time period from 1958 to 2001. The ratio of the solar potentials used in both in codes CARI and EPCARD, respectively, is plotted in the upper curve (left scale).

wind and irregularities carried by the solar wind, can be described by a complicated model considering processes of convection and diffusion. The net result of this shielding model is identical to the effect, which a negative electrical potential would have, against which the positively charged cosmic ray particles move in. This potential does not exist in reality and cannot be measured. Its virtual strength can be derived from measured particle fluxes impinging on earth and based on the LIS, which must also be assumed to define a starting point. That means that the LIS and the modulation potential are closely correlated and that a comparison of modulation potentials for different models makes only sense if both use the same LIS. However, the primary spectra used in EPCARD and the boundary conditions used in LUIN differ significantly. Therefore identical modulation potentials of both codes do not mean identical situations of cosmic ray primary spectra impinging on earth.

Therefore, for the study of the altitude effect on the difference between both codes, in Figure IV.19 the date January 1998 was chosen which is not too far from solar minimum, where the solar potential does not change much in the time period before and after. The data sequence is approximately the same as in Figure IV.17, i.e. with increasing total effective dose at this date. The altitudes were varied between 29000 ft and 41000 ft. It is observed that the dose ratios may change by up to approximately 30 % in this range of flight levels where the larger differences between both programs occur for the lower flight levels and for the northern long-range routes.

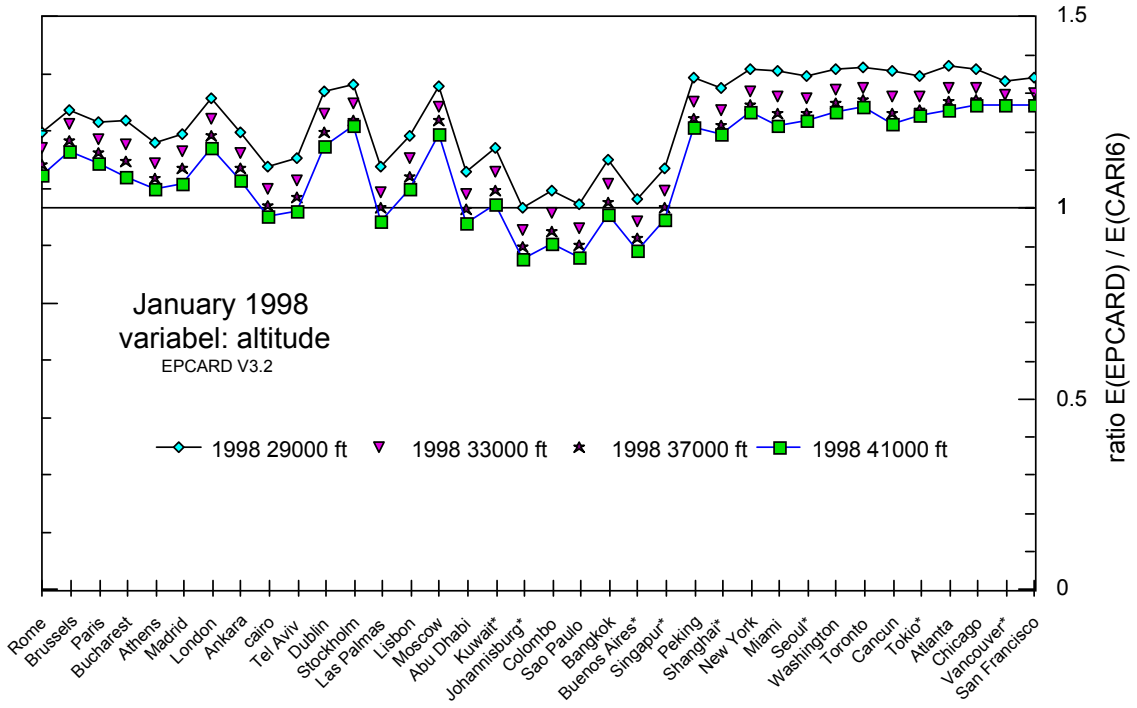

Figure IV.19 Ratio of effective dose calculated with EPCARDv3.2 and CARI6 for January 1998 close to solar minimum. The flight altitude is varied from 29000 to 41000 ft for the flight routes from Munich and Frankfurt

.

Finally, the influence of the solar modulation to the calculation results was studied by changing the date of flight between January 1990 and January 2001 keeping the flight level constant to 37000 ft. The results are shown in Figure IV.20 where the data are arranged in the same order as in Figure IV.16: For the period of solar maximum (1990/1991), the EPCARD results are clearly below those of CARI. They remain below or are equal to the CARI results for southern long-range routes, but are again higher for the northern long-range routes. It is also seen that for the latter ones the difference between both codes are larger at periods with decreasing solar activity (1992 to 1996) than at periods of increasing activity and reaching solar maximum conditions (1998 to 2001).

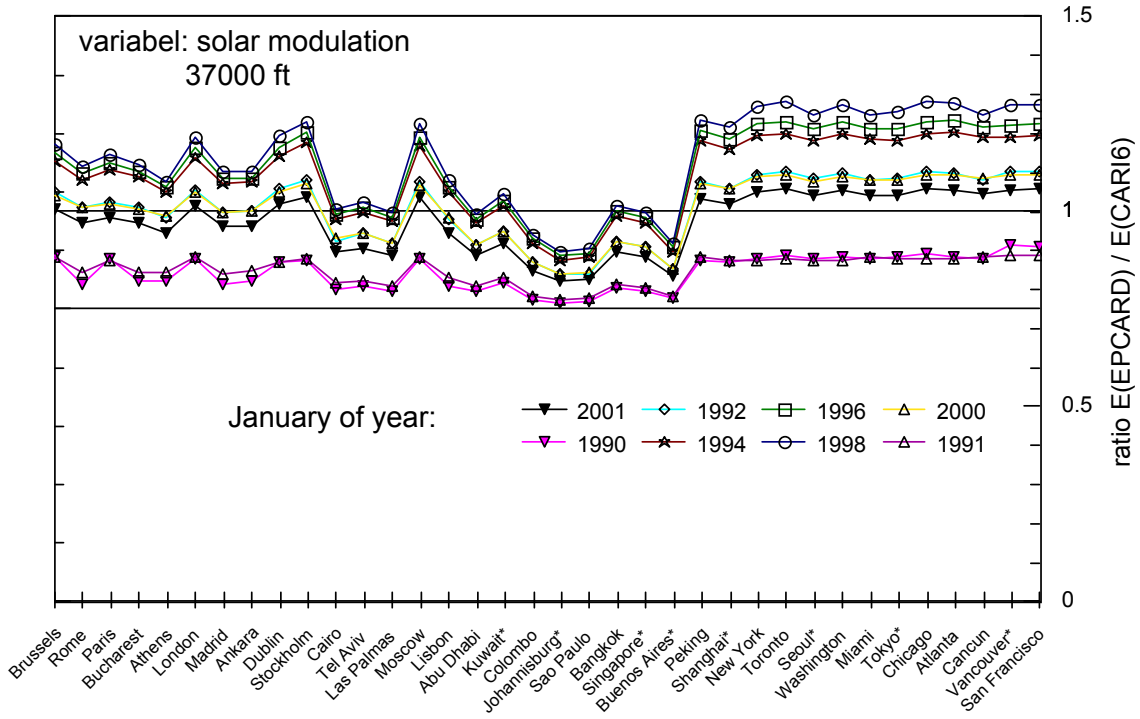

Figure IV.20 Ratio of effective doses calculated with EPCARDv3.2 and CARI6, for constant flight altitudes and variable solar modulation. The data are arranged as in Figure IV.16.

IV.6 Influence of flight altitude and solar modulation to route doses

In the following figures data are given for specific route doses when the cruising level and the solar modulation is changed. From Figure IV.16 only six destinations are selected, with the same simplified flight scheme, and the effective dose calculated using EPCARD and CARI.

Figure IV.21 depicts the influence of the cruising level. It is observed that the doses differ approximately by a constant factor when the flight level ist changed, e.g. a factor 5 when comparing flights to Lissabon and San Franzisco, respectively. It is also obvious that the change in cruising level from 41000 ft to 37000 ft, the dose is reduced by about 20%, independently from the destination; a change down to 29000 ft reduces the dose by a factor of about 2.

In Figures IV.22 and 23 the influence of the solar modulation to the calculated route dose is depicted. The cruising altitude is kept to 37000 ft and the year varied from 1990 to 2002, to cover the time period from maximum of solar cycle 22 to maximum of solar cycle 23. For the highest exposure considered, i.e. for the destination San Francisco, the effective dose rises from 55 µSv to 110 µSv, when the calculation is conducted with EPCARDv3.2 in January 1990 and January 1998; when employing CARI-6, the respective values are 60 µSv and 85 µSv.

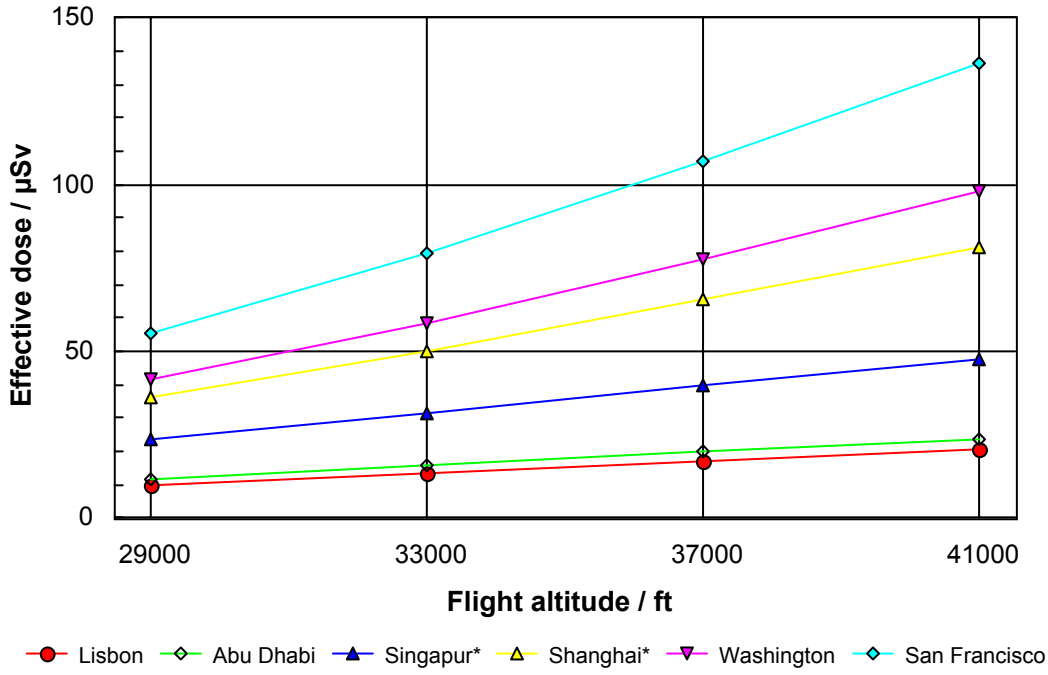

Figure IV.21 Influence of the cruising level to effective dose. Calculated effective dose, *E*, for six flight routes from MUC resp. FRA(*) to selected destinations depending on the flight altitude (one way). The selcted time was January 1998, i.e. close to solar minimum activity. The simplified flight scheme was 30 min ascent and descent each and at the indicated cruising altitude. The destinations are sorted due to total effective dose.

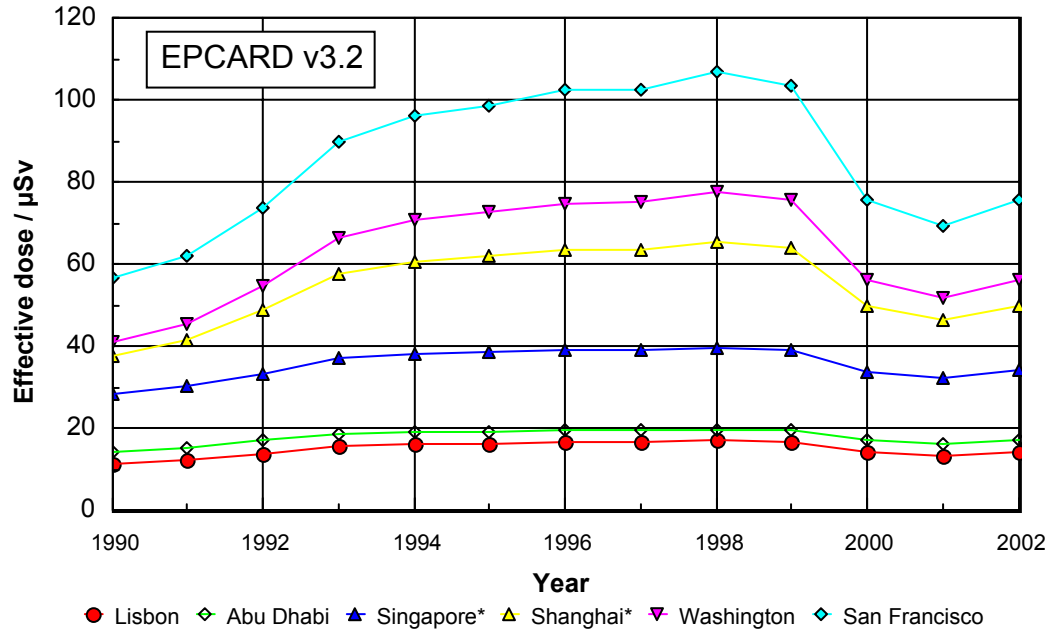

Figure IV.22 Influence of the solar modulation on effective dose (EPCARD). Calculated effective dose, *E*, for the flight routes of Figure IV.21 in the time period between both solar maxima (ca. 1990 and 2001) for Janury of each year and a cruising altitude of 37000 ft.

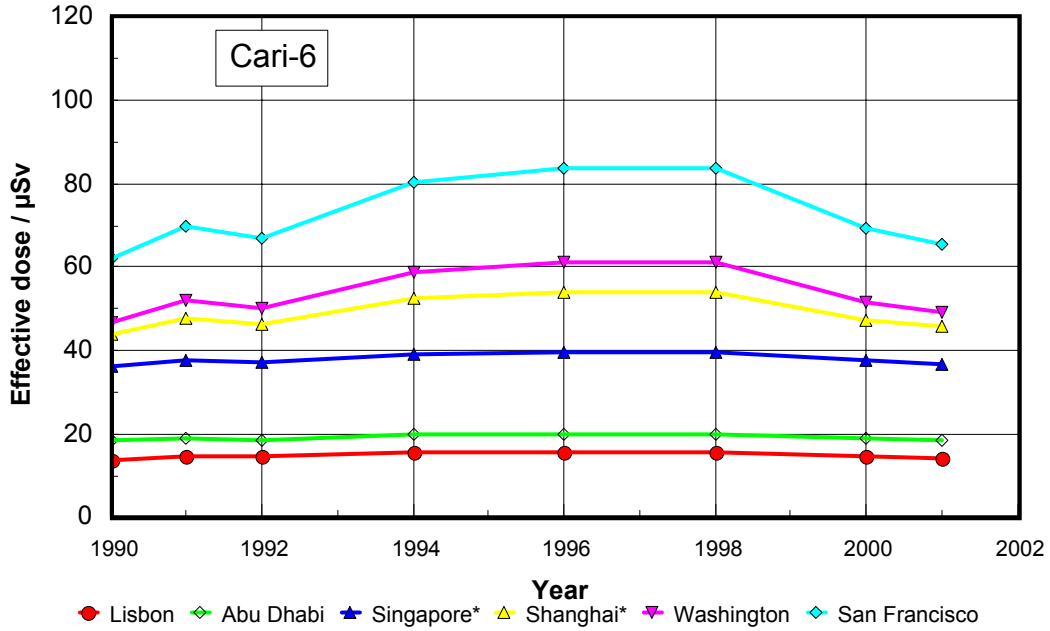

Figure IV.23 Influence of the solar modulation on effective dose (CARI-6).

IV.7 Comparison of calculated dose rates with selected experimental findings

The following experimental data were obtained during a number of flights with a series of different experimental devices on board. These data refer to the operational quantity ambient dose equivalent, $H^*(10)$. The instruments are calibrated in terms of this quantity. However, uncertainties may still occur from a lack of knowledge of their energy dependence of response, or with respect to their different responses to the different types of cosmic radiation components. Therefore, the data of some devices may require corrections with respect to the effects mentioned.

The experimental data are compared with calculated data employing EPCARDv3.2 (2002).

From the full set of experimental data available, obtained during different periods of the solar cycle, the data shown in the table below were selected.

Table IV.2 Selected experimental findings used for some detailed analysis

Institution	Period of time	Experimental devices	Figure
RMC	1999	TEPC	IV.24 - 28
GSF	1992-1993	ABH[§] and scintillation dose rate meter	IV.29-31
PTB/ACREM	1997-1999	NM500x[§], scintillation dose rate meter and high pressure ionisation chamber	IV.32-33

[§] Commercially available as NM500x. NM500x and SMN500x are the trade names of Fa.MAB-Münchener Apparatebau, D-82008 Unterhaching, for the Anderson&Braun REM counter with extended energy range ("ABH").

Following preliminary observations are made:

1. RMC-Data

It is assumed that the TEPC measures total ambient dose equivalent. Therefore, the total dose equivalent obtained from the calculation including contributions from neutrons, protons, charged pions, photons, electrons and muons are used for comparison.

The overall result is shown in Fig. IV.24: the ratio of calculated to experimental data is plotted versus cut-off rigidity. As evaluated experimental data, the filtered (smoothed) data are used. A linear fit through the data results in a ratio of 1.08 at 0 GV and 0.82 at 16 GV.

This trend does not appear very dramatic with respect to radiation protection purposes. One reason from the experimental side may be that at low dose rates the device has apparently some kind of lower experimental threshold somewhere below 1 μSv/h. This is observed e.g. in Figure IV.25. By this truncation the average dose rates may be slightly biased and elevated.

In Figures IV.25 through 27 some of the individual flights are depicted. In order to reduce the statistical uncertainties, the experimenters calculated in a first step 5-minutes averages. In a second step, they employed a digital filter (S-G) after Savitzky and Golay [SAG64]. Therefore, some structure in the resulting data are not of physical nature, but are artificial due to the filter characteristics of the smoothing technique, reproducing the width of the filter employed. Taking this behaviour into account, most of the measurements appear in very good agreement with the calculations.

2. GSF-Data

The GSF data were obtained during solar maximum of solar cycle 22. Data were obtained with an NM500x neutron moderator detector with lead converter, and a low-level radiation scintillation dosemeter. It is assumed the neutron monitor detects the neutron radiation with well-known energy dependence of response. This response characteristic is applied to the calibration situation and the spectral situation as available for aviation altitudes. The scintillation dosemeter is assumed to measure the dose from protons, pions, electrons, muons and photons. In Figure IV.29 the neutron results are depicted, in Figure IV.30 the ionising components, and in Figure IV.31 the sum of both.

The agreement between experimental and calculated data appears to be remarkable. However, some more work with respect to the study of the response characteristic appears necessary.

3. PTB/ACREM-Data

Part of the experimental devices employed by PTB was the same as those of GSF. This is of special interest, because the measurements of both institutions covered nearly a full period from solar maximum to solar minimum. The PTB used a special calibration technique, adjusting the weighted sum of the readings of the NM500X Remmeter and the high pressure ionisation chamber (IC) to the TEPC findings. Where necessary, the adjusted reading of the scintillation dose meter was used instead of the IC reading. The overall results were shown in Figure IV.11a, b.

Here, a trial was now made to use the same calibration procedure as for the GSF measurements.

In Figure IV.33 the data of the scintillation dosemeter are compared with the sum of the calculated ionising contribution. It appears that the assumption of the correction factor R may lead to an overestimation of the experimental data for this radiation contribution.

In the present view it appears that all data are very consistently in agreement with the calculated data. Further analysis is under work.

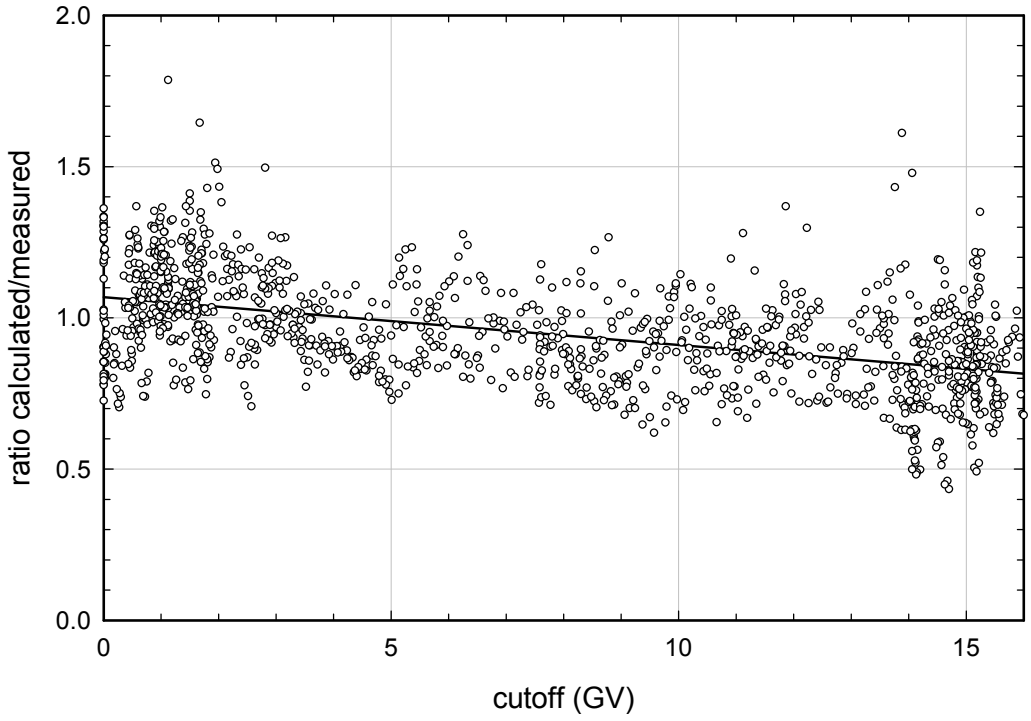

Figure IV.24 Ratio of total ambient dose equivalent rate, $\dot{H}^*(10)$, calculated with EPCARD32 to experimental results obtained during RMC flights #4,5,7,8,10,18,19,21,24-38, and 54-56.
The S-G-filter is applied to the 5 min averaged experimental data of the TEPC. A trend analysis results in a value of 1.10 at 0 GV cutoff, and in a value of 0.8 at 16 GV.

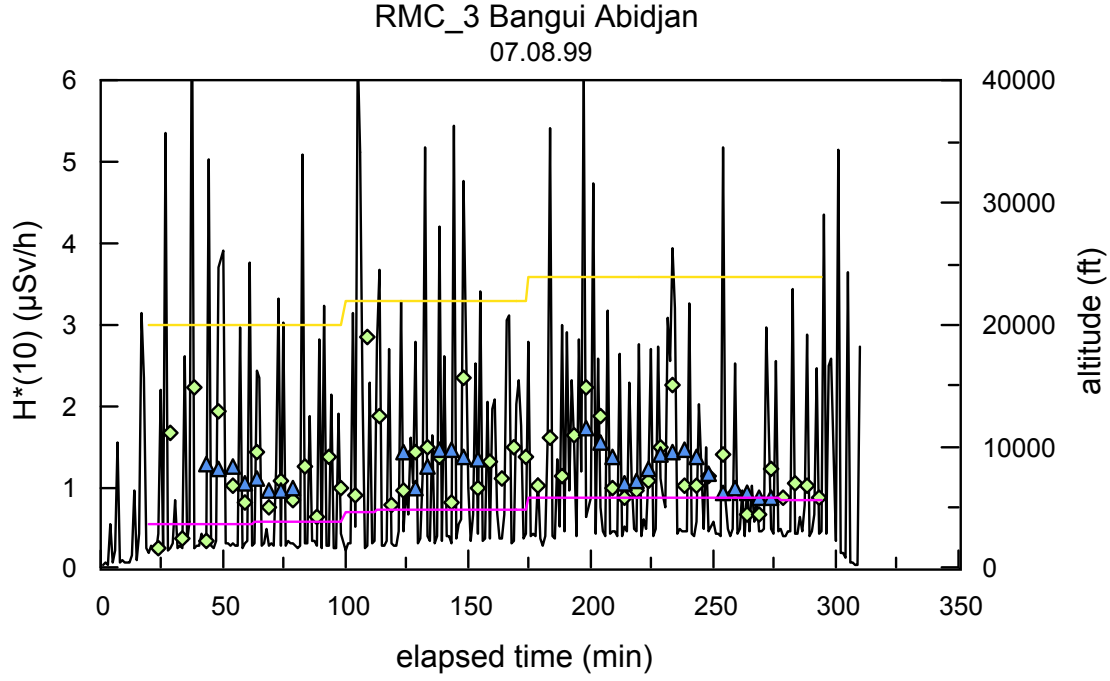

Figure IV.25 Experimental data obtained during RMC-flight #3 compared with the calculated total ambient dose equivalent, $\dot{H}^*(10)$. The vertical lines represent the individual data, the open diamonds the 5 min averages, the closed triangles the S-G-filtered data, and the lower step curve the calculated data (all left scale). The upper step curve depicts the altitude profile flown.

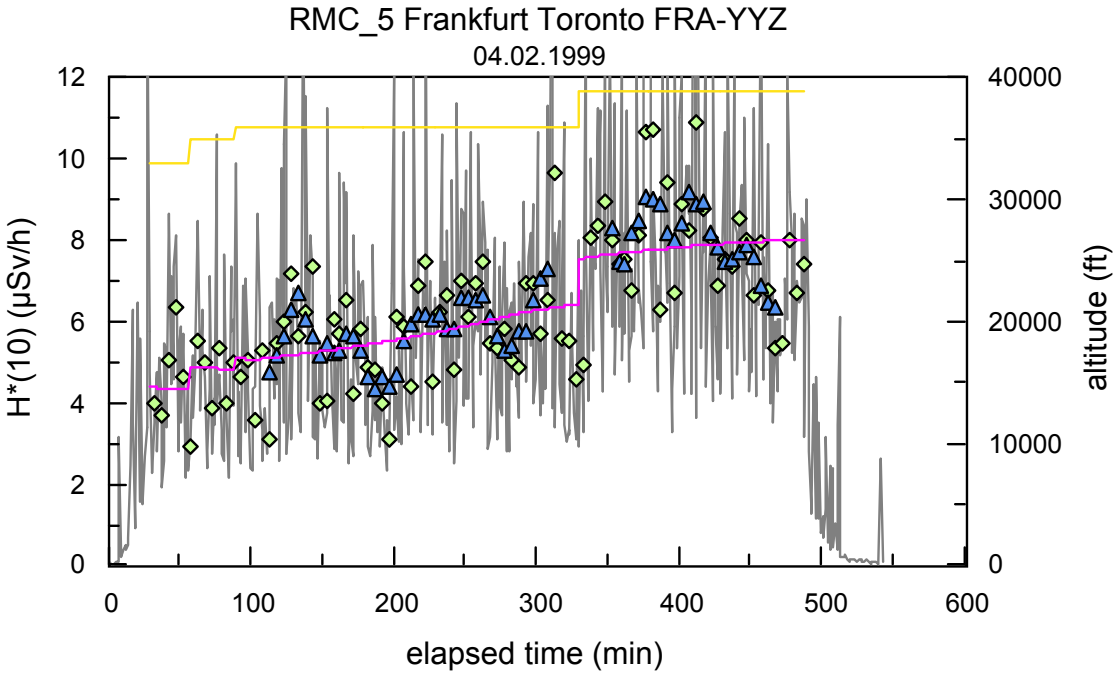

Figure IV.26 Same as Figure IV.25, experimental data obtained during RMC-flight #5.

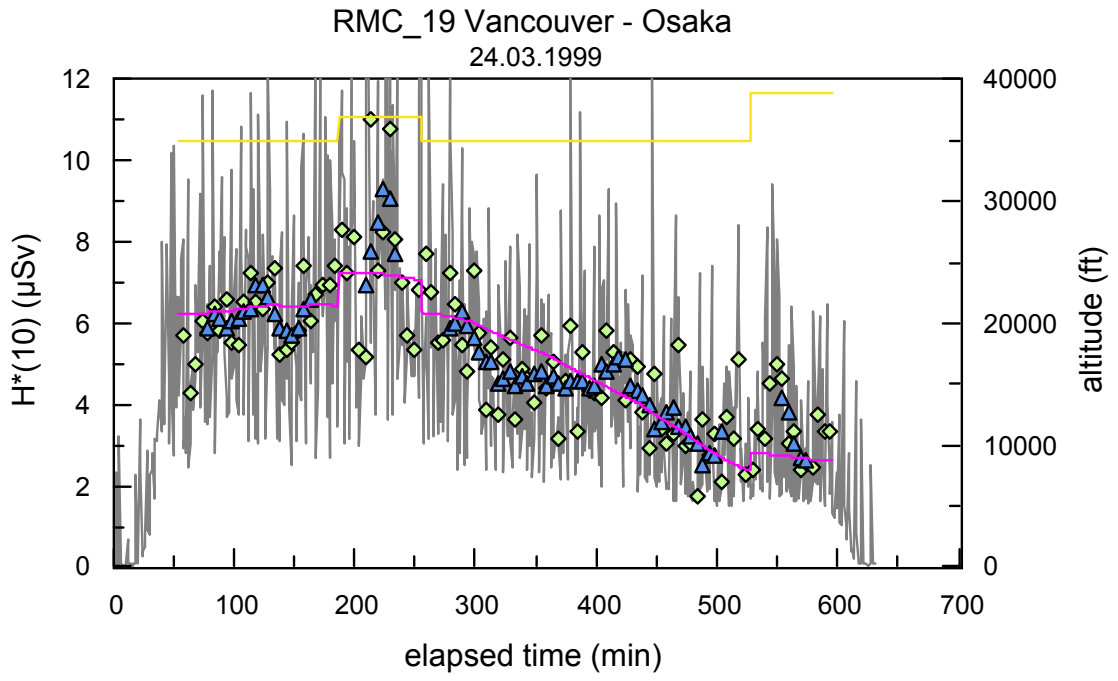

Figure IV.27 Same as Figure VI.25, experimental data obtained during RMC-flight #19 en route from Vancouver to Osaka

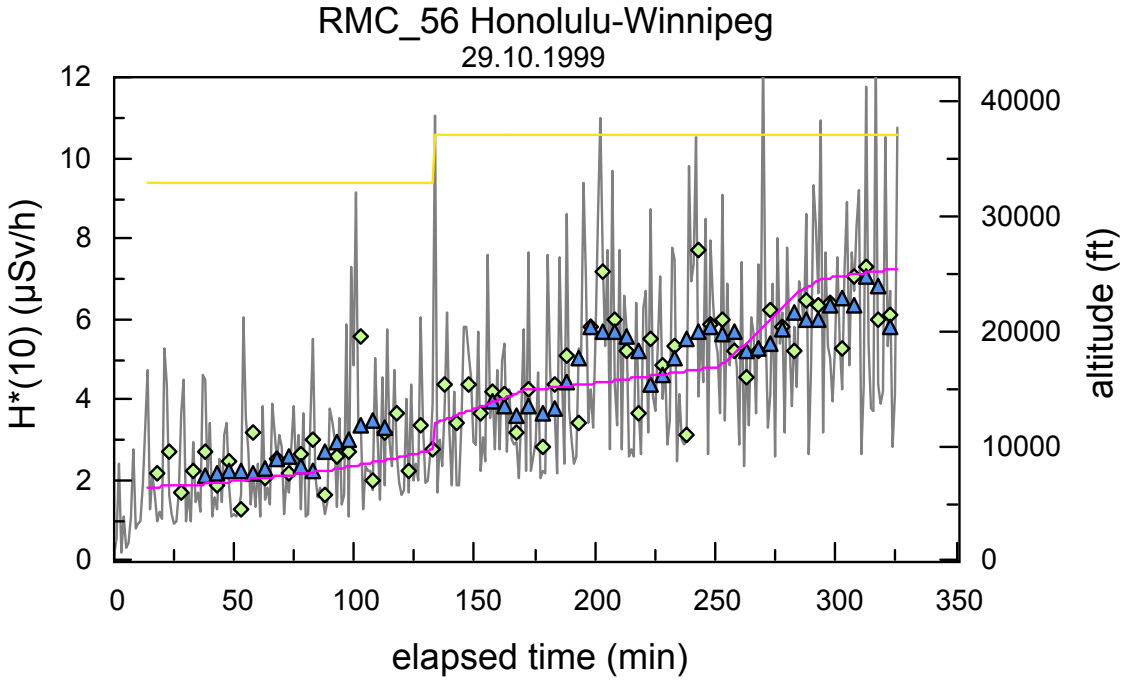

Figure IV.28 Same as Figure IV.25, experimental data obtained during RMC-flight #56 en route from Honolulu to Winnipeg

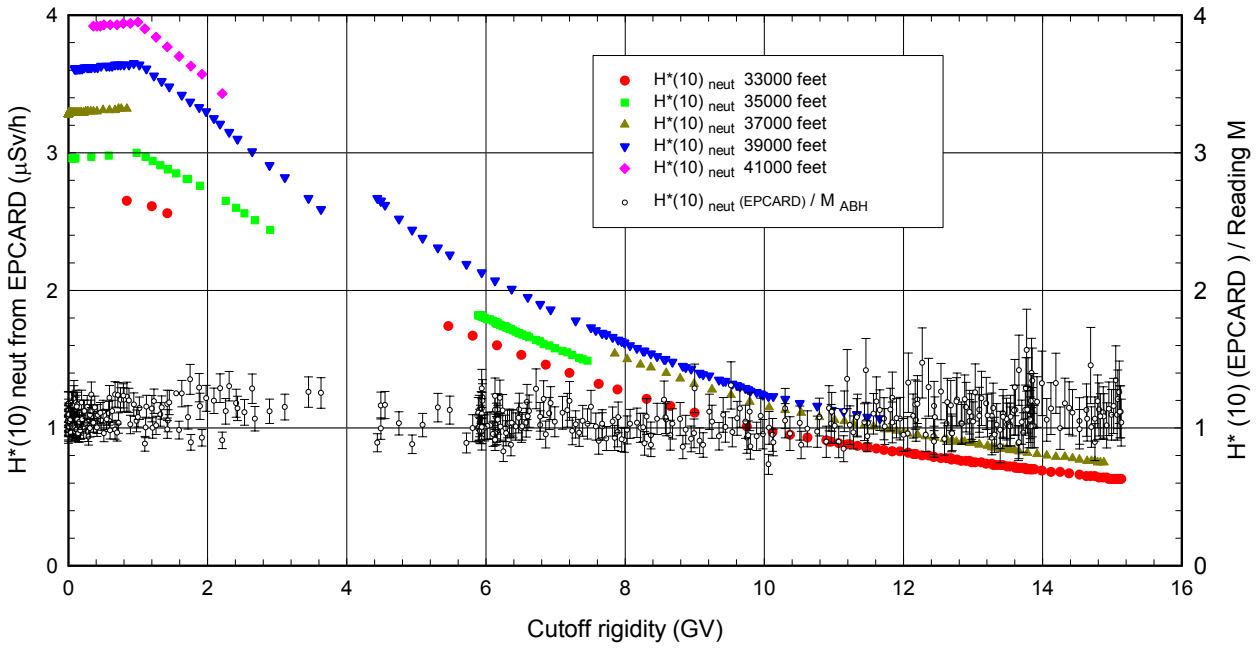

Figure IV.29 Experimental and calculated data obtained by GSF.
Ratio of the calculated neutron ambient dose equivalent rate and the experimentally determined ones (right scale) for five flights between geomagnetic north pole (cutoff rigidity =0GV) and geomagnetic equator conducted by the GSF. The full (coloured symbols) represent the ambient dose equivalent rate calculated with EPCARD (left scale), the open circles the ratio of the calculated data to the experimental ones with error bars for the ±1s statistical uncertainty of the experiments. The experimental data are corrected for the differences of the neutron spectra in the atmosphere to those of the calibration conditions, but not for the contribution of protons to the reading. The mean ratio is 1.07·(1±0.1).

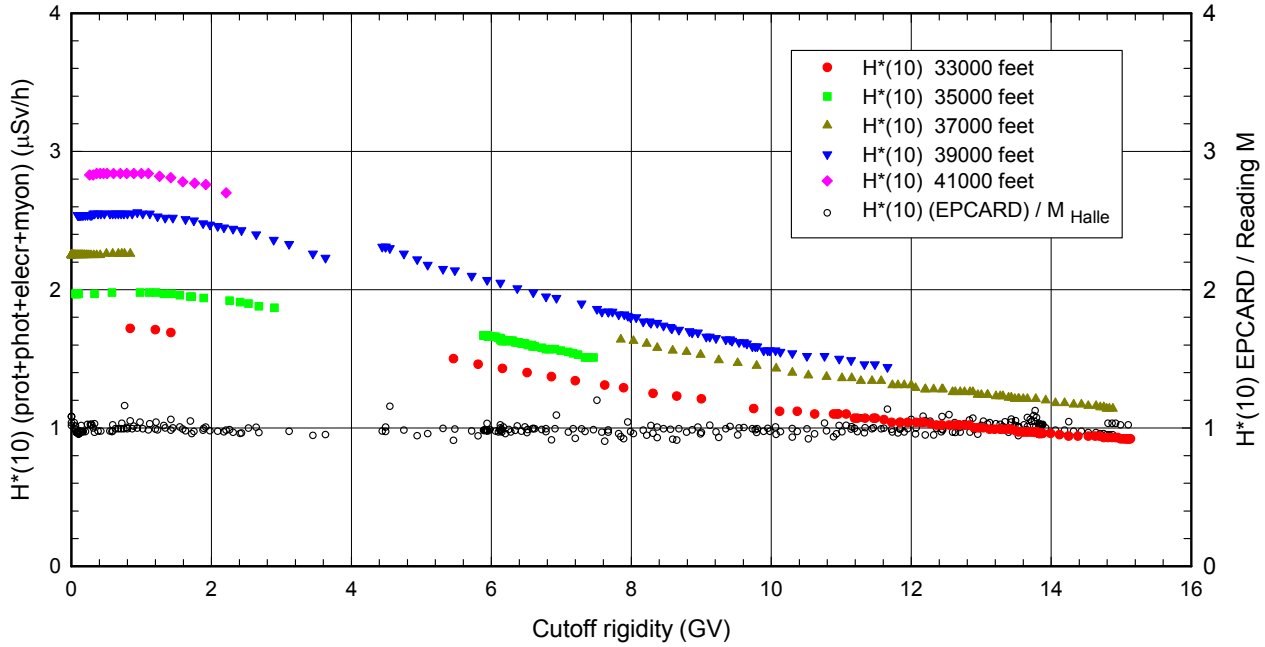

Figure IV.30 Same as Fig. IV.29 for the sum of dose equivalent rates of protons (plus pions), photons, electrons and muons. Measurements were conducted with a scintillation counter.

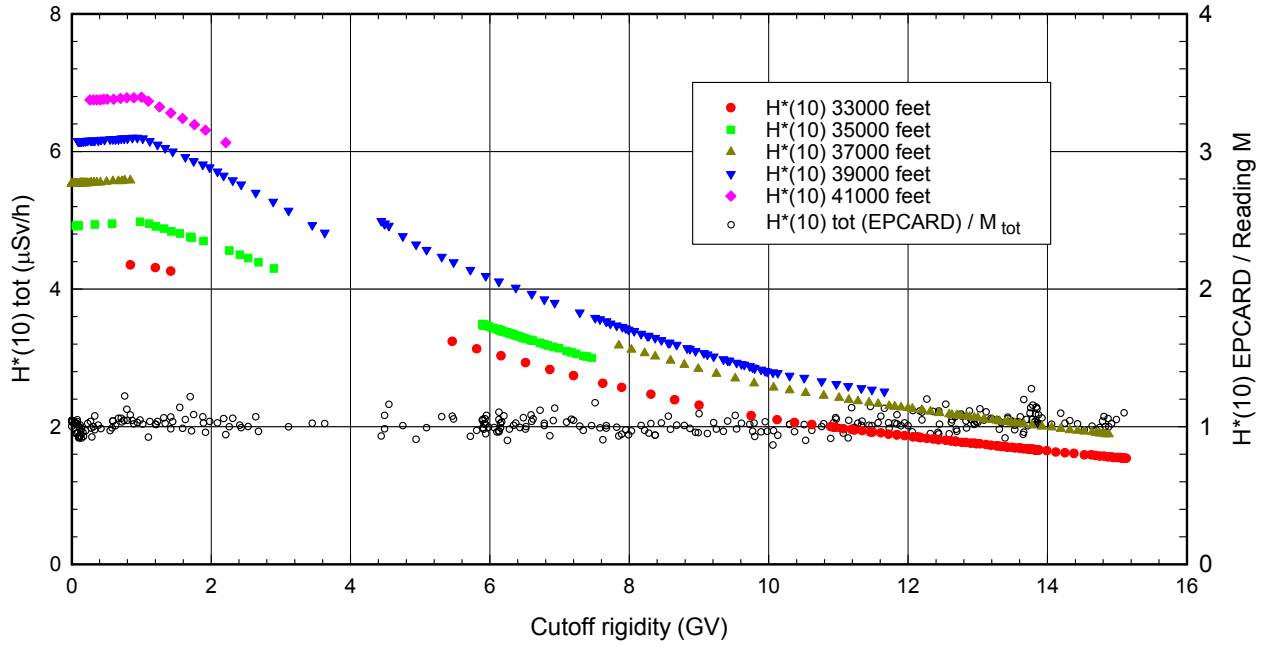

Figure IV.31 Same as Figures IV.29 and 30, results for the total ambient dose equivalent.

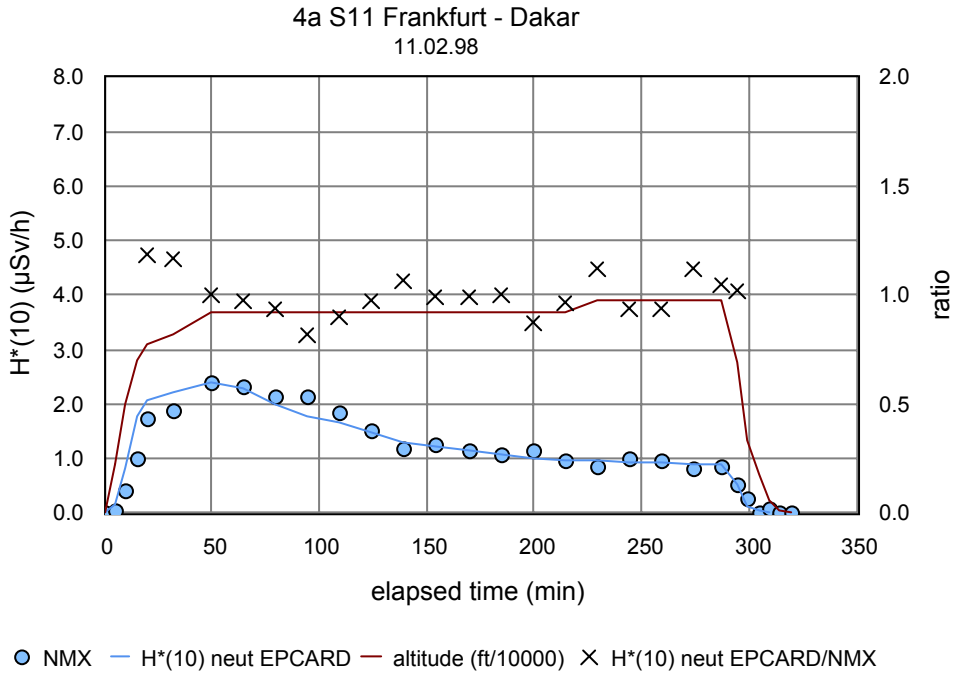

Figure IV.32 Experimental and calculated data obtained by PTB/ACREM with NMX neutron monitor at around solar minimum. The ratio of calculated to experimental data is depicted with crosses (X). The flight covers cutoff rigidities between 4 and 14 GV.

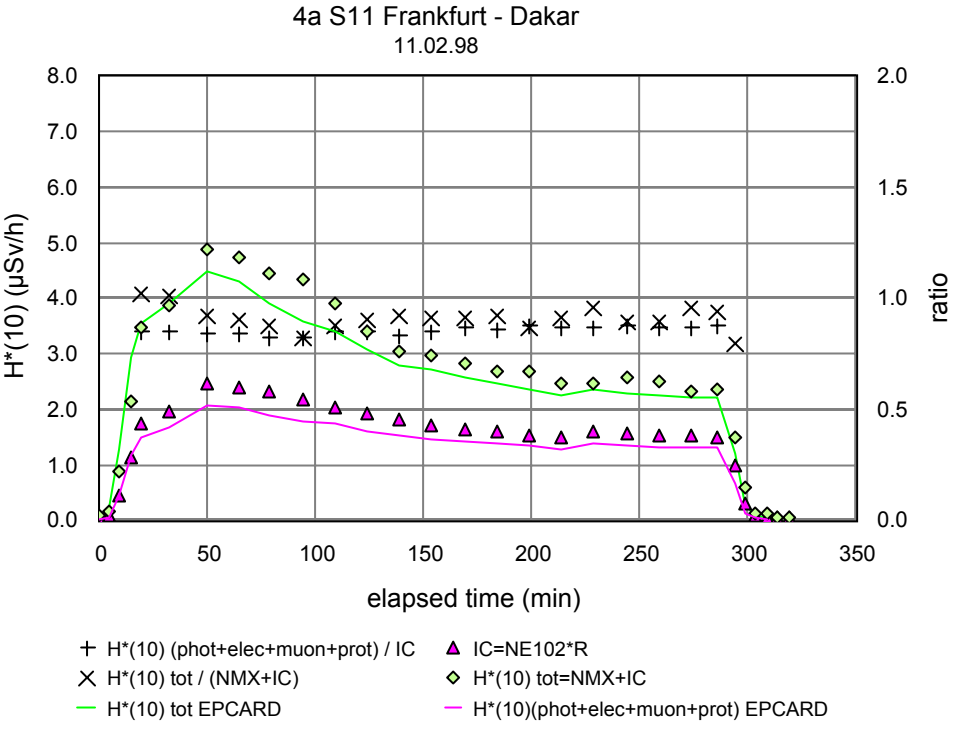

Figure IV.33 Same flight as in Figure IV.32. Shown are: measurements with the scintillation detector (NE102) sum of calculated ionising contribution (SUM), experimental dose rate (H*tot) for the total doses and calculated total dose rate (H*totEPC32).

IV.8 References

[CJG04] http://www.cami.jccbi.gov/AAM-600/Radiation/600radio.html

[SLH02] Schraube, H., Leuthold, G., Heinrich, W., Roesler, S., Mares, V. and Schraube, G. EPCARD - *European program package for the calculation of aviation route doses - User's Manual*. GSF - National Research Center on Environment and Health, GSF-Bericht 08/02 ISSN 0721 – 1694 (2002), and http://www.gsf.de/epcard.

[ISO00] ISO 14146:2000. *Radiation protection—Criteria and performance limits for the periodic evaluation of processors of personal dosemeters for X and gamma radiation*. International Organisation for Standardisation, Geneve, 5 p. (2000)

[OFD92] O'Brien, K., Friedberg, W., Duke, F. E., Snyder, L., Darden, E. B. J. and Sauer, H. H. *The exposure of aircraft crews to radiation of extraterrestrial origin.* Radiat. Prot. Dosim. **45**(1), 145-161 (1992).

[BAD97] Badhwar, G. D. *The radiation environment in low-earth orbit*. Radiation Research **148**, S3-S10 (1997).

[SAG64] Savitzki, A. and Golay, M. J. E. *Smoothing and differentiation of data by simplified least squares procedures.* Analytical Chemistry **36**(8), 1627-1639 (1964).

V Uncertainties in aircraft crew dose assessments

V.1 Introduction

Any estimation of exposure is accompanied by uncertainties. The acceptability of the magnitude of an uncertainty depends on the purpose for which the estimation is made. Aircraft crew exposure is estimated mainly for radiation protection purposes and the general requirements on uncertainties in this field are therefore given first in this chapter. Following this, the uncertainties, which accompany the experimental determinations, are presented and analyzed. A survey of experimental dosimetry methods and their calibration is presented. Both the statistical (Type A) uncertainties and those evaluated by other means (Type B) are summarized [ISO95]. The uncertainties related to calculation procedures are briefly described. Finally, some examples of actual exposure level variations based on a theoretical estimation and/or actual long series experimental measurements are given.

V.2 Radiation protection requirements on the estimation of the effective dose

International and national requirements for the assessment of doses to individuals, where they exist, are derived, in general, from ICRP and ICRU recommendations. In ICRP Publication 75 'General Principles for the Radiation Protection of Workers' [ICRP97] the following is stated: *'The overall uncertainty at the 95% confidence level in the estimation of effective dose around the relevant dose limit may well be a factor of 1.5 in either direction for photons and may be substantially greater for neutrons of uncertain energy, and for electrons. Greater uncertainties are also inevitable at low levels of effective dose for all qualities of radiation'.* ICRU in Report 47 [ICRU92] recommends that '*in most cases, an overall uncertainty of one standard deviation of 30% should be acceptable'* (instrumental uncertainties only, see also ICRU Report 66 [ICRU01]). This is broadly consistent with the ICRP requirements.

The radiation exposure of aircraft crew is due to complex multi-component fields, in which the dose is complicated to determine. Nevertheless, one of the objectives of the dose determination programme should be to meet the general requirement for the assessment of an effective dose at or near dose limits, so that the uncertainty of calculations or measurements should be no greater than a factor of 1.5 at the 95% confidence level. This may be applied to doses at or near an annual dose of 1 mSv to take account of the dose target for the 'child to be born'.

V.3 Uncertainties related to measurements and calculations

V.3.1 General requirements

The range 0.7 to 1.5 at the 95% confidence level noted above, corresponding to one standard uncertainty of about 21%, is usually considered to apply to the estimate of E. The quantity determined by measurement, however, is the operational quantity ambient dose equivalent, $H^*(10)$. This quantity may be treated as a surrogate for the protection quantity, E, with or without a correction factor applied appropriate for the radiation field in aircraft.

The uncertainty of laboratory calibrations for the operational quantity, $H^*(10)$, is commonly far less than 21%, typically 5%, in a specific well known radiation field. However the dose equivalent response of devices is frequently appreciably energy and angle dependent. The response characteristics of all devices should be determined prior to use. Either the determination of the response is required for the radiation field in which it is to be used, or it should be possible to calculate the response in this field from the knowledge of the field and of the detailed energy and angle dependence of response of the device. Sufficient angle response data should be available such as to enable, at a minimum, the estimation of the isotropic response. Where needed and where available, the ICRU conversion

coefficients to the relevant quantity should be used [ICRU98] extended to higher energies using the values of Pelliccioni and colleagues [PEL00]. For instruments, which are intended to measure a specific component of the radiation field, the response to the other components needs also to be investigated. Some detectors might have intrinsic radioactivity in the detector, which may need to be corrected for.

V.3.2. Reported instrument and detector characteristics

To assess the components of the uncertainties and the overall accuracy of values of ambient dose equivalent determined by measurements, detailed information about the instruments and their calibrations are needed and these are given in Appendix A.

It can be concluded from the information in Appendix A that:

- The reference fields at the Physikalisch-Technische Bundesanstalt (PTB), calibration in which assures traceability to international standards, have been most important for the interpretation of most instruments' results. Other fields used for calibration are the low LET radiation fields at national secondary standards laboratories, which also assures traceability, the high-energy neutron fields at Université Catholique Louvain, and the The Svedberg Laboratory (TSL), Uppsala, as well as the high-energy proton fields at TSL. Neutron detectors were in many cases calibrated also using common radioisotope sources (AmBe, Cf, PuBe). The CERF (CERN EU Reference Field) high-energy reference neutron facility at CERN has been widely used for calibrations and comparisons of instruments [MIT02]. Agreement with other instruments in the CERF field is often taken as a demonstration of the capability of an instrument to determine the neutron dose component on board aircraft acceptably well.
- Some laboratories have adopted similar approaches to calibrate the instruments. For example, Kiel University, RMC, ARCS and PTB might be expected to report similar results under otherwise identical conditions, as they would appear to use the same calibration procedure, in principle an in-flight calibration against a TEPC instrument from PTB. On the other hand, the DIAS stack derives a high-LET ambient dose equivalent component from an independent method of calibration. The NRPB passive survey instrument uses field-specific calibration coefficients derived from determinations of the instrument's energy and angle dependence of response folded with the energy distribution of the field in aircraft assuming isotropic irradiation. The ANPA stack, and NPI (MDU unit) make use of a combination of a low-LET beam calibration and a calibration in the CERF field, as well as the neutron sources already mentioned. The NAUSICAA instrument used by IRSN, and the CIEMAT detector set, are calibrated in fields of radioactive neutron sources and a low LET source. The SSI instruments are calibrated in a low-LET gamma beam and the response to other LET components is estimated from the knowledge of the response to some of those radiation types.

V.3.3 Measurement statistical uncertainties (Type A)

The statistical uncertainty of onboard measured exposure depends on the type of detector and/or the method used for its evaluation, and on the dose rate and total dose. The uncertainty reported by the different groups for TEPCs is typically about 5% (one standard uncertainty) for a one hour measurement. The sizes of the TEPCs are sufficient to make the absorbed dose determination accurate (at for instance 2 μGy within a couple of percent). However, an important uncertainty is caused by the relatively low frequency of high LET events, which deposit only a minor fraction of the dose, but which may contribute a much larger fraction of the ambient dose equivalent. This will determine the statistical uncertainty in the quality factor. The uncertainties are illustrated in Figure V.1, which shows a flight profile measured with the acquisition time 10 minutes by means of a TEPC (NAUSICAA) (Appendix A3) along a route from Tokyo to Paris [BOT00]. The lower smooth curve shows D, while the higher, strongly fluctuating curve shows the total $H^*(10)$. To reduce the influence of the statistical uncertainties in the comparison of measured and calculated data, routes for which the integral dose

equivalent value is less than 10 μSv have been avoided in the comparisons (see Chapter IV). Qualitatively the same statistical characteristics as for a TEPC are valid also for Si-diode spectrometer devices, DOSTEL and LIULIN (see Appendix A).

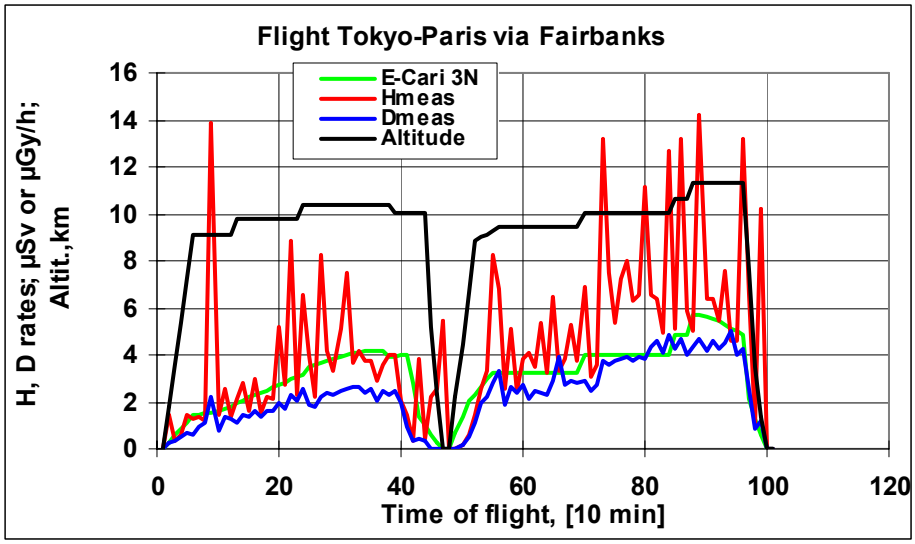

FigureV.1: Flight profiles for flight Tokyo – Fairbanks – Paris; measured data obtained with NAUSICAA TEPC.

For active detectors, which do not determine LET distributions- ionization chambers, scintillation counters, G-M tubes and moderator based neutron monitors, the statistical uncertainty is reported to be low even for short acquisition times. Passive detectors are generally less sensitive. Single track etch detectors may need to be exposed for a few hundred hours for acceptable statistical uncertainty. To reduce this, stacks of detectors are often used. The measurement time needed to receive a statistical uncertainty of ± 15 % (2s) for different detectors are estimated in Table V.1. With active low LET measuring instruments the goal is achieved within few tens of minutes. If single passive personal dosemeters are used the corresponding times are long and may become comparable with the annual limits of flight hours for air crew.

Table V.1: Typical number of flight hours necessary to achieve at 4 μSv h^{-1} a relative statistical uncertainty of less than ±15 % (2*s*). It is assumed that half of the total dose equivalent comes from each of the two LET components, or from the neutron and non-neutron components.

Detector Equipment	Measured component	Approximate Time (hours)
NRPB passive survey box	total	30
Various single - TLD	non-neutron	50 - 500
Various single - track etch detector	neutron	300 - 1000
Single - bubble detector (1 bubble per 1 μSv)	neutron	150
Electronic personal dosemeter (H_{min} ~ 1 μSv)	non-neutron	4
Ionisation chamber, scintillator, Geiger Muller	non-neutron	0.2
Tissue Equivalent Proportional Counter	total	0.5 -2
Tissue Equivalent Proportional Counter	non-neutron	0.2
Si-diode energy deposition spectrometer LIULIN	total	2
Si-diode energy deposition spectrometer LIULIN	non-neutron	0.2
"Rem-meters", LINUS included	neutron	0.5

V.3.4 Measurement Type B uncertainties

The more important uncertainties belonging to this category have been listed under general requirements above (V.3.1). For measurements in complex mixed radiation fields a distinction can be made generally between the type B uncertainties for devices for which the reading is directly related to the energy absorbed, and those for devices for which the reading is proportional to the frequency of a specific effect, for example that of events giving an energy deposit above a given threshold. However, for the range of particle types and energies (and LET) of the fields in aircraft, it is found to be necessary that all devices to determine ambient dose equivalent (with the possible exception of the DIAS approach for the neutron and heavy charged particle components), need to be calibrated in reference fields in terms of ambient dose equivalent. In some cases, the analysis of the results of the calibration requires additional input from calculations of the device response characteristics. Reference fields are not available for all the components of the fields in aircraft. Various calculations and corrections become necessary introducing an additional component of type B uncertainty. Since the energy distributions of the different components of the field in aircraft are approximately independent of altitude and cut-off, for both general types of device a calibration established in a similar radiation field would reduce the uncertainty of an instrument reading. A suitable field for the neutron component is the CERF neutron field at CERN, however the traceability to international standards has to be established.

For dosemeters which are intended to measure only the low-LET dose equivalent component the unwanted response to neutrons introduces another uncertainty. However, whereas neutrons contribute about 50% of the total dose equivalent in a field onboard aircraft, the contribution to the total absorbed dose in tissue and tissue equivalent proportional counters is only about 10%. In metal walled ionization chambers and in TLDs, the neutron kerma (for the energy distribution for the fields being considered) is lower than in tissue. For TLDs, in general, the relative light conversion efficiency for the secondary charged particles is also low overall. As a result, the component of type B uncertainty due to unwanted neutron response is unlikely to exceed about 5% in terms of total $H^*(10)$.

Moderator based neutron monitors need to be modified to improve the high-energy response, for example with lead or other high atomic number material. Most of those neutron monitors are also sensitive to high-energy protons: this effect is unlikely to increase the reading by more than about 10%.

The descriptions in Appendix A give some information on the magnitude and importance of type B uncertainties, but they are not always described in a comparable way. Type B standard uncertainties for TEPC measurements of total ambient dose equivalent are typically about 15% for example. Some indications of the uncertainties for low LET instruments can be deduced from onboard experimental results. It was observed, for example, that the response of Si-diode based electronic personal dosemeters is typically about 30% lower than the reading of a metal walled ionisation chamber, and GM-tube based instruments have given, in some cases, much larger results than would be expected for calibration in a ^{137}Cs photon field and the assumption that the instrument is only sensitive to low-LET radiation. (See Appendices A1, A4, A7, [KYL01], etc.).

V.4 Variations of flight profiles

Owing to the variation in flight profiles for the same route, estimates of route doses from single, or small numbers of measurements, may not be representative. The variability of route doses can be estimated from extended series of measurements for the same route.

Since March 2001, several long-term monitoring runs onboard a Czech Airlines aircraft have been made using a Si-spectrometer LIULIN (see Appendix A4). More than 600 individual flights were covered during this study [SPD03], mostly over the North-Atlantic. Navigation data were available for

all these flights. The results obtained allowed the estimation of the variations of route dose values for normal commercial flights. The results are presented in Table V.2, together with the variations of dose values calculated by means of codes CARI 6 and/or EPCARD 3.2.

Table V. 2 Variations of route doses for the flights between Prague and New York: period March-December 2001, 73 flights to, 73 flights from New York.

Method	Prague – New York[1)]				New York – Prague[1)]			
	Min	Max	Average	$2s$[2)]	Min	Max	Average	$2s$[2)]
	μSv			[%]	μSv			[%]
CARI6–E (ISO)	31.2	43.2	36.6	15.0	27.2	39.2	32.0	16.0
EPC – E(ISO)	34.1	49.0	40.2	16.9	29.3	43.8	35.2	17.2
EPC – H*(10)	29.2	41.3	34.2	16.3	25.0	37.2	29.9	16.7
LIULIN - H*(10)	26.3	54.2	35.7	23.6	22.4	38.7	30.9	20.1

[1)] For New York – JFK and Newark airports together

[2)] Relative standard deviation for an individual flight

One can see that the variations of the calculated total effective dose values and/or those of $H^*(10)$ are very similar, equal to about 16%. It should be mentioned that these flights covered the period between 22nd March and 6th December 2001, with heliocentric potential varying between 814 and 1022 MV. The variations of values deduced from experimental measurements are about 4 to 8% higher, owing to the uncertainty related to experimental statistical variations, mostly in the neutron contribution. This effect is also seen in the more clearly different minimum and maximum values of experimental compared to calculated data.

Even if the calibrations had been made in an identical way and if the measurements had been made with similar instruments, the daily variation of the solar wind may influence the outcome of such a comparison. Measurements on identical geographical positions and altitudes but performed on different dates may not necessarily agree to better than 10% to 20 %.

V.5 Uncertainties related to calculations

The uncertainties related to the calculations are discussed in some detail in the previous two chapters. The main sources of uncertainty are the result of:

- Basic information on the galactic cosmic ray particle spectra, including the influence of solar activity on the spectrum at the top of atmosphere
- Uncertainties in cut-off rigidity taken from geomagnetic characteristics
- Methods of taking the changes in solar activity into account
- Basic characteristics of transport codes and the cross section data used
- Statistical uncertainties in the integral fluence and fluence energy distributions
- Choice of conversion coefficients used to convert secondary particle spectra to effective dose and ambient dose equivalent

The individual uncertainties related to these factors are important and in some cases not fully known. The agreement of the calculated results obtained with the different codes is illustrated in Table VI.3, where 28 flight routes, somewhat arbitrarily chosen from the results available in the report, and spread over most of the solar cycle, are investigated with most of the codes. The two independent codes EPCARD and CARI have been used to calculate the effective dose for all the flights and the mean value of the ratio is 1.14 ± 0.16 (one standard deviation). The mean value of the ratio of the values for $H^*(10)$ from EPCARD and FREE is 1.00 ± 0.12. These uncertainties reflect the differences in assumptions on which the codes are based. As a first estimate and assuming the codes are equally reliable, a specific route dose expressed in effective dose cannot be determined to better than about 15% and the corresponding value for $H^*(10)$ is about 10 %. This is in line with the data shown in the graphs in Chapter IV.

Van Dijk has looked at the uncertainties associated with assessing aircraft crew doses by means of calculation methods (DIJ03). He considered the actual variation in flight routes and the consequent variations in the (calculated) doses, and treated this as a type A (statistical) uncertainty. For the routes investigated, the values obtained ranged from 4 to 21%. The type A uncertainty in the estimate of annual dose would be much less. The effect of using the planned route, from a simple algorithm LIDO (Lufthansa Integrated Dispatch Operation) profiles, as opposed to the actual flight path, was treated as a type B (systematic) uncertainty, and values obtained were ranged from 2 to 19%. The effect of the model used (CARI, EPCARD, Lewis [LEW01] and Ferrari [FER01]) was also treated as a type B uncertainty, and a value of 10% estimated. Van Dijk concluded that the total uncertainties in the estimated doses for single flights, obtained by summing the three components in quadrature, ranged from 11 to 27% for the twelve routes examined. This was considered in acceptable agreement with the requirement of a total uncertainty of 21%. If an alternative method using a global average dose rate for all flights, with route doses calculated as the product of this value and the number of flight hours, the author concluded that it was doubtful that the uncertainty in the results would comply with the ICRP recommendations.

V.6. Conclusions

The descriptions of methods given in the Appendix show that many different kind of detectors have been used to produce the results included in this report, with some instruments calibrated using independent methods. It is therefore concluded that the data bank includes results from independent measurement methods. Two of the calculation methods (CARI/FREE and EPCARD) are based on almost completely independent models and thus relatively independent calculated results are also included in the report.

The measurement uncertainty of the experimentally determined ambient dose equivalent rates evaluated in Chapter III is about 25% (coverage factor of 2). The agreement between measured and calculated values of ambient dose equivalent route doses is generally within a range of a factor of 1.3 (see Chapter IV). The mean ratio of measured route doses to values calculated using EPCARD is 1.03 with an uncertainty of 0.26 (coverage factor of 2). The uncertainty in the values of ambient dose equivalent and effective dose calculated for routes are estimated to be about 25% and 30% respectively (coverage factor of 2) when calculated for the actual flight path, but the analysis of van Dijk indicates that for calculations using planned flight profiles (as opposed to the actual flight paths), the uncertainty can extend up to about 50%. The information on experimentally determined uncertainties in Appendix A is not always sufficiently detailed for it to be easy to compare or summarize. However, for the TEPCs the Type B uncertainty is reported to be 30% (coverage factor of 2). The corresponding statistical uncertainty is typically 18% (coverage factor of 2) after one hour of measurement. For several other instruments, which do not require a determination of the LET, the statistical uncertainty is smaller. The combined uncertainty for a TEPC is about 35% (coverage factor of 2), which is larger than the uncertainty (25%) reported in Chapter III. However, for both calculated results and measured results the uncertainty is within the requirement set by the ICRP for radiation protection (± 42 % at the 95% confidence level). Further analyses are needed to better understand the uncertainties in aircraft crew dosimetry. The databank compiled during this project, together with the appendices, will be useful for such investigations.

V.7 References

[BOT00] Bottollier-Depois J.F., Chau Q., Bouisset P., Kerlau G., Plawinski L., Lebaron-Jacobs L., *Assessing exposure to cosmic radiation during long-haul flights*, Radiation Research. **153** 526-532 (2000).

[DIJ03] van Dijk J.W.E.: *Dose Assessment of Aircraft Crew in the Netherland.* Radiat. Prot. Dosim. **106** 25-32 (2003).

[FER01] Ferrari A., Pellicioni M., and Rancati T. *Calculation of the Radiation Environment caused by Galactic CosmicRays for Determining Aircraft Crew Exposure.* Radiat.Prot.Dosim. **93** 101-114 (2001).

[ISO95] BIPM, IEC, IFCC, ISO, IUPAC, IUPAP and OIML*: Guide to the Expression of Uncertainty in Measurement*, First Edition, corrected and reprinted 1995, ISBN 92-67-10188-9, (ISO: Geneva),(1995).

[ICRP97] International Commission on Radiological Protection. *Publication 75. General Principle for the Protection of Workers.* (Pergamon Press: Oxford)(1997).

[ICRU83] International Commission on Radiation Units and Measurements. *Publication 36. Microdosimetry. (ICRU:* Bethesda) (1983).

[ICRU92] International Commission on Radiation Units and Measurements. *Publication 47. Measurement of Dose Equivalents from External Photon and Electron Radiations. (ICRU:* Bethesda) (1992).

[ICRU98] International Commission on Radiation Units and Measurements. *Publication 57. Conversion Factors for Use in Radiological Protection Against External Radiation. (ICRU:* Bethesda) (1998).

[ICRU01] International Commission on Radiation Units and Measurements.. *Publication 66. Determination of Operational Dose Equivalent Quantities for Neutrons. (*NTP:Ashford), (2001).

[MIT02] Mitaroff, A. and Silari, M. *The CERN-EU High-Energy Reference Field (CERF) Facility for Dosimetry at Commercial Flight Altitudes and in Space*. Radiat.Prot.Dosim. **102** 7-22 (2002).

[KYL01] Kyllönen, J.-E., Lindborg, L. and Samuelsson, G. *Cosmic Radiation Measurements On-board Aircraft with the Variance Method.*. Radiat. Prot. Dosim. **93** 197-205 (2001).

[LEW01] Lewis B.J., McCall M.J., Green A., Bennet L.G., Pierre M., Schrewe U.J., O'Brien K. and Felsberger E. *Aircraft Crew Exposure from Cosmic Radiation on Commercial Airline Routes.* Radiat.Prot.Dosim. **93** 293-314 (2001).

[PEL00] Pelliccioni, M. *Overview of Fluence to Effective Dose and Fluence to Ambient Dose Equivalent Conversion Coefficients for High Energy Radiation Calculated using the FLUKA Code*. Radiat. Prot. Dosim. **88** 279-297 (2000).

[SPD03] Spurný, F. and Datchev, Ts. *Long-term Monitoring of Onboard Aircraft Exposure Level with Si-diode based Spectrometer.* 34th COSPAR Scientific Assembly, Houston, October 2002, Adv. Space Research **32** 53-58 (2003).

VI Summary, conclusions and recommendations

VI.1 Summary

The results of measurements, which are reported here, mainly from laboratories in Europe, have been obtained using a wide variety of instrument types, and different methods of calibration, response characterization and interpretation. The results obtained with this broad range of instruments and methods show very good agreement. This has been clearly demonstrated in the results given in this report for the experimentally determined values of dose rates and route doses (see Chapters III and IV). Almost all results are within ±25% (about two standard deviations) of the mean value, and the good agreement implies that standard uncertainties are probably somewhat less than estimated by the laboratories who have made the measurements (see Chapter V and Appendix A). The overall accuracy is as good as, if not better than that achieved generally in routine operational radiation protection measurements. This good agreement is illustrated in the following four tables. In Table VI.1 results are shown of ambient dose equivalent rates for similar altitudes, cut-offs and stage of solar cycle determined as part of an EC supported research project completed in 1998 [OSU99] and 1999 [BEC99]. In Tables VI.2, VI.3 and VI.4, results are shown of determinations of route doses obtained with different instruments and methods during the same flight, made under a current EC-funded research programme [BOT04].

Table VI.1: Measured ambient dose equivalent rates at temperate latitudes (40° – 60^0 N) measured during the time period 1995-1998.

Altitude	Investigator	$H^*(10)$ rate ($\mu Sv\ h^{-1}$)	
		Neutron	Total
10 km (33 000 ft)	ANPA passive (TLDs, bubble detectors, etched track detectors, fission foils and electronic dosemeter)	2.9 (0.3)[(a)]	4.6 (0.6) [(a)]
	ANPA active (ionization chamber, extended range remmeter,)	2.8 (0.5)	4.9 (0.5)
	ARCS (TEPC)	2.7 (0.4)	4.6 (0.7)
	PTB (extended remmeter and ionization chamber)	2.8 (0.3)	4.9 (0.5)
10.6 km (35 000 ft)	DIAS (Etched track with full analysis)	3.2[(b)] (0.3)	----
	USAAR (HANDI TEPC)	3.5 (0.8)	5.7 (0.8)
	SSI (SIEVERT variance TEPC)	3.1 (0.3)	5.1 (0.3)
	NRPB (TLDs, and etched track)	3.8[(c)] (0.6)	5.4 (0.8)
	ARCS (TEPC)	3.4 (0.9)	5.6 (0.8)
	PTB (extended remmeter and ionization chamber)	3.6 (0.9)	5.9 (0.6)
16 km (53 000 ft)	NRPB	7.8[(c)] (1.0)	12.1 (1.6)
	DIAS	7.1[(b)] (0.6)	----
	ANPA passive	6.1 (0.5)	11.0 (0.5)
20 km (67,000 ft)	NRPB	9.2[(c)] (1.3)	13.4 (1.8)
	NASA (multisphere spectrometer)	8.5	----

[(a)] One standard deviation on instrument reading
[(b)] All primary and secondary charged particles of $LET_{200} > 5\ keV\mu m^{-1}$.
[(c)] Neutron plus neutron-like interactions of protons

There are a number of methods of calculation which use the results of radiation transport codes to compute values of ambient dose equivalent or effective dose (generally without taking account of the presence of the aircraft, passengers, fuel etc.) in order to assess the doses of aircraft crew, for example CARI (using LUIN), EPCARD (using FLUKA), FREE (using PLOTINUS), PC-AIRE (using results of experimental measurements inside aircraft), SIEVERT (using the data from CARI or EPCARD), and the algorithm of Pelliccioni (using FLUKA). The effect of shielding, scattering and secondary particle generation by the aircraft fabric, passengers, cargo and fuel, would be to decrease doses by about 10 %, depending on aircraft type, loading etc. [FER04], that is, the results of most methods of calculation should be conservative. From the examples of route doses given in Table VI.5, it can be seen that there is generally good agreement between the results of different methods of calculation, for all altitudes and geographical locations. There are larger differences, up to 30%, between the results of different transport codes for effective dose rates than between results for ambient dose equivalent rates - agreement within 20 to 25% (two standard deviations). This seems mainly to be a result of differences in the calculated primary proton fluence rate amplified by the use of a proton radiation weighting factor of 5 in the definition of effective dose, as distinct from the mean quality factor for protons of about 1.5 for ambient dose equivalent. (It should be noted that ICRP are, at present, considering changes to both the neutron and proton radiation weighting factors). The greatest sources of uncertainty in the values from calculations are from the imprecise knowledge of the primary proton fluence rate at the top of the atmosphere and its energy distribution, and the significant uncertainties in the (double differential) interaction cross sections.

Table VI.2: Integral **a**mbient dose equivalent values obtained using different TEPC systems for the one-way flight NRT-FAI-CDG in 2002.

System - Laboratory	$H^*(10)$ Low LET (μSv)	$H^*(10)$ High LET (μSv)	Total (μSv)
Hawk TEPC - ARCS	25	41	66
Hawk TEPC - IRSN	27	32	59
Hawk TEPC - RMC	22	32	54
Sievert TEPC – SSI	25	47	72
Average	24 (2)[(a)]	38 (7)[(a)]	62 (7)[(a)]

[(a)] One standard deviation

Table VI.3: Integral ambient dose equivalent measured with different methods for the round trip CDG-FAI-NRT measured in 2002.

Method	Non-neutron component (μSv)	Neutron component (μSv)	Total (μSv)
TEPC	49	69	118
Silicon detector	58	84	142
GM counter	78	-	-
EPD	65	-	-
TLDs + etched track	51	77	124
Bubble detector	-	67	-
Average	54 (5)[(a)]	76 (9)[(a)]	129 (10)[(a)]

[(a)] One standard deviation

Table VI.4: Integral ambient dose equivalent and effective dose calculated with the different models for the round trip CDG-FAI-NRT and comparison with the experimental average value (measurements from 2002).

Model	Non-neutron component (μSv)	Neutron component (μSv)	Total (μSv)
EPCARD 3.2, *E*-ISO	83	61	142
EPCARD 3.2, *H**(10)	51	71	122
CARI 6, *E*-ISO	-	-	132
PCAIRE 6.5.3, *E*-ISO	-	-	130
PCAIRE 6.5.3, *H**(10)	-	-	106
Average *E*-ISO	83	61	$135 \pm 7^{*}$
Average *H**(10) calculated	51	71	$114 \pm 11^{*}$
Average *H**(10) measured	54 (5)[(a)]	76 (9)[(a)]	129 (10)[(a)]

(a) One standard deviation

VI.2 Conclusions

Results of measurements and calculations presented in this report show that there is good agreement between different methods of experimentally determining ambient dose equivalent rates at aircraft altitudes for the galactic component of cosmic radiation. Further, there is also agreement between the results of experimental determinations and calculations of this quantity. This gives partial support to the approach of basing determinations of effective dose for aircraft crew on the results of calculations, with verification of the calculation method by comparisons of experimental and calculated determinations of ambient dose equivalent. The experimental determinations of ambient dose equivalent should be traceable to national standards. The total uncertainty of measured values of average route doses is about 25% (coverage factor of 2). The total uncertainty in the values of effective dose calculated by the programs described in this report are estimated to be about 30% (coverage factor of 2), but perhaps extending up to 50% if the calculations are based on planned rather than actual flight profiles. The uncertainties for the assessment of doses to aircraft crew would appear to meet the accuracy requirements of ICRP and ICRU.

VI.3 Recommendations

Since the publication in 1997 of the Commission's recommendations on the implementation of Title VII of the Council Directive (RP 88)[EUR 97], there has been much research carried out on both measurement techniques and calculation methods, as shown by the results in this report. The Working Group believes that a revision of RP 88 would be timely and appropriate – the data included should be updated and the advice given may need to be reconsidered, as it may no longer be valid. An example of data, which may usefully be considered, is given in Figure VI.1. Accordingly, the Working Group recommends that the Article 31 Expert Group should give consideration to the revision of RP 88.

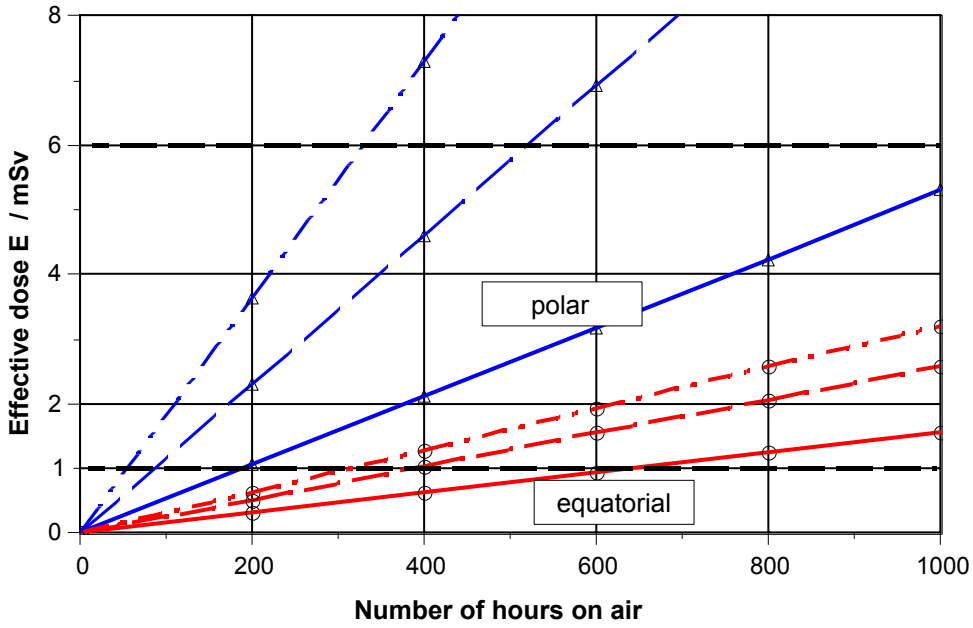

Figure VI.1 Diagram to enable a first estimate of the minimum number of flight hours, which are needed to obtain annual effective dose values of 1 mSv and 6 mSv. The calculations were performed for Jan. 1998, i.e. around solar minimum activity and therefore about the highest possible doses from cosmic radiation at flight altitudes. The three lowermost lines are for the equatorial region, the three uppermost for the polar region. For each region, the flight altitudes chosen are 30000 ft (upper line), 40000 ft and 50000 ft (lower line).

Table VI.5: Comparisons of route doses calculated by different programs. Calculated doses for selected flight routes obtained with the codes CARI, EPCARD, FREE and PCAIRE in terms of effective dose, *E*, and ambient dose equivalent, *H**(10). The doses are valid for the solar modulation conditions at the indicated date.

Flight route	Date	*E* EPCARD	*E* CARI-6	*H** (10) EPCARD	*H** (10) FREE	*H**(10) PCAIRE (Helio)
		(μSv)	(μSv)	(μSv)	(μSv)	(μSv)
Helsinki - New York (JFK)	27-Mrz-98	49.7	37.5	42.7	36.6	35.6
Copenhagen - Bangkok	13-Dez-98	30.2	26.3	26.5	24.7	26.5
Paris - Washington	14-Jan-98	54.5	41.9	45.5	41.7	
Paris - New York	21-Aug-96	43.7	35.4	32.8	30.4	
San Francisco - Paris	04-Mrz-96	76.2	62.4	64.4	62.6	
Paris - San Francisco	03-Mrz-96	84.9	69.9	71.3	69.8	
London - Tokio 1997/06	Jun-Jul 97	67.0	54.3	57.4	55.3	
Prague - Dubai	14-Mai-92	18.2	19.5	15.9	18.7	
Prague - Moscow	17-Dez-92	8.7	7.6	7.4	7.5	
Prague - Stockholm	11-Jan-93	7.6	6.3	6.4	6.1	
Paris - Prague	31-Jan-95	3.6	3.0	3.1	2.9	
Oslo - Prague	29-Mrz-99	7.1	5.3	6.0	5.5	
Frankfurt - Fairbanks	29-Sep-97	50.8	40.6	43.5	41.7	40.8
Frankfurt - New York	27-Okt-97	43.0	32.0	36.7	29.9	31.2
Frankfurt - Dakar	11-Feb-98	16.0	17.1	14.1	16.1	16.7
Frankfurt - Bahrain	22-Mrz-98	15.9	14.9	14.0	13.2	15.6
Madrid - Santiago de Chile	13-Mrz-01	27.5	34.4	24.9	32.5	24.4
Madrid - Mexico City	02-Apr-01	41.3	38.6	35.7	38.6	30.9
Madrid - Paris Orly	27-Apr-01	3.5	3.5	3.0	3.6	3.0
Madrid - New York	28-Apr-01	24.3	21.9	20.9	21.2	17.6
Madrid - Miami	13-Jun-01	27.0	24.4	23.6	23.9	22.2
Madrid - Johannesburg	11-Aug-01	17.7	21.4	16.1	20.1	12.1
Madrid - Stockholm	21-Aug-01	12.0	11.8	10.3	11.5	10.4
Madrid - Buenos Aires	12-Sep-01	20.9	24.1	18.9	22.9	13.0
Zürich - Toronto	09-Jun-99	59.4	48.3	49.3	49.2	50.2
Montreal - London	06-Mrz-99	47.8	37.0	39.8	37.3	39.1
Vancouver - Honolulu	10-Sep-99	14.2	11.8	12.5	11.7	13.2
Vancouver - Ottawa	18-Sep-99	29.2	21.2	24.4	21.0	22.3

VI.5 Future work

Although considerable progress has been made within the research programmes carried out during the last full solar cycle, there remains a need for research and development support in this new area of radiation protection for a number of reasons:

(i) The annual doses are significant compared to mean annual doses of radiation workers in the nuclear and medical sectors. More than 50% of the doses are due to high-LET radiation, and the workforce has a large young female component.

(ii) The radiation field is unique in terms of both the range of particle types and energies, and additional response characterization of instruments is needed. National regulations in Member States require validation by measurement of dose estimates made using calculation methods. There is a need to define procedures and common approaches to analysis, calibration and traceability of such measurements.

(iii) There has been no complete assessment of the accuracy of measurement or calculation methods; this is desirable.

(iv) There is a need for co-operative procedures between Member States to share information on solar particle events which give increased dose rates at aviation altitudes, to define common procedures for the notification of such events, and to summarize assessments of resultant doses to aircraft crew.

It may also be thought useful to maintain an expert group on aircraft crew dosimetry instrumentation in order to ensure the quality of dosimetry and record keeping generally, but also for possible epidemiological investigations.

VI.6 Acknowledgements

The EURADOS Working Group members and contributors to the report would like to thank Aer Lingus, Air Emirates, Air Canada, Air France, Air New Zealand, Alitalia, Austrian Airlines, British Airways, Czech Airlines, Finnair, Iberia, Icelandair, Lufthansa, NASA, Scandinavian Airlines System and Varig for their assistance. In some instances, unpublished results have been included of research part-funded by the European Commission, Directorate-General Research, under the auspices of the European Commission RTD Programme: Nuclear Energy (Euratom Framework Programme V, 1998-2002) Contract N° FIGM-CT-2000-00068. Valuable comments have been received from J.W.E.van Dijk, NRG Radiation&Environment, Arnhem, The Netherlands.

VI.7 References

[BEC99] Beck, P., Ambrosi, P., Schrewe, U., O'Brien, K., *ACREM, Aircrew Radiation Exposure Monitoring*, Final Report of European Commission contract no. F14P-CT960047 OEFZS Report G-0008, November (1999)

[BOT04] Bottollier-Depois J.F., Trompier, F., Clairand, I., Spurny, F., Bartlett, D.T., Beck, P., Lewis, B., Lindborg, L., O'Sullivan, D., Roos, H. and Tommasino, L. *Exposure of Aircraft to Cosmic Radiation: On-board Intercomparison of various Detectors*, Radiat. Prot. Dos., 2004 (in press).

[EUR97] European Commission, *Recommendations for the implementation of Title VII of the European Basic Safety Standards Directive (BSS) concerning significant increase in exposure due to natural radiation sources*, European Commission Report Radiation Protection 88, (Luxembourg: European Commission), (1997).

[FER04] Ferrari, A., Pelliccioni, M. And Villari, R. *Evaluation of the Influence of Aircraft Shielding on the Air Crew Exposure through an Aircraft Mathematical Model,* Radiat. Prot. Dosim. **108** 91-105 (2004).

[OSU99] O'Sullivan, D, Tommasino, L., Schraube, H., Grillmaier, R., Bartlett, D.T., Lindborg, L., Heinrich, W and Silari, M. *Investigations of Radiation Fields at Aircraft Altitudes*, Final Report of European Commission contract no. F14P-CT950011 (Dublin: Dublin Institute for Advanced Studies:) (1999).

A.1 Cosmic Radiation Exposure Measurements by the Royal Military College of Canada

B.J. Lewis, L.G.I. Bennett, A.R. Green, M. McCall, M. Pierre and B. Ellaschuk
Department of Chemistry and Chemical Engineering
Royal Military College of Canada
PO Box 17000
Kingston, Ontario
CANADA K7K 7B4

A.1.1 Experimental Procedure

Since radiation effects vary with altitude, geomagnetic latitude and heliocentric potential, the primary goal of the research at the Royal Military College (RMC) of Canada was to obtain data covering these parameters that were valid for the complex spectrum at aircraft altitudes. The complete details of the study are given in Ref. 1.

The only single instrument for a complete measurement of the cosmic mixed-radiation field is a tissue equivalent proportional counter (TEPC). It provides not only an indication of the total dose equivalent (with a simulation of a tissue-equivalent site with a diameter of 2 μm), but also the microdosimetric distribution of the radiation as a function of the lineal energy. The lineal energy can be used as a surrogate measurement of the linear energy transfer (LET) for the cosmic radiation spectrum. The TEPC used in this study had a 5"-diameter detector built by Far West Technology, and was designed by Battelle Pacific Northwest National Laboratories to be an extremely portable instrument (Figure 1). This instrument fits into any overhead bin and is powered by batteries which last up to five days of operation. It is simple to operate (off/on switch only) and stores a microdosimetric spectrum every minute for up to thirty days of operation.

The TEPC was calibrated initially by the manufacturer using ^{137}Cs and ^{252}Cf sources. This calibration was checked routinely with an internal ^{244}Cm source, which, in normal operation, is shielded from the detector cavity by a magnetic shutter. For the majority of the in-flight measurements, aircrew turned on the TEPC prior to takeoff and off after landing, and provided positional data consisting of the flight course and altitude history. Since the TEPC has its own internal clock, the measurements could then be correlated to the aircraft position (geomagnetic latitude and altitude) at one-minute intervals. The stored data were downloaded at the laboratory to provide an output of absorbed dose rate, $\dot{D}$, and dose equivalent rate, $\dot{H}$, and the average quality factor, $\overline{Q}$, of the radiation field.

In addition to the portable TEPC, different types of passive and active detectors were also used on several scientific flights to measure the individual low-LET (ionizing) and high-LET (neutron) components of the mixed-radiation field in the RMC study (which can be appropriately summed for comparison to the TEPC results). Other portable instruments used in this study included: (i) temperature-compensated neutron bubble detectors (BD-PND) from Bubble Technology Industries (BTI); (ii) a battery-powered Eberline FHT 191 N ionization chamber (IC); (iii) aluminum oxide (Al_2O_3) thermoluminescent detectors (TLD's); (iv) a Siemens Electronic Personal Dosemeter (EPD); and (v) a passive dosemeter box assembled by the National Radiological Protection Board (NRPB) in the United Kingdom, which contained 30 TLD's and 24 polyallyldiglycol carbonate (PADC) track-etch detectors.

A.1.2 Ground-Based Measurements

In support of the in-flight study, the operation of the TEPC was verified and calibrated using several common radioisotopic sources, such as ^{137}Cs, ^{252}Cf, ^{241}Am-^{9}Be and ^{239}Pu-^{9}Be. As detailed in Appendix A, the TEPC response was also evaluated with a mono-energetic neutron source from 0.144 to 14.8 MeV at the Physikalisch Technische Bundesanstalt (PTB), along with neutron bubble detectors that had been employed extensively in earlier studies to measure the neutron component of the cosmic field.

A.1.3 At-Altitude Measurements

Dosimetric measurements and microdosimetric spectra were taken on board 62 worldwide flights flown at altitudes between 4.5 and 12.4 km from September 1998 to October 1999. A typical dose distribution for a trans-Atlantic flight is shown in Figure 2. For a portion of these flights at altitudes greater than 8.5 km, values of the frequency mean lineal energy, $\bar{y}_F$, the dose mean lineal energy, $\bar{y}_D$, and the average quality factor, $\overline{Q}$, were obtained from TEPC spectral data summed over an entire flight (Table 1). On all flights, the $\overline{Q}$ values are greater than 1 and the $\bar{y}_D$ values are greater than 10 keV/μm, which indicates a significant high-LET (> 10 keV/μm) contribution to the radiation field.

The dose equivalent arising from the neutron (i.e., high-LET) component of this field was measured using BDs or the PADC detectors of the NRPB box. In addition, on some flights, the dose equivalent arising from the non-neutron (i.e., mainly low-LET) component was measured independently using either an IC, TLDs or an EPD. Both the TLDs and NRPB box correspond to integrated values over several flight legs. Table 2 shows different methods for estimating the total dose equivalent with these various combinations of instrumentation.

An estimate of the low-LET dose equivalent can also be obtained from the TEPC by including only those data points at lineal energies less than 10 keV/μm. The TEPC gamma measurements in Table 2 are always ~10-15% lower than that measured by the IC. This systematic discrepancy suggests that the IC is responding to ionizing particles with higher lineal energy values as well. The EPD readings are also consistently lower than the IC measurements by at least 20%. The low-LET dose equivalent (from the IC or TLD's) can be summed with the high-LET (neutron) value to obtain an estimate of the total dose equivalent. This procedure results in a value which is ~90% of that measured by the TEPC. This slight discrepancy can be related to the fact that the IC and TLD's are referenced to a photon-equivalent field (i.e., with a mean quality factor $\overline{Q}$ = 1), and therefore do not take into account an enhanced quality factor for those ionizing particles actually present in the cosmic spectrum with lineal energies greater than 10 keV/μm (such as protons). In addition, there is an under response of the BDs to neutrons of very high energy where the microscopic cross sections of the superheated detector liquid are known to decrease with increasing energy. Thus, the summed results from the various independent equipment are self-consistent with the TEPC results.

The database of the TEPC measurements for the various RMC flights are included with this report. For those flights where complete path information was available, the total ambient dose equivalent rate (H*(10)) is given as a function of time and the actual flight path (i.e., latitude, longitude and altitude). In addition, a route dose (in units of H*(10)) is further provided for all flights along with the departure and arrival locations, and flight profile (i.e., time at altitude). Comparisons of these latter data to theoretical calculations with the CARI-6, EPCARD and PC-AIRE aircrew exposure prediction codes are also given assuming a great circle route.

A.1.4: Instrument Calibration

TEPC (External Source Calibration)

Before using the TEPC to monitor radiation at jet altitudes, it is necessary to know the response of the TEPC relative to the ambient dose equivalent, H*(10). In other words, the TEPC must be calibrated in a known field of interest in order to obtain a multiplication factor, *f*, which can be applied to H_{TEPC} such that

$$H^*(10) = fH_{TEPC} \; . \qquad [A.1]$$

The response of the TEPC was compared to H*(10) in polyenergetic neutron reference fields (^{252}Cf and AmBe) and in monoenergetic neutron beams at the PTB. The results from the polyenergetic neutron fields are given in Table A.1, while the results from the mono-energetic neutron beam measurements are shown in Figure A.1.

These measurements show that H_{TEPC} is systematically higher than $H^*(10)$ by an average of ~15% (excluding the measurement at a neutron energy of 0.144 keV, where the TEPC is known to under-respond since the range of the recoil proton is less than the TEPC diameter). In addition, comparison to a calibrated ^{137}Cs gamma source shows that the TEPC over-responds to gamma rays by approximately 10%. Based on these various results, *f* in Equation (A.1) is taken as 1/1.15.

TEPC (Internal Alpha Source Calibration)

The TEPC also contains an internal alpha source (i.e., ^{244}Cm) which can be used for calibration since the cosmic ray spectrum also contains particles of higher LET. Thus, the value of *f* in Equation (A.1) can also be confirmed by examining the position of the peak generated by the internal source. This source emits 5.8-MeV alpha particles with virtually no gamma rays. The stopping power (S/ρ) of these particles in the detector can be evaluated with a Monte Carlo analysis using the SRIM-2000 code, assuming an atomic composition of: H (10.3 wt%), C (56.9 wt%), N (3.5 wt%) and O (29.3 wt%) for propane gas of density $\rho = 1.68 \times 10^{-5}$ g cm^{-3} (at 20°C and 7 torr). From the SRIM analysis, it can be seen that the stopping power is relatively constant for a high-energy alpha particle (i.e., until it has slowed down and is near the end of its range), where $(S/\rho) \sim 856$ MeV cm^2 g^{-1}. It is therefore possible to determine the amount of energy (ε) imparted to the counter gas using the relation

$$\varepsilon = (S/\rho)\rho_t d_t \; . \qquad [A.2]$$

Hence, with an $(S/\rho) \sim 856$ MeV cm^2 g^{-1}, a tissue site density $\rho_t = 1$ g/cm^3 and tissue sphere diameter, $d_t = 2$ μm, the energy imparted by the 5.8-MeV alpha particle in the current detector cavity is $\varepsilon = 171$ keV. This value is in excellent agreement with that reported in the literature (i.e., 170 keV for a 2-μm site size).[2] From the definition of the lineal energy *y*

$$y = \frac{\varepsilon}{\bar{\ell}} = 1.5\frac{\varepsilon}{d_t} \qquad [A.3]$$

where, for the simulated tissue site, the mean chord length $\bar{\ell} = (2/3)\, d_t$. A lineal energy peak is therefore predicted to occur with Equation (A.3) at a value of 128 keV/μm. The actual spectrum measured by the TEPC consists of a single peak with a maximum near 148 keV/μm (consistent with an original calibration by the manufacturer to a peak position of 150 keV/μm). Thus, this actual peak occurs at a lineal energy which, again, is ~15% higher than that predicted by theory (128 keV/μm). The absorbed dose calculation will be directly affected by this same factor, which further supports the use of the proposed value of *f* in Equation (A.1).

A.1.5 References

1. B.J. Lewis, M.J. McCall, A.R. Green, L.G.I. Bennett, M. Pierre, U.J. Schrewe, K. O'Brien and E. Felsberger, "Aircrew Exposure from Cosmic Radiation on Commercial Airline Flights," Radiat. Prot. Dosim. 93(4), 293-314 (2001).
2. U.J. Schrewe, H.J. Brede, P. Pihet and H.G. Menzel, "On the Calibration of Tissue-Equivalent Proportional Counters with Built-In α Particle Sources," Radiat. Prot. Dosim. 33(1-4) 249-252 (1988).

Table A.1: Response of RMC TEPC to Polyenergetic Neutron Reference Fields

Source	Reference (H*(10)) Dose Rate [μSv/hr]	Measured Dose Rate[a,b] [μSv/hr]	Relative Difference [%]
^{252}Cf	996 ± 24	1165	16.9
Am(Be)	11.8 ± 0.6	14.2	20.6

a. For y>10 kev/μm (neutrons only).
b. Corrected for backscattering (using shadow cone).

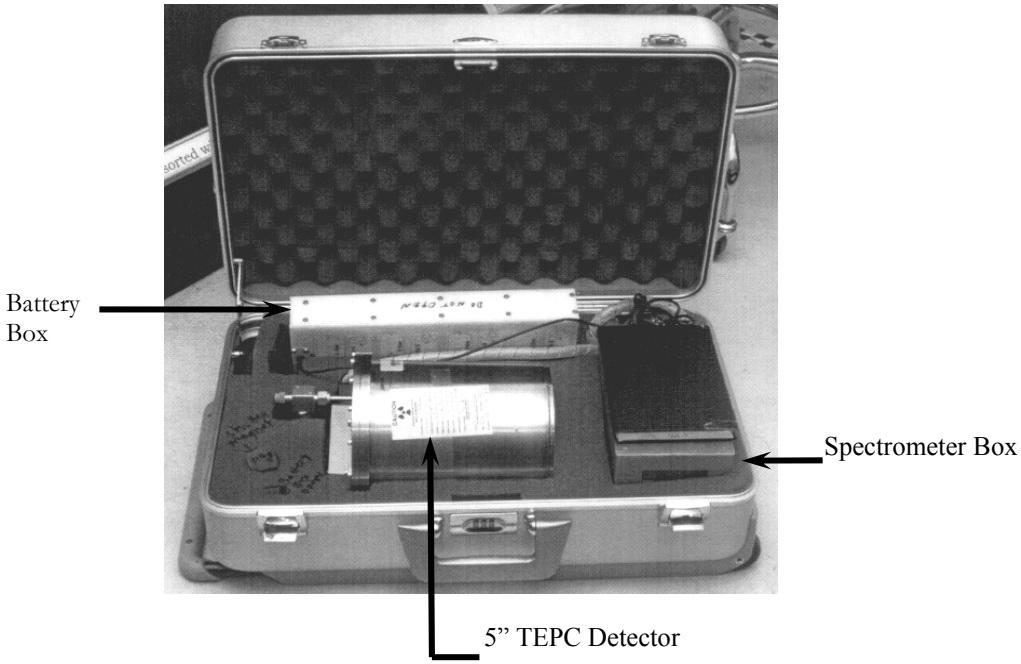

Figure A.1.1. Arrangement of TEPC components in the carry-on case.

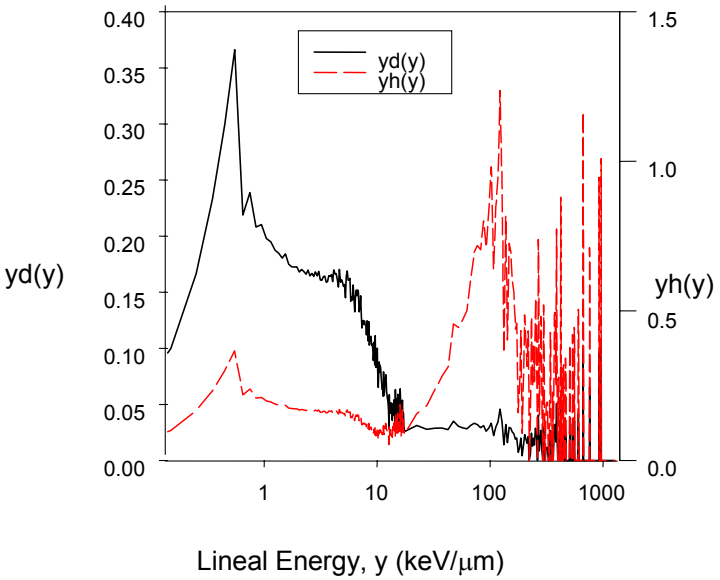

Figure A.1.2. Microdosimetric absorbed dose and dose equivalent distributions on a 7-hour flight between Toronto and Zurich at an altitude of 11.2 km.

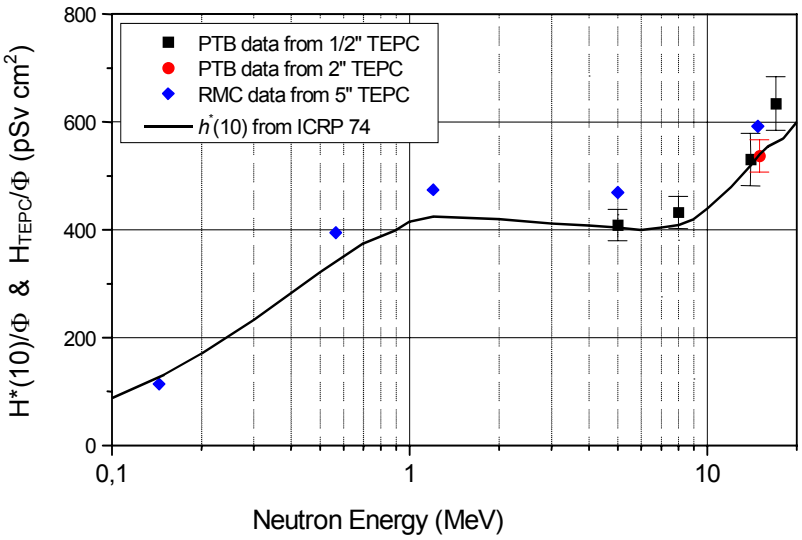

Figure A.1.3 Response of RMC TEPC compared to H*(10)/Φ at selected neutron energies. The response of the RMC TEPC, H_{TEPC}/Φ, is compared to H*(10)/Φ values given in ICRP-74 (solid line). Responses of PTB-owned TEPC's are also shown for comparison.

A 2 National Radiological Protection Board

D T Bartlett, L G Hager and R J Tanner
National Radiological Protection Board, Chilton, Oxon OX11 0RQ, United Kingdom.

A2.1 Instrument Description

The NRPB passive survey instrument consists of a glass reinforced polyester (GRP) box of dimensions 255 x 250 x 125 mm containing a central block of 36 etched track detectors arranged in 6 mutually orthogonal stacks of 6 dosemeters in order to have, in aggregate, a response approximately independent of the direction characteristics of the radiation field, 30 thermoluminescence dosemeters(TLDs), and 2 electronic personal dosemeters (EPDs) to record the time profile of the radiation field. The total mass is 4 kg. One of the larger faces of the box is the lid and top of the box. The top generally faces up during measurements in aircraft, and the normal to this surface defines the reference direction of the instrument for calibration. Two boxes are prepared for each measurement, one as a background control.

The 15% determination limit (that is the dose which can be determined with a 15% statistical uncertainty) is 100 μSv for the estimation of total ambient dose equivalent. However, this still means that, in general, several return flights are required to make a measurement of acceptable uncertainty. This is not necessarily a disadvantage where average route doses are being determined. An important consideration, which applies, to a greater or lesser extent, to all devices used to measure such complex radiation fields, is that some *a priori* information on the radiation field is needed to interpret the instrument response.

Figure A2.1: The NRPB passive survey instrument (PSI)

A2.2 Approach

The cosmic radiation field in aircraft comprises mainly photons, electrons, positrons, muons, protons and neutrons. There is not a significant contribution to dose equivalent from energetic primary heavy charged particles (HZE) or fragments. Details of the composition may be found elsewhere[1,2,3,4] . For dosimetric purposes the field can be divided into low and high (> 5-10 keV μm^{-1}) LET components. The low LET energy deposition can be determined using TLDs. The TLD used should have little response, ideally none, to the high LET component, and an LET-independent absorbed dose response for the low-LET component. With choice of appropriate TL phosphor and suitable calibration, the absorbed dose to tissue can be determined. The high-LET component can be measured using poly allyl diglycol carbonate (PADC, also known by the trade name CR-39®) in terms of particle fluence distribution in LET. After the application of the LET/quality factor relationship and with a correction for material composition and density, a determination of tissue dose equivalent can be made to a good approximation[5].

An alternative approach, which is adopted here, is to determine separately two slightly different components, the non-neutron component and the neutron component, which includes neutron-like dose equivalent contribution by high-energy protons. The non-neutron component is determined with TLDs and corresponds to the low-LET component corrected for any neutron contribution. The neutron component plus the nuclear interaction component of the high-energy proton part of the field is determined using PADC detectors with suitable calibration.

A2.2.1 Non-neutron component

The non-neutron component comprising photons and directly ionising particles is determined using TLDs. Standard lithium fluoride (^{7}LiF:Mg,Ti, 30% loaded PTFE disc) two element dosemeters are used. From an analysis based on photon interaction coefficients calculated by Hubbell[6], tabulations of electron[7] and proton[8] stopping powers, and data on muon stopping powers[9,10,11], it is concluded that relative to a ^{137}Cs calibration in terms of tissue kerma, the TLDs will give an estimate of absorbed dose to a small mass of tissue for all non-neutron components, to within 5%[12]. The energy ranges taken into account include the majority of the contributions to dose[4,13]. Further, the results of calculations by Ferrari *et al.*[14] would indicate that for the non-neutron component of the field at aircraft altitudes, the depth-dose profile is not pronounced. It is a reasonable approximation, therefore, to apply an ambient dose equivalent calibration of the PSI for a ^{137}Cs photon field to the non-neutron or neutron-like field as a whole, with an estimated systematic error of no more than 10%. However the particle type and energy dependence of ambient dose equivalent response for the non-neutron component of the field in aircraft is being investigated further.

In aircraft, the contribution of HZE particles to total ambient dose equivalent is small[5], and the lower light conversion efficiencies of these higher LET particles will reduce their contribution to the dosemeter reading further. The HZE dose contribution is not considered further.

The ^{7}LiF detectors will have some response to the neutron component of the radiation field. Energy deposition from direct nuclear interactions in the detectors and heavy recoils and low energy recoil protons from interactions in the dosemeter holder will be about 1/3 of total neutron kerma, but will have lower relative light conversion efficiency, in the range of 10 to 50% of that to energy deposition for the calibration field. The energy transfer from neutrons to energetic recoil protons will be approximately 2/3 of the total neutron kerma in the material of the passive survey instrument[15], the total kerma factor being similar to that for soft tissue. For energy deposition by the resultant secondary proton energy spectrum, a light conversion efficiency in the range 50 to 100% may be assumed[16,17]. The neutron component of the

radiation field is about 15% of the total in terms of tissue absorbed dose. Thus the contribution from the neutron (and neutron-like) component to the response of the TLDs is about 5-10%.

The proton fluence and dose distributions in energy at aviation altitudes are peaked around a few hundred MeV[3,4,18], with little dose deposited (at 10 mm depth) by incident protons of energies below 100 MeV or above 10 GeV. Below 100 MeV, protons deposit almost all energy by electromagnetic force (Coulomb) interactions. At higher energies, progressively larger fractions are deposited in a two-stage process with secondary particles being produced by initial strong force interactions, such that at 5 GeV almost all energy deposition by protons is via these neutron-like interactions[19]. Integrated over the proton spectrum, about 20% of proton dose, that is 5-6% of the total non-neutron dose component, is deposited by secondary particles from the neutron-like interactions. This analysis is consistent with a mean quality factor for total proton dose of between 1.5 and 2, in agreement with detailed calculations[20]. The neutron-like interactions of protons will be registered by the neutron detectors with similar efficiency to neutrons (see below). After taking into account the lower light conversion efficiency of the TLDs for the products of the neutron-like interactions (as in the above consideration of neutron component), a small correction of 2-3% needs to be applied to the response of the TLDs in order to avoid 'double counting' the protons. Taken together, the non-neutron and neutron detectors will, to a reasonable approximation, correctly determine ambient dose equivalent for the proton component. A factor of 0.92 is applied to the ambient dose equivalent (^{137}Cs calibration) to account for the contribution to the TLD signal from both neutron and neutron-like energy deposition.

A.2.2.2 Neutron component

The passive survey instrument uses NRPB personal neutron dosemeters with PADC detectors which are electrochemically etched and automatically read on a commercial photographic slide scanner with a standard personal computer using customised software[21,22,23]. The PADC detectors are used to estimate the neutron plus neutron-like component. Etched track detectors register charged particles by means of etchable damage to the detector structure. The type of material and method of processing (etching) to render the damage observable, determines a threshold rate of energy deposition or material damage along the charged particle track. This, in turn, determines the types, energies and angles of incidence of charged particles which are detected. Neutrons are detected via the secondary charged particles which they generate within the survey instrument.

The detector responds to particles which deposit energy in the etched volume of the detector with an LET above about 30 keV μm^{-1}. This means that, of protons incident on the detector rear surface, only those of energy less than about 1 MeV at the surface to be etched are detected by electromagnetic force interactions. Higher energy protons are only detected via other particles generated elsewhere in the instrument as a result of the strong force component of the total interaction cross-section. The proton energy spectrum at each detector will be modified from that incident on the outside of the passive survey meter by slowing down and other interactions. If it is assumed that there is partial radiation equilibrium (the survey meter is about 6 g cm^{-2} thick), the proton energy distribution at a detector will be similar to the distribution incident on the box, and will have little fluence below 2 MeV. It is estimated that about 10-20% of the detector reading will be the result of protons' neutron-like behaviour.

The instrument reading integral response characteristic is obtained by folding the monoenergetic response characteristics (see below) with the neutron energy distribution at aircraft altitudes. This is used to convert the values of readings of the PADC detectors obtained for in-flight measurements, to estimate the sum of the neutron component and the nuclear interaction part of the high-energy proton component of ambient dose equivalent for the radiation field being assessed

A 2.2.3 Neutron Fields and Calibration Procedures

Measurement of the energy dependence of neutron fluence response of the passive survey instrument has been carried out for the energy range 144 keV to 19 MeV at the Physikalisch-Technische Bundesanstalt (PTB) (but the 19 MeV results are still to be analysed) and in the 60, 68, 96 and 173 MeV quasi-monoenergetic beams at the Université Catholique Louvain (UCL) and the The Svedberg Laboratory (TSL), Uppsala University. All irradiations were carried out to a total fluence corresponding to an ambient dose equivalent in the range 1-3 mSv. The reference point for the instrument was taken to be the centre of the sensitive volume of the PADC detectors.

The neutron irradiation facilities at the PTB national standards laboratory are well characterized. For the irradiations reported here, the scatter component in terms of ambient dose equivalent was less than 1%; and the total uncertainty in the fluence was between 4 and 5%[24]. The box was positioned with the front face of the instrument at a distance of 50 cm from the target. The neutron fields provided at UCL, a description of which may be found in the papers by Dupont *et al.*[25] *a*nd Schuhmacher *et al.*[26], and in [24], are quasi-monoenergetic. The average energy of the peak of the fluence distribution for the neutron beam used was 60.2 MeV, with a width of about 2 MeV. The beam is monitored with a fission chamber and a plastic scintillator. The absolute neutron fluence is determined using a proton recoil telescope. The fraction of neutron fluence within the peak (E_n > 56 MeV) is 0.32 (fraction of H*(10) of 0.26). The fluence energy distribution above 5 MeV has been determined using time-of-flight techniques. Below 5 MeV, Φ_E has been assumed constant. The relative uncertainty in the total fluence was determined to be 7%. The box was moved through the beam in such a way as to achieve uniform irradiation. The neutron fields provided at TSL, a description of which may be found in the paper by Condé[27], are also quasi-monoenergetic. The average energies of the peaks of the fluence distributions for the neutron beams used were 68, 96 and 173 MeV, with a width of about 2 MeV. The neutron beam is monitored by means of a thin film breakdown counter (TFBC)[28,29,30]. There are some data on the neutron energy distribution above about 30 MeV determined from both measurements and calculations (see Prokofiev[31] and references therein). Calculated distributions[31] have been used in these investigations for the 68 and 96 MeV neutron beams. The distribution for the 174 MeV beam was extrapolated from published data for a 160 MeV beam[31]. Below about 40 MeV, the fluence energy distributions (Φ_E) have been extrapolated to lower energies with Φ_E constant. The ratio of peak fluence to total depends on peak energy, but is about 0.4. The uncertainty on the peak fluence was about 10%. The uncertainties in the total fluences are estimated to be 30-35%, when the significant uncertainties in the energy distributions are taken into account. Irradiations were carried out at a distance of 18 m, such that the beam encompassed the entire box.

The results of the measurements are given in Table A.2.1 Both the fluence and ambient dose equivalent dependence of response characteristics are given. The fluence to ambient dose equivalent conversion coefficients were taken from the International Commission on Radiation Units and Measurements Report 57[32] extended to higher energies using values calculated by Ferrari and Pelliccioni[33]. In the case of the quasi-monoenergetic fields, the fluence response characteristic for the fluence peak was determined by an iterative fitting method to subtract the instrument reading due to non-peak neutrons. For each TSL neutron field, but starting with the lowest peak neutron energy, a first estimate of the peak energy fluence response characteristic was taken from results for single detector irradiations with monoenergetic protons for energies at, or close to, the peak neutron energies. Together with the results of the lower neutron energy response determinations, a full set of energy response characteristics were constructed and folded with the energy distributions for the non-peak beam component. The instrument reading calculated thus was subtracted from the observed reading to obtain the instrument response for the peak neutron energy. This value was then substituted for the value of the proton response of single detectors and the procedure repeated.

Several iterations were carried out to obtain a final value of the peak response which, when included in the response characteristics, gave agreement of calculated and observed instrument readings. The statistical (type A) uncertainties for the instrument readings are combined in quadrature with the total standard uncertainties on the neutron fluences to give the standard uncertainties shown (1 s).

Radiation Field	Net tracks per unit fluence (isotropic exposure) ($cm^2\ 10^{-6}$)[a]	Net tracks per unit ambient dose equivalent (mSv^{-1})
144 keV (PTB)	2.25 (0.38)[b]	17.7 (1.1)[b]
542 keV (PTB)	14.4 (1.3)	42.9 (3.9)
1.13 MeV (PTB)	30.3 (2)	71.5 (4.7)
2.5 MeV (PTB)	41.8 (2.3)	100 (5.5)
5 MeV (PTB)	38.5 (1.7)	95.1 (4.2)
8 MeV (PTB)	35.3 (1.4)	86.3 (3.4)
14.8 MeV (PTB)	48.7 (2.4)	90.9 (4.5)
18.73 MeV (PTB)	In progress	
60.2 MeV (UCL)	53 (5)	74 (7)
68 MeV (TSL)	42 (13)	106 (33)
95 MeV (TSL)	30 (9)	83 (25)
100 MeV (iThemba)	In progress	
100 MeV (iThemba)	In progress	
173 MeV (TSL)	20 (6)	68 (20)

(a) Average for three angles of incidence

(b) Statistical uncertainty (1 s) on instrument reading added in quadrature to total ` standard uncertainty on fluence.

Table A2.1: Energy Dependence of Response of NRPB Passive Survey Instrument

The fluence energy dependence of response shown is folded with the calculated fluence energy distribution at aircraft altitudes[2,3], to obtain the instrument reading integral response characteristic for aircraft measurements. An estimate of the uncertainty in the integral response characteristic due to the uncertainty in the measured response characteristics of 13% is obtained by folding the values plus or minus one standard deviation. The uncertainty due to the uncertainty in the calculated energy distribution is yet to be investigated. Table A.2 shows the isotropic field instrument integral response characteristic for the neutron field in aircraft, plus the calculated and measured response characteristics for the CERF energy distribution. For neutron energies below 144 keV for which no response measurements have been made, extrapolation of the response has been made based on the response characteristics for a single PADC detector for isotropic irradiation[23]. Given the large uncertainties in the response data there is good agreement. The range of calculated integral fluence and ambient dose equivalent response characteristics for the two energy distributions are shown for the ± 1 s limits of the monoenergetic and quasi-monoenergetic response characteristics.

Neutron field	Reading per unit fluence[a] (cm^{-2} 10^{-6})	H*(10) weighted conversion coefficient (pSv cm^{-2})	H*(10) integral response characteristic (mSv^{-1})
Roesler *et al.*[2,3] 246 g cm^{-2}	18.9 (16.5-21.3)[b]	230	82 (72-93)
Rancati *et al.*[36,38,39] CERF	25.5 (21.4-29.8)[b]	260	97 (82-115)
CERF measured[b]	29.8 (2.0)[c]		

(a): For isotropic irradiation (average of three orientations)
(b): Range for envelope of integral response characteristic ± 1 s
(c): Standard deviation (s) of repeated measurements

Table A2.2 Comparison of calculated and measured readings of NRPB Passive Survey Instrument

Frequent checks on the repeatability of measurements using different batches and sheets of PADC, have been made with the survey instrument in the simulated cosmic radiation neutron field which has been designed and provided at CERN. The facility has been developed and characterized jointly with the EC for the calibration, characterization and intercomparison of the responses of instrument and dosemeters for the purpose of the determination of the neutron component of the cosmic radiation fields at aircraft altitudes, is known as CERF (CERN-EU high-energy Reference Field facility)[34,35,36]. The reference fields are created by beams of high energy protons and pions with momenta of either 120 GeV c^{-1} (positive or negative) or 205 GeV c^{-1} (positive) incident on a copper target, 0.5 m long. There is massive concrete shielding at the side of the beam at the target positions, and, depending on target position, either iron or concrete shields above. Well-characterized reference fields are located both at the side of the target area and on the roof shields. The radiation field in each calibration position has been calculated by using the Monte Carlo code FLUKA[36,37,38,39]. Behind the concrete shields, the neutron radiation field replicates the major components of the neutron component of the cosmic radiation field in aircraft. The CERF neutron field has a wide direction distribution. The PADC batch and sheet variability of the CERF non-isotropic integral response characteristic is shown in Figure A.2.

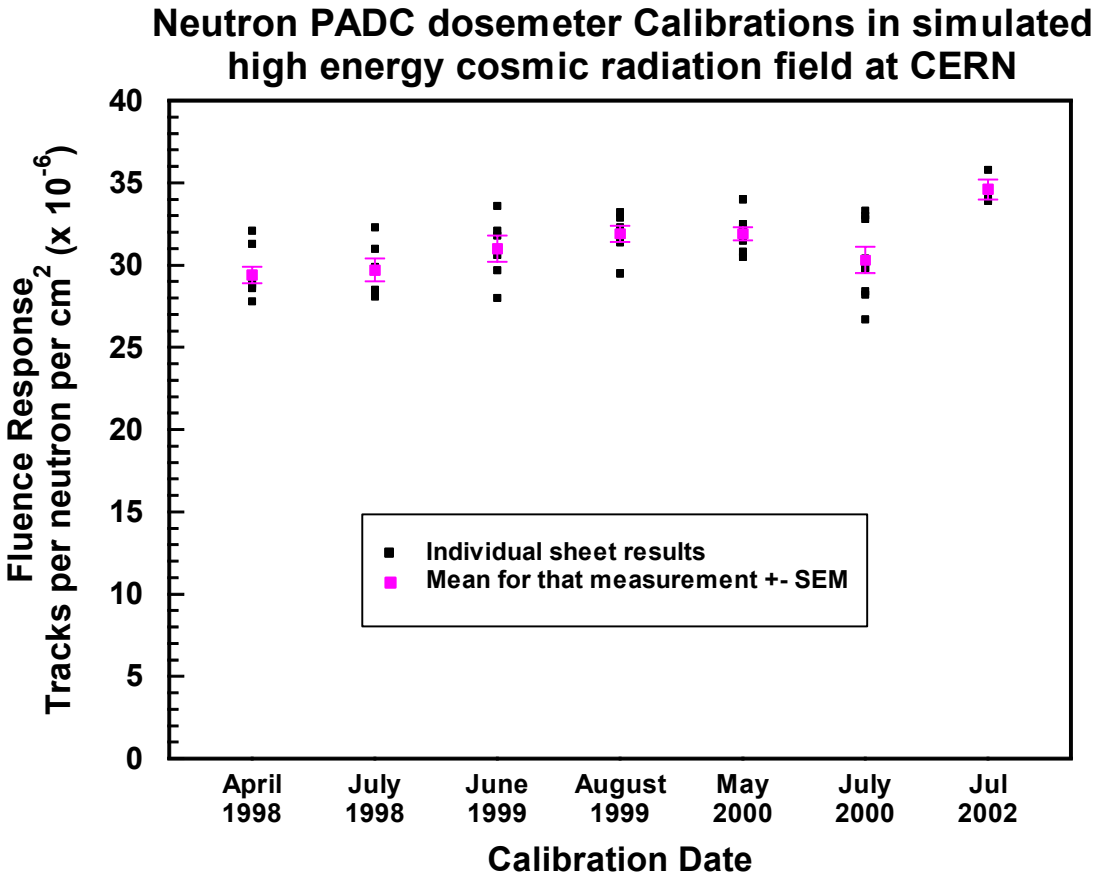

Figure A2.2 Repeatability results at CERF

A2.3 References

1 O'Brien, K. *The Cosmic Ray Field at Ground Level*. Proc. 2nd Int. Conference on Natural Radiation Environment, August 1972, Honiton, USA. Report Conf-720805-PC, 15–54, (US Dept of Commerce: Gaithersburg) (1972).

2 Roesler, S, Heinrich, W, and Schraube, H. *Calculation of Radiation Fields in the Atmosphere and Comparison to Experimental Data*. Radiat. Res.**149** 87-97 (1998).

3 Heinrich, W, Roesler, S, and Schraube, H. 'Physics of Cosmic Radiation Fields'. Radiat. Prot. Dosim. 86 , pp253-258 (1999).

4 Ferrari, A., Pelliccioni, M. and Rancati, T. *Calculation of the Radiation Environment caused by Galactic Cosmic Rays for Determining Air Crew Exposure.* Radiat. Prot. Dosim. **93** 101-114 (2001)

5 O'Sullivan, D., Zhou, D., Heinrich, W., Roesler, S., Donnelly, J., Keegan, R., Flood, E. and Tommasino, L. *Cosmic Rays and Dosimetry at Aviation Altitudes.* Radiat. Meas. **31** 579-584 (1999).

6 Hubbell, J H, and Seltzer, S M. *Tables of X-ray Mass Attenuation Coefficients and Mass Energy-Absorption Coefficients, 1 keV to 20 MeV for Elements Z = 1 to 92 and 48 Additional Substances of Dosimetric Interest.* National Institute of Standards and Technology Report NISTIR 5632, (US Dept of Commerce: Gaithersburg) (1995).

7 International Commission on Radiation Units and Measurements. ICRU Report 37 *Stopping Powers for Electrons and Positrons*, (ICRU: Bethesda) (1984).

8 International Commission on Radiation Units and Measurements. ICRU Report 49 *Stopping Powers and Ranges for Protons and Alpha Particles*, (ICRU: Bethesda) (1993).

9 O'Brien, K. *The Response of LiF Thermoluminescence Dosimeters to the Ground-Level Cosmic-Ray Background*. Int. J. Appl. Radiot. Isotop., **29**, 735–739 (1978).

10 Stevenson, G R. *Dose and Dose Equivalent From Muons*. European Laboratory for Particle Physics, CERN/TIS-RP/099 (1983).

11 Höfert, M. *Dosemeter Response to Muons*. Radiat. Prot. Dosim., **20**, 149–154 (1987).

12 Bartlett, D.T., Hager, L.G., Irvine, D. and Bagshaw, M. *Measurements on Concorde of the Cosmic Radiation Field at Aviation Altitudes,* Radiat. Prot. Dosim. **91** 365-376 (2000)

13 Schraube, H., Leuthold, G., Roesler, S. and Heinrich, W., *Experimental and Theoretical Basis of Aviation Route Dose Calculation*, Rad. Res. Congress Proceedings **2** 724-727 (2000).

14 Ferrari, A., Pelliccioni, M. and Rancati, T. *Study of the Dosimetric Characteristics of CosmicRadiation at Civil Aviation Altitudes* Radiat. Prot. Dosim. **102** 305-314 (2002)

15 Savitskaya, E N, and Sannikov, A V. *High Energy Neutron and Proton Kerma Factors for Different Elements*. Radiat. Prot. Dosim., **60**, 135–146 (1995).

16 Jahnert, B. *Thermoluminescent Research of Protons and Alpha Particles with LiF (TLD-700)*. Proc. 3rd Int. Conf. Luminescence Dosimetry, Risø, 1971. Risø Report 249, pp1031-1039 (Risø: Denmark) (1971).

17 Benton, E.R., Frank, A.L. and Benton, E.V. *TLD efficiency of ^{7}LiF for Doses Deposited by High-LET Particles* Radiat. Meas. **32** 211-214 (2000)

18 Ferrari, A, and Pelliccioni, M. *Fluence to Dose Equivalent Conversion Data and Effective Quality Factors for Flight Energy Neutrons.* Radiat. Prot. Dosim., **76** (4), 215–224 (1998).

19 Stevenson, G.R., Private Communication. (1997)

20 Pelliccioni, M. *Fluence to Dose Equivalent Conversion Data and Radiation Weighting Factors for High Energy Radiation.* Radiat. Prot. Dosim. **77** (3), 159–170 (1998).

21 Bartlett, D T, Steele, J D, Tanner, R J, Gilvin, P J, Shaw, P V, and Lavelle, J. *Ten Years On : The NRPB PADC Neutron Personal Monitoring Service.* Radiat. Prot. Dosim., **70** (1–4) 161–163 (1997).

22 Steele, J D, Bhakta, J R, Bartlett, D T, and Tanner, R J. *Development of a Reader for Track Etch Detectors Based on a Commercially Available Slide Scanne.r* Radiat. Meas. **31** 179-184(1999).

23 Tanner, R.J., Bartlett, D.T. and Hager, L.G. *Recent Enhancements to the Understanding of the Response of the NRPB Neutron Personal Dosemeter* Radiat. Meas. (2001)

24 Alberts, W.G., Arend, E., Barelaud, B., Curzio, G., Decossas, J-L., d'Errico, F., Fiechtner, A., Grillmaier, R., Meulders, J-P., Ménard, S., Roos, H., Schuhmacher, H., Thévenin, J-C., Wernli, Ch. And Wimmer, S. *Advanced Methods of Active Neutron Dosimetry for Individual Monitoring and Radiation Field Analysis (ANDO).* PTB Report PTB-N-39 (1999).

25 Dupont, C., Leleux, P., Lipnik, P., Macq, P. and Ninane, A. *Study of a Collimated Fast Neutron Beam* Nucl. Instrum Meth. **A256** 197-206 (1987).

26 Schuhmacher, H., Brede, H. J., Dangendorf, V., Kuhfuss, M., Meulders, J.P., Newhauser, W.D. and Nolte, R. *Quasi-monoenergetic Neutron Beams with Energies from 25 to 70 MeV* Nucl. Instrum Meth. **A421** 284-295 (1999).

27 Condé, H., Hultqvist, S., Ollson, N., Rönnqvist, T., Zorro, R., Blomgren, J., Tibell, G., Håkansson, O., Jonsson, O., Lindholm, L., Renberg, P.-U., Brockstedt, A., Ekström, P., Österlund, M., Brady, F.P. and Szeflinski, Z. *A Facility for Studies of Neutron-induced Reactions in the 50-200 MeV Range*. Nucl. Instrum. Meth. **A292,** 121-128 (1990).

28 Tommasino, L., Klein, N. and Solomon, *Thin-film Breakdown Counter of Fission Fragments.* P. J. Appl. Phys. **46** 1484-1488 (1975).

29 Prokofiev, A.V. and Olsson, N. *Fission Fragment Detection Efficiency of Thin-film Breakdown Counters in Sandwich Geometry* Uppsala University Report UU-NF 01#5 (2001).

30 Prokofiev, A.V. Smirnov and Renberg, P-U. *A Monitor of Intermediate-Energy Neutrons Based on Thin-film Breakdown Counters*, Uppsala University Report TSL/ISV-99-0203 (1999).

31 Prokofiev, A.V. *Nucleon-induced Fission Cross Sections of Heavy Nuclei in the Intermediate Energy Region* Ph.D. Thesis Uppsala University (2001)

32 International Commission on Radiation Units and Measurements, *Conversion Coefficients for Use in Radiological Protection Against External Radiation* ICRU Report 57 (ICRU: Bethesda) (1998)

33 Ferrari, A. and Pelliccioni, M. *Fluence to Dose Equivalent Conversion Data and Effective Quality Factors for High Energy Neutrons.* Radiat. Prot. Dosim. **76** (4), 215–224 (1998).

34 Höfert, M, and Stevenson, G R. *The CERN-CEC Reference Field Facility* Proc. Annual Nucl. Soc. 8th Int. Conf. Radiation Shielding. Arlington, Texas, USA, April 1994, pp635 (1994).

35 Stevenson, G R, Fassó, A, Höfert, M, and Tuyn, J W N. *Dosimetry at High Energy Accelerators.* Radioprotection **31** (2), pp193–210 (1996).

36 Mitaroff, A. and Silari, M. *The CERN-EU High- energy Reference Field (CERF) Facility for Dosimetry at Commercial Flight Altitudes and in Space.* Radiat. Prot. Dosim. **102** 7-22 (2002).

37 A. Fassò, A. Ferrari, J. Ranft, P. R. Sala, G. R. Stevenson and J. M. Zazula. *FLUKA92*. In Proc. Workshop on Simulating Accelerator Radiation Environment, Santa Fe, 11–15 January 1993, Ed, Palounek, A, Los Alamos LA-12835-C, 134. (1994)

38 Rancati, T, and Ferrari, A. Personal Communication (1996).

39 Birattari, C., Rancati, T., Ferrari, A., Höfert, M., Otto, T., and Silari, M. *Recent results at the CERN-EC high energy reference facility.* In: Proceedings of the SATIF-3 meeting, May 12-13, 1997, Sendai, Japan OECD-AENEA, pp219-234, (1998).

A3 Institute for Radiation Protection and Nuclear Safety, IRSN

J.F. Bottollier-Depois, I. Clairand and F. Trompier ,
IRSN, BP 17, F-92262 Fontenay-aux Roses, France

A 3.1 Instrumenation

The IRSN uses two different TEPC's, the Nausicaa system described below and the Hawk system (from Far West Technology) described in section A1 by B. Lewis and colleagues.

A 3.2 Description of the Nausicaa system

The Nausicaa system, used by the Institute for Radiation Protection and Nuclear Safety (IRSN) for measurements of cosmic radiation aboard aircraft, was developed in collaboration with the French space agency (CNES) for space projects.

The detector used in Nausicaa is a Tissue Equivalent Proportional Counter (TEPC). It is sensitive to directly ionising particles (ions, electrons and gamma rays) as well as to neutrons via the charged secondary particles created by them in the walls of the counter. The sensitive volume is a 5 cm x 5 cm cylinder filled at low pressure (33 hPa) with a gas « equivalent » to biological tissue. This gas is based on propane: 50% C_3H_8, 40% CO_2 and 5% N_2. The detector simulates a 3 micron-long biological site located inside the organism at a depth of 1 cm (Nguyen, 1985).

Incident radiation produces electrons in the gas which are collected on the central anode. The collected charge is proportional to energy deposited. Each event detected is analysed using a pulse height analysis (PHA) method and stored to produce the lineal energy distribution spectrum, d(y); y (0.15 - 1200 keV/µm) is the energy deposited divided by the average chord length of the detector. The system uses a logarithmic amplifier because of the dynamic range of y (10^4) and a 256 multi-channel analyser. There is a relationship between y and the linear energy transfer (LET) which is related to the quality factor (q(LET)) as defined in the ICRP, publication 60. The sum of the deposited energy for each event divided by the mass of gas provides the absorbed dose (D), an assessment of the dose equivalent (H) and the mean quality factor (Q = H/D) of the radiation. An internal source of alpha particles (^{244}Cm) is used to adjust the high voltage of the system for calibration in terms of y. Calibration factors in terms of ambient dose equivalent are determined in the laboratory with a ^{60}Co source for LET lower than 4 keV/µm and with a AmBe neutron source for higher LET.

A 3.3 References

Nguyen V.D., Bouisset P., Kerlau G., Parmentier N., Akatov Y., Siegrist M., A new experimental approach in real time determination of the total quality factor in the stratosphere, Radiat. Prot. Dosim., Vol 48, 41-46, 1993.

Bottollier-Depois J.F., Chau Q., Bouisset P., Kerlau G., Plawinski L., Lebaron-Jacobs L., Assessing exposure to cosmic radiation during long-haul flights, Radiation Research, Vol 153, 526-532, 2000.

Bottollier-Depois J.F., F. Trompier, I. Clairand, F. Spurny, D. Bartlett, P. Beck, B. Lewis, L. Lindborg, D. O'Sullivan, H. Roos, and L. Tommasino , Exposure of Aircraft to Cosmic Radiation: On-board Intercomparison of various Detectors, Radiat. Prot. Dos., 2004 (in press).

A 4 Department of Radiation Dosimetry, Nuclear Physics Institute, Academy of Sciences of the Czech Republic, Prague

F. Spurný, I. Kovář, K. Turek, B. Vlček
Nuclear Physics Institute-Department of Radiation Dosimetry, Academy of Sciences of the Czech Republic, CZ 18086, Praha 8, Czech Republic

A4.1. Introduction

Dose measurements on board of aircraft presented in this document were carried out over a long period, from 1991 to 2001. In the period up to 1999, three main campaigns were realised:

- the first one during mostly 1991 and 1992 years, just after publication of ICRP 60 recommendations;
- the second around 1994, when Czech Airlines tried to increase the average flight altitude for some of aircraft in use; and
- the third one during 1999 to verify the procedure developed to perform routine individual dosimetry of Czech aircrew [SPU02b].

During these runs, different combinations of active and passive instruments were used; the combination depending on the actual availability of instruments. The last run, during 2001, was carried out primarily to test the use of the MDU-Liulin semiconductor spectrometer for on board dosimetry. All methods and dosimeters are described together, following the radiation field component mostly characterized by means of each of them. The results obtained were published for the first three runs in [SPU02c], results with Liulin in [SPD03].

A4.2. Equipment Used to Characterize Non-neutron Component

A4.2.1. Active Measuring Facilities

A4.2.2. Electronic Personal Dosimeters (EPD)

Three types of EPD's were tested onboard aircraft during the period mentioned:

- DMC90 facility commercially available from Merlin-Gerin [DMC91]. Its sensitive element is a semiconductor (Si) detector. It can measure the dose equivalent rate up to of the order of Sv/h; minimum integrated dose equivalent value is μSv.
- Dosemeter CAFP which has been developed in the Joint Institute of Nuclear Research, Dubna, Russia [BAM95]. Its sensitive element is also a semiconductor (Si) detector. It can measure the dose equivalent rate up to of the order of 10 mSv/h; minimum integrated equivalent value is 10 nSv.
- Individual Personal Dosemeter D222 commercially available from ZMA Ostrov nad Ohří, Czech Republic. Its sensitive element is a small GM counter. It can measure the low LET radiation dose equivalent up to the order of 10 mSv/h; minimum integrated dose equivalent is 1 μSv.

A4.2.3. Other Instruments

A4.2.3.1. High Pressure Ionization Chamber Reuter Stokes 112 [RSS88]

High pressure argon-filled steel ionization chamber is available from the Reuter Stokes; it is taken as a reference instrument for the environmental external radiation measurements. Facility with the electronics available can measure the exposure rate from the values corresponding to a fraction of natural background up to ambient dose equivalent rates of the order of 1 mSv/h.

A4.2.3.2. Scintillation Counter for Environmental Radiation Measurements NB 3201

This facility [VIE90] is also devoted to the environmental external radiation measurement at the level of natural background. Its sensitive element is a plastic scintillator with a small NaI:Tl crystal incorporated to compensate the energy dependence.

A4.2.3.3. Thermoluminescent Detectors (TLD´s) [AKS90]

Thermoluminescent Al_2O_3:C detectors were used primarily to characterize the non-neutron contribution to the total equivalent dose. They have been studied in our laboratory for several years, including theirs responses to high LET charged particles [SPU93]. Their thermoluminescence yield („light conversion factor“) decreases with the increase of LET of the particle transferring the energy above few keV/μm much more rapidly than for other “classical” TLD´s, like TLD 100, etc.

A4.2.4. Calibration of Instruments Dedicated to the Characterization of the Non- neutron Component

Detectors and instruments devoted to the characterization of this component of onboard radiation field were primarily calibrated in etalon beam of ^{60}Co photons. The readings have been treated in terms of ambient dose equivalent H*(10). The same detectors were also tested in CERF high energy radiation reference fields [HOF94]. It was found that the response of PED based on the Si-diode was, when expressed as mentioned above, about 30% lower than for other instruments. This was taken into account in the interpretation of the direct readings of these instruments on board
All these detectors have also some response to the neutron component. It is known, that, relative (in terms of tissue kerma) response of “classical” TLD’s to fast neutrons does not exceed 10 %, for high energy neutrons it can reach up to 50% [SPU92]. Taking into account the composition of onboard radiation field, the contribution of neutrons to TLD’s response would not exceed 5% (see also chapter **A2** of this Annex). It could be a little higher for RSS 112 chamber, due to its higher relative sensitivity to neutrons.
Total uncertainty of established ambient dose equivalent values depends not only on the response to neutrons but also on the statistical reliability of measurements. This component of
relative uncertainty (2 σ here and for all other estimations) is less than ± 5 % for RSS 112 and/or NB 3201, for EPD’s depends on the total exposure level (flight time). For short haul flights it can reach up to ± 15 %. As far as TLD’s is concerned, they were found to be usable only for several long haul flights together.

A4.3. Equipment Used to Characterise Neutron Component

A4.3.1. Moderator Type Dose Equivalent Meter NM 2

This facility was commercially available from Nuclear Enterprises, it is based on Anderson-Braun counter [AND64] with a BF_3 proportional counter in the centre of cylindrical moderator. The equipment used during our studies measured the dose equivalent rate averaged over the different integration time; 380 seconds were generally used onboard aircraft. The range of dose equivalent rate covered was between 300 nSv and 1 mSv/h.

A4.3.2. Bubble Damage Neutron Detectors (BDND) [ING91]

Detectors were developed and are commercially available from Bubble Technology Industries, Chalk River, Canada. The types tested and used (PND, BD100R) detect neutrons from about 100 keV, in terms of equivalent dose are roughly energetically independent from 200 keV to about 10 MeV. Both PND and BD100R tested had nominal sensitivity about 1 bubble per 1 μSv of H*(10) of AmBe neutrons.

A4.3.3. Bubble Damage Spectrometer [BDS96]

Bubble damage spectrometer was also developed and is commercially available from Bubble Technology Industries, Chalk River, Canada. It represents 6 sets of detectors with 6 different thresholds in neutron energy: 0.01; 0.10; 0.60; 1.0; 2.5; and 10 MeV. It should be emphasized that these thresholds as well as their general sensitivity depends on the temperature during the exposure. The detector units are reusable by means of recompressing with the equipment furnished together with detector units.

A4.3.4. Neutron Dosemeter Based on an Electrochemically Etched Track Detector

Polyallyldiglycolcarbonate track detector available from Pershore, Ltd., UK, is used as the sensitive element. It detects neutrons from the energy about 100 keV. Two methods of etching were used [TUR93]. One consisting of chemical pre-etching (CE) followed by high frequency electrochemical etching (ECE), the second one consisting of subsequent low and high frequency ECE. Samples were during irradiation covered by polyethylene (PE), 2 mm thick.

A4.3.5. Superheated Drop Detectors with ASM reader

Detectors used were developed and they are commercially available from APFEL Enterprises Inc. (New Haven, USA). The principle of their function is based on the suspensions of over-expanded halocarbon and/or hydrocarbon droplets which vaporise upon exposure to the high LET recoils from neutron interactions. Their basic properties have been recently described and discussed [DER94]. Three types of SDD capsules have been used, with neutron energy threshold 0.1, 1.0 and 6.0 MeV. Apfel Survey Meter (ASM) was used for the reading; it is based on an acoustic effect accompanying each vaporization event.

A4.3.6. Calibration of Instruments Dedicated to Characterise Neutron Component

Detectors and instruments devoted to characterise neutron component of onboard radiation field were calibrated using a bare AmBe and/or ^{252}Cf radionuclide neutron source. The reading was treated in terms of ambient dose equivalent H*(10).
The same detectors were also regularly tested in CERF high energy radiation reference fields [HOF94]. For higher neutron energies their response decreases. The responses of passive neutron detectors relatively CERF neutron reference values [MIT02] as established during the 2002 runs at CERF are presented in Table 1 [SPU02a].

Table 1: Relative responses of passive neutron detectors to neutrons of CERF high energy radiation field (top concrete shield)

Neutron detector	Relative response to CERF reference values
BD 100R - BTI	0.72±0.07
PND - BTI	0.53±0.06
SDD 100 - Apfel	0.72±0.05
PADC combined etching	1.02±0.15
PADC two frequency EC etching	0.45±0.07

As far as the NM 2 “rem-counter” is concerned, it was used only during the first run of our studies. The calibration performed at this period showed, that its response in CERF high energy reference field is, relatively to reference values equal to 0.54±0.04 [SPU94]. All these calibration factors were considered to interpret direct reading of these instruments onboard.

Total uncertainty of established ambient dose equivalent values depends not only on the uncertainty of correction factors mentioned above but also on the statistical reliability of measurements. This component of relative uncertainty (2 σ) was less than ± 10 % for NM 2, for all types of bubble detectors depends on the total exposure level (flight time). Generally, we used 10 detectors of each type during a flight. For short haul flights the statistical component of uncertainty can therefore reach up to ± 40 %, for long haul flights is typically about ± 15 %.
As far as PADC neutron dosemeter is concerned, it was find to be usable only for several long haul flights together, total relative uncertainty was generally not better than ± 30 %.

A4.4. Equipment Used to Characterise Full Radiation Field

A4.4.1. Tissue Equivalent Proportional Counter (TEPC)

In this work the NAUSICAA TEPC equipment, developed in France [BOU92] (see also chapter **A 3** of this Annex) was used in several, mostly long haul, flights during the first and second run of our measurements. Its sensor is a cylindrical low gas pressure TEPC. Its sensitive volume is filled with a propane based tissue equivalent gas mixture at the pressure corresponding to a tissue target with a diameter of 3 μm. The counter wall thickness is equivalent to 10 mm of tissue. The NAUSICAA equipment measures directly the lineal energy between 0.15 and 1500 keV/μm. The instrument is calibrated with a ^{60}Co photon source for low linear energy transfer (LET) region (below ~10 keV/μm), and in the field of AmBe neutron source for high LET region (above ~10 keV/μm). The actual performance of the equipment is regularly checked by means of an internal ^{244}Cm alpha particle source. It can be used in the fields of radiation with the equivalent dose rates between ~ 1μSv/h and several mSv/h. The uncertainty of results obtained with this equipment is discussed and analysed in several other chapters of this Annex.
Our experience showed that the total uncertainty of integral values of ambient dose equivalent during a long haul (more than 6 block-hours) is about ± 15 %.

A4.4.1. Semiconductor Spectrometer MDU [DAC99]

The Mobile Dosimetry Unit (MDU) monitors simultaneously the doses and numbers of energy deposition events in a semiconductor detector. It is managed through specially developed firmware. After switching on, the MDU starts to measure the spectrum of energy deposition events. The acquisition time is variable. The data are stored in a flash memory (0.5 MB) which later is used to recalculate the time of the measurement. The amplitude of the pulses is proportional to the energy deposited in the detector. The adjustment of the energy scale is made through the 60 keV photons of ^{241}Am. The amplitudes are digitised and organised in a 256-channel spectrum. The dose D in Si [Gy] is calculated from the spectrum as:

$$D = K.*\Sigma(E_i*A_i)/MD,$$

where MD is the mass of the detector in [kg]; E_i is the energy loss in the channel **i;** A_i is the number of events in it; and K is a coefficient.

The response of the equipment was studied in the reference gamma (^{60}Co) and fast neutron (AmBe, ^{252}Cf) fields and in on-Earth high energy reference fields (CERF). It was observed that there is a principal difference in the shape of impulsion's spectra of the energy deposited in Si for low and high LET radiation [SPD02]. It was also observed that the spectra of energy deposition observed onboard aircraft are similar to these registered in CERF field. On the base of that we divided the spectra of energy deposited in Si on the part corresponding mostly to non-neutron and/or neutron component of onboard radiation field. Calibration factors used were deduced from the *H*(10)* reference values in on-Earth low and high energy (CERF) reference fields. The results obtained are taken as apparent ambient dose equivalent, H_{app}, in onboard radiation field. Typical results of comparison of data obtained using this procedure with the values as calculated by means of CARI 6 code are presented in the Figure 1 [SPD03].

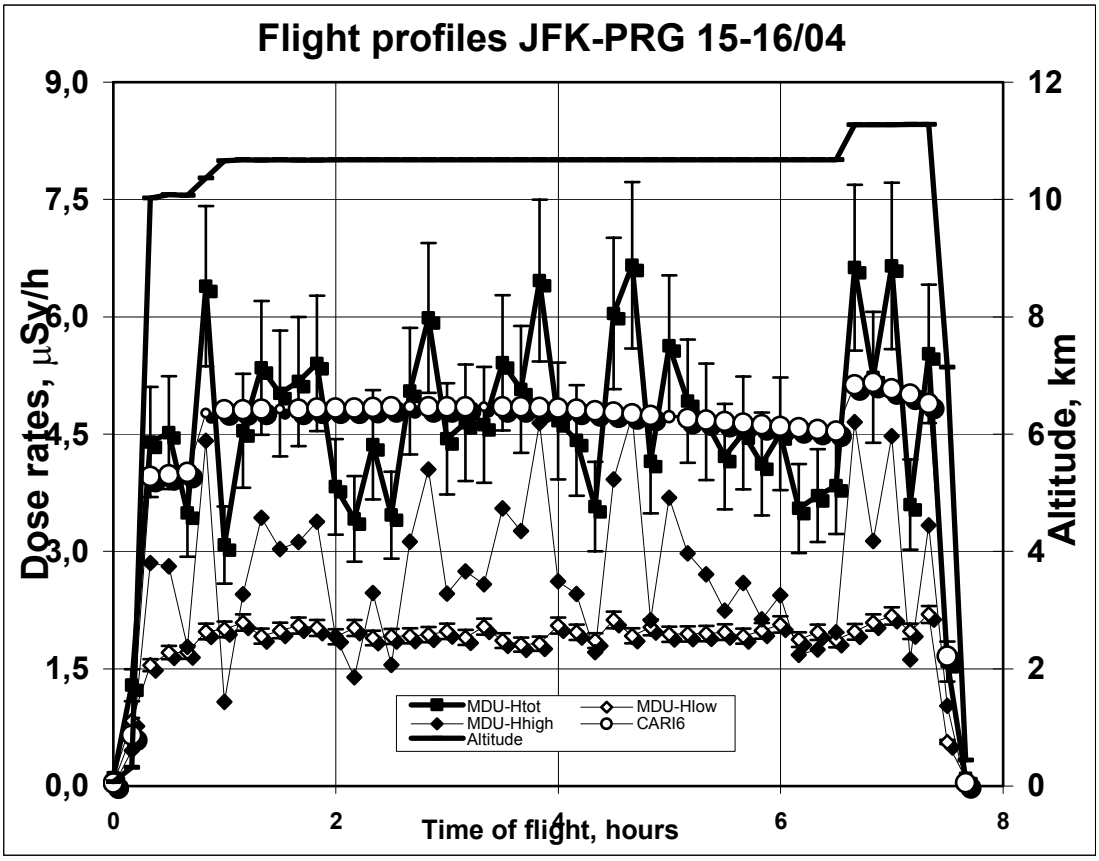

Figure 1: Comparison of apparent ambient dose equivalent rates as measured with MDU-Liulin equipment with effective dose rates as calculated by means of CARI 6 code.

Similar comparison was also made with the results obtained by means of EPCARD code. The Table 2 presents its results for about 400 flights realised during the four long-term monitoring series onboard of a A310-300 aircraft of Czech Airlines during 2001 year [SPD03].

Table 2: Relative deviations, in % of total H*(10), of EPCARD 3.1 calculated and MDU data interpreted using the procedure mentioned

Route	Relative deviation in %, for the 2001 flight period			
	22/03 – 07/05	30/05 – 24/07	29/08 – 16/10	25/10 – 10/12
PRG - JFK	0.1±5.3	-11.5±4.8	-5.7±3.7	-6.6±5.1
JFK - PRG	0.5±6.0	-11.2±5.9	-5.6±4.0	-7.1±4.6
PRG - YYZ	-1.8	-9.1±1.5	-3.7±2.9	-
YYZ - PRG	9.8	-8.91.0	-3.1±2.9	-
PRG - YUL	2.6±6.9	-8.8±5.2	-5.2±3.6	-5.9±4.8
YUL - PRG	0.6±3.8	-10.1±3.5	-0.5±5.0	-2.5±4.0
PRG - DXB	-6.7±2.8	-	-13.7±0.1	-
DXB - PRG	-8.8±6.4	-	-6.8±2.7	-

There are some variations of deviations following the period of measurements and, also one systematic difference. The values calculated by means of EPCARD code are always relatively (in

average about 7-8 %) lower for the flights to and from Dubai (DBX) to Prague (PRG) as compared with the flights above North Atlantic, to New York (JFK), Toronto (YYZ) and/or Montreal (YUL). Nevertheless, in all cases these deviations are fully conform to the requirements of individual radiation protection as defined in ICRP 75; we are still continuing to work on the improvement of interpretation procedure.
On the base of these results and, also, on the results of several direct comparisons with TEPC data [BOT03], it is estimated that the values of H_{app} differ from $H^*(10)$ values not more than about 20% for low LET component, about 30% for total (both $2\sigma_{rel}$).

REFERENCES

[AKS90] Akselrod M.S., Kortov V.S., Kravetsky D.J., and Gottlib V.I.: "Highly Sensitive Thermoluminiscent Anion-Defect α-Al_2O_3:C Single Crystal Detectors." Radiat. Prot. Dosim. 33, 119-122 (1990)

[AND64] Anderson I.O., and Braun J.A.: "A Neutron Rem Counter:, Nukleonik 6 (1964), p. 237-241

[BAM95] Bamblevskij V.P.: private communication, Dubna 1995

[BDS96] Bubble Damage Spectrometer Manual; BTI, Chalk River, 1996

[BOU92] Bouisset, P. et al., 1992. Description de l'instrument NAUSICAA conçu pour effectuer des mesures instantanées de H,D, et du spéctre TLE en champs complexes, In Proc. IRPA 8, Montréal, mai, pp. 463-466

[BOT03] Bottollier-Depois, J.-F., Spurný, F., etal.: „DOSMAX contract: Common flight Paris-Tokyo round trip via Fairbanks April, 2002", Rapport SDOS IRSN, in preparation

[DAC99] Dachev, Ts.P. et al. Detailed Study of the SPE and their Effects on the Dose Rate and Flux Distribution Observed by LIULIN Instrument on MIR Space Station, Radiat. Measur., 30 (3) (1999) 317-325.

[DER93] d'Errico F., and Alberts W.G.: „Superheated - Drop (Bubble) Neutron Detectors and Their Compliance with ICRP-60". Radiat. Prot. Dosim.54, (1994), p.357-360

[DMC91] "Dosimétre DMC 90 Manual." Merlin Gérin Radioprotection, 35226, Lamaron, France, 1991

[HOF94] Höfert M., and Stevenson G.R., 1994. The CERN-EC high energy reference field facility. In Proc. of the 8th Inter. Conf. on Radiat. Shielding, Arlington, Texas

[ING91] Ing H.: "Bubble Technology Industries Report". Chalk River 1991

[MIT02] Mitaroff A., Silari M.: "The CERN-EU high energy reference field (CERF) facility for dosimetry at commercial flight altitudes and in space"; Radiat.Prot.Dosim. 102 (2002) 7-22

[RSS88] RSS 112 Manual, Reuter Stokes Ltd., 1988

[SPD02] Spurný F., and Dachev Ts.: „Aircrew onboard Dosimetry with a Semiconductor Spectrometer"; Radiat.Prot.Dosim. 100(2002), p. 525-528

[SPD03] Spurný F., Dachev Ts.: "Long-term monitoring of the onboard aircraft exposure level with Si-diode based spectrometer", **sollicited speach** at the 34th COSPAR, Houston, Oct. 10-19, Adv. Space Research 32, (2003), No 1, 53-58

[SPU92] Spurný F.: "Dosimetric characteristics of proton, neutron and negative pion beams at the phasotron in Dubna", Radiat.Prot.Dosim. 44,(1992), 397-404 (**invited paper**)

[SPU93] Spurný F., and Votočková I.: "Response of TLD's to protons and alfa particles with energies to 10 MeV."(in czech) Nuclear Energy Safety 1(39), 176-180 (1993)

[SPU94] Spurný F., Votočková I., and Turek K.: „Equipment and Detector's Calibration at CERN High-Energy Reference Fields-II. May 1994"; Report IRD AS CR 391/94, Prague, May 1994

[SPU02a] Spurný F., Turek K., and Vlček B.: „Equipment and Detector's Calibration at CERN-CERF High-Energy Reference Fields - XVII. June-July 2002"; Report DRD NPI AS CR 508/02, Prague, August 2002

[SPU02b] Spurný F., Malušek A., and Kovář I.: "Individual dosimetry of czech company aircrew 1998-2000", Inter.Conf. on Occupational Radiation Protection: Protecting Workers against

Exposure to Ionising Radiation, IAEA, Geneva, August 26-30, 2002, Proc., p. 397-400
[SPU02c] Spurný, F.: „Exposure of Air Crew to Cosmic Radiation. Calculation and Experimental Approach"; in „*High Levels of Natural Radiation and Radon Areas: Radiation Dose and Health Effects"* : eds.:W. Burkart, M. Sohrabi, A. Bayer; Elsevier Science 2002, p. 121-129
[TUR93] Turek K., Spurný F., and Alberts W.G.: "On the Optimization of the Etching of CR 39 as Fast Neutron Dosemeter". Nucl. Tracks Radiat. Measur. 21, (1993), 299-302
[VIE90] Viererbl L., Nováková O., and Jursová L.: "Combined Scintillation Detector for Gamma Dose Rate Measurements", Radiat. Prot. Dosim. 32, 273-277, 1990

A.5 SWEDISH RADIATION PROTECTION AUTHORITY (SSI)

Jan-Erik Kyllönen and Lennart Lindborg
Swedish Radiation Protection Authority, S-171 16 Stockholm

A.5.1 Instrument Description

The Sievert-instrument (figure A.5.1) is based on two tissue-equivalent proportional counters (TEPC) used in the variance-covariance method.[1-5] The sensitive volume of each detector is 1.2 litres and cylindrical in shape with a height and a diameter of 11.5 cm each. The 5 mm wall is made of tissue-equivalent plastic A-150. With a propane-based tissue-equivalent gas filling of 1.45 kPa, the detector simulates a tissue volume of 2 µm mean chord length. Each detector is contained in a 3.9-litre vacuum tight container of 2 mm Al. The electric charge created in the detector gas is measured by an electrometer. An additional GM-tube is also included for use in parallel with the TEPC for studies of the low-LET radiation component. The measurements have demonstrated that it is sufficient to have one detector, as the covariance term is never large[3]. However, it has occasionally been valuable to have results from two detectors for the analysis.

A.5.2 Measurement principles

In the variance-covariance method, energy- or dose-weighted averages of the closely related microdosimetric quantities energy imparted (ε), lineal energy (y) and specific energy (z), are determined. The dose-mean energy imparted in a single event ($\bar{\varepsilon}_{1,D}$) is determined from measurements of the relative variance ($V_{r,gas}$) in a series of 100 ms long measurements of the energy deposition in the gas (E).[4]

$$\bar{\varepsilon}_{1,D} = \left(V_{r,tiss} - C_{r,tiss}\right)\bar{\varepsilon} = \left(\frac{\rho_{tiss}}{\rho_{gas}}\right)^2 \left(V_{r,gas} - C_{r,gas}\right)\left(\frac{\rho_{gas}}{\rho_{tiss}}\right)^2 \bar{E} = \left(V_{r,gas} - C_{r,gas}\right)\bar{E} \qquad (1)$$

The square of the density ratio between tissue and detector gas corrects for the smaller relative variance and the larger energy deposition in the gas compared with the microscopic tissue volume. The relative covariance between two simultaneously working detectors ($C_{r,gas}$) corrects for a possible variance contribution originating from a change of the mean dose rate in the radiation field itself. For propane-based tissue-equivalent gas and mixed photon and neutron fields, a mean energy spent per unit charge produced (W/e) of 28 J/C is used. The energy deposition in the gas is given by the average charge produced in the detector ($\bar{q}$) and W/e. The dose-mean lineal energy ($\bar{y}_D$) is calculated from the dose-mean energy imparted and the mean chord length of the simulated tissue volume.[4]

Assuming the quality factor (Q) to be a function of linear energy transfer to water (L) and substituting L with lineal energy (y), the dose-mean quality factor can be expanded in a power series of y

$$\bar{Q}_D = \int_0^\infty Q(y)d(y)dy = a + b\bar{y}_D + c\overline{y_D^2} + \ldots \approx a + b\bar{y}_D \qquad (2)$$

Here d(y) denotes the dose distribution of the lineal energy (y). The measured $\bar{y}_D$ is used in a first order approximation of the dose-equivalent given by

$$H^* = ND_{gas}\bar{Q}_D = \frac{N\bar{q}\,W/e\,(a + b\bar{y}_D)}{m_{gas}} \qquad (3)$$

Here N is a calibration factor determined in a ^{137}Cs gamma beam, D_{gas} is the dose to the detector gas and m_{gas} is the mass of the detector gas. The best choice of the constants a and b, minimizing the difference between H^* from eq. (3) and the ambient dose-equivalent $H^*(10)$, depends on the LET-distribution of the radiation field and the counter characteristics. For mixed fields with a low-LET component and a high-energy neutron component such as in the atmospheric cosmic radiation field, the best values have been determined to a=0.88 and b=0.09 μm/keV. For fields with lower neutron energies, another values on the constants should be used.[4]

A.5.3 Neutron Field Response Investigations

Response investigations have been performed at Physikalisch-Technische Bundesanstalt (PTB, Germany), at Université Catholique de Louvain (UCL, Belgium), at T. Svedberg Laboratory (TSL, Sweden) and in the cosmic neutron reference field (CERF) at CERN.[4-5] At PTB, measurements were performed in accelerator produced neutron beams between 71 keV and 14.8 MeV and in a moderated and an unmoderated field of ^{252}Cf by effective $H^*(10)$-energies of 1.77 MeV and 2.01 MeV, respectively. At both UCL and at TSL the neutron fields are "quasi-monoenergetic" with fluence peaks at 60 and 180 MeV respectively, and a band of neutrons at lower energies. At CERN the high-energy neutron field (CERF) the contribution to $H^*(10)$ comes mainly from two broad peaks, between 1 - 20 MeV and 50 - 200 MeV, respectively. It was shown that the $H^*(10)$ response of the instrument is within ±50% for neutrons between 1 and 180 MeV using the values a=0.88 and b=0.09 μm/keV in eq. (3) (figure A.5.2 and table A.5.1). It was also shown that in the cosmic radiation reference field (CERF) the instrument gives the same value of $H^*(10)$ within uncertainties as a single-event TEPC of the HANDI type.

A.5.4 In-flight Measurements

Two principally different methods have been used for the analysis of flight data showing no significant differences in the results.[3] In the first the radiation field in the atmosphere is assumed to be reasonably well characterized by one low-LET component and a high-energy neutron component. The response investigations showed that the dose-equivalent determined by eq.(3) was in agreement with a H^*-value based on a microdosimetric y-spectrum for the CERF field. If the atmospheric neutron spectrum is reasonably similar, then eq.(3) can be used directly on board aircraft.

The second method is based on the observation that single high-LET events can be identified in the multiple-event spectrum measured in the cosmic radiation field (figure A.5.3). A multiple-event distribution is the distribution of energy (or dose) at a specific dose level that is determined by the dose rate and the integration time. The energy in each measurement (0.1 s long) is deposited by many events, which in aircraft measurements are dominated by low-LET events. Measurements including a high-LET event will show up in the high-energy part of the distribution due to the low average dose in each single integration . Since the frequency of high-LET events is very low, the probability of having more than one such event in a 0.1 s long measurement is negligible. In this way it is possible to identify and to treat the high-LET events separately and reduce the multiple-event spectrum to events of low and medium-LET. The high-LET limit is defined as 150 keV/μm and the reduced multiple-event spectrum contains then only events below 150 keV/μm.

A measured energy deposition (ε_k) including a high-LET event can hence be interpreted as the sum of a single high-LET event ($\varepsilon_{h,k}$) and a low-LET multiple-event $G(\varepsilon)$. The quality factor for these high-LET particles are determined directly from the ICRP60 $Q(L)$-relation with y replacing L. The quality factor for the reduced low-LET multiple-event spectrum is given by eq (2) with a=0.73 and b=0.17 μm(keV)$^{-1}$ and the average quality factor can be written as

$$\overline{Q}_D = \int_0^{150} (a+by)d(y)dy + \int_{150}^{\infty} \frac{300}{\sqrt{y}} d(y)dy = (1-d_h)(a+b\overline{y}_{D,l}) + \frac{300}{N\varepsilon} \sum_{k=1}^{n} \sqrt{(\varepsilon_k - G(\varepsilon))\overline{l}} \qquad (4)$$

Here $\overline{y}_{D,l}$ is the dose-mean lineal energy for a spectrum with events below 150 keV/μm and d_h the dose fraction from the n events above 150 keV/μm.

Neither of the two methods gives direct information of the radiation field components. An estimation of the neutron component can be done by assuming the LET (or y) -distribution of the atmosphere to be the same as the sum of a CERF neutron field and a ^{137}Cs gamma beam. The neutron dose fraction (d_n) is then determined from the dose-mean lineal energies measured on-board ($\overline{y}_D$), in a ^{137}Cs gamma beam ($\overline{y}_{D,Cs}$) and in the CERF neutron field ($\overline{y}_{D,n}$) according to

$$d_n = \frac{(\overline{y}_D - \overline{y}_{D,Cs})}{(\overline{y}_{D,n} - \overline{y}_{D,Cs})} \qquad (5)$$

It should be noted that a division into ^{137}Cs- and CERF-equivalent dose fractions in terms of $\overline{y}_D$, is not equivalent to a division of the lineal energy distribution into a low- and a high-LET dose fraction. A comparison of dose fractions determined with single-event TEPC systems using the latter kind of separation should therefore be interpreted with caution.

A.5.5 Uncertainties

All uncertainties discussed in this section refer to standard uncertainties evaluated as type A or type B according to ISO.(6) The uncertainty in the $H^*(10)$-calibration in the ^{137}Cs-field is 5 %. The uncertainty introduced by the temperature dependence of the detectors is 1-2 %, and W/e is not known to better than 5 %. (7) Both methods for deriving an average quality factor have an estimated uncertainty of about 10 %. The correction to the route dose, which compensate for the lack of measured data during take-off and landing, has an uncertainty of about 1%. The uncertainty in H*due to the limitations in the response of the TEPC to primarily neutron is estimated to be 10%. One of the major uncertainty contributions at aviation altitudes is due to poor statistics of high-LET particle interactions.(3) As a consequence it is not possible to determine H^* on board aircraft with a better statistical accuracy than about 10-15% in a 1 hour measurement with the first method and with a detector of this size. When the high-LET particles are treated as single events, their importance will have a less weight and the statistical uncertainty will become smaller. Typically a relative standard deviation between 5 %and 7 % is observed in a one hour measurement during a north Atlantic flight. The combined A and B uncertainties in a 1-hour measurement of cosmic radiation is hence about 20 % (Table A.5.2) and about 17% in a 10-hour route dose determination. This is comparable with daily dose variations of 10-20% that may occur due to variations in solar activity.

A.5.6 References

1. Kyllönen, J.E., Lindborg, L. and Samuelson, G. *Paired TEPCs for Variance Measurements.* In: Microdosimetry: An Interdisciplinary Approach. Eds. D. Goodhead, P. O´Neill and H.G. Menzel (The Royal Society of Chemistry, Cambridge) Special Publication No 204 (1997)

2. Lindborg, L., Kyllönen, J-E., Beck, P., Bottollier-Depois, J. F., Gerdung, S., Grillmaier, R. E. and Schrewe, U. *The use of TEPC for reference dosimetry*, Radiat. Prot. Dosim. 61 (1-3) 119-124 (1999).

3. Kyllönen, J-E., Lindborg, L. and Samuelson, G. *Cosmic Radiation Measurements On-board Aircraft with the Variance Method*, Radiat. Prot. Dosim. vol. 93 No3, pp 197-205 (2001).

4. Kyllönen, J-E., Lindborg, L. and Samuelson, G. *The Response of the Sievert Instrument in Neutron Beams up to 180 MeV,* Radiat. Prot. Dosim. vol. 94 No3, pp 227-232 (2001).

5. Kyllönen, J-E., Lindborg, L. and Grindborg, J-E. *Response Investigations of a TEPC in High Energy Proton and Neutron Beams Using the Variance Method,* Presented at the 13th Symposium on Microdosimetry in Stresa, Italy, May 2001.

6. ISO, *Guide to the Expression of Uncertainty in Measurement,* International Organization for Standardization 1995.

7. IAEA, *Atomic and Molecular Data for Radiotherapy and Radiation Research*, IAEA-TECDOC-799, ISSN 1011-4289 (1995)

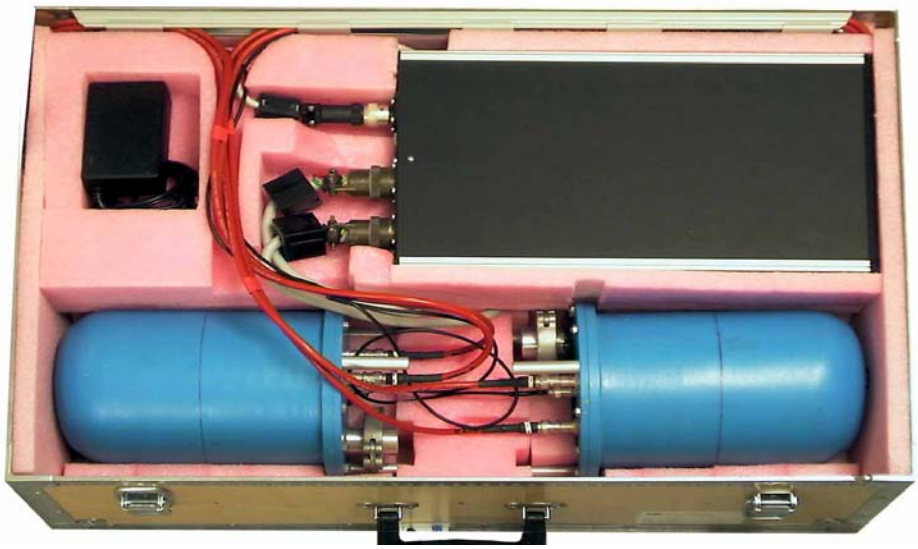

Figure A.5.1. The two TEPC detectors in the box used for cosmic radiation measurements onboard aircraft.

Table A.5.1. Measured dose-mean lineal energy ($\bar{y}_D$), conversion coefficients to D*(10) and *H*(10)* in neutron fields of different effective H*(10)-energies. A W/e-value of 30 eV has been used.

E_{eff} (MeV)	$\bar{y}_D$ (keV/µm)	D/Φ (pGy cm2)	H*/Φ (pSv cm2)
0.071	23 ± 5	4.8 ± 1.0	13.4 ± 3.4
0.144	41 ± 8	7.4 ± 1.5	31.9 ± 8.1
0.57	85 ± 15	18.7 ± 3.9	150 ± 39
1.77 [2)]	81 ± 15	29.9 ± 6.2	230 ± 60
2.01 [1)]	80 ± 15	31.5 ± 6.5	239 ± 63
5	64 ± 12	49.2 ± 10	306 ± 80
14.8	122 ± 23	79.6 ± 16	885 ± 238
34	121 ± 22	42.3 ± 9.1	468 ± 134
51	108 ± 12	68.4 ± 13	682 ± 154
69	109 ± 18	56 ± 13	562 ± 164
121	76 ± 8	21.7 ± 6.3	153 ± 51

[1)] ^{252}Cf-source. [2)] ^{252}Cf(D_2O. Cd)-source.

Table A.5.2. Standard uncertainties for a 1-hour TEPC measurement of cosmic radiation

Type	A (%)	B (%)
Dose (1 hour)	1	
Quality factor (1 hour)	6-13	
Temperature dependence		2
Calibration		5
Average ionisation energy		5
Approximations in method		10
TEPC response characteristics		10
Quadratic sum	6-13	16
Combined A & B	17-21	

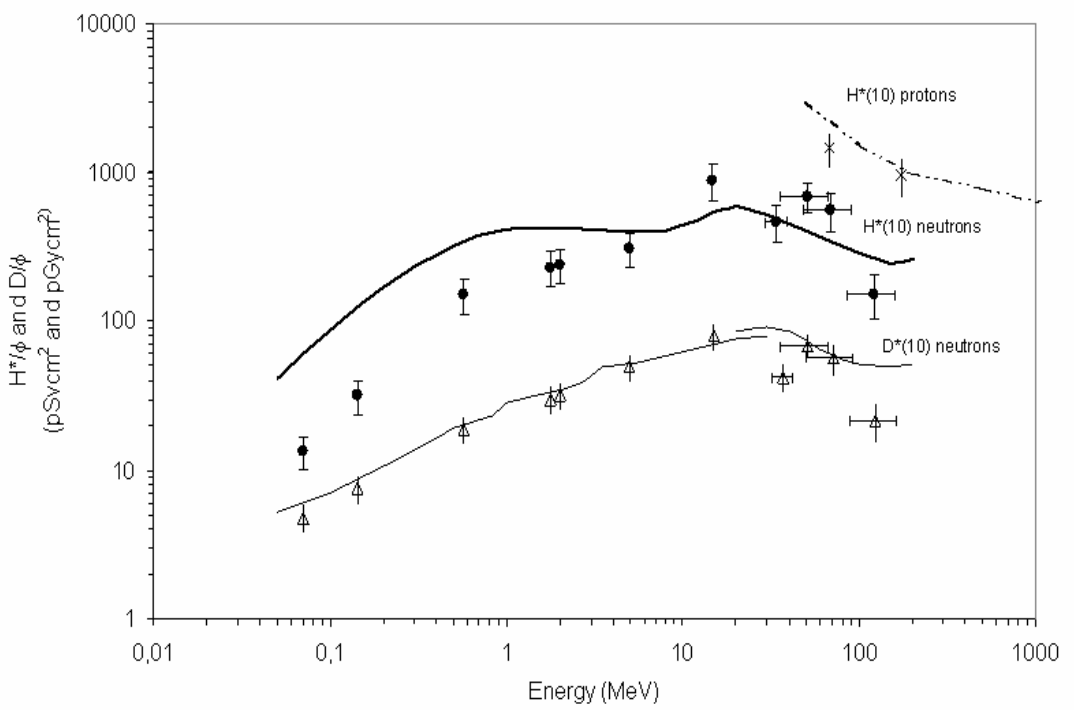

Figure A.5.2. Measured conversion coefficients from fluence to absorbed dose and dose-equivalent as a function of effective H*(10)-energy. The data are given with two combined standard uncertainties. Measured data for neutrons are shown as filled circles for H*, open triangles for D. The proton data are shown as crosses. The lines show coefficients to *D*(10)* and *H*(10)* from ICRP 74 and other references.

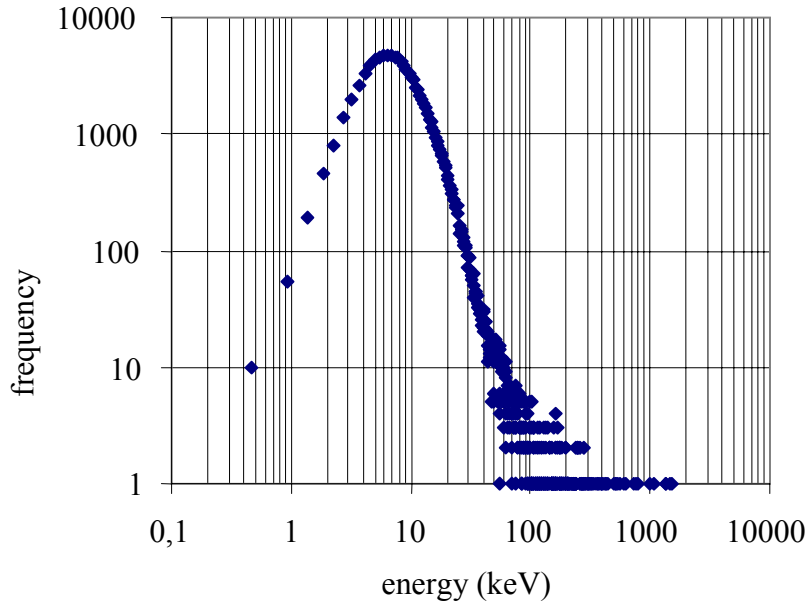

Figure A.5.3. Multiple-event spectrum (100 000 measurements, i.e. 3 hours) from 33 000 feet between N42W073 and N59W030, on the flight from New York to Helsinki 980328. Events of 300 keV correspond to lineal energies of about 150 keV/□m.

A.6 Dublin Institute for Advanced Studies

Determination Of LET Spectra And Charge Spectra at Aircraft Altitudes Using Solid State Nuclear Track Detector Techniques

D. O'Sullivan, D. Zhou, E. Flood, Dublin Institute for Advanced Studies, 5 Merrion Square, Dublin 2, Ireland.

A.6.1 Introduction

Solid State nuclear track detectors have been successfully employed in the study of cosmic radiation and its secondaries, over a wide charge and energy interval, since the late sixties. The technique has also been used in investigations of energetic particles originating on the sun. It was, therefore, natural that when it was decided some years ago to undertake an extensive study of cosmic and solar radiation at aircraft altitudes, that these detectors would provide an important contribution to the programme. Not all track detectors are suitable due to the nature of the radiation field at these altitudes in the Earth's atmosphere. Because of its high sensitivity and low ionization threshold for track registration, poly allyl diglycol carbonate (PADC) or CR-39 as it is also known, is ideal for aircrew investigations. Generally LET spectra above 5keV/μ can be determined as well as charge spectra for Z>1. Thus high LET spectra usually defined as LET ≥ 5keV/μm (as opposed to low LET ≤ 5keV/μm) can be measured conveniently by this method.

A.6.2 Experimental Method

(a) LET Spectra

Here we outline the methods used to investigate short range tracks produced by high LET particles which were generated mainly by neutron interactions in CR-39 detectors[1]. Stacks of CR-39 detectors were placed inside the cabin of each aircraft. The location was usually chosen to facilitate long term exposure of several months and generally close to the cockpit or in the panelling above the passenger compartment. The stacks consisted of up to 20 sheets of detector, each approximately 0.55mm thick. On recovery from the aircraft, the detector sheets were etched for either 20 hrs or 60 hrs in 6.25N NaOH at 60°C. Following etching the thickness of the detector layer removed, B, was estimated by both mass loss and thickness change measurements. Typical mean values found for the bulk etch rate were in the range $0.55 \leq Vg \leq 0.65$ μm/h.

The detectors were scanned to locate the recoil tracks produced predominantly by neutrons at these altitudes in the Earth's atmosphere. The magnification used for scanning depended on the track density observed. When a track signal was observed the ellipse major and minor axes were measured using the same magnification. The observed track depth distribution extends down to approximately 3 μm. The etch rate ratio (S) was calculated for each event from[2]:

$$S = \sqrt{1 + 4\left(\frac{a}{2B}\right)^2 \Big/ \left[1 - \left(\frac{b}{2B}\right)^2\right]^2} \qquad (1)$$

The relationship between the linear energy transfer, $LET_\infty(H_2O)$ and S was determined by calibrating the detectors mainly with protons and carbon ions over most of the range of LET values observed in these investigations[3]. The method used in this analysis assumes that in order to use equation (1), the etch rate of each track is constant over the length of each track. This of course will not be true for recoil tracks which are over-etched. Because of the nature of solid state nuclear track methods of analysis, this assumption gives rise to an approximation, which though unavoidable, can be estimated to a sufficient level of accuracy

for the investigation of radiation doses at civil aviation altitudes. The reference surface is the post etch surface in this investigation. All etched tracks that cross this surface are accepted for analysis. These include some tracks which are rounded at the bottom (over-etched) which may result from very low energy recoils that have penetrated the post etch surface or from particles which stopped in the layer removed by etching. Careful visual inspection of the tracks crossing the post etch surface revealed that only ≈5% of the sample showed definite signs of rounded tips but this is probably an underestimate due to the difficulty in recognizing short ranged stopping particles. The underestimate of S for these particles can be largely overcome by using a short etch time (20hrs) as mentioned earlier and the eventual LET spectrum above ≈180keV/μm, where most of these events lie, was constructed using this shorter etch time. In general an inspection of the LET versus range relationship for typical recoils show that in the worst case (a stopping oxygen nucleus) the underestimate in LET using equation (1) is ≈25%. This underestimate is reduced considerably as one goes to lower LET values. Detection efficiency was estimated by a combined investigation of registration efficiency and scanning efficiency. Registration efficiency was determined by estimating the loss of tracks (due to registration failure) for a sample of approximately 150 cosmic ray primary and secondary nuclei with 26>Z>1 penetrating the same detector stacks used for the LET work described here. The nuclei found in an optical scan of the detectors were followed to their stopping points, the final plate of their trajectory or to where they left the stack. Path lengths ranged from one to twenty detector plates and so the investigation involved several hundred cone pairs with etch rate ratios in the range 1.03<S<3.0. In no case was it found that a track expected to register on either top or bottom surfaces of a detector plate failed to do so, indicating a registration efficiency of 100%. Scanning efficiency was estimated by repeated independent scans of a fixed area of detector. An area of approximately 8 cm^2 was scanned under the same experimental conditions employed throughout this investigation, to detect penetrating primary and secondary cosmic ray nuclei as described above. Three experienced observers took part in the scanning. The resulting scans showed particle densities of 7.3, 7.5 and 7.6 particles/cm^2 for the three observers. The most experienced observer, who achieved a particle density of 7.5 initially, repeated the process and the second scan resulted in a density of 7.8 particles/cm^2. The results showed that scanning efficiency averaged approximately 96% overall giving a detection efficiency of the same value. LET values were binned and the differential fluence spectrum obtained using the formula:

$$\frac{d^3N}{dAd\Omega dLET} = \left(2\pi A \cos^2 \delta_{cut}\right)^{-1} \frac{dN}{dLET} \qquad (2)$$

The concept of δ_{cut} has been investigated in many previous experiments. Initially it was assumed that detection of particles was essentially 100% efficient between 90° and the etch rate ratio (S) dependent critical angle δ_{crit}. However it was found, particularly in the case of automatic systems, that 100% efficiency was attainable only to an angle δ_{cut} which was greater than δ_{crit}[4,5]. A relationship of the type $\delta_{cut} = \pi/2 - f\ (\pi/2 - \arcsin(1/S))$ expresses this situation. When f=1.0, $\delta_{cut} = \delta_{crit}$ and $\delta_{cut} > \delta_{crit}$ for all values when f < 1.0. Fig. 1 shows a plot of dip angle versus etch rate ratio S for a sample collected in the present work (at supersonic altitudes).

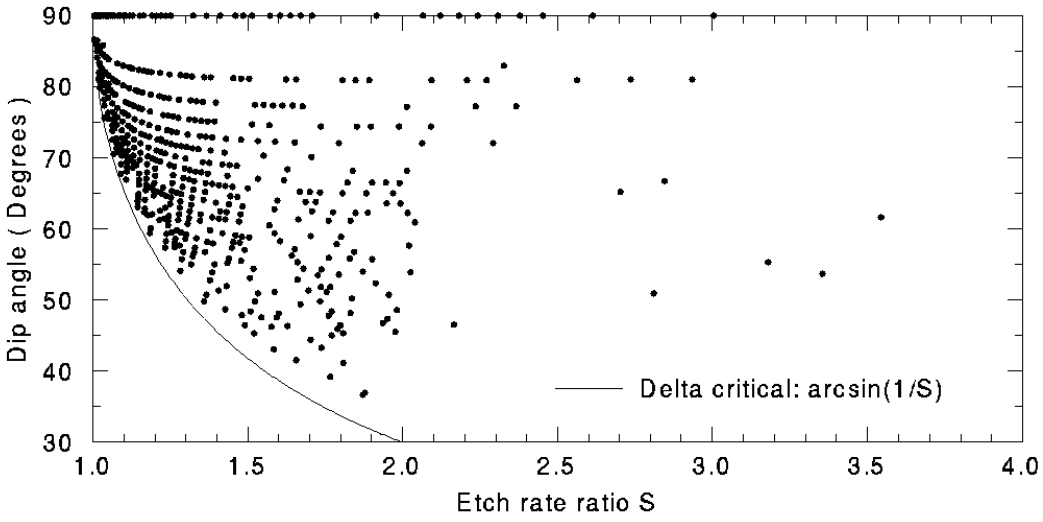

Fig. A.6.1. Dip angle versus etch rate ratio S for London-New York supersonic route

The fall off in the density of points near δ_{crit} which was very evident in previous work employing automatic systems[5]) is not very significant here and suggests that a δ_{cut} expression with $f \approx 0.95$ is appropriate in the present investigation. The average f value was calculated by determining the minimum dip value appropriate to each S value in Fig. A.6.1.

Because of the extended period during which the detectors are employed in this investigation background levels due to the exposure to α particles from radon were not insignificant and averaged approximately 20% of the track density when checked against control samples. Background subtraction was implemented at this stage. Measurement of the background was undertaken in the same way as described for the cosmic ray data and subtraction was done for each appropriate differential fluence bin of the LET spectrum. It is assumed that the angular distribution of the neutrons at these altitudes in the atmosphere is isotropic. Recent experiments by our group at supersonic and subsonic aviation altitudes show that this is true to an accuracy of ~93%. The absorbed dose (G_y) is then $=4\pi \times 1.6 \times 10^{-9} \times LET_\infty \times F$ where LET_∞ is the linear energy transfer (keV/μm) in water at the center of the relevant LET bin and F is the differential fluence in particles cm^{-2} sr^{-1} $(keV/\mu m)^{-1}$ in the same bin. The integral spectrum is generated by summing the differential spectrum from high LET to low LET.

Several exposures at the CERN Reference Field over the last 4 years have shown that this method for determining dose equivalent is consistent with data obtained by TEPC instruments for high LET (>5 keV/μm). Comparison of LET spectra by the method described also show very good agreement with predictions of the FLUKA code[1].

(b) Determination of Charge Spectra at Aircraft Altitudes

The procedures for these investigations are as follows[6,7]. Following exposure in aircraft (Concorde) the CR-39 detectors were etched for 50hrs at 60°C in 6.25N NaOH. Cosmic ray primary and secondary nuclei in the range $2 \leq Z \leq 4$ were located primarily during the high magnification scanning phase of these studies. The criterion for selection was that a pair of cones exist (one on the top surface and one on the bottom surface) corresponding to the passage of the particle through at least one sheet of detector. This allowed the discrimination of the higher energy cosmic ray particles from the overwhelming background of short range recoils (typically R≤50μm). For instance, helium nuclei generally registered in one sheet only since their ionisation decreases rapidly with energy and falls below the observable threshold. The energy interval over which helium nuclei were observed and measured in this experiment

was 7 MeV/n to 22 MeV/n, the former being defined by the minimum energy required to traverse one plate and the latter by ionisation threshold considerations. Nuclei with Z≥4 which traversed part or all of the detector stack were observable in several or all of the sheets. In order to facilitate following events from sheet to sheet it was required that the initial track picked up should have R≥2μm. This criterion, along with the consideration of the minimum energy required to traverse a single plate defined the energy intervals for the nuclei indicated in Table A.6.1. The observed differential fluence for each type is also shown. The charge of the individual particles was determined by measuring the etch rate gradient following calibration of the detectors with low energy protons and stopping carbon ions of initial energy of 85 MeV/N.

Table A.6.1: Differential Fluence of Cosmic Ray Nuclei at Supersonic Altitude (London-New York)

Nuclei	Energy Interval Detected	Differential Fluence Observed
	(MeV/n)	$(cm^2\ MeV/n)^{-1}$
He	7≤E≤22	$(3.43\pm0.49)\times10^{-3}$
Li	8≤E≤60	$(1.24\pm0.50)\times10^{-4}$
Be	10≤E≤150	$(3.06\pm1.53)\times10^{-5}$
B	11≤E≤155	$(2.98\pm1.49)\times10^{-5}$
C	13≤E≤250	$(4.07\pm1.36)\times10^{-5}$
N	14≤E≤400	$(1.39\pm0.62)\times10^{-5}$
O	15≤E≤800	$(5.46\pm2.73)\times10^{-6}$

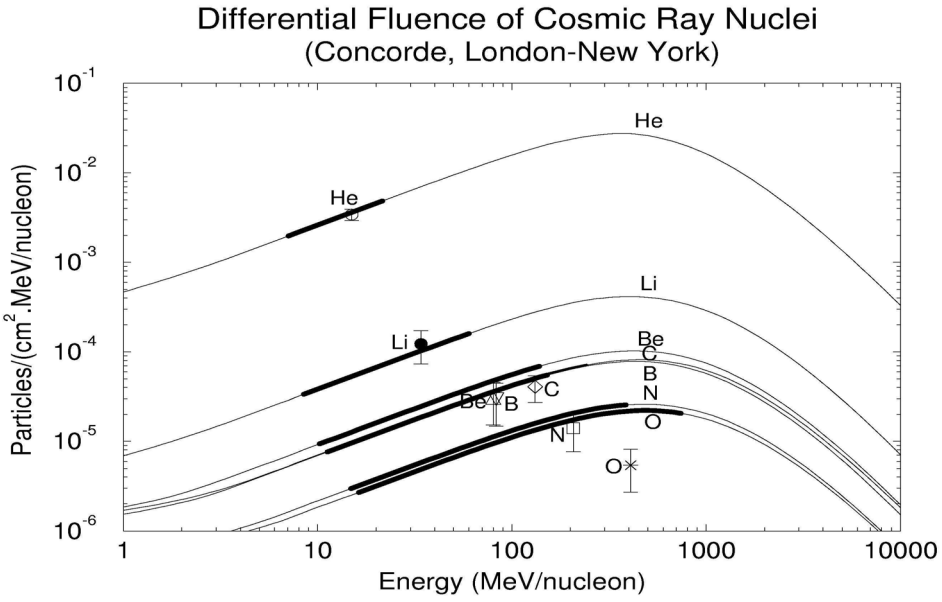

Figure A.6.2: A comparison of experimental and theoretical results for cosmic ray nuclei at supersonic altitude (London-New York)

Figure A.6.2 shows the observed differential fluence compared with the predictions of the Siegen University HITCODE programme. Agreement is very satisfactory except for oxygen nuclei. The charge spectrum extended as far as Z=26 at Concorde altitudes and up to Z=8 at typical subsonic flights.

A.6.2 References

1. D. O'Sullivan, D. Zhou, W. Heinrich, S. Roesler, J. Donnelly, R. Keegan, E. Flood and L. Tommasino. Cosmic Rays and Dosimetry at Aviation Altitudes. *Radiat. Meas.* 31 579-584, 1999.

2. G. Somogyi and S. Szalay. Track Diameter Kinetics in Dielectric Track Detectors. *Nucl. Instr. Meth.,* 109, 211-232, 1973.

3. GSF Report 12/98 Radiation Fields, Dosimetry, Biokinetics and Biophysical Models for Cancer Inducing Radiation (1996-1999). F*orschungzentrum für umwelt und Geshundheit, GmbH.* 1999.

4. K. Ogura, E.V. Benton, A. Frank and T. Atallah. Proton Response of CR-39. *Nucl. Tracks*. 12, 527-530, 1986

5. R. Keegan. LET Spectrum Generation and Proton Induced Secondary Contribution to Total Dose Measured in Low Earth Orbit. *Ph.D. Thesis, University College Dublin.* 1996.

6. D. Zhou, W. Heinrich, D. O'Sullivan, J. Donnelly, J. Byrne and E. Flood. Cosmic Abundance at Aircraft Altitudes in the Earth's Atmosphere. *Proc. 26th ICRC, Salt Lake City, USA, OG 1.1.27.* 1999.

7. D. O'Sullivan, A. Thompson and P.B. Price. Composition of Galactic Cosmic Rays with 20<E<1300 MeV/nucleon. *Nature Phys. Sci.* 243, 8-9. 1973.

A.7 CIEMAT

J.C. Saez Vergara[a], R. Dominguez-Mompell Román[b],
[a]CIEMAT, Servicio de Protección Radiológica, Av. Complutense 22, E-28040 Madrid, Spain
[b]IBERIA L.A.E., Servicio Médico, Zona Industrial Aeropuerto Barajas, E-28042 Madrid, Spain

A.7.1. Selection of instruments

Active (powered) dose rate monitors were selected from the commercially available instrumentation. In particular, high-energy neutron monitors recently available were targeted in order to check the real capabilities of such instruments in presence of high-energy neutrons. Table 1 presents the main characteristic of the selected instruments. According to the detectable component of radiation, the instruments have been divided into those designed to measure the non-neutron and the neutron components of the cosmic radiation. The non-neutron component approximately corresponds to the low-LET component (<10 keV·µm^{-1}) and the neutron component relates with the neutron and the nuclear interaction of the high-energy proton component of the field. Detailed information on the basis and operation of the different equipments can be found in references [1] to [7].

Table 1
Active instruments employed for dose rate measurements onboard IBERIA flights

Instrument	Detector type	Energy/LET range
Low LET or 'ionising' component:		
Reutes Stokes RS131	Pressure Ion Chamber	70 keV-8 MeV
Genitron GammaTracer	Geiger-Müller tubes	45 keV- 1.3 MeV
Eberline FH-40G	Proportional counter	45 keV- 1.3 MeV
High LET or 'neutron' component:		
Eberline SWENDI2	^{3}He tube + W moderator	Up to 5 GeV
MAB Linus SNM500X	^{3}He tube + Pb moderator	> 10 MeV
Far West Tech. HAWK	TEPC (12.7 cm diameter)	0.3-1024 keV·µm^{-1}

The instrument readings were converted to the quantity ambient dose equivalent, H*(10), using adequate conversion factors when needed. Regular calibrations were performed in the CIEMAT Secondary Standards Laboratory (Non-neutron component: ^{137}Cs and ^{60}Co photon beams) and the CERF[8] facility at CERN (Neutron component). For each instrument, the respective calibration factors obtained at CERF were constant within 5% during the last three years (2001 to 2003) as it is shown in Figure 1. The Figure also shows the relative response to the CERF of the instruments to others standard neutron sources (AmBe and ^{252}Cf bare). While the response of the SWENDI2 monitor to these sources was close the response at CERF, the Linus-SNM500X and the TEPC high-LET window offered about 15-20% over-response with the sources.

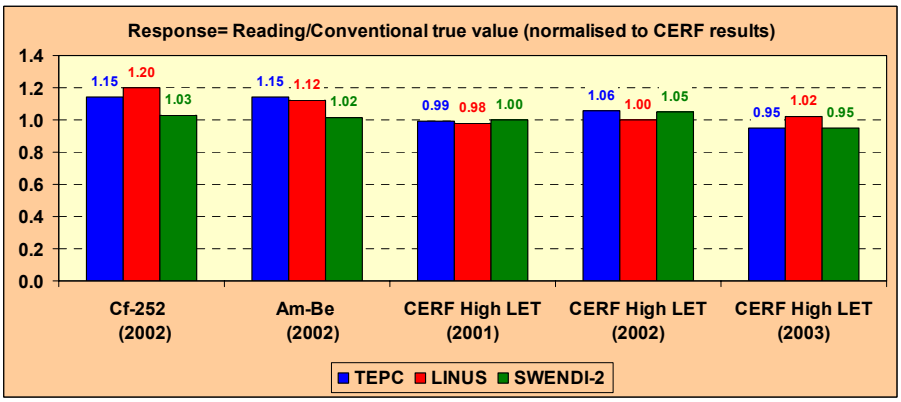

Figure 1: Response of the neutron instruments normalised to CERF: comparison with other neutron sources and changes during the three years 2001-2003.

A.7.2. Onboard measurements

The instruments were located on a modified aviation trolley (Figure 2)[7], with the exception of the RS131 due to its size. The trolley and the chamber were normally located at the forward galley. Due to safety reasons, all the instruments are battery operated during the flight and the autonomy (battery life) ranges from 6 hours (LINUS) to 3 years (GammaTracer). Each instrument records the entire flight (switching on before take-off, switching off after landing) and the integration time is 5 minutes, with the exception of TEPC which is automatically recording data (including two LET spectra) every minute. Geographic data (latitude, longitude and altitude) on the performed route are obtained automatically from a GPS mounted in the TEPC which needs a small antenna fitted in a window of the aircraft. The recorded data are stored in each instrument ranging the storage capability from 256 data (more than 21 hours) to practically unlimited (RS131 and TEPC).

After each flight, all the data are transferred and processed in a laptop with MS Excel templates to analyse the results. The route data are entered in the two codes employed in the Project: CARI-6 (FAA, USA)[9] and EPCARD 3.2 (GSF, Germany, developed under an EC Contract)[10]. A database with extensive information and analysis results of each flight is maintained at CIEMAT.

Aircrew monitoring in the Spanish airlines differs from the previous European studies due to the geographic situation of Spain (the most meridional european country) and economical and cultural links with America. In addition, Spanish isle territories (Canary and Balearic Islands) must be served with many flights. As a consequence, an important part of IBERIA flights goes to the Tropical and Equatorial regions, which means lower doses but also probably greater uncertainties (most of the published studies are focused in the North Hemisphere[11-16].

Figure 2: Installation of the instruments on-board: Left: Modified aviation trolley; Middle: Compensated neutron rem-meters and Pressure Ion Chamber (Center); Right: Trolley fixed in the forward galley in an Airbus-340 aircraft.

A.7.3. Results

The four instruments intended to detect the non-neutron component seems to be sensitive enough to detect the influence of flight operation parameters (altitude and latitude) with only 5 minutes integration period. In most flights, the three standard gamma probes agree in ±15% (5% when RS131 is compared with GammaTracer). By contrast, the TEPC (low LET

window) shows up to 20% underestimation in some flights. For the neutron component instruments, the sensitivity is poorer but it still permits to integrate within 5 minutes. The agreement between SWENDI2 and Linus-SNM500X results is also remarkable, but the TEPC high-LET window is giving 10% higher than the SWENDI2. Concerning the total dose, the sum of RS131 and SWENDI2 yields about 10% higher that those estimates obtained with the TEPC because some high-energy protons in the field can be detected, at least partly, by the ion chamber and the neutron monitor. None of the above mentioned ratios shows a clear dependence with the region of operation which means that all the instruments behave in a similar way irrespective of the latitude. Despite of these good results for the mean values, it should be mentioned that the differences when considering individual flights can reach 30%.

From the basic dose rate results obtained with each instrument, the following dose quantities are calculated:

- Route dose: integrated dose from take-off to landing.
- Mean dose rate during the flight (Route dose divided by the flight duration).
- Annual doses (Ambient dose equivalent, Effective dose), considering 800 flying hours per year (Flying hours are considered from take off to landing).

Figure 3 displays examples of flight dose rate profiles and dose estimates for three destinations in America (Chicago, Havana and Santiago de Chile).

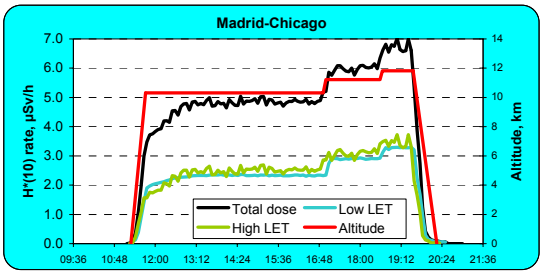

Departure date: 22/11/2002
Aircraft model: A340
Flight duration (h): 8.97 hours
Mean altitude (km): 10.7 km

	Route dose µSv	Mean dose rate µSv/h	Annual dose* mSv
CARI-6, E	37.9	4.23	3.38
EPCARD 3.2, E	43.3	4.82	3.86
EPCARD 3.2, H*(10)	36.7	4.09	3.27
TEPC, H*(10)	43.3	4.83	3.86
RS131+SWENDI2, H*(10)	41.9	4.67	3.74

* Computed for 800 flying hours (from take-off to landing)

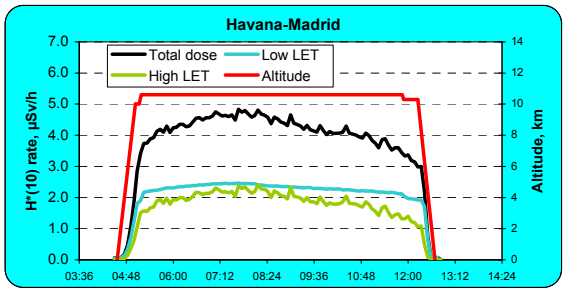

Departure date: 21/03/2002
Aircraft model: B747
Flight duration (h): 8.12 hours
Mean altitude (km): 10.6 km

	Route dose µSv	Mean dose rate µSv/h	Annual dose* mSv
CARI-6, E	28.2	3.47	2.78
EPCARD 3.2, E	31.6	3.89	3.11
EPCARD 3.2, H*(10)	27.2	3.35	2.68
TEPC, H*(10)	29.1	3.58	2.87
RS131+SWENDI2, H*(10)	30.5	3.76	3.01

* Computed for 800 flying hours (from take-off to landing)

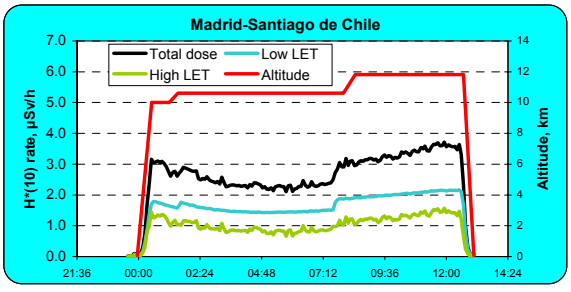

Departure date: 13/03/2001
Aircraft model: A340
Flight duration (h): 13.12 hours
Mean altitude (km): 11.0 km

	Route dose µSv	Mean dose rate µSv/h	Annual dose* mSv
CARI-6, E	34.4	2.62	2.10
EPCARD 3.2, E	27.5	2.10	1.68
EPCARD 3.2, H*(10)	24.9	1.90	1.52
TEPC, H*(10)	28.3	2.16	1.73
RS131+SWENDI2, H*(10)	34.9	2.66	2.13

* Computed for 800 flying hours (from take-off to landing)

Figure 3: Examples of experimental measurements onboard of IBERIA flights. Dose rates were taken from the tandem RS131 (Low LET) +SWENDI2 (High LET).

The Figure 3 clearly shows the effects of the altitude and latitude in the dose rate. Furthermore, the Figure illustrates how the neutron component (High-LET) increases with latitude over the non-neutron component (Low LET).

In the Spanish regulations, the use of computer codes such as CARI-6 or EPCARD 3.2 is admitted to compute the doses received by the air crew members in routine. However, they also mention the need to validate continuously the calculations by comparison with experimental measurements in representative routes. Based on the current requirements on accuracy for mixed fields [17], a performance ratio can be defined for each flight as the 'Computed value from the code' divided by 'Measured value with a reference instrument'. Acceptable values for this ratio will lie within 1.0±0.3 for a 95% confidence level, i.e., it will be acceptable to have an outlier every 20 studied flights.

The code EPCARD 3.2 provides dose estimates in terms of H*(10), which permits a direct comparison with the experimental results. The performance ratio for EPCARD 3.2 in terms of H*(10) fulfils the above criteria using any of the two experimental set up (TEPC or RS131+SWENDI2), obtaining the best results using the TEPC as the reference instrument[18].

As the CARI-6 code only provides results in terms of the effective dose, it is necessary to convert the measurements in terms of H*(10) to E. To this aim, for each flight the ratio E/H*(10) was calculated with the EPCARD 3.2 code, being applied to the corresponding experimental estimates of total H*(10). The performance ratio in terms of Effective dose for any combination of the two codes with the two experimental systems fulfils the established criteria, obtaining the best results in the combination EPCARD 3.2 vs. TEPC[18].

REFERENCES

1. GE Reuter Stokes. *RSS-131 User's Manual.* Part No. RSS131-O&M Revision F, March 2000.
2. Genitron Instruments. *GammaTracer Instruction Manual, 08/97.* Genitron Instruments Gmbh, 1997.
3. Olsher R.H., Hsu H.H., Beverding A., Kleck J.H., Casson W.H., Vasislik D.G., Devine R.T. *WENDI: An improved neutron REM meter.* Health Phys. 79 (2), 170-180, 2000.
4. Birattari C., Esposito A., Pelliccioni M., Rancati T., Silari M. *The extended range neutron rem counter LINUS: Overview and latest developments.* Radiat.Prot.Dosim. 76, 135-148, 1998.
5. Lewis B.J., Tume P., Bennet L.G.I., Pierre M., Green A.R., Cousins T., Hoffarth B.E., Jones T.A. and Brisson J.R. *Cosmic radiation exposure on Canadian-based commercial airline routes.* Radiat.Prot.Dosim. 86, 7-24, 1999.
6. Far West Technology. *Model FWAD-1 Hawk: Environmental radiation monitor with 5" tissue equivalent proportional counter. Operations and Repair Manual (revision A2) & Unit specific calibration document (Revision A, serial number 001).* Far West Technology, 2000.
7. J.C. Saez Vergara, A.M. Romero, R. Rodriguez, J.L.Muñiz, R. Dominguez-Mompell, F.Merelo, P.Ortiz, J. Ruano. *Monitoring of the cosmic radiation at IBERIA commercial flights: one year experience of in-flight measurements.* Proceedings of the Radiation Protection and Shielding Division Topical Meeting, Santa Fe, 2002. ISBN: 0-89448-667-5, CD ROM (2002).
8. A.Mitaroff and M. Silari, *The CERN-EU high-energy Reference Field (CERF) facility for dosimetry at commercial flight altitudes and in space,* Radiat.Prot.Dosim. 102, 7-22 (2002).
9. CARI-6 computer program. Developed at the Civil Aerospace Medical Institute (Federal Aviation Authority, USA). Free download from http://www.cami.jccbi.gov/aam-600/610/600Radio.html.

10. H. Schraube, W. Heinrich, G. Leuthold, V. Mares and S. Roesler. *Aviation route dose calculation and its numerical basis.* IN: Proceedings of the Tenth International Congress of the International Radiation Protection Association, Hiroshima, Japan. T-4-4, P-1a-45 (2000).More information also in www.gsf.de/EPCARD.
11. G. Reitz, K. Schnuer and K. B. Shaw, Eds. *Radiation Exposure of Civil Aircrew*, Proc. Workshop, Luxembourg, 1991, Radiat. Prot. Dosim., Vol. 48, 1993.
12. EURADOS, *Exposure of Air Crew to Cosmic Radiation*, report 1996-01, European Commission Report Radiation Protection 85. European Commission, Luxembourg, (1996).
13. M. Kelly, H-G. Menzel, T. Ryan T. and K. Schnuer, Eds. *Cosmic Radiation and Aircrew Exposure*, Proc. Workshop, Dublin, Ireland, 1998, Radiat. Prot. Dosim., Vol. 86, 1999.
14. U.J. Schrewe, *Global measurements of the radiation exposure of civil air crew from 1997 to 1999,* Radiat.Prot.Dosim. 91(4), 347-364 (2000).
15. B.J. Lewis, M.J. McCall, A.R. Green, L.G.I. Bennett, M. Pierre, U.J. Schrewe, K. O'Brien and E. Felsberger. *Aircrew Exposure from Cosmic Radiation on Commercial Airline Routes,* Radiat. Prot. Dosim. 93(4), 293-314 (2001).
16. B.J. Lewis, L.G.I. Bennet, A.R. Green, M.J. McCall, B. Ellaschuk, A. Butler and M. Pierre. *Galactic and solar radiation exposure to aircrew during a solar cycle.* Radiat.Prot.Dosim. 102, No. 3, 207-227 (2002).
17. International Commission on Radiological Protection, *Publication 75 General Principles for the Protection of Workers*, Pergamon Press, Oxford, (1997).
18. J.C. Saez Vergara, A.M. Romero, R. Rodriguez, and R. Dominguez-Mompell. *In-flight measured and predicted ambient dose equivalent and latitude differences on effective dose estimates***.** Presented at the 9th International Symposium on Neutron Dosimetry held in Delft (The Netherlands), September 2003. Proceedings to be published in Radiat.Prot.Dosim.

A.8 DOSTEL

Dr. R. Beaujean, University Kiel[1] and
Dr. Günther Reitz, DLR, Cologne

[1]University Kiel, Institut fuer Experimentelle und Angewandte Physik
Dosimetry in Luft- und Raumfahrt, Leibnerstrasse 11, D-24118

A.8.1 The DOSimetry TELescope (DOSTEL)

The DOSimetry TELescope DOSTEL, originally developed for spaceflight (Figure A.8.1), is based on two identical passivated implanted planar silicon (PIPS) detectors (Canberra Semiconductors) and designed to measure the energy deposit of charged particles. Both detectors have a thickness of 315 µm and a sensitive area of 693 mm^2. The distance of 15 mm between the two detectors yields a geometric factor of 824 mm^2 sr for particles arriving from the front when a coincidence in both detectors is required. The arrangement of the detectors is shown in Figure A.8.2.

Fig. A.8.1 DOSTEL as flown on Shuttle Missions and in airflight altitudes

Each detector is connected to an independent analogue signal section consisting of a charge sensitive amplifier (CSA) with 2pF integrating capacitor followed by a two-step pulse amplifier (PA1, PA2) and two peak detectors (Figure A.8.3). For noise reduction purpose, two RC-filters with equal individual time constants of 1µs are included in each detector signal line. Together with a multiplexed 8-bit ADC this design allows a pulse height analysis of the detector signals with different resolution for low and high energy deposits: 255 channels are used for an energy deposit of 0.3 – 77 MeV with a resolution of ~300 keV per channel, additional 255 channels for an energy deposit of 0.07 – 3.9 MeV with a resolution of ~15

keV per channel. The energy deposit for the low LET range in water is ~0.06 – 5.8 keV/µm and for the high LET range ~0.5 – 115 keV/µm (higher LETs are counted in channel 256).
The block diagram of the DOSTEL electronics is shown by Figure A.8.3. The digital signal section uses as main components an 8-bit MCU (68HC711), timer (68HC68T1), 1MB flash memory (E28F008SA) and 32 kB RAM (CXK58257AM-10LL). Scientific and housekeeping data are stored in the flash memory autonomously. The total power consumption of DOSTEL is 0.7 W from ± 10 V DC and +5 V DC. The size is 70x 70 x 100 mm³ with a mass of 0.6 kg.

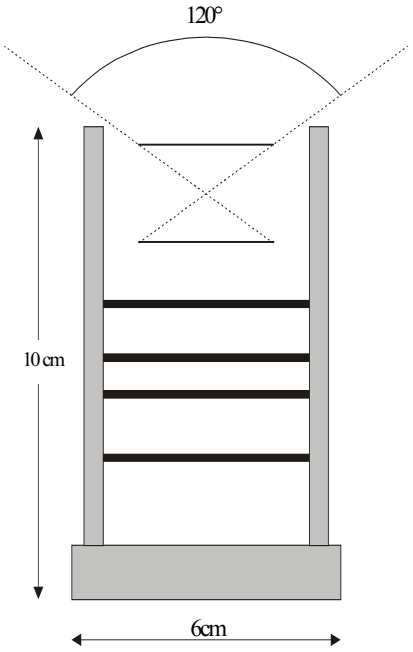

Fig. A.8.2 Detector arrangement

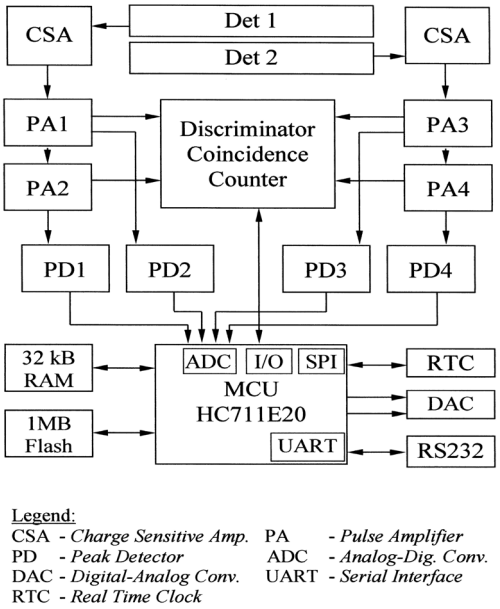

Fig. A.8.3 The block diagram of DOSTEL

The energy deposit response of the signals from the two DOSTEL detectors were calibrated by exposure to ^{241}Am in a vacuum chamber (pressure 0.1 hPa, distance 10 cm). The dead layer of the detectors, specified at about 0.1µm, can be neglected and the peak in the energy deposit spectrum is attributed to stopping alpha-particles of 5.48 MeV (their range in Si is about 28µm). For these calibration measurements with ^{241}Am the gain of the pulse amplifiers is reduced in order to yield the 5.48 MeV peak at the high end of the low energy deposit channels. Thus this method calibrates the CSA sensitivity including the RC-filter attenuation and the peak detectors. The ultimate response is calculated from the nominal gain of the pulse amplifiers (accuracy 2%). The overall linearity for the low and high energy deposit range was verified by using test pulses from a tail pulse generator.

Count and dose rates in the individual detectors are measured in the single-detector mode (6.93 cm^2, 315 µm, 4π sr), i.e. no coincidence between detectors D1 and D2 is required. LET(Si) values are deduced from the measured energy deposit in the individual silicon detectors in coincidence mode (120 degree viewing cone) using a mean pathlength of 364 µm at a density of 2.33 g/cm^3. This procedure does exclude short range secondary particles which may not trigger a coincidence and underestimate the LET for stopping particles. The energy deposit in Si is converted to LET (in water) using a conversion factor Si-to-water of 1.2, the mean quality factors are calculated using ICRP60.

Dose equivalent values for the DOSTEL aircraft measurements are calculated as follows:

a) DOSTEL count rates per (cm^2*s) versus residual atmosphere x (g/cm^2) are fitted by two exponential functions (interval 200-300 g/cm^2):

6.0*exp(-x/147) for high latitudes and 1.9*exp(-x/213) for low latitudes.

b) The count rates are multiplied by 6.93 cm^2* 3600 s and by the mean dose per count of $7*10^{-5}$ μG and $6.1*10^{-5}$ μG for high and low latitude respectively in order to obtain dose rates per hour in silicon (dose rates in silicon are converted to water by multiplying with 1.2).

c) These exponential laws are now compared to TEPC measurements published by Schrewe (ACREM, Rad. Prot. Dos., 91(4), 347-364) for the same time period. The slope of the DOSTEL measurements agree very well with the slope of the TEPC measurements both for high and low latitude regions (Fig. A.8.4). Therefore the free fitting parameter is just a factor which includes the mean quality factor and the mean DOSTEL response compared to the TEPC. The result for the altitude dependence of the dose equivalent rate (μSv/h) obtained by DOSTEL is

2.47*1.2*(0.25*6.93*6.0*exp(-x/147)) at high latitude,
1.77*1.2*(0.22*6.93*1.9*exp(-x/213)) at low latitude.

The value in parentheses is the measured DOSTEL dose rate in silicon (μG/h) versus the residual atmosphere x (g/cm^2).

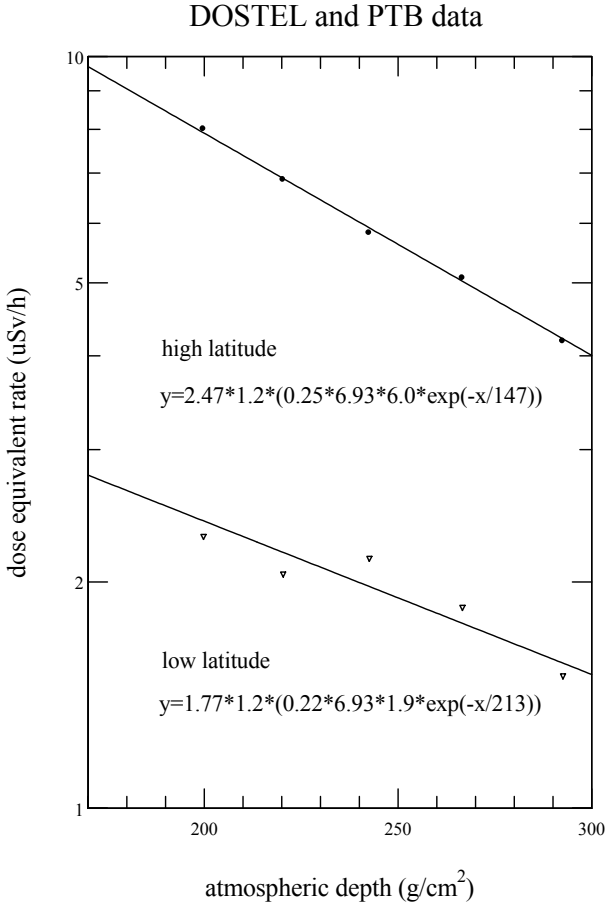

Fig. A.8.4. Altitude dependence of the dose equivalent (data points from PTB, curves for DOSTEL measurements as described in the text).

The described fit of the DOSTEL measurements to the PTB-TEPC data is used to deduce dose equivalent values for specific flights taking into account the latitude dependence by interpolation between the given mean quality factors for high and low latitudes. These data are compared to EPCARD calculations in Fig. A.8.5 (H. Schraube, GSF).

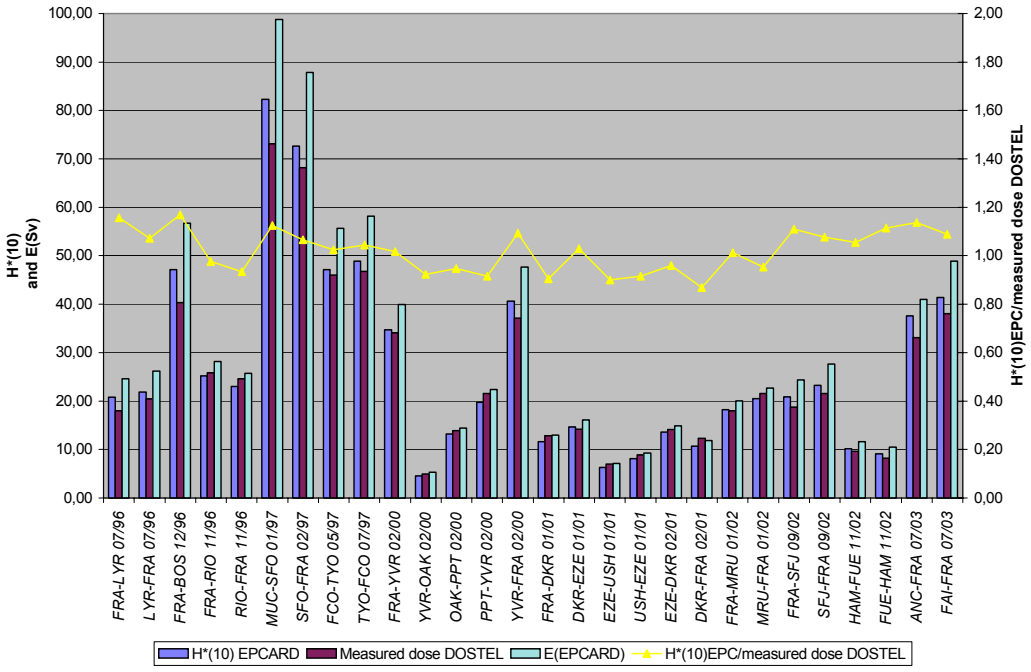

Fig. A.8.5. Comparison of DOSTEL dose equivalent values to EPCARD calculation for specific flights

A 9 Physikalisch Technische Bundesanstalt (PTB)

MEASUREMENTS OF THE RADIATION EXPOSURE OF CIVIL AIR CREW FROM 1997 TO 1999 U. J. Schrewe

A.9.1 INTRODUCTION

Between January 1997 and June 1999 the European Commission sponsored an international research project (referred to as ACREM, Air Crew Radiation Exposure Monitoring) implemented by the Austrian Research Centres Seibersdorf (ARCS), the Physikalisch-Technische Bundesanstalt (PTB), Braunschweig, and the Deutsche Lufthansa AG (DLH), Cologne, to investigate the dose assessment by active dosimetry for aircrew and to verify cosmic radiation transport calculations [1,8]. The in-flight measurement programme was performed with the help of Lufthansa Cargo aircraft between May 1997 and February 1999. The programme included ten measuring campaigns with 39 flight legs and a total measuring time of 195 h. The measuring activities were concentrated an the northern hemisphere, particularly an the North Atlantic and the North Pole regions, since these regions of the Earth combine a high air traffic density and high radiation exposure rates.

A.9.2 EXPERIMENTAL

The tissue-equivalent proportional counter (TEPC) [9] was used as the reference instrument for the determination of the ambient dose equivalent $H^*(10)$ [10-12]. Due to the low detection efficiency of the TEPC which complicates the investigation of the dose rate distributions as a function of geographical position and altitude, other dosemeter were used in addition and the combination of the readings served to estimate the total $H^*(10)$ value. This concept is similar to that proposed 30 years ago by Fuller and Day [13]. Dosemeters for directly ionising charged particles and photons, and neutron rem counters for the neutron component were found to be a suitable combination [7]. The ionising radiation was detected with various dosemeters otherwise used for environmental photon radiation dosemetry. Two neutron rem counters, NM and NMX of Andersson and Braun (A&B), and a third spherical rem counter, LB, were used. The NM is of conventional A&B design [14], whereas the NMX includes a lead insert 1 cm thick to extend the sensitivity to high energy neutrons [15]. The LB was specifically tailored to match with $h^*(10)$ from thermal to 20 MeV neutron energy [16,17], however, for higher energies the LB will underestimate $H^*(10)$ like the NM, since neither of them contains high-Z converter materials.

The TEPC measurements were performed with a HANDI (Homburg Area Neutron Dosemeter Instrument) and a special developed personal computer (PC)-based system. Both systems use spherical proportional counters of the Rossi type [9] with a cavity 56.9 mm in diameter. The HANDI provides absorbed dose and dose equivalent readings and the absorbed dose distributions $d(y)$ [9] with a resolution of 16 channels. However, the HANDI exclusively uses the $Q(L)$ relation from ICRP l5 [18]. The PC-based system was specifically tailored for the ACTREM in-flight measurements. The distributions $d(y)$ with 1024 channels were obtained by matching of the three linear pulse-height spectra and the dose equivalent distributions $h(y)$ were calculated by application of the quality factors $Q(L)$ to $d(y)$ where $Q(L)$ can be that defined by either ICRP 15 [18] or ICRP 60 [19].

In order to separate the dose fractions originating from the non-charged particles (mainly photons and neutrons) and from charged particles (mainly electrons, muons, protons and pions), in part of the measurements the TEPC sensor of the PC based system was surrounded by an active shielding detector, CACS (CACS = coincidence anticoincidence shield), which covers about 85% of the solid angle. The CACS was a cylindrical 24 anode wire chamber. The influence of the CACS an the dose measured with the TEPC is negligible. Application of the coincidence technique allowed the dose equivalent fraction originating from charged particles in the field to be separated with high efficiency. The timing resolution of the TEPC-CACS system was found to be smaller than 2 µs. In aircraft measurements where the radiation intensity produces only a few hundred events per second the TEPC the pulse heights furnished by the CACS were used to generate logic pulses of about 8 µs duration. The signals from the TEPC were split and measured as before using a quadruple ADC system coupled

to a PC and a second, identical quadruple ADC system being gated by the logic pulses from the CACS.

The aircraft position, i.e. the geographical longitude, L_g, and latitude, B_g, and the altitude, A, was furnished by cockpit instruments and manually recorded at intervals of 300 s together with the time (UTC). The data analysis required a correlation between dose measurements and aircraft position, which could be established an the basis of the statements of the time (UTC) associated with the dose measurements and the position records. The air pressure altitude in units of flight level, FL, was preferred to the true altitude since the radiation build-up and attenuation in the atmosphere depend on the mass of air above the aircraft and the civil air traffic at cruising altitudes always uses a flight level mesh of values which are multiples of 10 FL. (Under standard conditions, FL 1 corresponds to 30.48 m altitude.)

A.9.3 ANALYSIS OF THE MONITORING DATA AND RESULTS

The various data sets from the in-flight measurement as a function of time (UTC) were combined containing the date and the time, the geographical position, the magnetic latitude, the cut-off rigidity, the aircraft altitude and the dose equivalent readings from the monitors as well as the ratios of various monitor readings. Tabulations and figures to visualize the profiles for all flights have been given in a PTB Laboratory Report [5]. The monitoring data from the same altitudes were collected to obtain the distributions of global dose rates and of various monitor ratios for fixed altitude values. The amount of data for flight levels 280, 290, 310, 320, 330, 340, 350, 370 and 390 made such a procedure worthwhile [5]. The global distributions depend an the geographical position represented by the latitudes (B_g) and longitudes (L_g) which were converted to the geomagnetic latitude B_m = arc sin [0.982 sin(B_g) + 0.1886 cos (B_g) cos(Lg - 288.88°)]. The correlation of the dose equivalent rates with B_m is based on the expectation that the dipole component of the Earth's magnetic field is the dominant influence on the global cosmic ray distribution. The alternative is to use the cut-off rigidity, R_c, as parameter of the global dose rate distributions. The effective vertical cut-off rigidity as a function of geographical latitude and longitude was taken from a table in Shea et al. [20]. As discussed earlier [5], compared with B_m, R_c is the better suited parameter.

At aviation flight altitudes, the instruments respond in different ways to some components of the cosmic radiation and, for physical reasons some components cannot be detected by the instrument at all. Differences were observed between the dosemeter readings of the ionising component as well as between the neutron dose equivalent readings of the modified NMX rem counter and the other counters. The first can be explained by the influence of the muon component, the latter by the difference in the dose equivalent response to high energy neutrons [5]. The main difference of the NMX from standard rem counters (NM and LB) is that above 10 MeV the fluence response of the standard counters drops down to much lower values than the fluence-to-ambient dose equivalent conversion factor $h^*(10)$, while the NMX response is much better matched. It was found that the ratio of the rem counter readings varied only slightly with the geomagnetic latitude and altitude and even at mountain altitudes of 3600 m (at the Jungfraujoch Research Facility, Switzerland) and at altitudes of 70 m (PTB ground level), values similar to those at the flight altitudes were observed [11]. This observation indicates great similarity in shape of the energy distributions of the neutron fluence both globally and at all altitudes as already predicted by Monte Carlo computations [21,22]. The ratios $\overline{R}_{nn} = 1.75 \pm 0.11$ (reading from the NMX divided by the reading of the NM) and $\overline{R}_{nl} = 1.50 \pm 0.09$ (reading of the NMX divided by the reading of the LB) can be used in cosmic radiation fields to convert the NM and the LB readings to that of the NMX.

A.9.4 RESULTS OF THE FIELD CALIBRATION

The combination of two monitors, i.e. ionisation chamber IC and neutron rem Counter NMX with the response extended to measure high energy neutrons, has been adopted as a suitable monitor for the total dose equivalent. The sum of their readings was calibrated against the TEPC. Fig. A 9.1 shows distributions of the absorbed dose rate and the dose equivalent rate obtained an flights in the North Pole region (flights between Frankfurt and Chicago, and Frankfurt and Fairbanks).

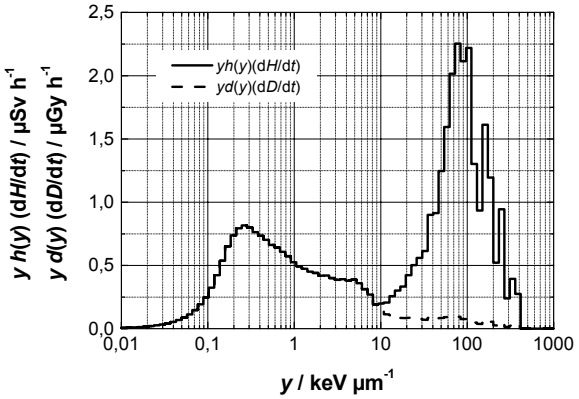

Fig. A 9. 1. Distributions of absorbed dose rate, d(y), and dose equivalent rate, h(y), as function of lineal energy y [9] from measurements during flights between Frankfurt and Chicago (Oct. 1998) and Frankfurt and Fairbanks (Feb. 1999). The distribution is the result obtained from a measuring time of 19,7 h and corresponds to a mean absorbed dose rate of (dD/dt) = 2,8 µGy h^{-1} and a dose equivalent rate of (dH/dt) = 6,0 µSv h^{-1}. The low-LET fraction (y < 10 keV μm^{-1}) accounts for 46%, the high-LET fraction (y > 10 keV μm^{-1}) for 54% of the total dose equivalent rate.

The "field calibration factor" [8] for the sum of the NMX and the IC readings is 0.96 ± 0.02. The statistical uncertainty is only 2% but many other factors contribute to the uncertainty [8]. The total uncertainty for TEPC dose equivalent measurements in cosmic radiation can be estimated at about 5% to 10% which justifies the use of 1.0 ± 0.1 as the "practical field calibration factor" for the sum of the NMX and the IC readings against the TEPC.

A.9.5 COINCIDENCE MEASUREMENTS WITH TEPC AND CACS

The dose equivalent distributions obtained from the TEPC PC system include all particles, charged and uncharged, while the dose equivalent distributions furnished by the TEPC-CACS system include only the charged particles. However, the coincidence efficiency of the TEPC-CACS system was lower than 100%. The coincidence losses from the pulse height processing were corrected by comparing the number of events in the gated and non-gated pulse height spectra of the CACS. The remaining reason for the loss of part of the CACS gate signals was that charged particles can pass through the apertures of the cylindrical CACS from top to bottom. The geometrical solid angle between the centre of the TEPC and the two apertures is about 15% of the total solid angle. If the charged particles are isotropically distributed in space, the coincidence efficiency would be 85%. When the CACS is operated in the horizontal position and assuming that the direction distribution is given by $I(\vartheta) = I_0 \cos^n \vartheta$ with $n \approx 2.2$, the coincidence efficiency would be 95%. Although the direction distribution at flight altitudes is not precisely known, it can be expected from previous work [24] that the exponent n increases with increasing altitude, and this would produce an even higher coincidence efficiency. It seems sufficient to assume a value of (90 ± 5)%.

Fig. A 9.2 shows the dose equivalent from the TEPC system together with the dose equivalent distribution simultaneously obtained from the TEPC-CACS system (with only the electronic but not the geometrical correction for the coincidence efficiency applied).

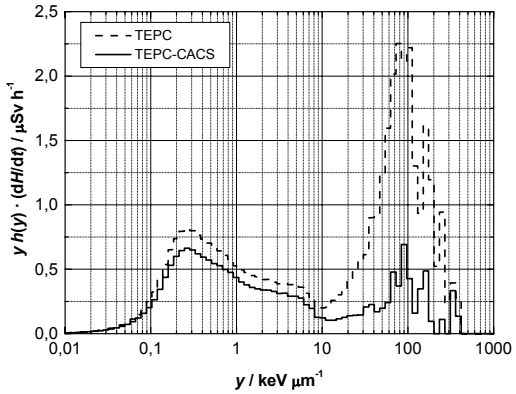

Fig. A. 9.2. Mean dose equivalent rate distributions from the TEPC as shown in Fig. 1 (dotted curve) together with the distribution of only those events from the TEPC which are due to charged particles (solid curve). The measurements were carried out simultaneously.

The TEPC dose equivalent was measured during flights between Frankfurt and Chicago, and Frankfurt and Fairbanks (the TEPC distribution shown is identical to that in Fig. 1). In the low-LET region (lineal energies lower than l0 keV·µm^{-1}), the TEPC-CACS and the TEPC distributions have a similar shape but the TEPC-CACS distribution covers only 80% of the events detected by the TEPC. Part of the losses are due to the finite coincidence efficiency of 90 ± 5%. When this correction is included in the TEPC-CACS, the low-LET dose equivalent rate still is only 90% of that from the TEPC. The difference may be attributed to a photon dose equivalent contribution of about 10 ± 5%. Experimental values of photon dose equivalent fractions which could be compared with the value given here have not yet been published, however, a 10% fraction of photons in the low-LET dose equivalent seems to be a reasonable number since annihilation and bremsstrahlung photons must certainly be present in cosmic radiation at flight altitudes [24].

The comparison between TEPC and TEPC-CACS in the high-LET region (lineal energies higher than 10 keV·µm^{-1}) reveals great differences. It is obvious that the greater fraction of the TEPC high-LET dose equivalent is caused by non-charged particles, i. e. neutrons, but a significant fraction is detected in the TEPC-CACS and this demonstrates the presence of a high-LET charged particle contribution. Photons, electrons and muons cannot, in general, produce the high-LET events. The contribution must be due to protons and pions. Theoretical estimations [25] indicate, however, that the pion dose fraction is much smaller than the proton dose fraction. Relative to the TEPC, the respective TEPC-CACS dose equivalent fraction is about 25%. With the same coincidence efficiency as before, i.e. 90 ± 5%, the high-LET dose equivalent is composed at a 30% fraction from protons (and pions) and a 70% fraction from neutrons.

A.9.6 CONCLUSIONS

The `field calibration' which has allowed a combination of two instruments to be calibrated against the TEPC as the reference instrument for ambient dose equivalent, is an essential step in our experiment. The "field calibration factor" of 0.96 determined supports the expectation that the IC nearly correctly measures the direct ionising component (electron, muon, proton, pion,...) and the photon dose fractions, while the lead-modified neutron rem counter is a suitable neutron dose equivalent meter at all neutron energies. Each of the instruments shows negligible sensitivity to that type of particle for which the measurement of the other one is best suited. It appears that the combination of IC and NMX can also measure to some extent the proton dose equivalent fractions, since the electromagnetic interaction of protons can be detected by the IC while the NMX can detect part of the dose equivalent fraction produced by the strong interaction of high energy protons. The NMX reading should, therefore, be attributed not only to the neutron dose equivalent but in part also to the strong interaction of protons (pions). This is important when theoretical and experimental partial dose equivalent fractions are compared.

The highest dose equivalent rates of the "ionising component" and the "neutron component" were found in the North Pole region and the lowest ones around the equator. For $B_m < 30°N$ (equator region) and for $B_m > 60°N$ (North Pole region), the spatial distributions are nearly constant. The measurements are not indicative of an enhancement of the dose rate in the vicinity of the magnetic poles. The present measurements are generally in agreement with previous evaluations [10,26]. In the lower altitude range beneath the "Pfotzer maximum" (about 25 km altitude), the altitude dependence of the cosmic radiation intensity is usually described by an exponential function. However, for the altitude range which is of greatest importance for civil aviation, 8.5 km (FL 280) to 11.9 km (FL 390), linear relations between dose equivalent rates and altitude were found to be fair approximations (cf. Fig. 4).

For the altitudes mainly investigated the dose equivalent rate distributions as a function of magnetic latitude B_m and cut-off rigidity R_c can be described by simple functions to allow rough estimates. The uncertainties of these estimates are approximately 10% to 15%.

The coincidence experiment with the TEPC and the CACS has unambiguously confirmed that almost the entire fraction (90%) of the low-LET radiation at flight altitudes is produced by charged particles, while only a small fraction (about 10%) may be attributed to photons. The high-LET dose equivalent contribution comprises a fraction of 30% from the incident charged particles, while the major part of 70% is to be attributed to neutrons.

A.9.7 References

1. Beck, P., Ambrosi, P., O'Brien, K., Duftschmid, K.E., Felsberger, E., Großkopf, A., Hornung, K., Kerschbaumer, S., Kindl, P., Körpert, K., Schmitzer, Ch., Schrewe, U.J., Winker, N. and Winter, M. *Active Air Crew Dose Assessment and TEPC Reference Investigations*. Proc. of IRPA Regional Symposium on Radiation Protection in Neighbouring Countries of Central Europe, Prague, 8.-12. September 1997, 76-79 (1998).
2. Beck, P., O'Brien, K., Kindl, P. and Felsberger, E. *Numerical Investigations of Radiation Exposure in Civil Aviation.* Proc. of IRPA Regional Symposium on Radiation Protection in Neighbouring Countries of Central Europe, Prague, 8.-12. September 1997, 80-83 (1998).
3. Beck, P., ACREM, Air Crew Radiation Exposure Monitoring. Active dosimeter and verification study of cosmic radiation transport code for air crew exposure assessment. Report of the Austrian Research Center Seibersdorf, **OEFZS-A-4317**, Ferbruary 1998
4. Beck, P., Bartlett, D.,O'Brien, K. and Schrewe, U.J. *In-flight Validation and Routine Measurements*. Radiat. Prot. Dosim. **86** 303-308 (1999).
5. Schrewe, U.J. *ACREM Air Crew Radiation Exposure Monitoring: Results from the In-Flight Measurement Program of the PTB: Summary of the Radiation Monitoring Data.* PTB-Laboratory Report **PTB-6.31-99-1**, Braunschweig, August 1999.
6. Schrewe, U.J. *ACREM Air Crew Radiation Exposure Monitoring: Results from the In-Flight Measurement Program of the PTB: Summary of Results from Calibration and TEPC Measurements.* PTB-Laboratory Report **PTB-6.31-99-2**, Braunschweig, October 1999.
7. Schrewe, U.J. *Radiation Exposure Monitoring in Civil Aircraft.* Nucl. Instrum. Meth. **A422,** 621-625 (1999).
8. Schrewe, U.J. Global Measurements of the Radiation Exposure of Civil Air Crew from 1997 to 1999. Radiat. Prot. Dosim. **94**, pp. 347-364 (2000).
9. ICRU. *Microdosimetry.* Report **36** (Bethesda, MD, USA: International Commission on Radiation Units and Measurements) (1983).
10. *Exposure of Air Crew to Cosmic Radiation*. edt. by McAulay, I.R., Barlett, D.T., Dietze, G., Menzel, H.G., Schnuer, K. and Schrewe, U.J., EURADOS **Report 1996-01**, Luxembourg, 1996.
11. Schrewe, U.J., Alberts, W.G., Alevra, A.V., Ferrari, A., Otto, T., and Silari, M. *Calibration Problems, Calibration Procedures and Reference Fields for Dosimetry in Flight Altitudes.* Rad. Prot. Dosim. **86,** 289-295 (1999).
12. Lindborg, L., Kyllönen, J.-E., Beck, P., Bottollier-Depois, J.-F., Gerdung, S., Grillmaier, R.E. and Schrewe, U.J. *The Use of TEPC for Reference Dosimetry.* Radiat. Prot. Dosim. **86**, 285-288 (1999).
13. Fuller, E. W. and Day, B., *Radiological Protection in SST Aircraft*. **CERN-71-16**, pp. 524-556 (1971)
14. Andersson, I.O. and Braun, J. *A. Neutron REM Counter.* Nukleonik **6,** 237-241 (1964).
15. Birattari, C., Ferrari, A., Nuccetelli, C., Pelliccioni, M. and Silari, M. *An Extended Range Neutron REM Counter*. Nucl. Instrum. Meth. **A 297,** 250-257 (1990).
16. Klett, A., Maushart, R., Burgkhardt, B., Fieg, G. and Piesch, E. *A New Neutron Dose Equivalent Rate Meter with Improved Energy Response in Terms of H*(10)*. In: Proc. 4th Conference on Radiation Protection Dosimetry, Orlando, FL, USA, 23-27 October 1994, **ORNL/TM-12817**, 227-233 (1994).
17. Burgkhardt, B., Fieg, G., Klett, A., Plewnia, A. and Siebert, B.R.L. *The Neutron Fluence and H*(10) Resonse of the New LB 6411 REM Counter*. Radiat. Prot. Dosim. **70,** 361-364 (1997).
18. ICRP: *Protection against Ionizing Radiation from External Sources*. Publication **15** (Pergamon Press, Oxford, New York, Toronto, Sydney, Braunschweig: The International Commission on Radiological Protection) (1970).
19. ICRU: *Fundamental Quantities and Units for Ionizing Radiation*. Report **60** (Bethesda, MD, USA: International Commission on Radiation Units and Measurements) (1998).
20. Shea, M. A., Smart, D. F., and McCall, J.R.. *A Five Degree by Fifteen Degree World Grid of Trajectory-determined Vertical Cutoff Rigidities*. Can. Jour. Phys. **46**, 1098-1101 (1968).
21. Rösler, S., Heinrich, W., and Schraube, H. *Calculation of Radiation Fields in the Atmosphere and Comparison to Experimental Data*. Radiat. Res. **149**, 87-97 (1998).
22. Kurochkin, I.A., Wiegel, B. and Siebert, B.R.L. *Study of the Radiation Environment Caused by Galactic Cosmic Rays at Flight Altitudes , at the Summit of the Zugspitze and at PTB Braunschweig*.

Radiat. Prot. Dosim. **83,** 281-291 (1999).
23. McCall, M.L. (private communication, 1999).
24. Allkofer, O.C. and Grieder, P.K.F. *Cosmic Rays on Earth*. Physics Data No. **25-1**, Fachinformationszentrum Energie, Physik, Mathematik, Karlsruhe, Germany (1984).
25. O'Brien, K. *The Cosmic Ray Field at Ground Level*. In: The Natural Radiation Environment II, Proc. Second Int. Symp. on the Natural Radiation Environment, August 1972, Houston, Texas. **COBF-720805** (Washington: NTIS) (1972).
26. *Die Ermittlung der durch kosmische Strahlung verursachten Strahlenexposition des fliegenden Personals*. Stellungnahme der Strahlenschutzkommission und Zusammenfassung eines Fachgespräches am 23. Mai 1996, published by the German Commission on Radiation Protection, Stuttgart; Jena; Lübeck; Ulm; (1997).

A 10 Austrian Research Center Seibersdorf

[1]P. Beck, [1]M. Latocha, [1]G. Stehno, S. Rollet, [2]A. Ferrari, [3]M. Pelliccioni, [4]R. Villari
[1]ARC Seibersdorf Research, Health Physics Division, A-2444 Seibersdorf, Austria
[2]CERN, 121 Geneva 23, Switzerland
[3]INFN, Laboratori Nazionali di Frascati, 00044 Frascati, Italy
[4]ENEA, Laboratori Nazionali di Frascati, 00044 Frascati, Italy

The work done by the Austrian Research Center Seibersdorf (ARCS) on measurements and simulation of the cosmic radiation is summarized in the following. Standard radiation equipment (GM-Counter, ionisation chamber, neutron monitor) as well as more sophisticated equipment as a Tissue Equivalent Proportional Counter (TEPC) have been used successfully for in-flight measurements. All instrumentation have been characterized in standard radiation photon and neutron fields. The response of a TEPC has been simulated by the Monte Carlo transport code FLUKA. Absorbed dose and dose equivalent distribution of lineal energy y have been determined for several kind of photon and neutron sources.

A 10.1 Instrumentation and Description

During EC projects ACREM (Air Crew Radiation Exposure Monitoring) and DOSMAX (Dosimetry of Aircrew Exposure to Radiation During Solar Maximum)ARCS investigated several active dose assessment methods for aircrew exposure:

Combination of conventional radiation protection instruments (ionisation chamber, neutron monitor)

Combination of conventional instruments and calculations (GM-counter combined with numerical calculations called together “ACREM system”)

TEPC

Tab. 1: *List of used detector systems.*

Detector	Instrument Type	to detect
TEPC	12,7 cm TEPC sphere, Far West type detector	Low LET / high LET
GM – counter	Robust standard military radiation survey meter	Non – neutron component
High pressure ionization chamber	Reuter Stokes Chamber	Non – neutron component
Neutron monitor	LB6411, Berthold	Neutron / hadronic component

All instruments were tested to be aviation qualified in certified laboratories according the regulations specified in EUROCAE ED-14c / RTCA DO-160C and DO-160D. Further electromagnetic interference (EMI) tests have been performed in running aircraft at ground. Environmental tests show the usability of the equipment under aviation conditions. To investigate solar events, ACREM and TEPC instruments were fix-installed at several aircrafts (Lufthansa, AUA, VARIG) for long-term in-flight investigations.

A 10.1.1 Combination of conventional radiation protection instruments

GM-Counter and Ionization chamber

The dose of direct ionizing particles and photons were monitored with two different radiation detector systems: GM counters (GM) and Ionizatuion Chambers (IC).

-The GM counter (GM) is a commercial available photon dose rate meter (SSM1), used as military and civil survey and environmental monitor. It is a many-sided programmable instrument (dose, dose rate, integration time, etc.) microprocessor controlled, with a serial input / output interface and works with a laptop based data acquisition system. Fig. A10.1 shows the transportable measurement equipment and data acquisition system.

Fig. A10.1*: High integrated and transportable measurement equipment for measuring the non neutron component using an external GM-detector and a PC controlled data acquisition system.*

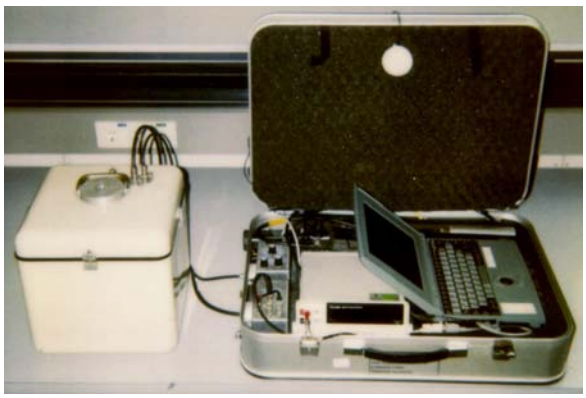

Fig.A10. 2*: The high pressure ionization chamber works at 2.5 MPa of argon gas, active volume of 8000 cm³ for measuring the non neutron component. The data acquisition unit is installed in an easy transportable bag. The white disk in the top of the bag cover shows the GPS antenna.*

The ionization chamber (IC) is a spherical high pressure argon gas ionization chamber with 254 mm diameter, this is an active volume of 8000 cm³ (Type: Reuters Stokes). The very low current measurement system has been special designed for measurements under aviation environmental conditions and works under software control of a note-book computer. The IC is well suited to be used for dosimetry in low intense environmental radiation. Fig.A10.1 and A10.2 show the IC detector and the transportable measurement bag which provides a automatic data acquisition controlled by a laptop [WIN99].

Neutron Monitor

The neutron monitor operated by ARCS is a spherical, moderated rem counter, using a ^{3}He detector, type: Berthold, LB 6411, (LB). It has been designed to measure H*(10) for neutron energies from thermal up to 20MeV (Fig.A10.3).

Fig.A10.3*:Dosimeter for the neutron component: The LB (marked by LB 6411) is a spherical rem counter specifically tailored to correctly measure H*(10) in the entire energy region from thermal to 20 MeV.*

One analysed approach is using a combination of the ionization chamber (IC) and the neutron monitor (NM). Using the reference TEPC instrument, a calibration factor for the combination of both detectors have been determined by field calibration during in-flight investigations.

A10.1.2 Combination of conventional instruments and calculations

Another method is the active on-board routine-dose-assessment monitor called ACREM (Air Crew Radiation Monitor), which combines measurements with one radiation detector (small and reliable GM-counter) and cosmic-ray transport calculations. A block diagramm of this system is shown in Fig.A10.4. For each flight co-ordinate a conversion factor from the non-neutron radiation component to ambient dose equivalent is calculated and used to multiply with the GM counter reading. Using a cosmic ray transport code for the calculation of the conversion factors, the ACREM instrument provides air-crew dose assessment and active real-time monitoring. The results agree with the above mentioned method of combined instruments within less than 10%. A picture of the ACREM system fixed installation is shown in Fig.A10.5.

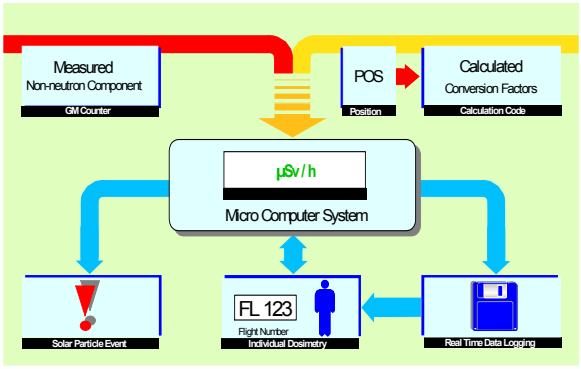

***Fig.A10.4**: ACREM dose assessment approach. GM-measurements are combined with trasnport calculations. A table of conversion factors gives for each geographical position, the relation of the calculated total dose to the non-neutron dose component.*

***Fig. A10.5**: Fix-installation of the airborne qualified ACREM system for active aircrew dose assessment.*

A 10.1.3 TEPC

The used reference instrument is a spherical TEPC (TE-sphere: 12.6 cm, "large TEPC", Far West Technology, Inc., Goleta, USA) operated with an ARCS developed low noise linear-preamplifier, logarithmic amplifier and a commercially available portable multi-channel analyser (MCA) [KER98] (is not in the references!). The MCA contains a programmable high voltage supply, a main amplifier and an 8192 channel ADC. The whole system operates software controlled with a note-book computer based data acquisition system. The pulse-height spectra and frequency distribution $f(y)$ were obtained with one logarithmic amplifier for more than 4 decades by the logarithmic amplifier. The dose distributions $d(y)$ were calculated by $d(y) = y\,f(y)$. The dose equivalent distributions $h(y)$ were calculated by applying the quality factors $Q(y) \cong Q(L)$ to $d(y)$, *i. e.* $h(y) = Q(y)\,d(y)$. The counter volume is large enough to achieve good statistics of environmental measurement during 1000 s. The selected measuring time in-flight altitude was 1000s. The TEPC pulse height spectra and corresponding start/stop times (UTC) were automatically and continuously stored in PCs. Fig. A10.6 shows the airborne proofed TEPC detector. Since 2000 a transportable TEPC called HAWK manufactured by Far–West[FAR00] is used in a hand luggage sized bag, shown in Fig.A10.7.

Fig. A10.6*: The transportable and airborne proofed ARCS TEPC reference detector in a robust transport bag.*

Fig.A10. 7*: Transportable TEPC - HAWK detector.*

A 10.2 Instrument Calibration

All instruments have been investigated in different photon (energies up to 7 MeV) and neutron (energies up to 66 MeV) radiation fields at several European research laboratories (PSI, PTB, ARCS, CERN). The standard neutron rem-counter (used as neutron monitors) gives a response comparable with the specification of the manufacturers. For high energetic neutrons their response is significantly lower than the fluence to ambient dose equivalent conversion function h*(10).

The dose equivalent response of the photon dosimeters (GM-counter, ionization chamber) were less than 1% for neutrons of energies between 0,5 MeV and 66 MeV. In the low energy region, around 200 keV a response of about 10% could be observed. The uncertainty of photon contribution in this radiation field conditions is about in the same dose rate range. In photon radiation fields the neutron monitors show no measurable dose response, even by using photon dose rates by a factor of 100 higher compared to the conditions in flight altitudes. Repeatable, unexpected higher readings for the first 20 s at Co-60 conditions were observed for the Berthold neutron monitors (LB). The dose equivalent responses of all photon dosimeters used are close to one for energies up to 1 MeV photons. At 7 MeV photon energy the GM –counter shows a 25% higher response compared to results of the ionization chamber.

This standard calibration of dosimeters used for air crew dose assessment in reference fields makes it possible to compare instruments under standard conditions (or conditions close to these). The essential step in the calibration described for cosmic radiation in the athmosphere is the field calibration. Consideration of the fundamental principles of a TEPC allows the conclusions that the TEPC is at present the best suited instrument to perform the "field calibrations" in cosmic radiation at flight altitudes.

The fluence response of a TEPC (even used without build-up caps providing secondary charged particle equilibrium) will be greater than the conversion function h*(10) thus, the dose equivalent measurement with such a system will still be a conservative estimate of the ambient dose equivalent in the neutron energy range up to 66 MeV.

A 10.3 In-flight Investigations and Results

During 10 in-flight investigations (36 city pair destinations, 220 flight hours) between May 1997 and February 1999 the solar potential ranged between 474 MV and 650MV. Between the flight levels from FL 260 to FL 390 measurements from 85° geographical northern latitude and about 35° geographical southern latitude have been performed. The position of the aircraft has been documented in time intervals of 300s cockpit data and 15s GPS measurements. The instruments measurement intervals

were integrated to 300s (ionisation chamber, GM-counter, neutron monitor). The intervals for the TEPC investigations was in general 30 minutes, partly 60 minutes at low dose rates, to get a higher statistical certanty of the measurement.

For an appropriate comparison of the in-flight data, the same flight position and solar condition have to be considert. For comparing all geographical co-ordinates, geomagnetic latitudes have been calculated using a simple dipole model:

$$sin(B_m) = sin(B_P) \cdot sin(B_g) + cos(B_p) \cdot cos(L_g - L_p)$$

B_m ... magnetic latitude in degrees.
B_p, L_p ... latitude and longitude of the magnetic North pole (1990: 79.13°N, 288.88°E) in degrees.
B_g, L_g ... geographical latitude and longitude in degrees.

Fig.A10.8 and Fig.A10.9 show examples of in-flight investigations and comparision of results. The dependence of the dose equivalent rate for the combination of a lead modified rem counter and an ionization chamber (NMX+IC by PTB-Braunschweig), the ACREM instrument, a large volume TEPC and the LUIN99 results in terms of effective dose of the geomagnetic latitude for 9.5 km to 11.9 km (31,000 ft to 39,000ft). The results show a good agreement within about 20% and better.

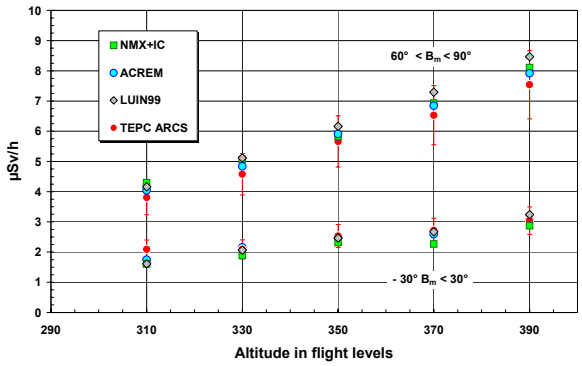

***Fig.A10.8**: Dose equivalent rate for a range of typical sub-sonic flight-altitudes between 9.5 km (31,000 ft) and 11.9 km (39,000ft) for a combination of the lead modified rem counter and an ionization chamber (NMX+IC), the ACREM instrument, a large volume TEPC and the LUIN99 calculations. Data where given for magnetic latitude B_m above 60° N and B_m between –30° and +30° in the equator region.*

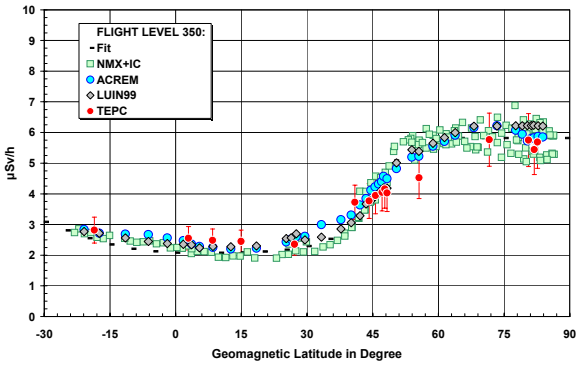

***Fig.A10. 9**: Dependence of the dose equivalent rate for a combination of a lead modified rem counter and an ionization chamber (NMX+IC), the ACREM instrument, a large volume TEPC and the LUIN99 results in terms of Effective dose of the geomagnetic latitude for FL 350, i.e. 10.7 km (35,000 ft)*

A 10.4 Monte Carlo simulations of the TEPC reference instrument

A Tissue Equivalent Proportional Counter (TEPC) is a standard instrument for measurements in a mixed radiation field. Particular in aircrew radiation dosimetry the TEPC is of major interest for usage as reference instrument [ROS94], [SIM95], [BEC99]. It measures the microdosimetric distribution of absorbed dose as a function of the lineal energy y over several order of magnitude and for different kind of nuclear particles. Folding this distribution with the quality function, dose equivalent is provided. Numerical simulations are necessary to understand the instrument response to unknown sources and to evaluate the relation between different dosimetric quantities such as absorbed dose, ambient dose equivalent and effective dose. For this purpose, the Fluka code [FAS01] is used to simulate the energy deposition and particles fluence rate inside a TEPC [BEC03]. Fluka is a Monte

Carlo code able to simulate transport and interaction of electromagnetic and hadronic particles in any target material over a wide energy range (from 20 TeV down to 1 keV for all particles and down to thermal energy for neutrons). Fluka is widely used for both basic research and applications in radiation protection and dosimetry, radiobiology, radiotherapy and cosmic ray calculations.

TEPC Simulation with Fluka

The geometrical model simulated with Fluka consists of a 3-D structure centered in the TEPC which takes into account the Hawk assembly. The TEPC detector is supposed to be irradiated by different kind of particles and energies, impinging on the lateral wall and transported through all the structure. The average energy deposition, and hence absorbed dose, from the source particles is calculated inside the gas.

The low pressure of the gas requires large numbers of MC calculations to achieve a reasonably statistic accuracy for the simulation results. The analysis of at least 10 different runs with 10^6-10^7 source particles is used to estimate the different moments in order to assess the statistical convergence. The uncertainty of the total absorbed dose in the gas is about 1%. That requires around 10-15 hours of CPU time for each calculation on a dual Intel Xeon, 1.8 GHz processor with 1GB RAM based on a Linux operating system. The lower energy cut-off used for electrons and photons is 1 keV. Neutrons are transported down to thermal energies, using a multigroup cross-sections data set appositely selected for FLUKA from the most recent evaluations.

The total energy deposited inside the TEPC gas is a small fraction (e.g. 10^{-6}) of the incoming photon energy. A careful check of the sensitivity of the calculations to different instrument parameters has been done [BEC03]. In particular, it has been found out, that the energy spectrum of the source, the gas composition and the structure around the TEPC have most influence on the final results. Beside average quantities, Fluka has the unique capability to score energy deposition on an event by event basis between given energy limits distributed over e.g. 1024 channels. This provides the lineal energy distribution.

Microdosimetric spectra

Fluka calculates the deposited energy in a given energy range as a function of the energy channel. Each channel has a lower and upper energy limit, from which the average energy can be calculated. The corresponding lineal energy y is given dividing the average deposited energy in each channel by the mean chord length of the microdosimetric volume. In Fig.A10.11 a comparison of the dose distribution yd(y) simulated with Fluka and measured with two different Hawk systems is shown for a ^{60}Co source. The distribution shows a range of the lineal energy from 10^{-2} to 10^3 keV/µm. As expected for a low-LET radiation, the main part of the contribution is below 10keV/µm. While the lower threshold of the measurements seems to be at 0.5 keV/µm, the simulation calculates values below this threshold. It has been published that some other TEPC systems are also able to measure below a threshold of 0.5 keV/µm i.e. 0,1 keV/µm [TAY02]. To take into account this missing part of the spectra, the measurements are usually presented with a linear interpolation below the threshold (shown as a dashed line in the figure. To correct this missing part for calculation of the absorbed dose values an extrapolation with a ^{60}Co spectra has been applied.

The same comparison is done for a neutron source of 0.5 MeV, shown in Fig.A10.12. For neutrons the microdosimetric spectrum shows that the dose contribution comes mostly for lineal energy larger than 10keV/µm (called high-LET).

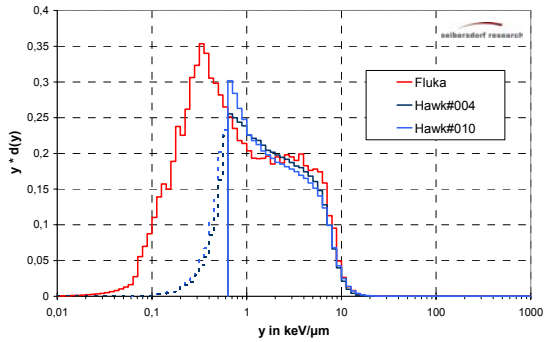

***Fig.A10.11**: Microdosimetric spectra yd(y) vs. y for a ^{60}Co source. Comparison between simulation and measurements*

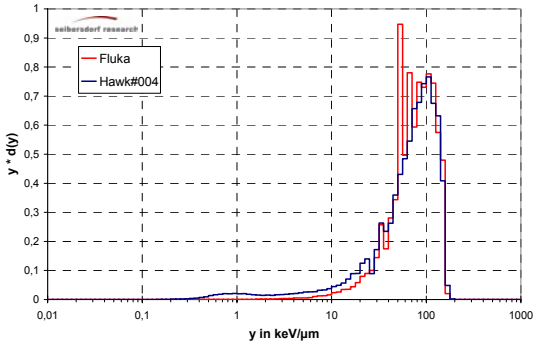

***Fig.A10.12**: Microdosimetric spectra for a 0.5 MeV neutron source. Comparison between simulation and measurements*

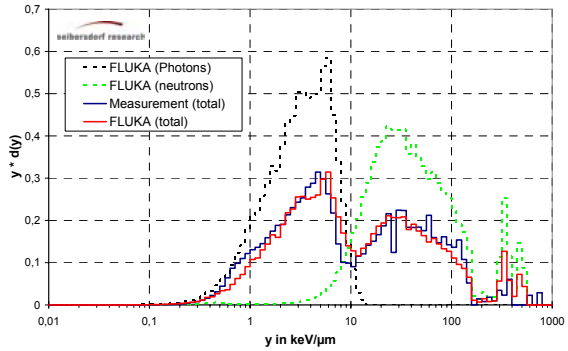

***Fig. A10.13**: Microdosimetric spectra for an ^{241}AmBe source. Comparison between simulation and measurements.*

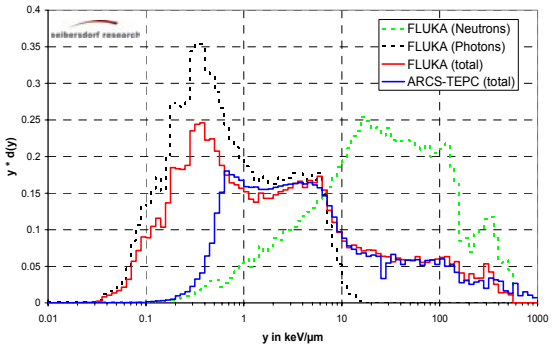

***Fig. A10.14**: Microdosimetric spectra for the CERF-facility. Comparison between simulation and measurements*

A comparison for an ^{241}AmBe source, without any lead cap, is shown in Fig.A10.13. In these spectra both the neutron and photon components are clearly discernible.

Since Fluka can handle high energy radiation, the simulation of the microdosimetric spectra expected in the CERF facility [MIT02] was also carried out. The measurement with the ARCS-TEPC was done on top of the concrete roof-shield, in position CT10 [AUT03]. For the simulation the spectral fluence rate for neutrons and photons were considered at the same position. It has been taken into account that the photon fluence is about a factor of two higher than the neutron one on the concrete roof shield due to (n,γ) reactions. Fig.A10.15 shows the comparison of the simulated microdosimetric spectrum by Fluka and ARCS-TEPC measurements. The figure distinguishes also the contribution from neutrons (green dots) and photons (black dots) calculated with FLUKA. It should be pointed out that some additional components are not taken into account in the simulation: Such as muon coming from secondary beams in neighbouring beam lines and not under direct control of the experiment. However, the simulated and measured spectra are in good agreement [ROL04].

TEPC response to cosmic ray field

The main components of the radiation field at civil aviation altitude have been calculated using the Monte Carlo transport code FLUKA as described in detail in [FER01] .The energy spectra for neutrons, protons, photons, electrons, positrons and muons in free atmosphere were calculated at 10580 m altitude. Some of these spectra are shown in Figures (15-18)a. The primary spectra entered in

the simulations correspond to a solar deceleration potential (SDP) of 465 MV and to a vertical cut-off rigidity r_c= 0.4 GV.

These spectra have been used as sources for the irradiation of the TEPC as described before The absorbed dose distribution is calculated as a function of lineal energy inside the TEPC for all the different kinds of particles and spectral energies distributions and is shown in Figures 15-18b. The corresponding input fluence rate and energy distribution is shown in figure 15-18a. All figures are normalized to one source particle. As expected, the bulk of the distribution for high LET particles, such as neutron, appears mainly above y = 10 keV·µm-1. The distribution of low LET particles, such as electrons, photons and positrons, is very similar and below y = 10 keV·µm-1. The charged pions and muons distribution is below 100 keV·µm-1. The total absorbed dose distribution is computed summing up the contribution of each particle weighted with its relative fluence value in Fig.A10.19.

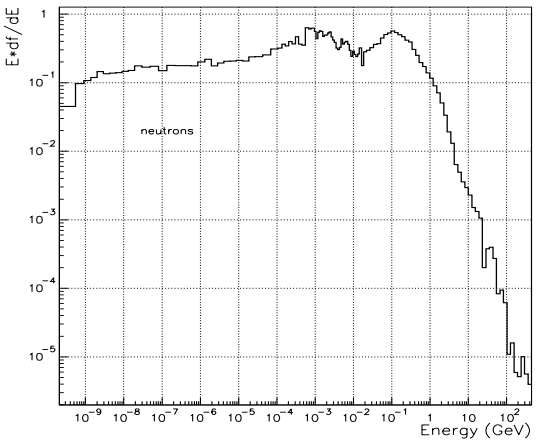

*Fig. **A10.15a**: Spectral neutron fluence as calculated by FLUKA*

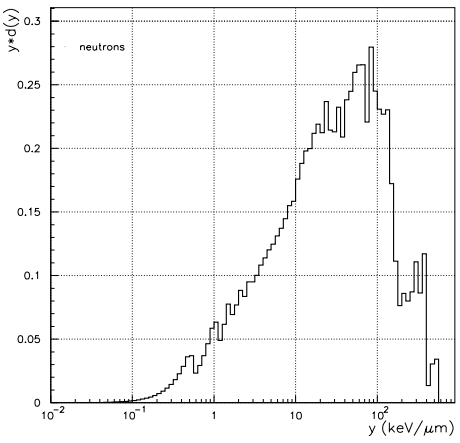

***Fig.A10.15b**: Microdosimetric neutron spectra y·d(y) as seen by the FLUKA simulated TEPC*

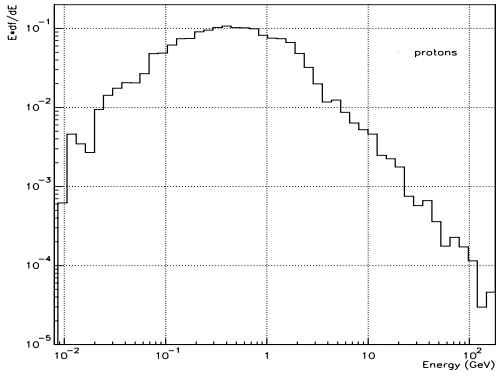

***Fig. A10.16a**: Spectral proton fluence as calculated by FLUKA.*

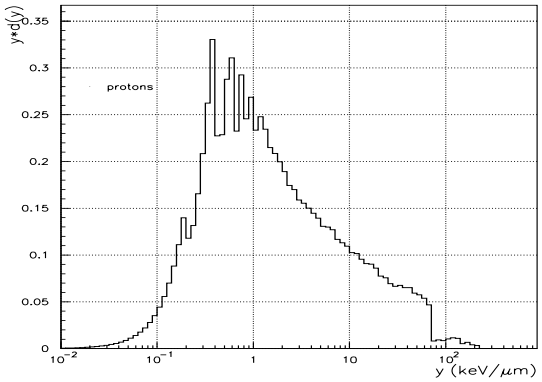

***Fig.A10.16b**: Microdosimetric proton spectra y·d(y) as seen by the FLUKA simulated TEPC.*

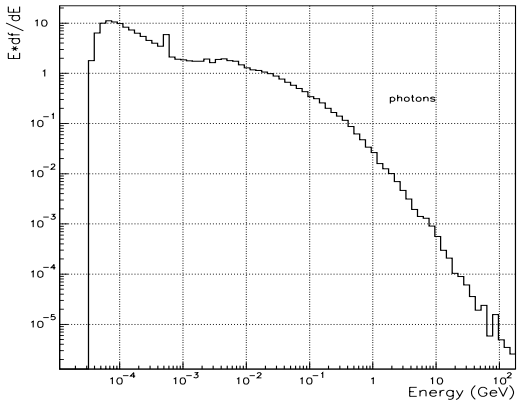

***Fig. A10.17a**: Spectral photon fluence as calculated by FLUKA.*

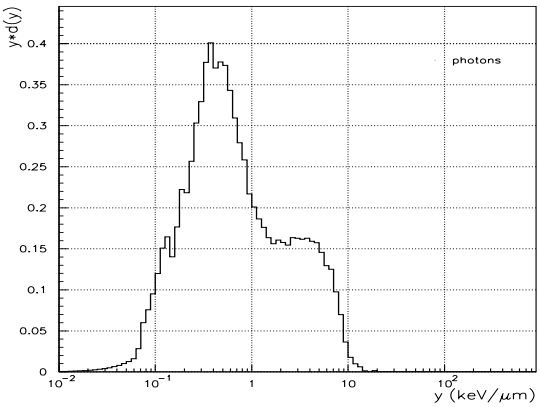

***Fig.A10.17b**: Microdosimetric photon spectra y·d(y) as seen by the FLUKA simulated TEPC*

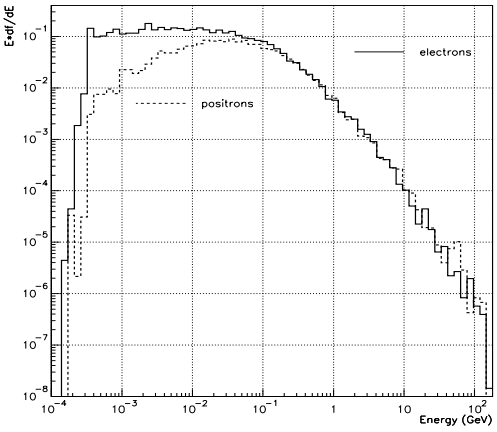

***Fig. A10.18a**: Spectral electron and positron fluence as calculated by FLUKA.*

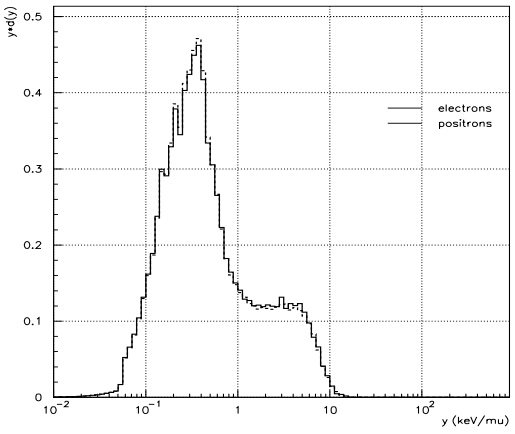

***Fig. A10.18b**: Microdosimetric electron and positron spectra y·d(y) as seen by the FLUKA simulated TEPC*

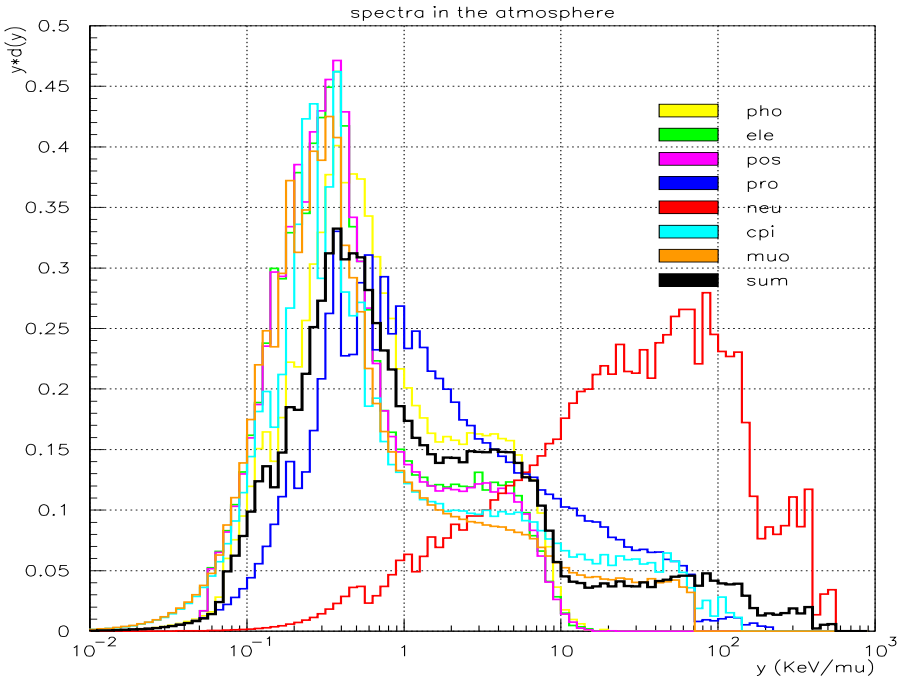

***Fig. A10.19**: Measured microdosimetric spectrum for all the particles. The total absorbed dose distribution is computed summing up the contribution of each particle weighted with its relative fluence value.*

For all of them the corresponding ambient dose equivalent distribution is calculated folding the absorbed dose rate with the ICRP-74 quality factor as a function of linear energy transfer.

For example, in Fig.A10.20 the absorbed dose distribution (black) is shown together with the red curve resulting from the multiplication of the region above 10 keV/μ with the Q factor. The integral below the two curves is the dose equivalent. The average Q calculated over all the spectral distribution is 2.

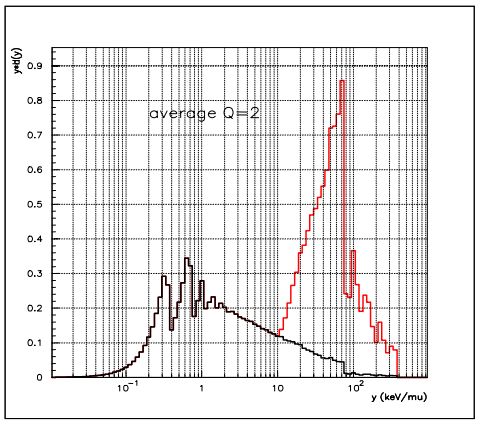

***Fig.A10.20**: Simulated absorbed dose (black) and dose equivalent (black+red) distribution for protons*

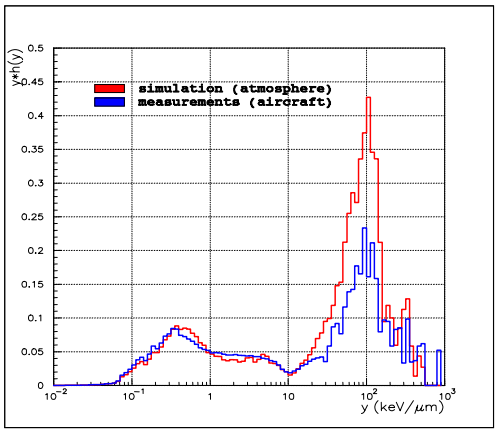

***Fig. A10.21**: Microdosimetric spectra y·h(y) due to all particles as seen by the FLUKA simulated TEPC compared to the measured one, normalized to the absolute fluence*

A comparison of the simulated and measured ambient dose equivalent rate distributions is shown in Figure 21, for a measurement time of one hour. The HAWK was installed on board of a Lufthansa aircraft A340 flying between Frankfurt and Vancouver on March the 10th, 2003. The instrument was positioned in the business class on a left window seat, row 12, close to two passengers. Both curves are normalized to the absolute values of the ambient dose equivalent. The measurements onboard the aircraft show a good agreement with the simulation in free atmosphere for the low LET part. For the high LET region a significant reduction can be observed [BEC04].

Conclusions on TEPC Simulation of reference instruments and on-board measurements

The comparisons between the simulated and measured microdosimetric spectra in photons, neutrons and mixed radiation fields are in good agreement. It has also been used to calculate the radiation field at aircraft altitudes to simulate the TEPC response to this field. The microdosimetric spectra were calculated in the free atmosphere for each kind of particle produced during the atmospheric shower. TEPC simulation have been compared with TEPC in-flight measurements done at the same geographical position, altitude and same solar condition. TEPC measurements within the aircraft show an reduced ambient dose equivalent rate of about 25% compared to calculations in free atmosphere.

References

[ROS94] Rossi, H. H. and Zaider, M., *Microdosimetry and its Applications*, Springer (1994).

[SMI95] Schmitz, Th.,Walker, A.J., Kliauga, P., Zoetelief, *Design, Construction and Use of Tissue Equivalent Proportional Counter*, Rad. Prot. Dos. Vol. 61, No. 4., (1995).

[BEC99] Beck, P., Schrewe U., O'Brien, K., Ambrosi, P., *ACREM, Air Crew Radiation Exposure Monitoring*, OEFZS-G-0008, November 1999.

[FAR00] Far West Techn. Inc., *Environmental radiation monitor with 5 inches tissue equivalent proportional counter*, Operations and repair manual, December 2000.

[FAS01] Fasso, A., Ferrari, A., Ranft, J., Sala, P.R., *FLUKA: Status and Prospective for Hadronic Applications* Proc. of the MonteCarlo 2000 Conference, Lisbon, October 23–26 2000, Springer-Verlag Berlin, p. 955-960 (2001).

[BEC03] Beck, P., Ferrari, A., Pelliccioni, M. and Rollet, S., *TEPC simulation with Fluka*, ARCS Report, ARC-G-0004/03 June 2003

[ICR83] International Commission on Radiation Units and Measurements, *Microdosimetry*, ICRU Report 36, 1983

[TAY02] Taylor, G.S., Bently, R.D., Conroy T.J., Hunter R., Jones J.B.L., Pond, A. and Thomas D.J., *The Evaluation and use of a portable TEPC system for measuring in flight exposure to cosmic radiation, Radiat. Prot. Dosim. Vol.99(1-4), pp. 435-438, (2002).*

[MIT02] Mitaroff, A. and Silari, M., *The CERN-EU High-Energy Reference Field (CERF) Facility for Dosimetry at Commercial Flight Altitudes and in Space*, Rad. Prot. Dos. Vol.102, No. 1. pp.7-22 (2002).

[AUT03] Autischer, M. , *Kalibriermessungen mit dem Tissue Equivalent Proportional Counter (TEPC)*, Diplomarbeit der Technischen Universität Graz, 2003.

[FER01] Ferrari, A., Pelliccioni, M. and Rancati, T., *Calculation of the radiation environment caused by galactic cosmic rays for determining air crew exposure*, Radiat. Prot. Dosim.93(2) 101-114, (2001).

[ROL04] Rollet, S., Beck, P., Ferrari, A., Pelliccioni, M. and Autischer, M., *Dosimetric considerations on TEPC FLUKA-simulation and measurements*, pres. at neutron dosim. Symp., Delft Oct 2003 to be published in Radiat. Prot. Dosim., (2004).

[BEC04] Beck, P., Ferrari, A., Pelliccioni, M., Rollet S. and Villari R., Fluka simulation of TEPC response to cosmic radiation, pres. at neutron dosim. Symp., Delft Oct 2003 to be published in Radiat. Prot. Dosim., (2004).

A 11. Agenzia per la Protezione dell'Ambiente e dei Servizi Tecnici - APAT

L. Tommasino, R.K. Jain, N.L. Singh, and S.P. Tripathy
APAT, Via V. Brancati 48
00144 Roma
Italy

A 11. Passive Multidetector system - (ANPA-stack)

A 11.1 New Detection Principles of the ANPA-stack

Passive detectors are very attractive for in-flight measurements, because of their small size, low weight, lack of need of electrical power and of the stringent requirements for the environmental parameters (temperature, vibration and interference with the on-board instrumentation).
A passive multidetector stack was developed at the Italian National Agency for Environmental Protection (ANPA-stack), which makes it possible to measure directly-ionizing radiations, low- and high-energy neutrons, and HZE particles (1,2).
The stack consists of several types of passive devices, namely recoil- and fission-track detectors, bubble detectors, thermo-luminescent dosemeters, and an electronic personal dosemeter. Most of these detectors have been used on earth for the assessment of the occupational exposure (3), or in outer space for cosmic-ray physics and/or for the assessment of the dose received by astronauts (4-6).
A great deal of efforts and new developments have been required to make these detectors useful for in-flight measurements (7-9) with special regards to the use of large-area detector stacks.
Even though this multidetector system presents the complexity typical of cosmic ray stacks, the scanning of many different types of detectors is relatively simple and rapid, as required for dosimetric applications.
In particular, a simple microfiche reader can be useful to scan large areas of different types of neutron detectors for the counting of both fission-induced aluminum spots or electrochemically etched recoil tracks.
For all these techniques, the detection principle is based on high-LET particle-induced avalanche processes, which greatly facilitate the registration of tracks.
These avalanche processes are based on bubble formation, electrical breakdowns in thin film capacitors, spark- or electrochemical-breakdown induction at track sites (3,10).
A major drawback of damage-track detectors is their large and unpredictable background. This problem has been finally solved by using the detection principle of counting coincidence-track events on matched-pair of detectors, not only for long-range particles but also for very short tracks induced by neutron recoils (7-9,11-14).

Fig.A.11.1 illustrates the different types of coincident events which may be induced with particle tracks. In Fig.A.11.1a, the etched range of the particles is so long that it may cross different track detectors in a stack. This coincidence method has been successfully exploited for the registration of high energy charged particles-HZE in cosmic rays since the early discovery of damage track detectors (4). This same coincidence method can be applied for short-range particles, provided that the paired detectors are thin enough to be crossed by the etchable range of the charged particles. In the past, this method (Fig.A.11.1b) has been successfully exploited with such short range particles as fission fragments crossing two thin polyester films (7,12,15). Coincident spots are observed on geometrically matched Al replicas obtained after spark counting etched-track holes in thin plastic films irradiated under the pair configuration. Similar coincident spots can be produced by neutron-recoils in matched pair of 12 m-thick cellulose nitrate films (2).

Another novel coincidence method is proposed in Fig.A.11.1c, where the etchable track ranges are so short that they do not cross any of the detectors, but they just penetrate both of the matched detector surfaces. These tracks are typically produced by neutron-induced recoils in polycarbonate and CR-39 detectors (7-8). The only way to produce coincident spots with these tracks is through the electrochemical etching-(ECE) processes. For short range tracks, this type of etching can be considered just the converse of the chemical etching, since the short-range recoil tracks keep enlarging under ECE processes, while they may disappear from view under chemical etching (10).

Fig.A.11.2 shows coincidence events produced by ECE spots on two paired polycarbonate detectors. As it can be easily seen, the identification of coincidence events is very simple, in spite of the poor image of the microfiche reader.

When compared with the responses of detectors based on counting tracks on a single surface, the response of the detectors based on the coincidence-method present the following advantages:
(i) consistently low background
(ii) relatively flat response
(iii) detector with different neutron-energy thresholds.
In order to obtain these novel detectors, tens of man-years of research and development have been required (1,7-9,11-16).
To conclude: different new detectors have been developed thanks to the novel strategy described above, which exploits some of the most successful principles of radiation detection (with particular regard to the detection of cosmic rays) such as:
-the use of avalanche processes to facilitate the registration of nuclear tracks;
-the use of coincidence-counting to increase the signal-to-noise ratio.
The ANPA-stack is formed by replicates of so many different types of passive detectors that by appropriate choices of the particular detectors to be used, it is possible to obtain ad-hoc stacks for a variety of different applications. In the following, only those stacks, which have been extensively applied in the past, will be described, such as the stack for:

- the measurement of HZE particles with Z>10
- the spectrometry of low-and high-energy neutrons
- the evaluation of the hardness ratios of neutron-spectra
- the dosimetry of the galactic cosmic radiations.

A 11.2 Stack for HZE-particle measurement.

Measurements of HZE particles are complex and time-consuming especially because of the presence on the detector surface of a large track density due to the interaction of neutrons with the detector material. These tracks have a length typically less than 100 μm and can be differentiated from those due to HZE particles, which have usually a length >> 100 μm. This discrimination can be achieved by using a stack of 12 μm thick cellulose nitrate (LR-115 from Kodak) and 20 μm thick polycarbonate films. After exposure, the thin films are etched and spark counted (17). Coincidence counting in several different thin-film detectors can be easily carried out by shining light through the stack of properly matched large area replicas, induced on the sparked thin-aluminum electrode (2).
This registration method makes it easy to identify particles with $Z \geq 10$ over large detector surfaces. The ANPA-stack has been exposed for 50 hours at 40 km altitude on a balloon (2), for 350 hours on the Concorde and for about 1000 hours on the route Milan-Los Angeles (18,19)
In the case of the balloon exposure, 50 particles with $Z \geq 10$ on a detector area of 225 cm^2 have been registered, while on the Concorde, only one single event has been detected on the same area. None of these particles has been registered on the subsonic flights. For what concerns the measurements of particles with $Z < 10$ it is necessary to use the method employed at the Dublin Institute of Advanced Studies- DIAS (2,6), which is by far less rapid but relatively much more sensitive and accurate.

A 11.3 Stack for neutron spectrometry

The basic requirements for a stack for neutron spectrometry (based on the unfolding procedures) is to have different detectors, which have a known response as a function of the neutron energy and chosen in such a way that all the parts of the expected energy range are included. In order to cover both the low-and the high-energy range of neutrons, two categories of detectors have been chosen which are based respectively on the registration of neutron-induced particle-tracks in organic materials and neutron-induced fission fragments in heavy elements (7-8). The other spectrometer available, which make it possible to cover both the low- and the high-energy range of neutrons consists of multisphere hydrogenous moderators, supplemented by different thickness of lead shielding to extend the response to high energy neutrons (20,21).
This multisphere system (upper part of Fig. A.11.3) is not convenient for on-board neutron spectrometry because of the limited room available in passenger aircraft.
However, this spectrometer has been used on dedicated flights made available by the NASA under the High-Speed Research Program (21,22).
When compared with the multisphere spectrometer, the passive ANPA-stack (lower part of Fig. A.11.3) is compact like a portable computer and does not require any technical assistance for on-board measurements.
Fig.A.11.4 shows the responses versus the neutron energy of 8 different neutron detectors contained in the ANPA-stack. They can be divided in the two following categories (1,7-9,13-14):

(I) known detectors such as bubble detectors (BD-100R) and recoil-track detectors based on counting track-spots on a single surface (CR-39-1, PC-1, and LR-115-1).
(II) new detectors based on coincidence counting of paired spots CR-39-2, PC-2, LR-115-2, and bismuth.
Because of its simplicity and compactness, the ANPA-stack has been exposed on passenger aircrafts simply by asking pilots to take the stack on board.
In Fig. A.11.5, the spectrum taken with the passive stack spectrometer flown along the Milan-Los Angeles route (23,24) is compared with those taken on the top of the concrete reference radiation facility at CERN (25) and at high-altitude at 0.8 GV geomagnetic cutoff rigidity (22). This figure shows that the in-flight spectrum measured by Golhagen at al. (22) by a multisphere spectrometer does not have as large a high-energy peak as that obtained at CERN (25). It is clear from Fig.A.11.5 that the spectra obtained by the multisphere spectrometer have different shapes and they are also different from that obtained by the ANPA-stack. In this last spectrum, the peak at high neutron energies is clearly located at about 300 MeV instead of 100 MeV as for the other two spectra. This 300 MeV peak-energy is consistent with the minimum of the neutron cross sections of O, C, and N (26). As an aside, it is also important to mention that the proton fluence at aviation altitudes is peaked around a few hundreds of MeV (27). Incidentally, the spectrum obtained with the ANPA-stack has not been corrected for the proton component of the cosmic ray field as for the Goldhagen spectrum (22). In order to improve the knowledge of the high-energy part of the neutron spectrum, new investigations have been undertaken to develop detectors for high energy neutrons based on fission reactions.
In particular, these fission detectors make it possible to evaluate the spectrum hardness which, in case of neutron dosimetry, represents a simple alternative to neutron spectrometry.

A 11.4 Stack for the evaluation of the hardness ratio of neutron spectra

Neutron induced fission cross-sections for some heavy nuclei (^{235}U, ^{238}U, ^{232}Th, ^{209}Bi) are internationally recommended as secondary standards for neutron flux monitoring in the energy region above 20 MeV (28,29). Extensive investigations have been carried out in the 1990s to study the response of the Bi-fission detectors for the measurement of high energy neutrons (9,11,12,16).
In addition to bismuth, other heavy nuclei such as gold and tantalum have been studied for the detection of high energy neutrons through fission-induced reactions (13). In spite of the low fission cross-sections of these materials, sufficiently high sensitivity was achieved with the multi-detector stack developed at ANPA. These achievements are important, since these detectors make it possible to exploit the excellent characteristics of the fission reactions in bismuth, gold and tantalum for the measurements of high energy neutrons, such as:
-excitation functions well above 20 MeV which eliminate the influences of low energy neutrons,
-smooth variation of the cross-section with neutron energy,
-mono-isotopic and non-radioactive materials, which make them easy to transport and handle.
However, in order to cover both the low- and high-energy range with the same detecting method, it was decided to use neutron-induced fission reactions in thorium. ^{232}Th fissile radiators can be safely handled at accelerator facilities but its use outside laboratories is hampered by its radioactivity. For in-flight measurements, it could be possible to use thin films of the alloy made by manganese and only a small percentage of thorium (2-4%), such as that used in the past for aircraft engine parts. A radiator with only a small percentage of thorium could indeed be used thanks to the large signal-to-noise ratio of the ANPA stack.

The response of these detectors has been extensively investigated at the quasi-monoenergetic neutron beam facility at The Svedberg Laboratory of the Uppsala University in cooperation with the Khlopin Radium Institute (KRI). This cooperation was facilitated by the fact that the V.G. Khlopin Radium Institute (KRI) and Uppsala University (UU) were carrying out a joint program of (n,f) cross-section measurements in the energy region between 30 and 180 MeV (30). The cooperation between ANPA, the Svedberg laboratory and the KRI group, even though it was just accidental, made it possible to measure neutron induced fissions in bismuth, gold, tantalum by two different techniques (namely the spark counting of etched through holes (17) and the thin film breakdown counter (31,32)), by which accurate calibrations of different detectors have been obtained. The accurate knowledge of the detector response in the neutron energy range from 30 MeV to 180 MeV is very important because the prediction power of available nuclear reaction models and codes (for these neutron energies) is yet not reliable (30) and because the peak of cascade neutrons falls within this energy range.

For neutron energy greater than 200 MeV, it is possible to derive the neutron cross-section values and thus the detector responses from the extensive data-base available on protons (13,33).
Fig. A.11.6 shows the fission-cross section of bismuth, gold, tantalum, and thorium obtained with the procedures described above. The response of fission-fragment track detectors for neutrons of different energies is proportional to the product of the fission cross-sections, $\sigma(n,f)$, and the fluence at the same energy. For this reason, the response ratio for any given detector can be easily calculated if both the neutron spectrum and the cross-sections are known. These detector ratios have been calculated for most of the high-energy spectra available respectively at CERN, high-altitude mountains and at civil aviation altitudes, as reported in Table A.11.1. All these spectra can be divided in two broad categories formed respectively by spectra (with number from 1 to 8) with the evaporation peak larger than that at high-energy (such as in the spectrum obtained by Goldhagen *et al.*[22]) and vice-versa (such as the spectrum obtained at the CERN facility by Mares and Schraube[25]). Table A.11.1 reports the values of the hardness ratios of these two categories of spectra.
Extensive measurements have been carried out at CERN on the high-energy field [32] with the ANPA-stack containing all the fission-fragment detectors described above (13-14). The ratios of the track densities for different detector combinations have resulted in the following: Th/Bi=4.3±0.4; Bi/Au=13±1 and Th/Au=56±7. These values are reported in the last row of table A.11.1. It is clear from this table that the two categories of spectra have two different sets of values for the above hardness ratios. In particular, the experimentally measured ratio of Bi/Au at the CERN facility is the same as those calculated for the facility from the two spectra available (number 9, 10) but it is different from those evaluated for the spectra with numbers from 1 to 8. The other two experimental ratios at the CERN facility (i.e. Th/Bi and Th/Au), which are representative of the spectrum hardness, are closer to those evaluated from the spectra with number from 1 to 8 than to those calculated from the CERN type of spectra (number 9-12).
From these data it appears that the low-energy part of the spectrum on the top of the concrete facility at CERN is similar to that of the atmospheric spectra (no 1-8), while the high energy part of the CERN spectrum is different from that of the atmospheric spectra. In particular, the data seem to indicate that the true shape of the cosmic-ray-neutron spectrum is closer to that of the Goldhagen spectrum (22). The difference between the Goldhagen spectrum and that obtained with the ANPA-stack could be explained by the fact that the latter has not been corrected for the proton component of the cosmic ray field.

Table A 11.1 Hardness ratios for spectra respectively with a larger peak at low-energy (1-8) and a larger peak at high-energy (9-12). Last row: Hardness ratios measured at CERN with the ANPA-stack.

Spectrum number		**Bi/Au**	**Th/Bi**	**Th/Au**
1	Calculated spectrum at altitude 17.5 km (Merker, 1973) [34]	**3.8**	**13**	**49**
2	Calculated spectrum at depth 50g.cm^{-2} (Armstrong *et al.*, 1973) [35]	**3.7**	**12**	**44**
3	Calculated spectrum at 23.5 km (Hajnal, 1991)[36]	**3.5**	**10**	**35**
4	Measured spectrum at Milan-Los Angeles route (Tommasino, 1999) [23]	**3.6**	**9.4**	**33.8**
5	Measured spectrum at chacaltaya mountain-altitude (Zanini *et al.,*2001)[24]	**3.7**	**11**	**41**
6	Calculated spectrum at 200 g.cm^{-2}, 4.6 GV cutoff (Roesler *et al.*, 1998)[37]	**3.6**	**11**	**40**
7	Calculated spectrum at 56 g.cm^{-2}, 20 km altitude (Goldhagen *et al.*, 2002) [22]	**3.7**	**11**	**41**
8	Calculated spectrum at 10580 m (Ferrari *et al.*, 2001)[38]	**3.7**	**11**	**41**
Mean		**3.7±0.1**	**11±1**	**41±5**
9	Calculated spectrum at CERN top concrete (Heinrich *et al.,* 1999) [27]	**4.2**	**17**	**70**
10	Measured spectrum at CERN top concrete (Mares and Schraube, 1997) [25]	**4.7**	**18**	**84**
11	Measured spectrum at Zugspitze mountain-altitude (Schraube *et al*, 1997)[20]	**4.5**	**18**	**83**
12	Measured spectrum at PTB site, 1025 g.cm^{-2} (Kurochkin *et al.*, 1999)[39]	**4.7**	**19**	**87**
Mean		**4.5±0.2**	**18±1**	**81±8**
Measured values at CERN		**4.3±0.4**	**13±1**	**56±7**

A 11.5 Stack for the dosimetry of the galactic cosmic rays.

The most convenient dosimeters of the stack for the assessment of the in-flight exposure are respectively (18,19):

-The bubble dosimeters and the bismuth-fission detectors for the assessment of the dose of low- and high-energy neutrons respectively.

-The TLD detectors for the dosimetry of the non-neutron component (40).

The simplicity and the compactness of these detectors make them particularly convenient for repeated measurements in given routes, as needed for the study of the reproducibility of route doses. For high energy neutrons, this dosimetric system makes use of the bismuth fission track detectors. With the bismuth stack, typically used at present, it is possible to measure the flux of cosmic ray neutrons with energy greater than 50 MeV for a single long-haul flight with a standard deviation better than 20%. In practice, this is the only

detector, which has its principal response at energies above 50 MeV (8). The possibility to obtain the selective measurements of the dose of high energy neutrons is of interest, specially because they produce nuclear disintegrations (stars) in tissue. The selective monitoring of the dose due to star-producing radiations should be considered a minimum course of action, because of the limited knowledge of the radiobiological effects of this radiation (41).

The dosimetric ANPA-stack has been developed with the specific goal in mind to make use of a system which does not require any technical assistance both on earth and on-board. Some problems may arise when using TLD detectors (sensitive to the terrestrial radiation and to the X-ray from the security scanning system) and thermal neutron detectors (because of their abundance at sea level). Detectors of thermal neutrons are not included in the dosimetric ANPA-stack simply because the exposure to thermal neutrons at flight altitude is negligible (22,41).

To overcome the problem of the TLD exposures to terrestrial gamma radiation, the ANPA-stack has been supplemented by an electronic personal dosemeter, which makes it possible to differentiate the in-flight exposure from that received on earth.

The neutron-dosimetry response of the ANPA-stack has been studied with mono-energetic beams of low- and high-energy neutrons at different facilities within Europe and North-America (18).

Inter-comparisons exercises have been carried out at the CERN-high-energy neutron-beam facility (18) using the ANPA-stack together with the CR-39 stack from the Dublin Institute of Advanced Studies – (DIAS-stack) and two tissue-equivalent proportional counters from the University of Saarland–(USAAR HANDI). The response of all these neutron dosimeters is sensitive to both low and high energy neutrons. Table A.11.2 reports the responses of these dosimeters relative to the CERN tissue-equivalent proportional counter - (CERN-TEPC).

It appears clear from this table that there is a good agreement between the responses of all four dosimeters with that of the TEPC from CERN.

Table A.11.2 Response of different neutron dosemeters relative to that of CERN-TEPC

USAAR-HANDI/CERN-TEPC	0.88
USAAR-HANDI/CERN-TEPC	1.02
ANPA-stack/CERN-TEPC	0.95 ± 0.1
DIAS-stack/CERN-TEPC	1.18 ± 0.12

On-board comparison of measurements have been made with the same dosimetric systems, once both ANPA-stack and the DIAS-stack have been supplemented with TLDs dosimeters for the measurements of the non-neutron response (18,19).

For this comparison, correction has been made for the exposure of the stack below 8 km, where the real-time instrumentation was switched off.

The average values of the total ambient dose equivalent rates along the three different routes for both passive and real-time instrumentation are reported in Table A.11.3

Table A 11.3 Comparison of in-flight measurements.

DOSIMETRIC SYSTEM	AMBIENT DOSE EQUIVALENT RATE (μSv/h)
MILAN - TOKYO (8 return flights)	
TEPC (USAAR)	4.7 ± 0.4
STACK (ANPA)	4.7 ± 0.4
STACK (DIAS)	4.9 ± 0.6
ROME - RIO DE JANEIRO (18 return flights)	
TEPC (USAAR)	2.3 ± 0.3
STACK (ANPA)	2.1 ± 0.2
STACK (DIAS)	2.4 ± 0.3
MILAN - LOS ANGELES (10 return flights)	
TEPC (USAAR)	4.7 ± 0.6
STACK (ANPA)	4.7 ± 0.5
STACK (DIAS)	4.8 ± 0.6

The values obtained with three different dosimetric systems are highly consistent. The total agreement among values obtained with very different dosimetric systems is of particular significance. Within one standard deviation all the measured values are the same. The dose rates are mean values over many repeated measurements for the same route and the same aircraft.
The standard deviation includes both the uncertainty of the measurements and the variation of the route among the many different flights. Since one standard deviation is only about 10% of the mean measured value, it is safe to conclude that the route doses are highly reproducible.
From the extensive investigations carried out in the past, the dosimetric stack has been used on 107 long-haul flights. For a given route such as Rome-Tokyo, all the data (in terms of the ambient dose equivalent) per flight at different phases of the solar cycle, for two different aircrafts (Boeing 747 and 767), at different locations within the 767 aircraft are the same within less than 20%.
When these data are compared with those obtained in the 1970s, they are 40% higher (19). According to all the data gathered so far, it is safe to state that most of the 40% difference is due to the different dosimetric quantities used and to the fact that the contribute to the total dose from high energy neutrons was missing in the earlier measurements.

A 11.6. Solar flares: retrospective or prospective dosimetry

The investigations on the aircrew exposure carried out to date by most of the laboratories are dealing with the galactic cosmic radiations, which represent a radiation source always available and relatively constant. By contrast with galactic cosmic rays, solar flares radiation is totally unpredictable and extremely variable in terms of energy spectrum, intensity, direction, and duration.
Most of the dosimetric systems used on-board so far for the galactic cosmic rays may not be appropriate for the solar cosmic rays dosimetry, which requires:
-the estimate of low-and high-energy neutron-dose in an unknown spectrum,
-the knowledge of the field geometry to evaluate the effective dose, E,
- the simplicity, the reliability, the roughness, the low cost of both the detectors and their maintenance i.e. all the requirements typical of a detector system which should be operated for decades prior to the detection of an extremely rare event. The last requirements are very important since solar flares, which may cause a significant increase of exposure at flight altitudes , may occur decades apart. The most suitable detectors for solar cosmic rays are those based on the registration of neutron-induced particle tracks in plastics, the responses of which have been extended to energies above 200 MeV by using monoenergetic protons beams from different accelerator facilities from PSI, TSL, DUBNA, etc.(14). Fig. A.11.7 shows all the responses

obtained to-date (14) for detectors based neutron-induced particles in three different track detectors (CR-39, PC, LR-115). The data shown in Fig.A.11.7 are consistent with those obtained by Spurny (42). As already observed by Spurny (42), there is a good continuity among the neutron- and proton-data, which justifies the calibration approach adopted.
Among all the detectors reported in Fig. A.11.7, the simultaneous use of the CR-39 and polycarbonate detectors (8) appears to be the best choice for the assessment of the neutron dose due to solar flare radiation respectively because of:
-the low background when counting coincident track spots in matched surfaces of paired detectors,
-the possibility to measure the neutron incident angle with these detectors (43),
-the large decrease in the response ratios between CR-39 and polycarbonate versus the neutron energy, which may be useful to estimate the neutron energy.
Another important characteristic of these two detectors is that they can be both found as consumer products in aircraft and could be used for retrospective dosimetry. Indeed, in passenger aircrafts, it is possible to find two different types of neutron detectors and/or dosemeters formed respectively by polycarbonate and CR-39 plastic materials. While the CR-39 may be found essentially in eyeglass lenses (44-46), the polycarbonate, in addition to eyeglass lenses, can be found in different consumer products such as bottles, plastic cups for soft drinks, and CD-ROMs (47-49).
An interesting retrospective polycarbonate dosimeter which can be found on-board is the CD-ROM used for music or video (47-49). Some preliminary data have been already gathered with these devices by exposing them at CERN (50). However with the CD-ROMs it is not possible to measure the radiation incident angle and to ensure that they will survive (as consumer products) long-enough to be exposed to any of the extremely rare solar events.
In the past, simple systems for the electrochemical etching of test tubes, small bottles, cups, Petri dishes, and/or any container have been developed (43,51), which make it possible to use polycarbonate products with different shapes as retrospective neutron dosimeter.
In particular, polycarbonate bottles have been extensively investigated (43), which are typically used as containers of the bubble detectors (52). The Polycarbonate bottles can be very useful as back-up detectors for the bubble neutron dosimeters in case they happen to be used on board during a large solar flare event, which may be large enough to saturate the response of the bubble detectors. Incidentally, the counting of electrochemically etched tracks is very similar to that of counting bubbles and the same automatic systems can be used to count both devices.
For what concerns the use of these polycarbonate detectors for retrospective dosimetry, an attractive solution could be that to find polycarbonate cups, typically used for soft drinks.
To date, it was not possible to find these types of plastic cups on-board and the simplest way to make them available would be to convince the flight companies to use these cups on-board instead of those used at present. Unfortunately, these arrangements would be more close to prospective dosimetry than to the retrospective one. Moreover, even under these arrangements, we also need to carry out the dosimetry of the non neutron-component of the solar cosmic rays. To our knowledge, the retrospective assessment of the total exposure to solar cosmic rays can hardly be achieved with the limited number of items that it is possible to find on-board.
The only way to obtain the measurements of this exposure is through prospective dosimetry which, in addition to polycarbonate- and CR-39-detectors, requires TLDs and one electronic personal dosimeter, as for the stack for galactic cosmic rays.
Other important requirements for solar flare dosimeter based on CR-39 and polycarbonate detectors is to have a sufficiently high response to measure a total dose of about 100 μSv within 20%. This dose is only 5% of the dose of 2 mSv that aircrew typically receive on long-haul flights. Sufficiently large response can be achieved not only with CR-39 but also with polycarbonate through the use of large area detectors. To obtain information of the geometry of the radiation field which is needed, it is possible to take advantage of the strong angular dependence of both CR-39 and polycarbonate on the neutron incident angle (43).
To this end, tens of polycarbonate foils (characterized by a negligible cost) with 10cmx10cm areas can be placed at the 6 different surfaces of a cube. CR-39 is needed in relatively small quantities, since it is relatively more sensitive. For this reason, only 2 paired detectors can be placed on 3 mutually orthogonal stacks of the cube. Inside this cube there is enough room to keep the dosimeters mentioned above for the non-neutron component: the TLDs plus one electronic personal dosimeter.
The stack for the dosimetry of solar cosmic rays has more stringent requirements than that for galactic cosmic rays. For these reasons, the former stack can be also conveniently used for the galactic cosmic rays

dosimetry, which is needed for the evaluation of computer-evaluated doses. However, the stack for solar cosmic rays shows promise for application in space dosimetry, where solar flares are very frequent events.

REFERENCES

1. Tommasino L., Caggiati F., Cavaioli M., Notaro M., Teodori R., and Zhou D. Passive Multidetector Stack for the Assessment of Aircrew Exposure. Environment International **22**, S:115-119(1996).
2. Byrne J., O'Sullivan D., Tommasino L., and Zhou D. New Method for the Rapid Evaluation of $Z \geq 1$ Cosmic Ray Particles- Results from a Balloon Borne Experiment. Rad. Meas. **25**, 471-474A (1995).
3. Griffith, R.V.,and Tommasino, L. *Etch Track Detectors.* In Radiation Dosimetry. In: The Dosimetry of Ionising Radiations. Kase K., Byangard, B.B., Attix, F.H. Editors. (New York: Academic Press) Vol. **III** pp 323-426 (1991)
4. Fleischer, R.L.. Price, P.B., and Walker, R.M. Nuclear Tracks in Solids: Principles and Applications (Berkeley: University of California Press) (1975).
5. Frank, A.L., Benton, E.V., Armstrong, T.W., and Colborn, B.L. Neutron Fluences and Dose Equivalents measured with Passive Detectors on LDEF. Radiation Measurements 26, 833-839, (1996)
6. O'Sullivan D., Zhou D., Heinrich W., Roesler S., Donnelly J., Keegan R., Flood E., and Tommasino L. Cosmic Rays and Dosimetry at Aviation Altitudes. Rad. Meas. **31**, 579-584, (1999).
7. Tommasino, L., and M. Chavalli (1998) A new method for the dosimetry of nucleons and for the measurements of low concentrations of man-made or natural alpha-emitting radionuclides. Italian Patent (APAT) Patent N° 1300503
8. Tommasino L. *In-flight measurements of radiation fields and doses.* Rad. Prot. Dosim. **86**, 297-301 (1999).
9. Jain R.K., Prokofiev, A.V., Smirnov, A.N., Tommasino, L. Measurement of high energy neutrons by fission reactions. Rad. Meas. 34, 129-132 (2001)
10. Tommasino, L. Solid Dielectric Detectors with Breakdown Phenomena and their Applications in Radioprotection. Nuclear Instruments and Methods. 173, 73-83 (1980)
11. Jin H., Cavaioli M., Hajdas V., Prokofiev A.V., Smirnov A.N., and Tommasino L. Bismuth-fission Detectors for High Energy Nucleons: II. Proton and Neutron responses. Rad. Meas. **31**, 459-462(1999).
12. Zhou D., Cavaioli M., Jain R.K., Spurny F., Teodori R., and Tommasino L. Bismuth-Fission Detectors for High Energy Nucleons: I. Registration Characteristics. Rad. Meas. **31**, 455-458 (1999).
13. Tommasino, L. and Tripathy, S.P. Hardness Ratios of Different Neutron Spectra. Presented at the 9th International Symposium on Neutron Dosimetry held in Delft (The Netherlands. Sept.2003. Accepted for publication in Radiation Protection Dosimetry.
14. Tommasino, L. Advanced Passive Detectors for Neutron Dosimetry and Spectrometry. Presented at the 9th International Symposium on Neutron Dosimetry held in Delft (The Netherlands. Sept.2003. Accepted for publication in Radiation Protection Dosimetry.
15. Tommasino, L., Jain, R. K., O'Sulivan, D., Prokofiev, A. V., Singh, N. L., Smirnov, A. N., Tripathy, S. P., Viola, P. *Cosmic-ray neutron spectrometry by solid state detectors.* Radiat. Meas. **36**, 307-311 (2003).
16. Cross, W.G. and Tommasino L. Dosimetry of High Energy Neutrons and Protons by Bi-209 Fissions. Rad. Prot. Dosim. 70, 419-424 (1997); also Canadian Patent(AECL) Patent N° 859,262
17. Cross, W. G., Tommasino, L. A rapid reading technique for nuclear particle damage tracks in thin foils. Rad. Eff. 5, 85-89 (1970).
18. Curzio G., Grillmaier E., O'Sullivan D., Pelliccioni M., Piermattei S., Tommasino L. The Italian National Survey of Aircrew Exposure: I Characterization of Advanced Instrumentation . Radiation Protection Dosimentry. 93, 115-123 (2001).
19. Curzio G., Grillmaier E., O'Sullivan D., Pelliccioni M., Piermattei S., and Tommasino L. The Italian National Survey of Aircrew Exposure: II On-board Measurements and Results.Radiation Protection and Dosimetry. 93, 125-133 (2001).
20. Schraube H., Jakes J., Sannikov A., Weitzenegger E., Roesler S., and Heinrich W. The cosmic Ray Induced Neutron Spectrum on the Summit of the Zugspitze (2963m) Rad. Prot. Dos. 70, 405-408 (1997)

21. Goldhagen P.-EML Multisphere Neutron Spectrometer, Ion Chamber and Scintillation Counters. Paper presented at the Atmospheric Ionizing Radiation Investigators' Workshop. Preliminary Results and Lessons Learned from the June 1997 ER-2 Flights. NASA Langley Research Center, Hampton, VA, March 30-31, 1998.
22. Goldhagen, P., Reginatto, M., Kniss, T., Wilson, J.W., Singleterry, R.C., Jones, I.W., Van Steveninck W. Measurement of the energy spectrum of cosmic-ray induced neutrons aboard and ER-2 high-altitude airpalne. Nucl. Instrum. And Methods in Physics Research A, 476, 42-51 (2002)
23. Tommasino, L. *In-flight measurements of radiation fields and doses.* Radiat. Prot. Dosim., **86,** 297-301 (1999).
24. Zanini, A., Ongaro, C., Manfredotti, C., Tommasino, L. and Miranda Losa P. *Neutron Spectrometry At Various Altitudes in Atmosphere by Passive Detector Technique.* Il Nuovo Cimento **24** (4-5), 691-697 (2001).
25. Mares, V. and Schraube, H. High energy neutron spectrometry with bonner spheres. In: IRPA-symposium " Radiation Protection in Neighbouring Countries of Central Europe" 1997 Prague, September 8-12 (1997).
26. Savitskaya E.N. and Sannikov A.V.High Energy Neutron and Proton Kerma Factors for Different Elements. Radiat. Prot. Dosim. 60, pp135-146 (1995)
27. Heinrich, W., Roesler, S. and Schraube, H. Physics of Cosmic Radiation Fields. Rad. Prot. Dos. 86, pp253-258 (1999).
28. Carlson, A.D., Chiba, S., Hambsch, F. J, Olsson, N., Smirnov, A. N. *Update to nuclear data standards for nuclear measurements.* IAEA Report INDC (NDS)-368, Vienna, 1997; Proc. Int. Conf. On Nuclear Data for Science and Technology, Trieste, Italy, May 19-24, Pat II, p. 1223 (1997).
29. Condé, H. *Cross section standards above 20 MeV*. In Proc. Int. Conference of Nuclear Data for Science and Technology (Ed. J. K. Dickens, USA, Illinois), Gatlinburg, USA, May 9-13, 1, 53-59 (1994).
30. Eismont, V. P., Prokofiev, A. V., Smirnov, A. N., Condé, H., Elmgren, K., Olsson, N., Renberg, P. U., Neutron-induced fission cross sections of ^{181}Ta, nat W, ^{197}Au, ^{197}Hg, ^{208}Pb, ^{nat}Pb, and ^{209}Bi nuclei in the energy range 35-175 MeV. TSL Progress Report 1998-1999, Ed. A. Ingemarsson, Uppsala University, p.38 (2000).
31. Tommasino L., Klein N., Solomon P. Thin film breakdown counters of fission fragments. J. of Appl. Phys. 46, 1484-1488 (1975); also Italian Patent (ENEA) Patent N° 5052/A/74
32. Eismont, V. P., Prokofiev, A. V., Smirnov, A. N. Thin film breakdown counters and their applications (Review). Rad. Meas. 25, 151-156 (1995).
33. Prokofiev, A. *Compilation and systematics of proton-induced fission cross-section data.* Nucl. Instr. and Meth. in Phys. Res. A **463**, 557-575 (2001).
34. Merker M. *Contribution of galactic cosmic rays to the atmospheric neutron maximum dose equivalent as a function of neutron energy and altitude.* Heath Phys. **25**, 524-527 (1973)
35. Armstrong, T.W., Chandler, K.C., Barish, J. *Calculations of neutron flux spectra produced in the earth's atmosphere by galactic cosmic rays.* J. Geophys. Res. **78**, 2715-2726 (1973).
36. Hajnal, F. and Wilson, J. W. *High-altitude cosmic-ray neutrons: A significant contributor to the radiation exposures at aircraft altitudes.* In: Seventh symposium on neutron dosimetry. Berlin: Nuclear Technology Publishing (1991).
37. Roesler, S., Heinrich, W. and Schraube, H. *Calculation of radiation fields in the atmosphere and comparision to experimental data.* Radiat. Res. **149**, 87-97 (1998).
38. Ferrari, A., Pelliccioni, M. and Rancati, T. *Calculation of the radiation environment caused by galactic cosmic rays for determining aircrew exposure.* Radiat. Prot. Dosim. **93**, 101-114 (2001).
39. Kurochkin, I.A., Wiegel, B. and Siebert, B. R. L. *Study of the radiation environment caused by galactic cosmic ray at flight altitudes, at the summit of the Zugspitze and at PTB Braunschweig.* Radiat. Prot. Dosim. **83**, 281-291 (1999)
40. Lucas, A.C. Hypersensitive dosemeters. Rad. Prot. Dos. 35, p219 (1991)
41. Reitz, G., 1993. Radiation Environment in the Stratosphere. Rad. Prot. Dosim. 48, pp5-20 (1993)
42. Spurny. F. Response of Some Solid State Nuclear Track Detectors to Protons with Energies from 0.01 to 10 GeV. Nucl. Tracks Radiat. Meas. 19, 127-128 (1991).
43. Lounis, Z., Cavaioli, M., and Tommasino, L. The Combined Use of Bubble Dosemeters and Electrochemical Etched Track Detectors. Rad. Prot. Dos. 59, pp299-302 (1995)

44. Fleischer, R.L. Serendipitous Dosimetry-An opportunity and an opportunity lost. Health Physics, 52, 219-221 (1987).
45. Hadley S.A., Meyer, N.R., Fleischer, R.L., and Cavallo, A. Eyeglass lenses for personal radon dosimetry. Health Physics 79, 242-250 (2000).
46. Fleischer, R.L., Meyer, N.R., Hadley, S.A., MacDonald, J., and Cavallo, A. Personal Radon Dosimetry from Eyeglass Lenses. Rad. Prot. Dos. 97, 251-258 (2001).
47. Pressianov, D., Van Deynse A., Buysse J. Poffijn, A. Meesen G.. Polycarnonates: a new retrospective radon monitor.In. Proceedings of IRPA Regional Congress on Radiation Protection in Central Europe. Cedex, France: International Radiation Protection Association. 716-722 (1999).
48. Pressianov, D., Buysse J., Van Deynse A., Poffijn, A. Meesen G. Polycarnonates: A long-term highly sensitive radon monitor. Nucl. Instrum. Methods A447, 619-621 (2000).
49. Pressianov, D., Buysse J., Van Deynse A., Poffijn, A. Meesen G. The Compact Disk as Radon Detector- A Laboratory Study of the Method. Health Physics 84, 642-651 (2003).
50. Pressianov, D., Poffijn, A., and Tommasino, L. Unpublished data
51. Tommasino L., and Zapparoli G (1977) A new method and apparatus for neutron dosimetry based on electrochemically etched container-shaped plastic detectors. Italian Patent (ENEA) Patent N° 49495/A/77
52. Ing, H.The Status of the Bubble-Damage Polymer Detector. Nuclear Tracks 12, pp49-54 (1986)

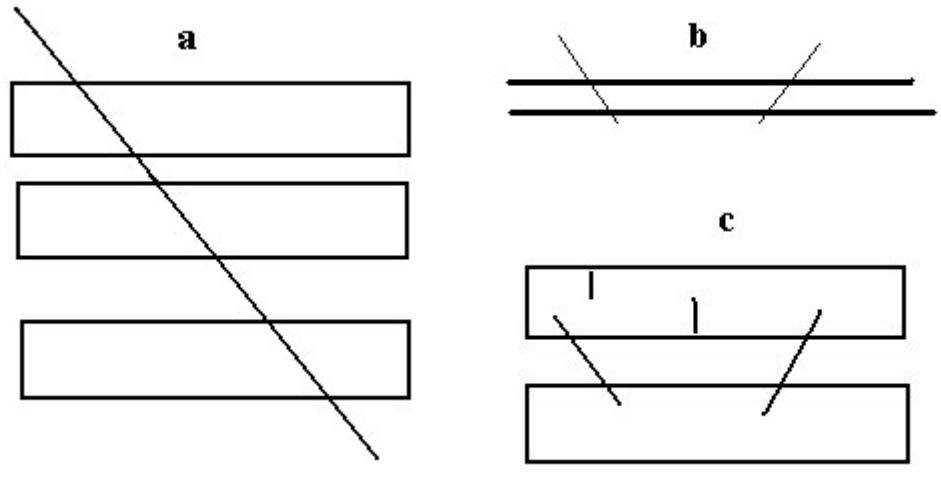

Figure A 11.1 Different Types of coincident events

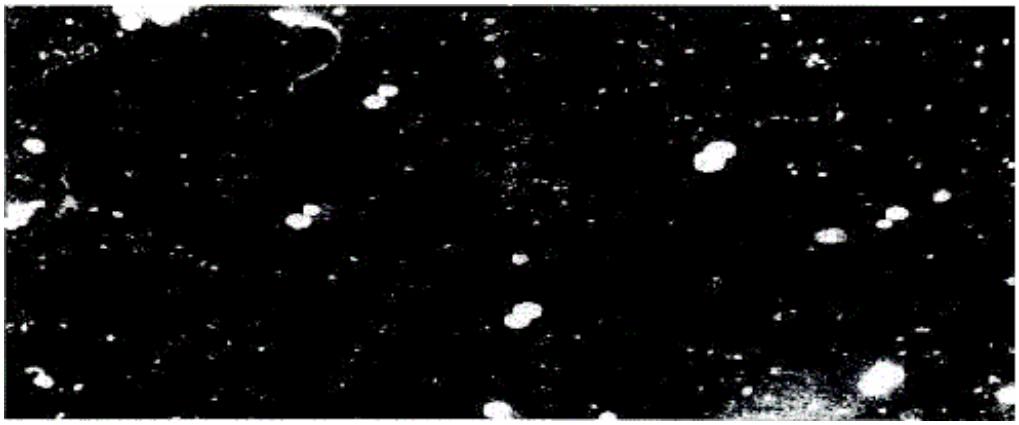

Figure A 11.2 Coincident events produced by neutron-recoil tracks in electrochemically etched polycarbonate

Figure A 11.3 Two different neutron spectrometers used for on-board measurements (20, 23)

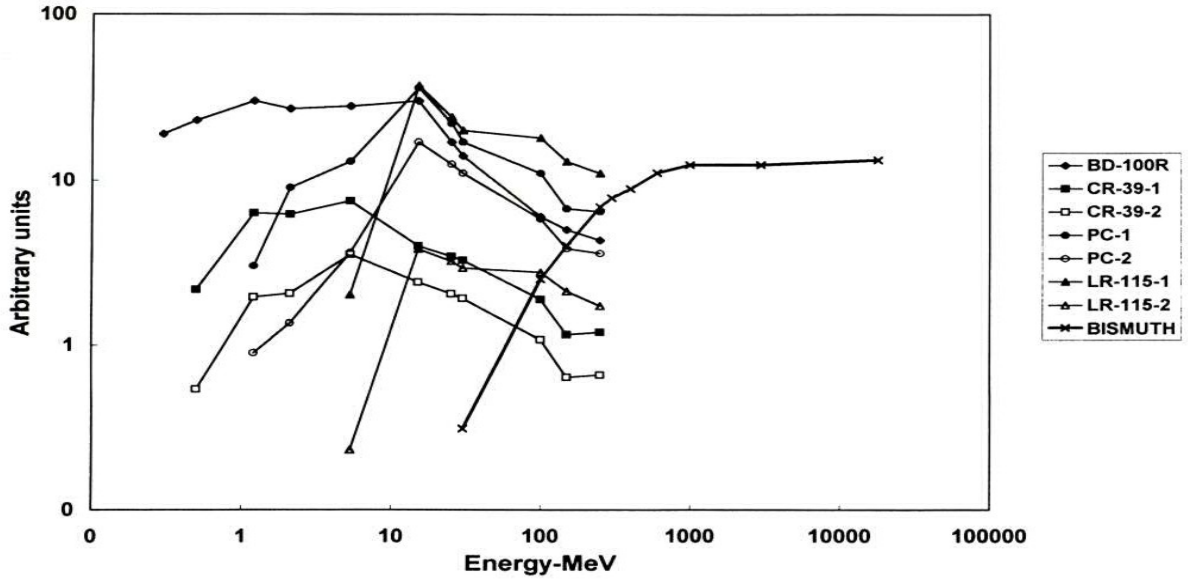

Figure A 11.4 Responses vs neutron energy of the different detectors of the ANPA-Stack

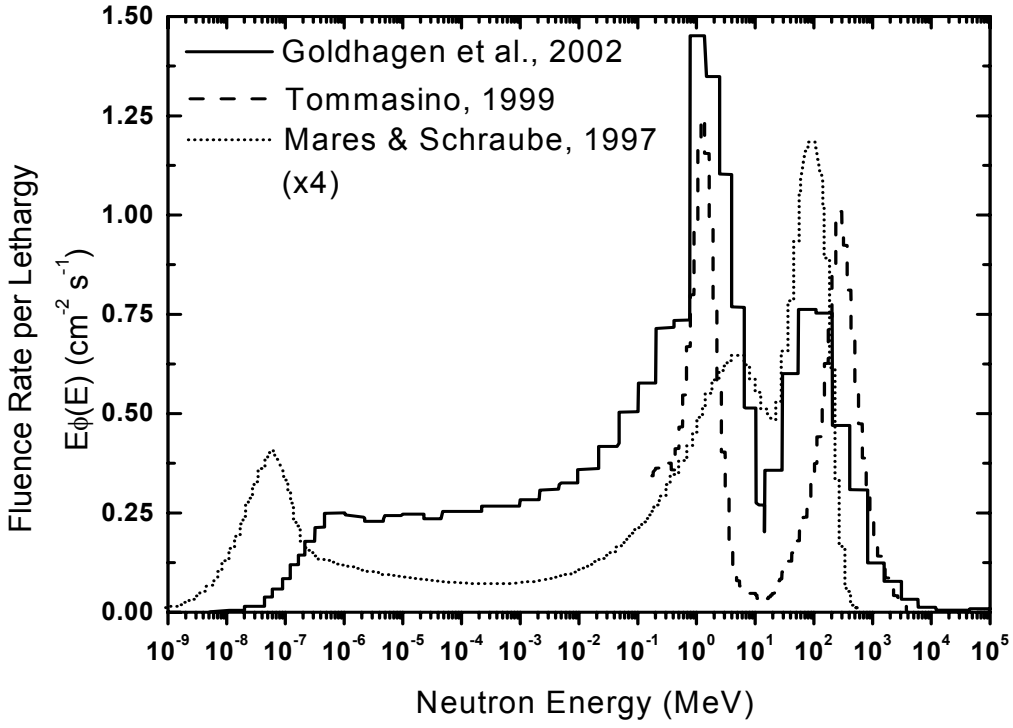

Figure A 11.5 Different neutron spectra obtained respectively with ANPA-stack on the route Milan-Los Angeles (23), with the multisphere spectrometer both at the CERN top of concrete facility (25) and on the NASA ER-2 high-altitude aircraft (22).

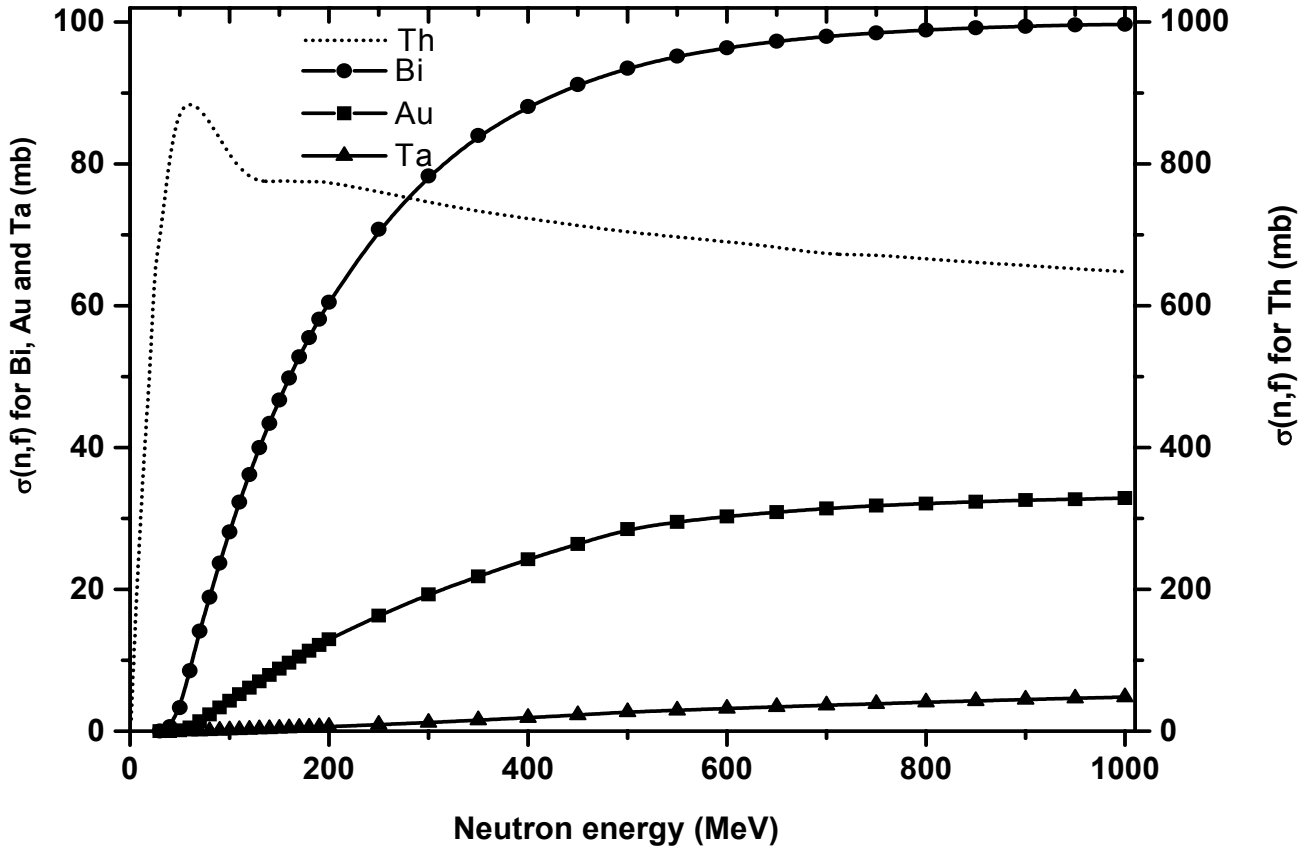

Figure A 11.6 The neutron fission cross-section, (□(n,f)), of ^{232}Th, ^{209}Bi, ^{197}Au and ^{181}Ta versus the neutron energy. The right hand ordinate is scaled for the thorium cross-section (13).

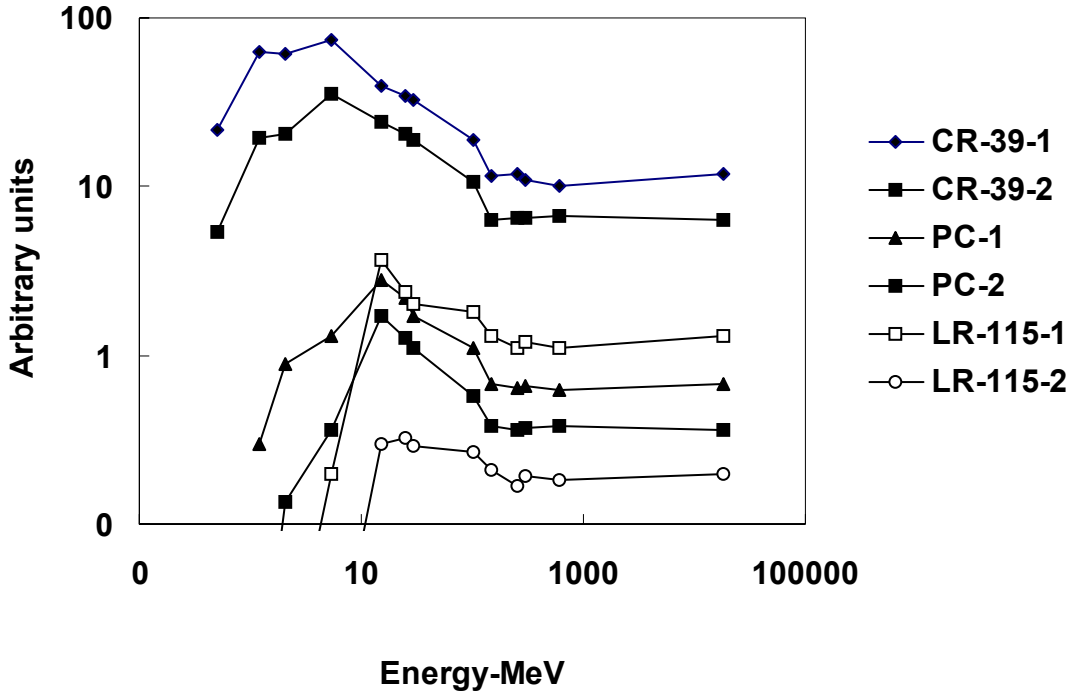

Figure A 11.7 Different detector responses versus the neutron energy

A12 Amira – Aviation Radiobiological Institute University of Munich

A.12.1 General description of amira – aviation

The instrument *amira-aviation* is specifically designed for aviation dosimetry. It consists of the prototype version of the active dosemeter *amira* (active monitoring in mixed radiation fields) combined with a mini PC and rechargeable batteries for extended power supply of both instruments. The instrument is sized 330mm, 225mm and 70mm, and its weight is 5.4kg. It can operate for about 150 hours without the need to recharge the batteries.

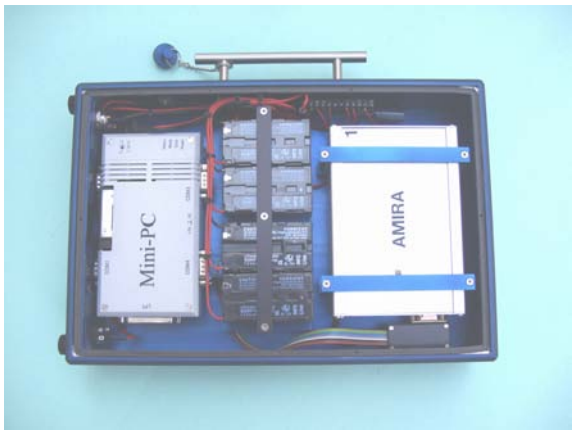

amira aviation ├──────┤ 10cm

A.12.1.1 Amira dosemeter:

Amira is an active dosemeter for radiation-protection purposes. It employs a tissue equivalent proportional counter, and is, therefore, well suited for measurements in mixed radiation fields including a neutron component (size: 148mm x 104mm x 42mm).

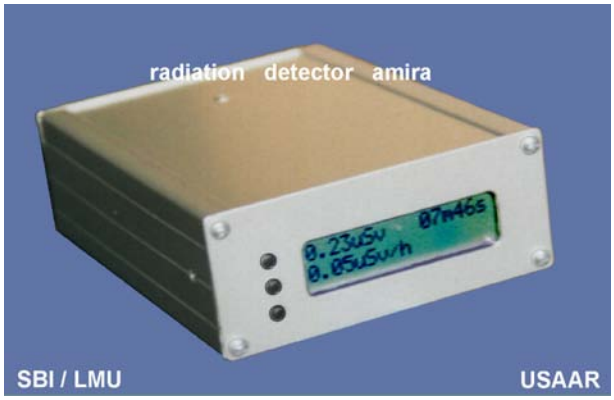

amira dosemeter

A.12.1.2 TEPC modul of amira dosemeter:

The instrument employs a simple geometry and a modular design of the detector which consists of a stack of three identical A-150 slices with half cylindrical grooves on each side. The slices are produced by a moulding technique. The sensitive volume of the detector comprises 24 cylindrical TEPC elements of 60mm length and 3mm diameter each, arranged in two layers. This permits a flat and compact design of the entire detector is attained. The large elongation of the cylinders reduces considerably the complexity of the design, the fabrication, and the use of the detector. Neither field tubes nor helices are necessary (see assessment of resolution). Because of the small diameter of the cylinders, the gas pressure inside the detector needs to be comparatively high - it is adjusted to simulate a diameter of 1µm in tissue - which reduces problems of counting-gas purity.

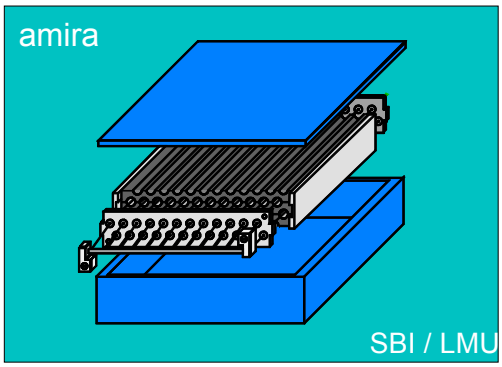

Diagram of the TEPC-modul*;* size of the detector module (95mm x 70mm x 16mm*)*.

A.12.1.3 Signal processing of amira dosemeter:

The miniaturized electronics has been developed by members of the Zentrum for Biophysik, Universität des Saarlands, this group had already developed, in the early 1990s, the well known HANDI system. The electronic system includes high voltage supply, charge sensitive preamplifier, quasi-logarithmic amplifier (four decades), filter, peak detector, A/D converter, data processing, display, computer interface, and power supply (rechargeable batteries). All components are optimised towards minimum power consumption. The measured absorbed dose and equivalent dose and the corresponding rates are calculated and displayed every five seconds, and an alarm function with readily set dose-rate threshold is provided. The accumulated single event spectrum can be transferred to a computer to be displayed and analysed in detail.

A.12.1.4 Assessment of resolution of amira dosemeter:

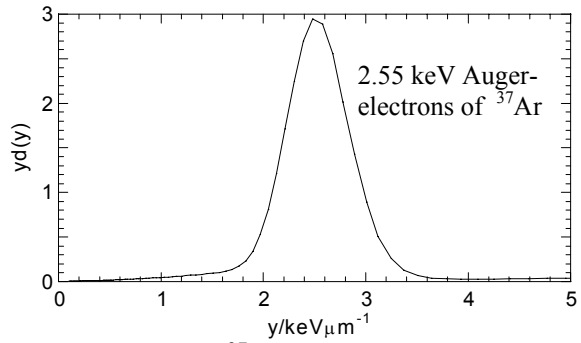

Microdosimetric distribution of ^{37}Ar admixed to the gas filling of the detector module. The resolution is close to the optimal resolution achieveable with proportional counters.

A.12.1.5 Performance of amira dosemeter:

In calibration measurements at PTB in monoenergetic neutron fields the dosemeter was found to underestimate for AP-exposure $H^*(10)$ at low neutron energies by up to 34% and to overestimate it by up to 82% for higher neutron energies up to 60MeV and at perpendicular incidence (see fig. below).

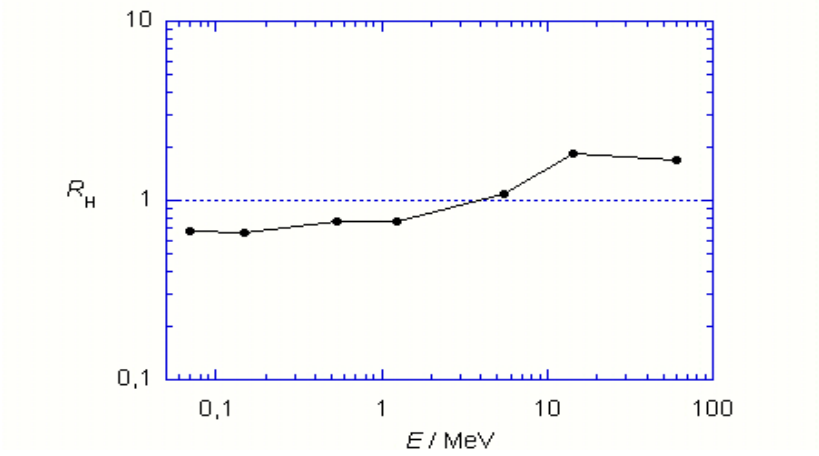

Equivalent dose response, R_H, of detector module relative to H*(10) of the reference field in its dependence on neutron energy (AP-exposure to monoenergetic neutrons).

In typical radiation protection situations low or very low doses need to be determined where
the relative accuracy of the equivalent dose measurements is limited by poor statistics. With a series of short measurements - at dose rate roughly 1mSv/h - the relative accuracy of the determination of 10µSv in a neutron field from a bare ^{252}Cf-source was found to be better than 10% (standard deviation).

A.12.1.5 Major characteristics of amira dosemeter:

lineal energy range	0.2keV/µm ... 2000keV/µm
display	equivalent dose, equivalent dose rate, measurement time
alarms	build in alarm levels for dose equivalent rate
operating time	70h (4 NiMH batteries)
computer interface	RS232
weight	0.7 kg
size	l48mm x l04mm x 42mm

A.12.3 Operation and calibration of amira – aviation:

For repeated measurements during flights *amira aviation* is controlled by a mini PC. Each 30 minutes the measurement is interrupted, the accumulated single event spectrum is stored on a flash memory card, and a new measurement cycle is started.

The assembled *amira-aviation* instrument has been calibrated in the ^{137}Cs photon field of a secondary standard laboratory and the calibration has been checked in the neutron field of a ^{241}Am-Be neutron source.

A.13 In-flight experiments conducted by the GSF during and after the maximum of solar cycle 22

H.Schraube and D.F.Regulla
GSF - National Research Center for Environment and Health
Institute of Radiation Protection
D-85758 Neuherberg
Germany

A.13.1 Introduction

When the radiation exposure to air crew received a renewed attention by the ICRP, the GSF started an experimental program to determine the dose rate caused by cosmic radiation inside airplanes by mid of 1990. A total number of 23 flights were conducted, Deutsche Lufthansa Airlines did the flight organisation and the supply of the airplanes, and organisation support was received from the German Occupational Insurance Association (BG). Two flights were very short distance connecting flights and not considered. Three flight routes had a total dose of less than 10 μSv; the other flights were on medium and long distance destinations. Two series of flights were done with slightly different experimental equipment: the first one during mid of 1990 to early 1991, the second one from mid 1992 to early 1993. The latter one included two routes of specific interest: One over the geomagnetic North Pole and one over the South Atlantic in the region of the geomagnetic anomaly. All flights but one were passenger flights; the exception was a taxi flight with a B747 without passengers and even without the seat assembly. During nearly all flights the experimental devices were arranged in the upper deck of the aircraft (see Figure A.13.1). More details on the flight and experimental conditions are given elsewhere [1,2].

A.13.2 Experimental equipment and calibration

During the flights a number experimental devices was employed, which are described shortly as far as their data are presented here:

1. Two neutron monitors of type NE-NM2B [a]. One of these was with the original moderator of Anderson and Braun [3] design (AB-counter). The second one was equipped with an additional lead converter and a modified outer moderator (ABH-counter[b]). This moderator arrangement is similar to that proposed by Birattari et al.[4], and described and the response characteristics determined by Mares et al. [5]. The reading device of booth monitors was the original NE-NM2B instrument. The integration time was approximately 6 min in the most sensitive range 0 to 100 μSv/h, which was used throughout all flights.

The calibration of the neutron devices was conducted face on, following the method of ISO-8529-2 [6] (clause 6.3.4) using an AmBe-source, which was calibrated against the PTB standard. Additionally, the original, unmodified NM2B was calibrated at the PTB.

2. Two photon dosemeters of type DLM7908 [c]. These counters with polyvenyltoluen-scintillators of 75 mm diameter x 75 mm length are commercially available dosemeters designed for low level ambient doserate measurements with a nominal range of 0.03 to 100 μSv/h. Calibration of the scintillation detectors were done under secondary laboratory conditions at Cs^{137} and Co^{60} sources at the GSF.

[a] Nuclear Enterprises Technology, Ltd., Benham, Reading , Berkshire, UK
[b] Commercially available as NM500x from Fa.MAB-Münchener Apparatebau, D-82008 Unterhaching,
[c] Fa.Halle, Braunschweig, Germany

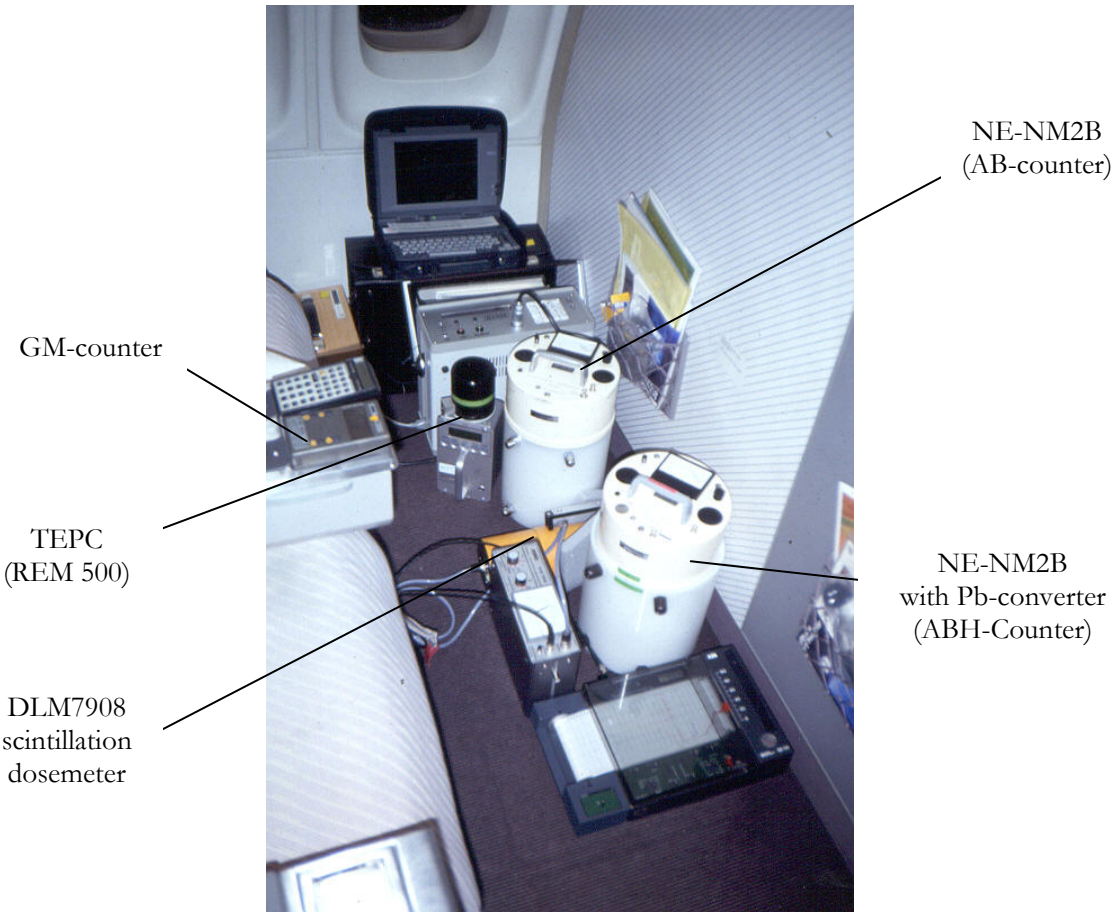

Figure A.13.1 Arrangement of experimental devices on the upper deck of a B747-400 during the measuring campaign of the GSF in 1992/93.

A.13.3 Data collection and evaluation

All data were collected and documented manually; for the flights 17 to 21, the data were taken after every integration period. For the earlier flights the reading intervals had to be extended due to the larger number of instruments to be observed by each of the attending scientists. The pilots provided geographic flight positions at reasonable time intervals, from which an interpolation could be done in the longitude-latitude domain with sufficient precision.

For the data evaluation the following procedures were applied:

1. For the neutron data corrections were applied to each reading of the to allow for the angular and energy response of the device, taking into account the spectral neutron fluence of both the calibration source and the cosmic neutron field at flight altitude. The corresponding correction factor, k_S, to be used for measurements in the cosmic radiation survey field is given by

$$k_C = \frac{\int_0^\infty R_\Phi(E_n)\cdot\Phi_E^C(E_n)\cdot dE_n}{\int_0^\infty R_\Phi(E_n)\cdot\Phi_E^S(E_n)\cdot dE_n} \cdot \frac{\int_0^\infty h_\Phi(E_n)\cdot\Phi_E^S(E_n)\cdot dE_n}{\int_0^\infty h_\Phi(E_n)\cdot\Phi_E^C(E_n)\cdot dE_n}$$

where E_n is the neutron energy, $\Phi_E^C(E_n)$ and $\Phi_E^S(E_n)$ are the spectral fluence (rates) in the calibration $^{(C)}$ field and in the survey $^{(S)}$ field; $R_\Phi(E_n)$ is the energy dependence of response of the instrument, and $h_\Phi(E_n)$ the coefficients to convert neutron fluence into ambient dose equivalent [7,8].

The energy range considered was 10^{-3}eV to 10 GeV, the response data taken from the literature [5] cited (see Figure A.13.2). For the direction of incidence it was assumed that the neutrons of the calibration field were incident to the detector front, while the cosmic radiation field in the aircraft was assumed as isotropic incident. Experimental and calculated neutron spectra were available from different sources [9-12] . The contribution of the reading due to protons is not corrected here to facilitate comparison with other measurements of the same type.

2. For the scintillation detectors, in some sections of the flights, one of the detectors showed inexplicable outliers of the reading. Due to the redundant devices available, the suspect values could be sorted out.

The responses of the scintillation detectors are not yet available in the full range of energies and particles encountered at flight altitudes; therefore, corrections to the readings are not possible at the time. However, qualitative considerations can be made: The contribution of neutrons to ambient dose equivalent is around 50% for flights at moderate latitudes (see, e.g. figure IV.3.3). To the remaining dose due to ionising radiation electrons contribute around 50%, protons (plus pions) 25%, muons and photons 12%, each. Protons and muons are sufficiently energetic to lose only part of their energy inside the scintillator (see chapter B.2). Electrons with a maximum of the energy spectrum at around 30 MeV will loose most of their energy or will even be stopped. Photons have their main energy range between 0.1 and 1 MeV and will be measured correctly, only the part in excess of a few MeV will possibly be slightly overestimated.

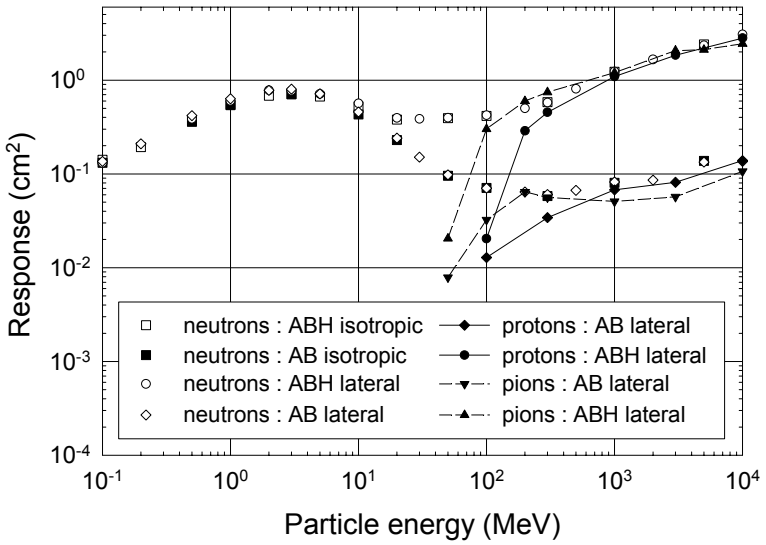

Figure A.13.2 Calculated neutron responses of the AB and ABH rem counters for lateral and isotropic irradiation, and for protons and pions at lateral incidence [5].

A.13.4 Results at flight and under laboratory conditions

In Figures A.13.3 and A.13.4, a specific aspect of the results obtained during the flights and under laboratory conditions is considered: The ratio of the both neutron detectors, which exhibit a considerably different response at energies in excess of 10 MeV, serves as a means to indicate spectral characteristic. A comparison of the in-flight data with those obtained in the (concrete shielded) CERN-fields [13] indicates a good similarity between the neutron fluence spectra. For the airborne experiments it appears that within the statistical uncertainty, there is no significant change in spectral shape, neither with changing altitude in the range 10700 m to 12500 m, nor with changing geomagnetic latitude from around 40° to 90°. The results at ground and mountain altitudes suggest that, here, the spectral shapes are slightly "harder", i.e. that the fluence contribution below around 10 MeV is somewhat less than inside the aircraft at flight altitudes.

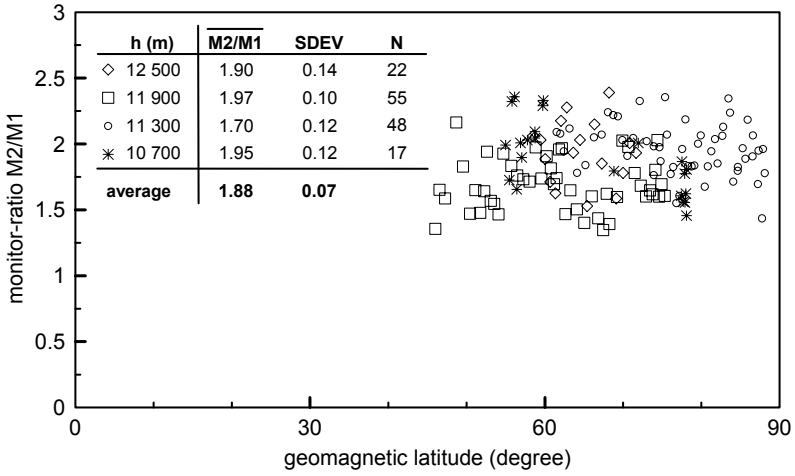

Figure A.13.3 Ratio M2/M1 of the reading of ABH- and AB-counter obtained during the 1992/93 flight campaign, for FL350 - FL410.

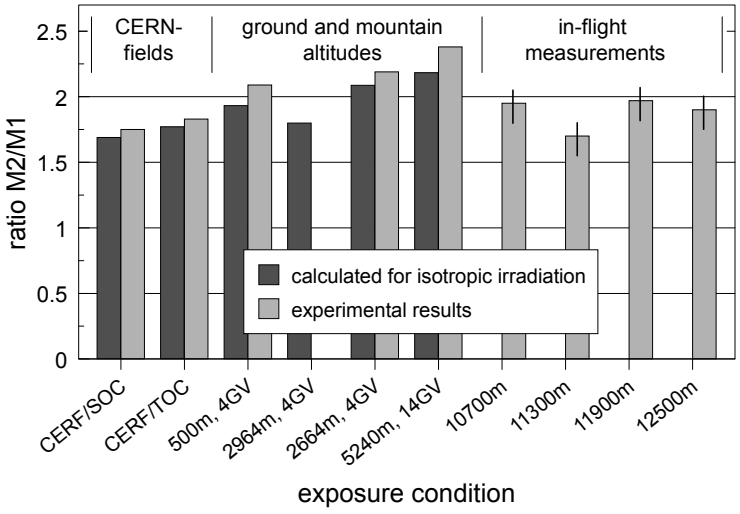

Figure A.13.4 Summary of ratios M2/M1 obtained at the CERF with , at ground- and mountain altitudes, and at the four flight levels [10].

A.13.5 References

[1] Regulla, D., David, J. *Radiation measurements in civil aviation*. Report GSF- (en) 41/91e (1993).

[2] Regulla, D., Schraube, H. *Radiation exposure of aircrews in civil aviation*. In: Strahlenbiologie und Strahlenschutz. 28.Jahrestagung des Fachverbands für Strahlenschutz e.V., Hannover, 23.-25.10.1996 (Hrsg.: G. Heinemann, H. Pfob). Köln: Verlag TÜV Rheinland, pp.375-380 (1996).

[3] Andersson, I., Braun, J. *A neutron rem counter*. Nukleonik **6**, 237-241 (1964).

[4] Birattari, C., Ferrari, A., Nuccetelli, C., Pelliccioni, M., Silari, M. *An extended range neutron rem counter*. Nucl.Instr.Meth. in Physics Research **A297,** 250-257 (1990).

[5] Mares, V., Sannikov, A.V., Schraube, H. *Response functions of the Anderson-Braun and extended range REM counters for neutron energies from thermal to 10 GeV*. Nucl. Instrum. Meth. Phys. Res. **A476**, 341-346 (2002).

[6] ISO-8529-2: Reference neutron radiations: Dosimetric fundamentals related to the basic quantities characterising the radiation field. International Organisation for Standardisation, Geneve (1998)

[7] Sannikov, A.V., Savitskaya, E.N. *Ambient dose equivalent conversion factors for high energy neutrons based on the new ICRP recommendations.* Radiat. Prot. Dosim. **70**, 383-386 (1997).

[8] ICRU-Report-66, Determination of operational dose equivalent quantities for neutrons. Journal of the ICRU International Commission on Radiation Units and Measurements **1** (3) 2001.

[9] Schraube, H., Jakes, J., Sannikov, A., Weitzenegger, E., Roesler S., Heinrich, W. *The cosmic ray induced neutron spectrum on the summit of the Zugspitze (2963 m)*. Radiat. Prot. Dosim. **70**(1-4), 405-408 (1997).

[10] Schraube, H., Mares, V., Roesler, S., Heinrich, W.: Experimental verification and calculation of aviation route doses. Radiat. Prot. Dosim. **86** (3), 309-315 (1999).

[11] Schraube, H., Heinrich, W., Leuthold,G., Mares,V., Roesler, S. *Aviation route dose calculation and its numerical basis.* In: Proc. 10th International Congress of the International Radiation Protection Association, Hiroshima, Japan. T-4-4, P-1a-45 (2000) 1-9. (http://www.oita-nhs.ac.jp/%7Eirpa10/CD-ROM/Full/topical.html)

[12] Roesler, S., Heinrich, W., Schraube, H. *Monte Carlo calculation of the radiation field at aircraft altitudes.* Radiat. Prot. Dosim. **98** (4), 367-388 (2002).

[13] Mitaroff, A., Silari, M. *The CERN-EU High-energy Reference Field (CERF) Facility for Dosimetry at Commercial Flight Altitudes and in Space.* Radiat. Prot. Dosim. **102** (1) 7-22 (2002).

A14 NPL/MSSL/VAA/CAA (PPARC) and ANZ Collaborative Project

G C Taylor[1], R H Iles[2], R D Bentley[2], J B L Jones[2,3], R Hunter[4], D Powell[5], D J Thomas[1]
1 National Physical Laboratory, Teddington, Middlesex TW11 0LW, UK
2 Mullard Space Science Laboratory, Holmbury St Mary, Dorking, Surrey, RH5 6NT, UK
3 Virgin Atlantic Airways Ltd, Manor Royal, Crawley, West Sussex, RH10 2NU, UK
4 Civil Aviation Authority, Aviation House, Gatwick Airport South, Gatwick, West Sussex, RH6 0YR, UK
5 Air New Zealand Ltd, Private Bag 92007, Auckland 1010, New Zealand

The MSSL/VAA/NPL/CAA collaboration has been collecting in-flight measurements of cosmic radiation doses with TEPCs since January 2000. By Summer 2003, data has been collected from over 700 flights, including well over 100 from Air New Zealand (ANZ). Unfortunately the analysis, particularly of the flight profile information, is lagging behind.

The instruments used in this study are commercial Hawk TEPCs (funded by a PIPSS Grant from PPARC, the UK Particle Physics and Astronomy Research Council), together with a prototype Hawk TEPC, obtained from Far West Technology, Goleta, California, USA.

The data offered for inclusion in this study were measured using the prototype TEPC (VAA flights) and commercial Hawk #006 (ANZ flights). The calibration of the prototype Hawk instrument is discussed elsewhere[1]. But to summarise, the prototype has been calibrated in NPL neutron and photon fields, and at the CERF high energy reference field facility. The calibration factor assumed for this instrument was 0.77, i.e. that it over-read by a factor of 1.3, and represents the calibration factor determined in the CERF field, having corrected for the muon background. It must be borne in mind, however, that there is an uncertainty associated with the CERF high energy field of approximately ±10%. The commercial Hawk has, thus far, not had a successful measurement run at CERF, despite several attempts. This is due to failings in both the available beam and the instrument itself. Consequently, the measurements are reliant on four cross calibration flights, performed in September 2001: one return flight from London to San Francisco and one return flight from London to Toronto. From this data the calibration factor for the commercial Hawk (relative to the prototype Hawk) was found to be 1.00 ± 0.02. This is discussed in detail elsewhere[2].

The prototype instrument's over-read of 30% is broadly in agreement with low energy neutron studies performed at NPL. Calculations have shown that a 'typical' TEPC over-reads by as much as 30% for a neutron energy of 2.5 MeV: this compares to 1.62 measured with the prototype TEPC (1.24 times the value for a 'typical' TEPC). Similar values have been obtained for 1.2 MeV (1.32 times the 'typical' value) and for 565 keV (1.28 times the 'typical' value).

This is further backed up by scaling the calculations of Alexeev et al.[3] to fit the response of the prototype in the MeV region, folding this with the neutron spectrum for the CERF field and comparing that to the H*(10) response (extrapolated from ICRP 74 using the (scaled) data of Sannikov reported in reference [2]) also folded with the same spectrum. This gave a theoretical over-read of x1.25. Given the approximations involved, this was only taken as being indicative of the TEPC's response. More significantly, the same process was repeated using the calculated neutron spectrum for an altitude of 35,000 feet rather than that of the CERF field, and yielded an over-read of x1.25.

Although the Hawk instrument uses a 5-inch TEPC, there is still a significant statistical uncertainty on the dose equivalent data collected. This is typically ±2% for complete long haul flights and ±4% for complete short haul flights.

All uncertainties stated above are quoted at the 68% confidence level.

The data provided for this report was taken from just 8 of the 700 flights performed by this collaboration, which is due to finish in November 2004. A comprehensive report will follow shortly thereafter.

ACKNOWLEDGEMENTS
We would like to thank Tom Conroy at Far West Technology, Nicky Horwood at the National Physical Laboratory and Rowena Dobson at Air New Zealand for their input to the project, and also Marco Silari and his team at the CERF Facility. Furthermore, the authors would like to thank the UK Particle Physics and Astronomy Research Council (PPARC) for funding the continuation of this measurement programme. The contribution provided by the UK DTI National Measurements Programme in Ionising Radiation in funding the staff at the National Physical Laboratory is also acknowledged.

[1] G.C. Taylor, R.D. Bentley, T.J. Conroy, R. Hunter, J.B.L. Jones, A. Pond and D.J. Thomas, *The evaluation and use of a portable TEPC system for measuring in-flight exposure to cosmic radiation*, Radiat. Prot. Dosim. 99(1-4), 435-438 (2002).

[2] G.C. Taylor, R.D. Bentley, N.A. Horwood, R. Hunter, R.H. Iles, J.B.L. Jones, D. Powell and D.J. Thomas, *TEPC Measurements in Commercial Aircraft,* Proceedings of the 9th Symposium on Neutron Dosimetry, Delft, The Netherlands, 28th September – 3rd October, 2003 (in press)

[3] A.G. Alexeev, T. Kosako and S.A. Kharlampiev, *Energy response of tissue equivalent proportional counter for neutrons above 20 MeV*, Radiat. Prot. Dosim. 78(2), 113-120 (1998).

A 15 Universität des Saarlandes Medizinische Fakultät : Microdosimetric Measurements of Dose Rates onboard Civil Aircraft

Rudolf E. Grillmaier and Stephan Gerdung
Fachrichtung Biophysik
Universität des Saarlandes
Medizinische Fakultät
66424 Homburg/Saar, Germany

A .15.I. Background

The investigations have been performed within the project "Study of Radiation Fields and Dosimetry at Aviation Altitudes" initiated and supported by the Commission of the European Community and attended scientifically by H.-G. Menzel. In this project participated Irish, Italian, German, Swedish and English teams and a team of CERN in Geneva. The project was coordinated by D. O`Sullivan from the Dublin Institute for Advanced Studies.[1] Included in this project was the Italian National Survey of Aircrew Exposure[2] performed under the responsibility of L. Tomassino from the Italian National Agency for Environmental Protection. For this survey the ALITALIA airline provided numerous free flights on the routes Milan-Los Angeles, Rome-Rio de Janeiro and Milan-Tokyo. (Table 1) The measurements reported here have been carried out within the frame of the Italian National Survey in close collaboration with teams of Italian scientists using different types of active and passive dose meters as well as particle detectors.

Table 1. Flight Routes and Number of Return- Flights

Flight-Route	No.of Flights	No.of Measm.
Milan – L A	10	ca. 650
Rome – Rio	18	ca. 300
Milan – Tokyo	8	ca. 550

A.15.2 Measuring device and principles

The measurements of dose and dose equivalent reported here have been performed using two hand held dosemeters (called HANDI), conceived and constructed by H.-G. Menzel et al.[3;4]. The systems are based on microdosimetric principles, equipped with low pressure tissue equivalent proportional counters[5]. Applying these principles the contribution of any single radiation event to absorbed dose is measured in a small volume of tissue equivalent material (simulating a diameter of about 1 m). Simultaneously the lineal energy of the traversing secondary particle is also determined as a measure of LET, so that the contribution of this event to dose equivalent can be calculated. Absorbed dose, dose equivalent, dose rates and measuring time can be read on a built-in display and can be transmitted to a PC. The microprocessor supported electronic system of the measuring device is able to record and to indicate the dose distribution (probability density of dose d(y)) produced by the radiation field, on dependence of the lineal energy (y), the so called lineal energy spectrum (Figure 2).

A.15.3 Measuring procedure

In order to get dose profiles of satisfying re-solution for the local positions of the aircraft and dose rates of sufficient accuracy (which is limited by the sensitivity of the detector) a compromise had to be found concerning the measuring time for a single measurement. Considering the expected dose rates and the sensitivity of the detectors it was decided, to set it to 30 minutes on the north atlantic route and on the route from Milan to Tokyo. On the route from Rome to Rio across the equator, where a smaller dose rate was expected, the measuring time was increased to 60 minutes. The total number of measurements during

a flight was determined by the measuring time and the duration of the flight. All instruments used by the Italian National Survey had been fixed on a board which was brought into the aircraft and fastened on the bottom of the passenger cabin in the aircraft.

A.15.4 Results

An Example of a dose profile (depending on the geomagnetic location and the flight altitude of the aircraft) measured on a flight from Milan to LA is given in Figure 1 indicating dose equivalent rates between 4 and about 8 µSv/h**.**

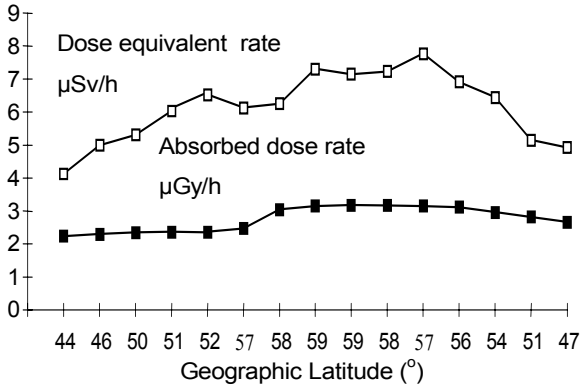

Figure 1. Dose profile on a flight from Milan to Los Angeles.

An excerpt of all 1500 pairs of absorbed dose and dose equivalent values is given in Table 2. As has been expected, the mean dose rates of the two flight routes across the northern hemisphere (geomagnetic latitude of at least 45°) are about the same whereas the dose rates on the route across the equator (where the magnetic shielding against cosmic rays is stronger) is significantly lower by a factor of about 1/2 . The mean radiation quality factor, indicating the contribution of high densely ionizing radiation to dose is also lower by a factor of 2/3 at the southern route. (The experimental standard deviation, s, of the dose rates is about 10% of the mean values.)

Table 2. Mean Values of Dose Rates and of Radiation Quality Factors

Flight Route	Mean Dose Rate (µGy/h)	Mean Dose Equivalent Rate (µSv/h)	Mean Quality Factor
Milan↔LA	2.15	4.82	2.24
Milan ↔Tokyo	2.10	4.70	2.23
Rom↔Rio	1.28	2.39	1.86

In figure 2 three microdosimetric spectra are shown. Two of them are measured at the same range of geomagnetic latitude above 60° north but at different altitudes (green: 8840 m, black: 11280 m). No real differences are to observe. The third one has been obtained at a flight across the equator(red:10670 m). A significant difference due to a lower contribution to dose at high LET values (leading to an increase of dose equivalent) is evident.

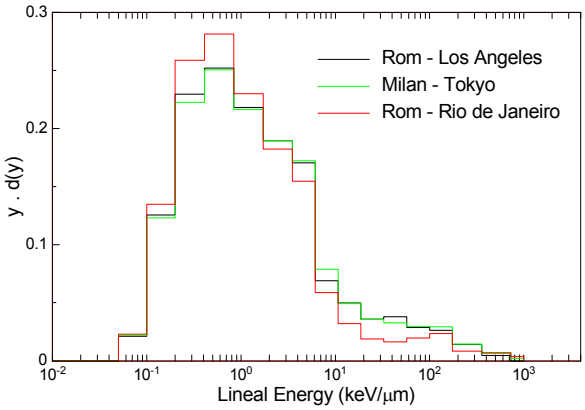

Figure 2. Lineal energy spectra of absorbed dose measured at different routes.

As already mentioned, not for all 1500 dose measurements (Table 1) the corresponding flight data are available. Results with varying cruising altitude during measurement have not been included in the evaluation. In total 956 single measurements could be related to cruising altitude and to geomagnetic position. These data are used to construct the dose rate dependence on altitude at a given small range of geomagnetic altitude and vice versa the dose rate dependence on geomagnetic latitude at a given altitude. Using the data the following regressions were found for a range of validity of 8.5 -11.6 km altitude and 12- 70^0 geomagnetic latitude (95% confidence intervals for parameters shown in parentheses):

(i) Dose rate (μGy/h) = a + b · Altitude (km) + c · (Geomagnetic Latitude (^{0}))^2,
a = -2.9 [-3.1; -2.7]; b = 0.41 [0.39; 0.43]; c = $2.64 \cdot 10^{-4}$ [$2.5 \cdot 10^{-4}$; $2.7 \cdot 10^{-4}$]

(ii) Dose equivalent rate (μSv/h) = a′ + b′ · Altitude (km) + c′ · (Geomagnetic Latitude (^{0}))^2,
a′ = -6.4 [-7.0; -5.8]; b′ = 0.86 [0.81; 0.92]; c′ = $7.2 \cdot 10^{-4}$ [$7.0 \cdot 10^{-4}$; $7.5 \cdot 10^{-4}$]

A .15.5 Acknowledgments

We wish to thank the Commission of European Communities, Directorate General XII for Sponsoring the project and Dr. H.-G Menzel for his continuing encouragement. We would also like to express our gratitude to the Italian National Agency for Environmental Protection ANPA and ALITALIA for their generous assistance. Last but not least we wish to thank Dr. Luigi Tommasino for initiating and managing the survey.

A .15.6 References

1. D. O`Sullivan, Study of Radiation Fields and Dosimetry at Aviation Altitudes, p. 83, Final Report of EC Contract Number: F14P-CT950011, Report 99-0-1, 1996-1999

2. G. Curzio, R.E. Grillmaier, D. O`Sullivan, M. Pelliccioni, S. Piermattei and L. Tommasino. Italian National Survey of Aircrew Exposure. p.39, Agenzia Nationale per la Protezione dell` Ambiente, Rome, 2000

3. A. Kunz, P. Pihet, E. Arend, H.G. Menzel: An easy-to-operate portable pules-height analysis system for area monitoring with TEPC in radiation protection. Nuclear Instruments and Methods in Physics Research A299 (1990) 696-701

4. Kunz, A., Arend, E., Dietz, E.,. Gerdung, S., Grillmaier, R.E., Lim, T. and Pihet, P. The Homburg Area Monitor HANDI: Characteristics and Optimisation of the Operational Instrument. Radiat. Prot. Dosim., 44(1-4), 213-218 (1992).

5. Gerdung, S., Pihet, P., Grindborg, J.E., Roos, H., Schrewe, U.J. and Schuhmacher, H. Operation and Application of Tissue Equivalent Proportional Counters in Design, Construction and Use of Tissue Equivalent Proportional Counters. Editors: Kliauga, P., Schmitz, T., Waker, A. and Zoetelief, H., Radiat. Prot. Dosim. 61(4) (1995).

A 16 Physikalisch-Technische Bundesanstalt (PTB) II

B. Wiegel[1], J. Wittstock[1], A.V. Alevra [2], M. Matzke [3]
[1] Physikalisch-Technische Bundesanstalt, Department "Neutron Radiation", Bundesallee 100, D-38116 Braunschweig, Germany.
[2] Development and Consulting, Krähenfeld 10A, D-38110 Braunschweig, Germany, retired from PTB.
[3] Haberweg 5, D-38116 Braunschweig, Germany, retired from PTB.

A 16.1 Introduction

During the EC project ACREM (Air Crew Radiation Exposure Monitoring) the PTB neutron dosimetry group measured for one specific flight route (Frankfurt – Fairbanks – Seoul / Seoul – Fairbanks – Frankfurt on June 14 to 19, 1998) neutron fluence rate spectra, averaged typically over 30 to 60 minutes. The ambient dose equivalent rates $dH^*(10)/dt$ were derived from the fluence spectra by applying the fluence-to-ambient dose equivalent conversion coefficients according to ICRP74. The non-neutron component was determined with an ionization chamber as described in Appendix A 9.

The neutron measurements were performed with a subset of the PTB Bonner sphere spectrometer (BSS) plus a spherical lead-modified survey meter LINUS. This spectrometer was not meant to be used as routine instrument but to demonstrate the capability of the BSS to determine spectrometric information as a basis of the dosimetric quantities even in such difficult environments.

A 16.2 Instrumentation and response functions

The PTB Bonner sphere spectrometer (BSS) consists of 12 polyethylene spheres with diameters from 7.62 cm (3") to 45.72 cm (18") and a ^{3}He-filled spherical proportional counter (type SP9, Centronic Ltd, UK) used as central thermal-neutron-sensitive detector, but also as bare or cadmium-shielded detector. The fluence response matrix of this BSS is mainly based on experimental calibration data obtained with thermal neutrons, with monoenergetic neutrons at 12 energies between 1.17 keV and 14.8 MeV, and with 55 MeV *quasi-monoenergetic* neutrons, Ref. [1] and references therein. The complete response matrix, covering the neutron energy range from 10^{-3} eV to 10^{10} eV, was obtained using calculated response functions for inter- and extrapolations [1].

Essential for the series of measurements presented here was the necessity to measure with all spheres used simultaneously. This implied the necessity to dispose of a large number of relatively calibrated SP9 counters and, for each of them, adequate electronics.

In order to establish a reduced but consistent set of Bonner spheres, optimised for the experiment in view, computational simulations of the measurements in aircraft were performed considering the neutron fields at flight altitudes to be similar to some other fields investigated by us, namely the cosmic-ray induced neutron natural background measured on the PTB site in Braunschweig [2] or high-energy calibration fields produced at CERN [3]. This resulted in the decision to use seven members of the PTB “C” BSS, namely the bare counter, 3", 4", 5", 6", 8" and 12", although the simulations have shown that the information brought by the 4" sphere is redundant. In spite of this redundancy the seven spheres chosen

are not able to obtain reliable spectral information above about 10 MeV, and for this reason the system was completed with a spherical, lead-modified neutron survey meter LINUS [4] routinely used at CERN. The fluence responses of the selected eight spheres are shown in Figure A 16.1. For better comparison of the response shapes in the high-energy part, the response of the spherical LINUS was magnified by a factor of four. The response function of the LINUS was calculated for a PTB SP9 counter as central detector on relative basis only. The absolute values being determined through supplementary calibrations. The calibrations were performed in the PTB bunker [5] with a bare ^{252}Cf source and a ^{241}AmBe source.

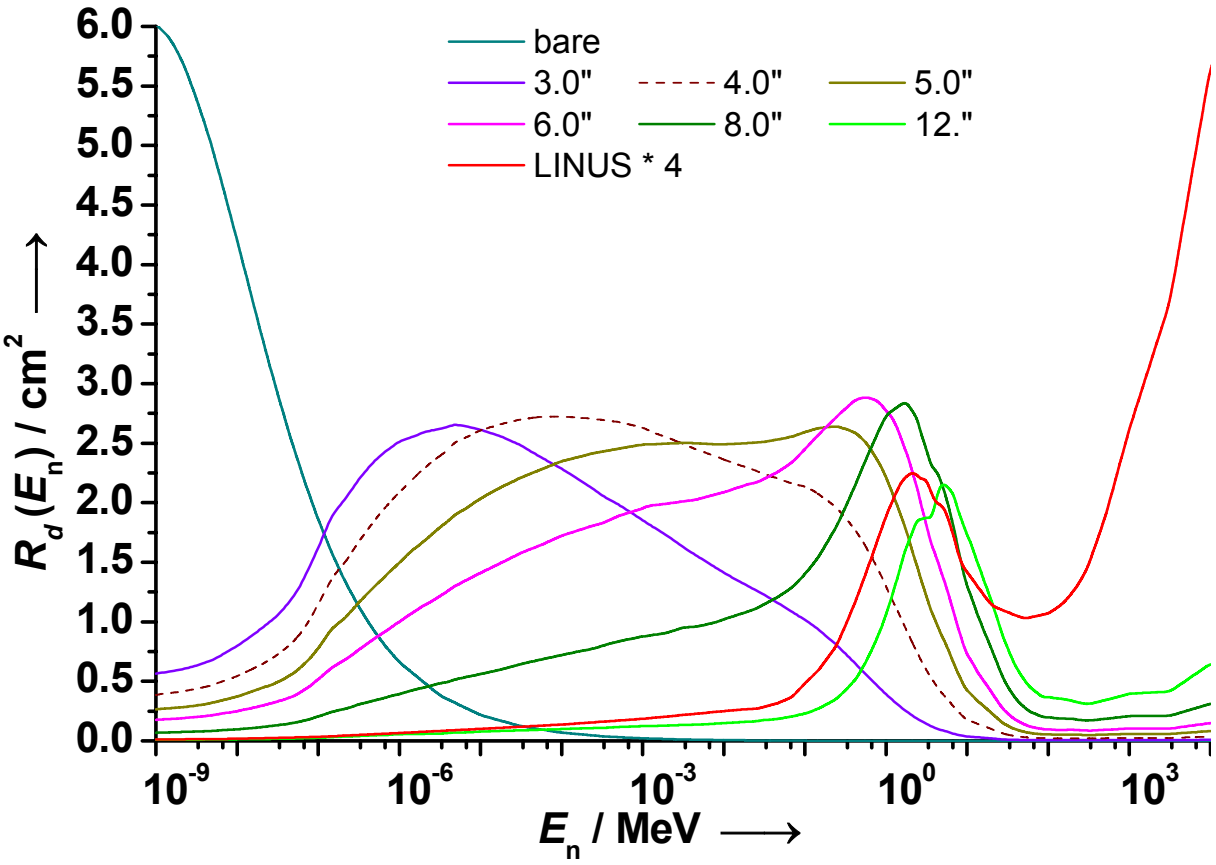

Figure A 16.1*: The fluence responses of the eight detectors used aboard the Lufthansa Cargo flight. For better comparison of the responses, the response of the spherical LINUS was magnified by a factor of four.*

A 16.3 Electronics

The electronics used for measurements in aircraft must fulfil some special requirements. First of all, this electronics must avoid any electromagnetic interference with the board instrumentation of the air plane. Also it is very convenient for the experiment to have at least the most sensitive parts of the analogue electronics used independent from the power supplied by the air plane. The use of compact and light instrumentation brings also important advantages.

As it was necessary in the present experiment to store simultaneously eight pulse height spectra, using eight analogue-to-digital converters (ADC) and eight multi-channel analysers, we used also eight analogue processors [6], small-sized, with low power consumption and specially built for such kind of experiments. Each of this analogue processors (AP) contains

the high-voltage supply for the detector, a charge-sensitive preamplifier, an internal pulse generator, a shaping amplifier with buffer and two discriminators. Four "A"-sized batteries placed inside the AP case ensure an autonomous operation of at least 120 hours. The multi-channel analysis was ensured by two 7074-Quad ADCs coupled each to a MCD4LAP-Multichannel-Analyser PC card (all produced by FAST ComTec, Germany).

A 16.4 Experimental arrangement

It was a new experience to simultaneously measure with eight detectors which had to be placed rather close together (close enough in order to occupy very similar positions with respect to the neutron field investigated, but far enough in order to avoid reciprocal perturbations like in-scattering or shadowing). In our compromise arrangement the eight detectors were installed in four aluminium cases, 100*50*50 cm^3, two in each case, together with the corresponding analogue processors. Each detector was placed at the centre of its "half-case" with the help of light materials. The smallest detectors (up to 6") were "suspended" in air by means of small aluminium rings and thin steel wires. The four aluminium cases were organised as follows: **A**) bare counter & 3" sphere, **B**) 5" & 6" spheres, **C**) 8" sphere & LINUS, **D**) 4" & 12" spheres, see Figure A.16.2.

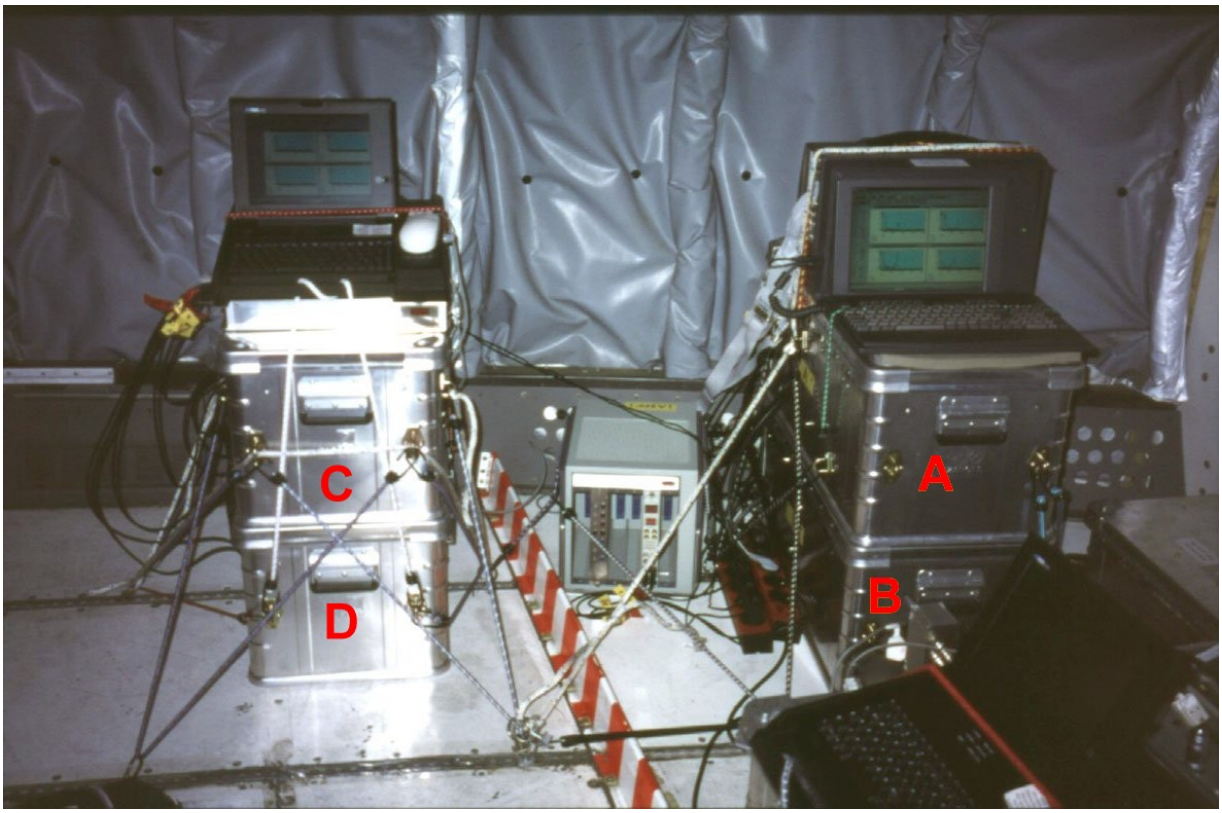

***Figure A 16.2**: The set up of the four aluminium cases aboard the Lufthansa Cargo flight, each containing two detectors.*

As concerns the arrangement in the case "**D**", it is quite sure that the 4" sphere (500g of polyethylene) has no influence on the reading of the 12" sphere. On the contrary, if there is an important reciprocal influence between various detectors, then the influence of the largest sphere used in the experiment, 12" (14 kg polyethylene), on the reading of the 4" sphere

should be the largest. Taking into account that the information brought by the 4" sphere is redundant, this influence can be quantified in a proper way.

The pulse height spectra from all eight detectors used were stored with integration periods of 30 to 60 minutes. This time interval was long enough to ensure a good statistical significance of the results, and short enough to let us consider that the flight parameters (altitude, geomagnetic latitude) did not change considerably during the measurement. In cases in which the air plane changed flight levels (FL), a new measurement was started before the altitude change and again after the new FL was reached.

With the Bonner sphere spectrometer we did not measure the non-neutron component. The dosimetric results of this component was taken from the measurements with an ionization chamber operated by our PTB colleague Ulrich Schrewe. For details of this instrument and the data analysis please see Appendix A 9.

A 16.5 Spectrometric and dosimetric results

There were all together 43 sets of measurements obtained during four flight legs. There were 15 sets of measurements obtained during a flight from Frankfurt to Fairbanks (denoted and numbered from FrFa01 to FrFa15), 13 sets from Fairbanks to Seoul (FaSe02 to FaSe14), eight sets from Seoul to Fairbanks (SeFa02 to SeFa09) and seven sets from Fairbanks to Frankfurt (FaFr02 to FaFr08).

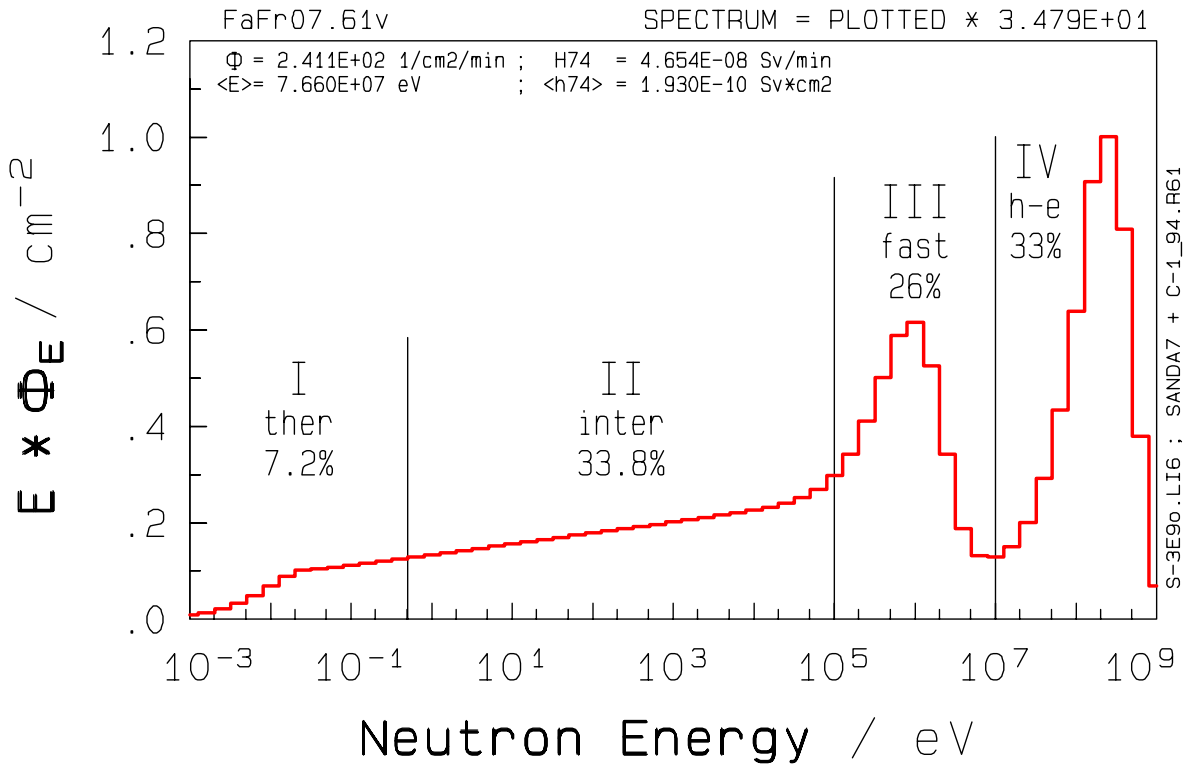

Figure A 16.3: *The spectral distribution of the neutron fluence, in lethargy representation, obtained from the FaFr07 data set, and typical for all spectral shapes obtained in this work.*

The analysis of the pulse-height spectra allowed us to extract the events due to neutrons and to establish the count rates for each detector. The unfolding of the data obtained in various

sets of measurements produced very similar results as concerns the shape of the resulting spectral distribution of the neutron fluence (a possible influence of the charged hadrons from the cosmic radiation was not considered).

As an example, Figure A 16.3 presents, in lethargy representation (areas below histogram proportional to neutron fluence), the neutron spectrum obtained from the FaFr07 data (measurement No. 7 during the flight from Fairbanks to Frankfurt at 10 km altitude, 80°N geomagnetic latitude). Some important integral quantities resulting from the spectrum, integral fluence rate, ambient dose equivalent rates and mean conversions factors (in terms of $H^*(10)$ according to ICRP74 [7]) are given numerically.

The result shows an important contribution of high-energy neutrons (energy region **IV**, above 10 MeV, named **h-e**) followed with decreasing energy by an "evaporation" distribution (region **III**, between 100 keV and 10 MeV, named **fast**), then slowed-down neutrons (region **II**, between 0.5 eV and 100 keV, named **inter**mediate), and finally a small contribution below 0.5 eV (region **I**, named **ther**mal) due to thermal and slowed-down neutrons.

A check of the solution spectrum for compatibility with the measurements is mandatory. Such a check, for the spectrum FaFr07, is given in Figure A 16.4. When the solution spectrum is folded with the fluence response matrix, the *calculated readings*, $\mathbf{C_d}$, are obtained, and in addition, the ratios $\mathbf{r_d = M_d / C_d}$, where $\mathbf{M_d}$ are the experimental readings. The deviations of the $\mathbf{r_d}$ values from unity should be comparable with their uncertainties, resulting in a *reduced chi-squared* value near unity.

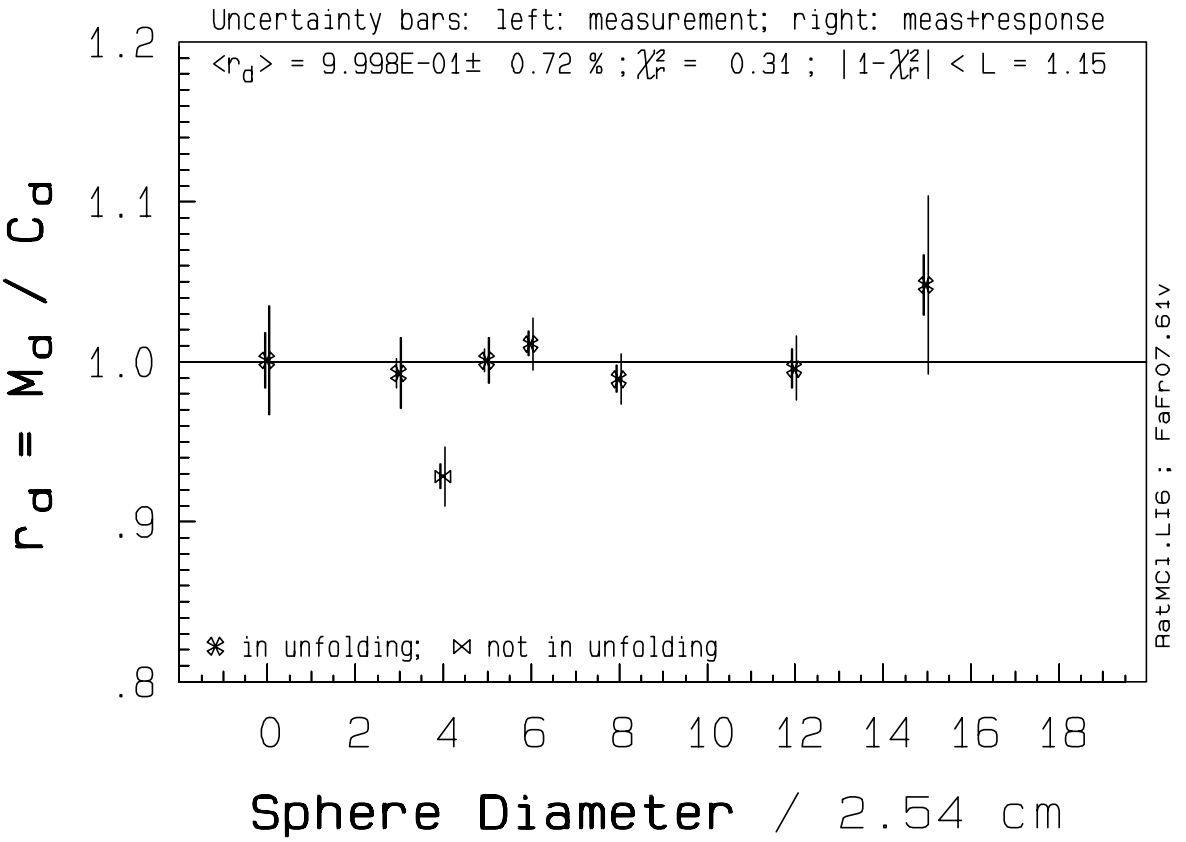

Figure A 16.4: *The ratios ($\mathbf{r_d}$) of measured ($\mathbf{M_d}$) to calculated ($\mathbf{C_d}$) readings of the detectors used to measure the spectrum shown in Figure A 16.3. The point with the abscissa 15" is due in fact to the spherical LINUS.*

The uncertainty bars associated to the points in Figure A 16.4 represent the statistical uncertainties (left bars) and the *total* uncertainties (right bars) which include those of the fluence responses used in folding and unfolding. The point with the abscissa 15" is due in fact to the spherical LINUS and indicates the highest uncertainties from all detectors used, the statistical due to low counting rates (similar to the bare counter) and the total due to higher uncertainties estimated for the fluence response available.

Figure A 16.4 shows good agreement between the solution spectrum from Figure A 16.3 and the measured readings of all detectors, except for the reading of the 4" sphere. This reading, which was not used to produce the result from Figure A 16.3, is by about 7% lower than a value consistent with the spectrum established in agreement with all other detectors. The situation shown in Figure A 16.4 is representative for all results obtained from the 43 sets of measurements which indicate a systematic influence of the vicinity of the 12" sphere on the readings of the 4" sphere.

The neutron spectrum from Figure A 16.3 is shown once more in Figure A 16.5, which uses a logarithmic scaling of the ordinate, under the name of FAI-FRA. For comparison, Figure A 16.5 shows also a spectrum named SEL-FAI which resulted from the SeFa04 set of measurements also performed at 10 km altitude, 3 flight hours north of Seoul, at a geomagnetic latitude of 36°N. The two aircraft neutron spectra differ in absolute fluence by about a factor of two, but their shapes are very similar. This statement is valid for all neutron spectra resulted from this series of measurements.

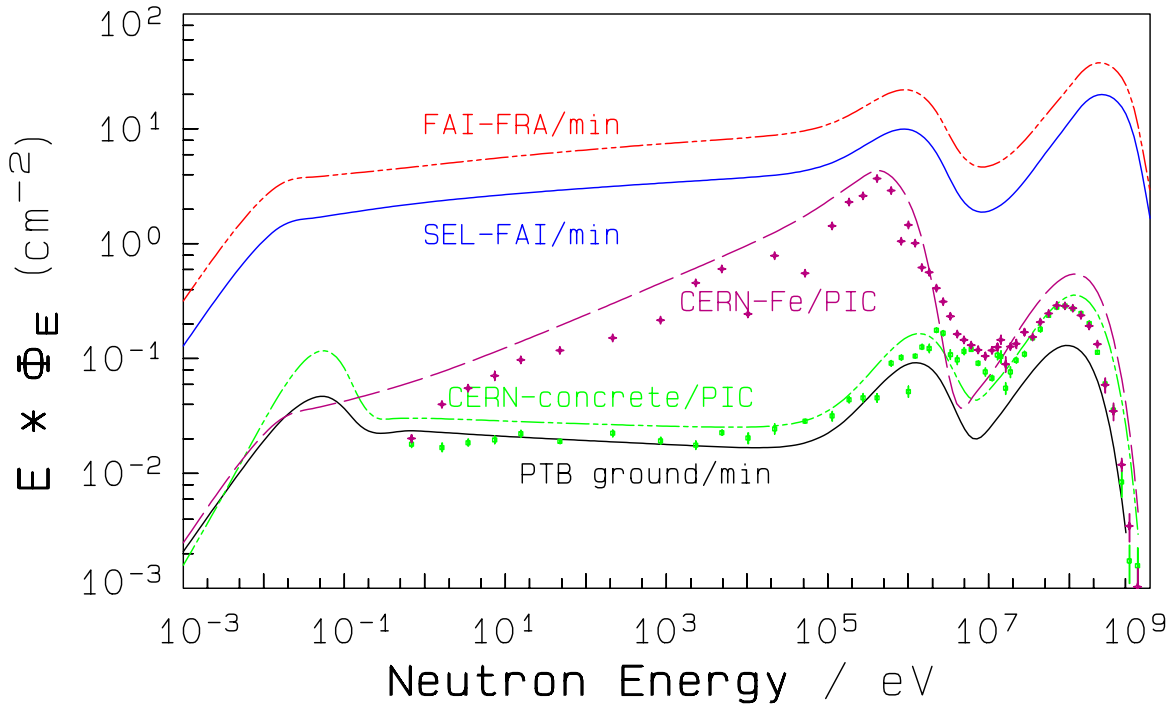

Figure A 16.5: *High-energy neutron spectra measured with the PTB "C" BSS. For the natural background [2] and aircraft spectra (FAI-FRA and SEL-FAI) the fluence rates are given per minute, for the two CERN spectra [3] the fluence rates are given per monitor (PIC) pulse. FLUKA calculations of the CERN spectra [8] are indicated by symbols.*

For further comparison, a few other high-energy neutron spectra measured with the PTB "C" BSS are given in Figure A 16.5. The cosmic-ray induced natural background measured on the PTB area [2] and, two neutron spectra measured in high-energy calibration fields produced at CERN [3], one behind concrete shielding, the other behind iron shielding. The CERN spectra are also compared with FLUKA calculations [8], indicating "reasonable" agreement especially for the concrete shielding. For the natural background and aircraft spectra the fluence rates are given per minute, for the two CERN spectra the fluence rates are given per monitor (Precision Ionisation Chamber, PIC) pulse.

From a comparison of the shapes of the spectra in Figure A 16.5 it may be concluded that the CERN concrete field is adequate for the calibration of dosimetric instrumentation used for monitoring the exposure to cosmic-ray-induced neutrons.

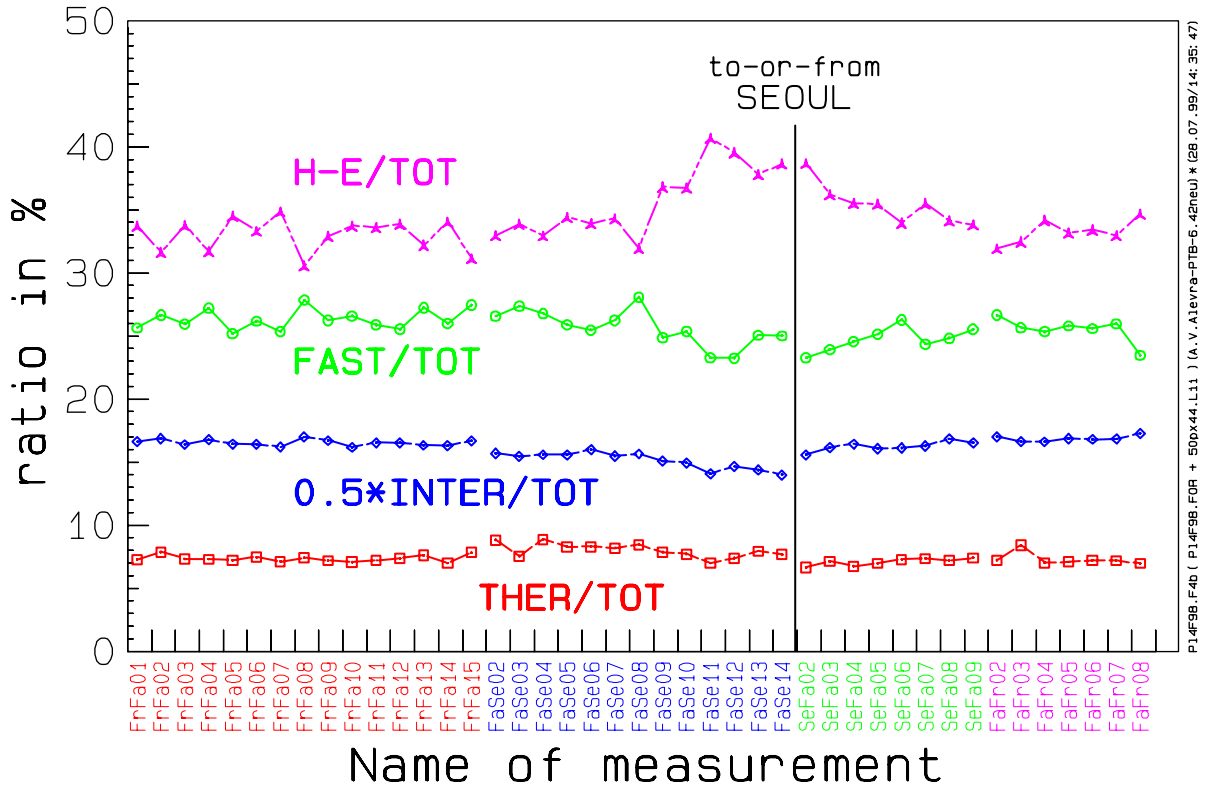

Figure A 16.6: *The ratios of the group fluences to total fluences for all four energy groups indicated in Figure A 16.3 and for all 43 measured spectra.*

Although the shapes of all neutron spectra obtained in this work are very similar, we have proceeded to a more detailed analysis of them. This analysis is shown in Figure A 16.6 were the ratios of the group fluences to total fluences are given, for all four energy groups indicated in Figure A 16.3 and for all 43 measured spectra. In order to obtain distinguishable plots, the ratios **inter**mediate/**tot**al were reduced by a factor two. While the ratios implying the **ther**mal and **inter**mediate regions show rather small fluctuations and variations, the ratios implying the **fast** and **h**igh-**e**nergy regions present not only some higher fluctuation, but also a trend of being systematically lower (**fast/tot**) or systematically higher (**h-e/tot**) in the spectra measured in the vicinity of Seoul (lowest values of the geomagnetic latitude encountered in this work).

The tendency seen in Figure A 16.6 is even more visible in Figure A 16.7 where the group-fluence ratios **h-e/fast** are plotted, together with the mean conversion factors, <h74>, calculated for the spectral distributions obtained. While the typical value of the **h-e/fast** ratio is about 120%-125%, in the vicinity of Seoul the ratio "jumps" to values of about 150%. Also the values of the mean conversion factor, <h74>, show a light increase in the vicinity of Seoul.

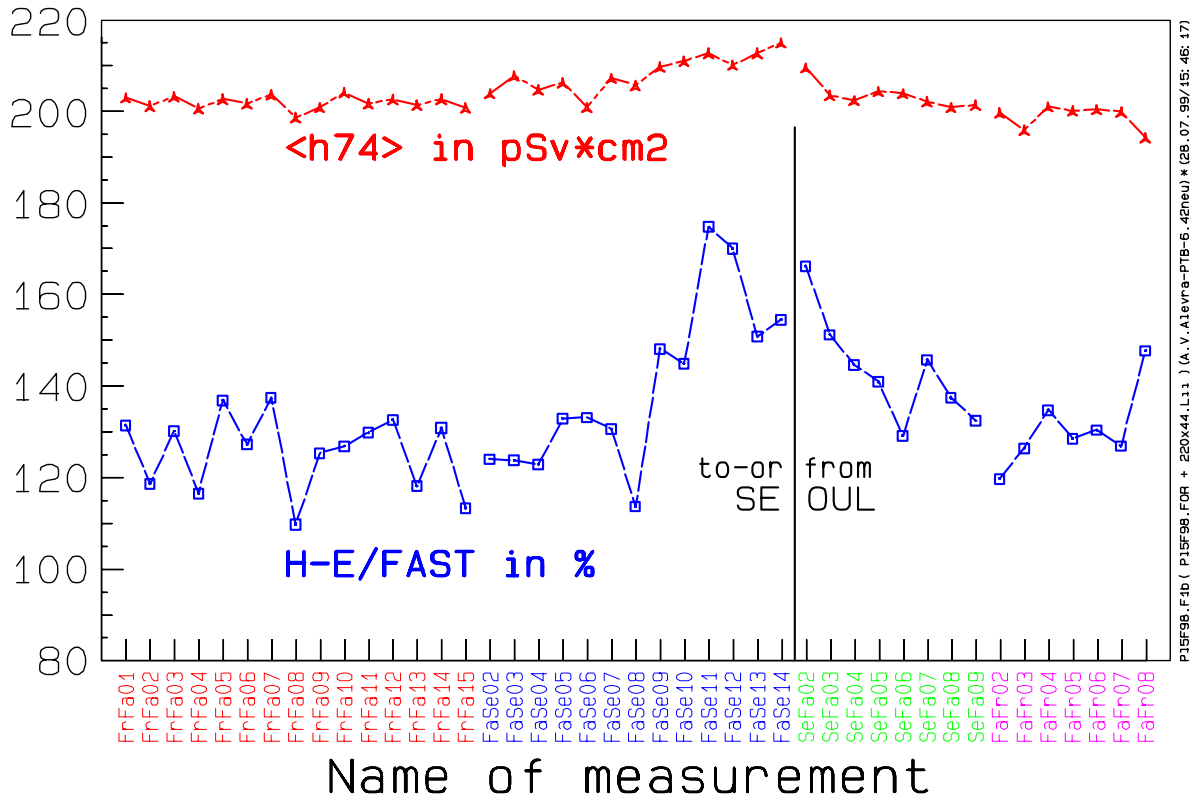

Figure A 16.7*. The group-fluence ratios* ***h-e/fast,*** *given in percent, and the mean conversion factors, <h74>, in pSv·cm^2, calculated for the spectral distributions obtained.*

The values we obtain for the **h-e/fast** ratio, give answer to a very controversial question, namely which of the components **h-e** or **fast** is larger. Even if we assume uncertainties up to ±20% for the fluence response of the LINUS in the high-energy range, our data clearly indicate the **h-e** component to be the **larger** one. As concerns the further increase of the **h-e** contribution in the vicinity of the equator, this relative effect is evident independently of the accuracy of the fluence response of the LINUS.

Figure A 16.8 shows the integral fluence rates, in cm^{-2}/minute and the integral ambient dose equivalent rates (according to ICRP74), in units of 10^{-8} Sv/hour, as resulted from the 43 neutron spectra. As practically all measurements took place at 10 km altitude, or slightly higher, the large decrease in magnitude of neutron fluence rate and dose equivalent rate are due to low geomagnetic latitude values in the vicinity of Seoul. The only exceptions are the results of two measurements made after the take-off from Fairbanks, FaFr02 and FaFr03, before the flight altitude of 10 km was attained.

Most data given in this appendix were already published in Ref. [9].

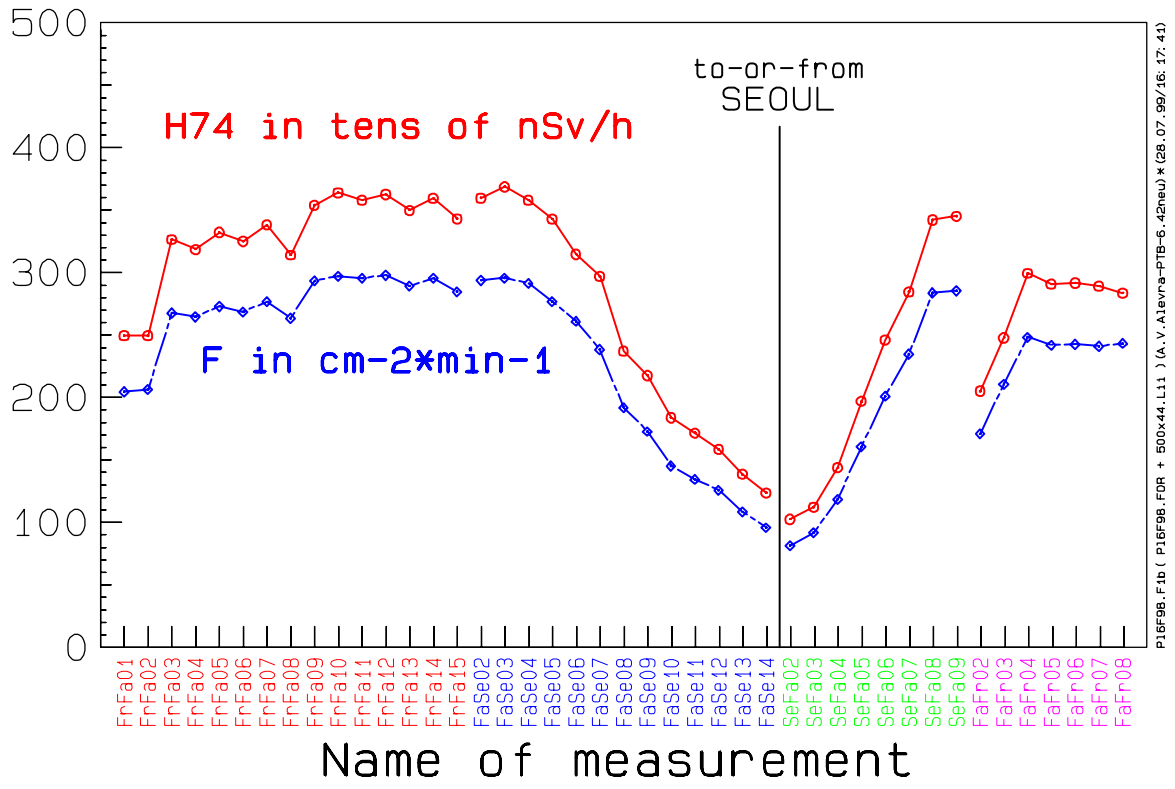

Figure A 16.8: *The integral fluence rates, in cm^{-2}/minute and the integral ambient dose equivalent rates (according to ICRP74), in units of 10^{-8}Sv/hour, as resulted from the 43 neutron spectra*

A 16.6 Comparison with dosimetric measurements

Two „classical“ survey meter, SNOOPY (produced by TRACELAB, USA) and LB6411 (produced by EG&G-Berthold, Germany), a cylindrical LINUS (cyLINUS) (Münchener Apparatebau, Germany) survey meter (a modified Anderson&Braun by adding an internal led shell to enhance the response at high energies) and its spherical version, a spherical LINUS (sphLINUS) were used simultaneously with the BSS to perform dosimetric measurements in terms of ambient dose equivalent rate according to ICRP74 (meaning also calibrations with ^{241}AmBe source).

The comparison of the survey meter readings with the BSS results is shown in Figure A 16.9 which displays the ratios survey meter reading to BSS result, in percent, for all four survey meters mentioned, and for all sets of measurement where they were used.

The agreement between the two variants of LINUS, i.e. the two instruments with enhanced responses to high-energy neutrons, and the BSS, is realised practically within ±10%. The “classical” survey meters, which give good results in neutron fields with energies below 10 MeV, show in this series of measurements under-estimations by roughly a factor of two. This result is perfectly understandable, taking into account that these instruments are practically not sensitive at all to the high-energy component which is very significant in the neutron fields investigated in the present work.

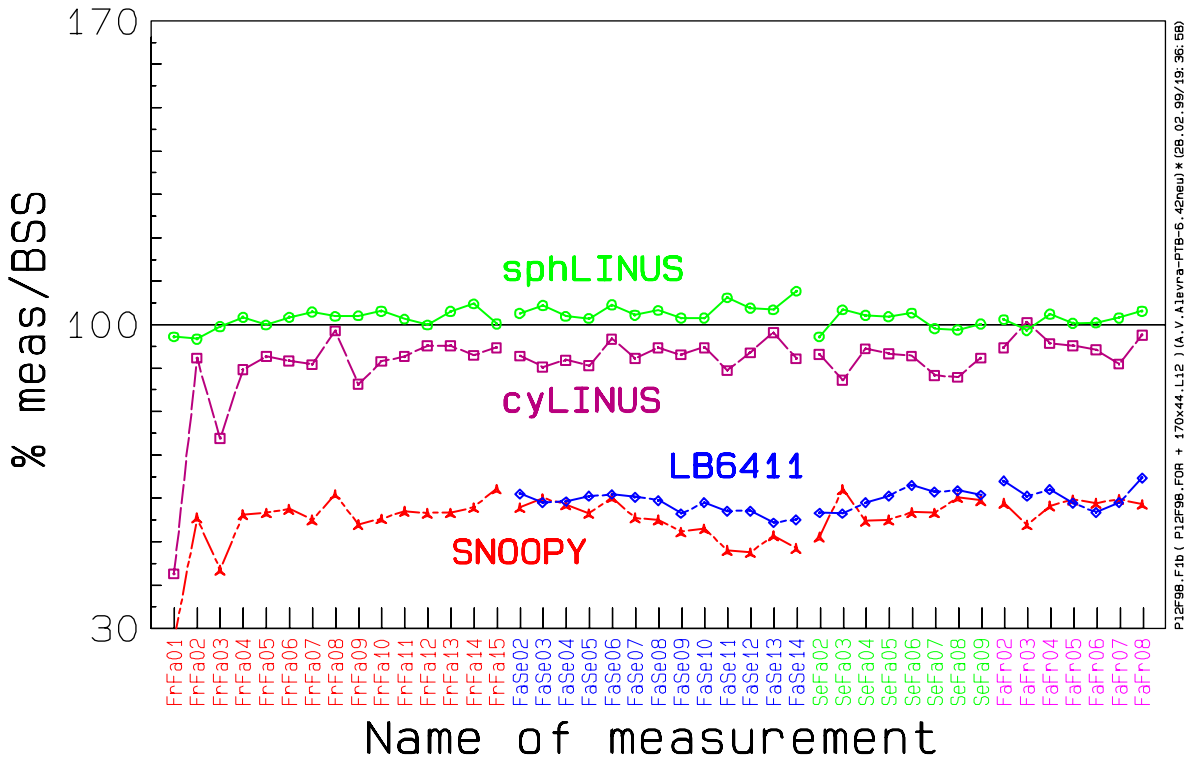

Figure A 16.9: *The ratios survey meter reading to ambient dose equivalent (BSS result), in percent, for all four survey meters used during this flight.*

A 16.7 Conclusion

During the EC project ACREM the PTB neutron dosimetry group used a Bonner sphere spectrometer (BSS) plus a spherical lead-modified survey meter LINUS to measure neutron fluence rate spectra for one specific flight route (Frankfurt – Fairbanks – Seoul / Seoul – Fairbanks – Frankfurt on June 14 to 19, 1998). With this flight path an altitude range from 9.5 km to 12 km and a range in geomagnetic latitudes between 26°N and 86°N were covered. For a total of 43 individual measurements, with measuring times between 30 and 60 minutes, the neutron fluence rate distributions were obtained from unfolding of the count rates of the eight detectors of the spectrometer.

It was shown that the measurements along the flight path produced very similar results as concerns the shape of the resulting spectral distribution of the neutron fluence. A more detailed analysis of the fluence rates in the **fast** and the **h-e** (high-energy) region shows slight changes in the shape of the spectra which are understood if one uses the appropriate flight parameters, namely altitude, longitude and geomagnetic latitude. For practical radiation protection dosimetry this slight change in the mean fluence-to-ambient dose equivalent conversion factors, <h74>, is negligible. However, as was demonstrated by the comparison of the dose rates derived from the Bonner sphere data and the conventional survey meters it is important to know the energy region in which the survey meter is sensitive to neutrons.

These spectrometric results can be used to justify the now common procedure to calculate route doses for the air crew personnel: a standard spectral shape of the neutron fluence is scaled by the according flight parameters and an appropriate monitor of the primary cosmic radiation and is integrated along the flight path.

A 16.8 References

[1] B. Wiegel and A.V. Alevra, *NEMUS - The PTB Neutron Multisphere Spectrometer: Bonner Spheres and More*, Nucl. Instrum. Meth. **A476**, 36-41 (2002)

[2] Alevra, A.V., Klein, H., Knauf, K., Wittstock, J. and Wolber, G., *Neutron Spectrometry and Dosimetry in the Environment and at Workplaces,* In: Proceedings of the IRPA Regional Symposium on Radiation Protection in Neighbouring Countries of Central Europe, Prague, 8-12 September 1997. Ed. J. Sabol, Prague (1997) pp 214-218.

[3] Alevra, A.V., Klein, H. and Schrewe U.J. *Measurements with the PTB Bonner Sphere Spectrometer in High-Energy Neutron Calibration Fields at CERN (CERN-CEC Experiment H6J93, July 1993).* PTB Report N-22, (*ISBN 3-89429-573-2*), Braunschweig, December 1994

[4] Birattari, C., Esposito, A., Ferrari, A., Pelliccioni, M., Rancati, T. and Silari, M., *The Extended Range Neutron Rem Counter LINUS: Overview and Latest Developments.* Radiat. Prot. Dosim. **76** (1998) pp 135-148

[5] Hecker, O. *Private communication.* PTB Braunschweig (June 1998).

[6] Ciobanu, M. and Alevra, A.V. *Low-Power Analogue Processor for Bonner Sphere Spectrometers.* In: Proceedings of the IRPA Regional Symposium on Radiation Protection in Neighbouring Countries of Central Europe, Prague, 8-12 September 1997. Ed. J. Sabol, Prague (1997) pp 506-509

[7] International Commission on Radiological Protection. *Conversion Coefficients for use in Radiological Protection against External Radiation (Adopted by the ICRP and ICRU in September 1995).* ICRP Publication 74, Pergamon Press, Oxford, 1997

[8] Roesler, S. and Stevenson, G.R. *July 1993 CERN-CEC Experiments: Calculation of Hadron Energy Spectra from Track-Length Distributions using Fluka.* CERN/TIS-RP/IR/93-47 (November 1993).

[9] Wiegel B., Alevra A.V., Matzke M., Schrewe U.J. and Wittstock J., *Spectrometry with the PTB Neutron Multisphere Spectrometer (NEMUS) at Flight Altitudes and at Ground Level*, Nucl. Instrum. Meth. **A476**, 52-57 (2002)

B 1 Institute for Radiation Protection and Nuclear Safety, IRSN

J.F. Bottollier-Depois, A. Biau, I. Clairand, D. Saint-Lô, M. Valero
IRSN, BP 17, F-92262 Fontenay-aux Roses, France
P. Blanchard
Air France, BP 10201, F-95703, Roissy-Charles de Gaulle, France
P. Dessarps
Direction Générale de l'Aviation Civile, F-75020 Paris, France
P. Lantos
Observatoire de Paris, F-92195 Meudon, France

B 1.1 Description of the SIEVERT calculation system

Due to their professional activity, flight crews may receive a dose of some mSv within one year. This is why the European regulations adopted in 1996 require the aircraft operators to monitor the exposure of their flight crews. In France, the Government delivered the SIEVERT system to employers: this dose assessment tool was developed by the French General Directorate of Civil Aviation (DGAC) and partners: the Institut de Radioprotection et de Sûreté Nucléaire (IRSN), the Paris Observatory and The French Institute for Polar Research and Technology (IFRTP).

In France, the Computerized System for Flight Assessment of Exposure to Cosmic Radiation in Air Transport, or "SIEVERT", is delivered to airlines for assisting them in the application of article 42 of the European Directive. This professional service is available on an Internet server accessible only to companies that applied for it to DGAC. However, a public section enables passengers to assess the dose received during a flight.

The system provides doses that consider the routes flown by aircraft. These values are calculated using models verified over several tens of flights with a satisfactory uncertainty margin. Also, in case of solar flare, the SIEVERT system allows assessing the impact with regard to the dose received.

SIEVERT is a tool suited for flight crew dosimetry for cosmic radiation. It requires no specific skill with regard to radioprotection within the airline. It generates no operating requirements for the personnel, as this is the case for personal dosemeters.

SIEVERT should provides a correct application of the regulation for at least three reasons. First, the results obtained are close enough to reality to avoid under-estimating the doses received by the personnel. Second, the radiation dose assessment mode is the same for all airlines. Third, if checks become required in the future, retrospective dose calculations might always be performed.

B 1.2 SIEVERT Operating Principle

The SIEVERT operating principle is simple. The company prepares a file of completed or planned flights and files it to the SIEVERT Internet address. The system then completes the file by adding the dose received during each flight. Doses are calculated, depending on flight characteristics, using IRSN-validated dosimetry data. The more detailed information with regard to the flown route, the more reliable the dose value. If the information is minimum, the dose is assessed from a standard route. At this stage, data is not nominal and the file of doses per flight can be stored for subsequent checks. The employers then have to total the doses received during routes flown by each crew member. This information is delivered to the individual concerned and communicated to the occupational physician and to IRSN.

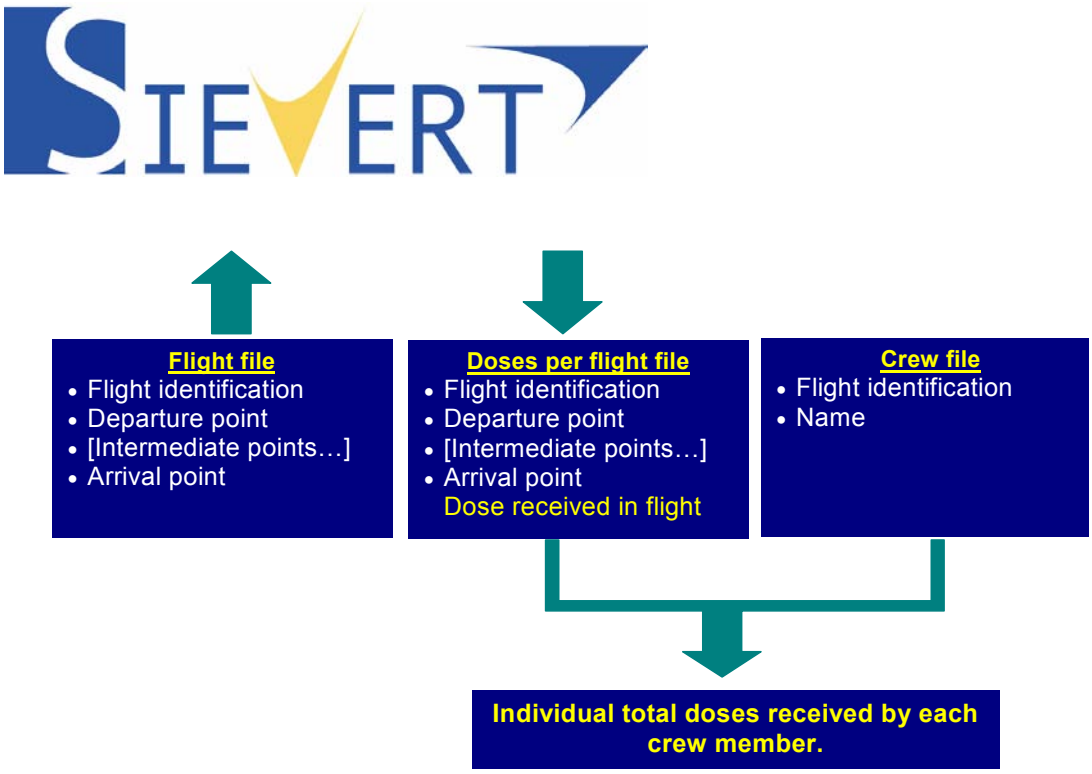

B 1.3 Dose Calculation with SIEVERT

Within SIEVERT, the airspace, divided into altitude, longitude and latitude areas, generates a 265,000-mesh cartography. Each mesh is assigned with a dose rate value. The SIEVERT computer assesses the time spent by the aircraft in each mesh and derives the dose received. The cumulative total of doses received in each mesh gives the dose received during the flight.

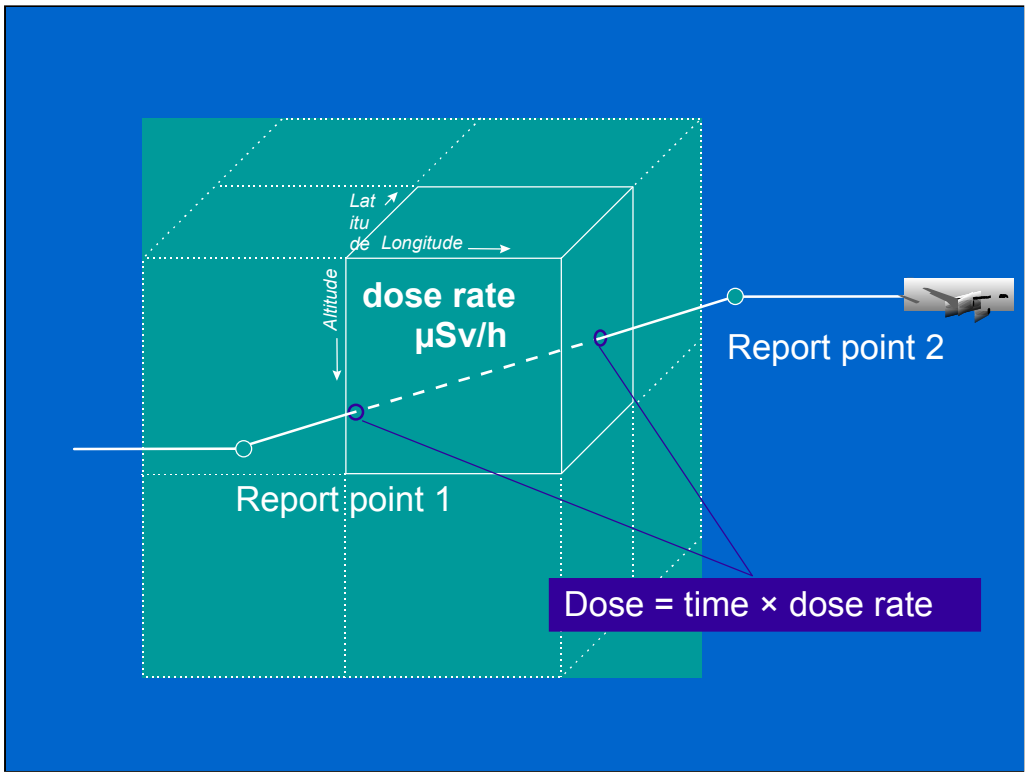

B 1.4 Validation of Dosimetry Data

Every month, IRSN calculates and validates the dose rate cartography. For this purpose, this Body is provided with various facilities. First, calculation allows to globally complete each mesh of the air space in a predictive manner, incorporating the sun activity cycles (the FAA software, CARI 6, is currently in use and the European EPCARD software might be used in the future). Radiation measurements, via dosemeters installed on ground and onboard aircraft, then allow confirming and, if required, correcting the values thus obtained. In case of noticeable solar flare, a specific cartography is created, then validated. The Paris Observatory astrophysicists are then called in support to estimate the flare impact. The time required to conduct this complex survey is long. It is thus necessary to wait for some weeks before calculating the doses received in flight during the flare.

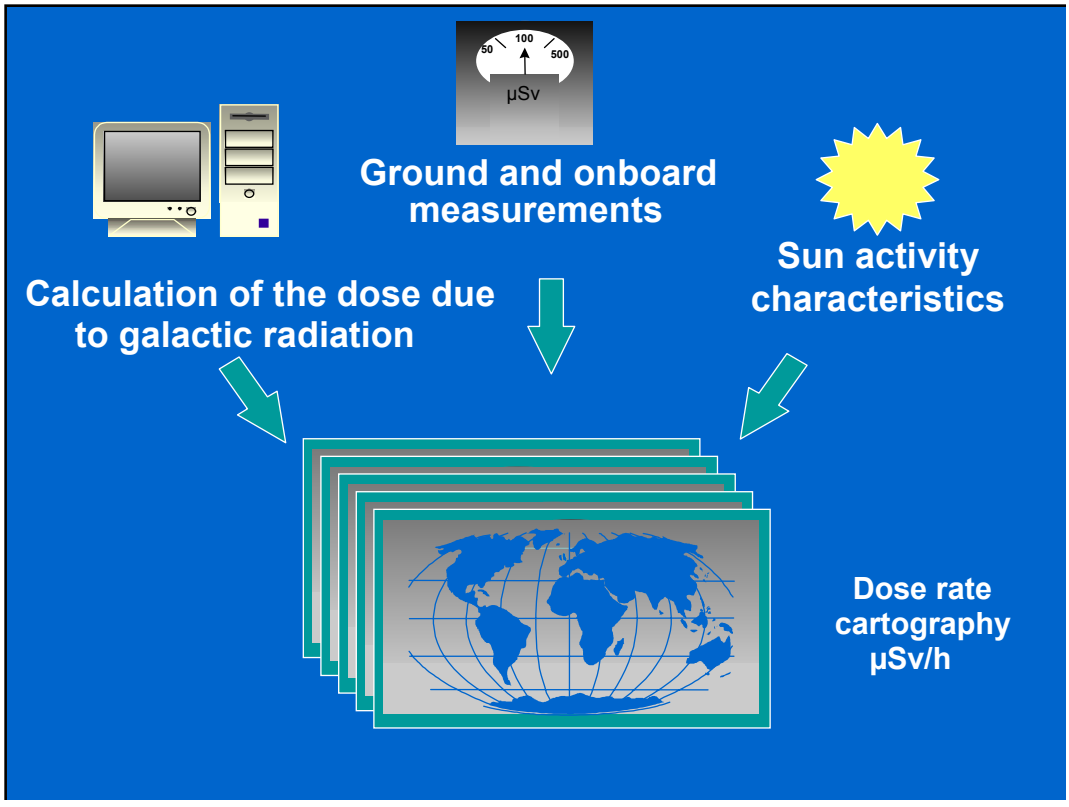

B 1.5 References

Bottollier-Depois J.F., A. Biau, P. Blanchard, I. Clairand, P. Dessarps, P. Lantos, D. Saint-Lô, M. Valero, Assessing exposure to cosmic radiation: the SIEVERT system, Radioprotection, vol 38, n°3, 357-366, 2003.

Lantos P., Fuller N., History of the solar flare radiation doses on-board aeroplanes using semi-empirical model and Concorde measurements, Radiat. Prot. Dos., 2003 (in press).

Lantos P., Fuller N., Bottollier-Depois J.F., Methods for Estimating Radiation Doses Received by Commercial Aircrew, Aviation Space and Environmental Medicine, vol 74, n°7, 746-752, 2003.

B.2 The Strategy and the Numerical Basis of the Program Package EPCARD

H.Schraube[1] , W.Heinrich[2] , S.Roesler[3], G.Leuthold[1] , and V.Mares[4]

[1] GSF - National Research Center for Environment and Health, D-85758 Neuherberg, Germany

[2] University of Siegen, Physics-Department, D-57078 Siegen, Germany

[3] CERN, TIS/RP, CH-1211 Geneva 23, Switzerland

[4] Ludwig-Maximilian-University, D-80539 München, Germany

B.2.1 Introduction

Galactic cosmic rays create secondary charged and uncharged particles in the Earth's atmosphere which are responsible for the radiation doses to individuals in airplanes. The dose rates and relative contribution of the single particles (neutrons, protons, pions, electrons, muons and photons) depend on the solar activity ("solar shielding"), the geographic position ("geomagnetic shielding") and on the flight altitude ("shielding effect of the atmospheric layer").

The routine determination of radiation doses to air crew requires the following scientific, numerical and administrative steps::

1. Calculation of particle fluence rates in the atmosphere at all solar and geomagnetic conditions as well as flight altitudes,
2. Final definition of quantities, quality factors and/or radiation weighting factors, and subsequent calculation of generally agreed fluence-to-dose conversion coefficients,
3. Consolidation of the calculated database and experimental validation,
4. General approval by national and international commissions,
5. Provision of a personal dose service which is subject to regular quality control. For this step the same requirements of precision of dose determination and record keeping apply as for any dosimetry service for occupationally radiation exposed individuals.

The basic physical processes and radiation components have been studied previously, however, the determination of dose quantities requires more physical information: Both operational (ambient dose equivalent) and risk related quantities (effective dose) contain non-physical information related to the radiation detriment to cells and organs. This is described by quality and radiation weighting factors, respectively. Therefore, the quantities can not be measured by direct dosimetric methods, though satisfying approaches are possible.

We have developed the computer program, EPCARD, for this purpose. It is a tool to calculate the radiation dose obtained by individuals along any aviation route at flight altitudes between 5000 m and 25000 m, both in terms of "ambient dose equivalent" and "effective dose". An extension of the flight levels is possible, if required. Dose rates and simulated instrument readings at any point in the atmosphere may be calculated for comparison with verification experiments.

EPCARD is based on the results of Monte Carlo radiation transport calculations which take into account all the physical processes and effects in detail. State of the art models are used to describe the flux of primary cosmic rays impinging at the top of the Earth’s atmosphere (NASA model of Badhwar, see below) and to the describe the nuclear reactions in the atmosphere (FLUKA Monte Carlo code, originally developed at CERN and lately extended considerably at INFN, details are given below). The fundamental knowledge gathered in different fields of physics is combined and used to make numerical predictions of particle fluence rates and energy spectra in the atmosphere without adjusting any parameters or boundary conditions.

The radiation transport calculations have shown that at commercial flight altitudes the spectral shapes of the particle fluences are essentially invariable. This permits the use of calculated conversion coefficients to determine the dose quantities from the calculated and experimental spectral data. This appears necessary especially for those radiation components whose dose contribution can not be experimentally separated, but may considerably contribute to the effective dose considering the radiation weighting factors required by the European Council [1], e.g. for protons.

B.2.2 Strategy

The strategy followed in developing EPCARD contains basically two steps (Figure B.2.1):

First, to establish the particle fluence rates in the Earth's atmosphere by Monte Carlo calculation. The most recent information on galactic cosmic rays described in reference [2] and by the NASA model (details are given below) is used as GCR-particle input. The calculations are conducted under all possible physical circumstances, i.e. solar modulation (solar minimum, solar maximum and reversals) and geomagnetic shielding conditions (between 0 and 17 GV cut-off rigidity). For the particle transport the most recent nuclear reaction models and cross section data are employed in FLUKA. All particles are treated separately.

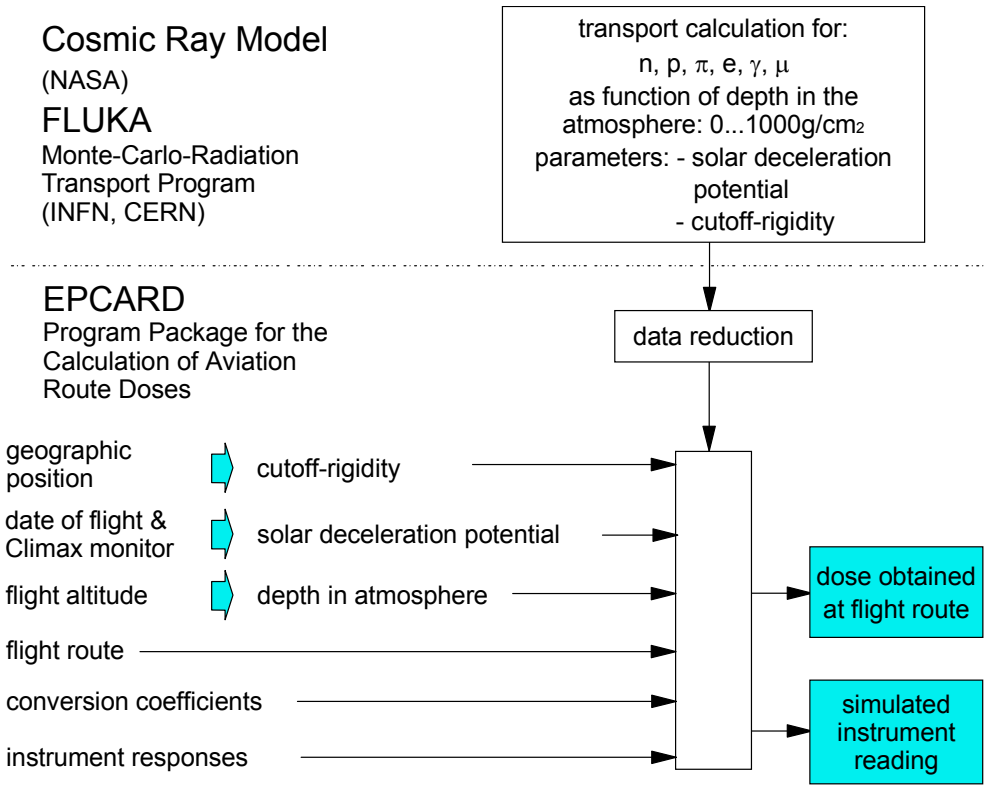

Figure B.2.1: Scheme of the data flow in EPCARD to calculate air crew doses

Secondly, to calculate fluence rates, dose rates and integral doses obtained by air crew along specific flight routes. For this purpose the fluence rates of all particles are systematically reduced to a matrix which fully describes the field conditions between the top of the atmosphere and ground level in physical parameters. For the determination of dose rates at specific places in the atmosphere, the cut-off rigidity is calculated for the respective geographic position from the data set of Shea and Smart (details are given below) to include important fine structures of the geomagnetic field. From the date and the Climax monitor reading (with a time delay of three months) the solar deceleration potential is derived. The flight altitudes of a certain flight profile are used to determine the respective depths in the

atmosphere. Between an arbitrary number of way points of a flight route, great circle navigation is assumed. A set of conversion factors for the respective particle type of interest is employed. These factors were derived in advance using the spectral shape obtained from the FLUKA calculations and energy dependent fluence-to-dose conversion coefficients (details are given below). As dose quantities, both "ambient dose equivalent" and "effective dose" (European Directive 96/29) are used. The set of conversion factors is assumed to be invariable within the required overall uncertainty of the calculation process. An option is prepared to employ a set of altitude-variable conversion factors. Finally, a set of mean instrument responses for each particle type may be used to derive simulated instrument responses which may serve for experimental verification.

B.2.3 Spectra of Primary Cosmic Rays

More than 80% of the dose at aircraft altitudes is caused by primary cosmic rays with energies below 100 GeV. In this energy range data from several independent direct measurements of the proton and helium spectra exist which were obtained with balloon-borne spectrometers [3-6]. More recently, spectra measured with the AMS detector on the Space Shuttle [7, 8] have also become available. At higher energies further direct and indirect measurements have provided information on the primary spectra which approximately follow a $E^{-\alpha}$-behaviour with a constant exponent α up to about 1000 TeV/nucleus. Compilations of these high-energy data as well as parameter-fits can be found, for example, in [9, 10].

Figure B.2.2 shows a summary of measured primary proton spectra (taken from [2]). All data were multiplied by $E^{2.7}$ in order to emphasise the spectral shape above 50 GeV/n which is not affected by solar modulation. As can be seen, the experimental data are consistent with each other and with the high-energy fits within approximately 25% for protons. The primary spectra used in the present calculations are shown in Figure B.2.2 as solid curves for the condition of the BESS experiment. They are based on spectra by Badhwar [11] which were scaled to match the recent experimental data. Recently, Badhwar [12] have provided us with updated spectra which are essentially in agreement with those used in the calculations. The spectra of heavier cosmic ray nuclei were also obtained from [11].

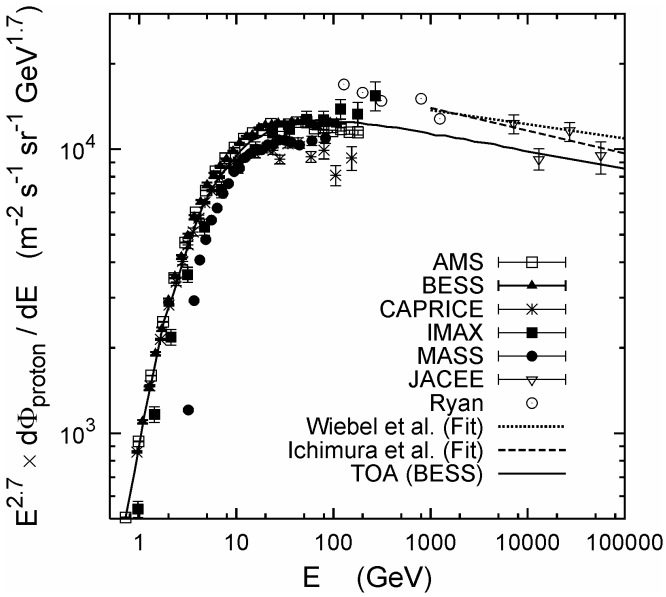

Figure B.2.2: Summary of direct measurements of the cosmic ray proton spectrum on top of the atmosphere (symbols). Dashed and dotted lines represent two fits to the data at higher energies. In addition, the spectrum used in the FLUKA calculations and as modulated for the condition of BESS experiment is shown (labelled "TOA (BESS)"). All spectra are multiplied by $E^{2.7}$ in order to emphasise the high-energy part.

Solar modulation of the primary spectra is described in the framework of a diffusion-convection model [11]. Within this model the modulation strength at a time is controlled by a single parameter ϕ (in MV), the so-called deceleration potential. This parameter is assumed to depend linearly on the Climax neutron-monitor count rate (prescaled by a time shift of 100 days).

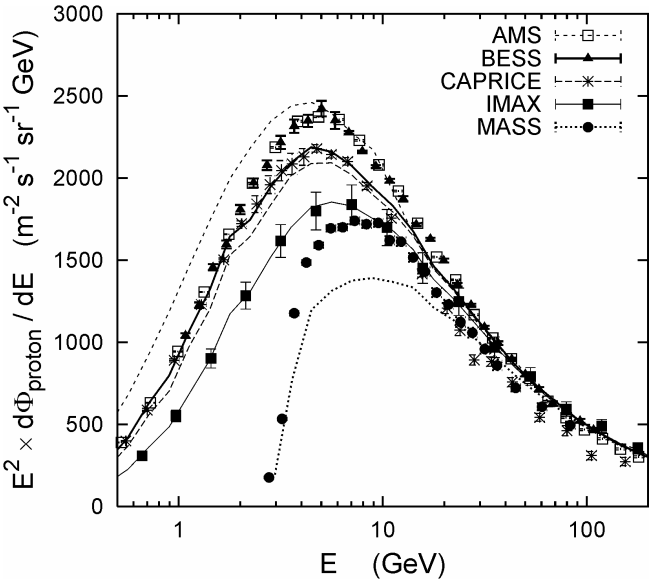

Figure B.2.3: Summary of measured proton spectra. Data as in Figure B.2.2 (symbols). Here, all spectra are multiplied by E^2 in order to emphasise the medium and low-energy part. The spectra used in the calculation and as modulated for the five measurement conditions are shown as curves.

Solar modulation affects the low energy part of the primary spectra for which data from balloon-borne and Space Shuttle measurements exist. Figure B.2.3 shows the measured proton spectra together with the spectra used in the calculation modulated with the dates and locations of these measurements [2]. The spectra are multiplied by E^2 so that equal areas on a semi logarithmic plot correspond to equal contributions to the energy fluence of cosmic radiation. Whereas good agreement is found for the IMAX- and CAPRICE-data the proton spectrum measured by MASS is underestimated by up to 30% below 20 GeV. This example demonstrates the uncertainty of the present knowledge of primary cosmic ray spectra, which is still one of the dominating uncertainties for the determination of doses at air flight level by model calculations.

The geomagnetic field acts as a shield against low-energy primary protons and nuclei. The rigidity cut-off below which protons and nuclei are deflected such that they are not able to enter the atmosphere depends on the location and direction of incidence on top of the atmosphere. The cut-off for vertical incidence is obtained from an one-by-one degree world grid of trajectory-determined cut-offs [13, 14]. These cut-offs are based on the 1990 International Geomagnetic Reference Field. Values range from zero at the geomagnetic poles to 17.6 GV at the geomagnetic equator. A dipole model of the Earth‘s magnetic field is used to correct these cut-offs for non-vertical directions (see [15] for further details). Figure B.2.4 shows the total nucleon spectrum for a solar modulation parameter of 465 MV, i.e. close to solar minimum, and different vertical rigidity cut-offs [2]. Note, that the rigidity cut-off translates into a kinetic energy cut-off which depends on the charge-to-mass ratio of the primary. This results in lower cut-offs for nuclei than for protons explaining the two-component structure in the nucleon spectra close to cut-off. In addition a spectrum for solar maximum and zero cut-off is shown. As can be expected already from this figure, the higher the rigidity cut-off is the lower is the effect of solar modulation on the radiation field in the atmosphere.

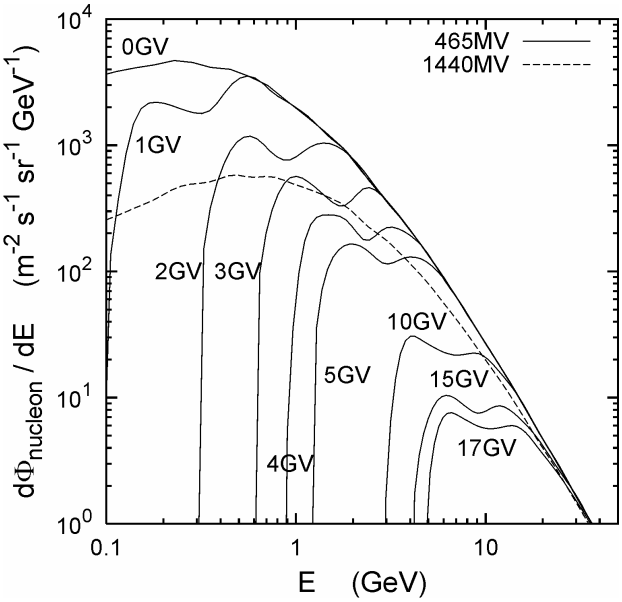

Figure B.2.4: Total nucleon flux for solar minimum modulation (465 MV) and different vertical rigidity cut-offs. In addition, the flux at solar maximum modulation (1440 MV) is shown.

B.2.4 Radiation Transport Calculations

The transport calculations of the primary GCR into the Earth's atmosphere were conducted by employing the transport code FLUKA. This is a multipurpose particle interaction and transport program with applications as diverse as proton and electron accelerator shielding, calorimetry, medical physics, beam design, high and low energy dosimetry, isotope production, etc. [16-18]. Recently, it has also been used successfully in space and cosmic ray studies [19, 15, 20-26].

In FLUKA, different physical models, or event generators, are responsible for the various aspects of particle production at different energies. These theoretical models have been directly tested against a large amount of nuclear experimental data, and have also been indirectly validated by comparisons with shower measurements, obtained both at accelerators [27-29] and in cosmic ray experiments [30, 31, 15, 32, 33].

Using FLUKA the spectral fluence rates for neutrons, protons, charged pions, electrons, photons and muons in the atmosphere have been calculated [34] for the following conditions which span approximately the extreme conditions for civil flight routes including the flight level:

- solar minimum, no geomagnetic shielding (cut-off rigidity of 0 GV), flight altitude of 15.3 km,
- solar minimum, highest geomagnetic shielding (cut-off rigidity of 17 GV), flight altitude of 9.6 km,
- solar maximum, highest geomagnetic shielding (cut-off rigidity of 17 GV), flight altitude of 9.6 km,
- solar maximum, no geomagnetic shielding (cut-off rigidity of 0 GV), flight altitude of 15.3 km.

The results are depicted in Figures B.2.5 through B.2.10 in the following way: The spectral particle fluence rates $d^2\Phi/dt \cdot dE$ (cm^{-2} s^{-1} GeV^{-1}), i.e. particle fluence per time interval dt and energy interval dE, are multiplied with the energy E, and divided by the energy integrated fluence rates (the normalisation factor is given in each figure for the respective curves). It can be seen in Figure B.2.5 and B.2.9 that the independence of the spectral shape on the flight conditions is almost perfect for neutrons and photons. Some differences can be observed for the charged particles (Figures B.2.6-8 and 10), however these differences are small. Based on this observation, constant conversion factors can be used to convert particle fluences into health physics dose quantities.

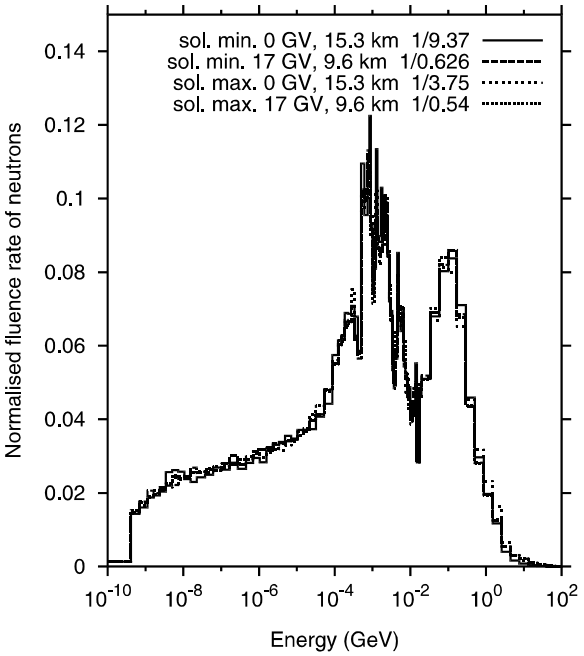

Figure B.2.5: Normalised spectral fluence rate of neutrons.

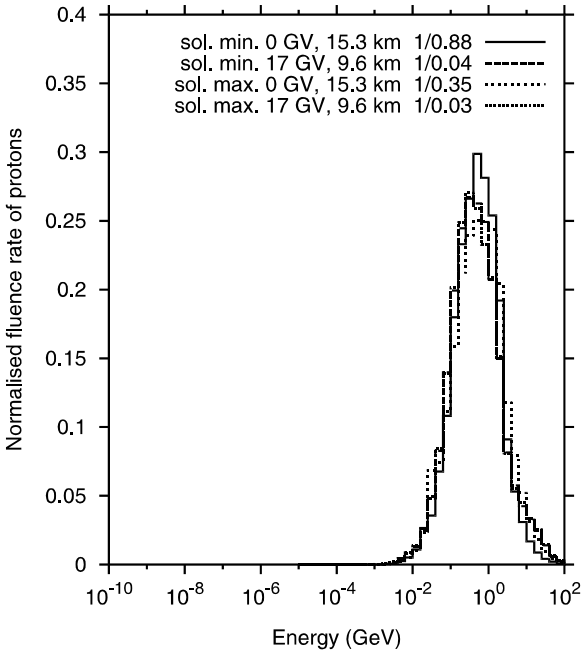

Figure B.2.6: Normalised spectral fluence rate of protons.

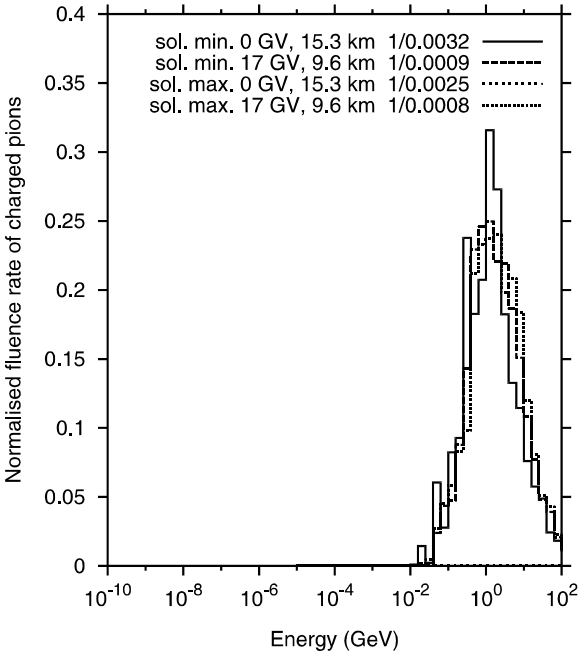

Figure B.2.7: Normalised spectral fluence rate of charged pions.

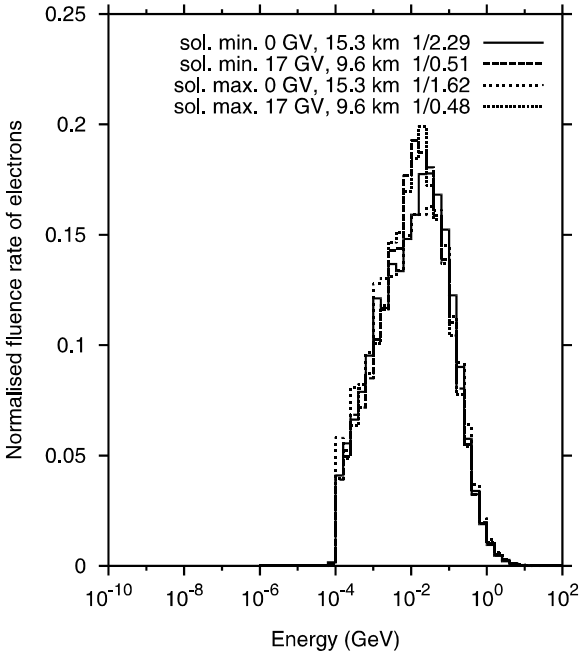

Figure B.2.8: Normalised spectral fluence rate of electrons.

The calculated fluence rates, integrated over the particle spectra, for all particles with exception of charged pions are presented in Figures B.2.12 to B.2.17, after conversion of atmospheric depth into flight altitudes. It was observed that the shape of the primary GCR spectra does influence to some extent the particle fluence with depth in the atmosphere, and the relative contribution of each specific component to the total particle fluence at a specified point. The uncertainties can be overcome by a comparison of calculated fluences or doses to experimentally ones for those components which are accessible with experimental means. The figures refer to solar minimum activity. Additionally, for neutrons the fluence rates at solar maximum activity are partly presented as well (Figure B.2.13). It should be emphasised again that the conditions are extreme ones, also with respect to solar activity

and geomagnetic shielding. The majority of flights are somewhere in between 3 and 10 GV geomagnetic shielding and for less extreme solar modulation conditions.

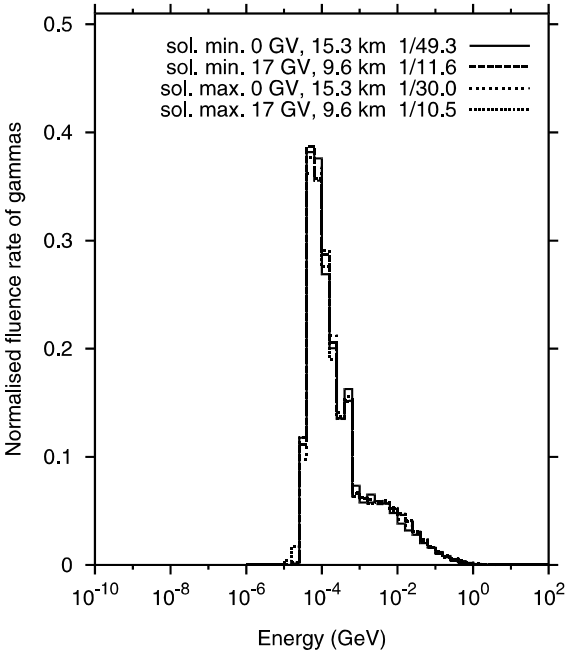

Figure B.2.9: Normalised spectral fluence rate of photons.

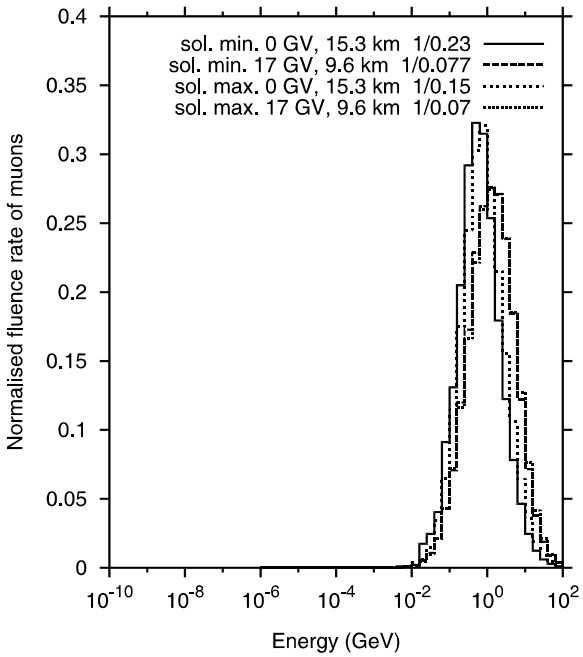

Figure B.2.10: Normalised spectral fluence rate of muons.

The FLUKA calculations are performed in air without the presence of an aircraft, i.e. at a point in the homogeneous medium air under particle equilibrium conditions, which may be assumed below the Pfotzer maximum [22]. Aircrafts have a wall thickness of several g/cm^2. If it is assumed that the chemical composition is not too far from air, i.e. aluminium instead of oxygen and nitrogen, then the effect of the wall would be equivalent to a somewhat lower flight altitude, approximately by 100 m, and a dose rate reduced accordingly.

B.2.5 Dose Calculation

Two health physics quantities are of interest in the context of the determination of the natural radiation exposure in the atmosphere:
i) The protection quantity effective dose which should give an estimate for the radiation risk. Its numerical values depend on radiation type and energy, and the irradiation geometry.
ii) The simplifying operational quantity ambient dose equivalent which is defined to be independent on the angle of radiation incidence, and additive with respect to any radiation component. Both quantities are described by conversion coefficients which are to be determined by radiation transport calculations for the respective phantom, for each of the six essential radiation components, and irradiation geometry.

The ICRU [35, 36] and the ICRP[37] have defined quality factors for secondary charged particles for the calculation of the ambient dose equivalent as operational quantity. On the other hand, for the determination of the effective dose the ICRP has recommended radiation weighting factors for the radiation components incident on the body. For both concepts, coefficients to convert particle fluence into the dose quantities may be found in the literature. For radiation energies below approximately 20 MeV, the data are well established [36]. In the high energy range, the INFN has published a series of data, and made them available on the WWW [38], but they require partly confirmation and amendments [39, 40] (see also [41, 42], where the data for H*(10) are discussed).

Table B.2.1: Averaged conversion coefficients for ambient dose equivalent, H*(10), and effective dose, E, used in EPCARD v3.0, v3.1(Dec. 2000) and v3.2 (Febr.2002)[1)].

particle	H*(10) / Φ (pSv cm^2)	E_{iso} / Φ (pSv cm^2)
neutrons	242	207
protons	919	3000
charged pions	799	1043
electrons	249	116
photons	2.70	6.02
muons	328	338

1) The uncertainties of the conversion coefficients are estimated to ± 10%.

As concluded above, the energy distribution of the relevant particles is essentially invariable for the flight altitudes considered here, i.e. in the range from 8000 m to 15000 m, and for all latitudes. Thus, one set of conversion factors for one quantity is sufficient for all altitudes and latitudes.

Using the energy dependent conversion coefficients, the conversion factors averaged over all spectra in Figure B.2.5 through B.2.10 were calculated. The results are listed in Table B.2.1 (taken from [46]). The data show that for neutrons the mean conversion coefficients of a number of experimental spectra with considerable high energetic components are practically the same as those for the calculated spectra of Figure B.2.5. It is also seen that the ambient dose equivalent, H*(10), exceeds somewhat the effective dose, E, for isotropic (ISO) and rotational (ROT) radiation incidence to the body, i.e. it appears to be a good and conservative estimate for the irradiation conditions expected in airplanes for the neutron component, which was also suggested earlier [42].

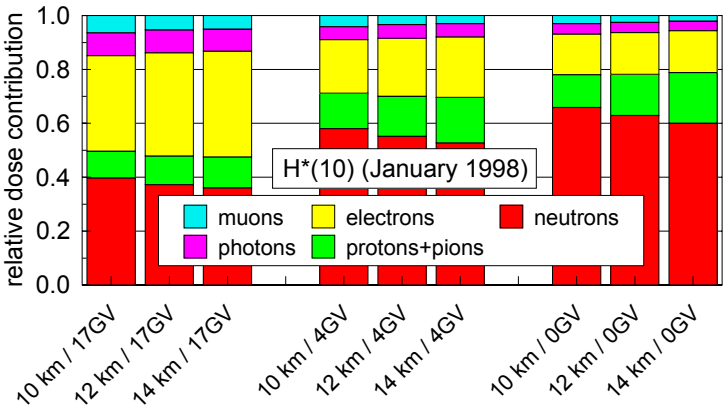

Figure B.2.11: Relative contribution to ambient dose equivalent from the six particle types at flight altitudes of 10, 12 and 14 km at 0, 4 and 17 GV cut-off rigidity and minimum solar activity.

The data of Table B.2.1 may be employed to convert the fluence rate data in Figures B.2.12 through 17 into dose rate data. This was done for flight altitudes between 10 and 14 km, minimum solar activity and for 0, 4 and 17 GV cut-off rigidity. The results in Figure B.2.11 exhibits the relative ambient dose equivalent of each of the radiation components. The contribution of charged pions is small (and disappears between the bars for protons and electrons in Figure B.2.11). With increasing latitude (0 GV is in the magnetic polar region), the relative neutron and proton contribution increases. The effective dose would be essentially determined by the neutron and proton components essentially because of the radiation weighting factor of 5 for protons other than recoil protons with energies in excess of 2 MeV, as proposed by the ICRP [37]. This is currently being reconsidered by the ICRP and by a number of other scientific institutions. The result of the international effort is expected in the near

future. As the computer programme EPCARD makes use of particle fluence matrices with a set of conversion factors, any essential and serious change in quality factors and/or radiation weighting factors for defined radiation components may be incorporated into the conversion data set without changing the whole data base from the scratch.

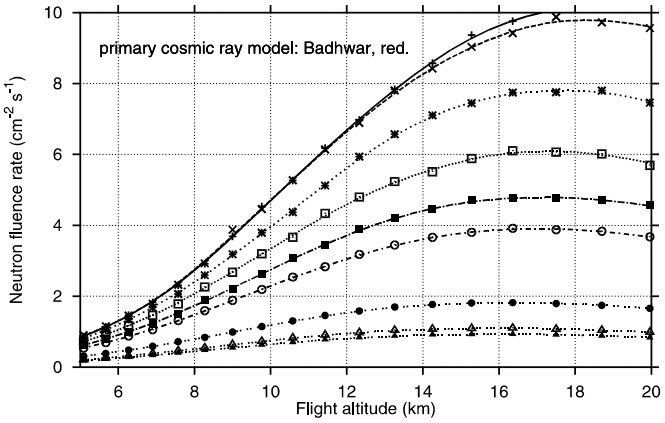

Figure B.2.12: Fluence rate as a function of atmospheric depth for neutrons at solar minimum activity and cut-off rigidities of 0, 1, 2, 3, 4, 5, 10, 15 and 17 GV (from top to bottom).

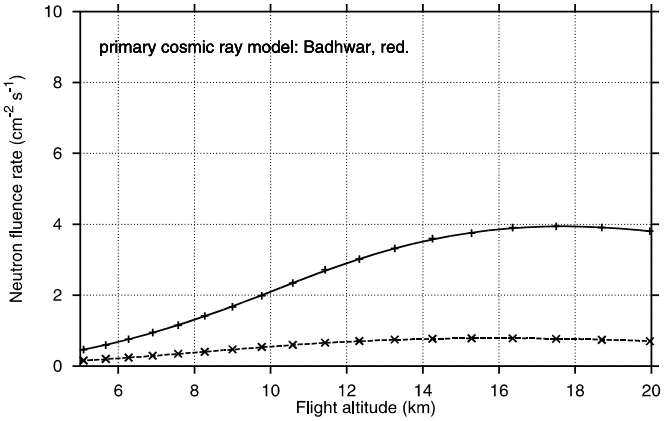

Figure B.2.13: Fluence rate as a function of atmospheric depth for neutrons at solar maximum activity, and at minimum (top) and maximum (bottom) cut-off rigidities.

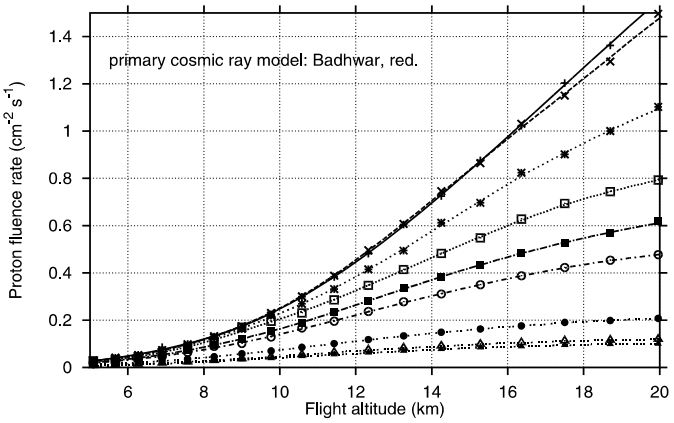

Figure B.2.14: Fluence rate as a function of atmospheric depth for protons at solar minimum activity, and different cut-off rigidities as in Figure B.2.12.

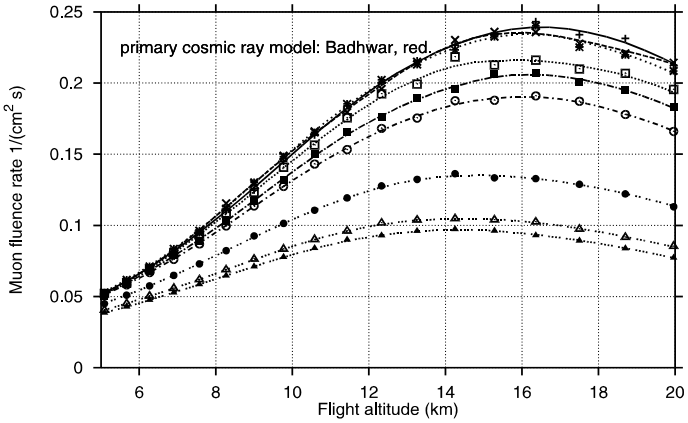

Figure B.2.15: Fluence rate as a function of atmospheric depth for electrons at solar minimum activity, and different cut-off rigidities as in Figure B.2.12.

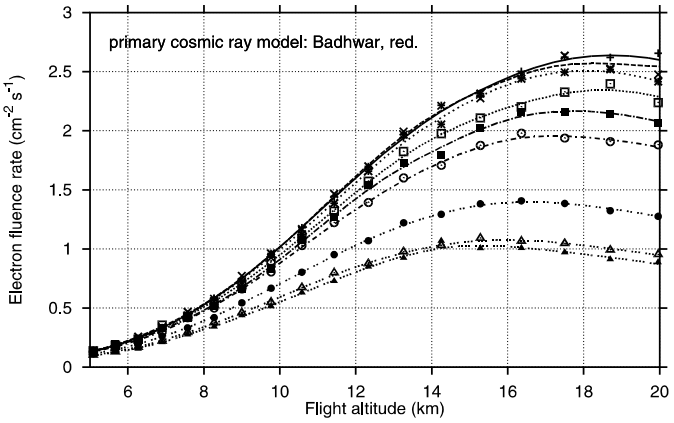

Figure B.2.16: Fluence rate as a function of atmospheric depth for muons at solar minimum activity, and different cut-off rigidities as in Figure B.2.12.

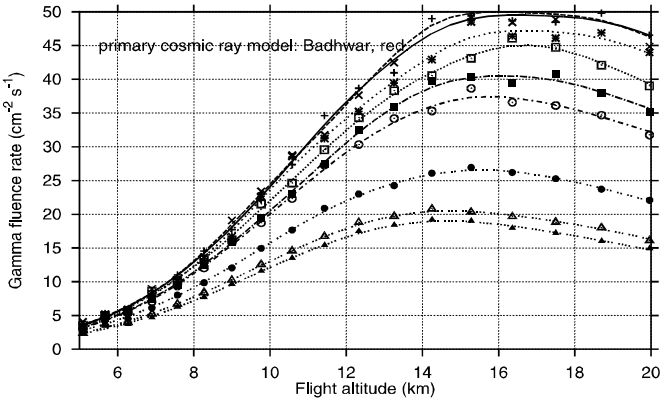

Figure B.2.17: Fluence rate as a function of atmospheric depth for photons at solar minimum activity, and different cut-off rigidities as in Figure B.2.12.

B.2.6 Discussion of the Reference Doses

We would like to refer to a recent publication [44] and discuss to some extent the problem of the quantities to be used. There are two motivations to use ambient dose equivalent, H*(d), as the operational quantity also for air flight conditions.

The first one is that this quantity - together with the personal dose equivalent, $H_p(d)$ - is the operational quantity to be determined under ground level conditions, i.e. at places where survey and personal dosimetry is mandatory. The ICRU found the depth d=10 mm as a good approach for these conditions.

H*(10) is well established in the system of radiation quantities of the ICRU, and has been introduced into most national regulations. It would be logical to keep this system for all occupationally radiation exposed individuals in an uniform way, if serious reasons do not contradict. One reason, of course, would be that the radiation exposure as a whole or for essential radiation components is not sufficiently assessed by the operational quantity.

The second motivation is more serious. As said above, all calculations (the analytical approaches as well as the MC-calculations) require experimental control and verification. Most devices are constructed to measure H*(10), or an approach to it with acceptable uncertainties, and are calibrated in terms of H*(10) under laboratory (reference) conditions. Therefore, most experimentalists do deliver their results in terms of H*(10). It is possible, of course, to transpose ambient dose equivalent, H*(10), into effective dose, E, and vice versa, by the relation

$$E = H^*(10) \cdot \frac{\int (E/\Phi) \cdot d\Phi_p/dE_p \cdot dE_p}{\int (H^*/\Phi) \cdot d\Phi_p/dE_p \cdot dE_p},$$

where $d\Phi_p/dE_p$ is the spectral fluence (rate) of the particle type, p, considered. H*(10) exhibits, for instance, the experimentally determined result for the specific particle or radiation type, if a discrimination against other radiation or appropriate corrections during the experiments were possible at all. (E/Φ) and (H^*/Φ) are the conversion coefficients as function of particle energy, E_p. These, and the spectral fluence (rates), $d\Phi_p/dE_p$, (see Figures B.2.5 through 10) have to be known explicitly with sufficient precision before the equation is employed. Part of the discussion on the conservative estimation by H*(10) suffers from the fact that data are available, but their uncertainties are not known.

In contrast to H*, the effective dose, E, is not a "receptor free quantity", but its numerical values depend on the orientation of the receptor (anthropomorphic phantom) in the field and on the direction distribution of the radiation field. Generally, it would be no problem to define one of the respective conversion functions for the effective dose, e.g. for isotropic incidence, as the "reference operational quantity" for flight conditions. The experimental devices have then to be calibrated in terms of this quantity, or the measurements have to be interpreted in the way described by the above equation. But this has to be agreed upon in the scientific and radiation administrative community.

B.2.7 Practical Aspects

As air crews are considered as occupationally radiation exposed persons by the European Directive, in principle the same requirements apply as for any other personnel to be surveyed by dosimetry services, e.g. in medical radiation diagnostic and therapy, and in nuclear industry: Precision of dose determination and quality assurance of the dose results, easy access to data listings for authorised people, easy recognition of excess of dose limits, evaluation of integrated personal doses during individual professional history, long term data maintenance, data protection (against unauthorised access) and data security (against loss). The only difference to the performance of standard routine service is that for air crews the doses are calculated for each flight segment, rather than measured during a time period. The responsibilities between dosimetry services and air companies could be divided by in the following way:

The air carrier(s) would be responsible for: i) delivering and up-date of the personal data, and delivering the personnel flight lists in time intervals as appropriate, ii) recalling the dose-lists, e.g. monthly, and taking care for the proper work plans and other measures required in Article 42.

The Personal Dose Service would be responsible for: i) maintenance of EPCARD, including up-dates of the physical data base, ii) taking care for a 24h world-wide access to the system, iii) providing all necessary measures for long term record keeping and data security.

The fluence or dose distribution of particles in the atmosphere which are produced by solar flare events have so far not been considered. Solar flares are extra-ordinary statistically observed radiation

events which may occur during certain periods of the solar cycle. In some of these events particle fluxes and particle energies may be high enough to produce a radiation level at air flight altitudes which is significantly increased in comparison to that one caused by the continuous galactic cosmic radiation. However, these are rare and transient phenomena for which the respective dose data may additionally be evaluated and recorded, as soon as accepted approaches for the dose description are available. This problem is currently treated by the 5th EU frame program. Any information on solar flares could then automatically be attributed to the individual members of the dose records if they were on-flight during that period of time.

B.2.8 Summary and Conclusions

The routine determination of doses to which air crews are exposed due to natural penetrating radiation requires to be based on the same principles as for any other occupationally radiation exposed individual. The calculations using the NASA model of primary cosmic radiation and Monte Carlo code FLUKA for description of particle interactions in the atmosphere deliver the basic information with respect to particle spectra, from which the averaged dose conversion factors are calculated, and with respect to particle fluence rate from which the numerical values of the dose quantities are derived for any depth in the atmosphere. The situation is somewhat facilitated as the spectral shapes do not change much at the flight levels considered, and a constant conversion factor may be used for every particle type which contributes to the total radiation dose.

Also the introduction of an altitude dependent conversion factor would be no problem, if higher than present standard altitudes were considered, or lower uncertainties required. Recently, it was found that this dependence of the conversion factors, $H^*(10)/\Phi$, is rather small and their values may change up to about ±10% in the range of civil flight altitudes, i.e. between 5 and 15 km, with respect to an arbitrarily chosen reference altitude of 11.4 km. The mean conversion factors, E/Φ, vary within ±12% for neutrons, protons and photons, but about ±20% for electrons [45].

Conversion factors for anthropomorphic phantoms to determine the effective dose, and the ICRU sphere phantom to determine ambient dose equivalent are not yet fully established. Especially, the radiation weighting factor for energetic protons requires further scientific consideration.

The precision of the dose calculation depends on the information of the primary galactic cosmic rays, on the modelling of the atmosphere and on the model for description of particle interactions in the atmosphere. Experimental data may be used to adjust the calculated ones. However, not all radiation components are accessible to direct measurements or are distinguishable against other particle types. EPCARD is the tool which permits to calculate the aviation route doses from the consolidated data matrix with calculated and experimental data which come from a number of internationally recognised institutes. It is designed in such a way that any interested air carrier may make use of it in the near future for dosimetry routine for his employees.

B.2.9 Technical Realisation

EPCARD version 3.2 [46], running as DOS-program on the lowest level standard PC at that time, was available to the members of the working group during their studies and data preparation for this EURADOS report.

In meantime, legal requirements became effective in some European member states. Consequently, a new version was developed, which takes into account specifically the requirements of the German Aviation Authorities and the German National Metrology Institute. This version 3.3 runs on MSWindows 98, 2000, NT and XP. An example of the input mask for the manual input, is given in Figure B.2.18. In dosimetry routine, the file input option of EPCARD for a large number of flights is preferable. The version 3.3_4, was approved by the German Authorities for the routine dose determination of the German undertakings operating aircraft in November 2003.

Both versions EPCARDv3.2 and $v3.3_x$ are identical as far as the physical content is considered, with exception of a minor data printing error in v3.2.

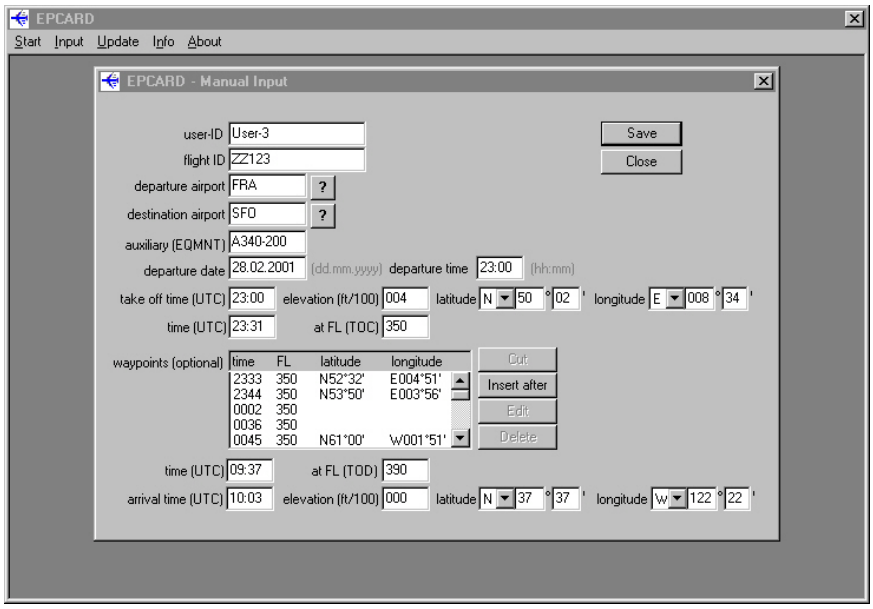

Figure B.2.18: Manual input window of EPCARDv3.3$_x$ with a flight example containing several waypoints.

B.2.10 Acknowledgements

The authors are grateful to Alfredo Ferrari, Milano, for providing the FLUKA-code and for valuable discussions and to late Gautam Badhwar, Houston, for providing the code for primary cosmic ray and the solar modulation model. Furthermore, the authors wish to thank the EU-contractors group for their valuable discussions, especially Denis O'Sullivan, Dublin, David Bartlett, Chilton, Rudolf Grillmaier, Saarbrücken, Lennart Lindborg, Stockholm, Marco Silari, Geneva, and Luigi Tommasino, Rome; and the sponsor of the group, Hans Menzel, Brussels and Geneva. This work was supported by the European Commission under contracts FI4P-CT950011a and B4-3040/99/135999/MAR/C1. Part of the work of S.R. was supported by the US-Department of Energy under contract DE-AC03-76SF00515.

B.2.11 References

1. European-Council *Directive 96/29/EURATOM laying down basic safety standards for the protection of the health of workers and the general public against the dangers arising from ionising radiation* (13 May 1996).
2. S. Roesler, W. Heinrich, and H. Schraube, *Monte Carlo Calculation of the Radiation Field at Aircraft Altitudes.* Radiat. Prot. Dosim. **98**(4), 367-388 (2002).
3. M. Boezio et al., *The cosmic-ray proton and helium spectra between 0.4 and 200 GV.* Astrophys. J. **518**, 457-472 (1999).
4. R. Bellotti et al., *Balloon measurements of cosmic ray muon spectra in the atmosphere along with those of primary protons and helium nuclei over midlatitude.* Phys. Rev. D **60**, 052002 (1999).
5. W. Menn et al., *The absolute flux of protons and helium at the top of the atmosphere using IMAX.* Astrophys. J. **533**, 281-297 (2000).
6. T. Sanuki et al., *Precise measurement of cosmic-ray proton and helium spectra with the BESS spectrometer.* Astrophys. J. **545**, 1135-1142 (2000).
7. J. Alcaraz et al., *Cosmic protons.* Phys. Lett. B **490**, 27-35 (2000).
8. J. Alcaraz et al., *Helium in near Earth orbit.* Phys. Lett. B **494**, 191–202 (2000)
9. M. Ichimura et al., *Observation of heavy cosmic-ray primaries over the wide energy range from ~ 100 GeV/particle to ~100 TeV/particle: Is the celebrated "knee" actually so prominent?* Phys. Rev. D **48**, 1949-1975 (1993).
10. B. Wiebel, *Chemical composition in high energy cosmic rays.* Report **WU B 94-08**, 1994.

11. G. D. Badhwar, *The radiation environment in low-Earth orbit.* Radiat. Res. **148**, S3-S10 (1997).
12. G. D. Badhwar, private communication, 1998.
13. D. F. Smart and M. A. Shea, *World grid of cosmic ray vertical cutoff rigidities for Epoch 1990.0,* In proceedings of 25th International Cosmic Ray Conference, pp. 401-404, Durban, South Africa, 1997.
14. D. F. Smart and M. A. Shea, private communication, 2000.
15. S. Roesler, W. Heinrich and H. Schraube, *Calculation of radiation fields in the atmosphere and comparison to experimental data*. Radiat. Res. **149**, 87-97 (1998).
16. A. Fasso, A. Ferrari, J. Ranft and P. R. Sala, *New Developments in FLUKA modeling of hadronic and EM interactions.* In Proceedings of The Third Workshop on Simulating Accelerator Radiation Environments (SARE-3) (H. Hirayama, Ed.), pp. 32-43. Proceedings 97-5, KEK, Tsukuba, Japan, 1997.
17. A. Fasso, A. Ferrari and P. R. Sala, *Electron-photon transport in FLUKA: Status.* To appear in Proceedings of the International Conference on Advanced Monte Carlo for Radiation Physics, Particle Transport Simulation and Applications, Monte Carlo 2000 (P. Vas, Ed.), Lisbon, Portugal, 2000.
18. A. Fasso, A. Ferrari, J. Ranft and P. R. Sala, *FLUKA: Status and perspectives for hadronic applications.* In: Proceedings of the International Conference on Advanced Monte Carlo for Radiation Physics, Particle Transport Simulation and Applications, Monte Carlo 2000 (P. Vas, Ed.), Lisbon, Portugal, 2000.
19. A. Ferrari, M. Pelliccioni and T. Rancati, *Calculation of the radiation environment caused by galactic cosmic rays for determining air crew exposure.* Radiat. Prot. Dosim. **93**, 101-114 (2001).
20. G. Battistoni, A. Ferrari, M. Carboni and V. Patera, *Monte Carlo study of the arrival time distribution of particles in Extensive Air Showers in the energy range 1-100 TeV.* Astropart. Phys. **9**, 277-295 (1998).
21. G. Battistoni, A. Ferrari and E. Scapparone, *Monte Carlo simulation of hadron production by atmospheric muons deep underground.* Nucl. Phys. B (Proc. Suppl.) **70**, 480-482 (1999).
22. W. Heinrich, S. Roesler and H. Schraube, *Physics of cosmic radiation fields*. Radiat. Prot. Dosim. **86**, 253-258 (1999).
23. A. Ferrari, M. Pelliccioni and T. Rancati, *The role of the quantities used in radiological protection for the assessment of the exposure to cosmic radiation.* Radiat. Prot. Dosim. **83**, 199-210 (1999).
24. G. Battistoni, A. Ferrari, P. Lipari, T. Montaruli, P. R. Sala and T. Rancati, *A 3-dimensional calculation of atmospheric neutrino flux.* Astropart. Phys. **12**, 315-333 (2000)
25. A. Fasso and J. Poirier, *Spatial and energy distribution of muons in γ-induced air showers.* Phys. Rev. D **63**, 036002 (2001).
26. J. Poirier, S. Roesler and A. Fass`o, *Distributions of secondary muons at sea level from cosmic gamma ray below 10~TeV.* Preprint astro-ph/0103030 (2001).
27. A. Fasso, A. Ferrari, J. Ranft, P. R. Sala, G. R. Stevenson and J. M. Zazula, *A comparison of FLUKA simulations with measurements of fluence and dose in calorimeter structures.* Nucl. Instrum. Methods A **332**, 459-468 (1993).
28. A. Ferrari and P. R. Sala, *The physics of high energy reactions.* In Proceedings of the workshop on Nuclear Reaction Data and Nuclear Reactors Physics, Design and Safety (A. Gandini and G. Reffo, Eds.), p. 424. World Scientific, Singapore, 1998.
29. A. Ferrari and P. R. Sala, *Intermediate and high energy models in FLUKA: Improvements, benchmarks and applications.* In Proceedings of the International Conference on Nuclear Data for Science and Technology, NDST-97 (G. Reffo, A. Ventura and C. Grandi, Eds.), p. 247. Societ`a Italiana di Fisica 59, Part I, Bologna, 1997.
30. V. Patera, M. Carboni, G. Battistoni and A. Ferrari, *Simulation of the electromagnetic component of Extensive Air Showers.* Nucl. Instrum. Methods A **356**, 514-525 (1995).
31. A. Ferrari and P. R. Sala, *Intermediate and high energy models in FLUKA: Improvements, benchmark and applications.* In Proceedings of the International Conference on Nuclear Data for Science and Technology, NDST-97 (G. Reffo, A. Ventura and C. Grandi, Eds.), p. 247. Societ`a Italiana di Fisica , Part I, Bologna, 1997.

32. A. Ferrari, T. Rancati and P. R. Sala, *FLUKA applications in high energy problems: From LHC to ICARUS and atmospheric showers.* In: Proc. The Third Workshop on Simulating Accelerator Radiation Environments (SARE-3) (H. Hirayama, Ed.), p. 165. Proceedings 97-5, KEK, Tsukuba, Japan, 1997.
33. A. Ferrari, J. Ranft and P. R. Sala, *The FLUKA radiation transport code and its use for space problems.* Physica Medica **XVII**, Suppl. 1, 72-80 (2000).
34. H. Schraube, W. Heinrich, G. Leuthold, V. Mares, and S. Roesler, *Aviation Route Dose Calculation and its Numerical Basis.* In: Proceedings of the Tenth International Congress of the International Radiation Protection Association (IRPA-10), Hiroshima, Japan, T-4-4 (2000).
35. ICRU-Report **39**, *Determination of Dose Equivalents Resulting from External Radiation Sources*, International Commission on Radiation Units and Measurements, Bethesda, Maryland, USA (1985).
36. ICRU-Report **57**, *Conversion Coefficients for Use in Radiological Protection against External Radiation*, International Commission on Radiation Units and Measurements, Bethesda, Maryland, USA (1998).
37. ICRP-Publication-60 1990 *Recommendations of the International Commission on Radiological Protection.* Annals of the ICRP, Pergamon Press **21**(1-3) (1991).
38. A. Ferrari, M. Pelliccioni and M. Pillon, www.inf.infn.it (1998).
39. V. Mares and H. Schraube, H. *The effect of the fluence to dose conversion coefficients upon the dose estimation from cosmic radiation in the atmosphere*. In print: Proc. of the Sixth Meeting of the Task Force on Shielding Aspects of Accelerators, Targets and Irradiation Facilities - SATIF6 (SLAC-Stanford, USA) (2003).
40. V. Mares and H. Schraube, *Conversion coefficients for cosmic radiation in the atmosphere.* In: Proc. Europ. IRPA Congress Towards Harmonisation of Radiatiation Protection in Europe. Oct.7-11, 2002, CD-ROM, ISBN 88-886-48-09-7 (2002).
41. H. Schraube, G. Leuthold, S. Roesler and W. Heinrich, *Neutron spectra at flight altitudes and their radiological estimation*, Adv.Space Res. **21**, 1727-1738 (1998).
42. H. Schraube, V. Mares, S. Roesler, W. Heinrich, *Experimental verification and calculation of aviation route doses*, Radiat. Prot. Dosim. **86**, 309-315 (1999).
43. H. Schraube, W. Heinrich, G. Leuthold and S. Roesler, *Experimental and theoretical basis of aviation route dose calculation*, In: Proc. 11th International Congress on Radiation Research, Dublin, July 18-23, 1999, Vol. 2, pp 724-727 (2000).
44. A. Ferrari, M. Pellccioni and T. Rancati, *The role of the quantities used in radiological protection for the assessment of the exposure to cosmic radiation.* Radiat. Prot. Dosim. **83**, 199-210 (1999)
45. V. Mares, S. Roesler, and H. Schraube, *Averaged particle dose conversion factors in air crew dosimetry.* Proc. 9th Symp. Neutron Dosimetry, Delft, Sept 28 - Oct 2, 2003. To appear in: Radiat. Prot. Dosim. (2004).
46. H. Schraube, G. Leuthold, W. Heinrich, S. Roesler, V. Mares, and G. Schraube, *EPCARD - European Program Package for the calculation of aviation route doses - User's Manual.* GSF - National Research Center on Environment and Health, GSF-Bericht **08/02** ISSN 0721 - 1694 (2002). see also www.gsf.de/epcard.

B.3 Description of the PCAIRE Code for Prediction of Aircrew Radiation Exposure

B.J. Lewis, M.J. McCall, L.G.I. Bennett, A.R. Green, B. Ellaschuk, M. Pierre, A. Butler and M. Desormeaux
Department of Chemistry and Chemical Engineering, Royal Military College of Canada, Kingston, Ontario, Canada K7K 7B4

Using the data in Section A 1, as measured by the Royal Military College (RMC) with a tissue equivalent proportional counter (TEPC), a model was derived to allow for the interpolation of the dose rate for any global position, altitude and date. Through integration of the dose-rate function over a great circle flight path or between various waypoints, a Predictive Code for AIrcrew Radiation Exposure (PCAIRE) was then developed to provide an estimate of the total dose equivalent on any route worldwide at any period in the solar cycle.

B.3.1. Model Derivation

The raw TEPC output from the flights can be processed to provide a dose equivalent rate (every minute). These data can be summed over five-minute intervals and then smoothed using a Savitzky and Golay method to reduce the relative error in the data to approximately 18%. This method of data treatment was applied to the TEPC spectral data obtained over the solar cycle. For instance, 36 flights were obtained near solar minimum conditions (i.e., at an average heliocentric potential (U) or deceleration potential (Φ) of 650 MV) and 14 flights were carried out near solar maximum conditions (i.e., at U = 870 MV and Φ = 970 MV). These data were used specifically for model derivation. This analysis resulted in the dose equivalent rate data plotted as a function of altitude and geomagnetic latitude as shown, for example, in Fig. B.3.1 (i.e., at $U = \Phi$ = 650 MV). This figure shows a consistent symmetry between altitude curves, which is due to the shielding effect of the atmosphere. The altitude A (in km) can also be related to an atmospheric depth h (in g/cm^2) (or atmospheric pressure p (in mbar)) in accordance with the relation:

$$h = \frac{p}{0.98} = \begin{cases} 1.02\,p_o\left[1 - 0.0227\,A\right]^{5.26}, & A \le 10.9 \\ 0.2276\,p_o\,\exp\left\{-0.1587\left(A - 10.94\right)\right\}, & A > 10.9 \end{cases} \qquad [1]$$

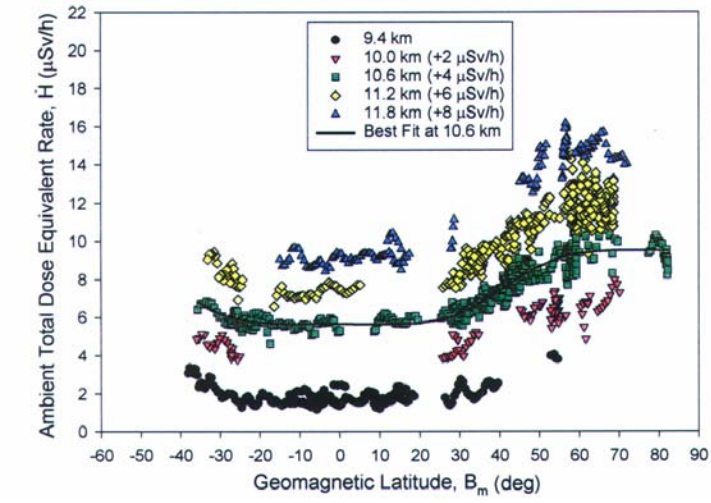

Figure B.3.1. Experimental dose rate data versus geomagnetic latitude for various altitudes. (The curves are displaced for improved clarity by the values given in the figure). The data correspond to a measurement period where on average $U = \Phi$ = 650 MV.

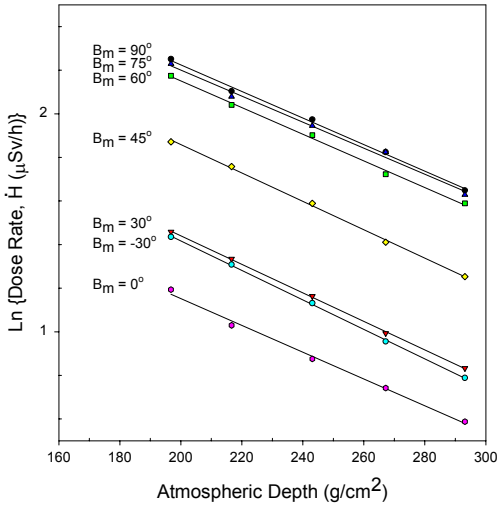

Figure B.3. 2. Plot of $\ln(\dot{H})$ versus atmospheric depth at various global positions.

where p_o = 1013.25 mbar. In fact, if the dose equivalent rate data are plotted in a semi-logarithmic fashion versus the atmospheric depth, h, a linear relationship results (see Fig. B.3.2). The slope of the resulting line corresponds to an effective relaxation length for the given particles in the atmosphere, ξ_s. An average slope of the resulting lines yields a value of ξ_s = 0.0068 cm^2/g, which is in excellent agreement with other literature values.[1,2] The parameter, ξ_s can be further refined as a function of the vertical cutoff rigidity R_c (in GV) using summed ambient dose equivalents from a lead-modified neutron rem counter (NMX) and an ionization chamber such that:[3]

$$\xi_s = \begin{cases} 0.0085\,\mathrm{cm^2\,g^{-1}}, & R_c \le 4\ \mathrm{GV} \\ -4.714\times10^{-4} R_c + 0.01039, & 4\ \mathrm{GV} < R_c < 11\ \mathrm{GV} \\ 0.0052\,\mathrm{cm^2\,g^{-1}}, & R_c \ge 11\ \mathrm{GV} \end{cases} \quad [2a]$$

At altitudes below 7.62 km (25 000 feet), the relaxation length, ξ_s, is reduced as follows:

$$\xi_{s,LowAlt} = \begin{cases} 0.6499\,\xi_s, & A \le 4.57\ \mathrm{km} \\ \left[0.6394 + 5.7\times10^{-5} e^{(1.1614A)}\right]\xi_s, & 4.57\ \mathrm{km} < A < 7.62\ \mathrm{km} \end{cases} \quad [2b]$$

This relaxation length can be used to normalize the data in Fig. B.3.1 to a specific altitude. In particular, the dose rate at 10.6 km (i.e., h_o = 243 g/cm^2) can be derived from the dose rate at any atmospheric depth according to the scaling function:

$$\frac{\dot{H}(h)}{\dot{H}_o} = e^{-\xi_s (h-h_o)}. \quad [3]$$

Normalizing all data in Fig. 1, for example, from various altitudes to 10.6 km in this manner yields Fig.B.3.3.

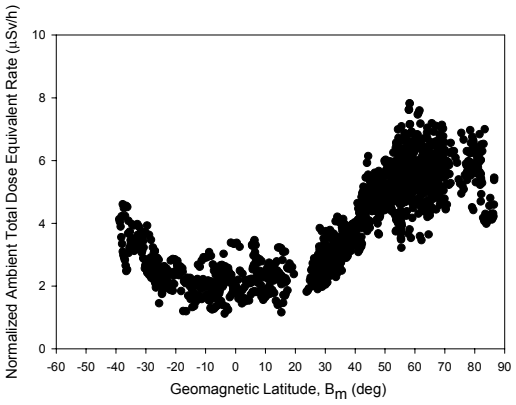

Figure B.3.3. Dose rate (normalized to 10.6 km) versus geomagnetic latitude.

Unfortunately, Eq. (3) cannot be extrapolated to altitudes near or above ~20 km because of the effect of secondary particle buildup. However, a more general function can be derived from mass balance considerations for the loss of primary particles and the formation of secondary particles in the atmosphere, such that:[4,5]

$$f_{Alt}(h) = e^{-\xi_s (h-h_o)} \left[\frac{1 - e^{-(k_o - \xi_s)h}}{1 - e^{-(k_o - \xi_s)h_o}} \right] + \frac{k_o - \xi_s}{\beta k_o} \left[\frac{e^{-k_o h}}{e^{-\xi_s h_o} - e^{-k_o h_o}} \right] \quad [4]$$

Here the parameter k_o accounts for the attenuation of primary particles in the atmosphere which is fitted to provide a maximum value of the function at the Pfotzer maximum. Based on FLUKA calculations, the altitude at which the Pfotzer maximum occurs will change with the latitude; for example, near the equator at R_c = 17.6 GV, the Pfotzer maximum is predicted to occur at 16.5 km, but shifts to a slightly higher altitude of 19 km at R_c = 0.7 GV nearer to the poles. To account for this effect, the attenuation coefficient for the primary particles is taken as $k_o \sim 0.016$ cm^2/g, which, with Eq. (2a) yields a Pfotzer maximum at the correct position as determined with Eq. (4). In Eq. (4), β is an effective proportionality constant for the production of secondary particles from primary-particle interactions. The parameter $\beta \sim 3$ as evaluated with a fitting of Eq. (4) to high-altitude data obtained with a TEPC on collaborative balloon-borne flights with the Italian Space Agency (Fig. 4(a)). This experiment was conducted on July 14 and July 23, 2001 at a geographical latitude and longitude of ~38°N and ~13°E ($R_c \sim 8.3$ GV) with a balloon ascent to 32 km. The first term in Eq. (4) (as previously proposed in Ref. 4) accounts for the buildup of secondary particles, whereas the second term is a correction for the contribution of primary particles to the dose equivalent, which is only important at high altitudes (i.e., > 20 km). Equations (3) and (4) are compared in Fig. 4(b), which reveals a simple exponential behaviour over the range of atmospheric depths in Fig. 2. Thus, Eq. (4) is able to account for the secondary particles including a maximum due to their buildup and an approximate exponential loss in the lower part of the atmosphere.

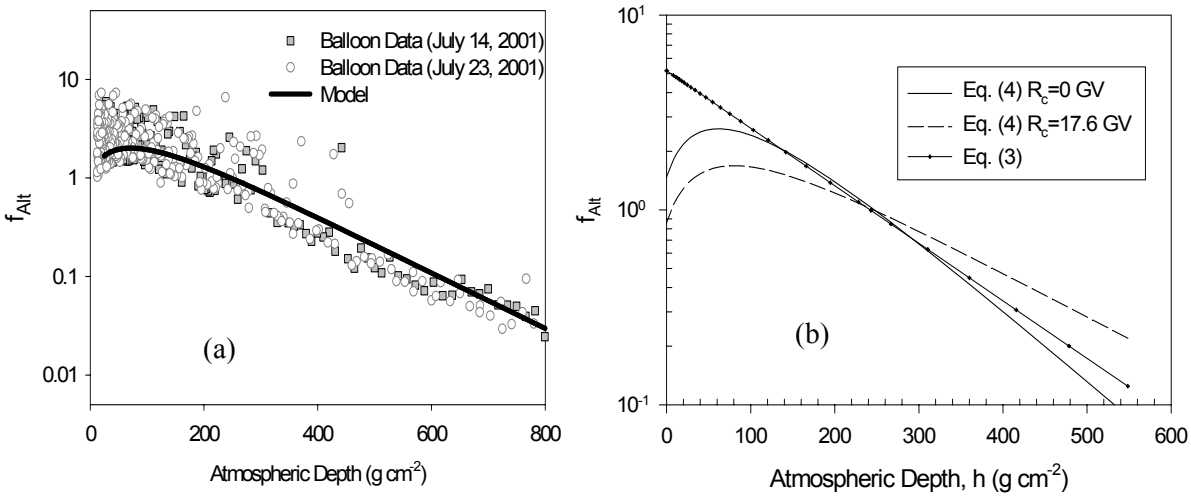

Figure B.3. 4. Comparison of: (a) Eq. (4) to measured TEPC dose rates obtained from balloon-borne experiments, (b) altitude correction function given in Eqs. (3) and (4).

On further examination of the symmetry around the equator in Fig. 3 (with a mirroring of data), it was seen that the north to south symmetry was not exact. This lack of symmetry is due in part to the 10.7° offset of the spin axis of the Earth with respect to the magnetic dipole axis, which gives rise to deviations in the magnetic field (in particular, the South Atlantic Anomaly). As well, the collected data do not span the full range of geomagnetic coordinates, which limits the ability of the correlation as a reliable method for interpolating the dose rate for any flight worldwide. To allow for the asymmetries of the magnetic field, the data can be plotted instead as a function of the vertical cutoff rigidity (R_c) (Fig. 5). The data in Fig. 5 in fact cover the full range of vertical cutoff rigidity of the Earth's field. A correlation of the global dose rate as a function of R_c is therefore possible for a given global position for different periods within the solar cycle. Symmetry was verified by differentiating data collected north of the equator with that south of the equator where such data indeed overlap. A best-fit polynomial to the data in Fig. B.5 provides the normalized dose rate f_i (in μSv/h) (at 10.6 km) as a function of R_c (in GV):

$$f_i = a_i + \frac{b_i}{1 + \exp\left\{\frac{R_c - c_i}{d_i}\right\}} \qquad [5]$$

The fitting parameters of the f_i function are tabulated in Table 1 for the two periods of the solar cycle.

Table B.3.1: Fitting Parameters for Dose Rate Function f_i

Fitting Parameters	i=1 (U = 650 MV and Φ = 650 MV)	i=2 (U = 870 MV and Φ = 970 MV)
a_i	2.0643	1.1744
b_i	4.5105	3.6392
c_i	5.0016	6.4170
d_i	2.7047	2.3073

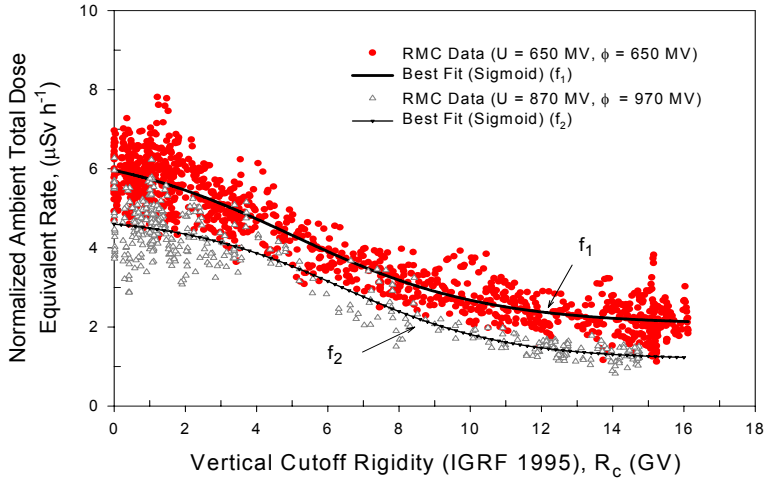

Figure B.3.5. Plot of ambient total dose equivalent rate (normalized to 10.6 km) versus vertical cutoff rigidity at U = 870 MV and Φ = 970 MV (near solar maximum conditions), and U = 650 MV and Φ = 650 MV (near solar minimum conditions).

In the original PCAIRE model of Ref. 4, in order to account for solar cycle effects, a normalizing function for the heliocentric potential was found based on theoretical considerations using the CARI 5E code. About 1350 CARI 5E runs were compiled for 23 flights worldwide at six-month intervals over a 28-year period at 10.6 km. The effective dose of each flight was normalized to a solar modulation potential of U = 650 MV. A correlation was developed to allow for interpolation of U for values from 400 to 1500 MV, where it is observed that there is also a slight dependence on the geomagnetic latitude B_m (in degrees) (which is more pronounced at higher latitudes), such that:[4]

$$f_{Helio}(U, B_m) = \begin{cases} \left[\frac{g_2 - g_1}{25}\right] |B_m| + g_1, & 0 \le |B_m| < 25 \\ g_2, & |B_m| \ge 25 \end{cases} \qquad [6a]$$

where g_1 and g_2 are explicit linear functions of U (in MV):

$$g_1(U) = -1.494 \times 10^{-4} U + 1.1026 \text{ and}$$
$$g_2(U) = -3.992 \times 10^{-4} U + 1.2696 \ . \qquad [6b]$$

Here f_{Helio} (as well g_1 and g_2) are normalized to a value of unity at 650 MV. Thus, to account for solar cycle effects, the normalized dose rate can be written as:

$$\dot{H}_o^U = f_1 \cdot f_{Helio} \qquad [7]$$

where f_1 is the function shown in Fig. 5 at $U = \Phi = 650$ MV. However, with the more complete set of measurements in Fig. 5 over the solar cycle, an experimental correlation is possible. For instance, using f_i as defined by Eq. (5) and Table 1, Eq. (7) can be replaced by the following equation, which is capable of employing the solar modulation model of either the Federal Aviation Administration (FAA) (via the heliocentric potential U) or the Johnson Space Centre (JSC) (via the deceleration parameter Φ) such that:

$$\dot{H}_o^U = \begin{cases} \dfrac{f_2 - f_1}{220}(U - 650) + f_1, & U \geq 650\,\text{MV} \\ f_1, & U < 650\,\text{MV} \end{cases} \qquad [8a]$$

$$\dot{H}_o^\Phi = \begin{cases} \dfrac{f_2 - f_1}{320}(\Phi - 650) + f_1, & \Phi \geq 650\,\text{MV} \\ f_1, & \Phi < 650\,\text{MV} \end{cases} \qquad [8b]$$

Note that Eqs. (8a) and (8b) and Eq. (7) (as used in the original model) are identical at $U = \Phi = 650$ MV.

Thus, Eq. (8) is used for the code development to allow for dose rate prediction for any global position and period in the solar cycle (with an appropriate choice of solar modulation model), with a correction for the effect of altitude via Eq. (4). Hence, it can generally be written:

$$\dot{H}(R_c, h; U, \Phi) = \dot{H}_o^{U \text{ or } \Phi} \cdot f_{Alt} \qquad [9]$$

The dose rate in Eq. (9) can be suitably integrated over a great circle path or between various way points for route dose prediction.

B.3.2. Comparison of RMC Model to Other Experimental Work

At the Physikalisch Technische Bundesanstalt (PTB) in Germany, measurements have also been conducted. In the PTB analysis, measurements with a neutron monitor and an ionization chamber were summed to produce a total dose equivalent rate. The instrumentation was flown on 39 flights worldwide.[3,6,7] The PTB data can be compared to the RMC data/model by similarly normalizing the former data to 10.6 km and plotting the dose equivalent rate versus R_c. From Fig. 1 of Section C.1, both studies were found to be in excellent agreement at $U = \Phi = 650$ MV where the best-fit curves for each of the data sets agree within 5%.

B.3.3. Code Development and Validation

The PCAIRE code was developed in a Visual C++ platform from the data analysis and the equations produced therein. This code was written to be user-friendly and requires minimal time for data input, calculation and data storage (Fig. 6). The code requires the user to input the date of the flight, the origin and destination airports, the altitudes and times flown at those altitudes. Look-up tables produce the latitude and longitudes of origin and destination, as well as the solar modulation potential. A great circle route is produced between the two airports, and the latitude and longitude are calculated for every minute of the flight. The vertical cutoff rigidity is calculated for a 3-epoch average based on the Shea et al. model in Ref. 8 or interpolated from IGRF-1995 tabulated data for the given geographical coordinates

along the flight path.[4] The at-altitude dose equivalent rate is then integrated along the great circle path at one minute intervals using the model of Eq. (9), which is based on the normalized correlations in Eq. (5) (or Fig. 5), and unfolded to the actual altitude flown (Eq. (4)) and the solar modulation potential for the date of the flight (i.e., Eq (8)). The user also inputs an ascent time, t_a, and descent time, t_d, from which the dose equivalent accumulated during ascent, H_a, and the dose equivalent accumulating during descent, H_d, can be calculated according to the equation:

$$H_{a,d} = \dot{H}_{i,f}^{U \text{ or } \Phi} \cdot \left(\frac{t_{a,d}}{2} \right) \qquad [10]$$

In this case, $\dot{H}_i^{U \text{ or } \Phi}$ indicates the dose equivalent rate calculated from Eq. (9) at the initial altitude over the originating airport and $\dot{H}_f^{U \text{ or } \Phi}$ indicates the dose equivalent rate calculated at the final altitude over the destination airport. The H_a and H_d are added to the at-altitude dose equivalent (integrated over a great circle path as described above) in order to provide an output of the ambient dose equivalent for the total flight. Using the conversion factors described in Section B.3.4, the code is also able to provide the effective dose for the total flight route. In addition, the code has the ability to model the routes via waypoints (where a great circle path is assumed between the given waypoints) or in a batch mode.

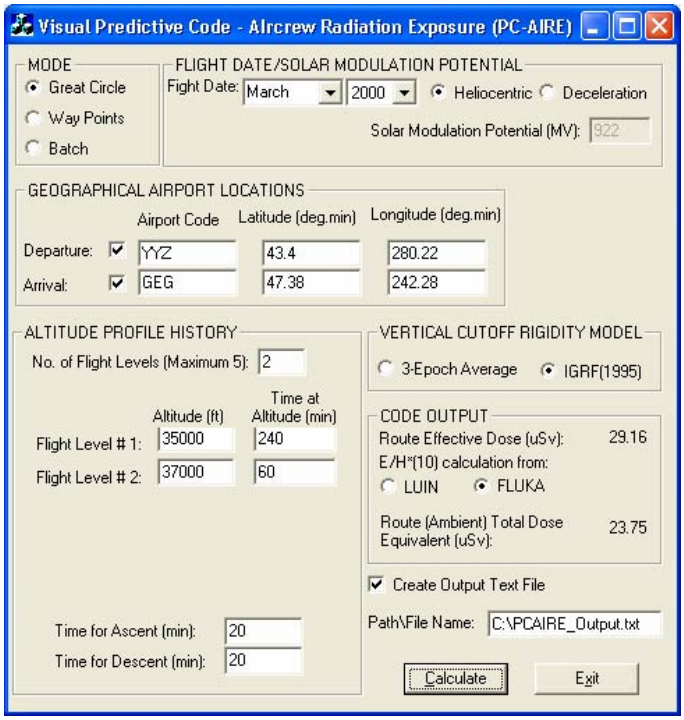

Figure 6. User interface for Visual PCAIRE.

The PCAIRE code was validated against TEPC data obtained at jet altitudes during different periods of the solar cycle. Figure 7(a) illustrates the predictive capabilities of PCAIRE under solar minimum conditions using an independent 26-flight TEPC data set which was collected in 1999 (i.e., these validation data were not part of the 36-flight data set used for model development in Fig. 5). Figure 7(b) shows PCAIRE predictions of the route dose equivalent for 16 flights measured close to solar maximum. As shown in the figures, the PCAIRE predictions of the validation flights are in good agreement with the TEPC measurements. Here the measured TEPC data have a relative error of ~18%, while the code has a predictive error of about 20% (which accounts for the uncertainty due to deviations in the flight path from a great circle route as well as uncertainties in the scaling functions for the altitude and solar modulation).

Figure 7. Plot of measured TEPC results versus PCAIRE code prediction of route dose equivalent using both solar modulation models for data obtained in (a) 1999 and (b) 2001.

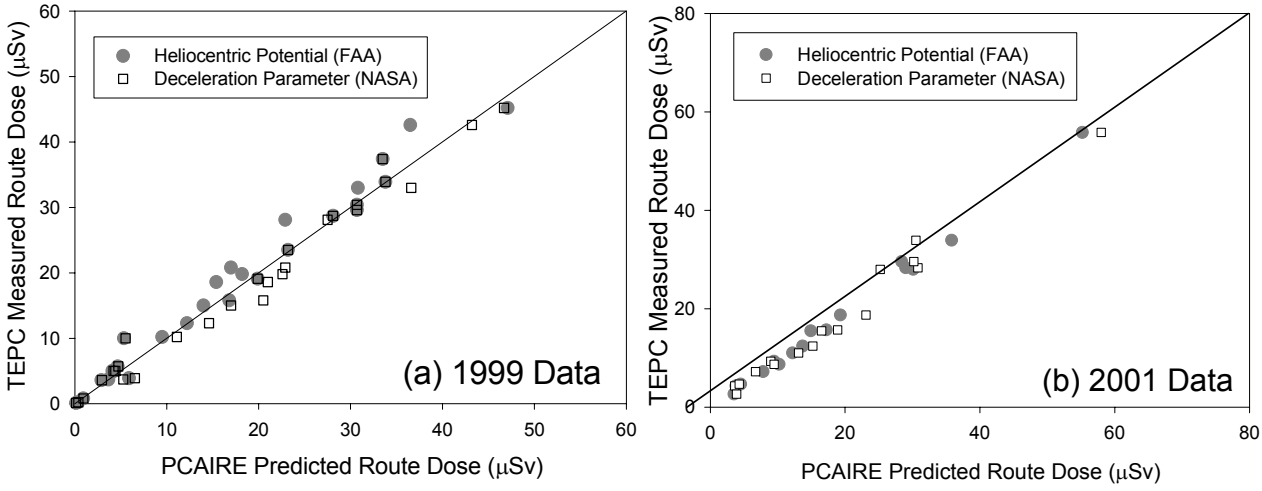

B.3.4. Effective Dose Estimation

The PCAIRE code provides a route dose in units of ambient dose equivalent, whereas legal regulation limits are generally given in terms of effective dose. For typical terrestrial situations, the ambient dose equivalent is a reasonable surrogate for the effective dose since it is a more conservative quantity. However, the ambient dose equivalent is no longer a conservative estimate of the effective dose for the complex high-energy cosmic spectrum, primarily due to the enhanced weighting factor of five for the protons.[9] This result can be clearly seen in Fig. 8(a), where the ratio of effective dose (E) to ambient dose equivalent (H*(10)) is greater than unity based on transport code calculations with FLUKA.[9] On the other hand, the transport code calculations with LUIN in Fig. 8(b) suggest that E/H*(10) is typically closer to unity. Consequently, in the PCAIRE code, an effective dose calculation is performed where the user has a choice of scaling function. Thus, utilizing a linear interpolation of the given functions in Figs. 8(a) and (b):[5]

$$f_{E/H^*(10)}^{FLUKA}(A,R_c)=\begin{cases} f_1(A), & 0\le R_c\le 0.4 \\ \{(f_2(A)-f_1(A))R_c+0.7f_1(A)-0.4f_2(A)\}/0.3, & 0.4<R_c\le 0.7 \\ \{(f_3(A)-f_2(A))R_c+12f_2(A)-0.7f_3(A)\}/11.3, & 0.7<R_c\le 12 \\ f_3(A), & R_c>12 \end{cases} \quad [11a]$$

where $f_1(A) = 0.97972 + 9.4307\times10^{-3}A + 1.3634\times10^{-3}A^2$, $f_2(A) = 1.0169 + 9.7771\times10^{-3}A + 9.2095\times10^{-4}A^2$ and $f_3(A) = 1.0822 + 3.7872\times10^{-4}A + 9.1674\times10^{-4}A^2$, or

$$f_{E/H^*(10)}^{LUIN}(A,R_c)=\begin{cases} f_1(A), & 0\le R_c\le 0.7 \\ \{(f_2(A)-f_1(A))R_c+12f_1(A)-0.7f_2(A)\}/11.3, & 0.7<R_c\le 12 \\ \{(f_3(A)-f_2(A))R_c+17.6f_2(A)-12f_3(A)\}/5.6, & R_c>12 \end{cases} \quad [11b]$$

where $f_1(A) = 0.84508 + 3.1555\times10^{-2}A - 2.4026\times10^{-3}A^2 + 8.1873\times10^{-5}A^3$, $f_2(A) = 0.88288 + 3.4036\times10^{-2}A - 2.6953\times10^{-3}A^2 + 7.7963\times10^{-5}A^3$ and $f_3(A) = 0.90765 + 4.1680\times10^{-2}A - 3.4292\times10^{-3}A^2 + 9.3997\times10^{-5}A^3$.

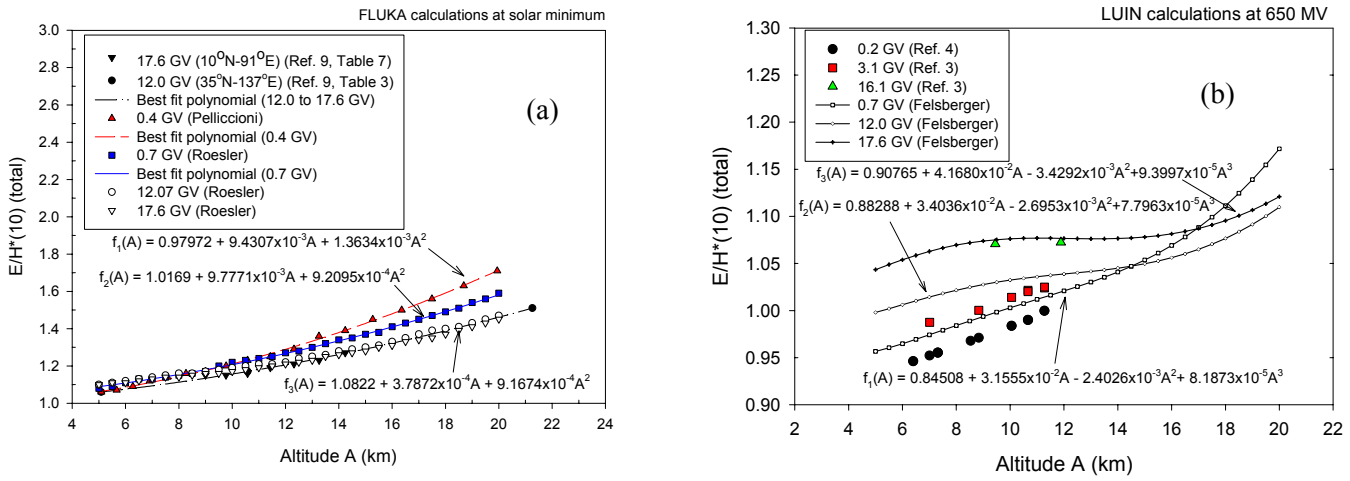

Figure B.3.8. Conversion factor from ambient dose equivalent to effective dose as derived from (a) FLUKA and (b) LUIN calculations.

In Eqs. (11a) and (11b), A is the altitude in km and R_c is the vertical cutoff rigidity in GV. These correlations correspond to conditions near a solar minimum; however, the effect of the solar cycle on the E/H*(10) ratio is small (i.e., typically within a few percent) especially at subsonic altitudes.[10] Thus, the ambient dose equivalent rate in Eq. (9) is multiplied by the chosen conversion function in Eqs. (11a) or (11b) to yield an effective dose, where Eq. (11a) will yield the more conservative estimate (i.e., by ~20% at subsonic altitudes). Hence, although the ambient dose equivalent estimates of FLUKA and LUIN do not vary significantly (see Fig. 1 of Section C.1), further investigation is clearly warranted to improve upon the effective dose calculation in order to reduce the observed discrepancy in Fig. 8 between the two transport codes. This discrepancy arises from the use of different environmental models, fluence-to-dose conversion coefficients and model approximations. In particular, the given result is principally due to a factor of two difference in the proton fluence rate.[4] Thus, a further investigation is important since an overly conservative estimate of effective dose could result in undue restrictions if such theoretically-based tools are used to manage the aircrew exposure.

B.3.5. Commercial Airline Application

As the PCAIRE model is comprised of simple correlations (e.g., Eqs. (2) and (4) to (11)), it can be readily employed as a kernel into an employee flight frequency database as needed for routine application to manage commercial aircrew exposure for a large number of personnel and flights (Fig. 9). As such, a PCAIRE*sys* code has been developed that is comprised of an underlying kernel model (written in VisualBasic) and a wrapper employing the structure queried language (SQL) of ORACLE. This code is therefore able to provide a secure interface with an airline database so that it can query the crew exposure in terms of such parameters as flight, date, crewmember and occupation (Fig. 9). This wrapper also permits data entry in batch mode or with waypoints for routine aircrew exposure assessment. Thus, the system is available on several platforms for use as: (i) a standalone application via desk top or web (individual users); (ii) a kernel incorporated into an airline's human resources system and flight database; and (iii) for Web/LAN batch-file processing as a separate data treatment centre.

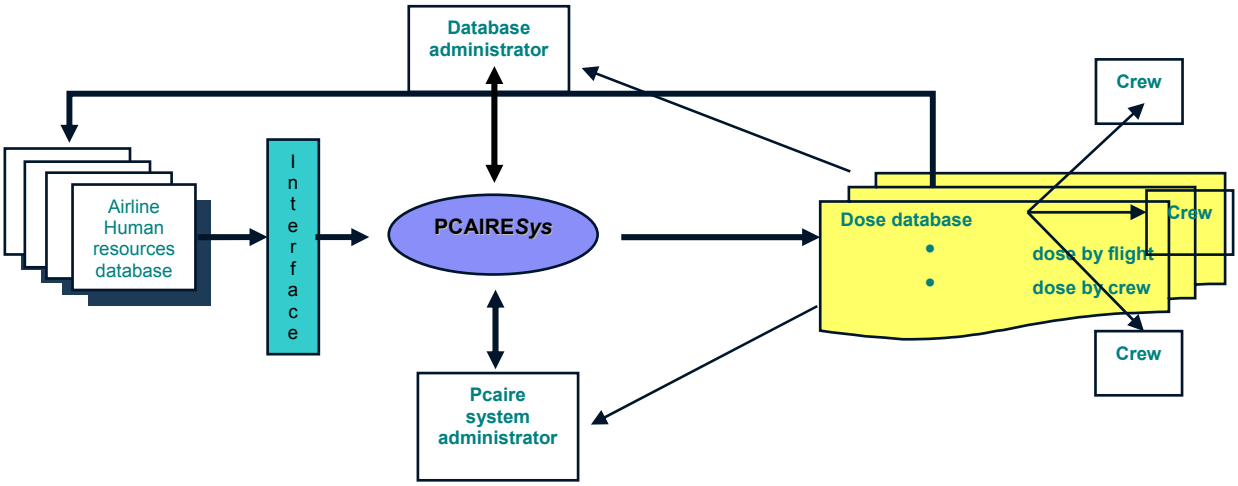

Figure 9. Operation environment for *PCAIRESys* for commercial application.

B.3.6 Acknowledgements

The authors would like to thank J.D. Servant of Transport Canada, and Dr. S. Kupca and C.J. Thorp of the Director General Nuclear Safety (DGNS) of the Department of National Defence, for their guidance of this study, and to acknowledge the discussions provided by Prof. K. O'Brien (Northern Arizona University), E. Felsberger (Technical University Graz), Dr. S. Roesler (CERN), Dr. H. Schraube (GSF – NCEH) and Prof. W. Heinrich (University of Siegen). The authors would like to further acknowledge the transport code calculations provided by E. Felsberger with LUIN, and Dr. S. Roesler and Dr. M. Pelliccioni (INFN, Laboratori Nazionali di Frascati) with FLUKA, and the equipment calibration of Dr. U.J. Schrewe (PTB). Additional gratitude is expressed to the employees and management of Air Canada, First Air, British Airways and Aerolinas Argentinas for their assistance and cooperation in the arrangement for measurements on board commercial flights. In particular, the authors wish to thank Capt. J. Nakielny, Capt. C.J. Saint-Martin and Dr. C. Thibeault of Air Canada, J. Lafrance of First Air and D. Irvine of British Airways, as well as Dr. A. Chee (Boeing) for the use of their data, Dr. A. Zanini (Italian Space Agency) for carrying out the experimentation for the balloon flights, and Dr. V. Ciancio (Universidad Nacional de la Plata) for collaboration on the Aerolinas Argentinas flights. Thanks are also due to 1 Canadian Air Division of the Canadian Forces, Air Operations at 8 Wing Trenton and the crewmembers of 437, 436 and 429 Squadrons for their cooperation and assistance in data collection on board military flights. In-kind and direct financial support for this work was received from Transport Canada, DGNS, ARP, NSERC and PCAIRE Inc.

B.3.7 References

1. L.D. Hendrick and R.D. Edge, "Cosmic-Ray Neutrons Near the Earth," Phys. Rev., 145 (4), 1023-1025, (1965).
2. R.H. Thomas, "Ionising Radiation Exposure Measurements at Commercial Jet Aircraft Altitudes," Radiat. Prot. Dosim. 48(1), 51-57 (1993).
3. U.J. Schrewe, "Global Measurements of the Radiation Exposure of Civil Air Crew from 1997 to 1999," Radiat. Prot. Dosim. 91(4), 347-364 (2000).
4. B.J. Lewis, M.J. McCall, A.R. Green, L.G.I. Bennett, M. Pierre, U.J. Schrewe, K. O'Brien and E. Felsberger, "Aircrew Exposure from Cosmic Radiation on Commercial Airline Flights," Radiat. Prot. Dosim. 93(4), 293-314 (2001).

5. B.J. Lewis, L.G.I. Bennett, A.R. Green, M.J. McCall, B. Ellaschuk, A. Butler and M. Pierre, “Galactic and Solar Radiation Exposure to Aircrew During a Solar Cycle,” Radiat. Prot. Dosim., in press.
6. U.J. Schrewe, “ACREM – Air Crew Radiation Exposure Monitoring: Summary of Results from Calibrations and TEPC Measurements,” PTB-6.31-1999-2, Physikalisch Technische Bundesanstalt, Braunschweig, Germany, October 1999.
7. U.J. Schrewe, “Radiation Exposure Monitoring in Civil Aircraft,” Nucl. Instr. and Meth. in Phys. Res. A, 422, 621-625 (1999).
8. M.A. Shea, D.F. Smart and L.C. Gentile, “Estimating Cosmic Ray Vertical Cutoff Rigidities as a Function of the McIlwain L-parameter for Different Epochs of the Geomagnetic Field,” Physics of the Earth and Planetary Interiors 48, 200-205 (1987).
9. A. Ferrari, M. Pelliccioni and T. Rancati, “The Role of the Quantities Used in Radiological Protection for the Assessment of the Exposure to Cosmic Radiation,” Radiat. Prot. Dosim., 83(3) 199-210 (1999).
10. A. Ferrari, M. Pelliccioni and T. Rancati, “Calculation of the Environment Caused by Galactic Cosmic Rays for Determining Air Crew Exposure,” Radiat. Prot. Dos. 93(2), 101-114 (2001).

B 4 Civil Aerospace Medical Institute Program CARI

W. Friedberg[1]

[1] Civil Aerospace Medical Institute, Federal Aviation Administration, P O Box 25082, Oklahoma City, OK 73125, USA

B.4.1 INTRODUCTION

CARI-6 is the latest in a series of computer codes designed to calculate the radiation dose accrued during aircraft flight. The primary differences between CARI-6 and its immediate predecessor, CARI-5, are a re-analysis of the primary spectrum and the expansion of the geomagnetic field models to include the IGRF 1995 field.[1]

B.4.2 CARI-6 DESCRIPTION

The CARI-6 computer program calculates the effective dose of galactic cosmic radiation received by air travelers on the shortest path (great circle route) between origin and destination airports. The path is the geodesic calculated by the computer program INVERSE, which takes into account the differences between the shape of the Earth and a perfect sphere.[2] CARI-6 relies on a database obtained by running LUIN99 at a variety of altitudes, latitudes, longitudes, and geomagnetic conditions, for dates back to January 1958. The physics of CARI-6 is the physics of LUIN99[3,4,5,6] (LUIN2000, the most recent version of LUIN, is a more user-friendly version of LUIN99; the results are the same).

B.4.3 References

1. D.F. Smart and M.A. Shea. World Grid of Calculated Cosmic Ray Vertical Cutoff Rigidities from IGRF 1995, personal communication (1999).

2. National Oceanic and Atmospheric Administration. INVERSE Version 2.00 (A computer program to calculate distances between locations on the surface of the Earth (1992)).

3. K. O'Brien. 'LUIN, a code for the calculation of cosmic ray propagation in the atmosphere (update of HASL-275)' Environmental Measurements Laboratory Report EML-338, Springfield, VA, National Technical Information Service, 1978.

4. K. O'Brien, and Gail de P. Burke, Calculated cosmic ray neutron monitor response to solar modulation of galactic cosmic rays, *Journ. Geophys. Res., 78*, 3013-3019, 1973.

5. K. O'Brien, W. Friedberg, D. F. Smart, and H. H. Sauer. The atmospheric and energetic particle radiation environment at aircraft altitudes. *Advances in Space Research* 644, 1739-48, 1998.

6. K. O'Brien, D. F. Smart, M. A. Shea, E. Felsberger, U. Schrewe, W. Friedberg, K. Copeland. World-Wide Radiation Dosage Calculations for Air Crew Members. *Advances in Space Research* 31(4):835-840, 2003.

B 5 IASON FREE

E. Felsberger[1,3], K. O'Brien[2], P. Kindl[3], Ch. Artner[1]

[1] IASON Graz, IASON Labormedizin GesmbH & Co KG, Feldkirchner Strasse 4, A-8054 Graz-Seiersberg, Austria

[2] Department of Physics and Astronomy, Northern Arizona University, Flagstaff, Arizona, AZ 86011, USA

[3] Technical University Graz, Technical Physics Department, Petersgasse 16/4, A-8010 Graz, Austria

B 5 – 1 INTRODUCTION

Due to the European Union Directive 96/29/EURATOM airlines belonging to the EU Member States are required to assess and limit their aircrews exposure. To support the air carriers to implement this legislative the flight-code FREE[1] was developed. Since in some Member States relative rigid Quality Assurance procedures were adopted, it was designed to take into account every relevant aspect of computational Aircrew Dosimetry.
FREE is the central piece within a series of professional commercial available Aircrew Dosimetry products.

B 5 - 2 OVERVIEW

FREE is a flight-code. A flight-code allows the direct introduction of an aircraft flight-trajectory by summing up the dose rates over a flight route and giving the complete dose for the whole flight. While the base-codes PLOTINUS and the SOLAR SUITE (see below) are comparatively slow and have a rather intricate format, FREE runs quickly by virtue of using an ultrafast access mechanism to its base-code results.
Because of being targeted for professional application FREE takes into account every relevant aspect of computational aircrew dose assessment: The flight-trajectory is taken into account in considerable detail, the modulation of the galactic cosmic ray (GCR) radiation field induced by the solar wind over the solar activity cycle (SAC) is handled correctly. Short term variations (Solar Particle Events, SPEs and Forbush Decreases, FDs respectively and other fast decreases in cosmic ray intensity) in the radiation field are also taken into account. FREE includes a database for calculating the complete radiation field in the atmosphere (of course with all transient effects) from the beginning of SAC 20 (November 1964) up to now.
FREE is designed and implemented on an modern component based Software Architecture (Zerbe, 1997, Schäpers, 1998). It consists of three main software modules: The flight-trajectory generator, the calculation engines (GCR incl. FDs/SPEs components) and an update possibility (see Figure B 5 - 1).

[1] Acronym for: Flight Route Effective Dose Estimation

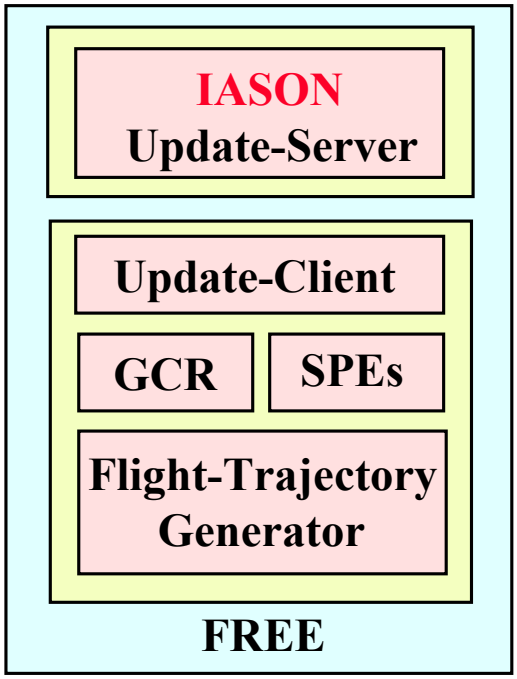

Figure B 5 - 1: FREE Main Software Modules

The central calculation engines, GCR and SPEs component, which perform the main dose calculations, are built upon high sophisticated cosmic ray transport-codes, which we denote here as so called base-codes.

B 5 - 3 THE BASE-CODES

Base-codes are the physical foundation of the FREE flight-code calculation components. Their results are built directly into the flight-code calculation engines (and approximate models), which integrate these data over the total flight-trajectory.
In contrast to the Monte-Carlo method deterministic analytical base-codes are used in our approach to enable extensive worldwide calculations in reasonable time frames without introducing of approximations, which effects are not exactly known. In the case of changed definitions of quantities or theory upgrades, the backend base-codes databases are simply completely recalculated.

- **B 5 – 3 - 1 PLOTINUS[2]**

PLOTINUS handles spatial variations of the radiation field induced by GCR and its variation in time with the Solar Cycle, but not SPEs. Its results have been demonstrated very good agreement with a large amount of in situ measurements.
The theory of PLOTINUS is described completely and in detail in O'Brien (2002a), therefore we present here only an short overview of the principle main parts.

The Primary Spectrum

The primary cosmic-ray spectrum used in the calculations described below is divided into twelve groups:

[2] Acronym for: Programmed Linear Operator for the Transport of Nuclear Showers

- The protons in the hydrogen flux, the unbound or free protons, and
- Eleven groups of primary nuclei.

Cosmic-ray proton spectra below 10 GeV are represented by the equation (Garcia-Muñoz, *et al*., 1975)

$$\varphi = 9.9\times10^{4}\left[E + 780\exp(-2.5\times10^{-4})\right]^{-2.65} \tag{1}$$

where E is in MeV/nucleon.

The cosmic-ray spectra above 10 GeV are represented by Peters' model

$$\log\varphi = \left\{a - 0.0495\left[11.9 + \log\left(1.7 + E^{2}\right)\right] + \log\left[0.0990\left(11.9 + \log\left(1.7 + \mathrm{E}\right)\right)/\left(1.7 + E\right)\right]\right\} \tag{2}$$

The eleven groups of nuclei plus hydrogen are obtained by normalizing each of these equations to the data of Gaisser and Stanev (1998).

The *shape* of the attenuation of the vertical muon flux underground depends sensitively on the *shape* of the primary spectrum. Represent the primary cosmic-ray spectrum by

$$\phi \propto E^{-\gamma} \tag{3}$$

where $\gamma = \gamma(E)$. The vertical muon flux then below ground depends on the values of γ. The magnitude of the cosmic-ray flux has already been determined by the normalization at 10.6 GeV.
In a gas such as air, the density-effect parameter, $\delta(E)$, in the muon stopping power is negligibly small. In solid matter, it has a magnitude and energy dependence such that the ionization loss is nearly constant as a function of energy and the stopping power can be represented accurately by

$$S_{\mu}(E) = 3.76(Z/A) + 7.34\times10^{-7}\left(Z^{2}/A\right) + 4.26\times10^{-7} \tag{4}$$

When dealing with muon fluxes underground, data are reduced to depth in "standard rock" which has a density of 2.65 g/cm^2, a mean atomic number of 11, a mean atomic weight of 22 and an ionization potential of 124 eV. In that case the muon stopping power is

$$S_{\mu}(E) = 1.88 + 4.463\times10^{-6}E \tag{5}$$

At low energies then, $S_\mu(E) = 1.88$, a constant, and it can be shown that at first the vertical muon spectrum attenuates as

$$\phi_\mu(x) \propto x^{-(\gamma+1)} \tag{6}$$

where x is the vertical depth in standard rock.

At high energies and therefore, great depths, $S_\mu(E) = bE$. This yields for the shape of the muon attenuation curve,

$$\phi_\mu(x) \propto \exp(-F\gamma bx) \tag{7}$$

where the constant $F = 0.93$ accounts for muon straggling.

Equations 6 and 7 are model-independent. Therefore, in that sense, they define the shape of the primary spectrum. Using Equations. 1 and 2, in combination with the data of Gaisser and Stanev (1998) to represent the primary spectrum yields the results shown in Figure B 5 - 2. Agreement is excellent.

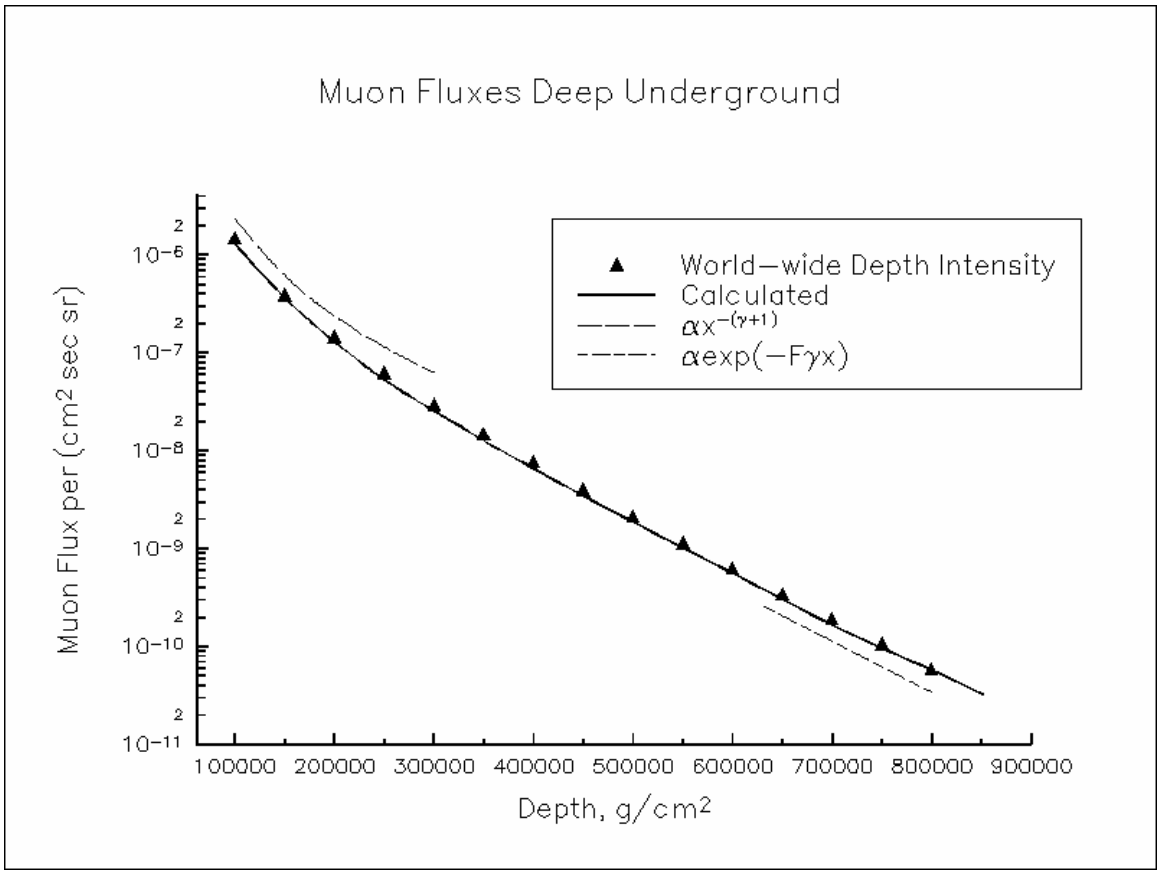

Figure B 5 - 2. Calculated and measured vertical muon intensity with depth underground. The points are from the world-wide depth intensity study of Larson (1968)

These boundary conditions when used in PLOTINUS work well throughout the whole atmosphere and at great depths below the surface of the earth. Equations 6 and 7 are independent of the form of the solution of the Boltzmann equation and of PLOTINUS. The chosen boundary condition works and works well as a function of latitude, altitude and solar activity.

PLOTINUS has the capability of adding a sheet of aluminum or aluminum-equivalent material between air-crew and the incident cosmic rays. As cosmic-rays are quite penetrating, it has not been felt necessary to use this feature. However, at great flight levels, above FL 500, say, it might have a significant effect on the incident complex nuclei which are more quickly attenuated than the incident nucleons and their secondaries.

Solar Modulation

Gleeson and Axford (1967) have shown theoretically that the effect on the galactic cosmic-ray spectrum of passage through the interplanetary medium is approximately the same as would be produced by a heliocentric potential with a magnitude at the earth's orbit equal to the energy lost per unit charge to that point by interacting with the solar wind.
This heliocentric potential model, being completely local, correctly describes the current state of the radiation field in the atmosphere as given by neutron monitor rates at the time of the flight, during the duration of the flight. Because of not being a forecast model, the heliocentric potential has now-cast capability (which is in use within FREE) and will correctly treat both Forbush decreases and fast decreases (See Section B 5 - 4 - 2).

Radiation Transport

PLOTINUS is based on an analytical theory of the transport of high-energy radiation through the earth's atmosphere. The transport of primary and secondary particles is described by a solution of the Boltzmann transport equation. The transport of secondary particles is based on a solution of the Boltzmann equation separable into longitudinal and transverse components, applicable to high-energy hadron-nucleus collisions. The longitudinal component is based on work by Passow (1962) and reported by Alsmiller (1965), and the tranverse component on the work of Elliott (1955) and Williams (1966). All secondary particles other than hadrons are mediated by meson production and decay. Cosmic rays consist of atomic nuclei ranging from hydrogen to nickel. PLOTINUS properly transports the primary nuclei. The breakup of primary nuclei as a result of collisions with atoms of air is treated by means of a generalized Rudstam (1966) formula. Thus the superposition approximation, which treats the incident nuclei as separate neutrons and protons, is not used in this code. Therefore an possibly important source of uncertainty - Kurochin, *et al.*, (1999) estimate the relative uncertainty of the superposition approach in the order of 20-25% at the maximum of the cascade - is eliminated in this code.
The theory on which PLOTINUS is based has also been applied to the atmospheres of other solar system bodies, *e.g.* Molina-Cuberos, *et al.*, (1999).

The Geomagnetic Field

A particle entering the earth's magnetic field must have sufficient momentum per unit charge, or rigidity to penetrate the earth's magnetic field and collide with air nuclei and produce atmospheric cosmic rays. That rigidity, a function of the particle's charge, and the zenith and azimuthal angles it makes with the earth's surface is called the "cutoff" rigidity and is expressed in GV (GeV/c per unit charge). Accurate vertical geomagnetic cutoff rigidities can be obtained by the numerical integration of cosmic-ray trajectories using mathematical models of the geomagnetic field. In PLOTINUS, the newest vertical cutoffs values as calculated from the International Geomagnetic Reference Field (IGRF) 95 coefficients are used (Shea, 2000).
Furthermore the entire cutoff distribution is used: all azimuths and zeniths for each location on the surface of the earth, not just the single vertical cutoff as do most other treatments[3]. The vertical cutoff distributions calculated by Shea (2000) include dipole and higher pole contributions to the geomagnetic field. However, the non-vertical cutoffs (Heinrich and Spill, 1979) (Roesler, 1998), assume the geomagnetic field is locally dipole.

Dosimetry of Cosmic Rays

Both effective dose and ambient dose equivalent are obtained from a simple convolution equation. Let $\phi_i, \left(i = p, n, \pi^{\pm}, \mu^{\pm}, e^{\pm}, \gamma\right)$ be the angular cosmic-ray fluxes calculated during a particular flight. Then the dose obtained during a flight is

$$X = \sum_i \int_0^{\pi/2} \sin(\theta) d\theta \int_0^{2\pi} d\omega \int_0^{\infty} dE \int_0^{\tau} dt \left\{ \phi_i\left[\theta, E, \vec{x}(t), t\right] \times K_j(E) \right\}, j = ED, H^*(10) \qquad (8)$$

where X is either *ED*[4] or *H*(10)*, θ is the angle the angular flux makes with the zenith, ω the angle the angular flux makes with the geographic pole, *E*, the kinetic energy of particles of type *i,* τ is the total time of the flight, *t*, a given time during the flight, $\vec{x}(t)$ is the location of the aircraft at a time *t* (latitude, longitude, altitude ($\vec{x}(t)$ is the flight path of the aircraft), $K_j(E)$ is the conversion factor from flux to dose rate, either ambient dose equivalent rate or effective dose rate (Pelliccioni, 1999, 2000).

- **B 5 – 3 - 2 THE SOLAR SUITE**

High-energy solar particles, produced in association with solar flares and coronal mass ejections, occasionally bombard the earth's atmosphere, resulting in radiation intensities additional to the already-present cosmic-radiation. These solar fluxes are also often distributed non-uniformly in space, so that fluxes measured by satellites at great distances from the earth and which sample large volumes of space around the earth do not alone accurately predict fluxes locally at the earth's surface.

[3] The complete cutoff-distribution is also taken into account within the flight-code FREE (see section B-5-4-2 The calculation engines)
[4] While the standard notation for effective dose is *E* rather than *ED*, the standard notation for energy is also *E.* To use *E* for both would create an ambiguity here.

When the earth is intercepted by a shock or other interplanetary disturbance, the induced current in the magnetosphere affects the geomagnetic field in a complex manner, changing the distribution of cutoff rigidities and usually reducing them. Consequently, access of these particles to the earth's vicinity during times of geomagnetic disturbance are not adequately described by using static geomagnetic field models.
Further, the flux may be distributed non-uniformly over the earth's surface. These factors make a straightforward calculation of the resulting radiation distributions from satellite data alone, or from the data obtained from a single high-latitude neutron monitor alone.

The SOLAR SUITE (O'Brien, 2000, 2002b) uses ground-level neutron monitor counting rates as adjoint sources of the flux in the atmosphere immediately above them in combination with the satellite data, to obtain solar-particle dose rates as a function of position over the earth's surface. The transport calculations were executed using PLOTINUS *q.v.*. This approach is a "first principles" approach. Aircraft fly within, at most, a few km of the ground where the neutron monitors are located. The monitor response reflects the fluxes actually impinging on them. Thus they reflect the local solar-particle environment. The monitor network of approximately 30 stations covers the globe from pole to pole.
The satellite particle energy spectra used by the SOLAR SUITE are obtained from data obtained by particle detectors aboard GOES satellites maintained by the NOAA Space Environment Center. These detectors measure the flux of energetic protons at geostationary orbit from energies of 600 keV to greater than 700 MeV (or momenta of 330 MeV/c to greater than 1300 MeV/c) in 11 discrete channels. The principal correction that had been applied to those data was a correction for the HEPAD response to backward fluxes through it, and subtraction of the background counting rates in each channel due primarily to galactic cosmic rays, their progeny, and to a lesser extent, instrument noise.

B 5 - 4 FREE FLIGHT-CODE IMPLEMENTATION

In general the physical base-codes do not fulfill the necessary requirements concerning calculation speed and ease of usage for routine operational application. Futhermore base-codes usually give only answers for point calculations for specific conditions and not provide integrated results along a flight-trajectory.
To meet all these requirements the introduction of a flight-code is necessary. The three main modules of the flight-code FREE are described in the following paragraphs.

- **B 5 - 4 - 1 FLIGHT-TRAJECTORY GENERATOR**

The flight-trajectory in space and time is the dosemeter of computational aircrew dosimetry (see Figure B - 5 - 3). The accuracy of the final results depends significantly on how precise this information could be introduced into the calculations. Dose variations of flights on the same flight route in the range of more than a factor of two are possible and furthermore systematic effects (e.g. reduction of general flight-trajectories to a simplified model, e.g. great circle calculation) can introduce errors in the range of up to 30 per cent (Felsberger, *et al.*, 2000). Therefore precise consideration of the flight-trajectory in time and space is absolutely crucial to reach good quality final results. FREE takes this importance into account by the flight-trajectory generator component.

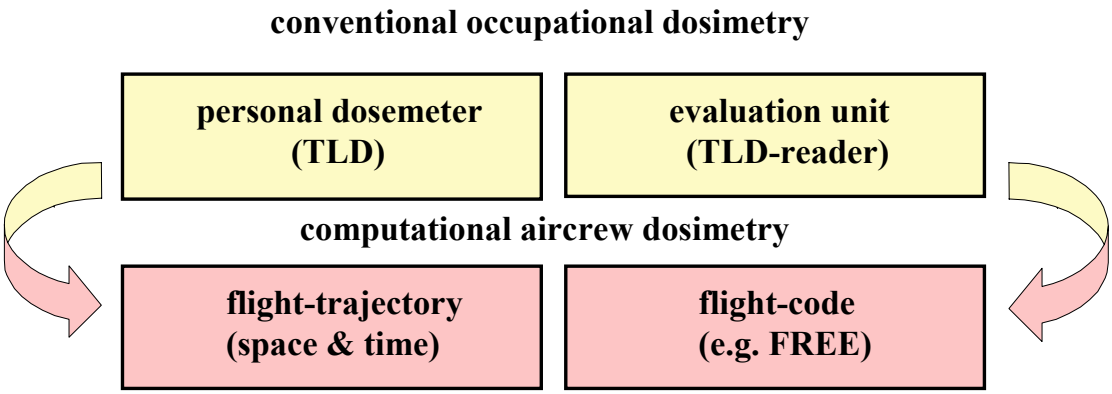

Figure B 5 - 3: Correspondence conventional occupational/computational Aircrew Dosimetry

The flight-trajectory generator reconstructs standard flight-trajectories from different input possibilities (see Figure B 5 – 4). The resulting flight-trajectories consist of a series of complete flight-trajectory points having a standard time binning of at least one minute. Available point information is correctly interpolated: altitude profiles linear, flight-leg points along great circle segments. Due to this open architecture any non standard flight-trajectories are supported easily.
When a flight profile is unavailable, an advanced model is used, which is aircraft-type dependent, and can generate flight time and flight-path information.
These existing flight-trajectory generation possibilities may be extended in the future.
Any special data demands are coupled to FREE by means of an user specific converter program. These modules form FREE standard flight-trajectories from any available proprietary airline specific data.

Possibility 1: Generation from complete flight-trajectory points in space and time

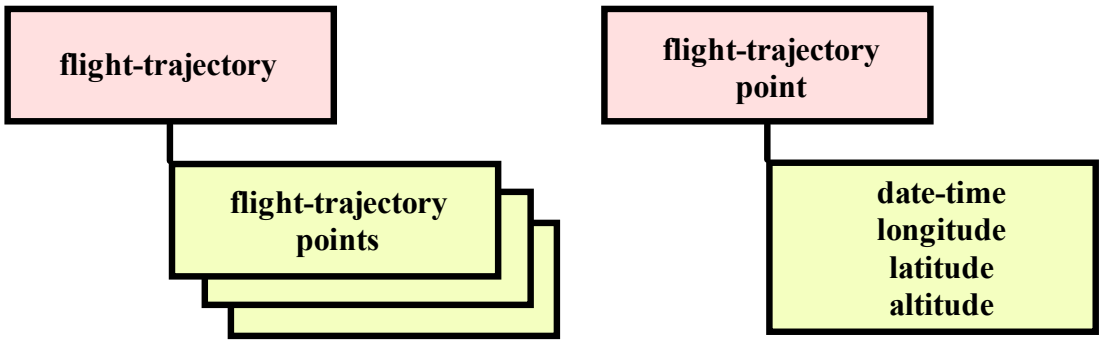

Possibility 2:Generation from flight-leg and altitude profile

- Flight-leg:

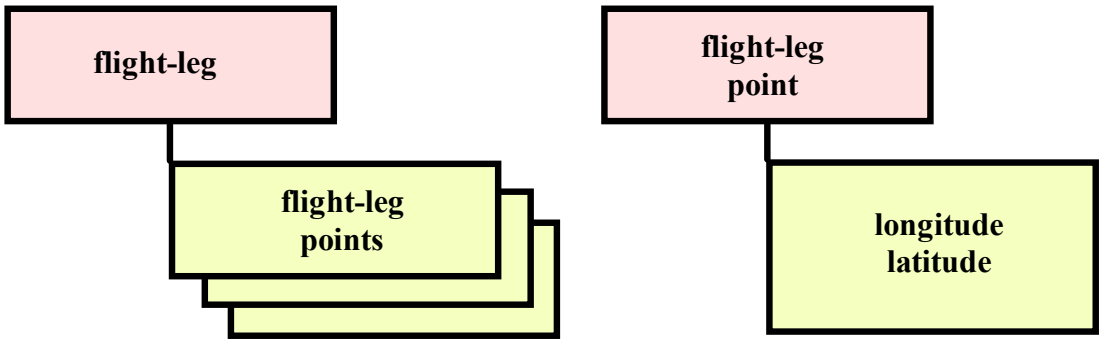

- Altitude profile: (Alternative: Flight-time/aircrafttype dependend model)

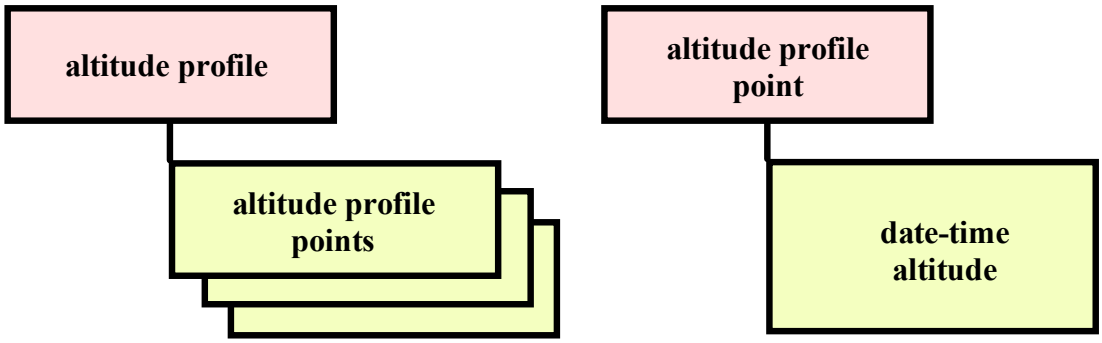

Figure B 5 - 4: Object model[5] of different flight-trajectory generation possibilities

- **B 5 - 4 - 2 THE CALCULATION ENGINES**

The calculation engines are the central dose assessment modules within FREE. They provide an ultrafast access mechanism to base-code results and approximate models respectively, which is definitely required for operational usage.

[5] The shadowed objects denote a collection/series.

Calculation engines give worldwide answers (every longitude/latitude, up to high altitudes) in the terms of dose rates[6] for either any solar activity or the duration of the special event in the case of short term variations.
Final flight-doses result from integration[7] of this time differential data over the complete flight-trajectory.

- **CGR COMPONENT**

The GCR component supplies the resulting radiation dose resulting from GCR impinging on the atmosphere and its variation with time in ultrafast access. Results can be given worldwide, up to 80 000 feets/24,4 km and for any solar conditions.
The GCR component obtains the necessary dose rate data from its base-code PLOTINUS. The ultrafast access mechanism is created by applying the "brute force method", also known as precalculation to the base-code PLOTINUS and reducing these results to a numerical function.
The radiation field in flight altitudes depends on altitude, the position within the earth magnetic field (latitude, longitude) and solar activity, hence the parameter space that is needed to be covered by precalculation is four dimensional. This parameter space was triangulated properly as follows:
The tridimensional spatial space was appropriately triangulated in altitude, latitude and longitude. The grid in altitude was created by dividing the altitude range from 0 until 80000 feet/24,4 km into some equally spaced atmospheric depth[8] regions. Additionally, to achieve very good precision for operational usage all common flight levels from 250 to 450 have been introduced separately as grid points. The complete altitude gridding was designed to achieve results that are within one per cent compared with the original base-code results of PLOTINUS.
The stronger dependency on latitude was taken into account by refining the grid in the meridional direction by a factor of three compared to its zonal subdivisions.
FREE takes into account the fact that there is not a 1-1 correspondence between the vertical cut-off and the radiation field below it, but that the radiation field is dependent on latitude and longitude (see section B 5 – 3 –1). The effect of this so called "yield approximation" is significant in flight altitudes, especially at low geomagnetic latitudes.
The final dataset in space consists of about 75000 single data points in three dimensions. To create continous access to the spatial parameter space this discrete dataset has been interpolated with advanced multivariate B-Spline methods (De Boor, 1972, 1978, 1979) (Visual Numerics, 2003).

Trivariate tensor product spline interpolation in space

The trivariate tensor-product spline interpolant to data (x_i, y_j, z_k, f_{ijk}), has the form:

[6] Except for the approximate FOA (First Order Approximation) method many physical quantities were calculated (scalar fluxes, absorbed/effective doses, ambient dose equivalents, ionizations) and are provided resolved for each particle type and other criteria.
[7] An efficient integration routine for integration of tabular data is used.
[8] The quantity atmospheric depth removes much of the complexity of dealing with the physics of a material which has a constantly changing density and is defined as the amount of absorbing mass of air per unit area above the point of interest. It is therefore equivalent to the quantity grammage often used in radiation physics.

$$\sum_{l=1}^{N_x}\sum_{m=1}^{N_y}\sum_{n=1}^{N_z} c_{nml} B_{n,k_x,t_x}(x) B_{m,k_y,t_y}(y) B_{l,k_z,t_z}(z) \tag{9}$$

where k_x, k_y, and k_z are the orders of the splines, t_x, t_y, and t_z are the corresponding knot sequences and c_{nlm} the tensor-product B-spline coefficients.
Tensor-product spline interpolants can be computed quite efficiently by solving repeatedly three univariate interpolation problems, that can be reduced to the well known *bivariate* tensor-product problem (De Boor, 1978, page 347).
The value of the resulting trivariate tensor-product spline (represented as a linear combination of tensor-product B-splines) at a given point is finally represented as:

$$S(x,y,z) = \sum_{l=1}^{N_x}\sum_{m=1}^{N_y}\sum_{n=1}^{N_z} c_{nml} B_{n,k_x,t_x}(x) B_{m,k_y,t_y}(y) B_{l,k_z,t_z}(z) \tag{10}$$

Linear interpolation in solar activity (time)

Solar activity is varies with the about 11 years solar cycle. However the simple model of an uniform smooth sinusoidal solar cycle is inappropriate. Furthermore during the last 50 year solar activity has been steadily increasing. All these difficulties are taken into account into FREE's solar activity handling.

To consider the 4th dimension of the parameter space, the solar activity, 18 complete spatial grids have been precalculated at certain solar conditions. Interpolation is done linearly, between the spatial results of the appropriate values of the heliocentric potential.
The gridding in solar activity was constructed non-uniformly to take into account the convex dependence of the results from the modulation parameter. It is finer at low heliocentric potentials (higher dose rates) and gets larger at high heliocentric potentials (lower dose rates), covering an extreme range from 0-3000 MV. (The extreme monthly averaged heliocentric potential values over the last three SACs are 400 MV for solar minimum and 1600 MV for solar maximum respectively.) This large range of values has been chosen to be prepared for non uniform solar cycles and to take large Forbush Decreases into account correctly (see Section B – 5-4-2, Forbush Decrease Model).

The final calculation is even not restricted to that (large) range, since values out of this range (0-3000 MV) are extrapolated, so the component works for any possible solar activity.

FREE GCR results have been compared sucessfully with a large amount of available experimental data.

o TRANSIENT VARIATIONS OF THE RADIATION FIELD

The radiation field in aircraft altitudes is not constant – it varies in time with the progress of the solar cycle. Furthermore transient effects maybe superimposed and can significantly modify the radiation field during the course of a flight. They may either increase the dose rate (ground level events, or GLEs) or reduce it (Forbush decreases (FDs)/fast decreases), see Figure B - 5 - 5.

FREE handles also these short term variations without compromises.

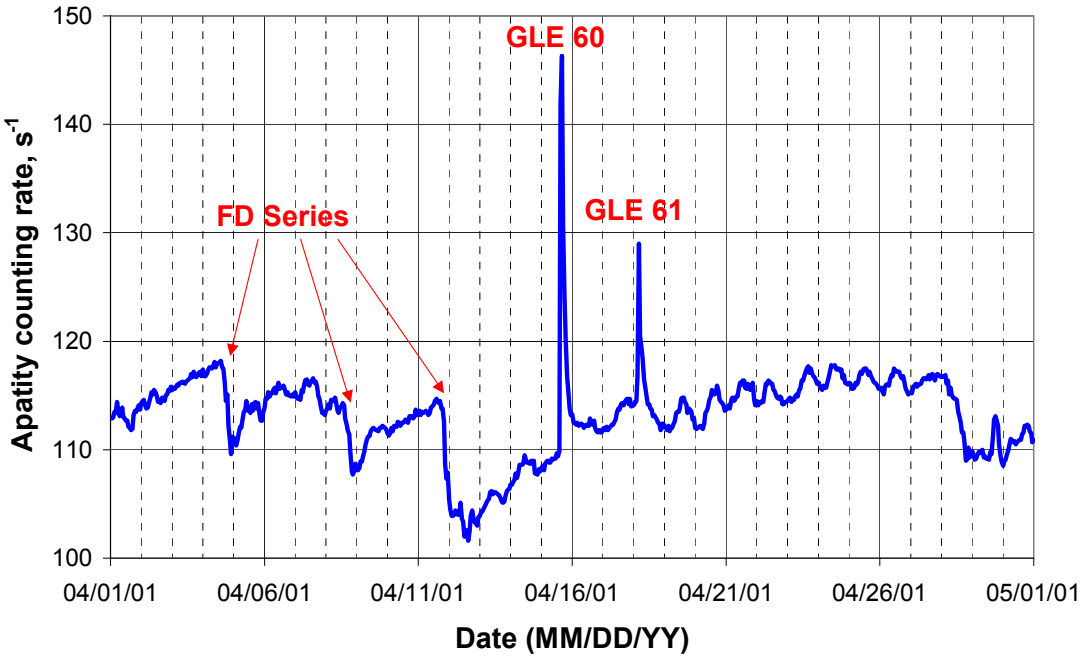

Figure B 5 - 5: Cosmic ray intensity April 2001, Apatity (2003)

- **SPEs COMPONENT**

Solar particle events can significantly enhance the radiation environment at aircraft altitudes. During large events additional doses contributions to individual flights for near polar subsonic flights of several mSv are possible (Dyer, 2001). Such large events are relatively seldom (~ one large event occurs per SAC), but it is important to have tools available to correctly take into account such effects.
The worst case event (GLE 5) from 23.Februray 1956 was even estimated by different sources to have very large effects (Armstrong, 1996) (Wilson, 2000).

The significant effect for additional doses in flight altitudes is the so called Ground Level Event (GLE). A GLE is a solar-particle-event that has a measurable effect on the worldwide neutron monitor network. Usually, an increase of more than two per cent count rate observed by at least two neutron monitor stations around the globe is regarded as a GLE. Aircrafts are flying near the earth surface, where the neutron monitors are located, so the GLE is the effect of choice that should be estimated to consider additional doses for the flying personnel.
Until today only 64 GLEs have been registered – so only a few solar particle events can reach aircraft altitudes (~ 1/year).

FREE considers GLEs by the means of two methods:

Adjoint Method

This method mirrors the approach that is described in Section B 5 – 3 - 2 the SOLAR SUITE and O'Brien (2002). The results are obtained by means of an ex-post-facto-

calculation and are provided with ultrafast access by an sophisticated cache data structure.
The Adjoint approach represents today's best available technical possibilities.
We have applied this approach to the series of September/October 1989 (GLE 42-45) to obtain the magnitudes of distribution from an representative selection of GLEs. Also an estimation of the worst case event (GLE 5) was made.
The results of these calculations clearly show the effect of the soft particle spectra associated with solar particle events, as compared to cosmic ray, resulting in a greater sensitivity to the geomagnetic field, and, unlike cosmic rays, the near-absence of a "knee" near 60° geomagnetic latitude.

FOA (First Order Approximation) Method[9]

The Adjoint method relies, to be correctly applied, on the availability of neutron monitor data, covering the complete geomagnetic field and needs a formidable computer time to be calculated.
However professional operational use needs fast dose estimations. Therefore an approximate method called First Order Approximation (FOA) was developed. This method is able to act as Now-Cast system, this means it is able to deliver its results in near real time.
This method gives only approximate results and cannot take into account different spectral differences and anisotropies.

The FOA-method is based solely on the relative increase over background of a single reference neutron monitor station, which is corrected to give finally dose rates:

$$\begin{aligned} \dot{E}_{\text{SPE-FOA}}(\text{RelInc}_{\text{NM}_{\text{Ref}}}, R_C, h) &= C_1 \times C_2 \times \text{RelInc}_{\text{NM}_{\text{Ref}}} \\ C_2 &= C_2(\text{RelInc}_{\text{NM}_{\text{Ref}}}, R_{C,}\ h) \\ C_1 &= const \end{aligned} \tag{11}$$

The correction factor C_2 is a function of relative increase (RelInc[10]), vertical cutoff rigidity (R_c) and of altitude (h). It was determined by an sophisticated numerical analysis of our Adjoint-Method results of GLE 5 and the series GLE 42-45. These events are believed to be a representative GLE series of all possible sizes.

$$C_2(\text{RelInc}_{\text{NM}_{\text{Ref}}}, R_C, h) = \frac{\dot{E}_{\text{SPE-Adjoint}}(\text{Date-Time}, R_C, h)}{\text{RelInc}_{\text{NM}_{\text{Ref}}}(\text{Date-Time})} \tag{12}$$

C_2 factors have been calculated from the Adjoint-Method results and the corresponding relative increases over background of the reference neutron monitor station according Equation 12 over the complete duration of the events. These results have been sorted into a three dimensional grid (with proper averaging). This grid has

[9] GLE 60 results of a preliminary FOA version have been used in to construct the solar flare model in Lewis, et al., 2002.
[10] Neutron monitor counting rates are taken into account only on a hourly basis, since this time binning is a reasonable granularity for aircrew dosimetry purposes and counting rates of neutron monitor stations are often not available in smaller time frames.

the dimensions relative increase, vertical cutoff rigidity, both with a suitable classification of data, and altitude.

This three dimensional regular data grid was finally numerically fitted with multivariate B-Spline methods using tensor-product cubic splines in all variables.

Trivariate tensor product spline fit

The trivariate tensor-product product spline approximant to gridded three dimensional data (x_i, y_j, z_k, f_{ijk}), specified by the three vectors x, y, z of length k, l, m respectively, to be fit using weighted least squares is given by:

$$\sum_{s=1}^{N_x}\sum_{t=1}^{N_y}\sum_{u=1}^{N_z} c_{stu} B_{stu}(x,y,z) \tag{13}$$

where c_{stu} are the tensor-product B-spline coefficients. These coefficients can be determined by solving the normal equations in tensor-product form as discussed in de Boor (1978, Chapter 17). The final result produces coefficients *c* minimizing

$$\sum_{i=1}^{k}\sum_{j=1}^{l}\sum_{p=1}^{m} w_x(i) w_y(j) w_z(p) \left[\sum_{s=1}^{K}\sum_{t=1}^{L}\sum_{u=1}^{M} c_{stu} B_{stu}(x_i, y_j, z_p) - f_{ijp} \right]^2 \tag{14}$$

where the function B_{stu} is the tensor-product of three B-splines of order k_x, k_y, and k_z. Specifically, we have

$$B_{stu}(x,y,z) = B_{s,k_x,t_x}(x) B_{t,k_y,t_y}(y) B_{u,k_z,t_z}(z) \tag{15}$$

The final approximating tensor-product spline, specified by order the orders k_i and the corresponding knot sequences t_i in the variables i (i=x,y,z), is given by:

$$S(x,y,z) = \sum_{s=1}^{N_x}\sum_{t=1}^{N_y}\sum_{u=1}^{N_z} c_{stu} B_{stu}(x,y,z) \tag{16}$$

The factor C_1 corrects the dose rates by 0,5 of the possible range of dose rates in the different relative increase classes in polar regions (which is most the important region). This number is nearly independent of altitude and was therefore chosen to be constant. So the final FOA results are designed to be rather conservative estimates.

FOA results have been compared very successfully with recent measurements of GLE 60 (Spurny, 2001) (Bartlett, et al., 2001).

FOA results of all GLE events from the beginning of SAC 20 until now (GLE 15 – GLE 64) are included within FREE. The following references and resources have been used to apply the method to available data and were of great help: (Kananen, et al., 1991)(Kudela, et al., 1993), (Shea, Smart, 1993), (Apatity, 2003), (Oulu, 2003).

To validate FOA results in operational use they are checked against the Ajoint Method. If the results are not within acceptable error limits, the FOA result is corrected by the better Adjoint method.

- **FORBUSH DECREASE MODEL**

Solar activity is a slowly varying parameter only on a large time scale, on a daily or weekly basis solar activity can fluctuate widely. These are the normal up and downs in the solar cycle. The effect is more pronounced at the more disturbed solar maximum times. The most obvious effect of this short term changes in solar activity is a Forbush decrease (Lockwood, 1971)(Cane 1996, 2000).
A Forbush decrease is a sudden decline in cosmic ray background intensity due to magnetic shielding effects and other interplanetary disturbances. Larger Forbush decreases (>4%) occur on average about every two month, more often in solar maximum times, more seldom in solar minimum times.

FREE takes Forbush Decreases and other fast changes in solar activity by routine application of the completely local heliocentric potential modulation model on a hourly basis. In this sense the disturbed conditions within a fast solar activity change are described by the usual quiet conditions applied with an different modulation parameter. So its easy to take into account all transient variations in cosmic ray intensity (except for GLEs, which are correctly described by the SPE component).

Larger Forbush decreases can reduce the doses up to the order of 20%. This FREE Forbush decrease model was successfully compared with recent measurements of such effects (Kyllönen, et al., 2001)(Schrewe, 1999)(Spurny, 2002).

- **B 5 - 4 - 3 UPATE COMPONENT**

FREE is a sophisticated flight code that takes also into account short term variation effects. Because of this level of detail it depends strongly on continuous data updates.
These data updates are managed by the update component, which consist of a server and a client part.
The server part is serviced at IASON, where experts monitor solar activity and provide data updates on a daily basis. The client part on user side works either in dynamic online mode over an internet communication channel or on request in offline mode on a file update basis.
Data updates consist of two principal parts:

1.) Solar Activity:

The heliocentric potential is obtained from high-latitude neutron monitor counting rates. As high-latitude monitors are unaffected by the geomagnetic field (and their cutoff is insensitive to magnetic activity), they may be used interchangeably—in case one of them should be down during a critical period. The potentials obtained are in “real time” and thus may be used immediately; allowing the correct treatment of

Forbush decreases and quick decreases which may have a significant effect on the cosmic-ray dose rate delivered during the hours of a given aircraft flight.
We do not depend on a single neutron monitor to determine solar activity level so that if one of our monitors is down a critical time, we can easily use another.

2.) GLEs:

Solar activity is monitored continuously. In the case of an GLE , FOA results are supplied with the next daily update cycle after the end of the event. FOA results are regularly checked against the more sophisticate Adjoint Method of the SOLAR SUITE as soon as possible.

- **B 5 – 5 SUMMARY**

A flight-code was developed for professional operation usage. It is able to take into account every aspect of computational aircrew dosimetry, data updates are provided through different update channels in short intervals.
The possibility of taking account of any shielding effect of the aircraft hull is also available.

Work partly supported by:

- Staatlich akkreditierte Prüf- und Überwachungsstelle
  STRAHLENMESSTECHNIK GRAZ – des Vereines zur Förderung der Strahlenforschung
  Steyrergasse 17, A-8010 Graz, Austria
- Institut für Technische Physik, TU-Graz, Petersgasse 16/4, A-8010 Graz, Austria

References:

Apatity (2003), PGI - Polar Geophysical Institute, *Cosmic Ray Station Website*, http://pgi.kolasc.net.ru/CosmicRay/, 2003

Armstrong, T. W., Alsmiller Jr., R.G. (1969), Calculation of the Radiation Hazard at Supersonic Aircraft Altitudes Produced by an Energetic Solar Flare, *Nuclear Science and Engineering*, 37, 337-343

Alsmiller, F. S. (1965). A general category of soluble nucleon-meson cascade equations, *ORNL-3746*, 1965

Bartlett, D., et. al. (2001). Investigation of Radiation Doses at Aircraft Altitudes during a Complete Solar Cycle. *Proceedings SOLSPA Space Weather Workshop*, Vico Equense Italy, 25-29 September 2001

Cane, H. V., Richardson, I.G., Rosenvinge, T.T. (1996). Cosmic Ray Decreases 1964-1994. *Journal of Geophysical Research*, 101, A10, 21561-21572

Cane, H. V. (2000), Coronal Mass Ejections and Forbush Decreases, *Space Science Reviews*, 93, 55-77

Dyer, C. (2001), Radiation Effects on Spacecraft & Aircraft, *Proceedings SOLSPA Space Weather Workshop*, Vico Equense Italy, 25-29 September 2001

De Boor, C. (1972). On Calculating with B-Splines, *Journal of Approximation Theory,* Vol. 6, 50-62

De Boor, C. (1978). A Practical Guide to Splines. Applied Mathematical Sciences 27, Springer Verlag New York Inc.

De Boor, C. (1979). Efficient Computer Manipulation of Tensor Products, *ACM Transaction on Mathematical Software*, Vol.5, No.2, June 1979, 173-182

Elliott, J. P. (1955), Milne's Problem with a Point-Source. *Proceedings of the Royal Society of London. Series A, Mathematical and Physical Sciences*, Vol. 228, No. 1174. (Mar. 8, 1955), 424-433.

Felsberger, E., O'Brien, K., Kindl, P. (2000) MOZAIC-Database Flightroute Calculations. *Unpublished Results*, Technical University Graz, Technical Physics Department

Gaisser, T.K., Stanev, T.(1998). Cosmic Rays, *European Physics Journal C*, 3, 132-137

Garcia-Muñoz, M., Mason, G.M., and Simpson, J.A, (1975). The anomalous ^{4}He component in the cosmic-ray spectrum at $\sim<$ 50 MeV per nucleon during 1972-1974. *Astrophysics Journal,* 202, 265-275

Gleeson, L. J., Axford, W. I., (1967), cosmic rays in the interplanetary medium. *Astrophysics Journal*, 149L, 115-118

Heinrich, W., Spill, A. (1979). Geomagnetic shielding of cosmic rays for different satellite orbits. *Journal of Geophysical Research, 84*, No. A8, 4401-4004

Kananen, H., Tanskanen, L.C., Gentile, L.C., Shea, M.A., Smart, D.F., (1991), A Quarter of a Century of Relativistic Solar Cosmic Ray Events Recorded by the Oulu Neutron Monitor. *22nd International Cosmic Ray Conference Contributed Papers*, 3, 145-148, Institute for Advanced Studies, Dublin, Ireland

Kudela, K., Shea, M.A., Smart, D.F., Gentile, L.C., (1993) Relativistic Solar Particle Events Recorded by the Lomnicky Stit Neutron Monitor, *23rd International Cosmic Ray Conference Contributed Papers*, 3, 71-74, The University of Calgary, Calgary, Canada

Kurochkin, I.A., Wiegel, B., Siebert, B. R. L. (1999). Study of the Radiation Environment caused by Galactic Cosmic Rays at Flight Altitudes, at the Summit of the Zugspitze and the PTB Braunschweig. *Radiation Protection Dosimetry*, 84, 4, 281-291

Kyllönen, J.-E., Lindborg, L., Samuelson, G. (2001). Cosmic Radiation Measurements on-Board Aircraft with the Variance Method. *Radiation Protection Dosimetry*, 93, 3, 197-205

Larson, M. O., (1968). Muon Fluxes Deep Underground, *PhD Thesis*, University of Utah, UMI Dissertation Services, 1968

Lewis, B. J., *et al.*, (2002), Galactic and Solar Radiation Exposure to Aircrew during a Solar Cycle, *Radiation Protection Dosimetry*, 102, 3, 207-227

Lockwood, J.A., (1971). Forbush Decreases in the Cosmic Radiation. *Space Science Reviews,* 12, 658-715

Molina-Cuberos, G. J., Lopez-Moreno, J. J., Rodrigo, R., Lara, L. M., O'Brien, K., (1999). Ionization by cosmic rays of the atmosphere of Titan, *Planetary and Space Science 47*, 1347-1354

O'Brien, K., Sauer, H., (2000). An Adjoint Method of Calculation of Solar-Particle-Event Dose Rates. *Technology*, 7, 449-456

O'Brien, K., (2002a). The Theory of Cosmic-Ray and High-Energy-Solar-Particle Transport in the Atmosphere, *Seventh International Symposium on the Natural Radiation Environment*, Rhodes, Greece, May 21, 2002

O'Brien, K., Sauer, H., (2002b). On the Atmospheric Response to Solar Particle Events. *34th Scientific Assembly of the Committee on Space Research (COSPAR)*, Houston, TX, October 17, 2002 (to be published in *Advances in Space Research*)

Passow, C., (1962). Phenomenologische Theorie zur Berechnung einer Kaskade aus schweren Teilchen (Nukleonenkaskade) in der Materie (Phenomenological theory for the calculation of a cascade of heavy particles (nucleonic cascade) in matter.) *Notiz A 285*, Deutsches Elektronen Synchrotron, Hamburg, 1962

Pelliccioni, M., (1999). Radiation Weighting Factors and Conversion Coefficients for High-Energy Radiation. *SATIF-4*, In. Proc. Workshop, Knoxville, 17-18 September 1998, 179-192 (OECD)

Pelliccioni, M., (2000). Overview of Fluence to Effective Dose and Fluence-to-Ambient Dose Equivalent Conversion Coefficients for High Energy Radiation calculated using the FLUKA Code. *Radiation Protection Dosimetry* 88(4): 279-297

Roesler, S., Heinrich, W., Schraube, H., (1998). Calculation of Radiation Fields in the Atmophere and Comparison to Experimental Data, *Radiation Research*, 149, 87-97

Rudstam, G., (1966). Systematics of spallation yields, *Zeitschrift für Naturforschung,* A21, 1027-1041

Schäpers, A., (1998). Kurze Leine-Lokale COM Server und Clients. *c't Magazin für Computertechnik*, 3/98, 174-181

Schrewe, U., (1999). ACREM Air Crew Radiation Exposure Monitoring, Results from the In-Flight Measurement Program of the PTB: Summary of the Radiation Monitoring Data. *PTB Laborbericht PTB-6.31-99-1*, Braunschweig, August 1999

Schrewe, U., (2000). Global Measurements of the Radiation Exposure of Civil Air Crew from 1997 to 1999. *Radiation Protection Dosimetry*, 91, 347-364.

Shea , M. A., Smart, D. F., (1993). Solar Proton Events: History, Statistics and Predictions, in *Solar-Terrestrial Predictions IV*, Vol.2, edited by J. Hruska, M.A.Shea, D.F. Smart and G. Heckman, 48-70, NOAA, Boulder

Shea, M. A., Smart, D. F., (2000). Cosmic Ray Implications for Human Health, *Space Science Reviews*, 93, 187-205

Spurny, F., Dachev, T. (2001). Measurements on Board an Aircraft during an Intense Solar Flare, Ground Level Event 60, on April 15, 2001 (Letter to the Editor), *Radiation Protection Dosimetry*, 95,3, 273-275

Spurny, F., (2001). Private Communication

Oulu (2003), University Oulu, *Cosmic Ray Station Website*, http://cosmicrays.oulu.fi/, 2003

Williams, M. M. R., (1966). Approximate Solutions of the Neutron Transport Equation in Two and Three Dimensional Systems. *Nucleonik*, 9, 7, 305-312

Wilson, J. W., (2000). Radiation environments and human exposures, *Health Physics*, 79, 5, 470-494

Zerbe, K., (1997). Bausatz – Einführung in COM, DirectX und ActiveX. *c't Magazin für Computertechnik*, *8/97,* 286-291

Visual Numerics (2003), Visual Numerics IMSL Mathematical & Statistical Libraries, http://www.vni.com/products/imsl/, 2003

B 6 Calculations for Cosmic Ray Dosimetry at Aircraft Altitudes using FLUKA

A. Ferrari*, M. Pelliccioni° and T. Rancati+

* CERN, 1211 Geneva 23, Switzerland

° INFN, Laboratori Nazionali di Frascati, 00044 Frascati, Italy

+ INFN, Sezione di Milano, via Celoria 16, 20133 Milano, Italy

B 6.1 Method of calculation

In order to determine radiation doses at aircraft altitudes, calculations of atmospheric showers initiated by the galactic component of cosmic rays were carried out using the Monte Carlo transport code FLUKA[1,2].

The main elements of atmospheric shower calculation are:

- primary spectra (protons and ions up to nickel), obtained from a NASA code[3];
- the superposition model for primary nuclei (since FLUKA did not transport nuclei and fragments with A>1 at the time of present calculations);
- the interplanetary modulation according to the actual solar activity for a given day;
- the vertical rigidities from NASA compilation interpolated in the Störmer dipole approximation.

Since the calculations started in the early 1999, the primary spectra entered in the simulations are updated to 1998. As an example, Figure B 6.1 shows the primary spectra for protons and alpha particles corresponding to a value of the modulation parameter (or deceleration potential), Φ equal to 465 MV.

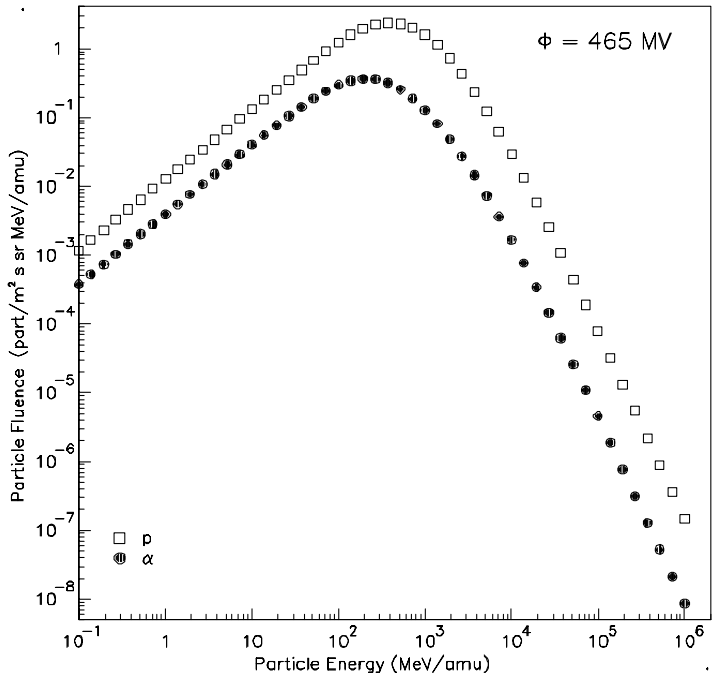

Figure B 6.1. Primary spectra (protons and alpha particles) entered in the calculations for solar activity corresponding to Φ =465 MV.

The spherical geometry of Earth and of its atmosphere (as a mixture of N, O and Ar) has been properly described. The atmosphere has been divided in 50 layers of different density, according to a parameterization of the standard atmosphere, down to about 0.1 g/cm^2.

The fluences of the secondary particles (neutrons, protons, photons, electrons, positrons, muons, charged pions) have been scored at different heights and geomagnetic locations. The assessment of the quantities of interest in radiological protection, namely effective dose rate and ambient dose equivalent rate, has been obtained by folding the scored particle spectra with appropriate sets of conversion coefficients. With the aim of comparing the results with those of other authors, the geometrical conditions of irradiation have been assumed to be isotropic. The conversion coefficients fluence to effective dose were taken from ICRP Publication 74[4] for low energy neutrons (from thermal to 20 MeV) and photons (below 50 keV) and according to ref. (5) for other particles and energies (Figure B 6.2).

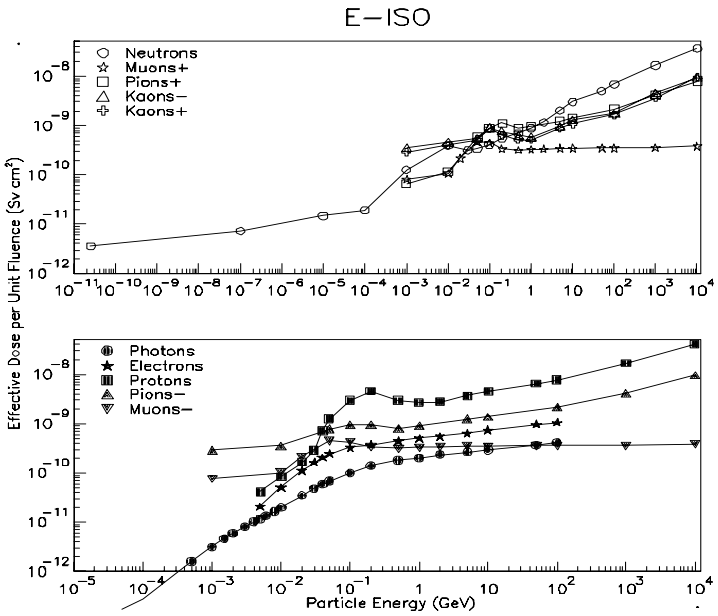

Figure B 6.2. Effective dose per unit of fluence for ISO irradiation as a function of particle energy (from ref.5).

As concerns the ambient dose equivalent, the conversion coefficients for low energy neutrons (from thermal to 12 MeV) were taken from ICRP Publication 74. Data for other particles and for neutrons of energy in excess of 12 MeV were taken from ref. (5) (Figure B 6.3).

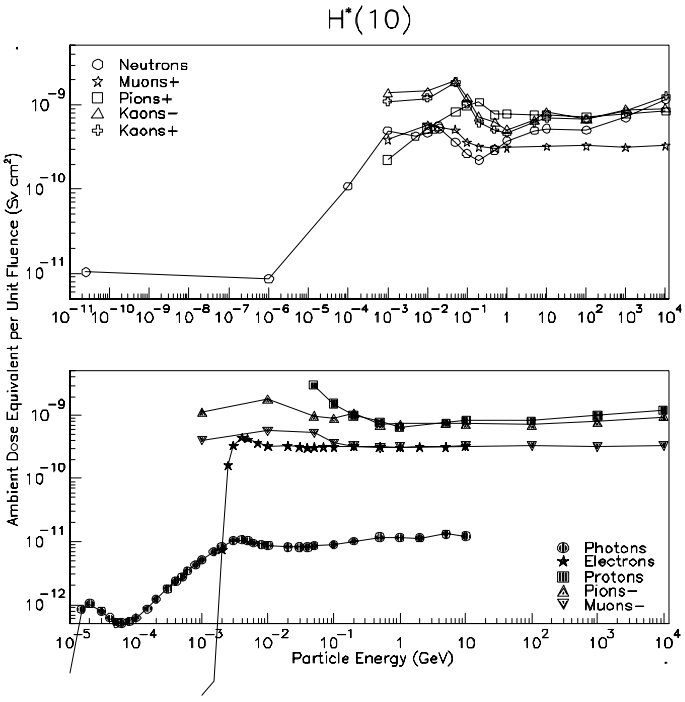

Figure B 6.3. Ambient dose equivalent per unit of fluence as a function of particle energy (from ref.5).

The simulations were carried out entering primary spectra corresponding to values of Φ equal to 465 MV (characteristic for minimum solar activity) and 1440 MV (characteristic for maximum solar activity), and for values of vertical cut-off rigidity, R_V, of 0.0, 0.4, 3.0, 6.1, 9.0, 12.0, 15.0 and 17.6 GV. Further calculations have been performed for values of Φ of 600, 800, 1000 and 1200 MV, but only for vertical cut-off of 0.4, 3.0 and 6.1 GV.

The calculated results as well as the comparison with the results of other codes and experimental measurements can be found in refs. (6,7,8). A summary of the calculated results, in form of graphical presentation, is given in the next sections.

B 6.2 Results

B 6.2.1 Influence of solar activity and geomagnetic shielding

The influence of solar activity and geomagnetic cut-off on the intensity of the various components of the radiation field at aircraft altitudes can be seen in Figures B 6.4 and B 6.5. Figures B 6.4 and B 6.5 show the calculated fluence rates of the hadron and the electromagnetic and muon components, respectively, as a function of altitude, for extreme values of vertical cut-off (0.4 and 17.6 GV) and modulation parameter (465 MV and 1440 MV). Since the solar modulation has little influence on the primary spectra for high values of the vertical cut-off, only the data at Φ 465 MV are plotted for the vertical cut-off of 17.6 GV. Because of lack of space the calculated results for positrons are omitted in these Figures.

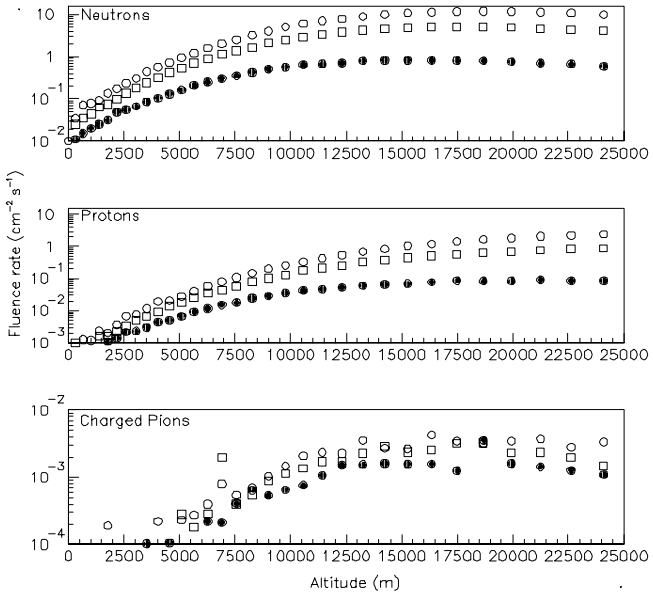

Figure B 6.4 Calculated hadron fluence rates as a function of altitude. ❍ **R_V=0.4 GV, Φ = 465 MV**. □ **R_V=0.4 GV, Φ =1440 MV**. • **R_V=17.6 GV, Φ =465 MV.**

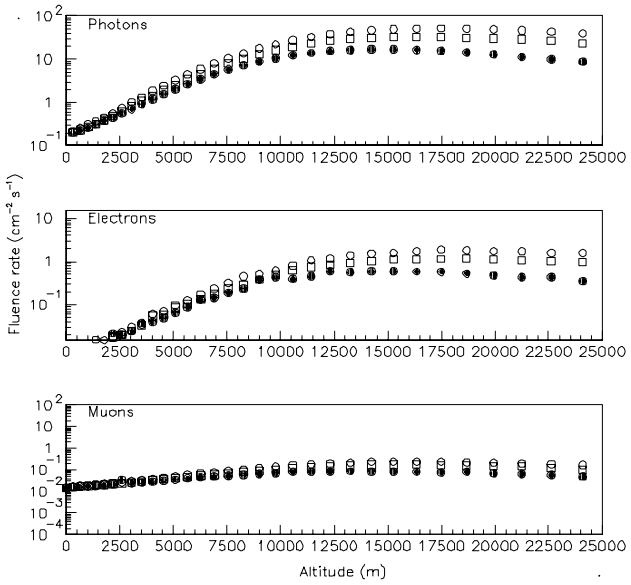

Figure B 6.5 Calculated electron, photon and muon fluence rates as a function of altitude. Key as Figure B 6.4.

Figure B 6.6 and B 6.7 show the effective dose rate as a function of altitude for several values of vertical cut-off rigidity and for the extreme values of the modulation parameter investigated (Φ = 465 and 1440 MV respectively). It is seen that the protection quantity may vary within a factor of about 2.0 due to solar modulation and up to a factor 15 due to geomagnetic latitude.

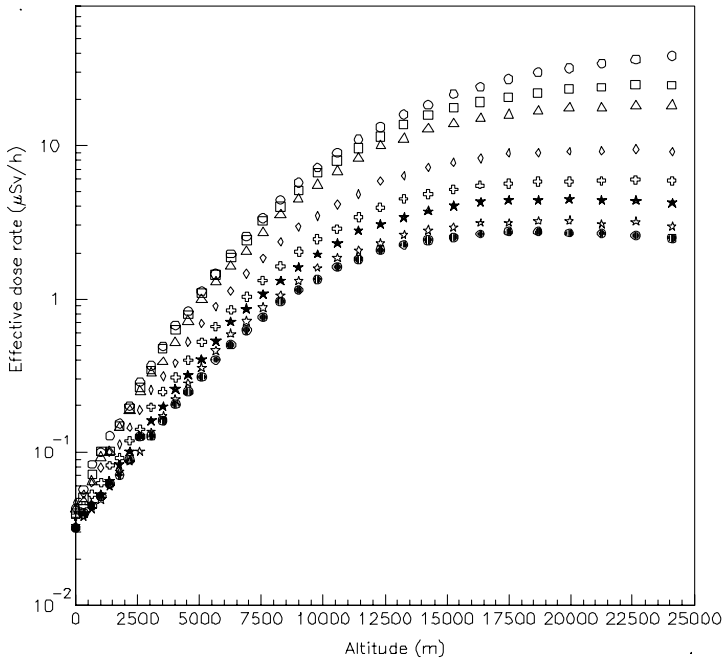

Figure B 6.6 Calculated effective dose rate as a function of altitude for several geomagnetic cut-off and Φ =465 MV. ❍ 0.4 GV. □ 2.0 GV. Δ 3.0 GV. ◊ 6.1 GV. ⍜9.0 GV. H 12.0 GV. I =15.0 GV. l 17.6 GV.

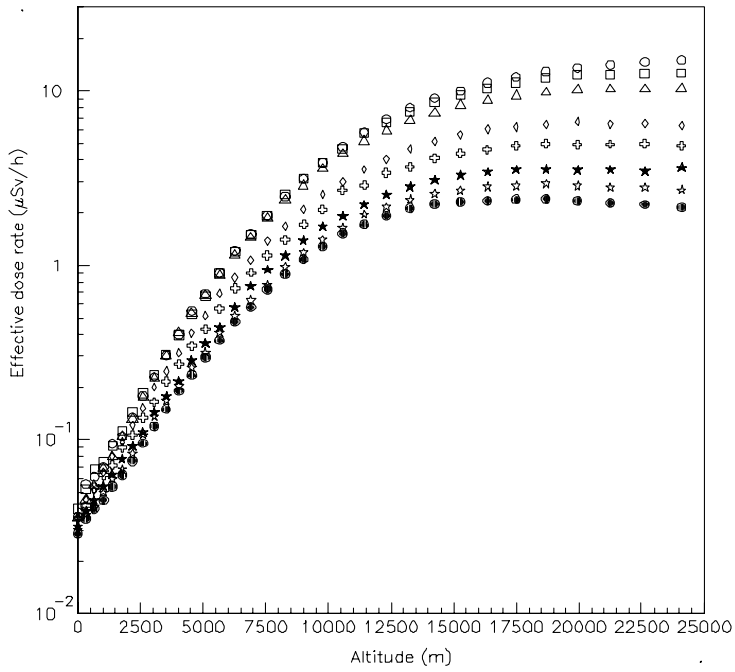

Figure B 6.7 Calculated effective dose rate as a function of altitude for several geomagnetic cut-off and Φ = 1440 MV. Key as Figure B 6.6.

B 6.2.2 Contributions of the various components of the radiation field

Figure B 6.8 illustrates, as an example at an altitude of 10580 m, the particle fluence rate for the various components of the radiation field, corresponding to Φ = 465 MV, as a function of the vertical cut-off rigidity. It can be noted that, in the region between 0 and 3 GV, the fluence rates of neutrons and protons are slightly decreasing, while those of other kinds of radiation are practically constant.

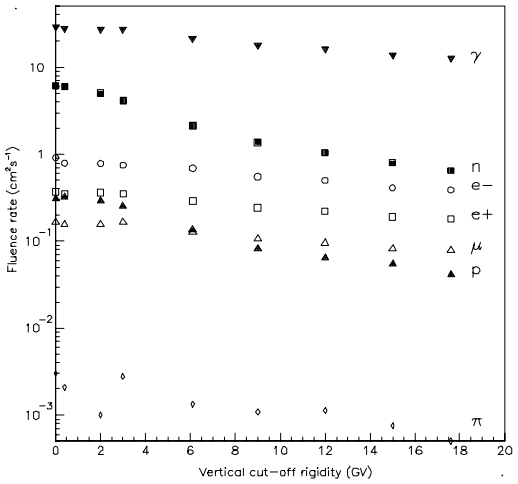

Figure B 6.8 Calculated particle fluence rate of the various components of the radiation field as a function of the vertical cut-off rigidity for an altitude of 10580 m and Φ =465 MV.

In order to highlight the contributions of the various types of secondary particles to the doses, Figures B 6.9 and B 6.10 show the effective dose rates and the ambient dose equivalent rates corresponding to the fluence rates of Figure B6.8, together with the total doses.

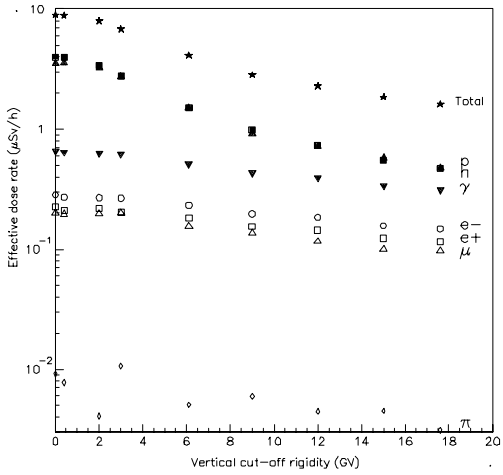

Figure B 6.9 Contributions of the various types of radiation to the effective dose rate as a function of the vertical cut-off rigidity for an altitude of 10580 m and Φ =465 MV.

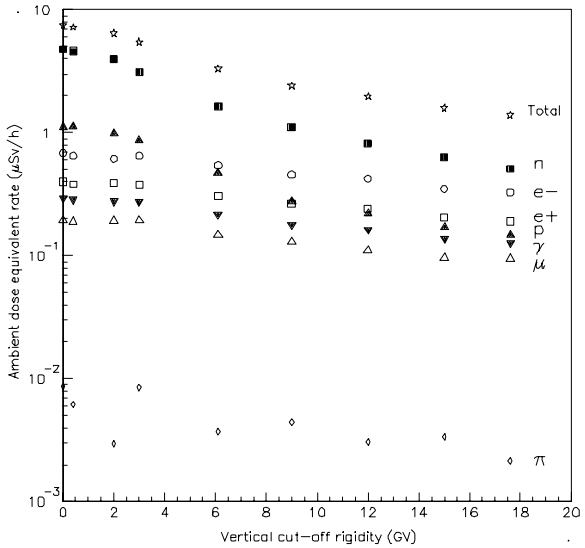

Figure B 6.10 Contributions of the various types of radiation to the ambient dose equivalent rate as a function of the vertical cut-off rigidity for an altitude of 10580 m and Φ =465 MV.

The effective dose rate and the ambient dose equivalent rate in the region 0.0-3.0 GV are primarily due to neutrons and protons. For vertical cut-off in excess of 3 GV, the major contribution to the ambient dose equivalent rate is due to neutrons and electrons. The neutron component varies between 29% and 44% of the total in the case of effective dose, and between 36% and 64% for the ambient dose equivalent.

The contribution of the individual secondary particles to both the quantities are constant up to 3.0 GV in the case of electrons, positrons, photons, muons and charged pions. Conversely, in this region, the contributions of neutrons and protons decrease as a function of the vertical cut-off at a higher degree than the fluence rates. As a result, the total effective dose rate and ambient dose equivalent rate are also slightly decreasing in this region.

B 6.2.3 Dependence of the doses on the various parameters

The calculated effective dose rates at flight altitudes (see Figures B 6.6 and B 6.7) have been analyzed with the aim to determine the dependence of the doses on the various parameter involved (altitude, vertical rigidity, solar activity).

As an example, Figure B 6.11 shows the calculated effective dose rate as a function of vertical cut-off for several flight altitudes ranging from 8270 m to 16360 m and Φ =465 MV. Conversely, Figure B 6.12 shows the calculated effective dose rate as a function of altitude up to 16360 m for several values of vertical cut-off and Φ =1440 MV.

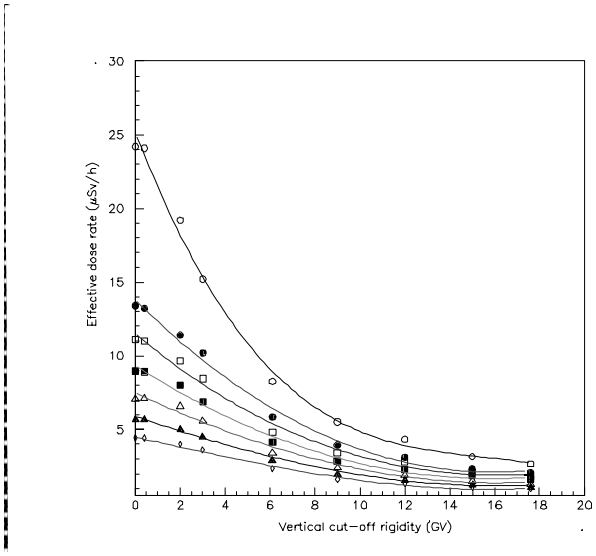

Figure B 6.11 Calculated effective dose rate as a function of vertical cut-off rigidity for various altitudes and Φ =465 MV. ◊ h=8270 m. □ h=9000 m. Δ h=9770 m. ■ h=10580 m. □ h=11430 m. l h=12320 m. ❍ h=16360 m.

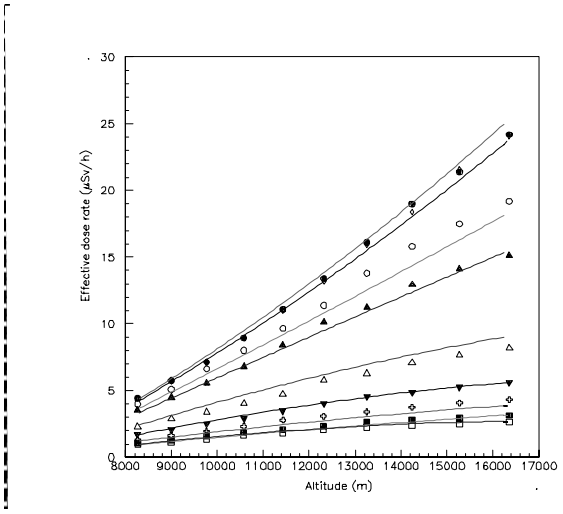

Figure B 6.12 Calculated effective dose rate as a function of altitude for various vertical cut-off rigidity and Φ =465 MV. l R_V=0.0 GV. ◊ R_V=0.4 GV. ❍ R_V=2.0 GV. s R_V=3.0 GV. Δ R_V=6.1 GV. t R_V=9.0 GV. 9 R_V=12.0 GV. ■ R_V=15.0 GV. □ R_V=17.6 GV.

The effective dose rate as a function of vertical rigidity can be approximated with polynomials of the third degree and as a function of altitude (from 8270 m to 16360 m) with polynomials of second degree. Therefore, simple equations have been proposed in ref. (8), giving the effective dose rate as a function of vertical rigidity in the altitude range from about 8000 m to 16500 m. The dose assessment performed by means of these equations approximate the calculated results within 10-15% or better.

For purposes of dose estimates for intermediate levels of solar modulation, Figure B 6.13 shows the ratio of the effective dose rates calculated for Φ =465 MV and Φ =1440 MV as a function of altitude for various vertical cut-off rigidity. It can be seen that ratios significantly different from unity are associated only to values of vertical cut-off less than about 9 GV.

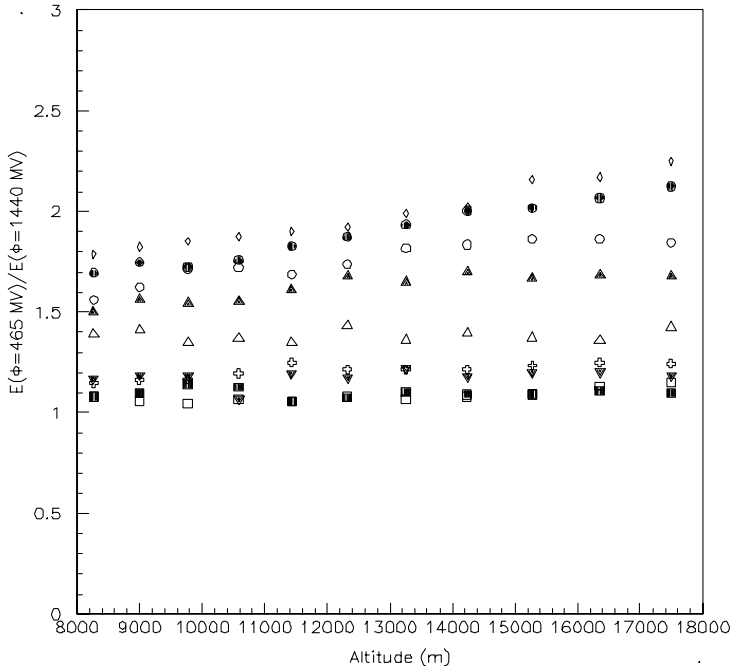

Figure B 6.13. Calculated ratio effective dose for Φ =465 MV to effective dose for Φ =1440 MV as a function of altitude for various vertical cut-off rigidity. Key as Figure B6.12.

Therefore, the dependence of the doses on the values of Φ has been better investigated by means of simulations carried out for vertical cut-off between 0.4 and 6.1 GV.

Figures B 6.14 shows the calculated effective dose rate as a function of the solar modulation parameter for two values of the vertical cut-off rigidity (0.4 and 3.0 GV) and three different altitudes.

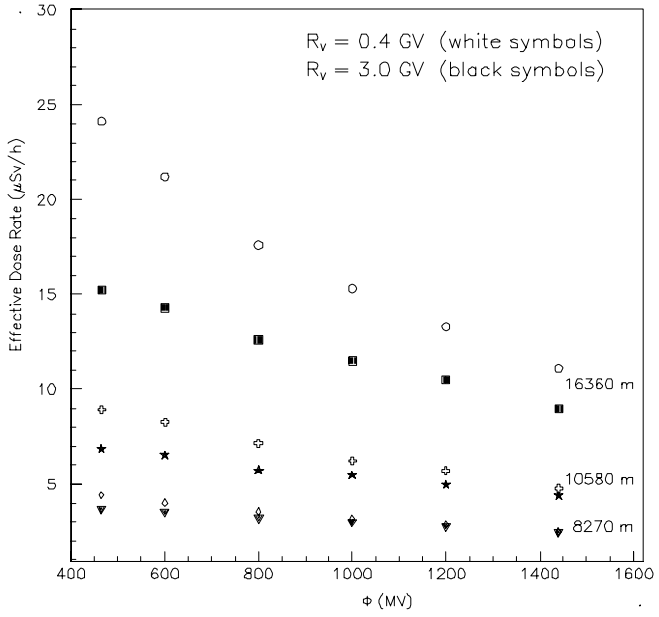

Figure B 6.14. Calculated effective dose rate as a function of the solar modulation parameter for two values of the vertical cut-off rigidity at different civil aviation altitudes.

The calculated results have shown that the linear dependence proposed in ref. (7) for the effective dose rate as a function of Φ can be considered as an acceptable approximation for R_V

greater than 3.0 GV, and below 3 GV when the altitudes do not exceed 10580 m. However, a better approximation of effective dose rate for the vertical cut-off rigidities of 0.4 and 3.0 GV can be derived from the plots of Figure B 6.14.

B 6.2.4 On the relationship between effective dose and ambient dose equivalent

As far as the ambient dose equivalent rate is concerned, Figure B 6.15 shows the calculated results from 9000 m to 25000 m on the sea level as a function of altitude for Φ =465 MV.

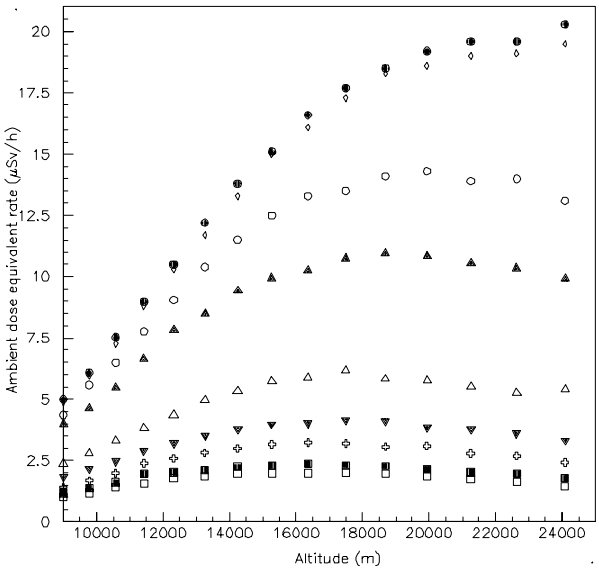

Figure B 6.15 Calculated ambient dose equivalent rate as a function of altitude for different values of the vertical cut-off rigidity and Φ =465 MV. Key as figure B6.12.

Figure B 6.16 shows the ratio effective dose to ambient dose equivalent at Φ =465 MV as a function of height above sea level for various geomagnetic cut-off. Depending on the geographical position and on the altitude, the underestimate of the operational quantity with respect to the protection quantity at aircraft altitudes varies up to about 40%. The main reason of that is the overestimation of E due to the enhancement of the proton contribution coming from an inappropriately high value of the radiation weighting factor recommended by ICRP for protons of energy above 10 MeV[9]. In order to have the ideal relation between protection and operational quantities, it should be enough to assign a value no greater than 2 to this component, as shown on Figure 9 of ref. (6).

Although the underestimate is within 15-20% at the usual flight altitudes, a dose evaluation based on H*(10) does not seem to be advisable. Due to legal and psychological reasons, in fact, a systematic underestimate of doses received by air crew members can not be accepted. However, since most devices are calibrated in terms of H*(10), the operational quantity can be useful in order to verify the predictions of Monte Carlo calculations.

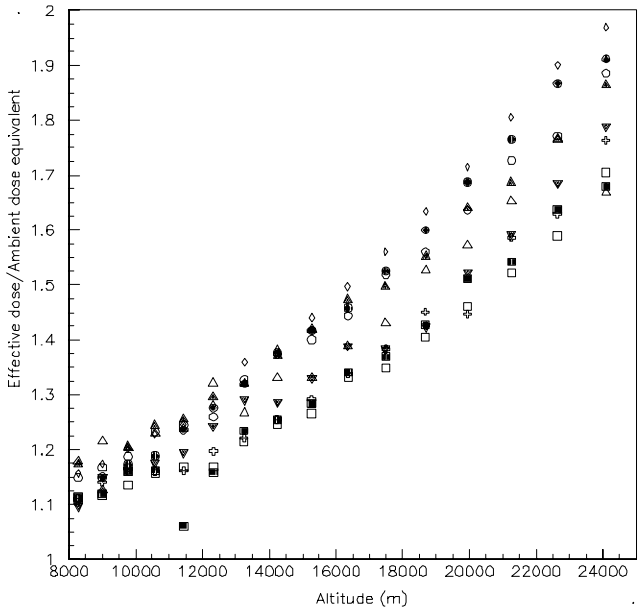

Figure B 6.16 Calculated ratio effective dose to ambient dose equivalent as a function of altitude for various vertical cut-off rigidities and Φ =465 MV. Key as Figure B6.12.

B 6.3 Conclusions

According to ICRP Publication 75[10], the overall uncertainty in the estimation of effective dose around the relevant dose limit may well be a factor 1.5 in either direction for photons and may be substantially greater for neutrons and for electrons. Greater uncertainties are also inevitable at low levels of effective dose for all qualities of radiation.

The calculated results and the simple equations proposed in ref. (7) allow determining the doses at aviation altitudes with a precision acceptable for scopes of individual dosimetry.

B 6.4 References

1. Fassò, A., Ferrari, A. and Sala, P.R. Electron-photon transport in FLUKA: status. Proceedings of the MonteCarlo2000 Conference, Lisbon, October 23-26 2000. Kling, A., Barao, F., Nakagawa, M., Tavora, L. and Vaz, P. - eds., Springer-Verlag Berlin, 159-164 (2001).
2. Fassò, A., Ferrari, A., Ranft, J. and Sala, P.R. FLUKA: status and prospective for hadronic applications. Proceedings of the MonteCarlo2000 Conference, Lisbon, October 23-26 2000. Kling, A., Barao, F., Nakagawa, M., Tavora, L. and Vaz, P. - eds., Springer-Verlag Berlin, 955-960 (2001).
3. O'Neill P.M. Program HIZ, private communication of L. Pinsky, Houston University, to A. Ferrari.
4. International Commission on Radiological Protection, Conversion Coefficients for use in Radiological Protection against External Radiation, ICRP Publication 74, Annals of ICRP, **26**, No. 3/4 (1996).
5. Pelliccioni, M. Overview of Fluence-to-Effective Dose and Fluence-to-Ambient Dose Equivalent Conversion Coefficients for High-Energy Radiation Calculated Using the FLUKA Code. Radiat. Prot. Dosim. **88**(4), 279-297 (2000).
6. Ferrari, A., Pelliccioni, M. and Rancati, T., The Role of the Quantities Used in Radiological Protection for the Assessment of the Exposure to Cosmic Radiation, Rad. Prot. Dosim. **83**(3), 199-210 (1999).
7. Ferrari, A., Pelliccioni, M. and Rancati, T., Calculation of the Radiation Environment Caused by Galactic Cosmic Rays for Determining Air Crew Exposure, Rad. Prot. Dosim. **93**(2), 101-114 (2001).

8. Ferrari, A., Pelliccioni, M. and Rancati, T., Study of the Dosimetric Characteristics of Cosmic Radiation at Civil Aviation Altitudes, Rad. Prot. Dosim. **102**(4), 305-314 (2002).
9. Pelliccioni M. Radiation Weighting Factors and High Energy Radiation, Radiat. Prot. Dos. **80**(4), 371-378 (1998).
10. International Commission on Radiological Protection, General Principles for the Radiation Protection of Workers, ICRP Publication 75, Annals of ICRP, **27**(1) (1997).